Genetic, Physiological and Biochemical Responses to Salinity Stress in *Pongamia pinnata*, a Sustainable Feed Stock for Biofuel

Thesis submitted to the University of Hyderabad for the award of

Doctor of Philosophy

By

SURESHBABU MARRIBOINA

Department of Plant Sciences
School of Life Sciences
University of Hyderabad
Hyderabad-500046
Telangana (India)

August, 2020

Regd No. 14LPPH08

Department of Plant Sciences
School of Life Sciences
University of Hyderabad
Hyderabad-500046

DECLARATION

I, Sureshbabu Marriboina, hereby declare that this thesis entitled "**Genetic, Physiological and Biochemical Responses to Salinity Stress in *Pongamia pinnata*, a Sustainable Feed Stock for Biofuel**" submitted by me under the guidance and supervision of Prof Attipalli R. Reddy is an original and independent research work. I also declare that it has not been submitted previously in part or in full to this University or any other University or Institution for the award of any degree or diploma.

Date: 31.08.2020

Name: Sureshbabu Marriboina

Signature: 31/08/2020

Regd. No.: 14LPPH08

Department of Plant Sciences
School of Life Sciences
University of Hyderabad
Hyderabad-500046

CERTIFICATE

This is certify that this thesis entitled "**Genetic, Physiological and Biochemical Responses to Salinity Stress in *Pongamia pinnata*, a Sustainable Feed Stock for Biofuel**" is a record of bonafied work done by Mr. Sureshbabu Marriboina, a research scholar for Ph.D. programme in Plant Sciences, School of Life Sciences, University of Hyderabad under my guidance and supervision. This thesis has not been submitted previously in part or in full to this University or any other University or Institution for the award of any degree or diploma.

Professor Atipalli R Reddy
(Supervisor)

Prof. Atipalli R. Reddy, FNASc
Dept. of Plant Sciences
University of Hyderabad
Hyderabad-500 046, India.

31/08/2020
(Head of the Department)

अध्यक्ष / HEAD
वनस्पति विज्ञान विभाग / Dept. of Plant Sciences
जैविक विज्ञान संकाय / School of Life Sciences
हैदराबाद विश्वविद्यालय / University of Hyderabad
हैदराबाद / Hyderabad-500 046, भारत / INDIA

(Dean of the School)

DEAN
School of Life Sciences
University of Hyderabad
Hyderabad - 500 046.

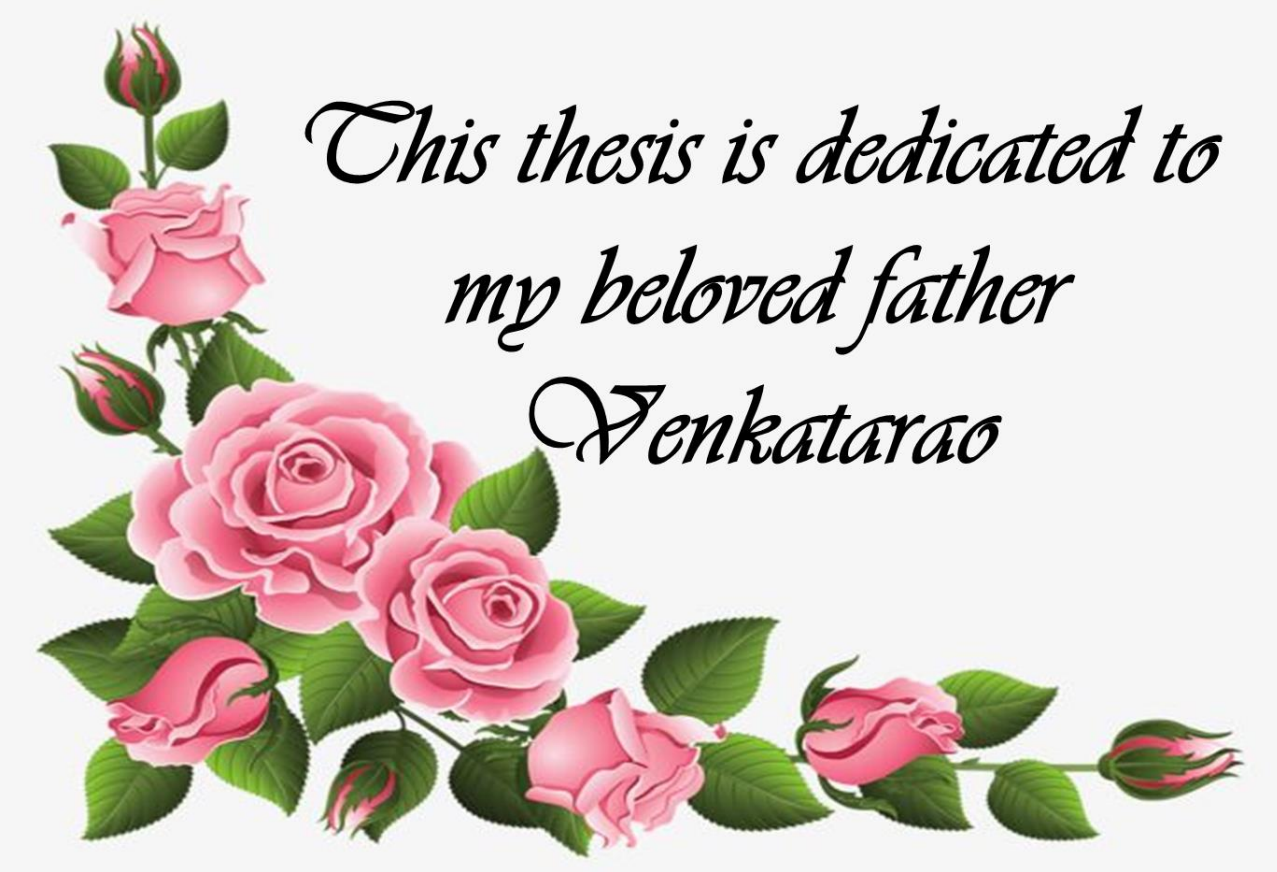
This thesis is dedicated to
my beloved father
Venkatarao

Acknowledgement

It’s a great privilege and honour for me to express my sincere gratitude to my supervisor Prof. Attipalli Ramachandra Reddy from bottom my heart for giving me opportunity to work under his guidance. I also extend my thanks for his invaluable guidance, constant suggestions, encouragement, and support throughout this work which helped me to develop new ideas in research and to improve scientific writing skills to a great extent.

I thank Prof. S. Dayananda, Dean School of Life Sciences; Prof. M. N. V. Prasad, Prof. Rammaiah, Prof. Reddanna, Former Deans, School of Life Sciences for allowing me to use the school facilities for my research work.

I thank Prof. G. Padamaja, Head, Department of Plant Sciences; Prof. Ch. Venkataramana, Former Head, Department of Plant Sciences for allowing me to use the school facilities for my research work.

I also thank Prof. A. S. Raghavendra and Prof. K. P. M. S. V. Padamsree, my Doctoral committee members for their valuable suggestions.

I would like to thank Prof. R. P. Sharma and Prof. M. N. V. Prasad for kindly providing their lab facilities.

I thank faculty members in the School of Life Sciences for sharing their knowledge which helped me developing new ideas in my research.

I thank Dr. Kapil Sharma for helping me in metabolomics and phytohormonal work, and Dr. A. Sebastian for helping me in atomic absorption spectroscopy work.

I thank Ms. Y. Anurupa Devi for helping me in bioinformatics analysis.

I thank Mr. Pavan for helping me in scanning electron microscope work and Ms. Nalini for helping me in confocal microscopy work.

I thank my seniors Dr. Debashree Sengupta, Dr. Sumit Kumar and Dr. K. Madhan Sekar for their valuable suggestions and support.

I also thank my seniors and present lab mates Dr. Chaitanya, Dr. M. Shalini, Dr. R. V. Sreeharsha, Dr. K. Seeta Rami Reddy, Tamna Singha, and Divya for maintaining healthy and cheerful environment in the lab.

I am thankful to my dearest friend A. Sattiraju for his love, caring, affection and support throughout my research.

I am thankful to my friends Dr. B. Bhuvana Chandra, Dr. M. Mohan Krishna, Dr. Rama Krishna, Dr. Varma, Dr. B. Ravi, M. Rajeshrao, S. Venkata Reddy, Trishla, Raju, Kishore, T. Veerashankar, V. Swaroop, Hyma, Ashwini, Rajesh, Durgeshwar and P. Pamuleti for their love and affection throughout my research tenure and also making my University days wonderful and memorable.

I thank Mr. Lakshman, and Mr. Satish for their help in maintaining the greenhouse and tissue culture lab work.

I also thank all the non-teaching staff members of Department of Plant Sciences and School of Life Sciences for their help with the official works during my research tenure.

I thank DBT and UPE for funding in the lab and DST-FIST, UGC-SAP and DBT-CREBB for funding the Department and School.

UGC-NET-JRF fellowship was gratefully acknowledged for assisting the financial help during my research in the form of junior and senior research fellowships.

I am thankful to my family members and my spouse E. Jyothi and my daughter Jashnica Cornelius Suresh for their unconditional love, care, affection, encouragement and moral support throughout my research tenure helping me to stay and focus on research work.

Sureshbabu

LIST OF FIGURES AND TABLES

List of Figures

Chapter 1

Chapter 2

Pongamia. The measurements were performed on the leaves of plants dark-adapted overnight illuminated with the following PAR intensities (0, 226, 412, 612, 846, 1263, 1732, 2638 and 3840 µmol photons m^{-2} s^{-1}). Error bar represents the mean ± SD (n =5).

Figure 3. Effect of salt stress on chlorophyll fluorescence of control and salt-treated *P. pinnata*. Changes in chlorophyll content (A), maximal photochemical efficiency of PSII (Fv/Fm) (B), effective quantum yields of regulated (YNPQ) (C), and non-regulated heat dissipation (YNPQ) of PSII (D) in control and salt-treated plants. Minimal fluorescence (F0) in one-month-old *P. pinnata* leaves after 1, 4 and 8DAS. Changes in the other fluorescence parameters include (E) maximum fluorescence (Fm), (F) coefficient of photochemical chemical quenching (qP). (G) Electron transport rate (ETR) and coefficient of non-photochemical chemical quenching (qN). (H) Apparent maximal photochemical efficiency of PSII (FV'/Fm'). Error bars represent the mean ± SD (n = 5).

Figure 4. Sodium, calcium, potassium and chloride ion content in leaves of 0 (control), 300 and 500 mM NaCl treated plants at (A) 1 DAS, (B) 4 DAS and (C) 8 DAS and in roots of 0 (control), 300 and 500 mM NaCl treated plants at (D) 1 DAS, (E) 4 DAS and (F) 8 DAS respectively. Variations in the ratios of K^+/Na^+, Ca^{2+}/Na^+ and Na^+/Cl^- in the leaves and roots of control and salt-treated plants (G-I). Error bar represents the mean ± SD (n = 6).

Chapter 3

Figure 1. Histochemical detection of lignin and suberin content in leaves of *P. pinnata*. For lignin visualization, sections were stained with HCl-phloroglucinol. Leaf sections of control (A-C) 300 mM (D-F) and 500 mM NaCl (G-I) treated plants at 1, 4 and 8 DAS, respectively. For suberin visualization, sections were stained with Sudan III. Leaf sections of control (J-L), 300 mM (M-O) and 500 mM NaCl (P-R) treated plants at 1, 4 and 8 DAS. Red arrows indicate lignin deposition and black arrows indicate suberin deposition. Cu: cuticle, Ue: upper epidermis, Xy: xylem, Ph: phloem, Lp: lignified parenchyma, Le: lower epidermis. Scale bars = 100 μm.

Figure 2. Histochemical detection of lignin and suberin content in roots *P. pinnata*. Staining was done similar to leaf sections explained previously. Lignin visualization in the root sections of control (A-C) 300 mM (D-F) and 500 mM NaCl (G-I) treated plants at 1, 4 and 8 DAS, respectively. Suberin visualization in the root sections of control (J-O), 300 mM (P-U) and 500 mM NaCl (V-A1) treated plants at 1, 4 and 8 DAS. Red arrows indicate lignin deposition and black arrows indicate suberin deposition. Ex: exodermis, P: phloem-enriched fraction, Xy: xylem, BEX: biseriate exodermis, MEX: multiseriate exodermis. Bars: black bars equivalent to 100 μm and red bars equivalent to 50 μm.

Figure 3. CLSM localization of Na^+ ions using Na^+ specific Coro Na-Green AM (green) and cell-wall binding propidium iodide (red) stains. Leaf sections from control plants (A-C), 300 mM NaCl (D-F) and 500mM NaCl treated plants (G-I) at 1, 4 and 8 DAS. Intensity of CoroNa-Green AM fluorescence in cytosolic and vacuolar compartments in the leaf sections (J). Root sections of control plants (K-M), 300 mM NaCl (N-P) and 500 mM NaCl treated plants (Q-S) 1, 4 and 8DAS. Intensity of CoroNa-Green AM fluorescence in cytosolic and vacuolar compartments in the root sections (T). Red lines were drawn to measure Na^+ fluorescence intensity. For quantification of Na^+ fluorescence intensity more than 20 images were pooled from five biological replicates in control and salt-treated plants. Error bar represents the mean ± SD (n=20).

Figure 4. Illumination of Na^+ ion fluorescence in leaves of control and salt-treated *P. pinnata*. Confocal images of leaves were stained with CoroNa-Green AM (green colour) and propidium iodide (red colour). (A, B and C) cross sections of leaves of control plants, (D, E and F), cross sections of leaves of 300 mM NaCl 1, 4 and 8DAS, (G, H and I) cross sections of leaves 500 mM NaCl 1, 4 and 8DAS respectively. Red arrows were drawn to measure Na^+ fluorescence intensity. Quantification of Na^+ fluorescence intensity more than 12 images were pooled from five biological replicates in control and salt-treated plants. Error bar represents the mean ± SD (n=12). Two-way ANOVA test was performed to measure P-values ns (not significant) * ($P<0.05$), ** ($P<0.01$) and * * * ($P<0.001$) respectively.

Figure 5. Illumination of Na^+ ion fluorescence in roots of control and salt-treated *P. pinnata*. Confocal images of roots were stained with CoroNa-Green AM (green colour) and propidium iodide (red colour). (A, B and C) cross sections of roots of control plants, (D, E and F), cross sections of roots of 300 mM NaCl 1, 4 and 8DAS, (G, H and I) cross sections of roots 500 mM NaCl 1, 4 and 8DAS, (J, K and L) magnified images of roots of control plants, (M, N and O) magnified images of roots of 300 mM NaCl 1, 4 and 8DAS, (P, Q and R) magnified images of roots 500 mM NaCl 1, 4 and 8DAS respectively. White arrows were drawn to measure Na^+ fluorescence intensity. Quantification of Na^+ fluorescence intensity more than 12 images were pooled from five biological replicates in control and salt-treated plants. Error bar represents the mean ± SD (n=12). Two-way ANOVA test was performed to measure P-values ns (not significant) * ($P<0.05$), ** ($P<0.01$) and * * * ($P<0.001$) respectively.

Figure 6. Our proposed model based to show the mechanism of high salinity tolerance in *Pongamia pinnata*. Suberized multiseriate exodermis and lignified walls of xylem vessels, cortical cells, tracheids of root and lignified vascular tissues of leaf are represented. Red line and red arrows: symplastic water and Na^+ transport through cytosol to enhance the Na^+ ion sequestration into the vacuoles of tracheids and xylem parenchyma cells; blue dashed lines: apoplastic water and Na^+ transport through suberized and lignified cell walls to reduce the excess deposition of Na^+ ions in the cytosol of leaf and root cells. Black arrows: water and solute transport though xylem vessels. Red color: suberin lamellae; pink color: cells with lignin deposition; green spots: vacuoles with Na^+ ions; white region with green border: empty vacuole. Abbreviations: vac, vacuole; ex, exodermis; cc, cortical cells; tra, tracheids; xyl, xylem vessel; xpc, xylem parenchyma cells; vas, vascular tissues.

Chapter 4

Figure 1. Effect of salt stress on plant morphology and levels of endogenous phytohormones in leaves and roots of *Pongamia pinnata*. (A) Shoot and root morphology of Hoagland's solution-grown P. pinnata plants after 30 days treated with three different salt concentrations 0 (control), 300 and 500 mM NaCl at three different

time points 1, 4 and 8DAS. The levels of endogenous hormones (B and I) zeatin, (C and J) IAA, (D and K) IBA, (E and L) MeJA, (F and M) SA, (G and N) ABA and (H and O) JA in leaves and roots of 0 (control), 300 and 500 mM NaCl treated plants at three different time points1, 4 and 8DAS respectively. Error bar represents the mean ± SD (n=6). Two-way ANOVA test was performed to measure *P*-values ns (not significant), * ($P < 0.05$), ** ($P < 0.01$) and * * * ($P < 0.001$) respectively.

Figure 2. Hierarchical cluster analysis and heat map of hormone-hormone correlation matrix in *P. pinnata* under different NaCl treatments. Each correlation value (based on Pearson correlation coefficient) corresponds to average of six biological replicates. HAC analysis performed among the hormones at each individual time points (A and D) 1DAS, (B and E) 4DAS, (C and F) 8DAS in leaves as well as (G and J) 1DAS, (H and K) 4DAS, (I and L) 8DAS in roots of 300 and 500 mM NaCl treated plants. The colour key and histogram show degree of correlation.

Figure 3. Heat map of metabolite changes in leaves of *P. pinnata* under salt stress. Log_2 ratios of the relative fold change values (1 to 12) of each metabolite is represented in the form of a single horizontal row portioned with six columns of two salt treatments (300 and 500 mM NaCl) and three different time points (1, 4 and 8DAS) respectively. Each metabolite value is an average of six biological replicates represented with different colour codes red or blue according to the scale bar. The colour scale indicates degree of correlation.

Figure 4. Heat map of hierarchical clustering of metabolite-metabolite correlations in leaves of 300 mM NaCl treated *P. pinnata* under salinity stress. Each correlation value (based on Pearson correlation coefficient) corresponds to average of six biological replicates. HAC analysis performed among the metabolite at each individual time points (A) 1DAS, (B) 4DAS and (C) 8DAS in leaves of 300 mM NaCl treated plants. (D, E and F) Detailed view of positively correlated metabolite correlations was shown in the form of table. HAC analysis performed among the metabolite at each individual time points (G) 1DAS, (H) 4DAS and (I) 8DAS in leaves of 500 mM NaCl treated plants. (J, K and L) Detailed view of positively correlated metabolite correlations was shown in the form of table. The colour key and histogram show degree of correlation.

Figure 5. Heat map of metabolite changes in roots of *P. pinnata* under salt stress. Log_2 ratios of the relative fold change values (1 to 12) of each metabolite is represented in the form of a single horizontal row portioned with six columns of two salt treatments (300 and 500 mM NaCl) and three different time points (1, 4 and 8DAS) respectively. Each metabolite value is an average of six biological replicates represented with different colour codes red or blue according to the scale bar. The colour scale indicates degree of correlation.

Figure 6. Heat map of hierarchical clustering of metabolite-metabolite correlations in roots of 300 mM NaCl treated *P. pinnata* under salinity stress. Each correlation value (based on Pearson correlation coefficient) corresponds to average of six biological replicates. HAC analysis was performed among the metabolite at each individual time points (A) 1DAS, (B) 4DAS and (C) 8DAS in roots of 300 mM NaCl treated plants. (D, E and F) Detailed view of positively correlated metabolite correlations was shown in the form of table. HAC analysis was performed among the metabolite at each individual time points (G) 1DAS, (H) 4DAS and (I) 8DAS in roots of 500 mM NaCl treated plants. (J, K and L) Detailed view of positively correlated metabolite correlations was shown in the form of table. The colour key and histogram show degree of correlation.

Figure 7. Circos plots showing correlations in the hormone-metabolite interactions in *P. pinnata* under different NaCl treatments. All 71 metabolites and 7 hormones were identified in the circle (order of metabolites mentioned in the Table 2, 3, 5 and 6). Each correlation value (based on Pearson correlation coefficient) corresponds to average of six biological replicates and analysis performed between the hormones-metabolites at each individual time points (A and D) 1DAS, (B and E) 4DAS, (C and F) 8DAS in leaves as well as (H and K) 1DAS, (I and L) 4DAS, (J and M) 8DAS in roots of 300 and 500 mM NaCl treated plants. Ribbon colour corresponds to degree of correlation (in leaves: blue (+ve correlation) and red (-ve correlation) and in roots: red (+ve correlation) and green (-ve correlation).

Figure 8. Relative mRNA expression levels of transporters in leaves of *P. pinnata* under salt stress conditions. Log_2 fold changes of NHX1, HKT1:1, SOS2, SOS3, CLC1, V-CHX1, CCX1, V-H^+ATPaseB subunit, V-H+ATPaseE subunit, PM-H^+ATP4.1,

PM-H^+ATP4.1-like, PM-H^+ATPase1, CNGC5, CNGC17, CDPK3, and, CDPK32 in leaves (A) and roots (B) of salt-treated plants of *P. pinnata* at 1, 4 and 8 DAS respectively when compared to their corresponding controls. Error bar represents the mean ± SD (n=6).

Figure 9. Relative mRNA expression levels of cell-wall enzymes and antioxidant enzymes in leaves of *P. pinnata* under Salt Stress Conditions. Log_2 fold changes of CAT4, FeSOD, MnSOD, Cu/ZnSOD1, Cu/ZnSOD1-like, POD, PAL1, PAL2, CAD2, and CAD6, in leaves (A) and roots (B) of salt-treated plants of *P. pinnata* at 1, 4 and 8DAS respectively when compared to their corresponding controls. Error bar represents the mean ± SD (n = 6).

Figure 10. The band intensities of transporter genes of semi-quantitative PCR analysis in leaves and roots of *P. pinnata* under three different salinity stress conditions 0, 300 and 500 mM NaCl at 1, 4 and 8DAS respectively.

Figure 11. Our proposed model based to show the mechanism of high salinity tolerance in *Pongamia pinnata*.

Chapter 5

Figure 1. Root morphology of hydroponically grown 30-days old *P. pinnata* seedlings treated with 500 mM NaCl for 4 days (A–C) when compared to corresponding controls.

Figure 2. (A) Percentage homology of Pongamia proteins with other related legume species and (B) percentage of differentially expressed proteins.

Figure 3. Schematic representation of secondary metabolic pathway. Relative expression of proteins related to Phenylproponoid pathway. Colour key represents fold expression and number indicates number of identified peptides; red colour: up-regulated proteins, green colour: down-regulated proteins, blue colour: unchanged proteins, yellow colour: control specific proteins, and violet colour: treated specific proteins. CHS: chalcone synthase, PAL: phenylalanine ammonia lyase. For protein abbreviations see in table 1.

Figure 4. (A) Relative fold expression of chalcone synthase proteins and (B) isoforms of seed storage proteins. For protein abbreviations see in table 1.

Figure 5. Relative fold expression of DEPs belongs to various metabolic pathways. Colour key represents fold expression and number indicates number of identified peptides; red colour: up-regulated proteins, green colour: down-regulated proteins, blue colour: unchanged proteins, yellow colour: control specific proteins, and violet colour: treated specific proteins. For protein abbreviations see in Table 1.

Figure 6. Schematic representation of carbohydrate metabolic pathway. The relative expression of proteins related to carbohydrate metabolism. Colour key represents fold expression and number indicates number of identified peptides; red colour: up-regulated proteins, green colour: down-regulated proteins, blue colour: unchanged proteins, yellow colour: control specific proteins, and violet colour: treated specific proteins. G6P: glucose-6-phosphatase, MTDH: mannitol dehydrogenase. For protein abbreviations see in Table 1.

Figure 7. Relative fold expression of DEPs belongs to various metabolic pathways. Colour key represents fold expression and number indicates number of identified peptides; red colour: up-regulated proteins, green colour: down-regulated proteins, blue colour: unchanged proteins, yellow colour: control specific proteins, and violet colour: treated specific proteins. For protein abbreviations see in Table 1.

Figure 8. Our proposed model for signalling transcription factors. Colour key represents fold expression and number indicates number of identified peptides; red colour: up-regulated proteins, green colour: down-regulated proteins, blue colour: unchanged proteins, yellow colour: control specific proteins, and violet colour: treated specific proteins. For protein abbreviations see in Table 1.

Figure 9. Relative fold expression of DEPs belongs to various metabolic pathways. Colour key represents fold expression and number indicates number of identified peptides; red colour: up-regulated proteins, green colour: down-regulated proteins, blue colour: unchanged proteins, yellow colour: control specific proteins, and violet colour: treated specific proteins. For protein abbreviations see in Table 1.

Figure 10. Relative fold expression of CYP450 family proteins.

Figure 11. Relative fold expression of DEPs. Colour key represents fold expression and number indicates number of identified peptides; red colour: up-regulated proteins, green colour: down-regulated proteins, blue colour: unchanged proteins, yellow

colour: control specific proteins, and violet colour: treated specific proteins. For protein abbreviations see in Table 1.

Figure 12. The distribution pattern of the chloroplasts across the root section. The bright-filed illumination of chloroplasts across the roots (green in colour) (A-D). The auto fluorescence of chloroplasts (Red in colour) (E-J). False colour was given to chloroplasts violet (G). The chloroplast auto fluorescence was excited with a blue argon laser (488 nm), and emitted light was collected from 660 to 731 nm. Red and White circles were drawn to show the chloroplasts.

Figure 13. Hierarchical cluster heat maps of up-regulated proteins and protein-protein correlations in roots of 500 mM NaCl treated *P. pinnata* at 4DAS. Each correlation value (based on Pearson correlation coefficient) corresponds to average of six biological replicates. HAC analysis was performed among the up-regulated proteins at 4DAS. Boxes were drawn to represent individual groups of DEPs. The colour key and histogram show degree of correlation. For protein abbreviations see in Table 1.

Figure 14. Hierarchical cluster heat maps of down-regulated proteins and protein-protein correlations in roots of 500 mM NaCl treated *P. pinnata* at 4DAS. Each correlation value (based on Pearson correlation coefficient) corresponds to average of six biological replicates. HAC analysis was performed among the down-regulated proteins at 4DAS. Boxes were drawn to represent individual groups of DEPs. The colour key and histogram show degree of correlation. For protein abbreviations see in Table 1.

Figure 15. Correlation networks of DEPs. (A) Up-regulated correlation network based on Pearson correlation coefficient with probability threshold $P < 0.0001$. Each node was represented with different colour based on degree of interaction. The order of interaction was green colour node > blue colour node > yellow colour node respectively. (B) Correlation network of the 53 proteins in cluster; box was drawn to represent zoom-in of the most highly interconnected core of proteins. (C) Down-regulated correlation network based on Pearson correlation coefficient with probability threshold $P < 0.0001$. Each node was represented with different colour based on degree of interaction. The order of interaction was red colour node > blue

List of Tables

Chapter 1

Chapter 4

Chapter 5

Symbols and abbreviations

DAS	Day after salt-treatment
ROS	Reactive oxygen species
SOS	Salt overly sensitive
ABA	Abscisic acid
JA	Jasmonic acid
MeJA	Methyl-jasmonic acid
IAA	Indole-3-acetic acid
IBA	Indole-3-butyric acid
SA	Salicylic acid
RWC	Relative water content
FW	Fresh weight
DW	Dry weight
TW	Turgid weight
A_{sat}	Light saturated net photosynthetic rate
g_s	Stomatal conductance
E	Transpiration rate
ANOVA	Analysis of variance
WUE	Water use efficiency
LC	Light responsive curve
IC	Induction curve
YII	Effective quantum yield of PSII
YNO	Actual quantum yield of non-regulated heat dissipation
YNPQ	Actual quantum yield of regulated heat dissipation/ non-photochemical quenching
NPQ	Non-photochemical quenching
PAR	Photosynthetic active radiation
PPFD	Photosynthetic photon flux density
Fv/Fm	Maximal photochemical efficiency of PSII
Fo	Minimal fluorescence
Fm	maximum fluorescence
qP	Coefficient of photochemical chemical quenching
ETR	Electron transport rate
qN	Coefficient of non-photochemical chemical quenching
FV'/Fm'	Apparent maximal photochemical efficiency of PSII
PSII	Photosystem II
Chl	Chlorophyll
BEX	Biseriate exodermis
MEX	Multiseriate exodermis
XPC	Xylem parenchyma cell

NHX	Na^+/H^+ antiporter
CHX	Cation/H^+ exchangers
CCX	Cation/Ca^{2+} exchangers
PCR	Polymerase chain reaction
RT-PCR	Real-time polymerase chain reaction
HAC analysis	Hierarchical cluster analysis
HKT1:1	High affinity transporter 1:1
CLC1	Chloride channel 1
CNGC	Cyclic nucleotide gated channels
CDPK	Calcium-dependent protein kinase
CATA	Catalase
SOD	Superoxide dimutase
POD	Peroxidase
PAL	Phenylalanine lyase
CAD	Cinnamyl-alcohol dehydrogenase

Table of Contents

Chapter 1

General Introduction, Experimental Design, and Objectives

Our mother Pongamia plant used in the study

Chapter 1 General introduction

Excess accumulation of soluble salts in the soil results in soil salinity. Soil salinization is a growing problem in arid and semi-arid areas. For the past three decades, over 800 million ha, which is about 6% of the total land mass has been converted to marginal saline lands (Munns and Gilliham, 2015). For the past three decades, over 800 million hectares which is about 6% of total land mass has been converted to marginal saline lands (Ismail and Horie, 2017; Marriboina and Reddy, 2020a). At present, about 1125 million hectares of land is polluted with salinity globally (Md-Hossain, 2019). Recent estimates showed that Australia occupied 38.4% saline land after Asia (33.9%), America (15.8%), Africa (8.6%) and Europe (3.3%) (Shahid et al., 2018). Global climatic changes and human interventions were further extended to salinization of cultivable lands. Human induced soil salinization at national level showed that Asia occupied 68.8% saline lands after Africa (19.3%), America (5.7%), Europe (5.0%) and Australia (1.2%) (Shahid et al., 2018). It was estimated that 50% cultivable lands will be salinized by the year 2050 due to increased global population and industrialization (Md-Hossain, 2019). Thus, marginal land cultivation is crucial to meet the global energy demand. On other hand, salinity causes yield losses on an average of 15-55% on every year (Zörb et al., 2018). Salinity or salt-induced land degradation was showed a greater impact on economic value and was estimated that approximately $27.3 billion was used to rehabilitate or modify the saline marginal lands towards agriculture productivity (Zörb et al., 2018).

Salt stress imposes salt-induced drought and ion toxicity on plants (Kaur and Nayyar, 2014). Both salt-induced drought and ion toxicity limit the plant growth and productivity. It is crucial to develop new strategies for salt tolerant crops to utilize the marginal saline lands towards sustainable agriculture productivity. Soil salinity is not only halt the plant growth and productivity but also changes the physiological and biochemical properties of soil (Shrivastava and Kumar, 2015). Thus, understanding the genetic, physiological and

molecular responses of plants are essential for optimizing plant performance under moderate saline water available conditions. In addition, studying soil texture and its chemical composition are also important to readjust the saline soils with amendments, which can mitigate the soil salinity and support plant growth (Rady, 2012).

Classification of higher plants based on salinity and their strategies

Based on salinity tolerance, plants are categorized into two groups glycophytes and halophytes. Glycophytes are salt sensitive plants including crop species, whereas halophytes are salt tolerant plants including shrubs and tree species. Halophytes can grow in soils with salt concentration of ~200 mM to ~500 mM NaCl (Yuan et al., 2019). Each halophyte species has adapted unique mechanisms to defend the salt toxicity. For example, the halophytic species *Atriplex* and *Chenopodium (Amaranthacea*e) contain a specialized bladders present in the epidermal cells, which helps in sequestering or excreting salt away from the tissues (Table 1) (Adolf et al., 2013; Guo et al., 2019). Additionally, quinoa accumulates free Na^+ and Cl^- ions in order to regulate osmotic imbalance (Adolf et al., 2013). According to Krishnamurthy et al. (2014) and Cheng et al. (2020), mangroves such as *Avicennia* species and *Bruguiera* species develop apoplastic barriers and salt glands to exclude salts from the tissues. Salt cress, *Thellungiella halophile* is a halophytic plant and a close relative of *Arabidopsis* operates vacuolar Na^+ sequestration mechanism to survive under extreme saline conditions (Wang et al., 2013).

Glycophytes such as barely, wheat, and rice were also developed salt tolerance by operating various strategies (Kamboj et al., 2015; Kumar et al., 2017; Quan et al., 2018). Low Na^+/K^+ ratio is one of the key strategies glycophytes can employ against salt stress to maintain Na^+ concentration inside the cell (Assaha et al., 2017). Xylem differentiation and xylem vessel pore size adjustments are other adaptive mechanisms to enhance the water

permeability across the plant under salt stress conditions (Escalante-Pérez et al., 2009). In addition, excess accumulation of Na^+ ions could inhibit the synthesis of photosynthetic pigments and thus net photosynthesis which leads to an imbalance between absorption and utilization of the energy during carbon fixation, resulting in excessive accumulation of reactive oxygen species (ROS) and disruption of the cellular redox homeostasis (Li et al., 2017). Plants have developed efficient antioxidative enzyme systems to maintain the redox state of the cell under such adverse environmental conditions (Rossatto et al., 2017). In addition, proton pumps and cation channels work together to maintain membrane potential and ion homeostasis under salt stress conditions (Falhof et al., 2016; Li et al., 2016; Liu et al., 2017). Based on the available information, we can summarize the basic plant responses to soil salinity as shown in Figure 1.

Salt-induced responses of plants

In general, salinity affects plant growth and development by decreasing the water potential of soil leading to reduced water uptake by roots (Shinozaki and Yamaguchi-Shinozaki, 1997). Salinity leads to uptake of Na^+ and Cl^- ions along with water. Thus, long term salinity and/or absence of efficient extrusion/sequestering mechanisms in plants result in accumulation of high concentrations of Na^+ and Cl^- in the cytosol causing ion homeostasis imbalance at cellular level. Salinity-induced decline in photosynthetic rates due to stomatal closure is an adaptive response (Shabala et al., 2012). However, excessive accumulation of Na^+ ions within photosynthetic tissues leads to toxicity and damage to the photosynthetic machinery which is detrimental to the plant. In order to survive, plants need to limit Na^+ transport into the shoot tissue by compartmentalizing the Na^+ into the root stele and vacuoles (Hasegawa, 2013; Benito et al., 2014; Julkowska et al., 2014) (Figure 1). In order to withstand the Na^+ toxicity, salt-tolerant

plant species develop certain morphological, physiological and biochemical mechanisms which include initiation of lateral roots, ion compartmentalization, biosynthesis of osmo-

Figure 1. Salinity-induced physiological, biochemical and molecular responses in plants

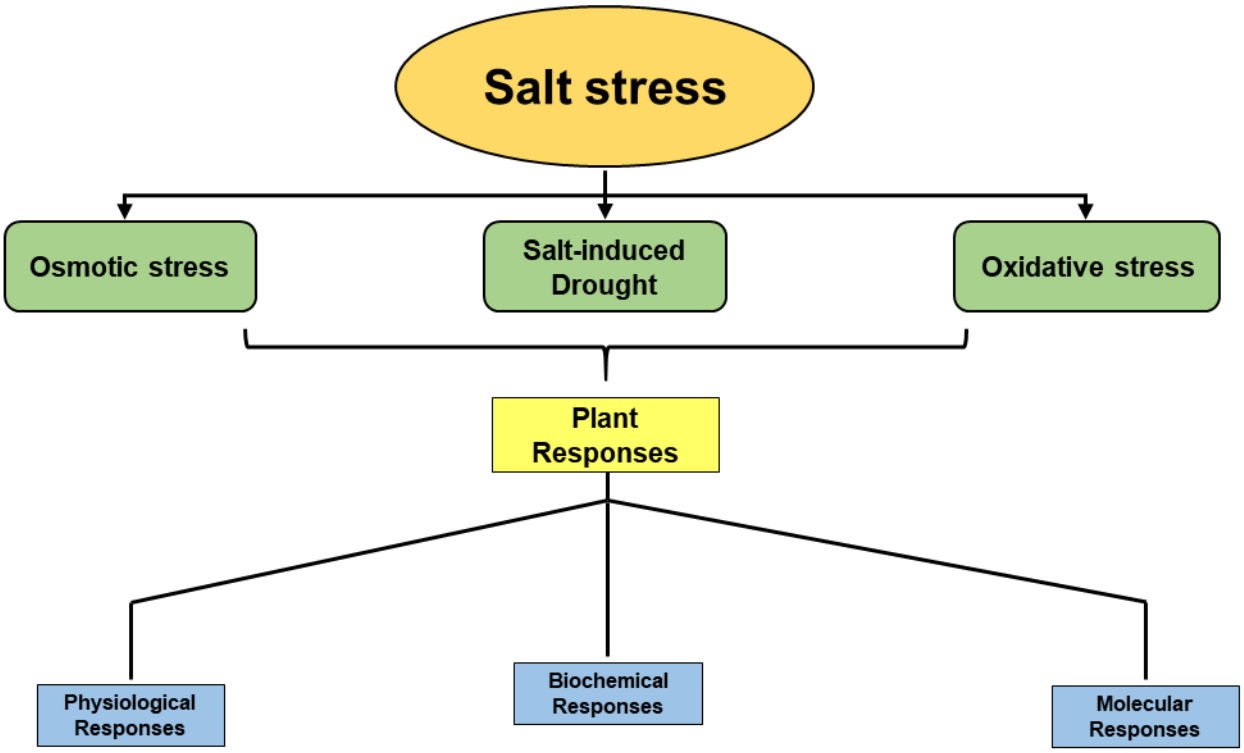

- Recognition of root salt signal
- Decreased stomatal conductance
- Decline net photosynthetic rate
- Reduced root growth rate
- Increased root relative water content
- Decreased root relative water content
- Turgor and osmotic adjustments

- Increased accumulation of Ca^{2+} ion content
- Na^{+} and K^{+} ion homeostasis, Na^{+}/K^{+} balance
- Increased accumulation of polyols or osmolytes
- Enhanced accumulation of phytohormones such as ABA, JA, IAA, zeatin and SA
- Increased production of Glucose and Sucrose
- Induction organic acid and cell wall carbohydrate synthesis

- Induction of stress responsive proteins
- Induction of anaerobic cycle regulatory proteins
- Increased accumulation of secondary metabolite proteins
- Induction of protein modifying enzymes such as protease inhibitors and chaperons
- Increased accumulation of cell wall related proteins
- Induction of glycoproteins

protectants andactivation of salt exclusion and/or sequestering pathways (Munns and Tester, 2008). Before responding to salinity stress, plants need to first perceive the stress signal and then transfer it through a series of signaling components to the final response *i.e.* expression of salt-responsive genes. Further, antioxidative defense system has been reported to play a key role in some members of both C_3 and C_4 plants, to neutralize the effect of stress-induced toxic levels of ROS. As ROS production is a continuous process, most of the antioxidative enzymes are constitutively expressed. Salt stress is known to induce expression of certain key enzymes including guaiacol peroxidase (POD) and ascorbate peroxidase (APX) which are considered as regulators of ROS and are required to maintain the ROS levels within physiological levels (Abogadallah, 2010). Most important mechanism for salt-tolerance in plants is through the salt overly sensitive (SOS) pathway, wherein salt stress perception by a salinity receptor (unknown), Ca^{2+} spikes (enhanced Ca^{2+} levels) are generated within the cytoplasm acting as secondary signals for activating the SOS pathway components.

Plants growing in saline soils, restrain the root cell wall expansion through increased deposition of lignin and suberin on the root cell walls to prevent excessive flow of toxic Na^+ ions through the apoplastic pathway and increase water retention in the roots (Shabala and Mackay, 2011). In addition, the increased number of lignified tracheary elements in the vascular tissues under salt stress also enhances the water permeability and greater selectivity for ion uptake in crops such as soybean and tomato (Neves et al., 2010). The accumulation of high amounts of Na^+ ions in the plants can also create ionic imbalance leading to osmotic stress, ion toxicity, and oxidative stress. To mitigate the effect of osmotic and ionic toxicity, plants are known to accumulate various compatible inorganic ions (K^+ and Ca^{2+}) and organic osmolytes (valine, glucose, fructose, sucrose, mannitol, pinitol, glycerol, and myo-inositol) (Gharsallah et al., 2016; Papazian et al., 2016).

Calcium ion (Ca^{2+}) is known as an intracellular second messenger and plays an important role in plant growth and development. It also plays an essential role in amelioration of sodium toxicity through activating several Ca^{2+} responsive genes and channels (Thor, 2019). In response to salt stress, plants produce several phytohormones such as abscisic acid (ABA), jasmonic acid (JA), methyljasmonic acid (MeJA), zeatin, indole acetic acid (IAA), indole butyric acid (IBA) and salicylic acid (SA), which play crucial role in sustaining its growth under extreme saline conditions. ABA is well-known stress induced phytohormone, critical for plant growth and regulates numerous downstream signalling responses (Tuteja, 2007). ABA causes stomatal closure to prevent excess water evaporation and regulate root growth under salinity stress (Zelm et al., 2020). Salt-induced endogenous accumulation of cytokinin improves salt tolerance in crop species by delaying leaf senescence and marinating photosynthetic capacity (Liu et al., 2012; Golan et al., 2017). According to Sahoo et al. (2014), the perfect harmony among phytohormones played a significant role in improving the salt tolerance in rice. However, the synergistic and antagonistic interactions between phytohormones are mostly depending on plant species and type of stress imposed on plants, but their interactions are still not clearly understood (Gupta et al., 2017). To combat against salinity-induced ROS damage, plants adapted jasmonates-directed anthocyanin accumulation to mitigate its negative effects (Ali and Baek, 2020). Further, JAs can positively regulate the endogenous ABA level to regulate the guard cell movement during salt stress (Siddiqi and Husen, 2019).

When plant exposed to salt stress, root is the primary organ in plant to sense and respond to salinity (Fu et al., 2019). Root acts as a physical barrier to restrict the Na^+ ion distribution across the plant (Marriboina and Reddy, 2020a). Auxin, one of the important phytohormone, plays a crucial roles in plants in order to adapt to changing environmental conditions. Auxin

plays important role in root meristem maintenance and root growth (Fu et al., 2019). The expression of auxin responsive proteins, auxin-induced proteins and auxin transporter-like proteins regulate root vasculature and involved in lateral root growth development (Péret et al., 2012). To avoid osmotic pressure imbalance, plants synthesize cell wall remodelling enzymes to protect cell wall turgor during salt stress (Tryfona et al., 2014; Saqib et al., 2019). In response to salt stress, plants also induce synthesis proteins related to secondary metabolism including flavonoid and anthocyanin biosynthesis. By induction of flavonoids and anthocyanins, plant can defend against ROS damage under salt stress (Chen et al., 2019). On the hand, plants also trigger antioxidant defense systems to cope with salinity-induced oxidative stress (Al-Kharusi et al., 2019). Alternations in cellular metabolism are essential for plant survival during conditions of salt stress (Kosova et al., 2018).

Table 1. Consolidated literature during the last decade on plant responses to salinity stress

	Growth stage	Salinity treatment duration	Techniques used	Response observed	References
Halophytes and mangroves					
Chenopodium quinoa	5 day old seedlings	100 or 400 mM NaCl stress for 21 days	Biochemical analysis, atomic absorption spectroscopy	Significant induction of SOD, organic solutes (soluble sugars, proline) and inorganic ions (Na^+ and K^+) in leaves.	Cai and Gao, (2020)
Avicennia marina	3 month old seedlings	600 mM NaCl stress for 10 days	CP-OES and anion chromatography, fluorescence photo-microscope.	Induction of root apoplastic barrier and root sodium exclusion.	Cheng et al., (2020)
Thellungiella halophila	50 day old seedlings	200, 400 or 600 mM NaCl stress for 15 days	Proteomics	Compartmentalizing Na^+ ions into cell vacuoles and accumulating osmolytes.	Wang et al., (2013)
Aeluropus littoralis	30 day old seedlings	200 or 400 mM NaCl stress for 72 h	Transcriptomics	Induction of jasmonic acid and abscisic acid signaling pathway.	Younesi-Melerdi, et al., (2020)
Mesembryanthemum crystallinum	14 day old seed lings and 28 day old seedlings	100 or 400 mM NaCl stress for 6 weeks and 500 mM NaCl stress for 14 days	Biochemical assay and physiological and gas exchange measurements	NaCl-induced ATP-synthesis in mitochondria and C_3 to CAM Transition.	Tran et al., (2020) and Guan et al., (2020)
Suaeda salsa	Six leaf stage saplings	100 or 500 mM NaCl stress for 7 days	Transcriptomics	Regulation K^+ ion homeostasis, ROS mitigation pathways, photoprotection of photosystem PSII and transcriptional regulation pathways.	Zhang et al., (2020)
Atriplex sp	Six leaf stage saplings	300 mM NaCl stress for 7 days	Transcriptome, RT-PCR and SEM analysis	High expression of sodium/potassium transporters (such as HKT1 and CNGC14) and ABA-dependent stomatal movements, photosynthesis and ROS pathways.	Yao et al., (2020)
Cakile maritima	Two leaf stage saplings	100 or 400 mM NaCl stress for 20 days	Metabolomics	Enhanced accumulation of amino acids (GABA, proline, glycine) and alterations in leaf sugar content.	Arbelet-Bonnin et al., (2020)
Salicornia europaea	Plants were observed contaminated soils	1M NaCl stress	Transcriptomics	Increased levels of K^+ and Ca^{2+} ions and enzymes S-adenosyl methionine, CP47 of light-harvesting complex II, photosystem I proteins, Hsp70 gene, ATP-dependent Clpproteases, ribulose bisphosphate carboxylase/oxygenase (Rubisco), phenylalanine ammonia-lyase (PAL), cytochromec oxidase (COX) and ATP synthase.	Furtado et al., (2019)

Plant	Growth stage	Salinity treatment duration	Techniques used	Response observed	References
Halogeton glomeratus	2 months old seedlings	100, 200, 300, 400 and 500 mM NaCl stress for 21 days	Proteomics	Sodium ion distributed into specific salt-storage cells, sequestration into vacuoles, and succulence of leaves.	Wang et al., (2015)
Bruguiera gymnorhiza	150 day old seedling	30 PSU (Practical Salinity Unit)	IRGA, PEA, and CP-MASS.	Enhanced leaf photosynthetic rate, capacity to regulate photoelectron uptake/transfer, and leaf succulence and increased accumulation K^+ and Ca^{2+} ions	Wang et al., (2020)
Rhizophora mangle	2 years old saplings	1, 10, 30, and 50 PSU for 10 days	steady-stateporomete, vapor pressure osmometer, and osmometer.	Decreased leaf stomatal conductance, whole-plant hydraulic conductance osmotic potential and substrate water potential.	Méndez-Alonzo et al., (2016)
Kandelia candel	Four leaf stage saplings	300, 450, and 600 mM NaCl stress for 3 days	Biochemical assays, flame photometer, proteomics	Na^+ compartmentalization and salt-induced expression of proteins related to protein folding, photosynthesis, energy metabolism and signal transduction	Wang et al., (2014)
Sonneratia alba	3 weeks old saplings	250 or 500 mM NaCl stress for 7 day	Transcriptomics	Up-regulation of proteins related to flavone and flavonol biosynthesis.	Feng et al., (2020)
Salt tolerant glycophytes and crop species					
Oryza sativa	Three leaf stage seedlings	140 mM NaCl stress	Genomics	Increased expression of genes related to OsMYB6, OsGAMYB, OsHKT1;4, OsCTR3, and OsSUT1.	Liu et al., (2019)
Triticum aestivum	After germination	50, 100, 150, and 200 mM NaCl stress	qPCR and genome wide analysis	High leaf Na^+ accumulation and root sodium extrusion pathways.	Genc et al., (2019)
Hordeum vulgare	20 day old seedlings	300 mM NaCl stress for 6 days	Biochemical analysis and proteomics	Up-regulation of proteins related to photosynthesis, reactive oxygen species (ROS) scavenging, and ATP synthase.	Zhu et al., (2020)
Cajanus cajan	Three weeks old seedlings	50, 100, and 150 mM of NaCl stress	Metabolomics	Enhanced accumulation of metabolites such as β-cyano-L-alanine and O-acetylsalicylic acid.	Biswas et al., (2018)
Cicer arietinum	7 day old seedlings	25 mM, 50 mM, 75 mM and 100 mM NaCl stress for seven days	Biochemical assays	High activities of catalase, Δ^1-pyrroline-carboxylate synthetase, superoxide dismutase, ascorbate peroxidase and glutathione reductase.	Kaur et al., (2020)

Plant	Growth stage	Salinity treatment duration	Techniques used	Response observed	References
Vigna radiata	After germination	100 mM NaCl stress for 8 days	Biochemical assays	Accumulation of osmolytes and enhanced activity of ROS scavenging enzymes such as GPOX and catalase	Tamang et al., (2016)
Glycine max	Three trifoliate stage seedlings	150 mM NaCl stress for 48 h	Root phosphoproteomics	Up-regulation of proteins related to chalcone synthase, chalcone isomerase, andcytochrome P450 monooxygenase,	Pi et al., (2016)
Medicago sp	7 day old seedlings	16.6 dS m^{-1} (Decisiemens)	Biochemical assays and RT-PCR	Up-regulation of genes related to transporters SOS1, SOS2, SOS3, HKT1, AKT1, NHX1, P5CS1, HSP90.7, HSP81.2, HSP71.1, HSPC025, OTS1, SGF29 and SAL1.	Sandhu et al., (2017)
Lotus japonicus	10 day old seedlings	25, 50, 100, and 150 mM NaCl stress for 28 days	Biochemical assays and flame photometer.	Enhancement of superoxide dismutase and glutathione reductase activities, and increased total and reduced glutathione content and lower Na^+ accumulation in leaves.	Melchiorre et al., (2009)
Pisum sativum	20 day old seedlings	2.5, 5.0, 7.5 and 10.0 dS m^{-1} for 40 days	Flame photometer	Accumulation of inorganic osmolytes Na^+, K^+ and Ca^{2+}.	Shahid et al., (2012)
Phaseolus vulgaris	3 week old seedlings	50, 100 and 200 mM NaCl stress for 7 days	Biochemical assays	Decreased photosynthetic pigments and accumulation of phenolic compounds, flavonoids and ascorbic acid	Taïbi et al., (2016)
Gossypium hirsutum	3^{rd} - 4^{th} stage leaf seedlings	100, 150 and 200 mM NaCl stress for 3 weeks	Biochemical assays and flame photometer.	Reduced stomatal conductance, transpiration and photosynthetic rate and ionic imbalance.	Hassan et al., (2014)
Nicotiana tabacum	3 week old seedlings	500 mM NaCl stress for 7 days	Proteomics	Enhanced accumulation of osmolytes, such as proline and myo-inositol, and changes in GABA shunt, and biosynthesis of aromatic amino acids.	Zhang et al., (2011)
Helianthus annuus	10 day seedlings	50, 150 and 250 mM NaCl stress for 30 days	Biological assay	Reduced activity of glutathione reductase (GR) and ascorbate peroxidase (APX), and superoxide dismutase (SOD).	Taher et al., (2018)
Arachis hypogaea	14 day seedlings	200 mM NaCl stress for 48 h	Transcriptome	Up-regulation of MYB, AP2/ERF, WRKY, bHLH, and HSF.	Zhang et al., (2020)
Zea mays	After germination	9.5 dS cm^{-1} for four weeks	Proteomics	High abundance of proteins involved in reactions to oxidative stress, dehydration, respiration, and translation	Soares et al., (2018)

Adapting the anaerobic respiration, plants are able to cope with the cellular energy demands under salinity stress (Kürsteiner et al., 2003; Luo et al., 2017). Assimilation of nitrogen is crucial for the plant to synthesize of new proteins, which play crucial role in cellular process during salt stress. Expression of protease inhibitors and heat shock proteins in response to salinity might enhance the cellular protein turnover by inhibiting the protein degradation and misfolding of proteins during salt stress (Haq et al., 2019). According to Kobayashi et al., (2013) salt-induced chloroplast accumulation in roots showed an increase in root photosynthesis, carbon assimilation rate and root biomass.

In the present agriculture scenario, Salinity is one of the major environmental constraints limiting plant growth and productivity and is becoming more extensive in the arid and semi-arid areas (Munns and Gilliham, 2015). Global climate change, inadequate water supply and excessive irrigation are further expanding the marginalization of arable lands, thereby limiting their availability for crop production (Shabala, 2013; Quinn et al., 2015; Sharma et al., 2016). To date, attempts to extend the crop productivity on saline lands had limited success, due to the failures in determining plant responses to salt stress owing to the high physiological and genetic diversity among various plant species and spatio-temporal heterogeneity of soil salinity (Jones et al., 2014; Pandolfi et al., 2016; Shabala et al., 2016). Indeed, salt tolerance is a complex trait governed by multiple genes intertwining with various physiological and biochemical mechanisms. A comparative understanding of physiological and morphological adaptive mechanisms evoked interest among researchers worldwide over the past few decades, to sustain crop productivity on marginal lands Dwindling fossil fuel resources has raised attention towards renewable energy resources to meet global energy demand in future. Oil seed-producing perennial halophytes are now gaining importance as a renewable energy resource (Chhetri et al., 2008). Biofuels are a viable substitute

for fossil fuels providing greater environmental benefits over fossil fuels by reducing the emission of GHGs (green house gases) and minimizing their negative impact on human and environment. Growing salt-tolerant perennial halophytes for sustainable bioenergy production on marginal lands will create a win-win situation between energy and land use competition without interfering productive arable land (Quinn et al., 2015). Interestingly, Pongamia can serve as a good alternative for the utilization of marginal saline lands associated with economic gain. *Pongamia pinnata* belongs to family *Fabaceae* is indigenous to the Indian subcontinent and also distributed to other temperate Asian regions including China, Japan, Malaysia, Australia, and Pacific Islands (Scott et al., 2008; Sangwan and Sharma, 2010). Pongamia is a medium-sized fast-growing tree with oil-rich seeds and is capable of adapting to wide agro-climatic conditions (Kesari et al., 2010; Wang et al., 2011). Although Pongamia does not possess salt adaptive characters such as leaf salt bladders, succulence, and trichomes like mangroves, it can still endure up to sea saline concentration (3% NaCl). Based on its physiological and molecular characteristics under salt stress, Pongamia is classified as transition species (intermittent species between glycophytes and halophytes), semi-mangrove or mangrove associate (Wang et al., 2013; Jiang et al., 2017). To deal with high salinity conditions, trees like mangroves and mangrove associates have evolved intricate response regulatory mechanisms during their evolution (Parida and Jha, 2010).

Although, the physiological and biochemical responses of several crop species in response to salinity stress, the responses of tress species to high salinity are not well known. It is crucial to elucidate the critical changes in responses to salinity which will help to improve tree species and to grow in marginal lands.

Objectives

Beased on above background information we framed the following objectives:

- To analyse the morphology and photosynthetic performance of *Pongamia pinnata* under medium and severe salinity stress conditions both in terms of concentration as well as duration of exposure by utilizing a hydroponic growth system.

- To elucidate the salt management strategies in leaves and roots of *Pongamia pinnata*, subjected to salinity stress.

- Analysis of integrative molecular, phytohormonal and metabolomic responses of *Pongamia pinnata* under medium and severe salinity stress conditions.

- Characterization of dynamic Pongamia root protein modulation in response to high salinity stress through proteome approach.

Plant material, growth conditions and experimental design

Plant material

Seeds of Pongamia accession TOIL 12 were obtained from Tree Oil India Limited (TOIL), Zaheerabad, Hyderabad, Telangana. The TOIL 12 Pongamia accession was chosen for this study based on its consistent high yields of three years over 300 accessions of Pongamia.

Plant growth, conditions and salinity treatment

Pongamia seeds were germinated on moist cotton for 10 days at 25°C in the dark. The germinated seedlings were grown in a long cylindrical glass tube (5 cm diameter X 60 cm length) filled with full-strength Hoagland No. 2 basal salt mixture (Himedia) solution adjusted to pH 5.75 ± 0.02 for 30 days. The solution was replenished every seven days (Chen et al., 2017). The hydroponic experiment was carried out in a plant culture room maintained at 24°C with a 16 h photoperiod and relative humidity maintained approximately at 60%. For salinity treatment, 30 days old plants (n = 20–30) were selected and subjected to 300 and 500 mM NaCl concentrations with an increment of 100 mM NaCl per day. Control plants were maintained with fresh Hoagland nutrient solution. Plants were harvested at an interval of 1 day after stress-treatment (1DAS), 4 and 8DAS. Fresh weights of leaf and root were measured immediately after harvest. Dry weights of control and treated plants were determined after drying at 70°C for 3 days. Control and treated samples were harvested at each time interval, flash frozen in liquid nitrogen and stored at –80°C prior to analysis.

Figure 2. **Growth and morphology of soil, and hydrophonically grown TOIL12 *Pongamia pinnata* seedlings.**

(A) Seeds of TOIL12 *Pongamia pinntata,*

(B) Seedlings were grown 20 liter pots, filled with sand and soil mix (1:3) in green house (University of Hyderabad, Hyderabad) under optimum conditions,

(C) Morphology of 30 day old Pongamia seedlings (controls),

(D) Seedlings of 30 days were treated with two different salt concentratons 300 mM and 500 mM NaCl for 15 days,

(E) Seedlings were grown hydroponicaly in a long cylinderical tube (1 liter capcity) filled with full-strength Hoagland solution in growth chamber (University of Hyderabad, Hyderabad) under optimum conditions,

(F) Morphology of 30 day old Pongamia seedlings,

(G) Seedlings of 30 days were treated with two different salt concentratons 300 mM and 500 mM NaCl for 8 days.

Plant material, growth conditions and experimental design

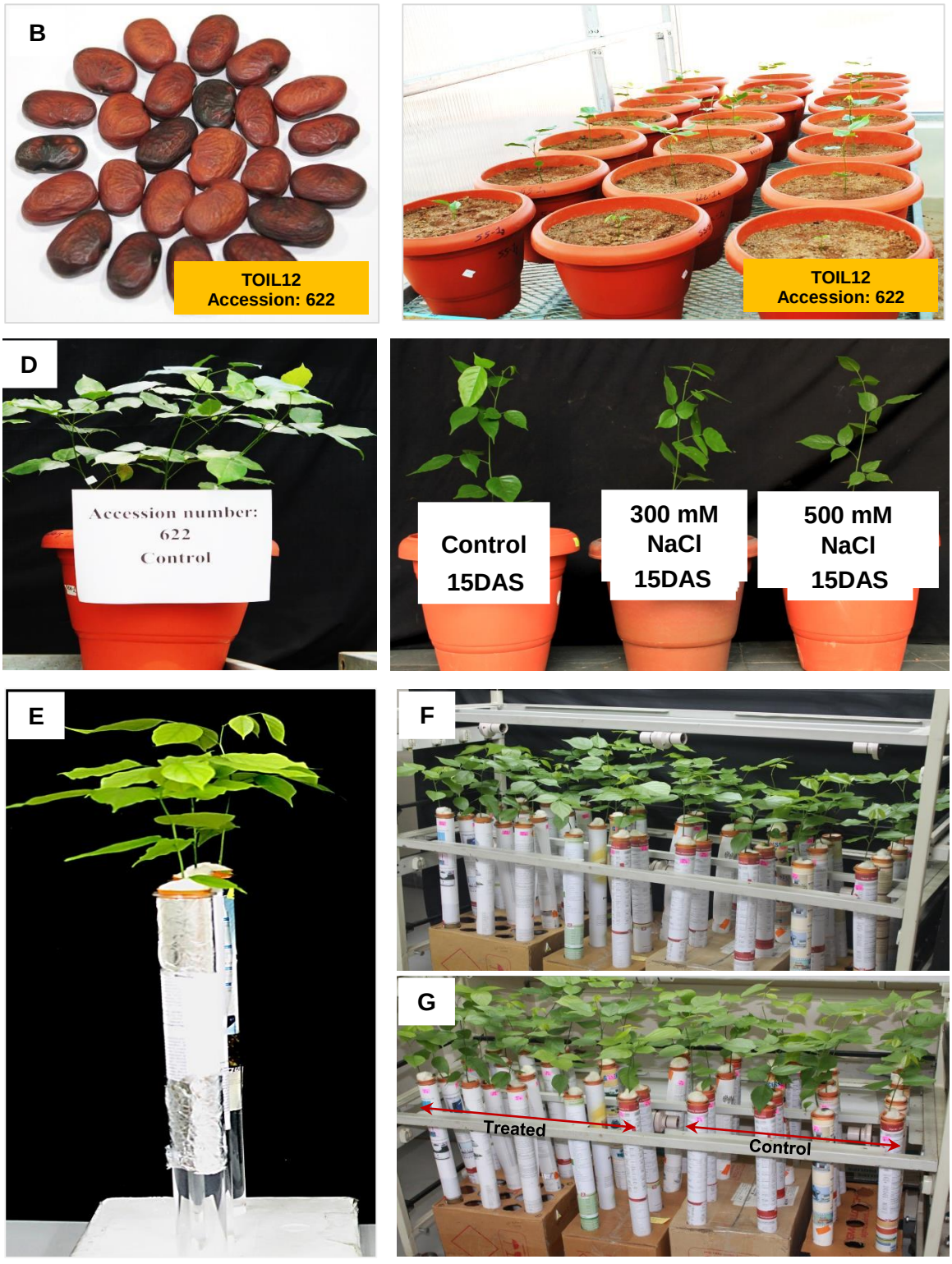

Chapter 2

Salt stress-induced changes in photosynthetic activity and ion contents in *Pongamia pinnata* (L.) pierre

Chapter 2 Introduction

Salinity is one of the major environmental constraints limiting plant growth and productivity and is becoming more extensive in the arid and semi-arid areas (Munns and Gilliham, 2015). Global climate change, inadequate water supply, and excessive irrigation are further expanding the marginalization of arable lands and thereby limiting their availability for crop production (Shabala, 2013; Quinn et al., 2015; Sharma et al., 2016). To date, attempts to extend the crop productivity on saline lands had limited success due to failures in determining plant responses to salinity owing to the high physiological and genetic diversity among various plant species as well as spatio-temporal heterogeneity of soil salinity (Pandolfi et al., 2016; Shabala et al., 2016). Indeed, salt tolerance is a complex trait governed by multiple genes intertwining with various physiological and biochemical mechanisms. A comparative understanding of physiological and morphological adaptive mechanisms evoked interest among researchers worldwide over the past few decades to sustain crop productivity on marginal lands (Jones et al., 2014). However, it is also essential to understand the detailed anatomic and molecular level mechanisms leading to salinity tolerance in plants.

Based on their survival strategies, halophytes are broadly classified as salt-secretors which excrete the salt through specialized glands on the leaves, and non-secretors exclude out the salt through specialized barriers in the roots (Parida and Jha, 2010; Wang et al., 2011; Jiang et al., 2017). However, the tolerance of all halophytes to salinity relies on controlled uptake and compartmentalization of Na^+, K^+, and Cl^- and the synthesis of organic 'compatible' solutes, even through salt glands are operative. Also, during salt stress, reduced water uptake may limit the intercellular CO_2 concentration in the leaf due to stomatal closure. In addition, excessive Na^+ decreases the synthesis of photosynthetic pigments and net photosynthesis which leads to an imbalance between absorption and utilization of the energy during carbon fixation, resulting in excessive accumulation of reactive oxygen species (ROS)

and disruption of the cellular redox homeostasis (Li et al., 2017). The accumulation of high amounts of Na^+ ions in the plants can also create ionic imbalance leading to osmotic stress, ion toxicity, and oxidative stress. To mitigate the effect of osmotic and ionic toxicity, plants are known to accumulate various compatible inorganic ions (K^+ and Ca^{2+}) and organic osmolytes (valine, glucose, fructose, sucrose, mannitol, pinitol, glycerol, and myo-inositol) (Gharsallah et al., 2016; Papazian et al., 2016). However, an integrated analysis to demonstrate the co-existing adaptive and defensive mechanisms for conferring overall tolerance under salinity stress is essential for gaining a thorough understanding of a specific plant's salt stress responses.

Oil seed-producing perennial halophytes are now gaining importance as a renewable energy resource (Chhetri et al., 2008). Growing salt-tolerant perennial halophytes for sustainable bioenergy production on marginal lands, will efficiently manage the energy and land use competition without interfering with productive arable land areas (Quinn et al., 2015). Interestingly, Pongamia can serve as a good alternative for the utilization of marginal saline lands associated with economic gain. Although Pongamia does not possess salt adaptive characters such as leaf salt bladders, succulence and trichomes like mangroves, it can still endure up to sea saline concentration (3% NaCl). Based on its physiological and molecular characteristics under salt stress Pongamia is classified as a transition species (intermittent species between glycophytes and halophytes), semi-mangrove or mangrove associate (Wang et al., 2013; Jiang et al., 2017). However, for in-depth analysis, a systematic and accurate salt exposure under non-limiting root proliferation conditions are essential to understand the mechanism of stress tolerance, specifically salinity stress in Pongamia.

In the present study, we aimed to analyse the physiological, biochemical, anatomical as well as molecular adaptive and defensive responses of *Pongamia pinnata* under medium and

severe salinity stress conditions both in terms of concentration as well as duration of exposure by utilizing a hydroponic growth system consisting of specialized elongated glass tubes, with periodic replacement of nutrient medium. The present study focuses on salt management strategies in leaves and roots of *Pongamia pinnata*, which can be highly useful for further studies on yield improvement of Pongamia under saline conditions.

Plant material, growth conditions, and salinity treatment

Seeds of *P. pinnata* accession TOIL 12 were obtained from Tree Oil India Limited (TOIL), Zaheerabad, Hyderabad, Telangana and were germinated on moist cotton for 10 days at 25°C in the dark. The germinated seedlings were grown in a long cylindrical glass tube (5 cm diameter X 60 cm length) filled with full-strength Hoagland No. 2 basal salt mixture (Himedia) solution adjusted to pH 5.75 ± 0.02 for 30 days. The solution was replenished every seven days (Chen et al., 2017). The hydroponic experiment was carried out in a plant culture room maintained at 24°C with a 16 h photoperiod and relative humidity maintained approximately at 60%. For salinity treatment, 30 days old plants (n = 20-30) were selected and subjected to 300 and 500 mM NaCl concentrations with an increment of 100 mM NaCl per day (Chen et al., 2017). Control plants were maintained with fresh Hoagland nutrient solution. Plants were harvested at an interval of 1 day after stress-treatment (1DAS), 4 and 8DAS. Fresh weights of leaf and root were measured immediately after harvest. Dry weights of control and treated plants were determined after drying at 70°C for 3 days. Control and treated samples were harvested at each time intervals, flash frozen in liquid nitrogen and stored at −80°C prior to analysis.

Relative water content

Freshly harvested leaves and roots of control and salt treated plants were used to estimate relative water content (RWC). Both leaves and roots of control and salt treated plants were weighed (fw) before immersed in double distilled water and kept in refrigerator at 4°C for 24 hours. After 24 hours, turgid weights (tw) of control and salt treated leaves and roots were measured. Further, both leaves and roots of control and salt treated plants were kept in hot air oven for drying at 70°C for 3 days and dry weights (dw) were measured. RWC values were calculated by using the following formulae $\mathrm{RWC}\ (\%) = \left[\frac{\mathrm{Lfw}-\mathrm{Ldw}}{\mathrm{Ltw}-\mathrm{Ldw}}\right] \mathrm{X}100$ where,

fw is the leaf fresh weight, tw is the leaf turgid weight and dw is the leaf dry weight. Further, Leaf relative water content represented as LRWC and root relative water content represented as RRWC.

Measurements of leaf gas exchange parameters

Leaf gas exchange measurements were performed by using an infrared gas exchange system (LI-6400/LI-6400XT, LI-COR Inc., Lincoln, NE, USA). All measurements were performed on fully expended 2nd and 3rd leaves of the plant between 10:00 and 13:00 hour. Gas exchange parameters such as light saturated net photosynthetic rate (A_{sat}), stomatal conductance (g_s) and transpiration rate (E) were measured in leaves of control and salt treated plants at 1, 4 and 8DAS. Leaf water use efficiency was calculated as A_{sat}/E.

Chl *a* fluorescence measurements were performed with a portable mini-PAM chlorophyll fluorometer (Walz, Germany). Whole plants were adapted in dark for 30 min prior to the analysis. Photosynthetic induction and light responsive curves were measured with the intensities of measuring light (<0.1 µmol photons m^{-2} s^{-1}), saturating pulse (3000 µmol photons m^{-2} s^{-1}), actinic light (170 µmol photons m^{-2} s^{-1}) and far-red light (7 µmol photons m^{-2} s^{-1}) respectively. The duration of actinic light and saturation pulses were 0.8 and 30 sec. Induction curve measurements were taken at ~780 PAR (photosynthetic active radiation) about 5 min to complete with 0.8 and 30 sec between saturating and actinic flashes of light and the light curve measurements were taken about 88 sec to complete with increasing intensities actinic light (~190 PAR to ~3000 PAR).

Chlorophyll a and b content

Concentration of chlorophyll *a* and *b* was calculated according to Arnon (1949). Freshly harvested control and salt treated leaves were cut into 1 cm length. The finely chopped leaves were ground in ice cold 80% acetone with precooled motor and pestle. The whole grounded

mixture was taken in 15 ml centrifuge tubes and centrifuged at 5000 rpm at 4°C for 15 minutes. Supernatant was collected in a fresh Eppendorfs tubes and kept in ice till absorbance was taken. The absorbance was taken at 645nm and 663nm against the 80% acetone blank.

The concentration of chlorophyll *a* and *b* was calculated as follows

Cholorophyll *a* concentration: $12.7\ (A663) - 2.69\ (A645)$

Cholorophyll *b* concentration: $22.9\ (A645) - 4.68\ (A663)$

Quantification of Na^+, K^+, Ca^{2+} and Cl^- ions

Accumulation of Na^+, K^+, Ca^{2+} and Cl^- in leaf and root tissues was determined as described in Munns et al. (2010), with some minor modifications. The collected samples were oven dried at 70°C for 3 days. Ions (Na^+, K^+ and Ca^{2+}) were extracted in 5 ml of Aqua Regia at 95°C for 60 min. The resulting solution was diluted and analysed for ions with an atomic absorption spectroscopy (GBC 932, Braeside, Australia). Chloride ion concentration was determined by titrimetric method (Korkmaz, 2001).

Statistical analysis

All measurements were taken five biological replicates and three technical replicates were constituted in each biological replicate. Significant differences at ***P < 0.001, **P < 0.01 and *P < 0.05 in various parameters estimated between control and salt treated plants were calculated by using one-way ANOVA. All the statistical and linear regression analyses were performed using the statistical package Sigma Plot 11.0.

Physiology and chlorophyll fluorescence analysis

In order to assess the level of salt tolerance of *P. pinnata*, 30 days hydroponically grown plants were treated with two different salt concentrations (300 and 500 mM NaCl) at three different time intervals 1, 4 and 8 days. After 8 days of salt treatment, leaves of 300 mM NaCl treated plants were healthy and green similar to leaves of control. However, leaves of 500 mM NaCl treated plants showed similar results till 4 days, while these plants exhibited minor senescence symptoms after 8 days of salt treatment (Figure 1A). High salinity significantly changed the gas exchange parameters such as A_{sat}, E and g_s (Figure 1B–D). The A_{sat} of both 300 and 500 mM NaCl treated was significantly decreased by ~25%, ~11%, and ~10%, in 300 mM NaCl treated leaves and ~54%, ~72%, and ~63% decrease was observed in 500 mM NaCl treated leaves at 1, 4 and 8DAS respectively. A significant reduction of ~50% (300 mM) and ~75% (500 mM) was observed in g_s as well as ~50% (300 mM) and ~83% (500 mM) decline was recorded in E, respectively for treated plants with respect to control plants. However, water use efficiency (WUE) showed significant increase by ~1.3, ~1.7 and ~1.5-fold in 300 mM NaCl treated plants as well as ~2.0, ~1.1 and ~1.6-fold up-regulation was observed in 500 mM NaCl treated plants at 1, 4 and 8DAS (Figure 1E). The leaf relative water content (LRWC) did not change significantly at 1, 4 and 8DAS, in 300 mM NaCl treated leaves, whereas 500 mM NaCl treatment showed significant changes at 4 and 8DAS (Figure 1F). At 1DAS, the percentage of LRWC was similar to the control leaf levels in 500 mM NaCl treated leaves. Further, the percentage root relative water content (RRWC) increased significantly in 300 mM NaCl treated roots at 8DAS, which were returned to pre-stress levels at 1 and 4DAS (Figure 1G). However, in 500 mM NaCl treated roots, the percentage of RRWC showed decrease or unchanged at 1, 4 and 8DAS.

To understand the changes in PSII photochemistry, components of quenching, photochemical utilization and photo-protective dissipation of excess excited energy in control and salt treated *P. pinnata*, were performed on light and dark-adapted leaves of 300 mM and 500 mM NaCl treatment at 1, 4 and 8DAS. After 20 min of dark adaptation, leaves of control and salt treated plants were subjected to various chl*a* fluorescence measurements such as induction curves (IC) (Figure 2A) and light responsive curves (LC) (Figure 2B). In 300 mM NaCl treated leaves, IC of PSII quantum yields such as effective quantum yield of PSII (YII), actual quantum yield of non-regulated heat dissipation (YNO), and actual quantum yield of non-regulated heat dissipation/ non-photochemical quenching (YNPQ) did not change significantly at 1, 4 and 8DAS, while the NPQ was significantly increased at 1, 4 and 8DAS. Further, the values of YII showed a significant decrease in 500 mM NaCl treated plants at 1, 4 and 8DAS. The NPQ was decreased significantly in 500 mM NaCl treated plants at 4 and 8DAS. However, at 1DAS, the NPQ values slightly decreased between 0.4 to 3.5 min and returned to control levels in 500 mM NaCl treated plants. Similarly, YNPQ values were significantly declined in 500 mM NaCl treated plants at 4 and 8DAS. The IC of YNPQ was decreased between 0.4 to 2.8 min which returned to control values in 500 mM NaCl treatment at 1DAS. However, the YNO levels significantly increased in 500 mM NaCl treated plants at 1, 4 and 8DAS. Accordingly, the LC of YII, NPQ, YNPQ, and YNO did not change much in 300 mM NaCl treated plants in 1, 4 and 8DAS. However, in 500 mM NaCl treated plants, the LC of YII, NPQ, and YNPQ decreased significantly at 1, 4 and 8DAS. Notably, LC of YNO was increased significantly in 500 mM NaCl treated plants at 1, 4 and 8DAS. Our results demonstrated that the chlorophyll contents (Chl *a*, Chl *b* and Chl *a*/*b*) were not changed much in both control and salt treated plants (Figure 3A).

Figure 1. Morphological and photosynthetic activity of control and salt treated *Pongamia pinnata*

(A) Plant morphology and physiological parameters of hydroponically grown 30-days old *P. pinnata* treated with 0 mM NaCl (Control), 300 mM NaCl and 500 mM NaCl for 1, 4 and 8DAS respectively,

(B) light-saturated net photosynthetic rate (A_{sat}) (μmol m^{-2} s^{-1}),

(C) Stomatal conductance (g_s) (mol m^{-2} s^{-1}),

(D) Transpiration rate (E) (mmol m^{-2} s^{-1}),

(E) Water use efficiency (WUE) (mmol m^{-2} s^{-1}),

(F) Leaf relative water content (LRWC),

(G) Root relative water content (RRWC). Error bars represent the mean ± SD (n = 5).

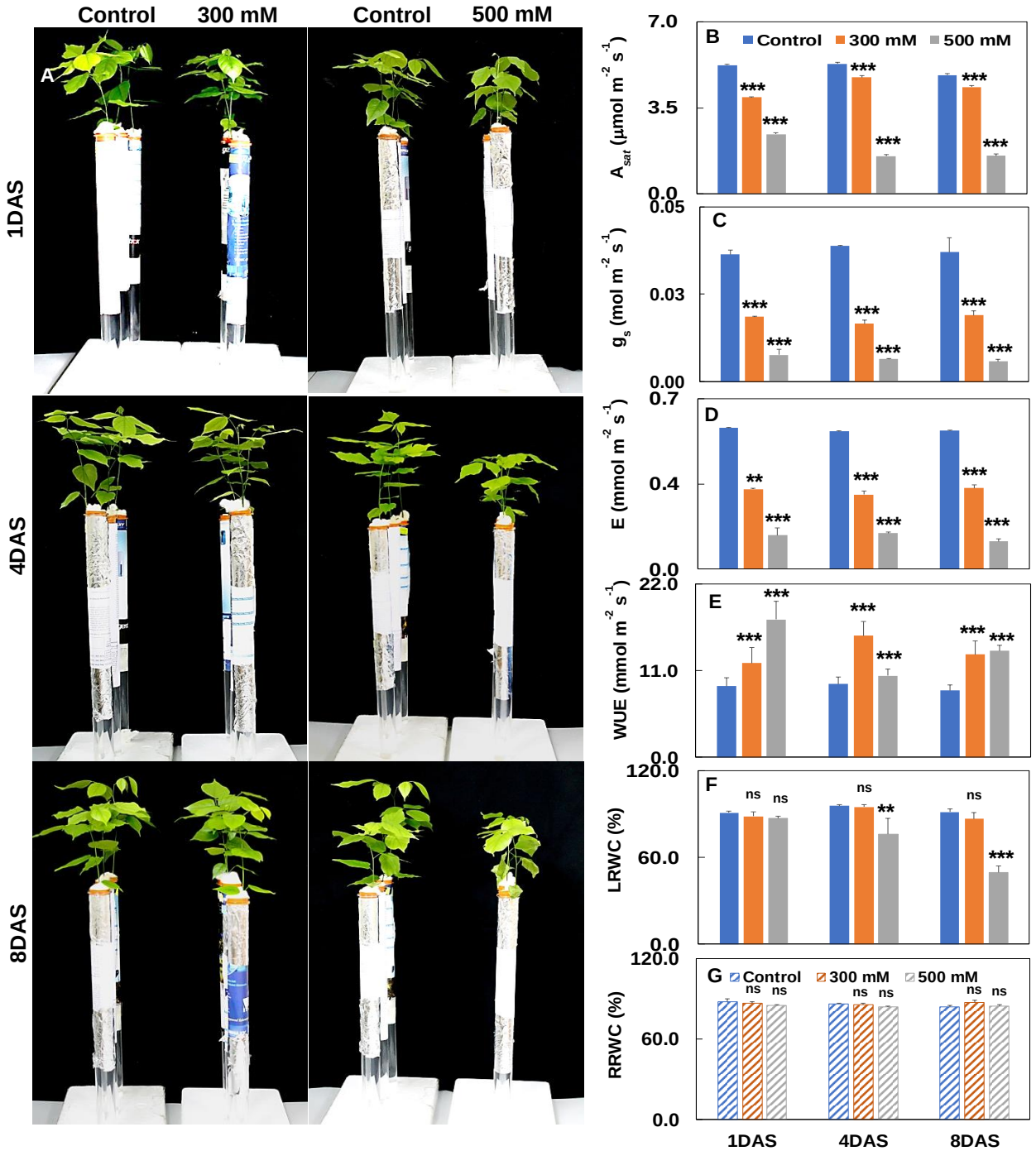
Control
300 mM
Control
500 mM
A
1DAS
4DAS
8DAS
B
Control
300 mM
500 mM
A_{sat} (µmol m^{-2} s^{-1})
7.0
3.5
0.0
C
g_s (mol m^{-2} s^{-1})
0.05
0.03
0.00
D
E (mmol m^{-2} s^{-1})
0.7
0.4
0.0
E
WUE (mmol m^{-2} s^{-1})
22.0
11.0
0.0
F
LRWC (%)
120.0
60.0
0.0
G
RRWC (%)
120.0
60.0
0.0
ns
**
***
1DAS
4DAS
8DAS

Figure 2. Effect of salt stress on chlorophyll fluorescence of control and salt treated *Pongamia pinnata*.

(A). Induction curves of PSII quantum yield (YII), NPQ, YNPQ, and YNO in control salt treated Pongamia. The measurements were performed on the leaves of plants dark-adapted overnight illuminated with a constant PAR intensity (850 µmol photons m^{-2} s^{-1}) for 6 min with time interval 24 sec.

(B). Light responsive curves of PSII quantum yield (YII), NPQ, YNPQ and YNO in control salt treated Pongamia. The measurements were performed on the leaves of plants dark-adapted overnight illuminated with the following PAR intensities (0, 226, 412, 612, 846, 1263, 1732, 2638 and 3840 µmol photons m^{-2} s^{-1}). Error bar represents the mean ± SD (n =5).

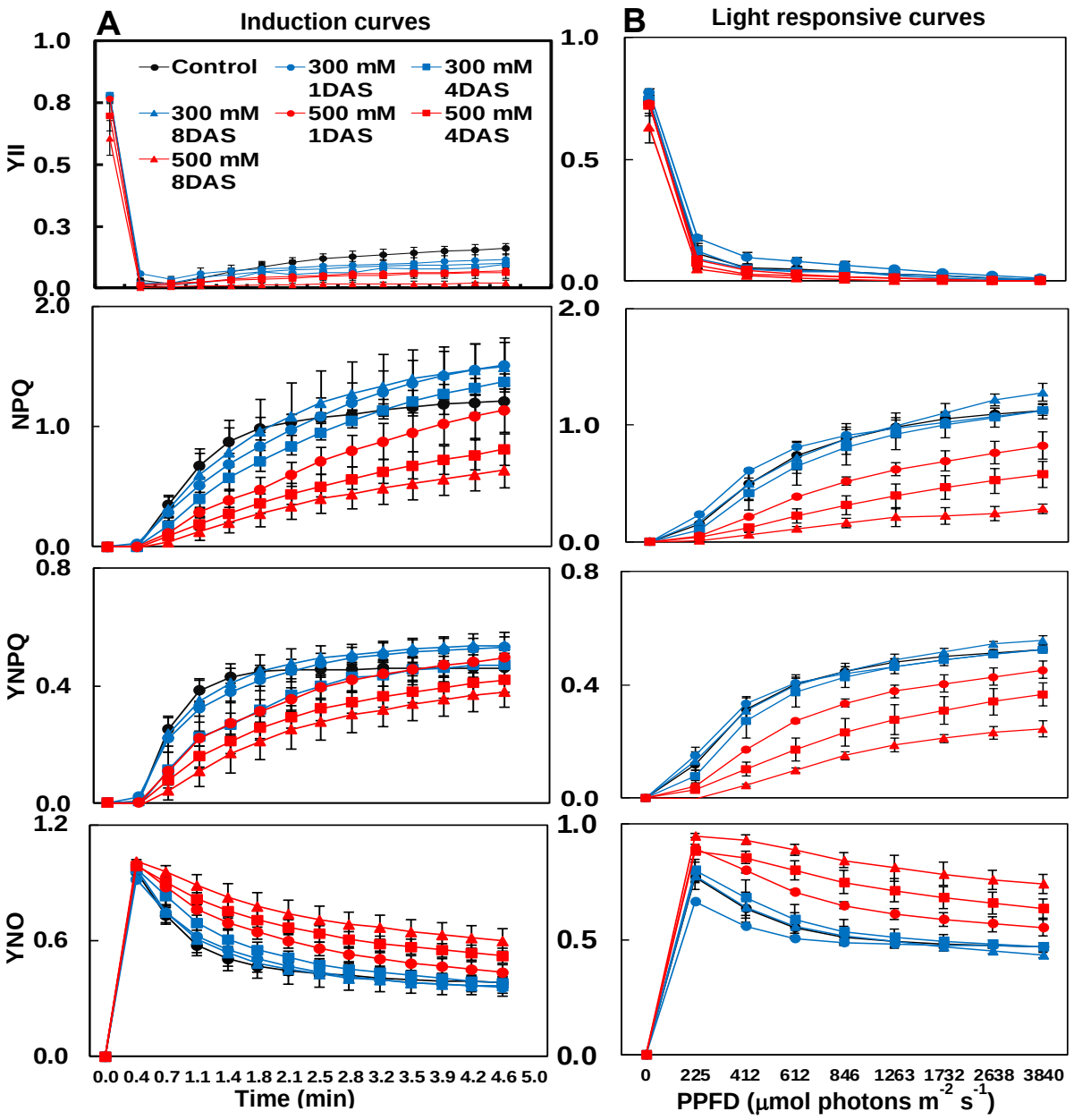
A
Induction curves
B
Light responsive curves
Control
300 mM 1DAS
300 mM 4DAS
300 mM 8DAS
500 mM 1DAS
500 mM 4DAS
500 mM 8DAS
YII
NPQ
YNPQ
YNO
Time (min)
PPFD (µmol photons m-2 s-1)

Figure 3. Effect of salt stress on chlorophyll fluorescence of control and salt treated *Pongamia pinnata*.

(A). Changes in chlorophyll content,

(B). Maximal photochemical efficiency of PSII (Fv/Fm),

(C). Effective quantum yields of regulated (YNPQ),

(D). Non-regulated heat dissipation (YNPQ) of PSII in control and salt treated plants, minimal fluorescence (Fo) in one-month-old *P. pinnata* leaves after 1, 4 and 8DAS,

(E). Changes in the other fluorescence parameters include maximum fluorescence (Fm),

(F). Coefficient of photochemical chemical quenching (qP),

(G) Electron transport rate (ETR) and coefficient of non-photochemical chemical quenching (qN),

(H). Apparent maximal photochemical efficiency of PSII (FV'/Fm'). Error bars represent the mean ± SD (n = 5).

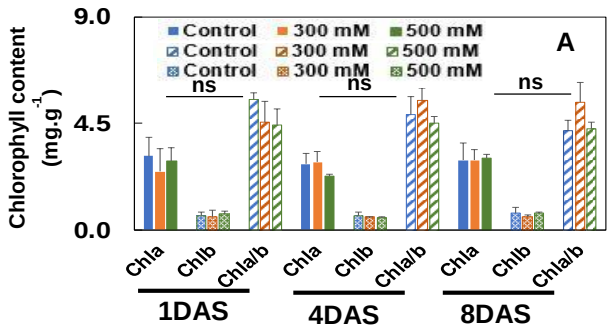
A
Control 300 mM 500 mM
Control 300 mM 500 mM
Control 300 mM 500 mM
Chlorophyll content (mg.g-1)
9.0
4.5
0.0
ns
Chla Chlb Chla/b
1DAS 4DAS 8DAS

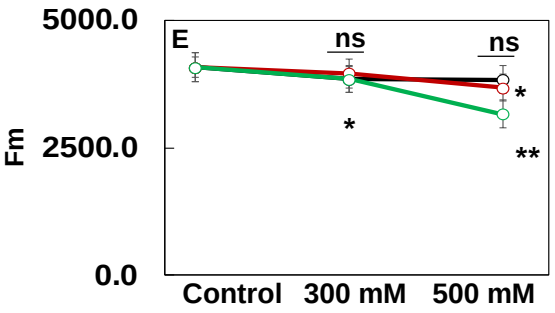
E
Fm
5000.0
2500.0
0.0
ns
*
**
Control 300 mM 500 mM

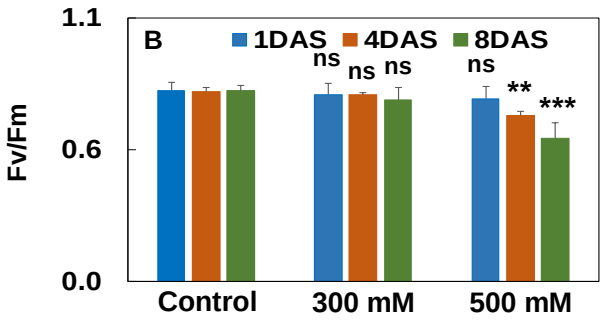
B
1DAS 4DAS 8DAS
Fv/Fm
1.1
0.6
0.0
ns
**
***
Control 300 mM 500 mM

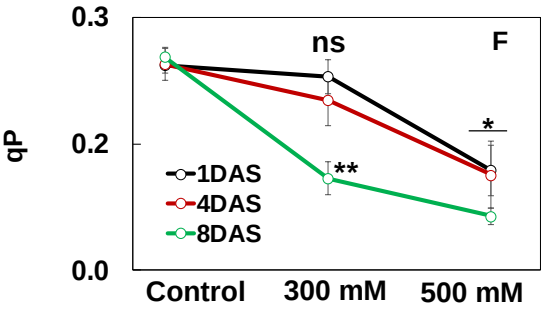
F
qP
0.3
0.2
0.0
ns
*
**
1DAS
4DAS
8DAS
Control 300 mM 500 mM

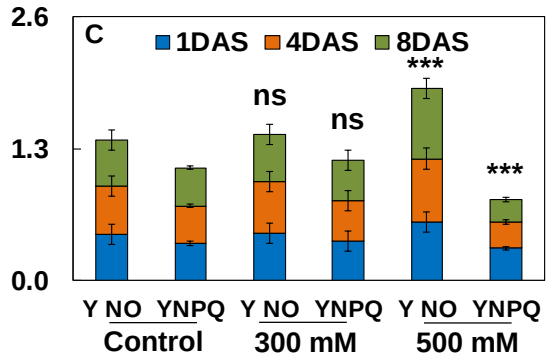
C
1DAS 4DAS 8DAS
2.6
1.3
0.0
ns
***
Y NO YNPQ
Control 300 mM 500 mM

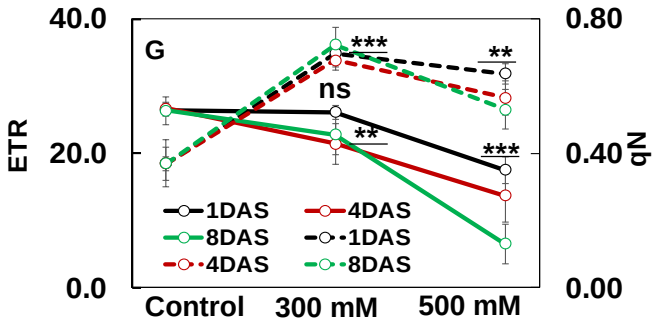
G
ETR
qN
40.0
20.0
0.0
0.80
0.40
0.00
ns
**
***
1DAS 4DAS
8DAS 1DAS
4DAS 8DAS
Control 300 mM 500 mM

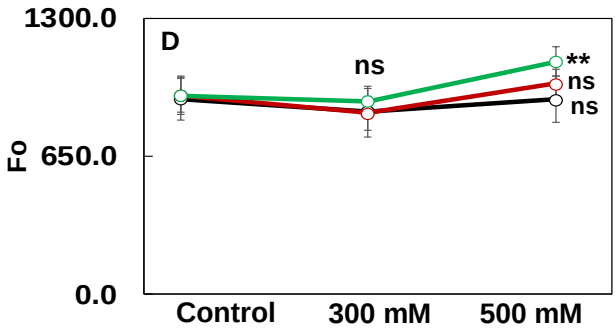
D
Fo
1300.0
650.0
0.0
ns
**
ns
ns
Control 300 mM 500 mM

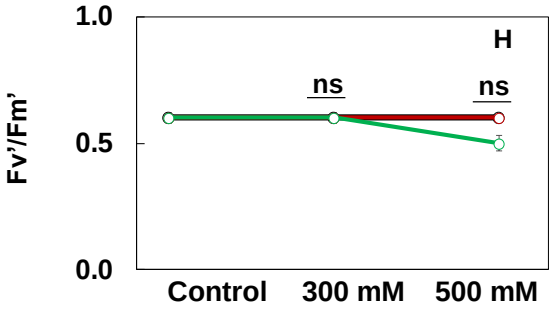
H
Fv'/Fm'
1.0
0.5
0.0
ns
ns
Control 300 mM 500 mM

Our results demonstrated that the chlorophyll contents (Chl *a*, Chl *b* and Chl *a*/*b*) were not changed much in both control and salt treated plants (Figure 3A). Similarly, there was no significant difference in the maximum quantum yield of PSII (Fv/Fm) of 300 mM NaCl treated plants at 1, 4 and 8DAS (Figure 3B). In 500 mM NaCl treated plants, Fv/Fm significantly decreased at 4 and 8DAS, while these levels remained similar to that of control at 1DAS. Further, the quantum yields of non-photochemical quenching (YNPQ) and constitutive heat dissipation (YNO) were significantly varied in control and salt treated plants. In 500 mM NaCl treated plants, YNO was significantly increased, while YNPQ values decreased significantly at 1, 4 and 8DAS (Figure 3C). However, YNO and YNPQ did not change significantly in 300 mM NaCl treated leaves at 1, 4 and 8DAS. The minimal fluorescence (Fo) and maximal fluorescence (Fm) levels did not change in 300 mM at 1, 4 and 8DAS as well as in 500 mM NaCl treated leaves at 1 and 4DAS, while these levels showed significant changes at 8DAS (Figure 3D and E). Initial exposure of 300 mM NaCl treated plants showed decrease or no change in photochemical quenching (qP) levels at 1, 4 and 8DAS, while these levels showed a significant decrease in 300 mM NaCl at 4 and 8DAS as well as in 500 mM NaCl treated leaves at 1, 4 and 8DAS (Figure 3F). Similarly, the electron transport rate (ETR) levels decreased in 300 mM NaCl treated leaves at 4 and 8DAS, but these levels remained unchanged at 1DAS (Figure 3G). In 500 mM NaCl treated leaves, the ETR levels decreased at all-time points. However, the qN levels were increased in both 300 mM and 500 mM NaCl treated leaves across all time points. The apparent maximal photochemical efficiency of PSII (Fv′/Fm′) levels were not changed significantly in both 300 and 500 mM NaCl treated leaves at 1, 4 and 8DAS (Figure 3H).

Figure 4. Sodium, calcium, potassium and chloride ion content in leaves of 0 (control), 300 and 500 mM NaCl treated plants at

(A) 1DAS, (B) 4DAS and (C) 8DAS and in roots of 0 (control), 300 and 500 mM NaCl treated plants at (D) 1DAS, (E) 4DAS and (F) 8DAS respectively. Variations in the ratios of K^+/Na^+, Ca^{2+}/Na^+ and Na^+/Cl^- in the leaves and roots of control and salt treated plants (G-I). Error bar represents the mean ± SD (n = 6).

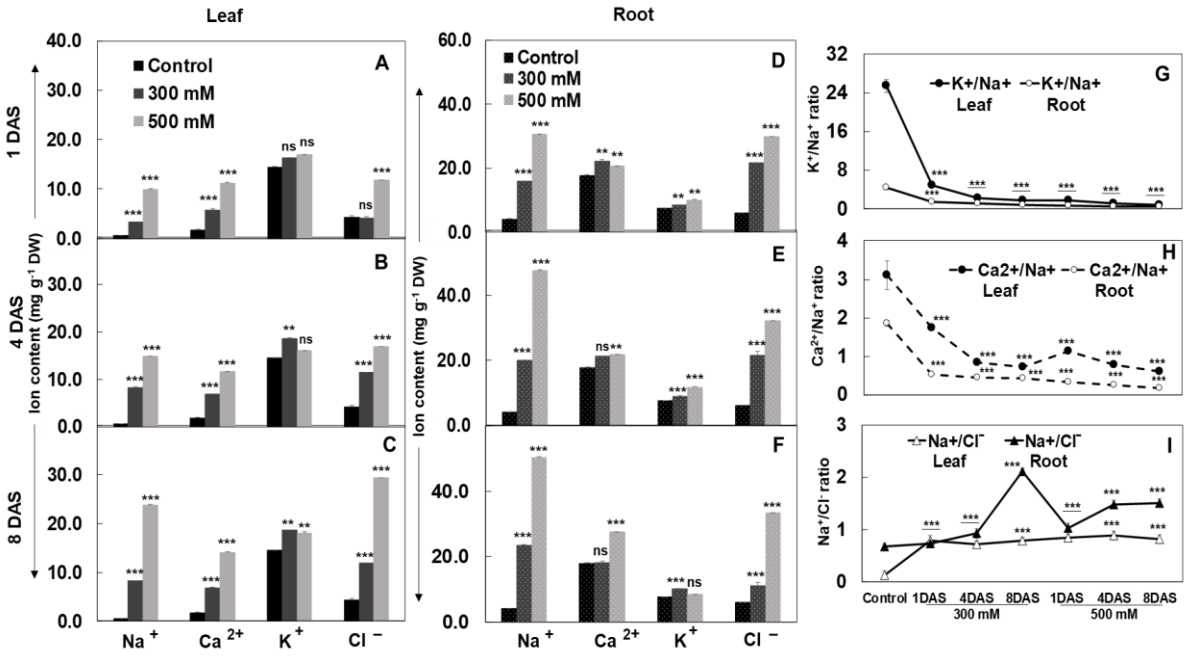
Leaf
Root
Control
300 mM
500 mM
1 DAS
4 DAS
8 DAS
Ion content (mg g-1 DW)
A
B
C
D
E
F
Na +
Ca 2+
K +
Cl −
K+/Na+ Leaf
K+/Na+ Root
K+/Na+ ratio
G
Ca2+/Na+ Leaf
Ca2+/Na+ Root
Ca2+/Na+ ratio
H
Na+/Cl- Leaf
Na+/Cl- Root
Na+/Cl- ratio
I
Control 1DAS 4DAS 8DAS 1DAS 4DAS 8DAS
300 mM
500 mM

Salinity-induced Na^+, K^+, Ca^{2+} and Cl^- ion homeostasis in leaves and roots of P. pinnata

In leaves, Na^+ and Ca^{2+} levels increased gradually in both 300 and 500 mM NaCl treated plants at 1, 4 and 8DAS. However, K^+ levels remained unchanged during 1DAS of both 300 and 500 mM NaCl treatment but got slightly enhanced at 4 and 8DAS of 300 mM salt stress and at 8DAS of 500 mM salt treatment. Correspondingly, Cl^- ion content was significantly enhanced at 1DAS in only 500 mM salt treated plants and 4 and 8DAS of both 300 and 500 mM NaCl treated plants (Figure 4A-C). Interestingly, in roots Na^+ and Cl^- ion content showed similar pattern of gradual accumulation in 300 and 500 mM salt treated plants at 1, 4 and 8DAS. However, Ca^{2+} levels were only slightly enhanced at 1DAS under 300 mM salt treatment and remained similar to controls during 4 and 8DAS, while 500 mM salt treated plants showed significant gradual increase in the Ca^{2+} content from 1 to 8DAS. Further, K^+ content also increased slightly in 300 mM NaCl treatment, which showed a gradual increase from 1 to 8DAS. However, in 500 mM salt treated plants, K^+ levels were enhanced only till 4DAS and declined again to control levels at 8DAS (Figure 4D-F). Also, K^+/Na^+ ratio declined significantly and consistently when compared to control in both leaves and roots under 300 and 500 mM salt treatment during all time points. However, leaf K^+/Na^+ ratio remained slightly higher than roots at all points except 8DAS of 500 mM NaCl treatment (Figure 4G). A similar trend was observed for Ca^{2+}/Na^+ ratios, wherein it declined significantly under both 300 and 500 mM salt treatment across all time points, but the leaf Ca^{2+}/Na^+ ratio was maintained at higher levels than roots (Figure 4H). In contrast, the Na^+/Cl^- ratio increased when compared to control plants in both leaves and roots under 300 and 500 mM salt treatments across all time points. The leaf Na^+/Cl^- ratios were higher than root Na^+/Cl^- ratios during all points, except at 1DAS of 300 mM NaCl treatment when both were same. Also, at 8DAS of 300 mM salt treatment, leaf Na^+/Cl^- showed unusually high values when compared to controls (Figure 4I).

Pongamia adapts to high salinity conditions through physiological adjustments

Pongamia exhibited a remarkable tolerance to salinity stress which is comparable with other established halophytes. Salt treated hydroponically grown Pongamia seedlings displayed no salt stress-induced symptoms such as wilting, yellowed leaves, leaf tip burning, chlorosis or necrosis in leaves till 8 days treatment indicating a strong adaptive mechanism to combat salinity-induced oxidative stress and ionic imbalance (Shabala and Mackay, 2011). Exposure of Pongamia to high salinity resulted in a significant decrease g_s, A_{sat} and E. Salinity can cause osmotic stress and minimize water uptake by roots resulting reduced A_{sat} and E. The WUE increased substantially in salt treated Pongamia seedlings. The higher WUE improves the level of salt tolerance since high WUE can reduce the salt uptake by roots and substantiate the water deficiency caused by salinity (He et al., 2009). Plants have developed various mechanisms to improve the RWC in order to withstand ion and osmotic imbalance caused by osmotic stress (Shabala et al., 2013). The reduced RWC as shown in this study is relatively a rapid adaptive strategy, which might allow the plants to accumulate the selective cations and compatible solutes to maintain cell or tissue turgor under high salinity stress (Negrão et al., 2017). The Fv/Fm levels were not changed significantly in 300 mM NaCl treated leaves which suggests that photoinhibition was not triggered. Although the maximum quantum yields of PSII did not change significantly, the ETR and qP levels in 300 mM NaCl treated leaves were progressively decreased as the time of salt exposure increased. The observed increase in the quantum yields of non-photochemical energy loss of PSII (NPQ and qN) might protect the photosynthetic apparatus against photodamage (Moradi and Ismail, 2007; Netondo et al., 2004). However, the leaves of 500 mM NaCl treatment showed a significant reduction in Fv/Fm at 4 and 8DAS.

After prolonged exposure of 500 mM NaCl stress, YII, NPQ, and YNPQ levels also showed a concomitant decline. In addition, decreased levels of Fv/Fm led to the gradual decrease in qP and ETR values (Zhou et al., 2018). Similar results were reported by in privet seedlings were treated with lead. The observed decline in chl *a* fluorescence parameters and increased levels of YNO could be the result of salt-induced irreversible damage to photosynthetic machinery (Maxwell and Johnson, 2000). As the seedlings showed no morphological salinity stress-induced damage and well maintained chlorophyll pigments in the leaves of treated plants, it was unlikely that the photosynthetic machinery was damaged (Santos et al., 2015; Marriboina et al., 2017). Further, the increased levels of qN may substantiate the photo-damage caused by YNO through a lutein dependent process (Santos et al., 2015).

Salinity-induced increase in Ca^{2+} and K^{+} ions in roots of salt treated P. pinnata effectively retained Na^{+} and Cl^{-} ions in root tissues and restricted their entry into leaf tissues

Atomic emission spectroscopy and titrimetric based quantification of Na^{+}, K^{+}, $Ca^{2+,}$ and Cl^{-} reveals that salt treated leaves and roots of *P. pinnata* showed different patterns of ion accumulation across all time points. The Na^{+} and Cl^{-} contents were significantly increased in both leaves and roots of salt treated plants. Our results showed that the levels of Na^{+} and Cl^{-} were significantly higher in roots than in leaves as well as maintenance of high Na^{+}/Cl^{-} ratio in roots than in leaves, suggesting that roots were actively involved in the ion sequestration in order to reduce the salt-induced toxic effect on areal parts of the plant (Marriboina et al., 2017; Wu et al., 2018). Initial exposure of 300 mM NaCl treatment did not induce the K^{+} content significantly in the leaves, while these levels increased at 4 and 8DAS. In contrast,

500 mM NaCl treated leaves showed significant increase only at 8DAS. Further, K^+ in roots showed significant increase in 500 mM NaCl treatment across all time points as well as in 300 mM NaCl treated roots at 1DAS. In general, high level of Na^+ inhibits the uptake of K^+ ions which results in growth impairment and may even lead to death of the plant (Gupta and Huang, 2014). The observed increase in K^+ content with an accompanying increase in Na^+ content in both leaves and roots enhances salt tolerance in *P. pinnata*. In addition, the steady-state increase of K^+ content in 500 mM NaCl treated roots with treatment time could be either due to increased magnitude of the NaCl-induced K^+ influx or decreased efflux of K^+ across cell and vacuolar membranes (Shabala et al., 2007). The results suggest that the increase in the K^+ level may be crucial to maintain osmoregulation caused by excess accumulation of Na^+ in the vacuole which in turn regulates protein stability under high salinity conditions (Hasanuzzaman et al., 2018). Low K^+/Na^+ ratio under salt stress indicates low selectivity for K^+ in the presence of high NaCl concentration (Taha et al., 2000).

The fact that K^+ is for the growth and survival of the plant raises, the question how *P. pinnata* and other salt-tolerant plant species cope along with low K^+/Na^+ and maintain ion balance under high salinity stress. A possible way to answer is the existence of strong adaptive mechanisms to compensate the low retention of K^+ in both leaves and roots under high salinity stress. In addition, the accumulation and compartmentation of Na^+ in the vacuole is energetically more efficient as compared with K^+ accumulation to maintain high K^+/Na^+ in the plant tissues under high salinity conditions (Taha et al., 2000). Similarly, Ca^{2+} levels were significantly increased in both leaves and roots of salt treated plants across all time points, while these levels did not show any significant change in 500 mM NaCl treated roots at 8DAS. Calcium is well known for its role in maintaining structural and functional integrity plant cell membranes, stabilizes cell wall and cellular structures regulates ion

transport across cell membrane and act as an intracellular second messenger under salt stress (Shabala et al., 2006; Hadi and Karimi, 2012). Further, the enhanced uptake of Na^+ into the vacuole conceals the significant increase in the Ca^{2+} levels resulting low Ca^{2+}/Na^+ ratio in both leaves and roots of Pongamia (Koksal et al., 2016; Chowdhury et al., 2018). However, the plants with low Ca^{2+}/Na^+ ratio showed no morphological stress symptoms with respect to the controls and it was unlikely that the cellular integrity and cell wall structures were damaged. Further, the transient increase in Ca^{2+} levels of salt treated plants might help the plant activating its salinity adaptive signaling pathways as well as the oxidative stress protective enzymes under salinity conditions (Hadi and Karimi, 2012).

In conclusion, the absence of salt-induced symptoms on leaves, less decline in the leaf photosynthetic parameters and continuous increase in the regulated heat dissipation of PSII confer salinity adaptive mechanisms in *P. pinnata*. Further, increased Ca^{2+} and K^+ minimizes the salt-induced damage in leaves and roots. Higher Na^+ content in the roots than leaves also revealed that Pongamia roots act as ultra-filters/ strong barriers to protect the leaves from Na^+ toxicity. The Na^+ probe fluorescence data reveals the existence of vacuolar Na^+ sequestration mechanism in the root and the confinement of Na^+ specific fluorescence to certain cells such as tracheid cells and xylem parenchyma showing strong salinity tolerance mechanisms effectively operating in the roots of *P. pinnata*. Our results highlight the key mechanisms, conferring high salt tolerance in Pongamia, which can be highly crucial for further research to develop Pongamia as a tolerant and sustainable biofuel tree crop.

Chapter 3

Determination of salinity stress-induced ion homeostasis, hydrophobic barriers Na^+ localization in leaves and roots of *P. pinnata* (L.) pierre

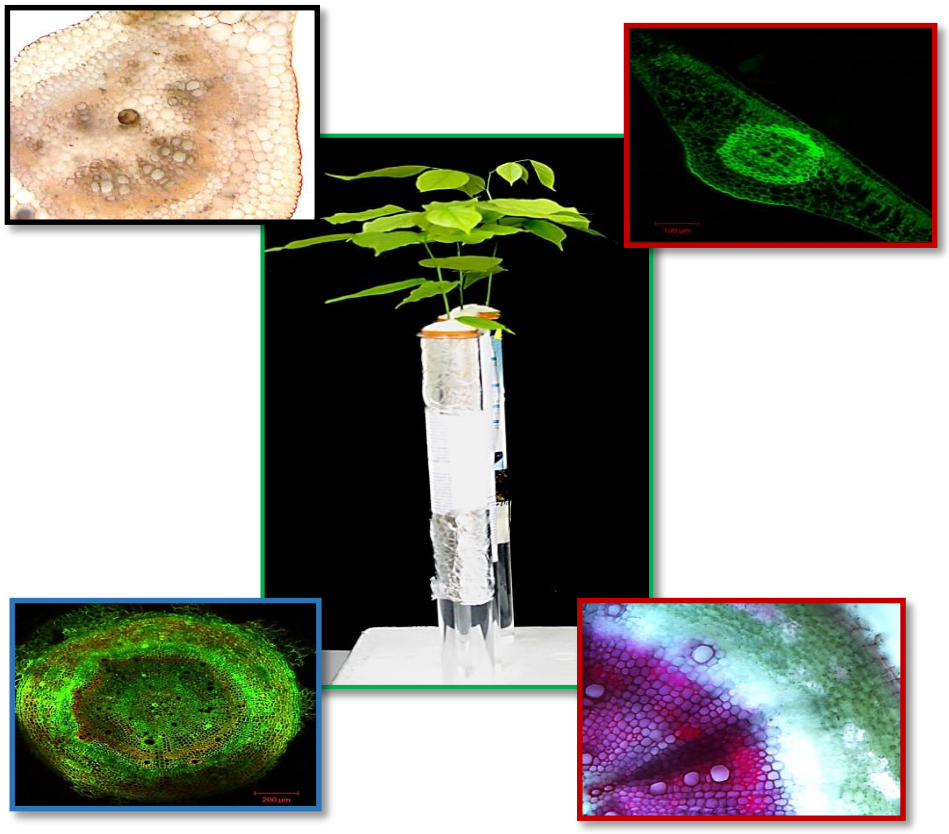

Chapter 3 Introduction

Continuous salinization of arable lands at an annual rate of 10% forecasts the possibility of approximately 50% of the total cultivated land area to be salinized by the year 2050 worldwide (Jamil et al., 2011). Thus, demands for initiating cultivation of economically important tree species in salinized lands, which are otherwise unfit for agricultural productivity is increasing in many parts of the world, as a potential alternative for optimum economic sustainability (Oh et al., 2012). A recent review on salt tolerance ability of trees discussed the wide variations in salinity tolerance among tree species which can thrive at soil salinities ranging from 200 to 450 mM (Polle and Chen, 2015). Despite having considerable reports on salt tolerance of trees, the underlying genetic, physiological and molecular basis for the trait is still superficial and limited mostly to poplars (Chen and Polle, 2010; Harfouche et al., 2014; Ma et al., 2014) and mangroves (Chen et al., 2010).

In general, salinity affects plant growth and development by decreasing the water potential of the soil leading to reduced water uptake by roots. Thus, both salinity and drought stress induce a set of common responses in plants owing to the osmotic stress signal (Shinozaki and Yamaguchi-Shinozaki, 1997). However, in addition to osmotic changes, salinity leads to uptake of Na^+ and Cl^- ions along with water. Thus, long term salinity and/or absence of efficient extrusion/sequestering mechanisms in plants result in accumulation of high concentrations of Na^+ and Cl^- in the cytosol causing ion homeostasis imbalance at cellular level. Salinity-induced decline in photosynthetic rates due to stomatal closure is an adaptive response (Shabala et al., 2012). However, excessive accumulation of Na^+ ions within photosynthetic tissues leads to toxicity and damage to the photosynthetic machinery which is detrimental to the plant. Thus in order to survive, plants need to limit Na^+ transport into the shoot tissue by compartmentalizing the Na^+ into the root stele and vacuoles (Hasegawa, 2013; Benito et al., 2014; Julkowska et al., 2014).

Plants growing in saline soils, restrain the root cell wall expansion through increased deposition of lignin and suberin on the root cell walls to prevent excessive flow of toxic Na^+ ions through the apoplastic pathway and increase water retention in the roots (Shabala and Mackay, 2011). According to Meyer et al. (2011) and Krishnamurthy et al. (2014), plants such as *Bruguiera* and *Iris germanica* possess layers of suberin and lignin coated exodermis (BEX and MEX) in roots, as well vascular tissues in leaves to enhance the water permeability under salt stress. In addition, the increased number of lignified tracheary elements in the vascular tissues under salt stress also enhances the water permeability and greater selectivity for ion uptake in crops such as soybean and tomato (Neves et al., 2010). Based on their survival strategies, halophytes are broadly classified as salt-secretors which excrete the salt through specialized glands on the leaves, and non-secretors exclude out the salt through specialized barriers in the roots (Parida and Jha, 2010; Wang et al., 2011; Jiang et al., 2017). However, the tolerance of all halophytes to salinity relies on controlled uptake and compartmentalization of Na^+, K^+ and Cl^- and the synthesis of organic 'compatible' solutes, even where salt glands are operative.

Most of the available information regarding salt tolerance mechanisms at physiological and molecular levels is limited to crops while only few reports are available for trees (Ma et al., 2014; Polle and Chen, 2015). At present, mangroves are the only known plant community that can tolerate up to 500 mM NaCl, which is equivalent to seawater salt levels (Wang et al., 2020). Ironically, in spite of being an excellent model for understanding high salinity tolerance in trees, mangroves are unsuitable for cultivation in salinized terrestrial lands (Oh et al., 2012). Hence identification of new tree species having high economic potential and salinity endurance as well as understanding the physiological and molecular responses in tree species is highly crucial. On the other hand, due to the dwindling fossil fuel resources,

a parallel strong demand has arisen for identification of certain tree species acting as potential sources for high quality biofuel production (Mathur and Vyas, 2013). This demand has recently led to the unravelling of a fast-growing leguminous tree *Pongamia pinnata* (L.) pierre (Synonym: *Millettia pinnata*), indigenous to India and Southeast Asia, whose non-edible seed oil was recognized worldwide as a potential feedstock for biodiesel production (Scott et al., 2008; Sangwan et al., 2010). Biodiesel production was reported from *Pongamia* seed oil through the consecutive acid and base-catalyzed dual step transesterification method (Naik et al., 2008). Apart from the seed oil, all other parts of the plant have also been implemented as crude drugs in Indian traditional medicine as well as for application as animal fodder and timber (Sangwan et al., 2010).

Fortunately, *P. pinnata* was found to display semi-mangrove characteristics, capable of operating both glycophytic and halophytic mechanisms, preferentially, for adaptation to salinity (Wang et al., 2011). Unlike mangroves, *Pongamia* does not exhibit physiological and anatomical adaptations to exclude Na^+ in order to endure salinity stress. Previous studies have shown partial salinity tolerance in Pongamia (Divakara et al., 2010; Kesari and Rangan, 2010; Wang et al., 2013). More recently, Huang et al. (2012), used salt-responsive transcriptome to demonstrate that *Pongamia* can overcome salt stress within 8 h after treatment. On the other hand, another report by Arpiwi et al. (2013), showed that some varieties of *P. pinnata*, collected from Kununurra, Western Australia and some parts of India did not tolerate salinity stress beyond 250 mM NaCl. Further, an integrated knowledge regarding the physiological and molecular responses of *P. pinnata* under salt stress is still at its incipient stage and needs proper characterization. However, a comprehensive analysis on the leaf and root responses as well as Na^+ localization patterns under different salt concentrations at both physiological and molecular level is not yet elucidated.

In the present study, we aim to analyze the salt tolerance of one month old *P. pinnata* plants under two different salt concentrations (300 and 500 mM NaCl) by targeting the underlying physiological and molecular responses in both leaves and roots. Nevertheless, the high tolerance of *P. pinnata* to soil salinity makes it an ideal target for cultivation in the marginal or degraded lands which are otherwise not suitable for food production.

Plant material, growth conditions, and salinity treatment

Seeds of *P. pinnata* accession TOIL 12 were obtained from Tree Oil India Limited (TOIL), Zaheerabad, Hyderabad, Telangana and were germinated on moist cotton for 10 days at 25°C in the dark. The germinated seedlings were grown in a long cylindrical glass tube (5 cm diameter X 60 cm length) filled with full-strength Hoagland No. 2 basal salt mixture (Himedia) solution adjusted to pH 5.75 ± 0.02 for 30 days. The solution was replenished every seven days (Marriboina and Reddy, 2020b). The hydroponic experiment was carried out in a plant culture room maintained at 24°C with a 16 h photoperiod and relative humidity maintained approximately at 60%. For salinity treatment, 30 days old plants (n = 20-30) were selected and subjected to 300 and 500 mM NaCl concentrations with an increment of 100 mM NaCl per day (Marriboina and Reddy, 2020b). Control plants were maintained with fresh Hoagland nutrient solution. Plants were harvested at an interval of 1 day after stress-treatment (DAS), 4 and 8DAS. Fresh weights of leaf and root were measured immediately after harvest. Dry weights of control and treated plants were determined after drying at 70°C for 3 days. Control and treated samples were harvested at each time intervals, flash frozen in liquid nitrogen and stored at –80°C prior to analysis.

Visualization of intracellular Na^+ ions through confocal laser scanning microscopy

Leaves and roots collected from and salt treated plants were segmented into 1 cm sections and incubated with 2.5% glutaraldehyde solution in 0.1 M MOPS buffer overnight at 4°C. For sodium illumination, tissues were stained with 5 µm Na^+ specific probe CoroNa-Green AM (Invitrogen) in the presence of 0.02% pluronic acid in 50 mM MOPS (pH 7.0) for overnight at room temperature. Samples were thoroughly washed with 50 mM MOPS (pH 7.0) several times, sectioned and immediately immersed in propidium iodide (Invitrogen) for 15 min. Cross sections of leaves and roots were examined under a laser scanning confocal

microscopy (Leica TCS SP2, Heidelberg, GmbH, Germany) as described by Oh et al. (2009), with some minor modifications. The cytosolic and vacuolar Na^+ fluorescence was calculated by LCS software (Heidelberg, GmbH, Germany).

Histochemical detection of lignin and suberin depositions in leaves and roots

Freshly collected leaves and roots of control and salt treated plant samples were incubated in 2.5% glutaraldehyde solution in 0.1 M MOPS overnight at 4°C and quickly cut into small thin sections. To check for lignin deposition, both leaf and root cross section were stained with phloroglucinol-HCl for 15 min. To check for suberin deposition, both leaf and root cross section were stained for overnight with sudan III stain. Stained leave and root cross-sections are examined with Leica DM6B (GmbH, Germany) light microscope (Krishnamurthy, 1999). In total five biological replicates were used and ~12 cross sections from each replicate were used for the examination.

Statistical analyses

Significant differences at ***$P < 0.001$, **$P < 0.01$ and *$P < 0.05$ in various parameters estimated between control and salt treated plants were calculated by using one-way ANOVA. All the statistical and linear regression analyses were performed using the statistical package Sigma Plot 11.0.

Salinity-induced hydrophobic barrier (suberin and lignin) formation in leaves and roots of P. pinnata

Characteristic magenta-pink colour of lignin from phloroglucinol-HCl was observed across all cross-sections of leaves and roots of control and salt treated plants (Figure 1 and 2). In leaves, under control conditions lignin deposition was faint in both lipid-parenchyma and xylem vessels of the vascular tissue at 1, 4 and 8DAS (Figure 1A–C). In treated leaves, lignification of xylem cells was slightly increased in 300 and 500 mM NaCl treatment at 1, 4 and 8DAS. Further, a lignified layer of lipid-parenchyma cells increased across the leaf axis in both 300 and 500 mM NaCl treatment at 1, 4 and 8DAS (Figure 1D–I). Sudan III staining was used to detect the suberin deposition across the cross-sections of leaves and roots of control and salt treated plants. Similar pattern of suberin deposition was observed in control and salt treated leaves at 1, 4 and 8DAS (Figure 1J–R).

In roots, under control and salt treated conditions, magenta-pink colour staining was detected in the cortical cells or xylem cells of 300 and 500 mM NaCl treatment at 1, 4 and 8DAS (Figure 2A–I). However, lignification gradually increased in the cortical cells or xylem cells of 300 and 500 mM NaCl treated roots at 1, 4 and 8DAS (Figure 2D–I). Also, a thin uniform suberized bilayer exodermis (biseriate exodermis (BEX)) was seen at 1, 4 and 8DAS (Figure 2J–O). Interestingly, a continuous band of suberized exodermis (multiseriate exodermis (MEX)) in salt treated plants was recorded. The cells of BEX and MEX showed thick layer of suberin deposition in 300 (Figure 2P–U) and 500 mM NaCl treated plants at 1, 4 and 8DAS (Figure 2V–A1).

Visualization of Na^+ ion sequestration in leaves and roots of P. pinnata

Significantly higher green fluorescence was observed in the symplasmic regions of 300 mM and 500 mM NaCl treated leaf sections at 1, 4 and 8DAS, when compared to the corresponding control sections (Figure 3A-I). Further, significant fluorescence intensity was

also observed in the apoplasmic regions of 500 mM NaCl treated leaves at 4 and 8DAS (Figure 3H and I). Further, the vacuolar and cytosolic Na^+ intensity was also measured in control and salt treated plants. The cytosolic Na^+ intensity did not change significantly in 300 and 500 mM NaCl treated leaves. However, the vacuolar Na^+ intensity was increased consistently in 300 and 500 mM NaCl treated laves at 1, 4 and 8DAS (Figure 3J).

On other hand, root tissue exhibited a completely different pattern of sodium compartmentalization in salt treated plants. The Na^+ fluorescence intensity was significantly increased in 300 and 500 mM NaCl treated roots at 1, 4 and 8DAS with respect to the controls (Figure 3K-S). Surprisingly, high intensity of sodium specific fluorescence was observed in the vacuolar region of salt treated plants. The profile distribution of Na^+ between cytosol and vacuole in roots of control and salt treated plants was shown in Figure 3T. The cytosolic Na^+ intensity was slightly changed in the 300 and 500 mM NaCl treated roots. However, the vacuolar Na^+ intensity was significantly increased in 300 and 500 mM NaCl treated roots at 1, 4 and 8DAS.

To investigate the pattern of Na^+ ion accumulation in leaves and roots of *P. pinnata*, a cell permeable Na^+ specific fluorescent probe CoroNa-Green AM was used (Figure 4 and 5). Leaf sections of control plants were showed no strong Na^+ specific fluorescence signal at 1, 4 and 8DAS. Similarly, leaf sections of 300 mM NaCl treated plants also showed no strong Na^+ specific fluorescence signal at 1 and 4DAS, whereas a Na^+ specific green florescence was observed in apoplasmic region at 8DAS. Conversely, we could observe a consistent increase in the Na^+ fluorescence signal in apoplasmic regions in leaf sections of 500 mM NaCl treated plants at 1, 4 and 8DAS. Further, roots followed a different pattern of fluorescence in both control and salt treated plants. We could observe no strong fluorescence signal in the cortical apoplasmic regions of control root sections at 1, 4 and 8DAS. However, a strong fluorescence

Figure 1. Histochemical detection of lignin and suberin content in leaves of *P. pinnata*. For lignin visualization, sections were stained with HCl-phloroglucinol.

1. Leaf sections of control (A-C) 300 mM (D-F) and 500 mM NaCl (G-I) treated plants at 1, 4 and 8DAS, respectively. For suberin visualization, sections were stained with Sudan III.

2. Leaf sections of control (J-L), 300 mM (M-O) and 500 mM NaCl (P-R) treated plants at 1, 4 and 8DAS.

Red arrows indicate lignin deposition and black arrows indicate suberin deposition. Cu: cuticle, Ue: upper epidermis, Xy: xylem, Ph: phloem, Lp: lignified parenchyma, Le: lower epidermis. Scale bars = 100 μm.

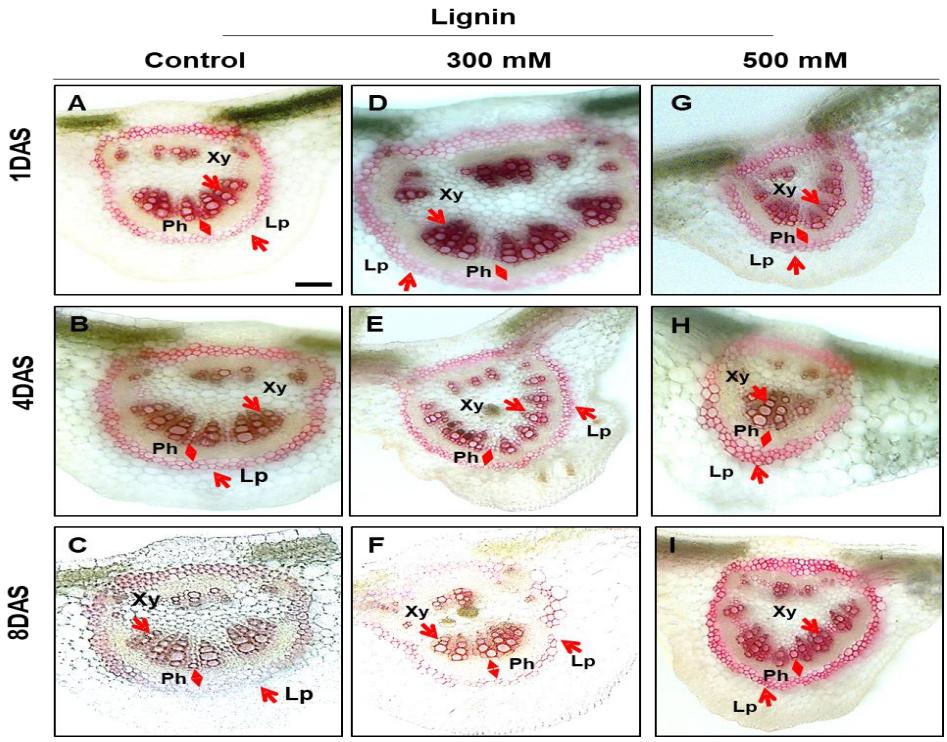
Lignin
Control
300 mM
500 mM
1DAS
4DAS
8DAS
A
B
C
D
E
F
G
H
I
Xy
Ph
Lp

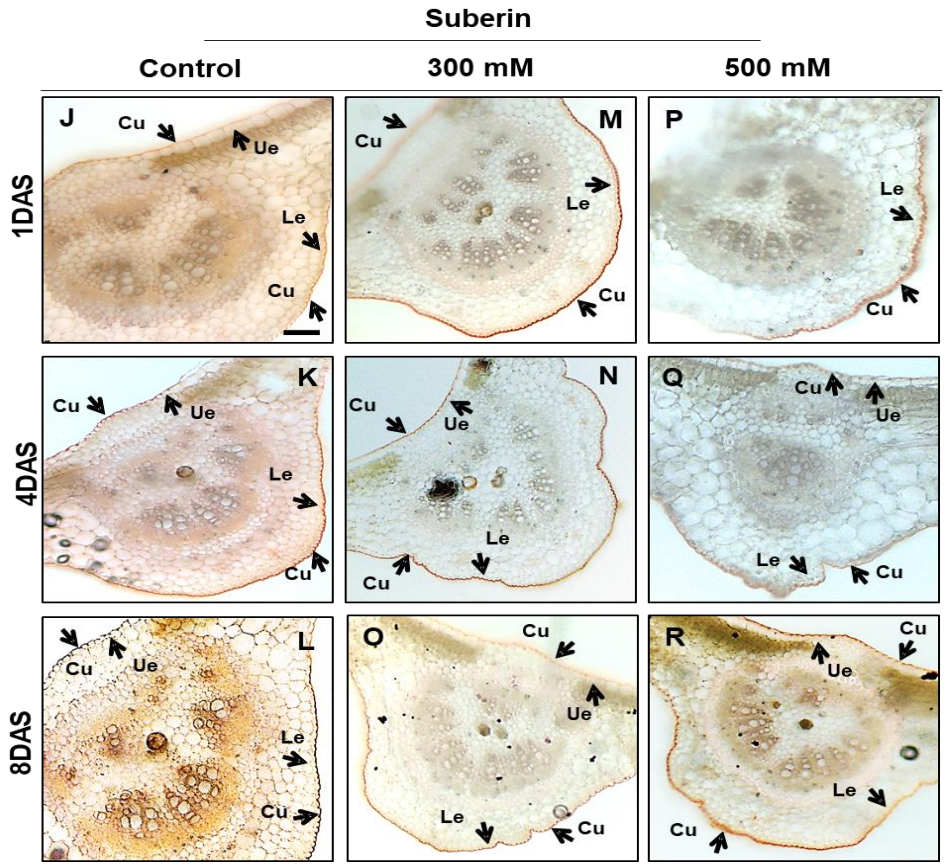
Suberin
Control
300 mM
500 mM
1DAS
4DAS
8DAS
J
K
L
M
N
O
P
Q
R
Cu
Ue
Le

Figure 2. Histochemical detection of lignin and suberin content in roots *P. pinnata*. Staining was done similar to leaf sections explained previously.

1. Lignin visualization in the root sections of control (A-C) 300 mM (D-F) and 500 mM NaCl (G-I) treated plants at 1, 4 and 8DAS, respectively.

2. Suberin visualization in the root sections of control (J-O), 300 mM (P-U) and 500 mM NaCl (V-A1) treated plants at 1, 4 and 8DAS.

Red arrows indicate lignin deposition and black arrows indicate suberin deposition. Ex: exodermis, P: phloem-enriched fraction, Xy: xylem, BEX: biseriate exodermis, MEX: multiseriate exodermis. Bars: black bars equivalent to 100 μm and red bars equivalent to 50 μm.

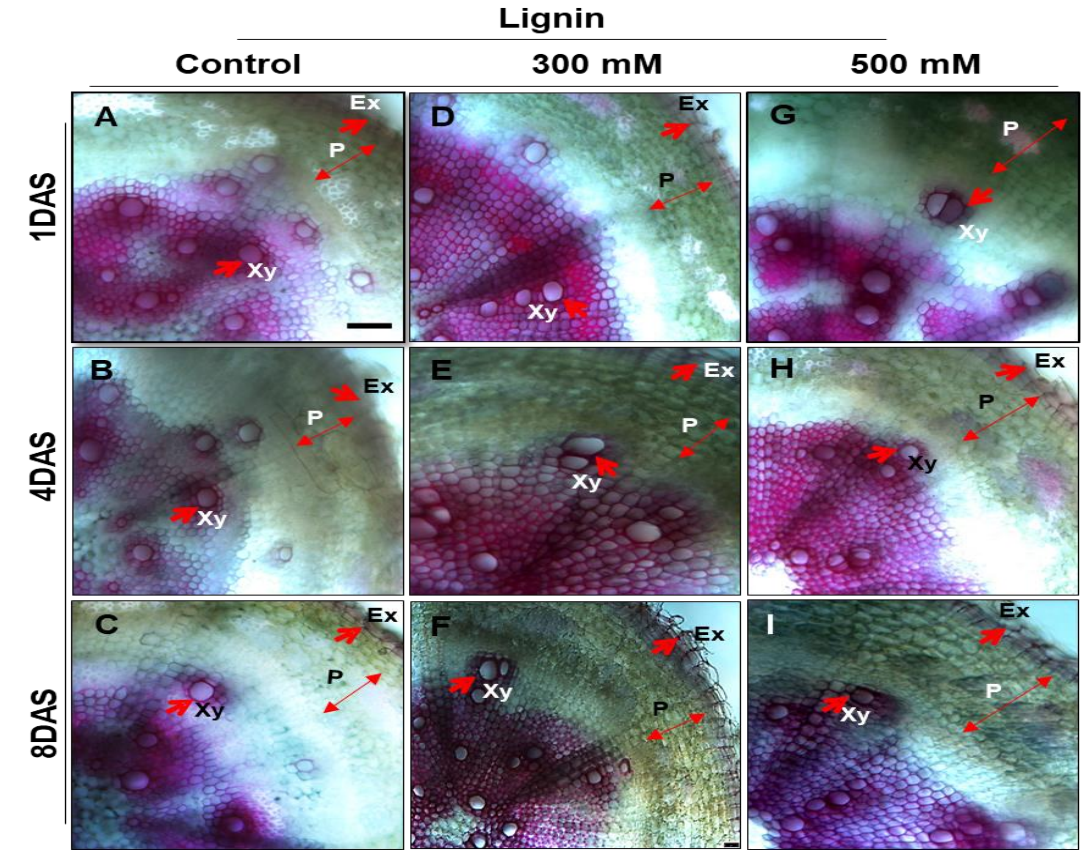
Lignin
Control
300 mM
500 mM
1DAS
4DAS
8DAS
A
B
C
D
E
F
G
H
I
Ex
P
Xy

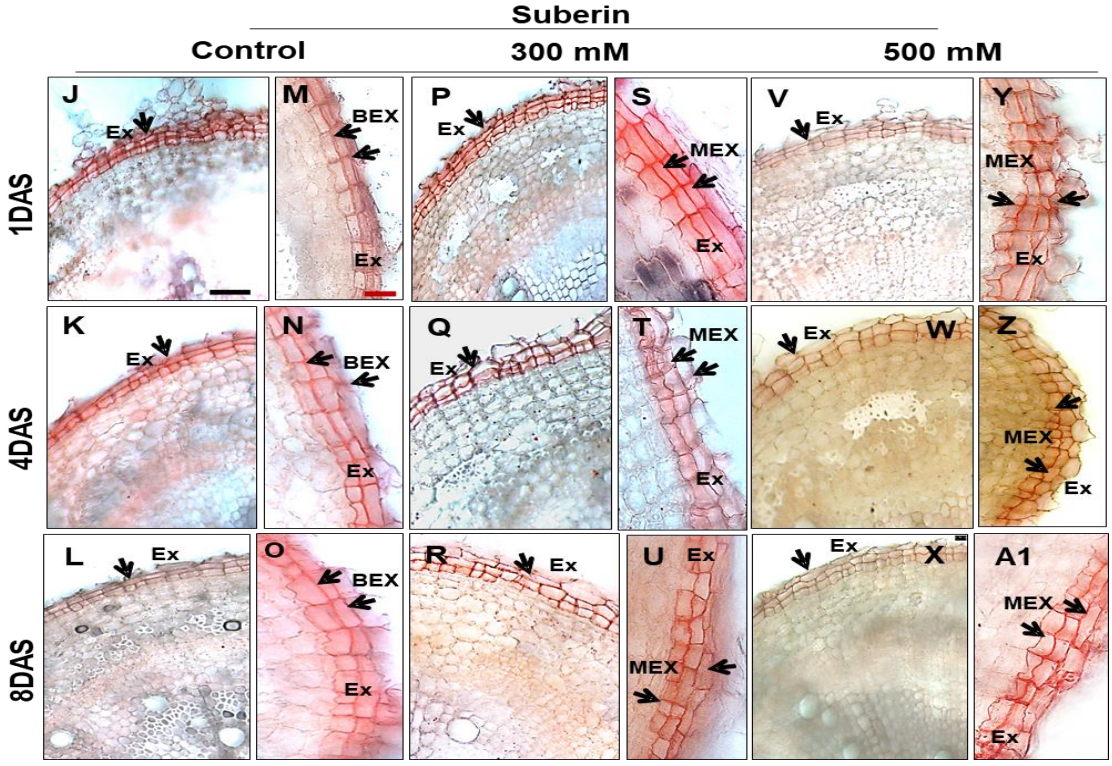
Suberin
Control
300 mM
500 mM
1DAS
4DAS
8DAS
J
K
L
M
N
O
P
Q
R
S
T
U
V
W
X
Y
Z
A1
Ex
BEX
MEX

signal was recorded in the cortical apoplasmic regions dose dependently in both 300 and 500 mM NaCl treated root sections at 1, 4 and 8DAS.

Figure 3. CLSM localization of Na^+ ions using Na^+ specific CoroNa-Green AM (green) and cell-wall binding propidium iodide (red) stains.

1. Leaf sections from control plants (A-C), 300 mM NaCl (D-F) and 500mM NaCl treated plants (G-I) at 1, 4 and 8DAS. Intensity of CoroNa-Green AM fluorescence in cytosolic and vacuolar compartments in the leaf sections (J).

Red lines were drawn to measure Na^+ fluorescence intensity. For quantification of Na^+ fluorescence intensity more than 20 images were pooled from five biological replicates in control and salt treated plants. Error bar represents the mean ± SD (n=20).

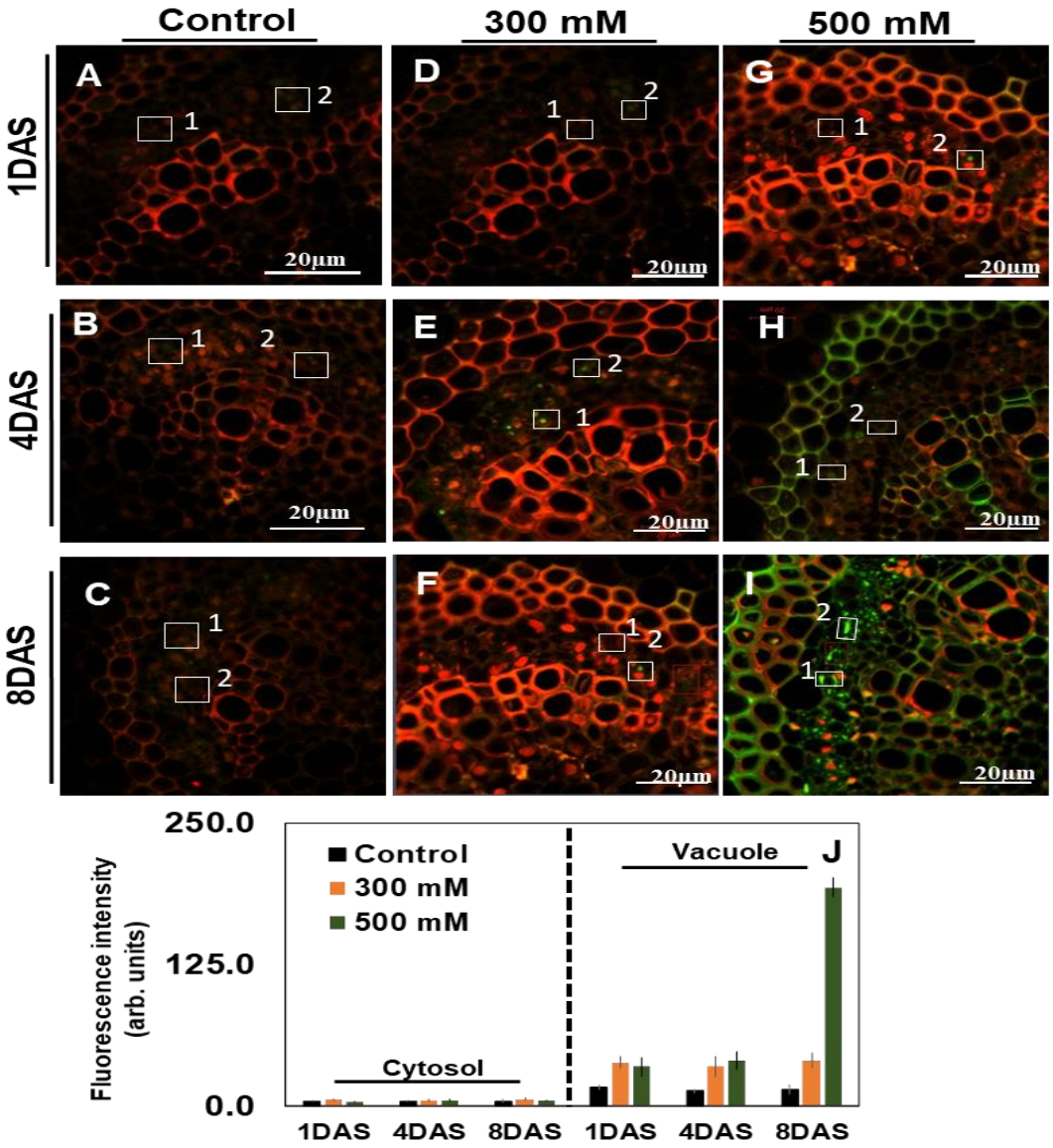
Control
300 mM
500 mM
1DAS
4DAS
8DAS
A
B
C
D
E
F
G
H
I
1
2
20µm
J
Vacuole
Cytosol
Control
300 mM
500 mM
Fluorescence intensity (arb. units)
250.0
125.0
0.0
1DAS
4DAS
8DAS
1DAS
4DAS
8DAS

Figure 3. CLSM localization of Na^+ ions using Na^+ specific CoroNa-Green AM (green) and cell-wall binding propidium iodide (red) stains.

1. Root sections of control plants (K-M), 300 mM NaCl (N-P) and 500 mM NaCl treated plants (Q-S) 1, 4 and 8DAS. Intensity of CoroNa-Green AM fluorescence in cytosolic and vacuolar compartments in the root sections (T).

Red lines were drawn to measure Na^+ fluorescence intensity. For quantification of Na^+ fluorescence intensity more than 20 images were pooled from five biological replicates in control and salt treated plants. Error bar represents the mean ± SD (n=20).

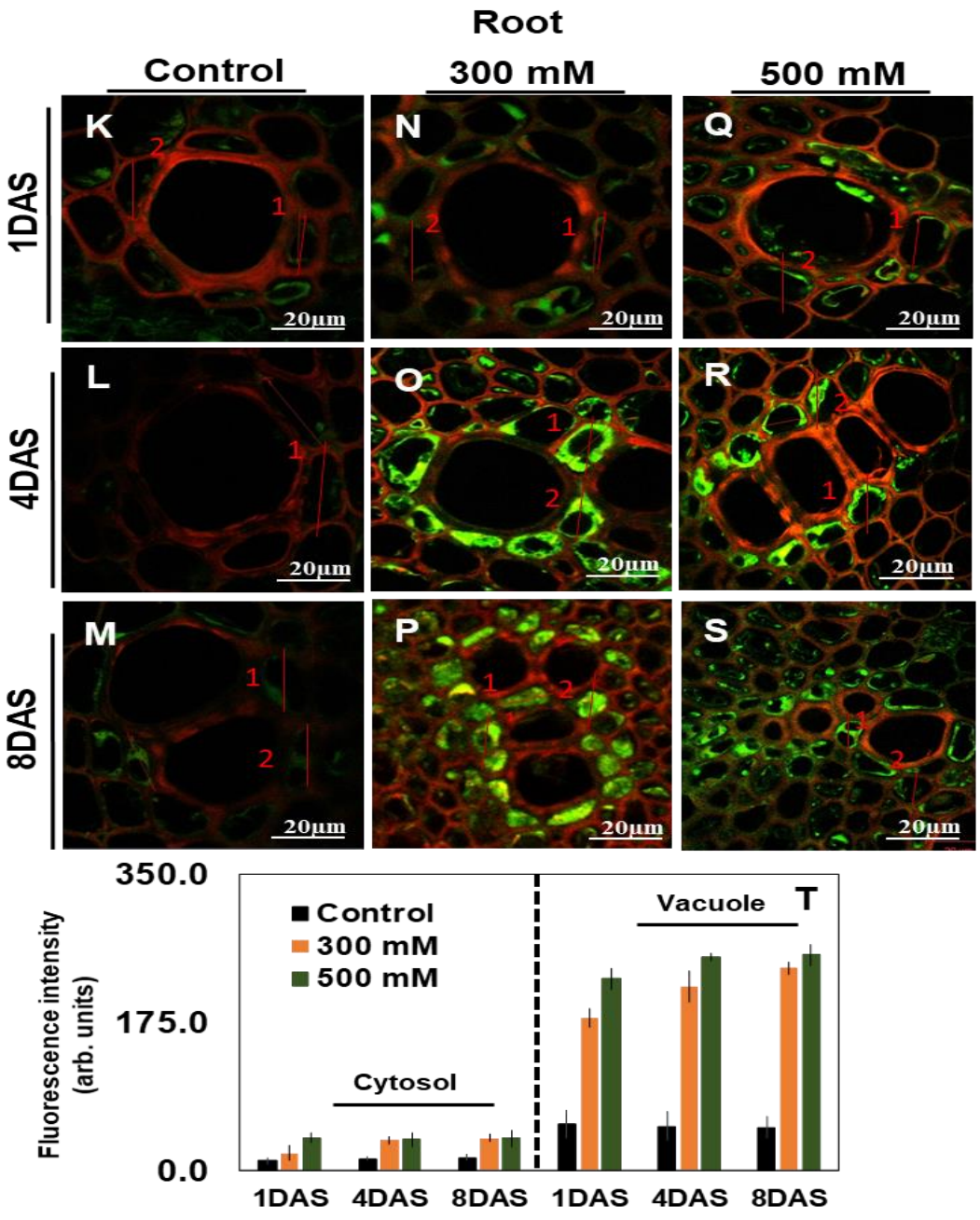
Root
Control
300 mM
500 mM
1DAS
4DAS
8DAS
K
N
Q
L
O
R
M
P
S
1
2
20µm
Fluorescence intensity (arb. units)
350.0
175.0
0.0
Control
300 mM
500 mM
Cytosol
Vacuole
T
1DAS
4DAS
8DAS
1DAS
4DAS
8DAS

Figure 4. Illumination of Na^+ ion fluorescence in leaves of control and salt treated *Pongamia pinnata*.

Confocal images of leaves were stained with CoroNa-Green AM (green colour) and propidium iodide (red colour). (A, B and C) cross sections of leaves of control plants, (D, E and F), cross sections of leaves of 300 mM NaCl 1, 4 and 8DAS, (G, H and I) cross sections of leaves 500 mM NaCl 1, 4 and 8DAS respectively.

Red arrows were drawn to measure Na^+ fluorescence intensity. Quantification of Na^+ fluorescence intensity more than 12 images were pooled from five biological replicates in control and salt treated plants. Error bar represents the mean ± SD (n=12). Two-way ANOVA test was performed to measure P-values ns (not significant) * ($P<0.05$), ** ($P<0.01$) and * * * ($P<0.001$) respectively.

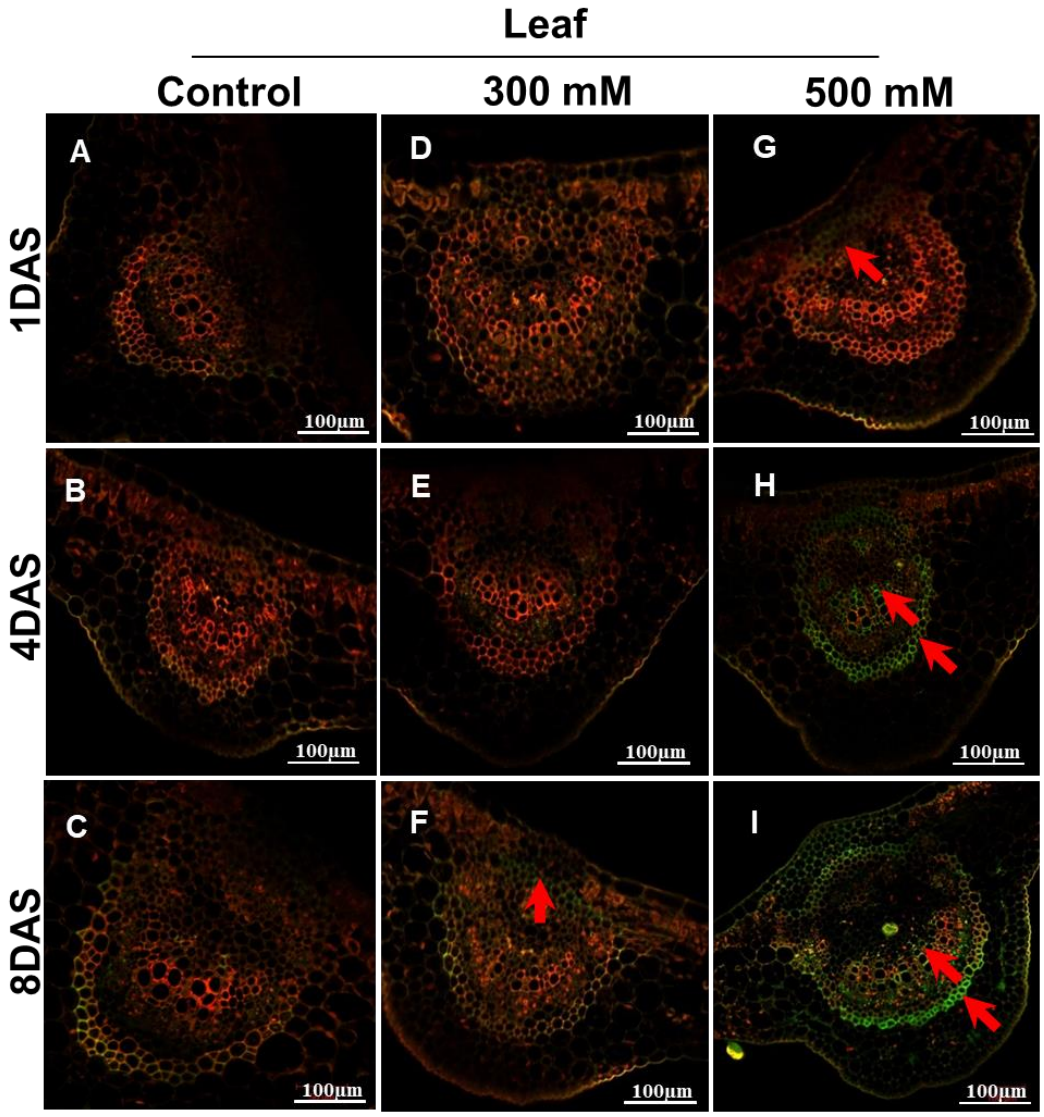
Leaf
Control
300 mM
500 mM
1DAS
4DAS
8DAS
A
B
C
D
E
F
G
H
I
100µm

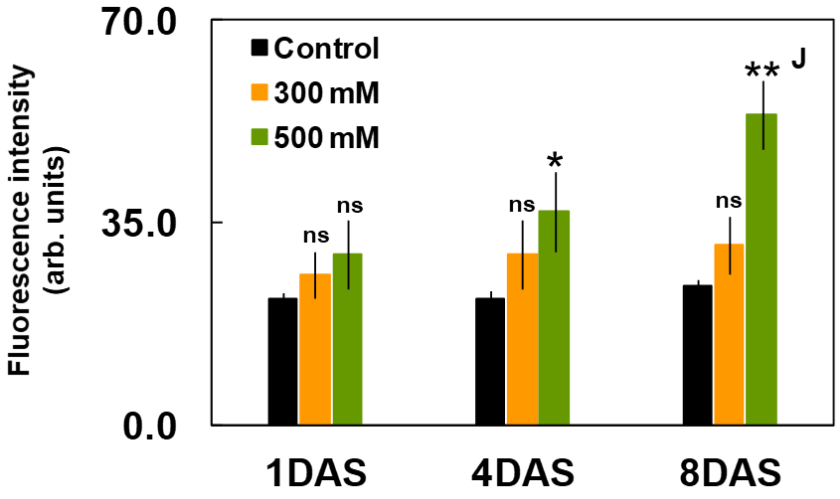
Fluorescence intensity (arb. units)
70.0
35.0
0.0
Control
300 mM
500 mM
ns
ns
ns
*
ns
** J
1DAS
4DAS
8DAS

Figure 5. Illumination of Na^+ ion fluorescence in roots of control and salt treated *Pongamia pinnata*.

Confocal images of roots were stained with CoroNa-Green AM (green colour) and propidium iodide (red colour). (A, B and C) cross sections of roots of control plants, (D, E and F), cross sections of roots of 300 mM NaCl 1, 4 and 8DAS, (G, H and I) cross sections of roots 500 mM NaCl 1, 4 and 8DAS, (J, K and L) magnified images of roots of control plants, (M, N and O) magnified images of roots of 300 mM NaCl 1, 4 and 8DAS, (P, Q and R) magnified images of roots 500 mM NaCl 1, 4 and 8DAS respectively.

White arrows were drawn to measure Na^+ fluorescence intensity. Quantification of Na^+ fluorescence intensity more than 12 images were pooled from five biological replicates in control and salt treated plants. Error bar represents the mean ± SD (n=12). Two-way ANOVA test was performed to measure P-values ns (not significant) * ($P<0.05$), ** ($P<0.01$) and * * * ($P<0.001$) respectively.

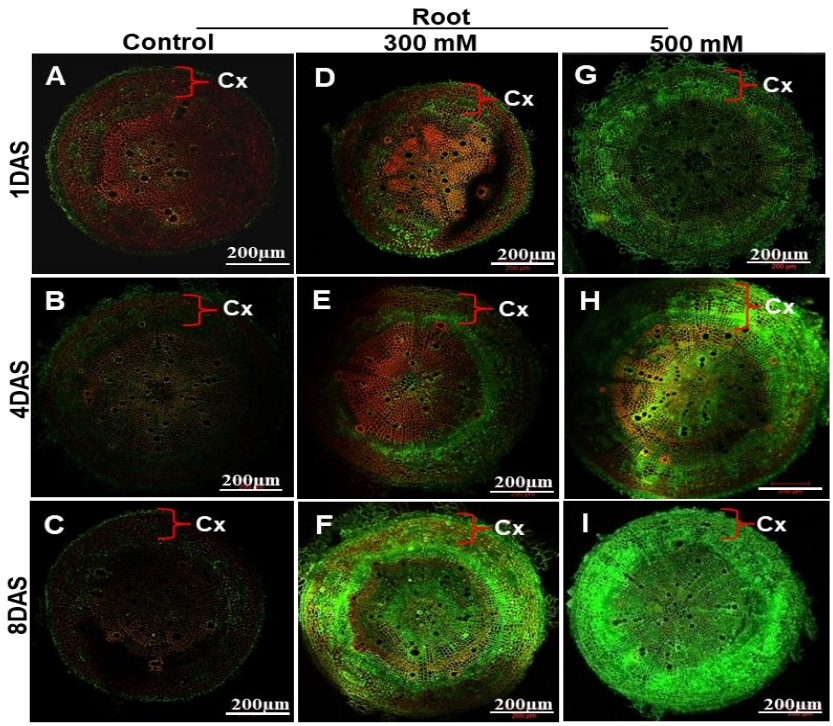
Root
Control
300 mM
500 mM
1DAS
4DAS
8DAS
A
B
C
D
E
F
G
H
I
Cx
200µm

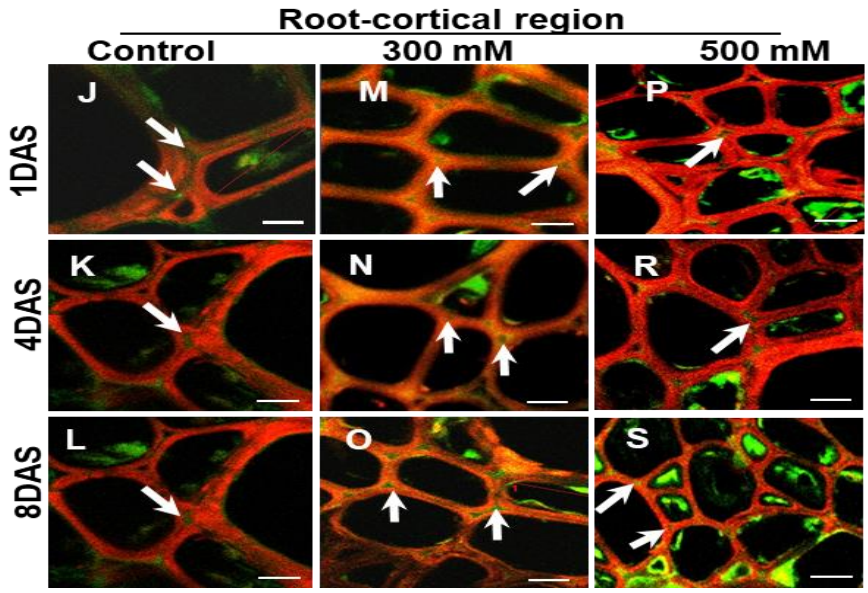
Root-cortical region
Control
300 mM
500 mM
1DAS
4DAS
8DAS
J
K
L
M
N
O
P
R
S

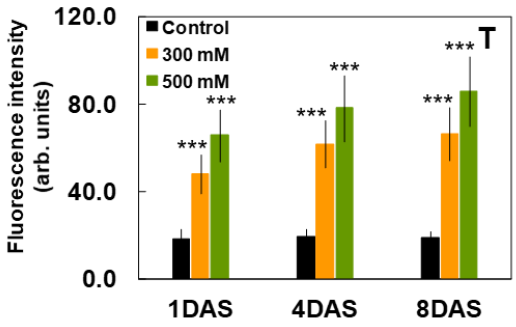
Fluorescence intensity (arb. units)
120.0
80.0
40.0
0.0
Control
300 mM
500 mM
***
T
1DAS
4DAS
8DAS

Figure 6. Our proposed model showing the mechanism of high salinity tolerance in *Pongamia pinnata*.

1. Suberized multiseriate exodermis and lignified walls of xylem vessels, cortical cells, tracheids of root and lignified vascular tissues of leaf are represented.

2. Red line and red arrows: symplastic water and Na^+ transport through cytosol to enhance the Na^+ ion sequestration into the vacuoles of tracheids and xylem parenchyma cells.

3. Blue dashed lines: apoplastic water and Na^+ transport through suberized and lignified cell walls to reduce the excess deposition of Na^+ ions in the cytosol of leaf and root cells.

4. Black arrows: water and solute transport though xylem vessels.

5. Red colour: suberin lamellae; pink colour: cells with lignin deposition; green spots: vacuoles with Na^+ ions; white region with green border: empty vacuole. Abbreviations: vac, vacuole; ex, exodermis; cc, cortical cells; tra, tracheids; xyl, xylem vessel; xpc, xylem parenchyma cells; vas, vascular tissues.

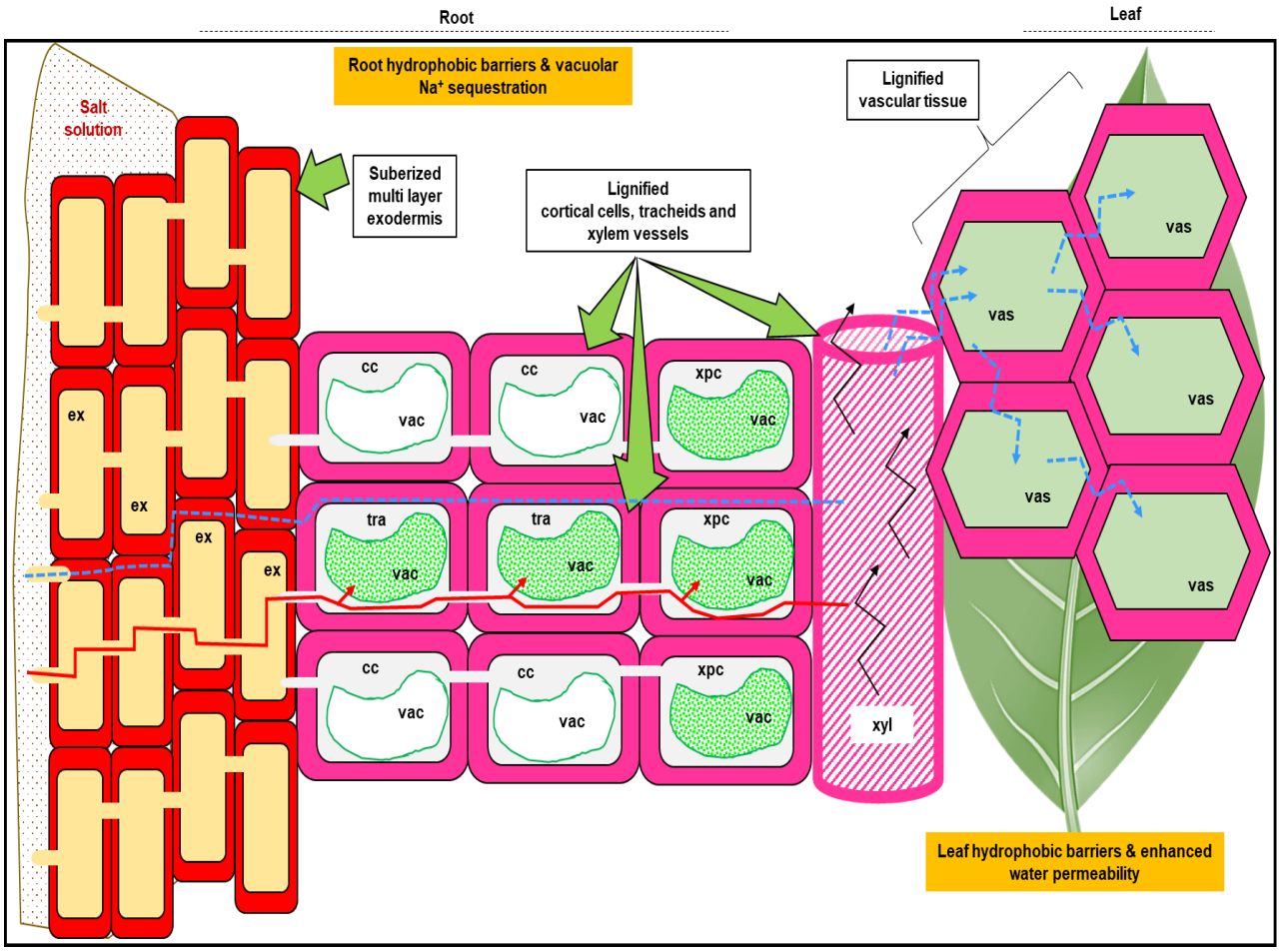
Root
Leaf
Root hydrophobic barriers & vacuolar Na+ sequestration
Lignified vascular tissue
Salt solution
Suberized multi layer exodermis
Lignified cortical cells, tracheids and xylem vessels
ex
cc
vac
tra
xpc
xyl
vas
Leaf hydrophobic barriers & enhanced water permeability

Salinity-induced multiseriate exodermis/ hydrophobic barrier formation in the roots of P. pinnata effectively enhanced the leaf and root water permeability and vacuolar Na^+ sequestration

Lack of morphological salt-induced stress symptoms, low Na^+ content in the salt treated leaves and unchanged root relative water content led us to examine the development of hydrophobic barriers in leaves and roots, which have been shown to restrict the ion uptake and water transport in some plants (Krishnamurthy et al., 2014). In this study, the structural development of exodermal layers of leaves and roots in *P. pinnata* were recorded. In roots, increased pattern of suberization was noticed in both 300 and 500 mM NaCl treated roots across all time points. Suberin is a complex biopolymer with a polyaliphatic domain that forms hydrophobic barriers in exodermis and endodermis, which mediates the symplastic transportation by regulating the unregulated apoplastic by flow of water and solutes. Enhanced deposition of suberin in the exodermis as evidenced in the roots result decreased uptake of Na^+ into shoot and increased retention of water in root under salinity stress. The results also corresponded with unchanged RWC content of root and low Na^+ ion content in leaves of 300 and 500 mM NaCl treatment. Interestingly, a third suberized multiseriate or multilayer exodermis (MEX) was formed periclinally to the existing biseriate or bilayer exodermis (BEX) in the salt treated roots of *P. pinnata* across all time points, while control roots did not exhibit MEX across all time points. Such multiseriate exodermis formation was reported in *Iris germanica* in response to varying environmental conditions, which restrict water and solute transport through apoplasmic route (Meyer et al., 2011). To the best our knowledge, this is the first study reporting on the identification of salt-induced multi-layered exoderm in *P. pinnata*. Moreover, at anatomical level, though we could not observe significant changes in suberization pattern between the cross sections of control and salt-

treated leaves, the cellular integrity of both 300 and 500 mM NaCl treated leaves was well maintained as similar to that of respective controls.

Histological cross sections of leaves and roots showed that salt treated plants showed high lignification of xylem vessels, xylem parenchyma cells (XPCs) and cortical cells with respect to controls across all time points. Increased salinity also resulted in number of lignified cells in xylem vessels, XPCs, and tracheids in the roots of Pongamia at all-time points. Presumably, increased number lignified tracheids, xylem vessels and its XPCs are adaptive strategies to high salinity stress aiming to restrict the Na^+ uptake through apoplastic flow as well as enhance the cell-to-cell pathway for water transport (Sánchez-Aguayo et al., 2004; Neves et al., 2010). Further, the numbers of tracheary elements in the vascular bundle of NaCl treated leaves were increased with increasing treatment time. Under salinity stress, the occurrence of high lignin content in the cell wall not only decreased the excess ion accumulation in the plant but also reduced the water uptake by several folds. The abundance of lignified xylem vessels may compensate for the salt-induced reduction in water uptake (Sánchez-Aguayo et al., 2004).

Roots of salt treated P. pinnata effectively sequestered Na^+ ions

Salt treated Pongamia leaves showed a consistent high intensity staining of the central vascular bundle region, while control leaves did not change in its Na^+ specific fluorescence across all time points. In addition, a high intensity of green fluorescence was observed in the cell walls (apoplastic region) of 500 mM NaCl treated leaves of Pongamia at 4 and 8DAS, which is due to increased accumulation of Na^+ ions in the apoplast. The results suggest that the higher accumulation of Na^+ ions may increase the availability of cation-binding groups in the cell wall matrix to enhance the apoplastic based Na^+ sequestration, which may act as an additional barrier to existing vacuolar Na^+ sequestration in order to protect the plant cellular

integrity from Na^+ toxicity (Byrt et al., 2018). In this study, we investigated the distribution of Na^+ between the cytosol and the vacuole in control and salt treated leaves of *P. pinnata* at 1, 4 and 8DAS. Interestingly, there was high vacuolar Na^+ intensity in 500 mM NaCl treated leaves only at 8DAS, while cytosolic Na^+ intensity did not change significantly in both 300 and 500 mM NaCl treated leaves across all time points. From the above observation, we infer that the small amount of sodium which escaped root barrier and reached salt treated leaves, is actively sequestered into the vacuole and cell wall matrix (apoplastic region) to attain structural and functional integrity of photosynthetic machinery under high salinity (Marriboina et al., 2017). The CoroNa-Green intensity increased with increasing salt concentration in both 300 and 500 mM NaCl treated roots. Further, the xylem companion cells which were surrounded by xylem vessels exhibited high levels of Na^+ specific fluorescence across the cross sections of both 300 and 500 mM NaCl treated roots, while the Na^+ specific fluorescence intensity level of adjacent cortical cells remained similar to that of controls.

The above data suggest that the XPCs might act as Na^+ ion specific filter barrier which restricts the entry of excess Na^+ ions (transported across the root either by symplastic or apoplastic origin) to the aerial parts of the plant. Corresponding with the observed dry weight-based Na^+ ion content that the leaves and roots accumulated. Further, intracellular Na^+ ion distribution pattern of Na^+ ions was investigated in the XPCs of both control and salt treated roots. The vacuolar Na^+ intensity of XPCs was significantly higher in roots of both 300 and 500 mM NaCl treated plants, while the cytosolic Na^+ intensity was remained unchanged. The Na^+ vacuolar sequestration and low cytosolic Na^+ content in the XPCs might favor the uptake of Na^+ ions from the xylem vessel, as the vacuolar Na^+ increased with salt treatment time. The absence of propidium iodide-stained cells across the cross-sections of

leaves and roots of salt treated plants suggest that the structural and functional integrity of cell and cellular components were well maintained even under high salt conditions (Oh et al., 2010).

In the present study, the apoplastic/ cell wall Na^+ specific fluorescence intensity was increased with treatment time in both 300 and 500 mM NaCl treated plants indicating that there was an apoplastic Na^+ sequestration (Gonzalez et al., 2012; Anower et al., 2017). The carboxylic residues of pectin in the cell wall may primarily serve as cation-binding matrix for Na^+ ion, contributing to apoplastic Na^+ sequestration (Gonzalez et al., 2012; Marriboina et al., 2017). The patterns of high apoplastic and vaculoar Na^+ contents might lead to lower Na^+ ion content in the cytosol which may facilitate the protection of cytosolic enzymes from sodium toxicity (Wu et al., 2018; Marriboina and Reddy, 2020a).

In conclusion, the absence of salt-induced symptoms on leaves, Further, increased Ca^{2+} and K^+ minimizes the salt-induced damage in leaves and roots. Higher Na^+ content in the roots than leaves also revealed that Pongamia roots act as ultra-filters/strong barriers to protect the leaves from Na^+ toxicity. The Na^+ probe fluorescence data reveals the existence of vacuolar Na^+ sequestration mechanism in the root and the confinement of Na^+ specific fluorescence to certain cells such as tracheid cells and xylem parenchyma showing the strong salinity tolerance mechanisms effectively operating in the roots of *P. pinnata*. At the anatomical level, formation of salt-induced suberized multiseriate exodermis in the roots and a greater deposition of lignin maximize the water permeability in the leaves and roots (Figure 6). In addition, suberin and lignin synthesis in the roots and leaves contribute towards the high salinity tolerance of *P. pinnata*. Our results also highlight the key mechanisms conferring high salt tolerance in Pongamia, which can be highly crucial for further research to develop Pongamia as a tolerant and sustainable biofuel tree crop.

Chapter 4

Phytohormonal and Metabolomic cross-talk

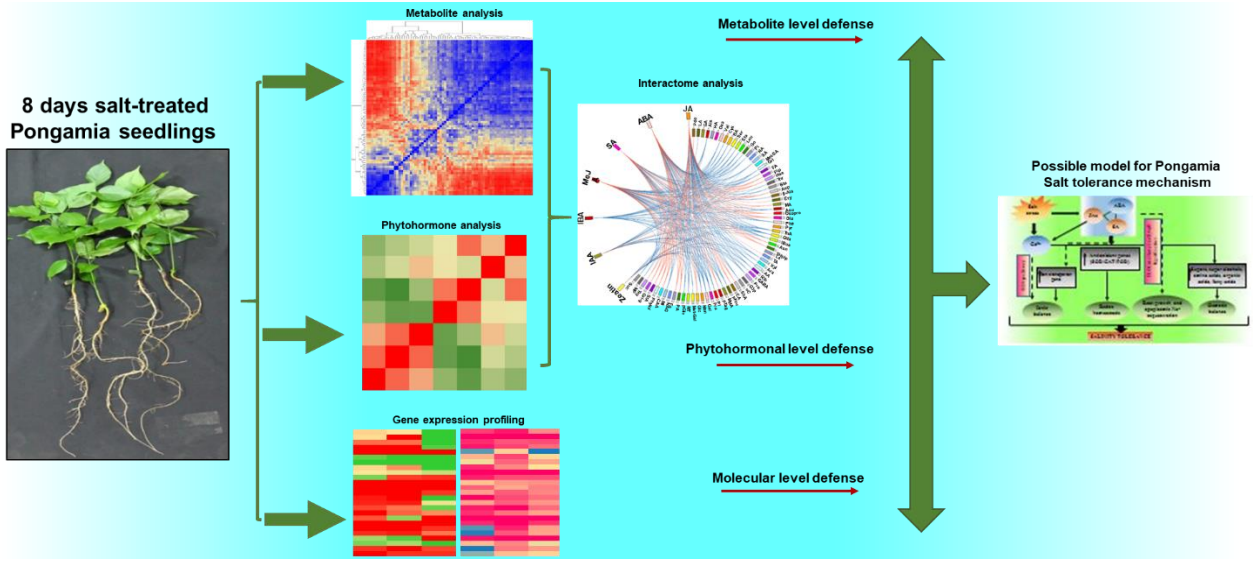

Chapter 4 Introduction

Soil salinization is a major environmental stress to limit plant growth and production which is closely associated with arable land degradation (Shahid et al., 2018; Marriboina and Reddy, 2020a). Approximately 1.5 million hectares of cultivable land is becoming saline marginal lands by every year because of high salinity levels and nearly 50% of arable lands will be lost by year 2050 (Md-Hossain, 2019). Global climate change, increasing population and excessive irrigation are further limiting the availability of cultivable land for crop production (Raza et al., 2019). To date, attempts are being made to extend the crop productivity on saline lands. However, progress of these attempts is greatly hampered by the genetic complexity of salt tolerance, which largely depends on physiological and genetic diversity of the plant and spatio-temporal heterogeneity of soil salinity (Morton et al., 2019). To address this issue, several plant species were introduced to rehabilitate the saline lands and certain economically important nitrogen fixing biofuel tree species are of immense importance not only for sustenance to saline marginal lands but also economic gain towards saline lands (Samuel et al., 2013; Hanin et al., 2016; Marriboina and Reddy, 2020a).

A comprehensive understanding of physiological, hormonal and molecular adaptive mechanisms is crucial to cultivate these tree species on saline marginal lands (Quinn et al., 2015). Plants growing in saline soils prevent the excess Na^+ ion disposition in the leaves in order to protect the photosynthetic machinery from salt-induced damage. The decrease in net CO_2 assimilation rate and optimum quantum yield of PSII (Fv/Fm) might substantiate the leaf performance under salt- induced drought stress. Calcium ion (Ca^{2+}) is known as an intracellular second messenger and plays an important role in plant growth and development. It also plays an essential role in amelioration of sodium toxicity through activating several Ca^{2+} responsive genes and channels (Thor, 2019).

In response to salt stress, plant produces several phytohormones such as abscisic acid (ABA), jasmonic acid (JA), methyl-jasmonic acid (MeJA), zeatin, indole acetic acid (IAA), indole butyric acid (IBA) and salicylic acid (SA), which plays crucial role in sustaining its growth under extreme saline conditions. ABA is well-known stress-induced phytohormone, critical for plants growth and regulating numerous downstream signalling responses (Tuteja, 2007). ABA causes stomatal closure to prevent excess water evaporation and regulate root growth under salinity stress (Zelm et al., 2020). Auxins and cytokinins are growth promoting phytohormones which interact to regulate various growth and developmental process such as cell division, elongation and differentiation. Salt-induced endogenous accumulation of cytokinin improves the salt tolerance in crop species by delaying leaf senescence and marinating photosynthetic capacity (Liu et al., 2012; Golan et al., 2017). Upon salt stress, the rise in endogenous SA levels can cause a significant reduction in the ROS and Na^+ accumulation across the plant, whereas SA deficient plant produced an elevated levels of superoxide and H_2O_2 (Yang et al., 2004). According to Sahoo et al. (2014), the perfect harmony among phytohormones played a significant role in improving the salt tolerance in rice. However, the synergistic and antagonistic interactions between phytohormones mostly depending on plant species and type of stress imposed on plants but their interactions are still not clearly understood (Gupta et al., 2017). To combat against salinity-induced ROS damage, plants adapted jasmonates directed anthocyanin accumulation to mitigate its negative effects (Ali and Baek, 2020). Further, JAs can positively regulate the endogenous ABA level and together they regulate the guard cell movement during salt stress (Siddiqi and Husen, 2019). JA and ABA together also regulate antioxidant status of the cell to enhance the survivability of plant towards osmotic stress. Additionally, JA and SA positively regulate the several protein coding genes which

are responsible for plant salt tolerance (Wang et al., 2020). Plants pre-treated with SA, alleviate salinity stress by decreasing Na^+ transport and by increasing H^+-ATPase activity (Jayakannan et al., 2013; Gharbi et al., 2018). Excessive deposition of salts in the cell and celluar compartments causes membrane depolarization. To counteract the salt-induced membrane depolarization, ABA regulates expression of numerous vacuolar and plasma membrane transporters such as vacuolar H^+-inorganic pyrophosphatase (H^+-PPase), vacuolar H^+-ATPase, Na^+/H^+ antiporter (NHX) 1, vacuolar pyrophosphatase (V-PPase) and plasma membrane H^+-ATPase (PM-H^+-ATPase) pumps (Fukuda and Tanka, 2006). According to Shahzad et al. (2015), exogenous application of JAs on maize improved salt tolerance by regulating Na^+ ion uptake at the root level. Proton pumps and cation channels such as H^+-ATPase pumps, cation/H^+ exchangers (CHXs) and cation/Ca^{2+} exchangers (CCXs) were involved in maintaining the membrane potential under salt stress conditions (Falhof et al., 2016; Li et al., 2016; Liu et al., 2017). Significantly, the expression of several isoforms of NHXs namely SOS (salt overly sensitive)1, NHX1, NHX2, NHX3 and NHX6 under salt stress to regulate Na^+ fluxes in and out of the cell (Dragwidge et al., 2018). Upon salt stress, plants activate a complex antioxidant defense mechanism to minimize oxidative stress damage by ROS under salt stress conditions (Xie et al., 2019). For the first time, we report here the mechanisms of salinity tolerance in Pongamia at molecular level with the help of hormonal, metabolomics, gene expression and computational approaches. Further, the assessment of tissue specific-phytohormone profiling elucidates the key role of specific hormones in conferring the tissue-specific associated mechanisms of salt tolerance in Pongamia. In addition, the correlation studies between the phytohormones enable to identify the crosstalk between phytohormones, which may regulate the growth and development in Pongamia under salt stress

(Maury et al., 2019). Time-course metabolic profiling and correlations under salt stress in Pongamia would certainly contribute to understand the biochemical changes involving metabolic pathways, which is crucial in plant adaptation to salinity stress conditions. The interaction studies between hormones and metabolites should certainly create new opportunities for the discovery of hormone-metabolite associates, which are very crucial to understand stress tolerant mechanisms (Cao et al., 2017). The present study provides an evidence for the hormone-metabolite interactions as well as novel hormone-metabolite associated signalling pathways to understand high salinity tolerance mechanisms in *Pongamia pinnata*.

Plant material, growth conditions and NaCl treatment

Pongamia seeds (accession TOIL 12) were obtained from Tree India Limited (TOIL), Zaheerabad, Hyderabad, Telangana. Freshly collected seeds were sterilized with 1% (v/v) hypochlorite solution for 5 min. Further, the seeds were kept for germination on moist cotton bed at 25°C in dark for 10 days after thoroughly washed with autoclaved distilled water. Germinated seeds were grown hydroponically in Hoagland No. 2 basal salt mixture (Himedia) solution (pH 5.75 ± 0.02) for 30 days. The seeds were kept for germination on moist cotton bed for 10 days at 25°C in dark after thoroughly washed with autoclaved distilled water. After radicle emergence, the germinated seeds were placed just above the nutrient medium (Hoagland No. 2 basal salt mixture (Himedia) solution (pH 5.75 ± 0.02)) level with help of parafilm in 50 ml falcon tubes (Genaxy) for 10 days. Further, the plants were grown initially in long cylindrical glass tubes (5 cm diameter X 30 cm length) for 10 days and then transferred to long cylindrical glass tubes (5 cm diameter X 60 cm length) before giving the salt stress treatment. The glass apparatus were designed in such a way to grow the plants without root limitation. We maintained following culture conditions 24°C temperature, 16 h light and 8 h dark, and relative humidity maintained approximately at 60%. In order to avoid hypoxic conditions nutrient solution was renewed on daily basis. Salinity stress treatment was given according to Marriboina and Reddy, (2020b). For salinity stress, two different salt concentrations (300 mM NaCl and 500 mM NaCl (sea water equivalents)) were used. For stress treatment, 30 days old plants (n = 20 to 30) were chosen and exposed to 300 and 500 mM NaCl stress with increment of 100 mM NaCl per day (Marriboina and Reddy, 2020b). Control plants were maintained in a fresh Hoagland's solution. Plants were harvested at an interval of 1, 4 and 8 days. Fresh weights of leaves and roots were measured immediately after harvest. Dry weights of control and treated plant tissues were determined after

drying at 70°C for 3 days. Control and treated samples were harvested at each time intervals, flash frozen in liquid nitrogen and stored at -80°C till analysis.

LC-MS analysis

The endogenous levels of phytohormones were quantified by LC-MS using a protocol described by Pan et al. (2010), with some modifications. Freshly harvested leaves and roots of control and salt treated plants were finely ground to powder with liquid nitrogen. Approximately 100 mg of powdered tissue was suspended in 500 μl of extraction solvent (2-Propanol:H_2O:HCl, 2:1:0.002, v/v/v) and kept in thermomixer at 4°C at 500 rpm for 30 min. The above step was repeated with addition of 1 ml ice cold dichloromethane. The resulting mixture was centrifuged at 4°C 13000g for 5 min and collected in fresh centrifuge tube. The sample tubes were placed in speed vac to evaporate extra solvent for 45 min. The final residue was dissolved in 70 μl of ice cold methanol followed by centrifugation at 13000g for 5 min. Finally, samples were taken into a transfer vial and were analysed by using Exactive™Plus Orbitrap mass spectrometer (Thermo Fisher, USA) coupled with UPLC (Waters, Milford, MA, USA).

LC-MS analysis was performed on an Aquity UPLC™ System equipped with quaternary pump, and auto-sampler to perform hormone analysis. For analysis, we used following conditions: capillary temperature 350˚C, sheath gas flow (N2) 35 (arbitrary units), AUX gas flow rate (N2) 10 (arbitrary units), collision gas (N2) 4 (arbitrary units) and capillary voltage 4.5 kV under ultrahigh vacuum 4e-10 mbar. Chromatographic separation was carried out in a Hyperreal GOLD C18 (Thermo Scientific) column (2.1×75 mm, 2.7 μM). Formic acid (0.1%, v/v) and acetonitrile with 0.1% formic acid were used as mobile phase A and B, respectively. A gradient elution program was performed using two solvents system, solvent A and B chromatographic run for 9 min at 20˚C. Hormones such as ABA, GA, JA and SA were

quantified by using all ion fragmentation (AIF) mode (m/z 50-450) with positive heated electrospray ionization (ESI) in negative ion mode. Similarly, hormones zeatin, indoleacetic acid (IAA), indolebutyric acid (IBA) and methyljasmonate (MeJA) were measured using Turbo Ion spray source in positive ion mode. All phytohormones were quantified by using standard calibration curves.

GC-MS analysis

The plant primary metabolites were analysed by GC-MS as described by Roessner et al. (2000). 100 mg of freshly collected leaves and roots were ground finely with liquid nitrogen and extracted with 1.4 ml of 100% methanol containing ribitol as internal standard. The mixture was kept at 70°C for 15 min and then mixed vigorously with 1.4 ml of water. Further, the sample was transferred in glass vial (GL-14 Schott Duran) and centrifuged at 4°C for 15 min at 542 rpm. The upper phase was taken in a fresh centrifuge tube and evaporated by using Speed Vac drying for 45 min. Finally, the samples were kept in -80°C for storage until analysis. For derivatization, the residue was dissolved in 80 μl of methoxyamine hydrochloride with pyridine at 30°C for 90 min, followed by 80 μl of MSTFA (N-methyl-N-(trimethylsilyl) trifluoroacetamine) and 20 μl of FAME mix (Sigma, 1 μg. μl^{-1} in hexane) at 30°C for 30 min.

The derivatized sample was analysed on a system LECO-PEGASUS GCXGC-TOF-MS system (LECO Corporation, USA) equipped with 30 m Rxi-5ms column with 0.25 mm internal diameter and 0.25 μm film thickness (Restek, USA). The ion, interference and source of injection temperatures were maintained at 200°C, 225°C and, 250°C, respectively. Chromatographic separation was carried out under following conditions: isothermal heating at 70˚C for 5 min, followed by 5˚C min^{-1} oven temperature ramp to 290˚C and final heating at 290˚C for 5 min. The flow rate of carrier gas (helium gas) was adjusted to 1.5 ml. min^{-1}. A

volume of 1 μl sample was used for analysis and injected in split less mode, and scan mass range 70 to 600 at 2 scans/ s.

Data sets were generated in the form of NETCDF files from ChromaTOF software 4.50.8.0 chromatography version (LECO Corporation, USA) GC-MS and were further exported to MetAlign 3.0 (www.metalign.nl). The MSClust software was used to adjust signal to noise ratio of ≥2, for baseline correction, noise estimation and identification of mass peak (ion-wise mass alignment). Non-repetitive (<3 samples) mass signals were discarded. The MSClust analysis was performed on the above results for the reduction of data and compound mass extraction. Further, the MSClust files were further exported to NISTMS Search v2.2 software for identifying compounds with the NIST (National Institute of Standard and Technology) Library and Gölm Metabolome Database Library (http://gmd.mpimp-golm.mpg.de/). Metabolite identity was given based on the maximum matching factor (MF) value (>700) and least retention index (RI) value. The intensity of each metabolite value normalized with internal standard ribitol value. Finally, only annotated metabolites were taken into consideration for further analysis.

Semi-quantitative PCR and quantitative RT-PCR analysis

In the present study, a total of 34 genes were analysed for their salinity-induced expression profiles. Direct primers were used for 22 genes based on available transcriptome shown by Sreeharsha et al. (2016) and Huang et al. (2012), while indirect primers were designed for 12 genes based on the available gene sequences of *Glycine max* from SoyKB (www.soykb.org) database since the transcriptome studies showed that *P. pinnata* was closely related to *G. max*. All genes were amplified by PCR using *P. pinnata* cDNA. The amplicons obtained based on *G. max* indirect primers as well as *P. pinnata* direct primers were sequenced for confirming the identity of target gene. Quantitative PCR analysis was performed on Eppendorf Realplex

Master Cycler (Eppendorf, Germany) using KAPASYBRFAST [Mastermix (2×) Universal; KAPA Biosystems] real-time PCR kit following manufacturer's instructions. For relative quantification analysis, 0.25 μg of RNA template was used, which was extracted from the pool of six biological replicates of both control and salt treated plants by using Sigma spectrumTM Total RNA kit (Sigma, USA) and cDNA synthesis was performed by using the PrimeScriptTM 1st strand cDNA synthesis kit (TAKARA, Japan). Target genes were amplified with the following cycling programme: 1 cycle at 95°C for 2 min, followed by 40 cycles of 30 s at 95°C, 30 s at 60°C and 20 s at 72°C, followed by the dissociation (melting) curve. The intensity of fluorescence was measured by using the Realplex software (Eppendorf, Germany). The limit and efficiency of each primer pair of both target and reference gene was allowed to measure accurate comparison of gene expression using the $2^{-\Delta\Delta C_T}$ method for relative quantification (the Applied Biosystems User Bulletin No. 2 (P/N 4303859)) (Livak and Schmittgen, 2001). The 18s rRNA was used as reference gene after confirming its consistency expression under salt stress.

Correlation and statistical analysis

To measure the linear dependence between the variables, Pearson's correlation coefficient was calculated using R statistical package. Heat maps were generated based on correlation values of metabolites and hormones. Circos plot represents the relationship between hormones and metabolites, which was generated based on correlation values of individual metabolites and hormones. The statistical significant differences of control and salt treatments were calculated by using one-way ANOVA at ***$P < 0.001$, **$P < 0.01$ and *$P < 0.05$.

Salinity-induced phytohormonal changes in leaves and roots of P. pinnata under progressive salt stress

Upon salt stress, Pongamia accumulated various hormones tissue specifically and time dependently. Accordingly, we quantified phytohormones by using LC-MS/MS analysis. All seven hormones zeatin, IAA, IBA, MeJA, SA, ABA, and JA were showed a significant increase in leaves of 300 and 500 mM NaCl treated plants at 1, 4 and 8DAS (Figure 1A-D). As shown in the Figure 1A-D, the hormone accumulation pattern was changed with the treatment time in leaves of 300 mM NaCl plants. At 1DAS, six hormones zeatin, IAA, IBA, MeJA, ABA, and JA were showed significant increase in leaves of 300 mM NaCl treated plants, while SA levels did not change significantly. Hormones such as zeatin, IAA, MeJA and JA showed significant up-regulation at 4DAS. IAA, ABA and JA levels were significantly enhanced in leaves of 300 mM NaCl treated plants at 8DAS. Moreover, in roots, the phytohormone levels varied with salt concentration and treatment time. Zeatin, IBA and MeJA levels increased significantly in roots of 300 mM NaCl treated plants at 1DAS. Similarly, zeatin and ABA levels showed significant up-regulation in 500 mM NaCl treated plants at 1DAS (Figure 1E). At 4DAS, only zeatin showed significant increase by ~3.7-fold in roots of 300 mM NaCl treated plants. In response to 500 mM NaCl treatment, MeJA and JA levels showed ~3.3 and 2.0-fold up-regulation in roots at 4DAS respectively (Figure 1F). At 8DAS, zeatin and IAA levels were increased by ~2.2 and 2.3-fold in roots of 300 mM NaCl treated plants respectively (Figure 1G). In response to 500 mM NaCl stress, only IBA levels showed significant increase by ~3.0-fold at 8DAS.

Correlation studies among hormones are essential to explore hormonal interactions under salt stress. Accordingly, correlation studies were performed based on stress treatment time. Each stress time point was grouped individually in the form of a correlation cluster matrix to show the

interactive responses of each individual hormone under salt stress. We observed significant correlation between JAs and IAA over time in leaves of 300 mM NaCl treated plants (Figure 2A-C). Similarly, JA showed significant correlation with MeJA in leaves of 500 mM NaCl treated plants across all-time points (Figure 2D-F). Jasmonates (JA and MeJA) and SA showed significant interaction with other hormones in roots of 300 and 500 mM NaCl at all-time points (Figure 2G-L).

Temporal metabolite profiling in leaves and roots of Pongamia pinnata under salt stress

The relative levels of metabolites in Pongamia under salt stress conditions were quantified by using gas chromatography-mass spectrometry (GC-MS) (Figure 3 and 5). A total of 71 metabolites were identified in both leaves (Table 1) and roots (Table 4), which are related to 12 carbohydrate metabolism, 22 organic acid metabolism, 15 amino acid metabolism, 6 cyclitol/ polyol metabolism, 6 fatty acid metabolism and 10 other miscellaneous metabolites.

In response to salinity stress, leaves accumulated a set of primary metabolites related to various metabolic pathways such as amino acid metabolism, carbohydrate metabolism, organic acid metabolism, polyol and fatty acid metabolism (Figure 3). Upon salt stress exposure, leaves accumulated various metabolites, which includes Suc, Fru, Man, pinitol, mannitol, myo-inositol, Phe, Val, butanoate, coumarate and myristate showed significant increase in both 300 and 500 mM NaCl treated plants at 1, 4 and 8DAS. Importantly, mannitol levels showed significant up-regulation by ~12 fold in leaves of 300 and 500 mM NaCl treated plants at 1, 4 and 8DAS. With increasing treatment time, Pongamia accumulated several metabolites related to cell wall synthesis and TCA cycle, which include Gal, Xyl, pGlc, pFru, Leu, fumarate, succinate and glutarate in leaves of 300 and 500 mM NaCl treated plants at 8DAS. Additionally, several other metabolites

Figure 1. Effect of salt stress on plant morphology and levels of endogenous phytohormones in leaves and roots of *Pongamia pinnata*.

(A) Shoot and root morphology of Hoagland solution-grown *P. pinnata* plants after 30 days treated with three different salt concentrations 0 (control), 300 and 500 mM NaCl at three different time points 1, 4 and 8DAS. The levels of endogenous hormones (B and I) zeatin, (C and J) IAA, (D and K) IBA, (E and L) MeJA, (F and M) SA, (G and N) ABA and (H and O) JA in leaves and roots of 0 (control), 300 and 500 mM NaCl treated plants at three different time points1, 4 and 8DAS respectively.

Error bar represents the mean ± SD (n=6). Two-way ANOVA test was performed to measure *P*-values ns (not significant), * ($P < 0.05$), ** ($P < 0.01$) and * * * ($P < 0.001$) respectively.

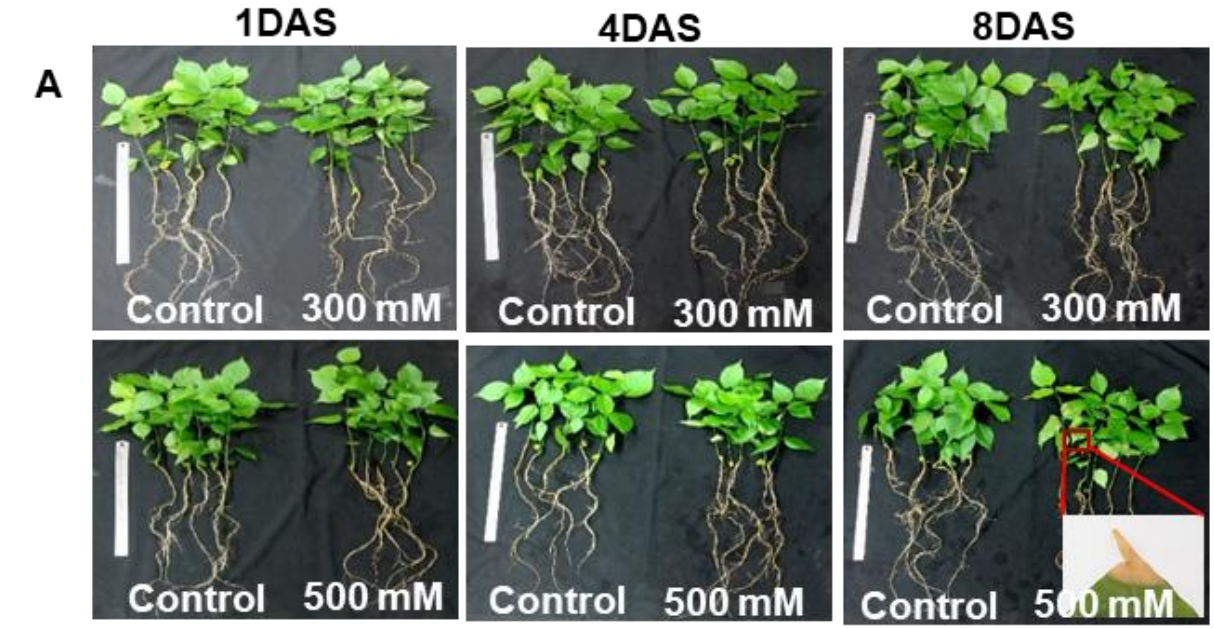
A
1DAS
4DAS
8DAS
Control
300 mM
Control
300 mM
Control
300 mM
Control
500 mM
Control
500 mM
Control
500 mM

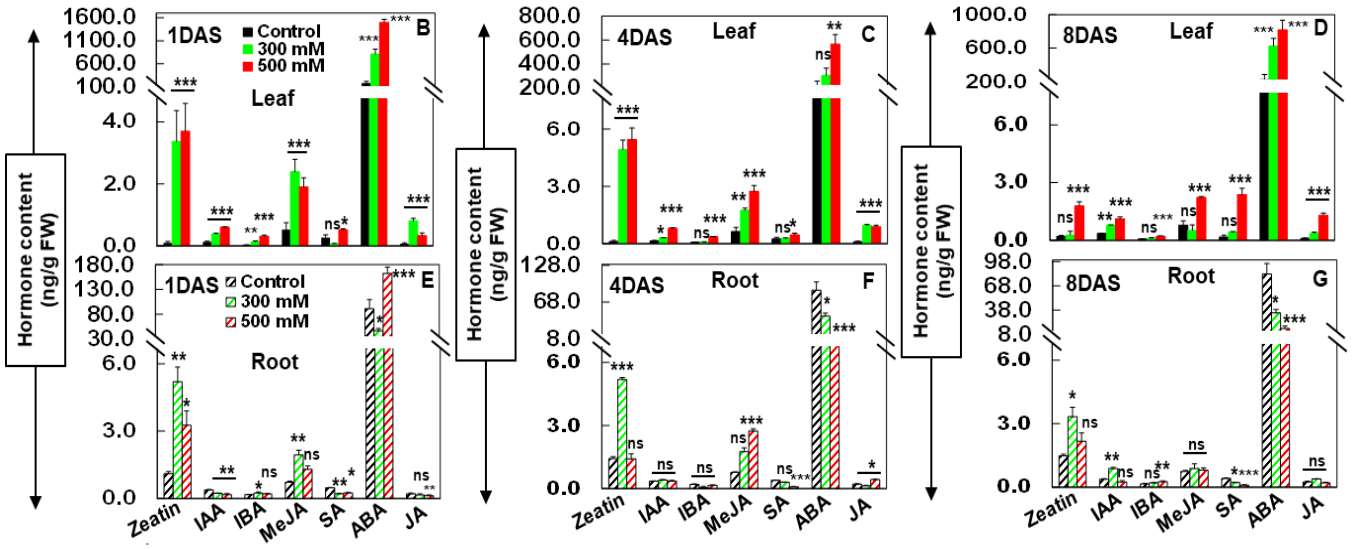
Hormone content (ng/g FW)
1DAS
Control
300 mM
500 mM
Leaf
B
Root
E
4DAS
Leaf
C
Root
F
8DAS
Leaf
D
Root
G
Zeatin
IAA
IBA
MeJA
SA
ABA
JA

Figure 2. Hierarchical cluster analysis and heat map of hormone-hormone correlation matrix in *P. pinnata* under different NaCl treatments.

Each correlation value (based on Pearson correlation coefficient) corresponds to average of six biological replicates. HAC analysis performed among the hormones at each individual time points (A and D) 1DAS, (B and E) 4DAS, (C and F) 8DAS in leaves of 300 and 500 mM NaCl treated plants. The colour key and histogram show degree of correlation.

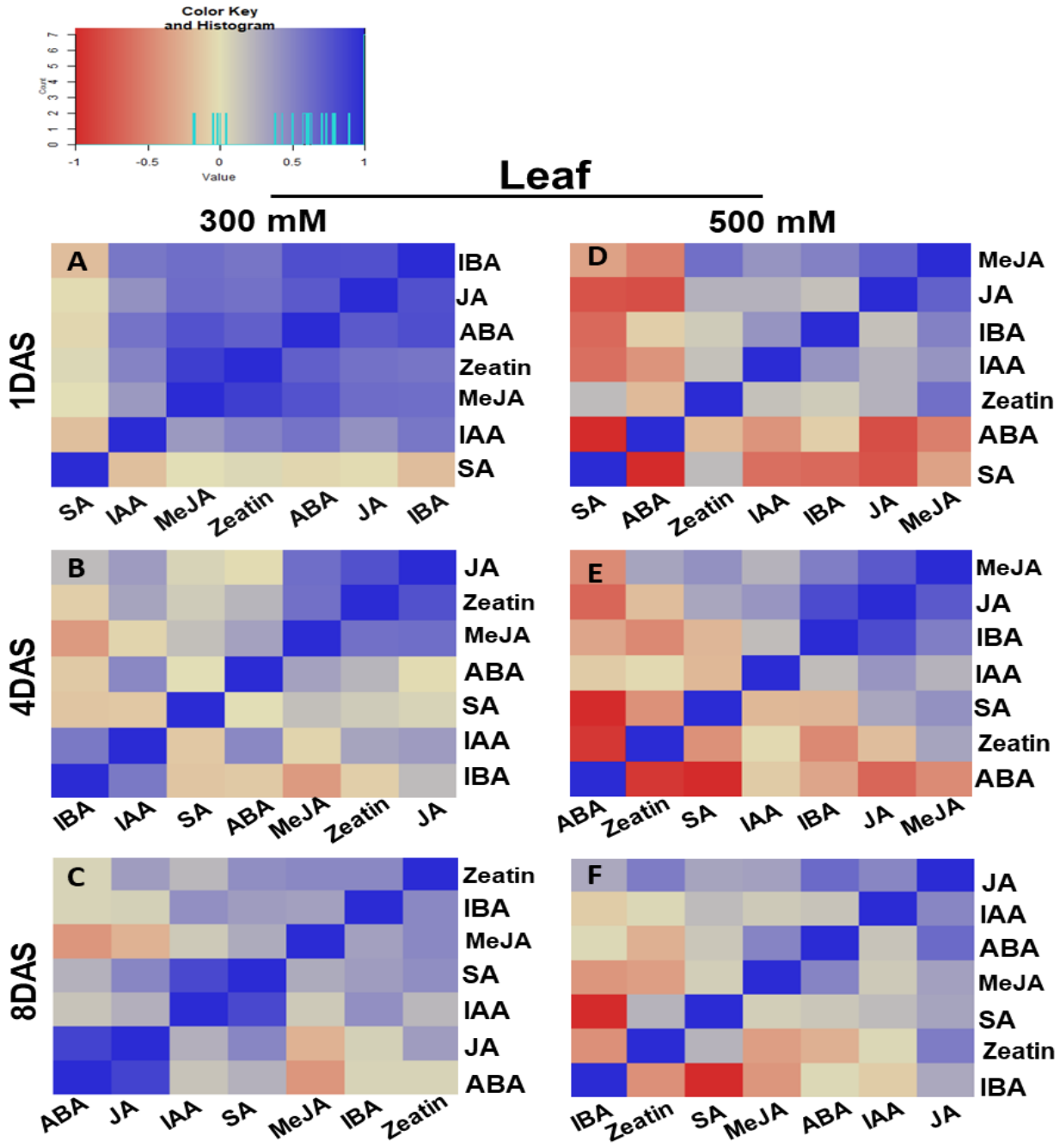
Color Key and Histogram
Count
Value
Leaf
300 mM
500 mM
1DAS
4DAS
8DAS
A
B
C
D
E
F
IBA
JA
ABA
Zeatin
MeJA
IAA
SA

Figure 2. Hierarchical cluster analysis and heat map of hormone-hormone correlation matrix in *P. pinnata* under different NaCl treatments.

Each correlation value (based on Pearson correlation coefficient) corresponds to average of six biological replicates. HAC analysis performed among the hormones at each individual time points (G and J) 1DAS, (H and K) 4DAS, (I and L) 8DAS in roots of 300 and 500 mM NaCl treated plants. The colour key and histogram show degree of correlation.

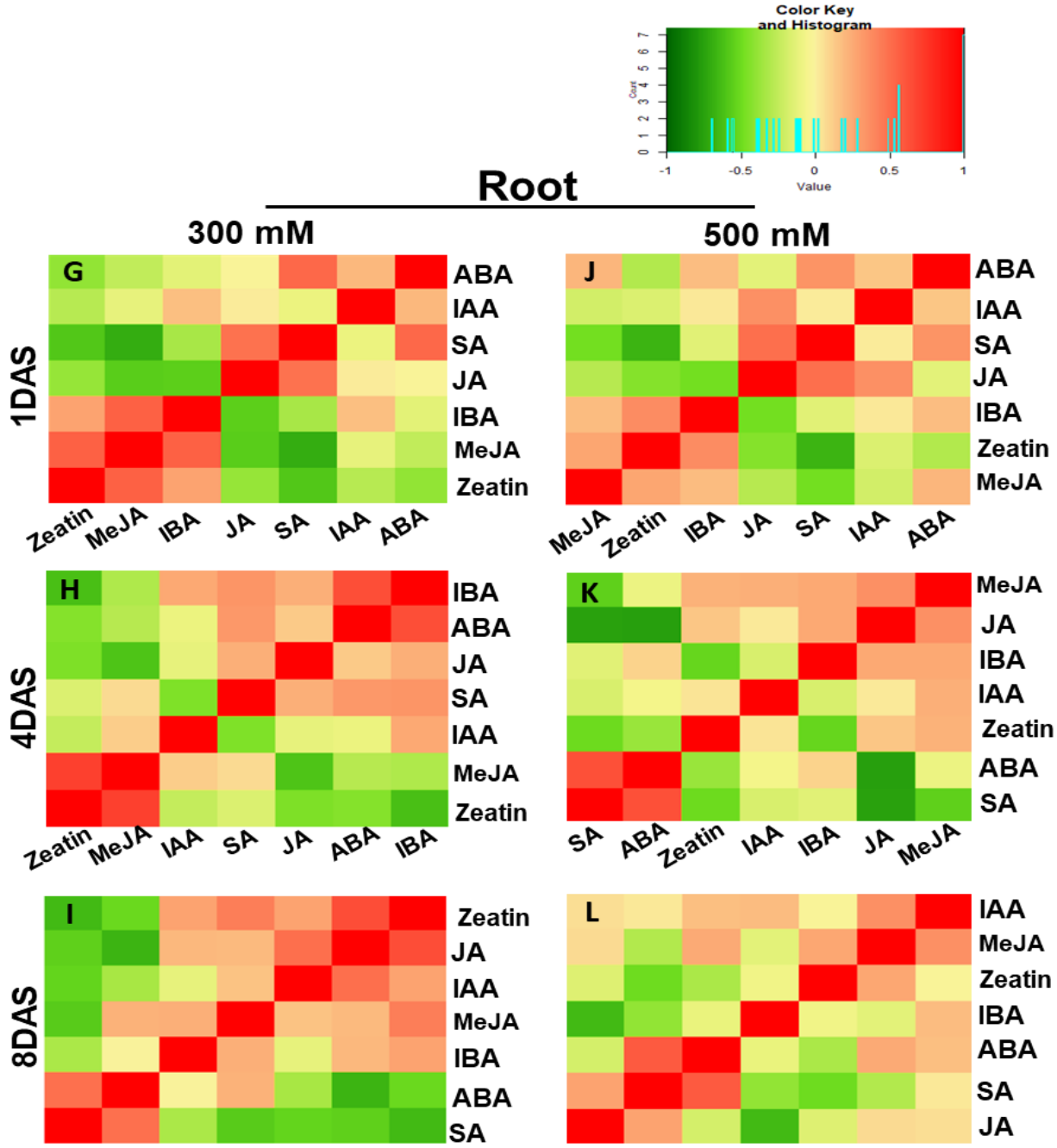
Color Key and Histogram
Count
Value
Root
300 mM
500 mM
1DAS
4DAS
8DAS
G
H
I
J
K
L
ABA
IAA
SA
JA
IBA
Zeatin
MeJA

were increased marginally in related to glycerol pathway, organic acid synthesis, amino acid metabolism and GABA shunt in leaves of treated plants across all-time points. In response to salt stress, roots accumulated a set of primary metabolites related to various metabolic pathways such as amino acid metabolism, carbohydrate metabolism, amino acid metabolism, polyol and fatty acid metabolism (Figure 5). Additionally, roots of salt treated plants also accumulated various metabolites related to cell-wall carbohydrates, carbohydrate alcohol, polyol, amino acid and fatty acid metabolism, which includes Gal, mannitol, NAG, myristate, laurate, palimitate, phytol and methyl-succinate showed significant increase in 300 and 500 mM NaCl treated plants at 1, 4 and 8DAS. Significantly, similar to leaves, mannitol levels showed significant up-regulation by ~12 fold in roots of 300 and 500 mM NaCl treated plants at 1, 4 and 8DAS. In addition, Pongamia leaves accumulated several metabolites related to Leu, glycerol, threonate and benzoate in roots of 300 and 500 mM NaCl treated plants at 8DAS. Several other metabolites also increased marginally relating to fatty acid, organic acid synthesis, amino acid metabolism and GABA shunt in leaves of treated plants across all-time points.

Correlation based clustering among metabolites in leave and roots P. pinnata under salt stress

In order to explore the relationship among the metabolites in Pongamia subjected to salt stress, hierarchical cluster analysis was performed on a total 60,492 elements of two different tissues leaf (30,246) and root (30,246) which include two different treatments 300 mM NaCl (15,123), 500 mM NaCl (15,123) and three time points 1, 4 and 8DAS (71 X 71 metabolite; 5041) (Figure 4 and 6). Correlation analysis was performed with Pearson correlation coefficients for each metabolite pair (Moing et al., 2011; Sánchez et al., 2012; Lombardo et al., 2011). The correlation values were clustered into six groups based on treatment time e.g. leaves of 300 mM NaCl

Figure 3. Heat map of metabolite changes in leaves of *P. pinnata* under salt stress.

Log_2 ratios of the relative fold change values (1 to 12) of each metabolite is represented in the form of a single horizontal row portioned with six columns of two salt treatments (300 and 500 mM NaCl) and three different time points (1, 4 and 8DAS) respectively. Each metabolite value is an average of six biological replicates represented with different colour codes red or blue according to the scale bar. The colour scale indicates degree of correlation.

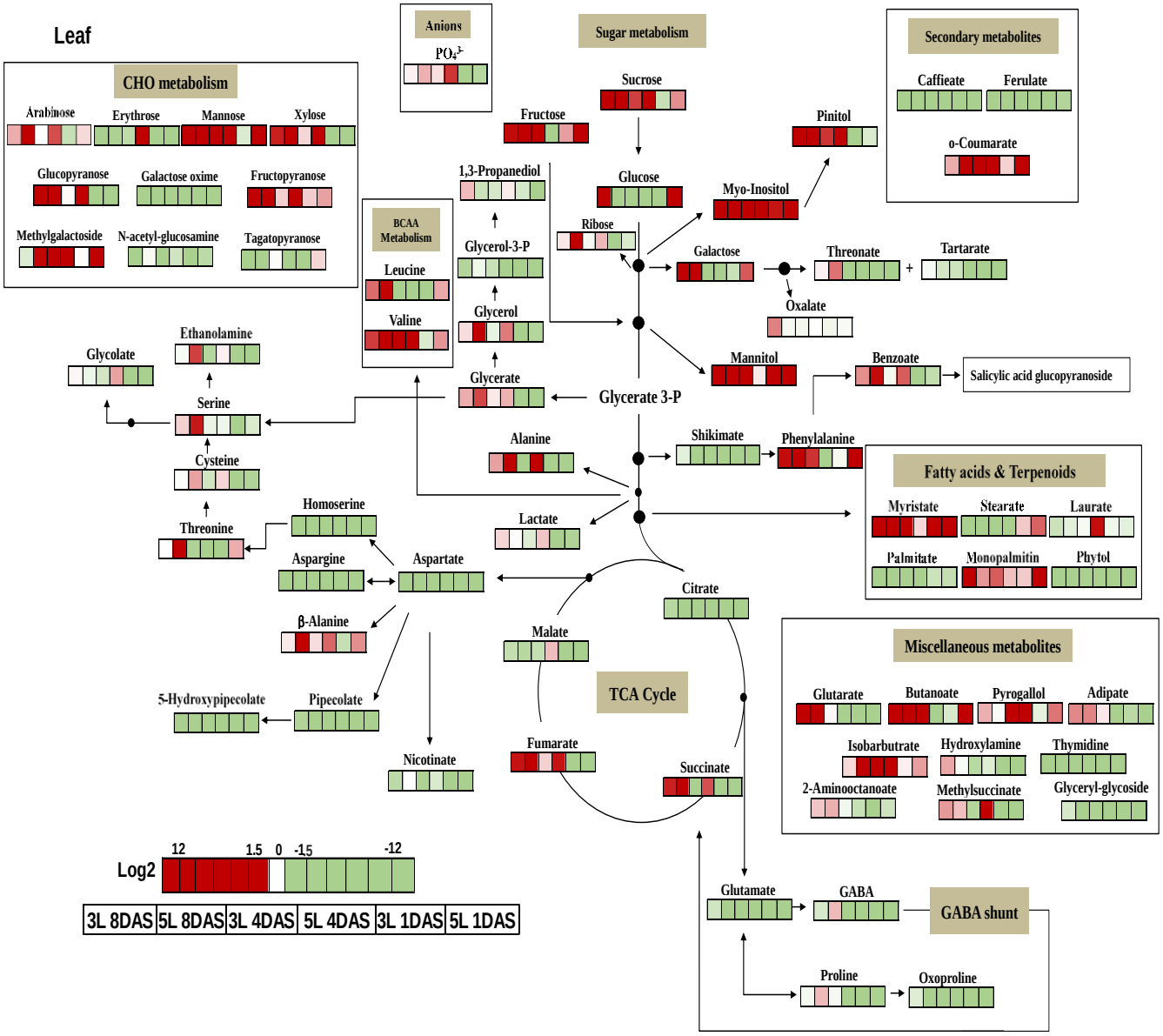
Leaf
CHO metabolism
Arabinose
Erythrose
Mannose
Xylose
Glucopyranose
Galactose oxime
Fructopyranose
Methylgalactoside
N-acetyl-glucosamine
Tagatopyranose
Anions
PO_4^{3-}
Sugar metabolism
Sucrose
Fructose
Glucose
Ribose
Secondary metabolites
Caffieate
Ferulate
o-Coumarate
Pinitol
Myo-Inositol
Galactose
Threonate
Tartarate
Oxalate
BCAA Metabolism
Leucine
Valine
1,3-Propanediol
Glycerol-3-P
Glycerol
Glycerate
Glycerate 3-P
Mannitol
Benzoate
Salicylic acid glucopyranoside
Ethanolamine
Glycolate
Serine
Cysteine
Threonine
Homoserine
Alanine
Shikimate
Phenylalanine
Fatty acids & Terpenoids
Myristate
Stearate
Laurate
Palmitate
Monopalmitin
Phytol
Lactate
Aspargine
Aspartate
β-Alanine
5-Hydroxypipecolate
Pipecolate
Nicotinate
Citrate
Malate
TCA Cycle
Fumarate
Succinate
Miscellaneous metabolites
Glutarate
Butanoate
Pyrogallol
Adipate
Isobarbutrate
Hydroxylamine
Thymidine
2-Aminooctanoate
Methylsuccinate
Glyceryl-glycoside
Log2
12
1.5
0
-1.5
-12
3L 8DAS
5L 8DAS
3L 4DAS
5L 4DAS
3L 1DAS
5L 1DAS
Glutamate
GABA
GABA shunt
Proline
Oxoproline

S.No		Control	1DAS				4DAS				8DAS			
			300 mM NaCl	P value	500 mM NaCl	P value	300 mM NaCl	P value	500 mM NaCl	P value	300 mM NaCl	P Value	500 mM NaCl	P value
	Amino acids													
1	Alanine	0.16 ± 0.0	0.00 ± 0.0	***	0.06 ± 0.0	***	0.06 ± 0.0	**	0.75 ± 0.1	***	0.23 ± 0.1	ns	1.99 ± 0.0	***
2	Valine	0.04 ± 0.0	0.03 ± 0.0	ns	0.06 ± 0.0	ns	0.13 ± 0.0	***	0.28 ± 0.1	**	0.09 ± 0.1	ns	0.64 ± 0.0	**
3	Cysteine	1.80 ± 0.3	0.67 ± 0.3	***	0.96 ± 0.2	***	1.24 ± 0.5	*	2.14 ± 0.8	ns	1.75 ± 0.3	ns	2.64 ± 0.3	*
4	Serine	1.61 ± 0.3	0.66 ± 0.2	***	1.19 ± 0.3	*	1.37 ± 0.6	ns	1.42 ± 0.5	ns	1.95 ± 0.4	ns	4.15 ± 0.3	**
5	Leucine	0.01 ± 0.0	0.00 ± 0.0	***	0.02 ± 0.0	ns	0.00 ± 0.0	***	0.00 ± 0.0	***	0.02 ± 0.0	ns	0.03 ± 0.0	***
6	Threonine	0.02 ± 0.0	0.00 ± 0.0	***	0.03 ± 0.0	ns	0.01 ± 0.0	***	0.00 ± 0.0	***	0.02 ± 0.0	ns	0.07 ± 0.0	ns
7	Aspartate	0.74 ± 0.2	0.03 ± 0.0	***	0.04 ± 0.0	***	0.15 ± 0.0	***	0.00 ± 0.0	***	0.31 ± 0.0	**	0.10 ± 0.0	***
8	Aspargine	1.75 ± 0.4	0.00 ± 0.0	***	0.00 ± 0.0	***	0.00 ± 0.0	***	0.00 ± 0.0	***	0.20 ± 0.0	***	0.20 ± 0.0	***
9	Proline	18.8 ± 1.2	5.38 ± 1.7	***	9.68 ± 1.2	***	17.4 ± 1.5	ns	5.24 ± 1.5	***	17.2 ± 1.5	ns	24.9 ± 1.2	*
10	Glutamate	4.49 ± 1.3	0.84 ± 0.3	***	1.52 ± 0.3	***	1.03 ± 0.3	***	0.00 ± 0.0	***	0.39 ± 0.7	*	1.32 ± 0.0	***
11	Homoserine	0.10 ± 0.0	0.00 ± 0.0	***	0.00 ± 0.0	***	0.00 ± 0.0	***	0.00 ± 0.0	***	0.01 ± 0.0	***	0.02 ± 0.0	***
12	β-Alanine	0.01 ± 0.0	0.01 ± 0.0	ns	0.01 ± 0.0	*	0.01 ± 0.0	ns	0.02 ± 0.0	*	0.01 ± 0.0	ns	0.15 ± 0.0	*
13	Oxoproline	3.99 ± 1.1	0.96 ± 0.2	***	1.52 ± 0.6	***	1.20 ± 0.5	***	0.00 ± 0.0	***	3.09 ± 0.7	ns	1.64 ± 0.3	***
14	Phenylalanine	0.10 ± 0.0	0.09 ± 0.0	ns	0.70 ± 0.0	***	0.24 ± 0.0	***	0.00 ± 0.0	***	0.28 ± 0.0	***	2.78 ± 0.3	***
15	GABA	3.61 ± 0.9	0.97 ± 0.3	***	1.63 ± 0.3	***	1.78 ± 0.4	**	1.06 ± 0.3	***	2.63 ± 0.4	*	4.81 ± 0.9	ns
	Sugars													
16	Erythrose	0.27 ± 0.1	0.12 ± 0.1	*	0.07 ± 0.0	**	0.16 ± 0.0	ns	0.99 ± 0.2	***	0.12 ± 0.0	*	0.14 ± 0.0	*
17	Xylose	0.02 ± 0.0	0.00 ± 0.0	*	0.01 ± 0.0	*	0.03 ± 0.0	ns	0.08 ± 0.0	***	0.06 ± 0.0	**	0.09 ± 0.0	***
18	Ribose	0.59 ± 0.1	0.29 ± 0.1	***	0.44 ± 0.1	*	0.55 ± 0.1	ns	0.79 ± 0.2	ns	0.66 ± 0.1	ns	1.99 ± 0.1	***
19	Fructose	0.17 ± 0.0	0.25 ± 0.0	ns	3.57 ± 0.2	***	0.88 ± 0.1	***	0.00 ± 0.0	***	0.46 ± 0.1	***	2.45 ± 0.1	***
20	Galactose	0.05 ± 0.0	0.03 ± 0.0	ns	0.09 ± 0.0	*	0.00 ± 0.0	***	0.00 ± 0.0	***	0.23 ± 0.0	***	2.09 ± 0.3	***
21	Mannose	0.10 ± 0.0	0.07 ± 0.0	*	0.93 ± 0.3	***	0.65 ± 0.3	**	1.54 ± 0.3	***	0.56 ± 0.1	***	1.53 ± 0.0	***
22	Glucose	0.04 ± 0.0	0.02 ± 0.0	***	0.17 ± 0.0	***	0.02 ± 0.0	***	0.00 ± 0.0	***	0.43 ± 0.0	**	0.00 ± 0.0	***
23	Arabinose	0.07 ± 0.0	0.05 ± 0.0	*	0.08 ± 0.0	*	0.07 ± 0.0	ns	0.15 ± 0.0	*	0.10 ± 0.0	ns	1.08 ± 0.1	*
24	Sucrose	6.79 ± 1.8	4.35 ± 1.0	**	10.8 ± 1.7	***	14.9 ± 2.4	***	25.3 ± 3.3	***	20.6 ± 3.5	***	33.4 ± 1.8	**
25	Fructopyronose	0.00 ± 0.0	0.00 ± 0.0	ns	0.00 ± 0.0	ns	0.00 ± 0.0	ns	0.59 ± 0.1	***	0.31 ± 0.1	***	0.04 ± 0.0	***
26	Glucopyranose	0.07 ± 0.0	0.03 ± 0.0	*	0.03 ± 0.0	*	0.07 ± 0.0	ns	1.31 ± 0.1	**	1.09 ± 0.2	**	1.58 ± 0.4	***
27	Tagatopyranose	0.02 ± 0.0	0.00 ± 0.0	***	0.02 ± 0.0	ns	0.02 ± 0.0	ns	0.00 ± 0.0	***	0.00 ± 0.0	***	0.00 ± 0.0	***
	Organic acids													
28	Lactate	0.26 ± 0.1	0.11 ± 0.0	***	0.14 ± 0.0	***	0.20 ± 0.0	*	0.33 ± 0.1	ns	0.30 ± 0.1	ns	0.2 6 ± 0.1	ns
29	Threonate	0.44 ± 0.1	0.06 ± 0.0	***	0.07 ± 0.0	***	0.17 ± 0.1	***	0.00 ± 0.0	***	0.47 ± 0.0	ns	0.78 ± 0.1	**
30	Glycolate	0.13 ± 0.0	0.00 ± 0.0	***	0.00 ± 0.0	***	0.09 ± 0.0	*	0.19 ± 0.0	***	0.13 ± 0.0	ns	0.11 ± 0.0	ns
31	Oxalate	0.17 ± 0.0	0.15 ± 0.0	ns	0.16 ± 0.0	ns	0.16 ± 0.0	ns	0.17 ± 0.0	ns	0.29 ± 0.1	ns	0.16 ± 0.0	ns
32	Nicotinate	0.28 ± 0.0	0.07 ± 0.0	***	0.10 ± 0.0	***	0.15 ± 0.0	***	0.21 ± 0.0	ns	0.16 ± 0.0	***	0.28 ± 0.1	ns
33	Succinate	0.67 ± 0.1	0.23 ± 0.0	***	0.27 ± 0.0	***	0.32 ± 0.0	***	1.37 ± 0.3	***	1.66 ± 0.2	***	6.26 ± 1.0	***
34	Methylsuccinate	0.06 ± 0.0	0.02 ± 0.0	***	0.02 ± 0.0	***	0.03 ± 0.0	**	0.27 ± 0.0	**	0.08 ± 0.0	ns	0.07 ± 0.0	ns
35	Glycerate	0.13 ± 0.0	0.00 ± 0.0	***	0.00 ± 0.0	***	0.14 ± 0.0	ns	0.18 ± 0.0	*	0.18 ± 0.0	ns	0.28 ± 0.0	***
36	Fumarate	0.06 ± 0.0	0.01 ± 0.0	***	0.02 ± 0.0	***	0.07 ± 0.0	ns	0.15 ± 0.0	***	0.15 ± 0.0	***	0.19 ± 0.0	***
37	Butanoate	0.00 ± 0.0	0.00 ± 0.0	ns	0.03 ± 0.0	*	0.02 ± 0.0	ns	0.00 ± 0.0	ns	0.03 ± 0.0	*	0.17 ± 0.0	*
38	Malate	28.0 ± 4.4	1.49 ± 0.3	***	3.94 ± 0.9	***	17.5 ± 3.5	***	36.8 ± 3.0	***	17.4 ± 3.9	***	15.8 ± 4.4	***
39	2-Aminooctanoate	58.7 ± 4.6	27.8 ± 4.7	***	39.2 ± 4.5	***	52.3 ± 5.4	ns	37.6 ± 3.2	***	74.6 ±. 6.2	*	81.5 ± 9.1	***
40	Glutarate	0.11 ± 0.0	0.03 ± 0.0	***	0.05 ± 0.0	***	0.11 ± 0.0	ns	0.00 ± 0.0	***	0.36 ± 0.1	***	0.67 ± 0.2	***
41	Isobarbiturate	0.00 ± 0.0	0.00 ± 0.0	ns	0.00 ± 0.0	ns	0.00 ± 0.0	ns	0.00 ± 0.0	ns	0.00 ± 0.0	ns	0.00 ± 0.0	ns
42	Tartarate	28.0 ± 5.9	9.20 ± 1.3	***	7.31 ± 0.9	***	18.8 ± 4.4	**	0.00 ± 0.0	***	26.5 ± 5.9	ns	19.8 ± 5.9	*
43	Citrate	6.10 ± 1.5	0.17 ± 0.0	***	0.02 ± 0.0	***	0.25 ± 0.0	***	0.38 ± 0.0	***	3.46 ± 0.8	*	2.07 ± 0.2	***
44	Benzoate	0.02 ± 0.0	0.01 ± 0.0	***	0.01 ± 0.0	***	0.02 ± 0.0	ns	0.04 ± 0.0	**	0.03 ± 0.0	ns	0.06 ± 0.0	*
45	o-Coumarate	0.00 ± 0.0	0.00 ± 0.0	ns	0.35 ± 0.0	**	0.30 ± 0.0	**	0.02 ± 0.0	**	0.00 ± 0.0	ns	0.00 ± 0.0	ns
46	Ferulate	0.03 ± 0.0	0.01 ± 0.0	*	0.02 ± 0.0	*	0.00 ± 0.0	***	0.00 ± 0.0	***	0.01± 0.0	**	0.00 ± 0.0	***
47	Caffeate	0.56 ± 0.1	0.00 ± 0.0	***	0.00 ± 0.0	***	0.02 ± 0.0	***	0.00 ± 0.0	***	0.07 ± 0.0	***	0.05 ± 0.0	***
48	Pipecolate	5.41 ± 1.0	0.14 ± 0.0	***	0.25 ± 0.0	***	0.88 ± 0.2	***	0.00 ± 0.0	***	2.91 ± 0.5	**	2.11 ± 0.7	***
49	5-Hydroxypipecolate	0.22 ± 0.0	0.00 ± 0.0	***	0.00 ± 0.0	***	0.00 ± 0.0	***	0.00 ± 0.0	***	0.06 ± 0.0	***	0.00 ± 0.0	***
	Polyols													
50	Glycerol	1.04 ± 0.3	0.41 ± 0.1	***	0.57 ± 0.1	***	0.86 ± 0.1	ns	1.79 ± 0.3	***	1.20 ± 0.2	ns	3.39 ± 0.9	**
51	Pyrogallol	0.01 ± 0.0	0.01 ± 0.0	ns	0.03 ± 0.0	ns	0.07 ± 0.0	*	0.23 ± 0.0	***	0.02 ± 0.0	ns	0.01 ± 0.0	ns
52	Shikimate	0.54 ± 0.1	0.15 ± 0.0	***	0.13 ± 0.0	***	0.25 ± 0.0	***	0.15 ± 0.0	***	0.44 ± 0.1	ns	0.22 ± 0.0	***
53	Pinitol	7.54 ± 0.0	3.61 ± 0.0	***	5.64 ± 0.0	**	17.3 ± 0.0	***	30.9 ± 0.0	***	34.1 ± 0.0	***	31.4 ± 0.0	***
54	Mannitol	0.00 ± 0.0	0.19 ± 0.0	*	0.33 ± 0.0	***	0.51 ± 0.1	***	0.00 ± 0.0	ns	0.16 ± 0.0	***	0.32 ± 0.0	***
55	Myo-Inositol	1.10 ± 0.2	2.86 ± 0.8	*	5.29 ± 1.3	***	7.77 ± 1.9	***	20.8 ± 4.9	***	7.59 ± 1.2	***	15.7 ± 2.4	***
	Fatty acids													
56	Laurate	0.00 ± 0.0	0.00 ± 0.0	ns	0.00 ± 0.0	ns	0.00 ± 0.0	ns	0.01 ± 0.0	***	0.00 ± 0.0	ns	0.00 ± 0.0	ns
57	Adipate	0.59 ± 0.1	0.34 ± 0.1	***	0.25 ± 0.0	***	0.65 ± 0.2	ns	0.04 ± 0.0	***	0.95 ± 0.3	***	0.97 ± 0.3	***
58	Myristate	0.00 ± 0.0	0.17 ± 0.0	***	0.14 ± 0.0	**	0.13 ± 0.0	**	0.00 ± 0.0	ns	0.19 ± 0.0	***	0.30 ± 0.0	***
59	Palmitate	0.58 ± 0.1	0.39 ± 0.0	ns	0.37 ± 0.0	ns	0.18 ± 0.0	***	0.00 ± 0.0	***	0.23 ± 0.0	***	0.12 ± 0.0	***
60	Stearate	0.53 ± 0.2	0.66 ± 0.2	ns	1.00 ± 0.2	**	0.26 ± 0.0	***	0.00 ± 0.0	***	0.23 ± 0.0	**	0.13 ± 0.0	***
61	Monopalmitin	0.00 ± 0.0	0.00 ± 0.0	ns	0.00 ± 0.0	ns	0.00 ± 0.0	ns	0.00 ± 0.0	ns	0.00 ± 0.0	ns	0.00 ± 0.0	ns
	Other metabolites													
62	1,3-Propanediol	0.16 ± 0.0	0.11 ± 0.0	**	0.00 ± 0.0	***	0.11 ± 0.0	**	0.17 ± 0.0	ns	0.21 ± 0.0	*	0.11 ± 0.0	**
63	Hydroxylamine	0.09 ± 0.0	0.01 ± 0.0	***	0.01 ± 0.0	***	0.05 ± 0.0	*	0.07 ± 0.0	ns	0.13 ± 0.0	*	0.09 ± 0.0	ns
64	Ethanolamine	1.69 ± 0.4	0.48 ± 0.1	***	0.84 ± 0.2	**	0.94 ± 0.3	***	1.80 ± 0.5	ns	1.59 ± 0.3	ns	3.68 ± 0.9	*
65	Phosphate	9.15 ± 1.1	3.93 ± 0.6	***	5.14 ± 1.2	**	10.4 ± 2.2	ns	20.8 ± 2.4	***	9.75 ± 1.4	ns	12.7 ± 1.3	*
66	Glycerol-3P	0.43 ± 0.1	0.08 ± 0.0	***	0.09 ± 0.0	***	0.28 ± 0.0	*	0.02 ± 0.0	***	0.23 ± 0.0	***	0.38 ± 0.1	ns
67	Methylgalactoside	0.13 ± 0.0	0.13 ± 0.0	ns	0.40 ± 0.0	**	0.71 ± 0.1	***	1.09 ± 0.6	***	0.10 ± 0.0	ns	0.35 ± 0.0	ns
68	N-Acetyl-glucosamine	0.05 ± 0.0	0.00 ± 0.0	***	0.03 ± 0.0	**	0.00 ± 0.0	***	0.04 ± 0.0	ns	0.01 ± 0.0	***	0.05 ± 0.0	ns
69	Phytol	0.57 ± 0.2	0.05 ± 0.0	***	0.05 ± 0.0	***	0.07 ± 0.0	**	0.13 ± 0.0	**	0.16 ± 0.0	**	0.04 ± 0.0	***
70	Glyceryl-glycoside	0.29 ± 0.0	0.04 ± 0.0	***	0.05 ± 0.0	***	0.15 ± 0.0	***	0.02 ± 0.0	***	0.21 ± 0.0	*	0.14 ± 0.0	***
71	Thymidine	0.03 ± 0.0	0.00 ± 0.0	*	0.00 ± 0.0	*	0.00 ± 0.0	*	0.00 ± 0.0	*	0.00 ± 0.0	*	0.00 ± 0.0	*

Table 1. Relative concentration and fold changes of major metabolites in leaves of *P. pinnata.*

S.No	1DAS	Abbreviation	4DAS	Abbreviation	8DAS	Abbreviation
1	Glycerol	**Gro**	Citrate	**CA**	Myo-Inositol	**MI**
2	Proline	**Pro**	Galactose	**Gal**	Glutarate	**Glta**
3	2-Aminooctanoate	**Asu**	N-Acetyl-glucosamine	**GlcNAc**	Succinate	**SA**
4	Fumarate	**FA**	Aspartate	**Asp**	Phenylalanine	**Phe**
5	Malate	**MA**	Oxoproline	**Oxopro**	Mannitol	**MT**
6	Asparagine	**Asn**	Caffeate	**CAA**	Fructopyranose	**pFru**
7	Ethanolamine	**Eta**	Glucose	**Glc**	Pinitol	**PI**
8	Aspartate	**Asp**	Leucine	**Leu**	Sucrose	**Suc**
9	5-Hydroxypipecolate	**5HPip**	Nicotinate	**NA**	Galactose	**Gal**
10	4-Aminobutanoate	**GABA**	Alanine	**Ala**	Fumarate	**FA**
11	Glutamate	**Glu**	5-Hydroxypipecolate	**5HPip**	Butanoate	**Bta**
12	Phosphate	**Pi**	Asparagine	**Asn**	Mannose	**Man**
13	Pipecolate	**Pip**	Glutamate	**Glu**	Myristate	**MytA**
14	Alanine	**Ala**	Pipecolate	**Pip**	Glucopyranose	**pGlc**
15	Glycerate	**Gri**	Homoserine	**Hse**	Fructose	**Fru**
16	Glycolate	**GA**	4-Aminobutanoate	**GABA**	Xylose	**Xyl**
17	Nicotinate	**NA**	Malate	**MA**	Glucose	**Glc**
18	Oxoproline	**Oxopro**	Palmitate	**PA**	2-Aminooctanoate	**Asu**
19	Citrate	**CA**	Glyceryl-glycoside	**Grl-g**	1,3-Propanediol	**Pdo**
20	N-Acetyl-glucosamine	**GlcNAc**	Hydroxylamine	**HA**	Adipate	**AA**
21	Cysteine	**Cys**	Shikimate	**ShiA**	Oxalate	**Oxa**
22	Tagatopyranose	**pTag**	Fumarate	**FA**	Benzoate	**BA**
23	Methylsuccinate	**Met-SA**	Ethanolamine	**Eta**	Leucine	**Leu**
24	Caffeate	**CAA**	Threonine	**Thr**	Glycerate	**Gri**
25	Glycerol-3-phosphate	**G3p**	Glycerol-3-phosphate	**G3p**	Hydroxylamine	**HA**
26	Serine	**Ser**	Methylsuccinate	**Met-SA**	o-Coumarate	**oC**
27	Hydroxylamine	**HA**	Phytol	**Phytol**	Lactate	**LA**
28	Glyceryl-glycoside	**Grl-g**	1,3-Propanediol	**Pdo**	Arabinose	**Ara**
29	Threonine	**Thr**	Threonate	**ThA**	Serine	**Ser**
30	Homoserine	**Hse**	Thymidine	**Thy**	Monopalmitin	**MP**
31	Tartarate	**TA**	Stearate	**StA**	Glycolate	**GA**
32	Threonate	**ThA**	Succinate	**SA**	Threonate	**ThA**
33	Succinate	**SA**	Tartarate	**TA**	Valine	**Val**
34	Benzoate	**BA**	Cysteine	**Cys**	Alanine	**Ala**
35	Ribose	**Rib**	Glycerol	**Gro**	Methylsuccinate	**Met-SA**
36	Pinitol	**PI**	2-Aminooctanoate	**Asu**	Glycerol	**Gro**
37	Glutarate	**Glta**	Oxalate	**Oxa**	Ribose	**Rib**
38	Adipate	**AA**	Glycolate	**GA**	Pyrogallol	**Pyr**
39	Leucine	**Leu**	Lactate	**LA**	Isobarbiturate	**IBua**
40	Glucose	**Glc**	Erythrose	**Ery**	Phosphate	**Pi**
41	Arabinose	**Ara**	Serine	**Ser**	β-Alanine	**Ba**
42	Lactate	**LA**	Ribose	**Rib**	Oxoproline	**Oxopro**
43	Shikimate	**ShiA**	Proline	**Pro**	Glutamate	**Glu**
44	Phytol	**Phytol**	Benzoate	**BA**	Laurate	**La**
45	1,3-Propanediol	**Pdo**	Glucopyranose	**pGlc**	Methylgalactoside	**Met-Gal**
46	Xylose	**Xyl**	Arabinose	**Ara**	Tartarate	**TA**
47	Glucopyranose	**pGlc**	Tagatopyranose	**pTag**	Threonine	**Thr**
48	Thymidine	**Thy**	Glutarate	**Glta**	Cysteine	**Cys**
49	Ferulate	**Fa**	Adipate	**AA**	Ethanolamine	**Eta**
50	Sucrose	**Suc**	β-Alanine	**Ba**	Shikimate	**ShiA**
51	Mannose	**Man**	Fumarate	**Fa**	4-Aminobutanoate	**GABA**
52	Erythrose	**Ery**	Butanoate	**Bta**	Pipecolate	**Pip**
53	Galactose	**Gal**	Xylose	**Xyl**	Malate	**MA**
54	β-Alanine	**Ba**	Phosphate	**Pi**	Thymidine	**Thy**
55	Valine	**Val**	Laurate	**La**	Glyceryl-glycoside	**Grl-g**
56	Pyrogallol	**Pyr**	Glycerate	**Gri**	Proline	**Pro**
57	Oxalate	**Oxa**	Fructopyranose	**pFru**	Glycerol-3-phosphate	**G3p**
58	Butanoate	**Bta**	Monopalmitin	**MP**	Aspartate	**Asp**
59	Laurate	**La**	o-Coumarate	**oC**	Nicotinate	**NA**
60	Palmitate	**PA**	Pyrogallol	**Pyr**	Citrate	**CA**
61	Phenylalanine	**Phe**	Myristate	**MytA**	Erythrose	**Ery**
62	Methyl-galactoside	**Met-Gal**	Mannose	**Man**	5-Hydroxypipecolate	**5HPip**
63	Isobarbiturate	**IBua**	Pinitol	**PI**	Caffeate	**CAA**
64	Fructose	**Fru**	Myo-Inositol	**MI**	Tagatopyranose	**pTag**
65	Monopalmitin	**MP**	Sucrose	**Suc**	Asparagine	**Asn**
66	Fructopyranose	**pFru**	Isobarbiturate	**IBua**	N-Acetyl-glucosamine	**GlcNAc**
67	o-Coumarate	**oC**	Fructose	**Fru**	Phytol	**Phytol**
68	Stearate	**StA**	Phenylalanine	**Phe**	Ferulate	**Fa**
69	Myristate	**MytA**	Valine	**Val**	Stearate	**StA**
70	Myo-Inositol	**MI**	Methyl-galactoside	**Met-Gal**	Palmitate	**PA**
71	Mannitol	**MT**	Mannitol	**MT**	Homoserine	**Hse**

Table 2. List of all 71 metabolites in 300 mM NaCl treated leaves of *P. pinnata* at 1, 4 and 8DAS and their abbreviations.

S.No	1DAS	Abbreviation	4DAS	Abbreviation	8DAS	Abbreviation
1	Asparagine	**Asn**	Threonine	**Thr**	Ethanolamine	**Eta**
2	Malate	**MA**	Pipecolate	**Pip**	Valine	**Val**
3	Proline	**Pro**	Tartarate	**TA**	Glycerol	**Gro**
4	Tartarate	**TA**	Homoserine	**Hse**	Sucrose	**Suc**
5	Pipecolate	**Pip**	Threonate	**ThA**	Benzoate	**BA**
6	Homoserine	**Hse**	Palmitate	**PA**	Proline	**Pro**
7	Threonate	**ThA**	Stearate	**StA**	Threonate	**ThA**
8	Glycerate	**Gri**	Glyceryl-glycoside	**Grl-g**	Phosphate	**Pi**
9	Glycolate	**GA**	Glycerol-3-phosphate	**G3p**	Xylose	**Xyl**
10	Nicotinate	**NA**	5-HydroxyPipecolate	**5HPip**	Ribose	**Rib**
11	Alanine	**Ala**	Adipate	**AA**	Fructose	**Fru**
12	Glycerol-3-phosphate	**G3p**	Proline	**Pro**	Arabinose	**Ara**
13	1,3-Propanediol	**Pdo**	GABA	**GABA**	2-Aminooctanoate	**Asu**
14	Hydroxylamine	**HA**	2-Aminooctanoate	**Asu**	Alanine	**Ala**
15	Glyceryl-glycoside	**Grl-g**	Aspartate	**Asp**	Galactose	**Gal**
16	2-Aminooctanoate	**Asu**	Oxoproline	**Oxopro**	Myristate	**MytA**
17	Fumarate	**FA**	Phenylalanine	**Phe**	Cysteine	**Cys**
18	GABA	**GABA**	Glutarate	**Glta**	β-Alanine	**Ba**
19	5-Hydroxypipecolate	**5HPip**	Glucose	**Glc**	Threonine	**Thr**
20	Aspartate	**Asp**	Glutamate	**Glu**	Butanoate	**Bta**
21	Ethanolamine	**Eta**	Asparagine	**Asn**	GABA	**GABA**
22	Cysteine	**Cys**	Fructose	**Fru**	Monopalmitin	**MP**
23	Adipate	**AA**	Leucine	**Leu**	Glutarate	**Glta**
24	Glycerol	**Gro**	Citrate	**CA**	Phenylalanine	**Phe**
25	Glutamate	**Glu**	Caffeate	**CAA**	o-Coumarate	**oC**
26	Citrate	**CA**	Galactose	**Gal**	Myo-Inositol	**MI**
27	Caffeate	**CAA**	Tagatopyranose	**pTag**	Mannose	**Man**
28	Oxoproline	**Oxopro**	Shikimate	**ShiA**	Pinitol	**PI**
29	Methylsuccinate	**Met-SA**	Ferulate	**Fa**	Fumarate	**Fa**
30	Shikimate	**ShiA**	Phytol	**Phytol**	Leucine	**Leu**
31	Lactate	**LA**	Butanoate	**Bta**	Isobarbiturate	**IBua**
32	Phytol	**Phytol**	Thymidine	**Thy**	Fructopyranose	**pFru**
33	Erythrose	**Ery**	Hydroxylamine	**HA**	Succinate	**SA**
34	Xylose	**Xyl**	Serine	**Ser**	Mannitol	**MT**
35	Glucopyranose	**pGlc**	Nicotinate	**NA**	Serine	**Ser**
36	Serine	**Ser**	N-Acetyl-glucosamine	**GlcNAc**	Glucopyranose	**pGlc**
37	Thymidine	**Thy**	Oxalate	**Oxa**	Adipate	**AA**
38	Succinate	**SA**	1,3-Propanediol	**Pdo**	Glycerate	**Gri**
39	Benzoate	**BA**	Mannitol	**MT**	Methylsuccinate	**Met-SA**
40	Pinitol	**PI**	Ethanolamine	**Eta**	Methyl-galactoside	**Met-Gal**
41	N-Acetyl-glucosamine	**GlcNAc**	Ribose	**Rib**	Lactate	**LA**
42	Glutarate	**Glta**	Cysteine	**Cys**	Hydroxylamine	**HA**
43	Phosphate	**Pi**	Myristate	**MytA**	Glycolate	**GA**
44	Ribose	**Rib**	Lactate	**LA**	N-Acetyl-glucosamine	**GlcNAc**
45	Laurata	**La**	Glycerate	**Gri**	Nicotinate	**NA**
46	Oxalate	**Oxa**	Monopalmitin	**MP**	Oxalate	**Oxa**
47	Ferulate	**Fa**	β-Alanine	**Ba**	Laurata	**La**
48	Palmitate	**PA**	Arabinose	**Ara**	Pyrogallol	**Pyr**
49	Tagatopyranose	**pTag**	Benzoate	**BA**	Glycerol-3-phosphate	**G3p**
50	Threonine	**Thr**	Glucopyranose	**pGlc**	Erythrose	**Ery**
51	Leucine	**Leu**	Malate	**MA**	Tartarate	**TA**
52	Pyrogallol	**Pyr**	Valine	**Val**	Thymidine	**Thy**
53	Isobarbiturate	**IBua**	Methylsuccinate	**Met-SA**	Ferulate	**Fa**
54	Valine	**Val**	Erythrose	**Ery**	Shikimate	**ShiA**
55	Arabinose	**Ara**	Glycerol	**Gro**	1,3-Propanediol	**Pdo**
56	β-Alanine	**Ba**	Isobarbiturate	**IBua**	Glyceryl-glycoside	**Grl-g**
57	Fructopyranose	**pFru**	Fumarate	**FA**	Malate	**MA**
58	Butanoate	**Bta**	Pyrogallol	**Pyr**	Homoserine	**Hse**
59	Methyl-galactoside	**Met-Gal**	Glycolate	**GA**	Phytol	**Phytol**
60	Myristate	**MytA**	Xylose	**Xyl**	Citrate	**CA**
61	Fructose	**Fru**	o-Coumarate	**oC**	Oxoproline	**Oxopro**
62	Myo-Inositol	**MI**	Succinate	**SA**	Caffeate	**CAA**
63	Mannitol	**MT**	Laurata	**La**	Pipecolate	**Pip**
64	Galactose	**Gal**	Fructopyranose	**pFru**	Glutamate	**Glu**
65	Stearate	**StA**	Methyl-galactoside	**Met-Gal**	Stearate	**StA**
66	Mannose	**Man**	Alanine	**Ala**	Palmitate	**PA**
67	Glucose	**Glc**	Myo-Inositol	**MI**	Tagatopyranose	**pTag**
68	o-Coumarate	**oC**	Pinitol	**PI**	5-HydroxyPipecolate	**5HPip**
69	Sucrose	**Suc**	Phosphate	**Pi**	Aspartate	**Asp**
70	Phenylalanine	**Phe**	Sucrose	**Suc**	Asparagine	**Asn**
71	Monopalmitin	**MP**	Mannose	**Man**	Glucose	**Glc**

Table 3. List of all 71 metabolites in 500 mM NaCl treated leaves of *P. pinnata* at 1, 4 and 8DAS and their abbreviations.

Figure 4. Heat map of hierarchical clustering of metabolite-metabolite correlations in leaves of 300 and 500 mM NaCl treated *P. pinnata* under salinity stress.

Each correlation value (based on Pearson correlation coefficient) corresponds to average of six biological replicates. HAC analysis performed among the metabolite at each individual time points (A) 1DAS, (B) 4DAS and (C) 8DAS in leaves of 300 mM NaCl treated plants. (D, E and F) Detailed view of positively correlated metabolite correlations was shown in the form of table. HAC analysis performed among the metabolite at each individual time points (G) 1DAS, (H) 4DAS and (I) 8DAS in leaves of 500 mM NaCl treated plants. (J, K and L) Detailed view of positively correlated metabolite correlations was shown in the form of table. The colour key and histogram show degree of correlation.

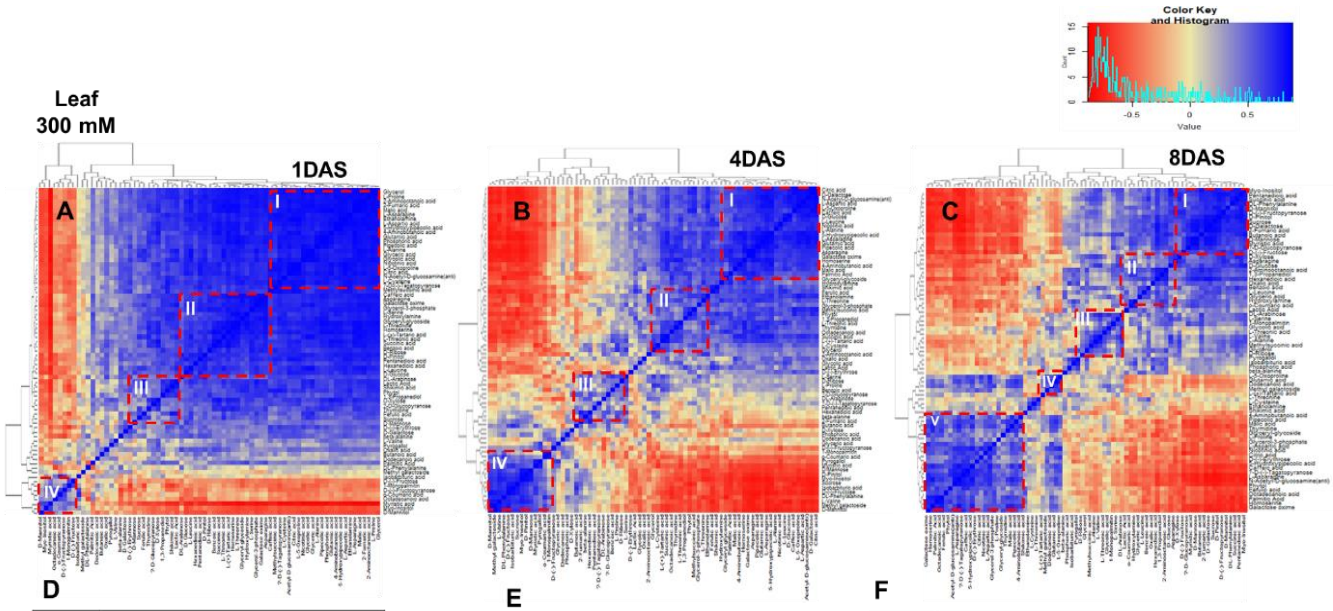

D

Group	1DAS
I	Gro, Pro, Asu, FA, MA, Asn, Eta, Asp, 5HPip, GABA, Glu, Pi, Pip, Ala, Gri, GA, NA, Oxpro, CA, GlcNAc, pTag, Cys, Met-SA, CAA
II	G3p, Ser, HA, Thr, Hse, TA, ThA, SA, BA, Rib, Pl, Glta, AA, Leu, Glc
III	LA, ShiA, Phytol, Pdo, Xyl, pGlc, Thy
IV	Fru, MP, pFru, oC, StA, MytA, Ml, MT

E

Group	4DAS
I	CA, Gal, GlcNAc, Asp, Oxpro, CAA, Glc, Leu, NA, Ala
II	5HPip, Asn, Glu, Pip
III	Met-SA, Phytol, Pdo, ThA, Thy, StA, SA, TA, Hse, GABA, MA
IV	MT, Met-Gal, Val, Phe, Fru, IBua, Suc, Ml, Pl, Man, MytA, Pyr, oC

F

Group	8DAS
I	Ml, Glta, SA, Phe, MT, pFru, Pl, Suc, Gal, FA, Ba, Man, Myta, pGlc, Fru
II	Asu, Pdo, AA, BA, Oxa, Leu, oC, HA
III	Ara, Ser, MP, Gri, ThA, Val, Ala, Met-SA, Gro, Rib
IV	Oxpro, Glu, LA, Met-Gal, TA
V	GABA, Pip, MA, G3p, Asp, NA, CA, Ery, 5HPip, CAA, pTag, Asn, GlcNAc, Phytol, Fa, StA, PA, Hse

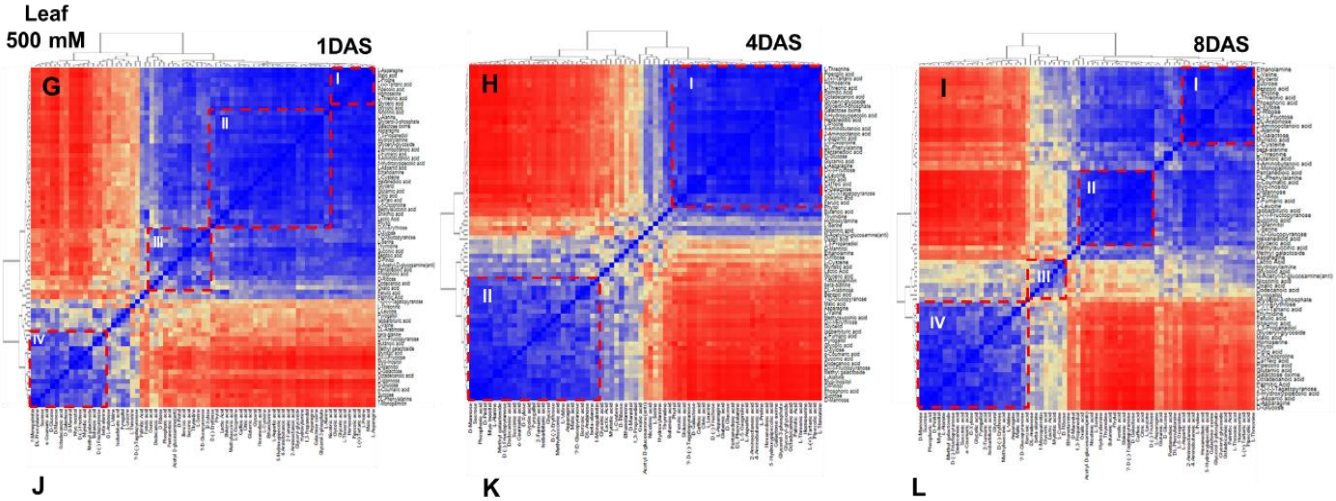

J

Group	1DAS
I	Asn, MA, Pro, TA, Pip, Hse, ThA, Gri, GA, NA
II	G3p, Pdo, HA, Grl-g, Asu, FA, GABA, 5HPip, Asp, Eta, Cys, AA, Gro, Glu, CA, CAA, Oxopro, Met-SA
III	Xyl, pGlc, Ser, Thy, SA, BA, Pl, GlcNAc, Glta, Pi
IV	Leu, Pyr, IBua, Val, Ba, pFru, Met-Gal, MytA, Fru, Ml, MT, Man, Glc, oC, Suc, Phe, MP

K

Group	4DAS
I	Thr, Pip, TA, Hse, ThA, PA, StA, Grl-g, G3p, 5HPip, AA, L-Pro, GABA, Asu, Asp, Oxopro, Phe, Glta, D-Glc, Glu, Asn, Fru, Leu, CA, CAA, Gal, pTag, ShiA, Fa, Phytol
II	Pdo, MT, Rib, Cys, LA, Gri, MP, Ba, Ara, BA, pGlc, MA, Val, Met-SA, Ery, Gro, IBua, FA, Pyr, GA, Xyl, oC, SA, La, pFru, Met-Gal, Ala, Ml, Pl, Pi, Suc, Man

L

Group	8DAS
I	Eta, Val, Gro, Suc, BA, Pro, ThA, Pi, Xyl, Rib, Fru, Ara, Asu, Ala, Gal, MytA
II	Glta, Phe, oC, Ml, Man, Pl, Fa, Leu, IBua, pFru, SA, MT, Ser, pGlc, AA, Gri
III	LA, HA, GA, GlcNAc, NA, Oxa, La, Pyr
IV	Fa, ShiA, Pdo, Grl-g, MA, Hse, Phytol, CA, Oxopro, CAA, Pip, Glu, StA, PA, pTag, 5HPip, Asp, Asn, Glc

treatment at 1DAS clustered into a group (Figure 4A and D; order of metabolite names and abbreviations were given in the Table 2), leaves of 300 mM NaCl treatment at 4DAS clustered into a group (Figure 4B and E; Table 2) and leaves of 300 mM NaCl treatment at 8DAS clustered into another group (Figure 4C and F; Table 2). In order to simplify the graphics, only strong correlations ($r \geq 0.6$) were showed separately in the tables. Similarly, leaves of 500 mM NaCl at 1DAS clustered into one group (Figure 4G and J; order of metabolite names and abbreviations were given in the Table 3), leaves of 500 mM NaCl at 4DAS clustered into one group (Fig 4H and K; Table 3) and leaves of 500 mM NaCl at 8DAS clustered into one group (Figure 4I and L; Table 3). In leaves of 300 mM NaCl treated plants, we observed high correlations within the organic acid group (e.g. CA:CAA:NA, 5HPip:Pip) and polyols (MI:MT). Although a significant correlation was not observed within the amino acid group, these levels showed strong interaction with organic acids (Asp:CA:NA:CAA, Asn:Pip:5HPip, GABA:MA) in leaves of 300 mM NaCl treated plants. Additionally, a strong positive correlation was observed between several metabolites such as fructose, myristate, mannitol and myo-inositol in leaves of 300 mM NaCl treated plants. In 500 mM NaCl treated plants, a significant correlation was observed within the amino acids group (Asp:Glu:Oxopro, Asn:Hse, Leu:Phe), organic acid group (e.g. 5HPip:CA:CAA, IBua:oC) and carbohydrate group (Xyl:pGlc, Man:pFru) at all-time points. Carbohydrates also showed interaction with other metabolites (Suc:Val, Xyl:SA:Pi, pGlc:SA) in 500 mM NaCl treated plants. Additionally, several metabolites showed a significant interaction within each other (e.g. Asp:Oxopro:Glu:5Hpip:CA:CAA:Grl-g, Man:pFru:MI:MT:oC:IBu, Asn:Hse:Pip) all time points. In the root dataset, the correlations among the metabolites were less pronounced when compared

Figure 5. Heat map of metabolite changes in roots of *P. pinnata* under salt stress.

Log_2 ratios of the relative fold change values (1 to 12) of each metabolite is represented in the form of a single horizontal row portioned with six columns of two salt treatments (300 and 500 mM NaCl) and three different time points (1, 4 and 8DAS) respectively. Each metabolite value is an average of six biological replicates represented with different colour codes red or blue according to the scale bar. The colour scale indicates degree of correlation.

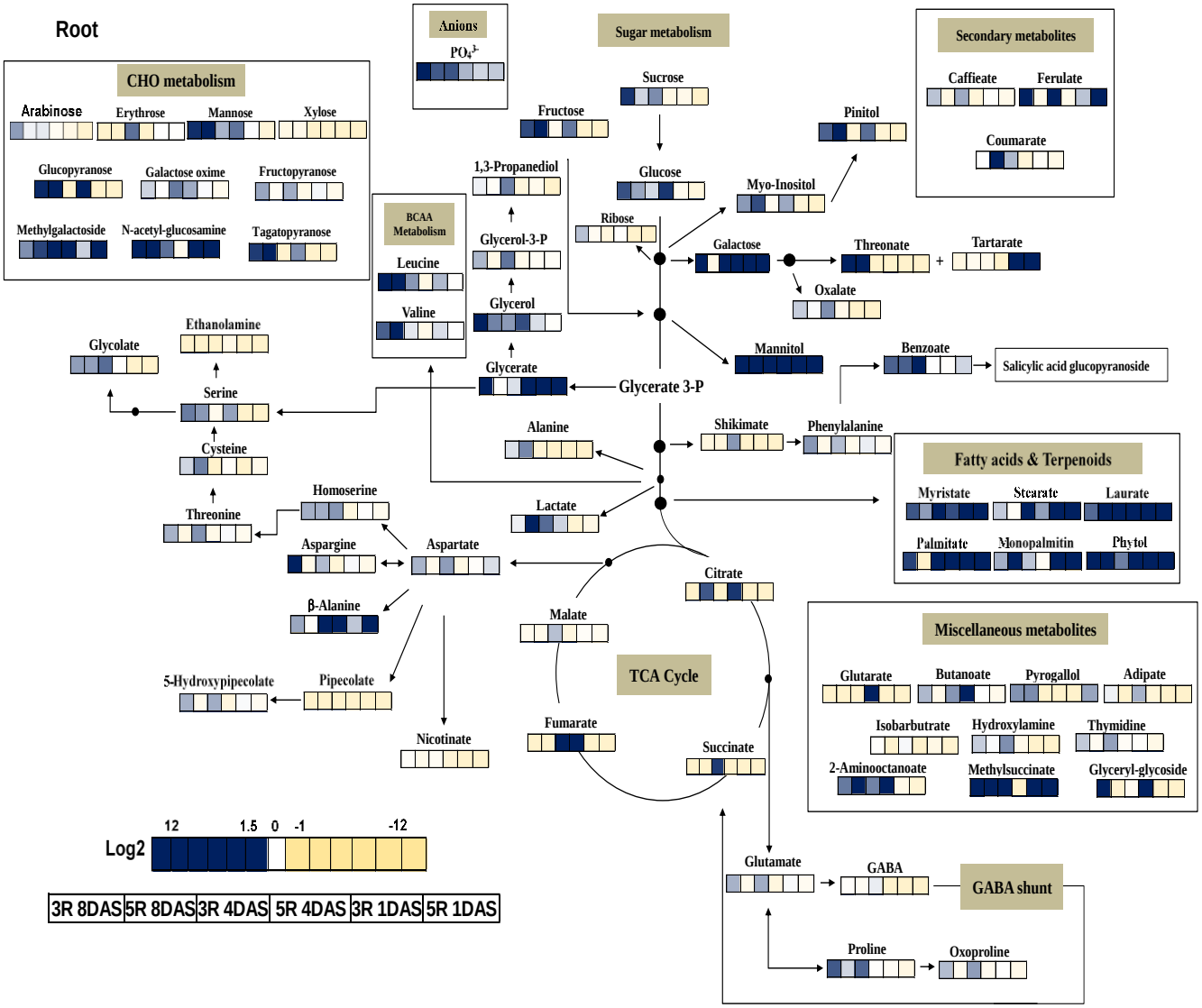
Root
CHO metabolism
Arabinose
Erythrose
Mannose
Xylose
Glucopyranose
Galactose oxime
Fructopyranose
Methylgalactoside
N-acetyl-glucosamine
Tagatopyranose
Anions
PO_4^{3-}
Sugar metabolism
Sucrose
Fructose
Glucose
Ribose
Galactose
Threonate
Tartarate
Oxalate
Pinitol
Myo-Inositol
Secondary metabolites
Caffieate
Ferulate
Coumarate
BCAA Metabolism
Leucine
Valine
1,3-Propanediol
Glycerol-3-P
Glycerol
Glycerate
Glycerate 3-P
Mannitol
Benzoate
Salicylic acid glucopyranoside
Ethanolamine
Glycolate
Serine
Cysteine
Threonine
Homoserine
Asparagine
Aspartate
Alanine
Shikimate
Phenylalanine
Lactate
Fatty acids & Terpenoids
Myristate
Stearate
Laurate
Palmitate
Monopalmitin
Phytol
Citrate
Malate
TCA Cycle
Fumarate
Succinate
β-Alanine
5-Hydroxypipecolate
Pipecolate
Nicotinate
Miscellaneous metabolites
Glutarate
Butanoate
Pyrogallol
Adipate
Isobarbutrate
Hydroxylamine
Thymidine
2-Aminooctanoate
Methylsuccinate
Glyceryl-glycoside
Glutamate
GABA
GABA shunt
Proline
Oxoproline
Log2
12
1.5
0
-1
-12
3R 8DAS
5R 8DAS
3R 4DAS
5R 4DAS
3R 1DAS
5R 1DAS

S.No		Control	1DAS				4DAS				8DAS			
			300 mM NaCl	P value	500 mM NaCl	P value	300 mM NaCl	P value	500 mM NaCl	P value	300 mM NaCl	P Value	500 mM NaCl	P value
	Amino acids													
1	Alanine	0.84 ± 0.3	0.11 ± 0.0	***	0.00 ± 0.0	***	0.47 ± 0.1	ns	0.23 ± 0.1	**	0.97 ± 0.7	ns	1.74 ± 0.5	*
2	Valine	0.00 ± 0.0	0.00 ± 0.0	ns	0.00 ± 0.0	ns	0.00 ± 0.0	ns	0.00 ± 0.1	ns	0.01 ± 0.0	*	0.03 ± 0.0	***
3	Cysteine	0.04 ± 0.0	0.02 ± 0.0	*	0.03 ± 0.0	ns	0.01 ± 0.0	*	0.03 ± 0.0	ns	0.04 ± 0.0	ns	0.07 ± 0.0	ns
4	Serine	0.21 ± 0.1	0.11 ± 0.0	*	0.10 ± 0.0	ns	0.17 ± 0.0	ns	0.33 ± 0.1	*	0.40 ± 0.2	*	0.35 ± 0.1	*
5	Leucine	0.00 ± 0.0	0.00 ± 0.0	ns	0.00 ± 0.0	ns	0.00 ± 0.0	ns	0.00 ± 0.0	ns	0.00 ± 0.0	ns	0.02 ± 0.0	**
6	Threonine	0.00 ± 0.0	0.00 ± 0.0	ns	0.00 ± 0.0	ns	0.00 ± 0.0	ns	0.00 ± 0.0	ns	0.00 ± 0.0	ns	0.00 ± 0.0	ns
7	Aspartate	0.00 ± 0.0	0.00 ± 0.0	ns	0.00 ± 0.0	ns	0.00 ± 0.0	ns	0.00 ± 0.0	ns	0.00 ± 0.0	ns	0.00 ± 0.0	ns
8	Aspargine	0.00 ± 0.0	0.00 ± 0.0	ns	0.00 ± 0.0	ns	0.00 ± 0.0	ns	0.00 ± 0.0	ns	0.00 ± 0.0	ns	0.00 ± 0.0	ns
9	Proline	1.48 ± 0.4	1.29 ± 0.4	ns	1.01 ± 0.2	*	3.05 ± 1.1	**	1.44 ± 0.7	ns	3.21 ± 0.9	***	1.80 ± 0.9	ns
10	Glutamate	0.00 ± 0.0	0.00 ± 0.0	ns	0.00 ± 0.0	ns	0.00 ± 0.0	ns	0.00 ± 0.0	ns	0.00 ± 0.0	ns	0.0 ± 0.0	ns
11	Homoserine	0.00 ± 0.0	0.00 ± 0.0	ns	0.00 ± 0.0	ns	0.00 ± 0.0	ns	0.00 ± 0.0	ns	0.00 ± 0.0	ns	0.00 ± 0.0	ns
12	β-Alanine	0.00 ± 0.0	0.00 ± 0.0	ns	0.01 ± 0.0	*	0.03 ± 0.0	***	0.01 ± 0.0	***	0.00 ± 0.0	ns	0.00 ± 0.0	ns
13	Oxoproline	0.00 ± 0.0	0.00 ± 0.0	ns	0.00 ± 0.0	ns	0.00 ± 0.0	ns	0.00 ± 0.0	ns	0.00 ± 0.0	ns	0.00 ± 0.0	ns
14	Phenylalanine	0.00 ± 0.0	0.00 ± 0.0	ns	0.00 ± 0.0	ns	0.00 ± 0.0	ns	0.00 ± 0.0	ns	0.00 ± 0.0	ns	0.00 ± 0.0	ns
15	GABA	0.39 ± 0.2	0.14 ± 0.0	***	0.16 ± 0.0	***	0.42 ± 0.1	ns	0.19 ± 0.0	**	0.37 ± 0.1	ns	0.33 ± 0.1	ns
	Sugars													
16	Erythrose	0.03 ± 0.0	0.03 ± 0.0	ns	0.03 ± 0.0	ns	0.06 ± 0.0	**	0.01 ± 0.2	ns	0.00 ± 0.0	**	0.00 ± 0.0	**
17	Xylose	0.02 ± 0.0	0.00 ± 0.0	**	0.00 ± 0.0	**	0.00 ± 0.0	*	0.01 ± 0.0	ns	0.01 ± 0.0	ns	0.01 ± 0.0	ns
18	Ribose	0.19 ± 0.1	0.09 ± 0.0	ns	0.07 ± 0.0	*	0.12 ± 0.0	ns	0.18 ± 0.1	ns	0.25 ± 0.1	ns	0.16 ± 0.0	***
19	Fructose	0.25 ± 0.1	0.13 ± 0.0	*	0.10 ± 0.0	*	0.20 ± 0.0	ns	0.46 ± 0.1	*	0.57 ± 0.1	**	1.15 ± 0.5	***
20	Galactose	0.00 ± 0.0	0.02 ± 0.0	***	0.01 ± 0.0	***	0.02 ± 0.0	***	0.01 ± 0.0	ns	0.10 ± 0.0	***	0.00 ± 0.3	ns
21	Mannose	0.06 ± 0.0	0.06 ± 0.0	ns	0.03 ± 0.3	ns	0.08 ± 0.0	ns	0.11 ± 0.0	ns	0.15 ± 0.0	ns	0.28 ± 0.1	***
22	Glucose	0.02 ± 0.0	0.01 ± 0.0	ns	0.01 ± 0.0	ns	0.02 ± 0.0	ns	0.04 ± 0.0	*	0.04 ± 0.0	**	0.02 ± 0.0	ns
23	Arabinose	0.04 ± 0.0	0.03 ± 0.0	ns	0.02 ± 0.0	ns	0.04 ± 0.0	ns	0.03 ± 0.0	ns	0.06 ± 0.0	*	0.04 ± 0.0	ns
24	Sucrose	15.1 ± 3.3	11.5 ± 3.4	*	5.50 ± 1.7	***	25.9 ± 2.4	***	10.6 ± 1.3	*	39.0 ± 5.5	***	18.4 ± 2.8	ns
25	Fructopyronose	0.00 ± 0.0	0.00 ± 0.0	ns	0.00 ± 0.0	ns	0.00 ± 0.0	ns	0.00 ± 0.0	ns	0.00 ± 0.0	ns	0.00 ± 0.0	ns
26	Glucopyranose	0.05 ± 0.0	0.02 ± 0.0	**	0.02 ± 0.0	**	0.03 ± 0.0	**	0.18 ± 0.1	**	0.14 ± 0.0	*	0.34 ± 0.1	***
27	Tagatopyranose	0.02 ± 0.0	0.00 ± 0.0	***	0.00 ± 0.0	***	0.01 ± 0.0	*	0.03 ± 0.0	ns	0.04 ± 0.0	**	0.07 ± 0.0	***
	Organic acids													
28	Lactate	0.28 ± 0.1	0.16 ± 0.0	**	0.20 ± 0.0	ns	0.57 ± 0.1	***	0.35 ± 0.1	ns	0.31 ± 0.1	ns	0.92 ± 0.4	***
29	Threonate	0.00 ± 0.0	0.00 ± 0.0	ns	0.00 ± 0.0	ns	0.00 ± 0.0	ns	0.00 ± 0.0	ns	0.02 ± 0.0	***	0.02 ± 0.0	***
30	Glycolate	0.02 ± 0.0	0.00 ± 0.0	***	0.00 ± 0.0	***	0.04 ± 0.0	***	0.02 ± 0.0	ns	0.03 ± 0.0	*	0.03 ± 0.0	ns
31	Oxalate	0.16 ± 0.0	0.14 ± 0.0	ns	0.10 ± 0.0	**	0.31 ± 0.1	***	0.11 ± 0.0	*	0.20 ± 0.0	ns	0.15 ± 0.0	ns
32	Nicotinate	0.02 ± 0.0	0.00 ± 0.0	***	0.01 ± 0.0	***	0.02 ± 0.0	ns	0.01 ± 0.0	ns	0.02 ± 0.0	ns	0.01 ± 0.0	ns
33	Succinate	0.26 ± 0.1	0.03 ± 0.0	**	0.02 ± 0.0	***	0.64 ± 0.2	***	0.03 ± 0.0	***	0.05 ± 0.0	***	0.02 ± 0.0	***
34	Methylsuccinate	0.00 ± 0.0	0.00 ± 0.0	ns	0.00 ± 0.0	ns	0.02 ± 0.0	***	0.00 ± 0.0	ns	0.03 ± 0.0	**	0.05 ± 0.0	***
35	Glycerate	0.00 ± 0.0	0.00 ± 0.0	ns	0.00 ± 0.0	ns	0.00 ± 0.0	ns	0.02 ± 0.0	***	0.00 ± 0.0	ns	0.00 ± 0.0	ns
36	Fumarate	0.00 ± 0.0	0.00 ± 0.0	ns	0.00 ± 0.0	ns	0.01 ± 0.0	**	0.02 ± 0.0	***	0.00 ± 0.0	ns	0.00 ± 0.0	ns
37	Butanoate	0.00 ± 0.0	0.00 ± 0.0	ns	0.00 ± 0.0	ns	0.00 ± 0.0	ns	0.00 ± 0.0	ns	0.00 ± 0.0	ns	0.00 ± 0.0	ns
38	Malate	00.0 ± 0.0	0.00 ± 0.0	ns	0.00 ± 0.0	ns	0.00 ± 0.0	ns	0.00 ± 0.0	ns	0.00 ± 0.0	ns	0.00 ± 0.0	ns
39	2-Aminooctanoate	4.20 ± 1.0	3.10 ± 1.7	ns	2.30 ± 1.0	*	7.50 ± 0.5	***	14.0 ± 3.3	***	7.80 ±. 1.7	***	14.4 ± 3.1	***
40	Glutarate	0.00 ± 0.0	0.00 ± 0.0	ns	0.00 ± 0.0	ns	0.00 ± 0.0	ns	0.01 ± 0.0	***	0.00 ± 0.0	ns	0.00 ± 0.0	ns
41	Isobarbiturate	0.00 ± 0.0	0.00 ± 0.0	ns	0.00 ± 0.0	ns	0.00 ± 0.0	ns	0.00 ± 0.0	ns	0.00 ± 0.0	ns	0.00 ± 0.0	ns
42	Tartarate	0.00 ± 0.0	0.00 ± 0.0	ns	0.00 ± 0.0	ns	0.00 ± 0.0	ns	0.00 ± 0.0	ns	0.00 ± 0.0	ns	0.00 ± 0.0	ns
43	Citrate	0.02 ± 0.0	0.00 ± 0.0	ns	0.00 ± 0.0	ns	0.00 ± 0.0	ns	0.05 ± 0.0	*	0.00 ± 0.8	ns	0.04 ± 0.2	*
44	Benzoate	0.01 ± 0.0	0.01 ± 0.0	ns	0.01 ± 0.0	ns	0.03 ± 0.0	***	0.01 ± 0.0	ns	0.02 ± 0.0	**	0.02 ± 0.0	*
45	o-Coumarate	0.00 ± 0.0	0.00 ± 0.0	ns	0.00 ± 0.0	ns	0.00 ± 0.0	ns	0.00 ± 0.0	ns	0.00 ± 0.0	ns	0.00 ± 0.0	ns
46	Ferulate	0.00 ± 0.0	0.00 ± 0.0	ns	0.00 ± 0.0	ns	0.00 ± 0.0	ns	0.00 ± 0.0	ns	0.00 ± 0.0	ns	0.00 ± 0.0	ns
47	Caffeate	0.00 ± 0.0	0.00 ± 0.0	ns	0.00 ± 0.0	ns	0.00 ± 0.0	ns	0.00 ± 0.0	ns	0.00 ± 0.0	ns	0.00 ± 0.0	ns
48	Pipecolate	0.00 ± 0.0	0.00 ± 0.0	ns	0.00 ± 0.0	ns	0.00 ± 0.0	ns	0.00 ± 0.0	ns	0.00 ± 0.0	ns	0.00 ± 0.0	ns
49	5-Hydroxypipecolate	0.00 ± 0.0	0.00 ± 0.0	ns	0.00 ± 0.0	ns	0.00 ± 0.0	ns	0.00 ± 0.0	ns	0.00 ± 0.0	ns	0.00 ± 0.0	ns
	Polyols													
50	Glycerol	1.47 ± 0.6	1.71 ± 0.5	ns	1.40 ± 0.2	ns	2.36 ± 0.2	***	3.39 ± 0.9	***	4.34 ± 1.2	***	2.63 ± 0.6	***
51	Pyrogallol	0.03 ± 0.0	0.00 ± 0.0	***	0.04 ± 0.0	**	0.01 ± 0.0	*	0.00 ± 0.0	***	0.05 ± 0.0	*	0.05 ± 0.0	**
52	Shikimate	0.01 ± 0.0	0.00 ± 0.0	ns	0.00 ± 0.0	ns	0.01 ± 0.0	ns	0.00 ± 0.0	ns	0.00 ± 0.0	ns	0.00 ± 0.0	ns
53	Pinitol	2.21 ± 0.6	1.26 ± 0.5	**	0.70 ± 0.1	***	1.29 ± 0.5	*	4.36 ± 0.6	**	4.61 ± 0.6	***	7.88 ± 1.9	***
54	Mannitol	0.00 ± 0.0	0.14 ± 0.0	***	0.68 ± 0.1	***	0.66 ± 0.1	***	1.01 ± 0.2	***	0.09 ± 0.0	**	0.21 ± 0.0	***
55	Myo-Inositol	1.55 ± 0.5	0.93 ± 0.1	ns	0.71 ± 0.1	**	1.30 ± 0.2	ns	2.32 ± 0.9	*	2.50 ± 0.8	***	3.58 ± 0.9	***
	Fatty acids													
56	Laurate	0.00 ± 0.0	0.00 ± 0.0	ns	0.00 ± 0.0	ns	0.00 ± 0.0	ns	0.00 ± 0.0	ns	0.00 ± 0.0	ns	0.00 ± 0.0	ns
57	Adipate	0.02 ± 0.0	0.00 ± 0.0	***	0.00 ± 0.0	***	0.03 ± 0.0	ns	0.01 ± 0.0	*	0.02 ± 0.0	ns	0.00 ± 0.0	***
58	Myristate	0.01 ± 0.0	0.08 ± 0.0	**	0.06 ± 0.0	***	0.04 ± 0.0	**	0.03 ± 0.0	***	0.03 ± 0.0	***	0.02 ± 0.0	*
59	Palmitate	0.02 ± 0.0	0.16 ± 0.2	*	0.17 ± 0.3	**	0.25 ± 0.4	***	0.14 ± 0.2	**	0.04 ± 0.0	*	0.00 ± 0.0	***
60	Stearate	0.02 ± 0.0	0.13 ± 0.0	***	0.24 ± 0.2	**	0.22 ± 0.0	***	0.03 ± 0.0	ns	0.03 ± 0.0	ns	0.02 ± 0.0	ns
61	Monopalmitin	0.00 ± 0.0	0.01 ± 0.0	***	0.01 ± 0.0	***	0.00 ± 0.0	ns	0.00 ± 0.0	ns	0.00 ± 0.0	ns	0.00 ± 0.0	ns
	Other metabolites													
62	1,3-Propanediol	0.13 ± 0.0	0.10 ± 0.0	**	0.00 ± 0.0	***	0.24 ± 0.0	**	0.08 ± 0.0	ns	0.14 ± 0.0	*	0.12 ± 0.0	**
63	Hydroxylamine	0.08 ± 0.0	0.00 ± 0.0	***	0.01 ± 0.0	***	0.13 ± 0.0	**	0.06 ± 0.0	ns	0.10 ± 0.0	ns	0.08 ± 0.0	ns
64	Ethanolamine	1.24 ± 0.4	0.19 ± 0.0	***	0.13 ± 0.0	***	0.14 ± 0.0	***	0.89 ± 0.5	***	0.63 ± 0.1	***	0.47 ± 0.1	***
65	Phosphate	14.8 ± 3.3	18.0 ± 2.3	*	19.0 ± 3.7	*	33.0 ± 4.7	***	20.8 ± 2.4	ns	51.6 ± 7.5	***	32.1 ± 4.2	***
66	Glycerol-3P	0.00 ± 0.0	0.00 ± 0.0	ns	0.00 ± 0.0	ns	0.00 ± 0.0	ns	0.00 ± 0.0	ns	0.00 ± 0.0	ns	0.00 ± 0.0	ns
67	Methylgalactoside	0.01 ± 0.0	0.01 ± 0.0	ns	0.05 ± 0.0	ns	0.08 ± 0.0	***	0.13 ± 0.2	***	0.02 ± 0.0	ns	0.03 ± 0.0	ns
68	N-Acetyl-glucosamine	0.00 ± 0.0	0.00 ± 0.0	ns	0.00 ± 0.0	ns	0.00 ± 0.0	ns	0.00 ± 0.0	ns	0.02 ± 0.0	***	0.00 ± 0.0	ns
69	Phytol	0.00 ± 0.0	0.00 ± 0.0	ns	0.00 ± 0.0	ns	0.00 ± 0.0	ns	0.00 ± 0.0	ns	0.00 ± 0.0	ns	0.00 ± 0.0	ns
70	Glyceryl-glycoside	0.00 ± 0.0	0.00 ± 0.0	ns	0.00 ± 0.0	ns	0.00 ± 0.0	ns	0.02 ± 0.0	*	0.02 ± 0.0	*	0.00 ± 0.0	***
71	Thymidine	0.00 ± 0.0	0.00 ± 0.0	ns	0.00 ± 0.0	ns	0.00 ± 0.0	ns	0.00 ± 0.0	ns	0.00 ± 0.0	ns	0.00 ± 0.0	ns

Table 4. Relative concentration and fold changes of major metabolites in leaves of *P. pinnata.*

S.No	1DAS	Abbreviation	4DAS	Abbreviation	8DAS	Abbreviation
1	Glutamate	**Glu**	Mannitol	**MT**	Sucrose	**Suc**
2	Oxoproline	**Oxopro**	Methyl-galactoside	**Met-Gal**	Phosphate	**Pi**
3	Butanoate	**Bta**	Ferulate	**Fa**	Threonate	**ThA**
4	Fructopyranose	**pFru**	β-Alanine	**Ba**	Pinitol	**D-PI**
5	Asparagine	**Asn**	Methylsuccinate	**Met-SA**	Glycerol	**Gro**
6	Threonine	**Thr**	Benzoate	**BA**	Methylsuccinate	**Met-SA**
7	5-Hydroxypipecolate	**5HPip**	Succinate	**SA**	Proline	**Pro**
8	Phenylalanine	**Phe**	Phosphate	**Pi**	Phytol	**Phytol**
9	Caffeate	**CAA**	Galactose	**Gal**	Serine	**Ser**
10	Homoserine	**Hse**	Laurate	**La**	Glycerate	**Gri**
11	Thymidine	**Thy**	Lactate	**LA**	Mannitol	**MT**
12	Benzoate	**BA**	2-Aminooctanoate	**Asu**	Tagatopyranose	**pTag**
13	Glycerol-3-phosphate	**G3p**	Glycerol	**Gro**	Glucose	**Glc**
14	Aspartate	**Asp**	Glycolate	**GA**	Glycolate	**GA**
15	o-Coumarate	**oC**	Sucrose	**Suc**	Laurate	**La**
16	Isobarbiturate	**IBua**	Proline	**Pro**	Fructose	**Fru**
17	Ferulate	**Fa**	Palmitate	**PA**	Glyceryl-glycoside	**Grl-g**
18	Oxalate	**Oxa**	Stearate	**StA**	N-Acetyl-glucosamine	**GlcNAc**
19	1,3-Propanediol	**Pdo**	Myristate	**MytA**	Leucine	**Leu**
20	Arabinose	**Ara**	Oxalate	**Oxa**	Galactose	**Gal**
21	Mannose	**Man**	1,3-Propanediol	**Pdo**	Palmitate	**PA**
22	Glucose	**Glc**	N-Acetyl-glucosamine	**GlcNAc**	Myristate	**MytA**
23	Malate	**MA**	Fumarate	**FA**	Benzoate	**BA**
24	Ethanolamine	**Eta**	Glutamate	**Glu**	Mannose	**Man**
25	Tagatopyranose	**pTag**	Oxoproline	**Oxopro**	Glucopyranose	**pGlc**
26	Glycolate	**GA**	Butanoate	**Bta**	Valine	**Val**
27	Hydroxylamine	**HA**	Thymidine	**Thy**	2-Aminooctanoate	**Asu**
28	Nicotinate	**NA**	Aspartate	**Asp**	4-Aminobutanoate	**GABA**
29	4-Aminobutanoate	**GABA**	Threonine	**Thr**	Adipate	**AA**
30	Adipate	**AA**	Leucine	**Leu**	Isobarbiturate	**IBua**
31	Alanine	**Ala**	Homoserine	**Hse**	Cysteine	**Cys**
32	Succinate	**SA**	Caffeate	**CAA**	Alanine	**Ala**
33	Ribose	**Rib**	Phytol	**Phytol**	Lactate	**LA**
34	Cysteine	**Cys**	Hydroxylamine	**HA**	Stearate	**StA**
35	Glyceryl-glycoside	**Grl-g**	Fructopyranose	**pFru**	Asparagine	**Asn**
36	Citrate	**CA**	o-Coumarate	**oC**	Butanoate	**Bta**
37	Myo-Inositol	**MI**	5-Hydroxypipecolate	**5HPip**	Aspartate	**Asp**
38	Sucrose	**Suc**	Asparagine	**Asn**	Threonine	**Thr**
39	Pinitol	**PI**	Phenylalanine	**Phe**	5-Hydroxypipecolate	**5HPip**
40	Shikimate	**ShiA**	Adipate	**AA**	Caffeate	**CAA**
41	Lactate	**LA**	4-Aminobutanoate	**GABA**	Thymidine	**Thy**
42	Fructose	**Fru**	Glycerol-3-phosphate	**G3p**	Glutamate	**Glu**
43	Serine	**Ser**	Erythrose	**Ery**	Oxoproline	**Oxopro**
44	Pyrogallol	**Pyr**	Arabinose	**Ara**	Homoserine	**Hse**
45	Glucopyranose	**pGlc**	Malate	**MA**	Glycerol-3-phosphate	**G3p**
46	Threonate	**ThA**	Glycerate	**Gri**	Hydroxylamine	**HA**
47	Xylose	**Xyl**	Mannose	**Man**	Oxalate	**Oxa**
48	Glutarate	**Glta**	Myo-Inositol	**MI**	Phenylalanine	**Phe**
49	Proline	**Pro**	Isobarbiturate	**IBua**	D-Fructopyranose	**pFru**
50	2-Aminooctanoate	**Asu**	Shikimate	**ShiA**	β-Alanine	**Ba**
51	Valine	**Val**	Monopalmitin	**MP**	Arabinose	**Ara**
52	Erythrose	**Ery**	Glucose	**Glc**	Pyrogallol	**Pyr**
53	Pipecolate	**Pip**	Glyceryl-glycoside	**Grl-g**	Myo-Inositol	**MI**
54	Fumarate	**FA**	Valine	**Val**	Methyl-galactoside	**Met-Gal**
55	Glycerol	**Gro**	Tartarate	**TA**	Ferulate	**Fa**
56	Methyl-galactoside	**Met-Gal**	Serine	**Ser**	Monopalmitin	**MP**
57	Leucine	**Leu**	Fructose	**Fru**	Ribose	**Rib**
58	β-Alanine	**Ba**	Alanine	**Ala**	1,3-Propanediol	**Pdo**
59	Palmitate	**PA**	Nicotinate	**NA**	o-Coumarate	**oC**
60	Myristate	**MytA**	Pipecolate	**Pip**	Shikimate	**ShiA**
61	Phosphate	**Pi**	Ribose	**Rib**	Fumarate	**FA**
62	Stearate	**StA**	Pinitol	**PI**	Tartarate	**TA**
63	Monopalmitin	**MP**	Citrate	**CA**	Xylose	**Xyl**
64	Phytol	**Phytol**	Cysteine	**Cys**	Malate	**MA**
65	Galactose	**Gal**	Xylose	**Xyl**	Citrate	**CA**
66	Laurate	**La**	Glutarate	**Glta**	Pipecolate	**Pip**
67	N-Acetyl-glucosamine	**GlcNAc**	Threonate	**ThA**	Nicotinate	**NA**
68	Glycerate	**Gri**	Tagatopyranose	**pTag**	Succinate	**SA**
69	Tartarate	**TA**	Pyrogallol	**Pyr**	Ethanolamine	**Eta**
70	Mannitol	**MT**	Glucopyranose	**pGlc**	Glutarate	**Glta**
71	Methylsuccinate	**Met-SA**	Ethanolamine	**Eta**	Erythrose	**Ery**

Table 5. List of all 71 metabolites in 300 mM NaCl treated roots of *P. pinnata* at 1, 4 and 8DAS and their abbreviations.

S.No	1DAS	Abbreviation	4DAS	Abbreviation	8DAS	Abbreviation
1	Hydroxylamine	**HA**	Leucine	**Leu**	Pinitol	**PI**
2	1,3-Propanediol	**Pdo**	Oxalate	**Oxa**	Phosphate	**Pi**
3	Ethanolamine	**Eta**	Hydroxylamine	**HA**	Laurate	**La**
4	Tagatopyranose	**pTag**	Threonine	**Thr**	Valine	**Val**
5	Glycolate	**GA**	Glycerol-3-phosphate	**G3p**	Glycerol	**Gro**
6	Sucrose	**Suc**	Fructopyranose	**pFru**	Glucopyranose	**pGlc**
7	Pinitol	**PI**	Oxoproline	**Oxopro**	Threonate	**ThA**
8	Adipate	**AA**	Malate	**MA**	Leucine	**Leu**
9	Alanine	**Ala**	N-Acetyl-glucosamine	**GlcNAc**	Phytol	**Phytol**
10	4-Aminobutanoate	**GABA**	Glutamate	**Glu**	Myo-Inositol	**MI**
11	Nicotinate	**NA**	Cysteine	**Cys**	Lactate	**LA**
12	Arabinose	**Ara**	Caffeate	**CAA**	Methyl-galactoside	**Met-Gal**
13	Ribose	**Rib**	Homoserine	**Hse**	Alanine	**Ala**
14	Myo-Inositol	**MI**	o-Coumarate	**oC**	Citrate	**CA**
15	Glyceryl-glycoside	**Grl-g**	Asparagine	**Asn**	Cysteine	**Cys**
16	Citrate	**CA**	1,3-Propanediol	**Pdo**	Mannose	**Man**
17	Succinate	**SA**	Succinate	**SA**	Tagatopyranose	**pTag**
18	Oxalate	**Oxa**	Phenylalanine	**Phe**	Mannitol	**MT**
19	o-Coumarate	**oC**	Isobarbiturate	**IBua**	2-Aminooctanoate	**Asu**
20	Xylose	**Xyl**	Aspartate	**Asp**	Fructose	**Fru**
21	Fructose	**Fru**	5-Hydroxypipecolate	**5HPip**	Monopalmitin	**MP**
22	Glutarate	**Glta**	Adipate	**AA**	Methylsuccinate	**Met-SA**
23	Threonate	**ThA**	Ferulate	**Fa**	Myristate	**MytA**
24	2-Aminooctanoate	**Asu**	Ethanolamine	**Eta**	Benzoate	**BA**
25	Shikimate	**ShiA**	Alanine	**Ala**	Pyrogallol	**Pyr**
26	Glucopyranose	**pGlc**	4-Aminobutanoate	**GABA**	N-Acetyl-glucosamine	**GlcNAc**
27	Proline	**Pro**	Shikimate	**ShiA**	Serine	**Ser**
28	Serine	**Ser**	Pyrogallol	**Pyr**	Glycolate	**GA**
29	Lactate	**LA**	Threonate	**ThA**	Glucose	**Glc**
30	Glutamate	**Glu**	Sucrose	**Suc**	Sucrose	**Suc**
31	Oxoproline	**Oxopro**	Arabinose	**Ara**	Arabinose	**Ara**
32	Butanoate	**Bta**	Glycolate	**GA**	Glycerol-3-phosphate	**G3p**
33	Asparagine	**Asn**	Ribose	**Rib**	Phenylalanine	**Phe**
34	Thymidine	**Thy**	Thymidine	**Thy**	Caffeate	**CAA**
35	Fructopyranose	**pFru**	Benzoate	**BA**	Butanoate	**Bta**
36	Caffeate	**CAA**	Proline	**Pro**	Asparagine	**Asn**
37	Homoserine	**Hse**	Monopalmitin	**MP**	5-Hydroxypipecolate	**5HPip**
38	Threonine	**Thr**	Valine	**Val**	Isobarbiturate	**IBua**
39	Phenylalanine	**Phe**	Tartarate	**TA**	Glutamate	**Glu**
40	5-Hydroxypipecolate	**5HPip**	Xylose	**Xyl**	Oxoproline	**Oxopro**
41	Isobarbiturate	**IBua**	Nicotinate	**NA**	Aspartate	**Asp**
42	D-Mannose	**Man**	Methylsuccinate	**Met-SA**	Ferulate	**Fa**
43	Malate	**MA**	Erythrose	**Ery**	Threonine	**Thr**
44	Cysteine	**Cys**	Pipecolate	**Pip**	Galactose	**Gal**
45	Glycerol-3-phosphate	**G3p**	Mannose	**Man**	Thymidine	**Thy**
46	Leucine	**Leu**	Phosphate	**Pi**	Nicotinate	**NA**
47	Aspartate	**Asp**	Butanoate	**Bta**	Glyceryl-glycoside	**Grl-g**
48	Glucose	**Glc**	Lactate	**LA**	Hydroxylamine	**HA**
49	Pipecolate	**Pip**	Tagatopyranose	**pTag**	Oxalate	**Oxa**
50	Fumarate	**FA**	Palmitate	**PA**	1,3-Propanediol	**Pdo**
51	Erythrose	**Ery**	Fumarate	**FA**	Ribose	**Rib**
52	Valine	**Val**	β-Alanine	**Ba**	Malate	**MA**
53	Glycerol	**Gro**	Glutarate	**Glta**	Glycerate	**Gri**
54	Benzoate	**BA**	Citrate	**CA**	Fructopyranose	**pFru**
55	Methylsuccinate	**Met-SA**	Glyceryl-glycoside	**Grl-g**	β-Alanine	**Ba**
56	β-Alanine	**Ba**	Pinitol	**PI**	Succinate	**SA**
57	Palmitate	**PA**	Fructose	**Fru**	Laurate	**La**
58	Stearate	**StA**	Myristate	**MytA**	Ethanolamine	**Eta**
59	Ferulate	**Fa**	Glucopyranose	**pGlc**	Glutarate	**Glta**
60	Myristate	**MytA**	Glucose	**Glc**	Erythrose	**Ery**
61	Pyrogallol	**Pyr**	Laurate	**La**	Palmitate	**PA**
62	Methyl-galactoside	**Met-Gal**	Phytol	**Phytol**	o-Coumarate	**oC**
63	Phosphate	**Pi**	2-Aminooctanoate	**Asu**	Proline	**Pro**
64	Phytol	**Phytol**	Glycerol	**Gro**	4-Aminobutanoate	**GABA**
65	N-Acetyl-glucosamine	**GlcNAc**	Methyl-galactoside	**Met-Gal**	Homoserine	**Hse**
66	Glycerate	**Gri**	Galactose	**Gal**	Tartarate	**TA**
67	Tartarate	**TA**	Glycerate	**Gri**	Stearate	**StA**
68	Monopalmitin	**MP**	Mannitol	**MT**	Shikimate	**ShiA**
69	Galactose	**Gal**	Stearate	**StA**	Xylose	**Xyl**
70	Mannitol	**MT**	Serine	**Ser**	Pipecolate	**Pip**
71	Laurate	**La**	Myo-Inositol	**MI**	Fumarate	**FA**

Table 6. List of all 71 metabolites in 500 mM NaCl treated roots of *P. pinnata* at 1, 4 and 8DAS and their abbreviations.

Figure 6. Heat map of hierarchical clustering of metabolite-metabolite correlations in roots of 300 and 500 mM NaCl treated *P. pinnata* under salinity stress.

Each correlation value (based on Pearson correlation coefficient) corresponds to average of six biological replicates. HAC analysis was performed among the metabolite at each individual time points (A) 1DAS, (B) 4DAS and (C) 8DAS in roots of 300 mM NaCl treated plants. (D, E and F) Detailed view of positively correlated metabolite correlations was shown in the form of table. HAC analysis was performed among the metabolite at each individual time points (G) 1DAS, (H) 4DAS and (I) 8DAS in roots of 500 mM NaCl treated plants. (J, K and L) Detailed view of positively correlated metabolite correlations was shown in the form of table. The colour key and histogram show degree of correlation.

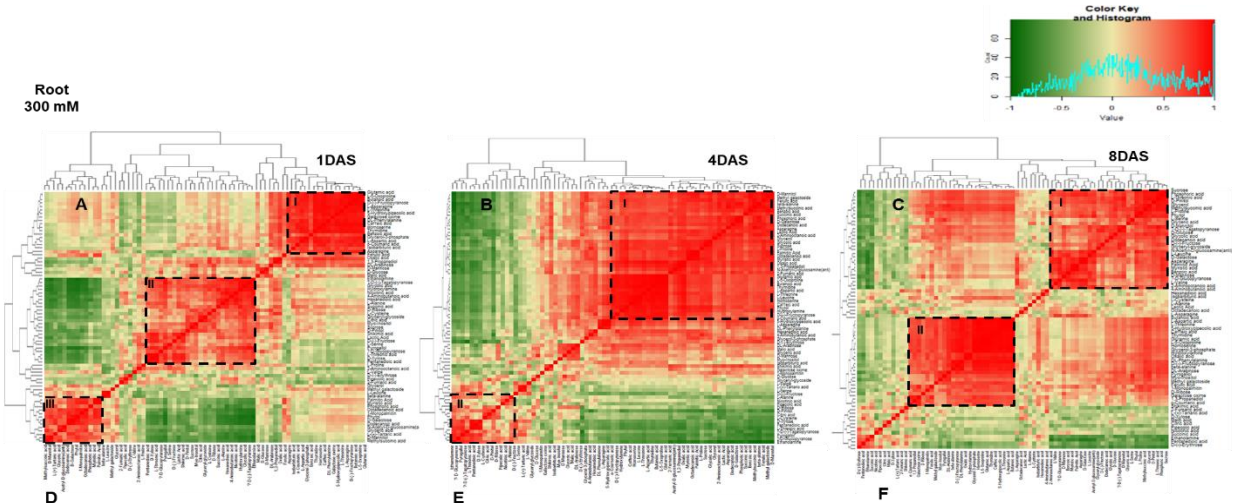

D

Group	1DAS
I	Glu, Oxopro, Bta, pFru, L-Asn, Thr, 5HPip, Phe, CAA, Hse, Thy, G3p, Asp, oC, IBua, Oxa, Pdo, Ara, Man, Glc
II	Eta, pTag, GA, HA, NA, GABA, AA, Ala, SA, Rib, Cys, Grl-g, CA, MI, Suc, PI, ShiA, LA, Fru, Ser, Pyr, pGlc, ThA, Xyl, Glta
III	PA, MytA, Pi, StA, MP, Phytol, Gal, GlcNAc, La, Gri, TA, MT, Met-SA

E

Group	4DAS
I	MT, Met-Gal, Fa, Ba, Met-SA, BA, SA, Pi, Gal, La, LA, Asu, Gro, GA, Suc, Pro, PA, StA, MytA, Oxa, Pdo, GlcNAc, FA, Glu, Oxopro, Bta, Thy, Thr, Leu, Hse, CAA, Phytol, HA, pFru, oC, 5HPip, Asn, Phe, AA, G3p, GABA, Ara, MA, Gri, Man, MI
II	Ala, NA, Pip, Rib, PI, CA, Cys, Xyl, Glta,, ThA, pTag, Pyr, pGlc, Eta

F

Group	8DAS
I	Suc, Pi, ThA, PI, Gro, Met-SA, Pro, Phytol, Gri, Ser, MT, pTag, Glc, GA, La, Fru, Grl-g, GlcNAc, Leu, Gal, PA, MytA, BA, Man, pGlc, Val, Asu
II	Bta, Asp, Thr, 5HPip, Thy, Glu, Oxopro, Hse, G3p, HA, Oxa, Phe, pFru, Ba, Ara, Pyr, MI, Met-Gal, Fa, MP, Rib, Pdo, oC, SA, Eta, Glta

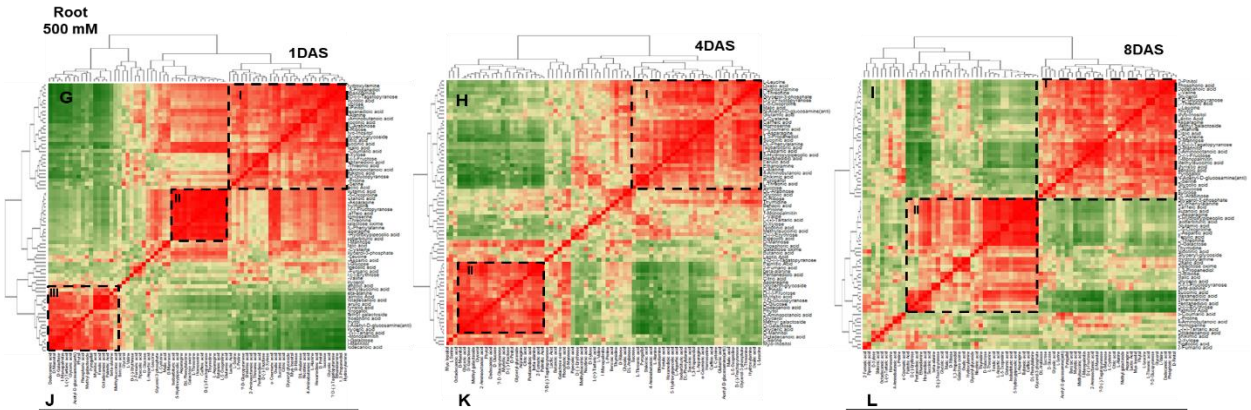

J

Group	1DAS
I	HA, Eta, Pdo, pTag, GA, Suc, PI, AA, Ala, GABA, NA, Ara, Rib, MI, CA, SA, Oxa, oC, Xyl, Fru, Glta, ThA, Asu, ShiA, pGlc, Pro, Ser, LA
II	Glu, Oxopro, Bta, Asn, Thy, pFru, CAA, Hse, Thr, Phe, 5HPip, IBua
III	Ba, PA, StA, Fa, MytA, Pi, Phytol, GlcNAc, Gri, TA, MP, Gal, MT, La

K

Group	4DAS
I	Leu, Oxa, HA, Thr, G3p, pFru, Oxopro, CAA, Hse, oC, Asn, Pdo, SA, Phe, IBua, Asp, 5HPip, AA, Fa, Eta, Ala, GABA, ShiA, Pyr, ThA, Suc, Ara, GA, Thy, Rib, BA, Pro
II	PA, FA, Ba, Glta, CA, Grl-g, PI, Fru, MytA, pGlc, Glc, LA, Phytol, Asu, Gro, Met-Gal, Gal, Gri, MT

L

Group	8DAS
I	PI, Pi, La, Val, Gro, pGlc, ThA, Leu, Phytol, MI, LA, Met-Gal, Ala, Man, pTag, MT, Asu, Fru, MP, Met-SA, MytA, BA, Pyr, GlcNAc, Ser
II	G3p, Phe, CAA, Bta, Asn, 5HPip, IBua, Glu, Oxopro, Asp, Fa, Thr, Gal, Thy, NA, Grl-g, HA, Oxa, Pdo, Rib, MA, Gri, pFru, Ba, SA, AA, Eta, Glta, Ery, PA

with leaf datasets. In roots of 300 mM NaCl treated plants, most of the metabolite levels showed significant correlation with each other (e.g. Glu:Oxopro:Thr:Phe:Hse:Ara:5Hpip:oC:Oxa:Pdo, PA:MytA:Gal:Gri:Met-SA:MT:Pi:Phytol:GlcNAc, pGlc:ThA:PI:pTag, Rib:Pyr:Glta:Eta, Suc:GA:Fru, HA:MI:SA) (Figure 6A-F; names and abbreviations were given in the Table 5). In 500 mM NaCl treated plants, a strong positive correlation was observed within the organic acid group (SA:Oxa) and carbohydrate group (pGlc:Fru) across all the time points (Figure 6G-L; names and abbreviations were given in the Table 6).In addition, several metabolites were associated significantly within each other (e.g. Oxopro:Asn:Thr:Phe:CAA:5Hpip:IBua:pFru:Thy, Ala:ThA, LA:Asu:PI, Rib:AA, HA:Pdo:Eta, Ba:Gal:Gri:PA, MytA:MT:Phytol) in 500 mM NaCl treated plants at all-time points.

Correlation based clustering between hormones and metabolites in leaves and roots of P. pinnata under salt stress

Figure 7 shows the interaction between hormones and metabolites in leaves and roots. In leaves, hormones including ABA, IBA, MeJA, zeatin and JA showed a positive correlation with MytA in leaves of 300 mM NaCl treated plants at 1DAS (Figure 7A). Hormones JA, MeJA and zeatin showed significant interaction with metabolites such as amino acids, carbohydrates, and organic acids in leaves of 300 mM NaCl treated plants at 4DAS (Figure 7B). In addition, JA and MeJA also showed strong association with carbohydrates and amino acids in leaves of 300 mM NaCl treated plants at 4DAS. At 8DAS, JA and ABA showed significant correlation with several metabolites MytA, Suc, Gal, Man and FA, while ABA and JA were showed significant interaction with metabolites pTag, organic acid group (NA, Pip, MA, 5Hpip, CAA), amino acids group (Hse, Asp, Asn), StA, and other metabolites (G3p, NAG, Grl-g) (Figure 7C). In leaves of 500 mM NaCl

treated plants, we could observe more interaction between hormones and metabolites including MeJA:IBA:zeatin:JA:IAA::carbohydrates, JA:MeJA:IAA:zeatin::organic acids, ABA:IBA:IAA:zeatin::amino acids, JA:IBA:IAA:SA:zeatin::polyols and fatty acids at 1DAS (Figure 7D). Increased interactions were also observed between hormones and metabolites namely JA:MeJA:zeatin::carbohydrates and cell-wallcarbohydrates, JA:MeJA:IBA:zeatin::organic acids, MeJA:IBA:IAA::amino acids, JA:MeJA:zeatin::polyols at 4DAS (Figure 7E). We recorded a significant positive correlation between hormones and metabolites namely MeJA:JA:ABA:SA::carbohydrates and cell-wall carbohydrates, JA:ABA:MeJA:SA::organic acids, JA:ABA:MeJA:IBA:IAA::amino acids, JA:ABA::polyols, fatty acids and JA:ABA:MeJA:IBA:zeatin::fatty acids in leaves of 500 mM NaCl treated plants at 8DAS (Figure 7F).

In roots, significant correlation between hormones and metabolites was recorded including JA:SA:ABA:MeJA:IBA:zeatin::carbohydrates, JA:MeJA:SA:ABA:IAA:SA::organic acids and MeJA:IBA::fatty acids in 300 mM NaCl treated plants at 1DAS (Figure 7G). At 4DAS, more positive interactions were seen between hormones and metabolites namely JA:ABA:ABA:SA:IBA::cell-wall carbohydrates, MeJA:JA:zeatin::polyols and MeJA:zeatin::fatty acids (Figure 7H). At 8DAS, a strong interaction was noticed between hormones and metabolites (JA:MeJA:ABA:zeatin::organic acids, JA:IBA:zeatin::amino acidand JA:zeatin::polyols) (Figure 7I). As the salinity progressed from day 1 to day 8, the positive interactions decreased in roots of 500 mM NaCl treated plants (Figure 7J-L). In roots of 500 mM NaCl treated plants, significant interaction was between hormones and metabolites namely ABA:SA:IBA:zeatin::organic acids at 1DAS, JA:SA:IBA::cell-wall carbohydrates,

Figure 7. Circos plots showing correlations in the hormone-metabolite interactions in *P. pinnata* under different NaCl treatments.

All 71 metabolites and 7 hormones were identified in the circle (order of metabolites mentioned in the table 2, 3, 5 and 6). Each correlation value (based on Pearson correlation coefficient) corresponds to average of six biological replicates and analysis performed between the hormones-metabolites at each individual time points (A and D) 1DAS, (B and E) 4DAS, (C and F) 8DAS in leaves as well as (H and K) 1DAS, (I and L) 4DAS, (J and M) 8DAS in roots of 300 and 500 mM NaCl treated plants. Ribbon colour corresponds to degree of correlation (in leaves: blue (+ve correlation) and red (-ve correlation) and in roots: red (+ve correlation) and green (-ve correlation).

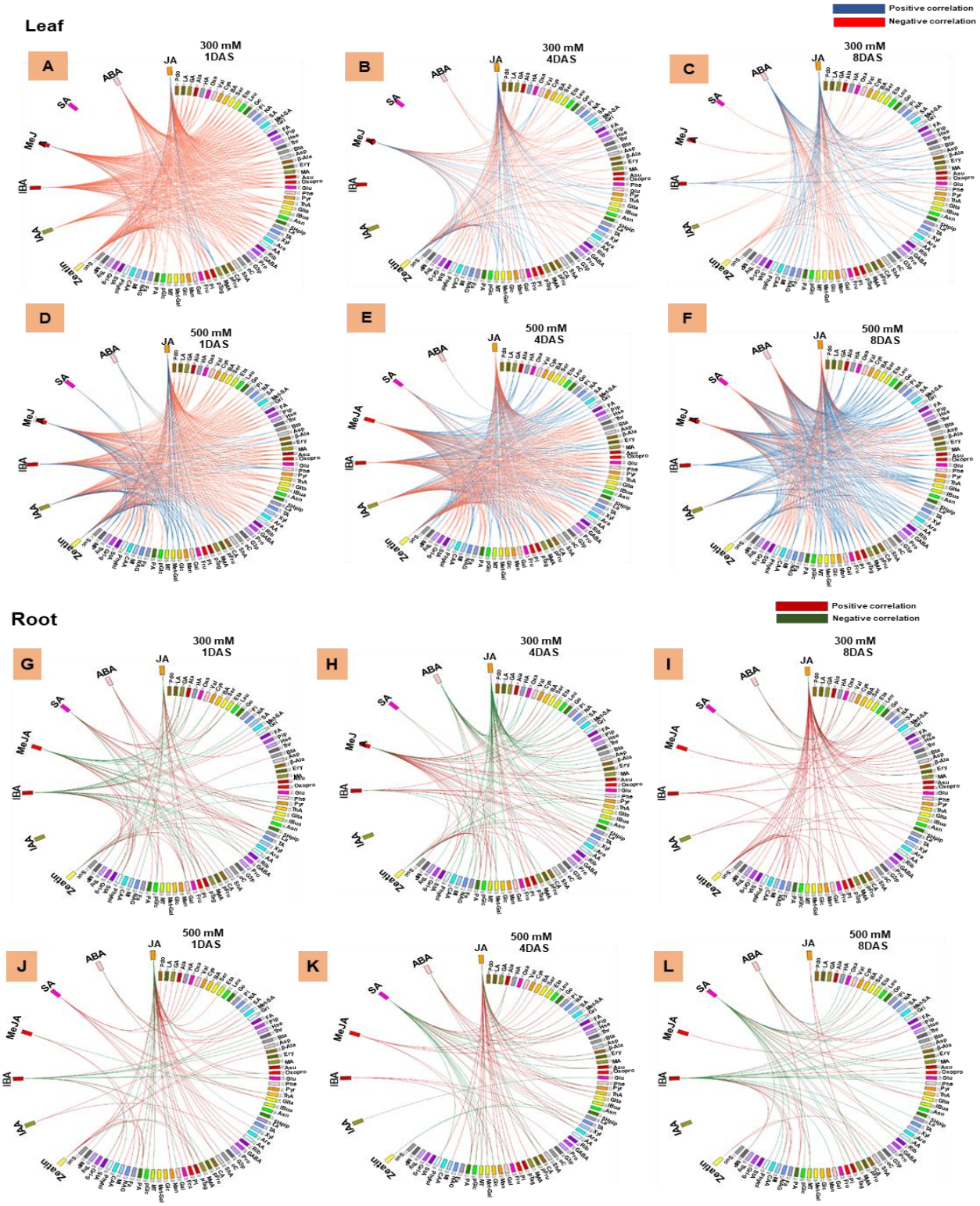
Leaf
Positive correlation
Negative correlation
A
300 mM
1DAS
B
300 mM
4DAS
C
300 mM
8DAS
D
500 mM
1DAS
E
500 mM
4DAS
F
500 mM
8DAS
Root
Positive correlation
Negative correlation
G
300 mM
1DAS
H
300 mM
4DAS
I
300 mM
8DAS
J
500 mM
1DAS
K
500 mM
4DAS
L
500 mM
8DAS
JA
ABA
SA
MeJ
MeJA
IBA
IAA
Zeatin

ABA:SA:JA:MeJA::organic acids at 4DAS, and ABA:SA::cell-wall carbohydrates, ABA:MeJA::organic acid at 8DAS respectively.

Differential expression of genes associated with ion transport and membrane potential in leaves and roots of P. pinnata

To assess the effect of salinity stress on the gene expression profile of Pongamia, we monitored the expression profile of several key salt-responsive genes including SOS pathway components (SOS1, SOS2 and SOS3), transporters (NHX1, HKT1:1, CLC1, V-CHX1, CCX1, V-H^+ATPaseB subunit, V-H^+ATPaseE subunit, PM-H^+ATPase1, PM-H^+ATPase4.1, PM-H^+ATPase4.1-like, CNGC5 and CNGC17), and calcium-dependent protein kinases (CDPK3 and CDPK32) (Figure 8). Sodium proton exchanger 1 (NHX1) was significantly up-regulated by ~2.6 and ~3.6-fold in leaves of 500 mM NaCl treated plants at 1 and 4DAS respectively, while these levels remained unchanged in leaves of 300 mM NaCl treated plants at all-time points and 500 mM NaCl at 8DAS respectively (Figure 8A). Further, the NHX1 gene expression was significantly increased only in 500 mM NaCl treated plants at 1DAS (Figure 8B). Interestingly, high affinity transporter 1:1 (HKT1:1) levels significantly increased by ~3.6 and ~2.0-folds in both leaves and roots of 300 mM NaCl treated plants at 1DAS. The SOS2 levels showed increase/ decrease in leaves of 300 and 500 mM NaCl treated plants, while these levels were unchanged in the roots of salt treated plants. SOS3 levels showed a significant up-regulation by ~3.9, ~2.0, and ~3.7-fold in leaves of 300 mM NaCl treated plants as well as ~5.9, ~6.0 and ~6.0-fold increase was observed in laves of 500 mM NaCl treated plants respectively. However, we did not observe much changes in expression levels of chloride channel 1 (CLC1) in both leaves and roots of salt

Figure 8. Relative mRNA expression levels of transporters in leaves of *P. pinnata* under salt stress conditions.

Log_2 fold changes of NHX1, HKT1:1, SOS2, SOS3, CLC1, V-CHX1, CCX1, V-H^+ATPaseB subunit, V-H^+ATPaseE subunit, PM-H^+ATP4.1, PM-H^+ATP4.1-like, PM-H^+ATPase1, CNGC5, CNGC17, CDPK3, and, CDPK32 in leaves (A) and roots (B) of salt treated plants of *P. pinnata* at 1, 4 and 8DAS respectively when compared to their corresponding controls. Error bar represents the mean ± SD (n=6).

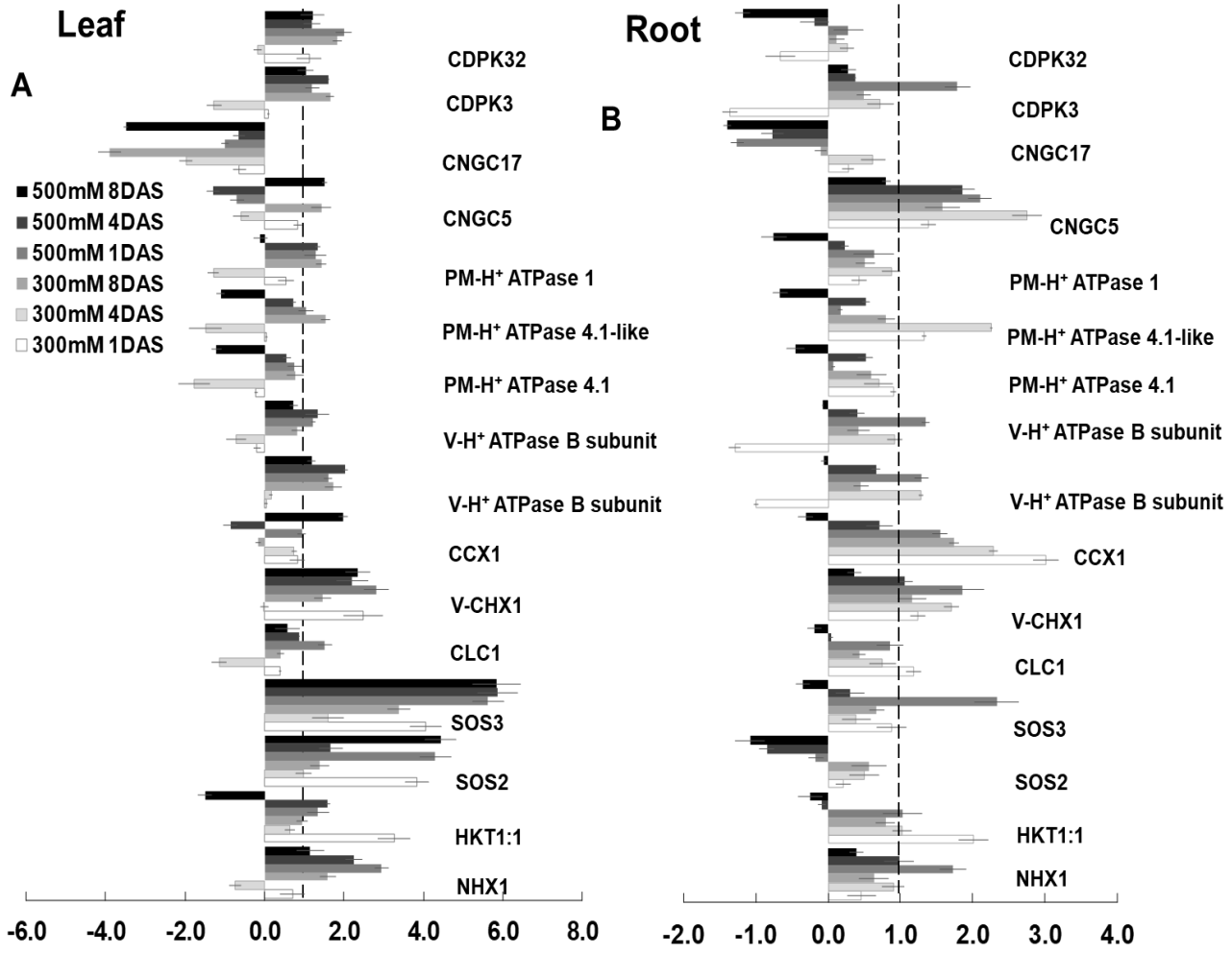
Leaf
A
500mM 8DAS
500mM 4DAS
500mM 1DAS
300mM 8DAS
300mM 4DAS
300mM 1DAS
CDPK32
CDPK3
CNGC17
CNGC5
PM-H+ ATPase 1
PM-H+ ATPase 4.1-like
PM-H+ ATPase 4.1
V-H+ ATPase B subunit
V-H+ ATPase B subunit
CCX1
V-CHX1
CLC1
SOS3
SOS2
HKT1:1
NHX1
-6.0 -4.0 -2.0 0.0 2.0 4.0 6.0 8.0
Root
B
CDPK32
CDPK3
CNGC17
CNGC5
PM-H+ ATPase 1
PM-H+ ATPase 4.1-like
PM-H+ ATPase 4.1
V-H+ ATPase B subunit
V-H+ ATPase B subunit
CCX1
V-CHX1
CLC1
SOS3
SOS2
HKT1:1
NHX1
-2.0 -1.0 0.0 1.0 2.0 3.0 4.0

Figure 9. Relative mRNA expression levels of cell-wall enzymes and antioxidant enzymes in leaves and roots of *P. pinnata* under salt stress conditions.

Log_2 fold changes of CATA4, FeSOD, MnSOD, Cu/ZnSOD1, Cu/ZnSOD1-like, POD, PAL1, PAL2, CAD2, and CAD6, in leaves (A) and roots (B) of salt treated plants of *P. pinnata* at 1, 4 and 8DAS respectively when compared to their corresponding controls. Error bar represents the mean ± SD (n = 6).

Figure 10. The band intensities of transporter genes of semi-quantitative PCR analysis in leaves and roots of *P. pinnata* under three different salinity stress conditions 0, 300 and 500 mM NaCl at 1, 4 and 8DAS respectively.

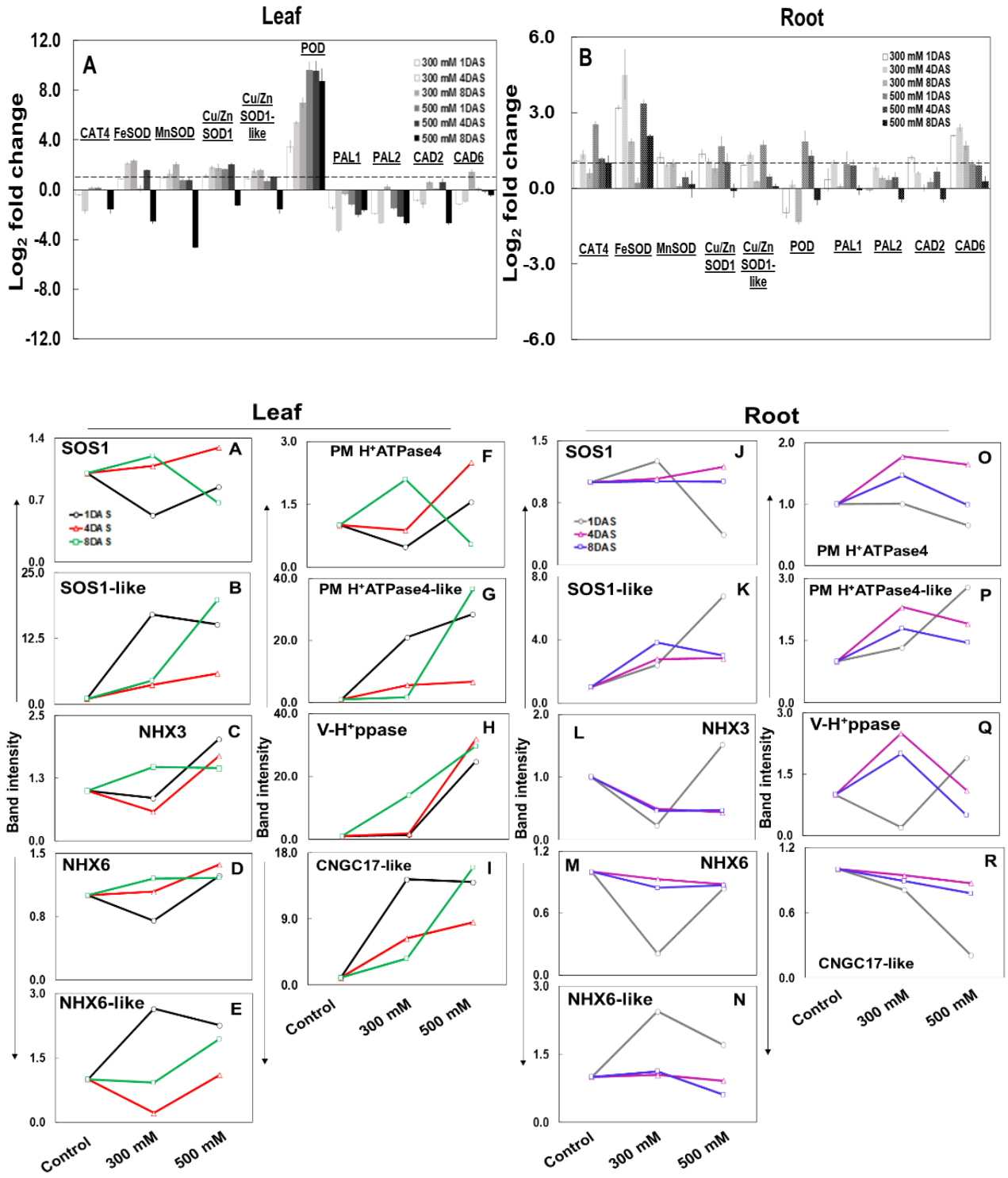
Leaf
Root
A
B
POD
CAT4 FeSOD MnSOD Cu/Zn SOD1 Cu/Zn SOD1-like PAL1 PAL2 CAD2 CAD6
300 mM 1DAS
300 mM 4DAS
300 mM 8DAS
500 mM 1DAS
500 mM 4DAS
500 mM 8DAS
Log2 fold change
SOS1
SOS1-like
NHX3
NHX6
NHX6-like
PM H+ATPase4
PM H+ATPase4-like
V-H+ppase
CNGC17-like
1DAS
4DAS
8DAS
Band intensity
Control
300 mM
500 mM

treated plants. The V-CHX1 levels were marginally induced in both leaves and roots of salt treated plants. Under salt stress, CCX1 levels were induced significantly by ~2.0-foldin 300 mM NaCl treated plants only at 8DAS, while these levels significantly increased by ~3.0, ~2.5 and 1.9-fold in roots of 300 mM NaCl treated plants, though these levels remained unchanged in 500 mM NaCl treated plants. Vacuolar proton ATPaseB subunit (V-H^+ATPaseB subunit) and V-H^+ATPaseE subunit expression levels were slightly induced in both leaves and roots of salt treated plants. We also monitored expression levels of three PM-H^+ATPase isoforms PM-H^+ATPase1, 4.1, 4.1-like in both leaves and roots of salt treated plants. The expression levels of PM-H^+ATPase1, 4.1, and 4.1-like genes were similar to those of control levels in leaves of salt treated plants, while PM-H^+ATPase4.1-like levels were marginally increased in roots of 300 mM NaCl treated plants only at 4DAS. The CNGC5 levels were decreased or increased in leaves of treated plants while these levels were significantly induced in roots of treated plants at 1, 4 and 8DAS. Furthermore, the expression level of CNGC17 gene was decreased/ unchanged in both leaves and roots of treated plants. Both CDPK3 and CDPK32 levels were increased/ unchanged in both leaves and roots salt treated plants. Gene primers for NHX3, NHX6, NHX6-like, SOS1, SOS1-like, H^+-ATPase4, H^+-ATPase4-like, CNGC17-like, and V-H^+ppase exhibited with multiple banding patterns their expression pattern significantly varied in leaves and roots of both control and salt treated plants (given in Figure 10).

Differential expression of genes associated with ROS homeostasis and cell wall modifications in leaves and roots P. pinnata

We monitored the expression levels of several key salt-responsive genes including antioxidant enzymes (catalase (CAT)4, iron superoxide dismutase (FeSOD), MnSOD, Cu/ZnSOD1, and Cu/ZnSOD1-like) and cell wall thickening enzymes (peroxidase (POD), phenylalanine lyase (PAL)1, PAL2, cinnamyl-alcohol dehydrogenase (CAD)2, and CAD6) (Figure 9A). Among the antioxidant genes CAT4 expression remained unchanged in leaves throughout the salt stress treatment and showed down-regulation at 8DAS in both 300 and 500 mM salt stress. In leaves, different isoforms of SODs showed gradual and significant up-regulation under 300 mM salt treatment from 1 to 8DAS. However, under 500 mM NaCl treatment, the SOD isoforms showed significant up-regulation only till 4DAS, but declined at prolonged stress treatment at 8DAS. Among the cell-wall strengthening genes, only POD showed a strong up-regulation in leaves of 300 and 500 mM NaCl treated plants at all-points, while the other genes (PAL1, PAL2, CAD1 and CAD2) did not show any significant induction. CAD 6 showed significant increase in 300 mM NaCl treatment at 8DAS, while these levels were significantly down-regulated in 300 mM NaCl 1 and 4DAS as well as in 500 mM NaCl treated plants at 1, 4, and 8DAS. In roots, the expression levels CAT4 were substantially up-regulated in 300 and 500 mM NaCl treated plants at 1, 4 and 8DAS respectively (Figure 9B). Among the antioxidant genes, CAT4 was significantly up-regulated only at 1DAS of 500 mM salt treatment. FeSOD also increased at all-time points in 300 mM salt treated plants and in 500 mM NaCl treatment at 4 and 8DAS. However, the expression levels of all other genes including MnSOD, Cu/ZnSOD1, Cu/ZnSOD1-like SOD, PAL1, 2, and CAD1, 2 and 6 were slightly changed in roots of salt treated plants.

Figure 11. Our proposed model to show the cross talk between phytohormones and metabolism in *Pongamia pinnata* subjected salinity stress.

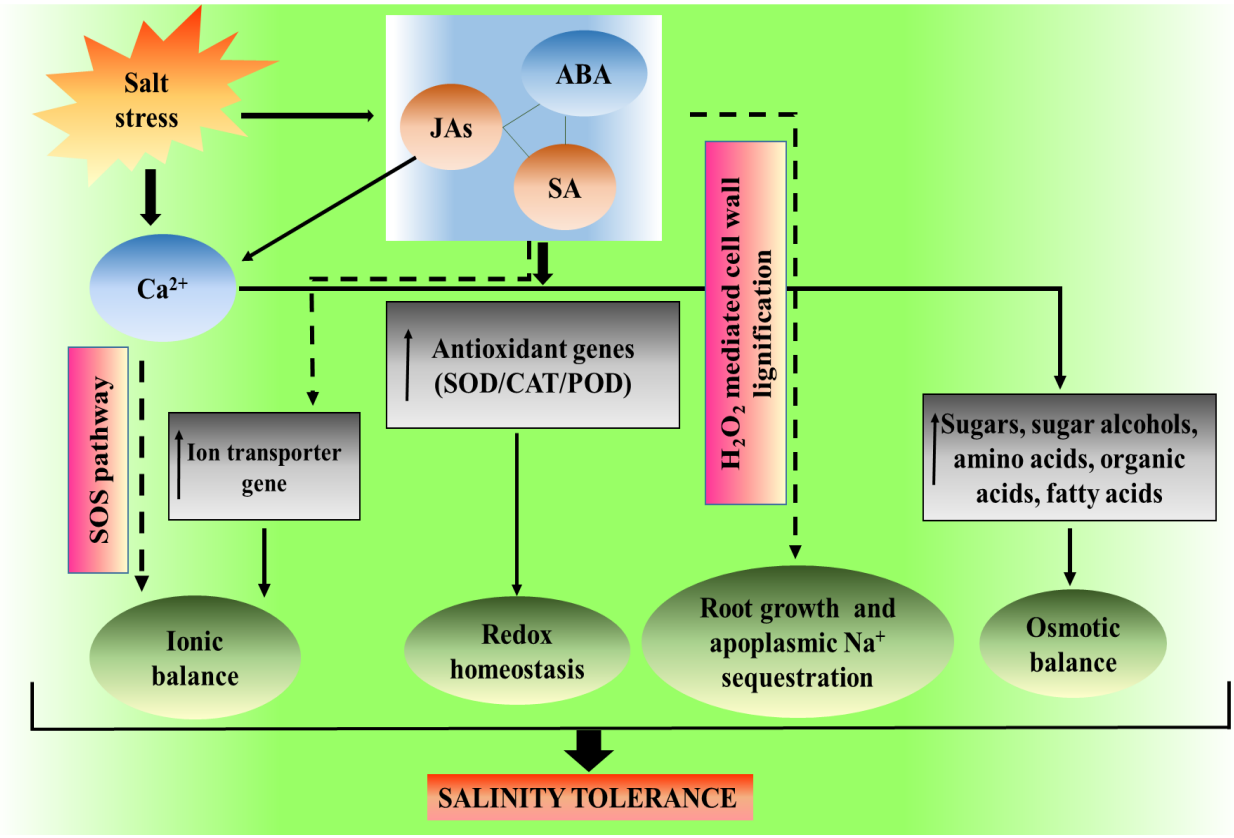
Salt stress
ABA
JAs
SA
Ca2+
SOS pathway
Ion transporter gene
Antioxidant genes (SOD/CAT/POD)
H2O2 mediated cell wall lignification
Sugars, sugar alcohols, amino acids, organic acids, fatty acids
Ionic balance
Redox homeostasis
Root growth and apoplasmic Na+ sequestration
Osmotic balance
SALINITY TOLERANCE

The consequence of salt-induced phytohormonal disturbance in leaves and roots of Pongamia

Developmental plasticity under stress conditions largely depends upon the interactions between hormones which regulate stress-adaptation responses and developmental processes. In this study, both leaves and roots of salt treated plants showed a significant diversity in hormone profile and their correlation patterns at all-time points. A significant correlation was observed among all hormones due to initial exposure of 300 mM NaCl stress in leaves. The rise in all hormones and correlation may be beneficial for the plant to maintain the growth under salt stress conditions (Sahoo et al., 2014; Fahad et al., 2015). Moreover, increased levels of zeatin in both leaves and roots of salt treated plants improved RRWC and stress-induced growth under salt stress conditions (Ghanem et al., 2011; Nishiyama et al., 2011; Wu et al., 2014; Melo et al., 2016).

A strong correlation was also observed between zeatin and JAs in leaves and roots of 300 mM NaCl treated plants. The interactive influence of cytokinin may substantiate JAs negative impact to promote plant survival under extreme saline conditions. The synergistic interaction between zeatin and JAs may also enhance the salt-induced vasculature in roots to enhance water uptake, which is also supported by the well maintained RRWC in roots of treated plants (Ueda and Kato, 1982; Nitschke et al., 2016; Jang et al., 2017). IAA levels were significantly increased in leaves of salt treated plants at all-time points, indicating that IAA might play an important role in Pongamia salt tolerance. Transgenic poplar plants, overexpressing *AtYUCCA6*gene associated with increased levels of auxin, showed delayed chlorophyll degradation and leaf senescence (Kim et al., 2012). The increased levels of IAA and IBA may due to tissue damage or cell lysis. However, our fluorescence studies clearly suggest the viable status of cells and tissue integrity. Therefore, increased IAA levels in Pongamia might help in

maintaining “stay-green” trait and steady levels of chlorophyll pigments under salt stress (Kim et al., 2012). Likewise, IBA levels also showed significant increase in both leaves and roots of salt treated plants, suggesting that enhanced IBA levels may also play a role in acquiring the stress-induced protective architectural changes in Pongamia (Tognetti et al., 2010). In addition, correlation studies revealed that IBA showed good interaction with IAA in leaves of 300 mM NaCl treated plants. It was evident that the plants deficient in both IAA and IBA expression levels showed defective plant growth and development (Spiess et al., 2014). Auxins also showed a strong association with JAs (JA and MeJA) in leaves and roots of salt treated plants, which might involve in promoting salt-induced growth and tissue integrity during salt stress (Cai et al., 2014; Fattorini et al., 2018; Ishimaru et al., 2018). A significant increase in JAs was detected in both leaves of salt treated plants. However, in roots, JA levels were maintained low till 4DAS, and restored to control levels at 8DAS. Conversely, MeJA levels were maintained high till 4DAS, while these levels returned to control levels at 8DAS. The results indicates that the two different forms of JAs are presumably interchangeable and might share common signal transduction pathway in Pongamia during salt stress (Diallo et al., 2014; Mitra and Baldwin, 2014; Cao et al., 2016; Li et al., 2017). An exogenous application of JAs reduced shoot growth, enhanced water uptake and cell wall synthesis in certain crop species (Kang et al., 2005; Uddin et al., 2013; Shahzad et al., 2015; Tavallali and Karimi, 2019). Previous studies suggest that the increased JAs level alleviate the toxic effects of salt stress by lowering the Na^+ and Cl^- ions accumulation across the plant (Shahzad et al., 2015). Correlation studies revealed that JAs showed a strong correlation with ABA in leaves of treated plants. The interactions between JAs and ABA may induce stomatal closure by triggering the stress-induced signalling pathways

in guard cells, preventing water loss from the leaves (Munemasa et al., 2011; Wang et al., 2016; Yang et al., 2018).

ABA levels were significantly increased in leaves of salt treated plants which might limit the stomatal conductance, water content, transpiration rate and carbon exchange rate (CER) by closing the stomatal apparatus (Skorupa et al., 2019). The observed reduction in ABA accumulation in roots might be due to ABA transfer from root to shoot or ABA exudation from the roots (Shi et al., 2015). The prolonged maintenance of higher ABA levels negatively impacts the plant growth, while transient increase helps in mitigation of salt stress by enhancing the stress responsive genes (Shi et al., 2015). Further, reduced ABA content may favour in maintaining RWC by regulating aquaporin proteins (Shi et al., 2015). The correlation studies revealed that ABA showed a strong interaction with SA in roots of salt treated plants, which improves plant growth under saline conditions, albeit the signalling mechanism is still unclear (Devinar et al., 2013). SA levels in roots were maintained little low at 1DAS and maintained high at 4DAS, while these levels returned to control levels at 8DAS. Exogenous application of SA on plants showed an improvement in LRWC and ROS homeostasis under salt stress (Jayakannan et al., 2013; Husen et al., 2018). The rise in SA levels might protect the leaves from salt injury by inhibiting necrosis signalling pathways and also regulate the leaf turgor by accumulating carbohydrate polyols (mannitol, pinitol, and myo-inositol) (Husen et al., 2018). The observed reduction in SA levels in roots may be due to the transportation of SA from root to shoot under salt stress conditions (Xu et al., 2017). Correlation studies revealed a positive correlation between SA and IAA in leaves of salt treated plants might help in maintaining the leaf cell extensibility to promote better plant growth under salt stress (Formentin et al., 2018; Shaki et al., 2019).

Enhanced cell-wall carbohydrates, carbohydrate alcohols, organic and fatty acids maintain cellular osmotic balance under salt stress

Pongamia exhibited significant changes in the metabolite levels including carbohydrates, amino acids, organic acids, polyol, and fatty acids. Interestingly, the rise in mannitol level (~12 fold), observed in both leaves and roots of salt treated plants at 8DAS, suggest that mannitol may serve as a major osmoticum in Pongamia. The increased levels of carbohydrate alcohols not only regulates the cellular osmotic potential but also provides non-enzymatic ROS scavenging protection under abiotic stress conditions (Abebe et al., 2003; Hossain et al., 2017; Dumschott et al., 2019). High levels of carbohydrates were recorded in both leaves and roots of treated plants at 8DAS. These carbohydrates are known to contribute to secondary call wall synthesis, while their accumulation alters the cell wall composition in Pongamia (Gilbert et al., 2009; Geilfus et al., 2017; Zhao et al., 2019). The rise in carbohydrates level may serve as osmolytes and immediate source of energy for a cell (Abdallaha et al., 2016).

The metabolic profile also indicate that enhanced levels of free amino acids such as β-Ala, Val, Leu, Ala, Thr, Cys and Phe in leaves and roots of treated plants at 8DAS. The increased levels of these free amino acids may provide continue nutrient and water uptake to support plant growth under salt stress condition and also contribute to tolerance by regulating several biological processes including biosynthesis of cell wall components, to protect the membrane protein integrity as well as stability of cellular macro-structures (Cao et al., 2017; Nasir et al., 2010). Interestingly, the accumulation of serine and glycolate are active components of photorespiration, which play a crucial role in protecting the photosynthestic apparatus by limiting the deposition of toxic photo-inhibitory metabolites (Hossain et al., 2017). Lactic acid accumulation may involve in the regulation of cytoplasmic pH, and production of pyruvate to maintain glycolysis under salt

stress condition (Felle et al., 2005; Hossain et al., 2017). Increased accumulation of saturated fatty acids might protect the membrane fluidity to protect the cell and cellular organelle from Na^+ toxicity and ion leakage (Shu et al., 2015; Atikij et al., 2019).

The correlation analysis between metabolites provides new insights for salinity studies in Pongmaia

In leaves, a strong correlation was observed among carbohydrates, fatty acids and polyols in treated plants suggesting that these metabolites may serve as first line 'osmolyte defense' against Na^+ ion osmotic imbalance, protecting the structural and functional integrity of the cell and cell membrane from osmotic imbalance (Gao et al., 2013; Conde et al., 2015). Further, the positive interaction between carbohydrates, intermediates of TCA cycle and polyols could serve as second line 'ion homeostasis defense' to maintain the intracellular pH and ion balance under salt stress (Guo et al., 2015). The positive correlation, observed between carbohydrates, polyols, amino acids and organic acids might serve as third line 'quick energy defense' suggesting an anaplerotic role for the TCA cycle and provide immediate carbon energy source under salt stress (Zhang et al., 2017). The association between carbohydrates and amino acids showed maintain C:N balance, which may ameliorate salt-induced stress in Pongamia (Nasir et al., 2010; Naliwajski and Skłodowska, 2018).

Our results also showed an increase in coumarate and benzoate in both leaves and roots, while significant increase was observed in caffieate and ferulate levels only in roots of salt treated plants. Increased levels of these metabolites could be beneficial to the plants for lignin biosynthesis as well as salicylic acid production, which may play defensive role under salinity stress (Chen et al., 2019). An increase in the accumulation of free amino acids Thr, Ala, Cys, and Leu might also involve in the production of pyruvate to maintain TCA cycle. Consistent with these results,

we observed a marginal induction of the GABA shunt. The induction of GABA shunt may serves as an alternative source for carbon in TCA cycle and support respiratory carbon metabolism under salt stress (Che-Othman et al., 2019; Seifikalhor et al., 2019). Further, we observed marginal increase in metabolites of glycerol pathway, which is essential in providing carbon source to glycolysis and triglyceride pathways. Moreover, glycerol is known to function as intra-cellular osmoticum under salt stress (Bahieldin et al., 2013; Igamberdiev and Kleczkowski, 2018).

In roots, the positive correlation between organic acids, carbohydrates and fatty acids may serve as line of 'ion homeostasis and osmolyte defense', regulating cellular pH, osmotic potential and membrane fluidity (Sakamoto and Murata, 2002; Guo et al., 2015). The enhanced correlation of secondary metabolites with these metabolites could serves as second line of 'antioxidant and cell wall barrier defense', where it enhances the tolerance to salinity by regulating pathways such as ROS detoxification and cell wall barrier synthesis (lignin biosynthesis) (Liu et al., 2018; Yang et al., 2018). The positive association of polyols may provide a continuous osmoticum at cellular level to mitigate the osmotic imbalance raised by the increase uptake of Na^+ ions into the vacuole (Slama et al., 2015).

The correlation analysis between phytohormones and metabolites provides new insights for salinity studies

Hormone association with fatty acids may favour the protein lipid modifications such as S-acylation and N-myristoylation, which correspond to the irreversible link of lipid (fatty acid) to the N-terminal amino acid residue of proteins. The lipid modification could be involved in regulation of several biological processes redox homeostasis, protein-membrane associations and protein stability under various environmental stresses (Boyle et al., 2016; Majeran et al., 2018).

The exogenous application of MeJA on shoots of soybean showed increased accumulation of cell wall SFAs to maintain growth under drought stress (Mohamed and Latif, 2017). Further, JA also showed strong interaction with organic acids and amino acids with the salinity treatment time suggesting that organic acids and amino acids may be involved in promoting salt-induced growth by regulating osmotic balance, ion homeostasis, carbon and nitrogen balance under salt stress (Sharma et al., 2018; Siddiqi and Husen, 2019). The results suggest that the increased interaction between hormones and metabolites may be beneficial to Pongamia in order to survive under extreme salinity stress (Sahoo et al., 2014; Formentin et al., 2018). The number of interactions between hormones and metabolites increased with increasing treatment time in roots of 300 mM NaCl treated plants. In contrast, the number interactions were decreased with the treatment time in roots of 500 mM NaCl treated plants. The high correlation between hormones and cell-wall carbohydrates and organic acids may enhance the water permeability as well as pH regulation under salt tress conditions. The increased association of hormones with organic acids may provide immediate source of carbon energy and osmotic balance under salinity stress conditions (Assaha et al., 2017; Böhm et al., 2018; Yang and Guo, 2018).

Salinity-induced alteration in expression of ion transporter genes

In the present study, Pongamia exhibited tissue specific expression of salt-responsive transporter genes including SOS1, NHXs, PM-H^+-ATPases, V-H^+-ATPases, CNGCs, and other transporter genes. The expression patterns of SOS1 and SOS1-like genes correlated with Na^+ fluoresence and Na^+ion content,indicating that SOS1 genes are responsible for low Na^+ levels in the leaves of Pongamia by increasing Na^+ loading into the xylem/ apoplastic region. Further, the expression levels of SOS1 and SOS1-like genes increased significantly in salt treated roots, which

may contribute to apoplastic Na^+ depostion under high salinity. The differential expression of SOS2 and SOS3in the both leaves and roots suggest their crucial role in salt tolerance of Pongamia through SOS pathway. In this study, we observed that the expression of NHX1 was unchaged upon 300 mM salt stress in both leaves and roots of Pongamia, while there was significant induction in 500 mM NaCl stress in both leaves and roots, which correlates with the low levels of Na^+ fluoresence intensity and Na^+content data in leaves of 300 mM NaCl treated plants. At high salt concentration (500 mM NaCl), Pongmia might induce NHX1 experssion to sequester Na^+ ions rapidly into the vacuole to mitigate the Na^+ toxicity. Similarly, in roots, induced NHX1 expression may indicate the vacuolar Na^+ sequestration. In contrast, NHX1 levels wereunaffected at intial impostion of stress, suggesting involvement of other NHXs isofoms for vacuolar Na^+ sequestration at intial stages of salt stress. The differential expresssion of other NHXs isoforms such as NHX3, NHX6 nd NHX6-like in both leaves and roots suggests their possible roles in ion homeostasis, plant growth and development under salt stress (Bassil et al., 2018; Dragwidge et al., 2018). In this study, expression of high affinity transporter (HKT)1:1 followed similar trend in both leaves and roots of salt stressed plants. Previous studies suggested that HKT family transporter proteins can mediate exclusion of $Na^+$from leaves and roots by translocating shoot-to-rootand root-to-shoot Na^+ delivery by withdrwaing Na^+ from xylem stream into phloem (Munns et al., 2012; Hill et al., 2013; An et al., 2017; Zhang et al., 2018). Induction of HKT1:1 expression upon initial imposition of salt stress in both leaves and roots may promote Na^+ exclusion tolimit Na^+ toxcity in the respective tissues (Zhang et al., 2018). However, with increasing salt stress treatment time, the marginal expression of HKT1:1genemay regulate the retrevial of Na^+ from the xylem (Davenport et al., 2007; Ali et al., 2016). The expression levels of CLC1 indicate that CLC1 may not be involved

in the Cl^- vacuolar sequestration (Wei et al., 2016). PM-H^+-ATPase family pumps playa crucial role in improving the salt tolerance by maintaing the intracellular pH balance, transmembrane potential and ion homeostasis under salt stress conditions (Olfatmiri et al., 2014; Falhof et al., 2016; Shabala et al., 2016). The diffrences in the expression levels of PM-H^+-ATPase isoforms could be due toconfigurational and/or post-translational modifications of these isforms under salt stress, which could promote growth under salinity stress. The increased expression of V-H^+-PPase and V-H^+-ATPaseB and E subunit in leaves of salt treated plants may control the depolarization of vacuolar membrane potential, which is generated by excess depostion of Na^+ ions in leaves of Pongamia upon prolonged salt exposure (Graus et al., 2018; Marriboina and Reddy, 2020a). An increased expression levels of V-CHX1 may involve in plant growth by improving cellular ion homeostasis, pH balance and osmoregulation under saline conditions (Guan et al., 2014; Qi et al., 2014; Liu et al., 2017). Enhanced experssion of CCX1 may involved in regulation of intracellular Ca^{2+} levels, which may help in vacuolar Na^+ sequestration, ROS and ion homeostasis under salt stress (Yong et al., 2014; Li et al., 2016; Corso et al., 2018). Differential expression of CNGC5, CNGC17 and CNGC17-like may induce Ca^{2+} derived reponses to mitigate the negative effects of salt stress (Wang et al., 2013; Saand et al., 2015).

Salinity-induced alteration in expression of antioxidant genes

Excess Na^+ accumulation in the plant causes ionic imbalance which results in ion toxicity, oxidative stress, and generation reactive oxygen species (ROS) (AbdElgawad et al., 2016). To combat the ROS induced cellular damage plant induces several antioxidant enzymes such as superoxide dismutase (SOD), catalase (CAT) and peroxidase (POD) (Reddy et al., 2004). In this study, the observed higher expression levels of the different SOD isoforms might protect the plants

at the onset of oxidative stress much before the cellular antioxidant signaling cascade initiates its function under high salinity. According to Gill and Tuteja, (2010), the H_2O_2 produced through SOD activity, provides an additional advantage to the plant by strengthening cell wall through lignin biosynthesis. Also, higher CAT4 expression levels in roots might help the plant to reduce the higher levels of H_2O_2 under high salt conditions. The lower expression levels of CAT4 in the leaves may reflect the dynamic and tissue specificity of the antioxidant system under high salt environment (AlHassan et al., 2017). Increased expression of POD in leaves and roots were well correlated with the respective lignin depositions. The classIII apoplastic peroxidases play a major role in maintaining the structural integrity of the cell wall under salt stress (Kim et al., 2012). In addition, the expression levels of several other cell-wall modifying and lignin biosynthesis genes were monitored which include, PAL1, PAL2, CAD1, CAD1-like, CAD2, and CAD6. The increased expression levels of both PAL1 and PAL2 in 500 mM NaCl treated roots might permit the plant to preserve the cell wall integrity under high salt environment (Lee et al., 2007). The consistent increase in the CAD1-like gene expression suggests its possible role in reinforcing the strength and rigidity of the cell wall to enhance the selectivity and permeability of cell wall for solute and water transport under high saline environment (Zhao et al., 2013). Salinity-induced Ca^{2+} levels not only counteract the Na^{+} toxicity but also activate numerous signaling pathways including JAs signaling.

Based on our correlation results, we hypothesize that JAs, SA and ABA play crucial role in the adaptation of Pongamia plants to high salinity stress. On the other hand, induction of metabolites such as a sugars, amino acids and polyols provides constant supply of nutrients and are also involved in conferring osmotic and ionic homeostasis under salinity stress.

The downstream effect of the above signaling pathways could influence the defense (antioxidant) and transporter gene expression patterns conferring redox homeostasis under salinity stress, ultimately leading to Na^+ ion exclusion and sequestration in the apoplasmic regions.

Chapter 5

Root proteomics and protein-protein cross-talk

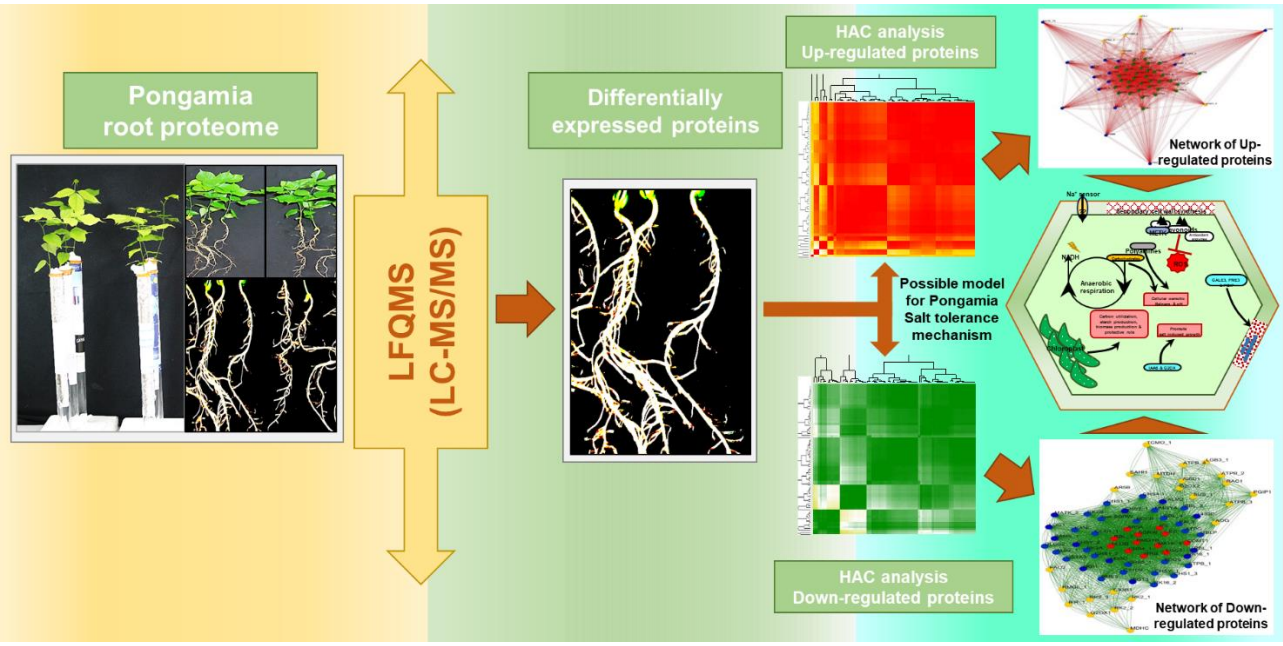

Chapter 5 Introduction

Crop productivity on saline marginal lands has limited success due to complex genetic diversity of the plant and spatio-temporal heterogeneity of soil salinity. Cultivation of economically or ecologically important tree species has been largely neglected mainly due to genetic and physiological robustness of these species (Tsai et al., 2018). Understanding the physiological and genetic diversity of tree species is crucial for sustenance of saline marginal lands towards economic gain (Samuel et al., 2013; Hanin et al., 2016). When the plants are exposed to salt stress, root is the primary organ to sense and respond to salinity (Fu et al., 2019). Root also acts as a physical barrier to restrict the Na^+ ion distribution across the plant (Marriboina and Reddy, 2020a). Of late, auxins are known to play a crucial role in plants to adapt changing environmental conditions. The expression of auxin responsive proteins including auxin-induced protein (IAA6), auxin transporter-like protein 2 (LAX2), and LAX3 regulate root vasculature were reported to beinvolved in lateral root growth development (Péret et al., 2012). Similarly, expression patterns of gibberellin 2-oxidase (G2OX) could regulate the active form of gibberellin levels and promote plant growth (Wang et al., 2019). Continuous accumulation of Na^+ ions inside the root cell exerts high osmotic pressure on cell wall (Horie et al., 2012) and to avoid this imbalance, plants synthesize cell wall remodelling enzymes including galactoside 2-alpha-L-fucosyltransferase (FUT1) and probable UDP-arabinopyranose mutase 1 (RGP1) to protect cell wall turgor during salt stress (Tryfona et al., 2014; Saqib et al., 2019). In response to salt stress, plants also induce synthesis of proteins related to secondary metabolism including flavonoid and anthocyanin biosynthesis to defend against ROS damage under salt stress (Chen et al., 2019). On the other hand, plants also trigger antioxidant defense systems to cope with salinity induced oxidative stress (Al-Kharusi et al., 2019). Antioxidant enzymes such as ascorbate peroxidase

(APX1), catalase4 (CAT4), and monodehydroascorbate reductase (MDAR) provide defense against ROS and also help maintaining superoxide levels under salt stress (Li et al., 2015; Sofo et al., 2015).

Metabolic modifications in cellular metabolism are essential for plant survival during conditions of salt stress (Kosová et al., 2018). With induction of pyruvate decarboxylase2 (PDC2), alcohol dehydrogenase class-3 (ADHX) and aldehyde dehydrogenase family 7 member (A1AL7A1), plant shifts carbohydrate pools to anaerobic respiration (Luo et al., 2017). Adapting the anaerobic respiration, plants can cope up with cellular energy demands under salinity stress (Luo et al., 2017). Additionally, expression of ACEA1 diverts the energy metabolism to the glyoxylate cycle to utilize carbon metabolism for the generation of necessary energy under salinity stress (Yuenyong et al., 2019). Assimilation of nitrogen is also crucial for the plant to synthesize new proteins, which might play significant role in cellular processes during salt stress. Expression of protease inhibitor and heat shock proteins, in response to salinity, enhanced the cellular protein turnover by inhibiting the protein degradation and misfolding of proteins during salt stress (Haq et al., 2019). Interestingly, induced chloroplasts accumulation in roots showed an increase in root photosynthesis, carbon assimilation rate and root biomass (Kobayashi et al., 2017).

Dwindling fossil fuel resources has raised attention towards renewable energy to meet global energy demands in future. To address this problem, several studies on non-food crops could be potential candidate species for renewable energy resources including *Pongamia pinnata*, *Jatropha curcas* and *Camelina sativa* (Mudalkar et al., 2014; Chaitanya et al., 2015; Singha et al., 2019). Interestingly, we have chosen Pongamia because of its high resilience to various agro-climatic conditions (Kesari and Rangan 2010). We report for the first time deeper insights of salinity

tolerance mechanisms in *P. pinnata* at root proteome level by using computational approaches. Marriboina et al., 2017; Marriboina and Reddy, 2020a). The interactions and crosstalk among different groups of proteins would certainly create new opportunities for discovery of new protein pathways, which are very crucial to understand stress tolerant mechanisms. The current study also provides an evidence for the protein interactions and associated signalling pathways to understand high salinity tolerance mechanisms in *Pongamia pinnata*.

Plant material, growth conditions, and salinity treatment

Pongamia pods (TOIL 12) were obtained from Tree Oil India Limited (TOIL), Zaheerabad, Hyderabad, Telangana. The pods were dried for three days at 6 h regular intervals under natural sunlight. For experimentation, uniform seeds were selected and germinated on moist cotton for 10 days at 25°C in dark. After 10 days, uniform seedlings were chosen and transferred carefully into a 50 ml falcon tubes (Genaxy, India) filled with full-strength Hoagland No. 2 basal salt mixture (Himedia) solution adjusted to pH 5.75 ± 0.02. The seedlings were grown in a long cylindrical glass tube (5 cm diameter X 60 cm length) after 10 days (Marriboina and Attipalli, 2020b). The solution was replenished every four days. 30 days old seedlings (n = 10) were taken and treated with 500 mM NaCl (~ 3% NaCl) for 4 days dose dependently by increasing 100 mM NaCl every day. Control plants were maintained with fresh Hoagland nutrient solution. All the hydroponic experiments were conducted in a plant culture room maintained at 24°C with a 16 h photoperiod and relative humidity about 60%. After 4 days of salt-treatment (DAS), roots were harvested quickly, frozen in liquid nitrogen and stored at – 80°C prior to analysis.

Root protein extraction

Whole roots of control and 500 mM NaCl treated plants were collected and finely ground in liquid nitrogen with motor and pestle. Total root proteins were extracted as described in Saravanan and Rose (2004) with some modifications. Approximately 1 g root powder was taken in 15 ml falcon tube (Genaxy, India) and suspended in 4 ml of extraction buffer containing 0.5 M Tris-HCl (pH 7.5), 0.7 M sucrose, 0.1 M KCl, 50 mM EDTA, 2% β-mercaptoethanol and 1mM PMSF. An equal volume of Tris-saturated phenol (pH 7.5) was added to the extract suspension after thorough mixing and the whole suspension was further mixed for 30 min at 4°C in a rotospin cyclomixer.

Tris-saturated phenol was prepared by mixing equal volume of Tris-HCl (pH 7.5) and phenol with continuous stirring for 3-4 h. The lower phenolic layer was separated and added equal volume of Tris-HCl (pH 7.5) with continuous stirring for 2-3 h. The lower phenolic layer was collected and stored in amber colour glass bottle at 4°C. The sample mixture was centrifuged at 5000 g for 30 min at 4°C. The upper phenolic phase was collected carefully and equal volume of extraction buffer was added to it. The above step was repeated one more time and phenolic phase was re-extracted. Four volumes of ice cold 0.1 M ammonium bicarbonate in methanol was added to the final collected phenolic phase, and incubated overnight at -20°C for protein precipitation. Next day, the samples were centrifuged at 10000 g for 30 min at 4°C. The pellet was washed thrice with ice cold methanol, twice with acetone and air dried for few minutes.

nLC-MS/MS analysis

100 µg of the final pellet was treated with 100 mM DTT for 1 h at 95°C followed by 250 mM iminodiacetic acid (IDA) for 45 min at room temperature in dark. The sample suspension was incubated with trypsin at 37°C for overnight digestion. The trypsin digested peptides were extracted in 0.1% formic acid solution at 37°C for 45 min. The solution was centrifuged at 10000 g and the supernatant was collected in fresh tube for vacuum drying. The final sample was solubilized in 20 μl of 0.1% formic acid. For separation of peptides, 10 μl of injection volume was loaded on C18 UPLC column and peptides separated Waters Synapt G2 Q-TOF for MS and MS/MS analysis.

For LC-MS analysis, 10 μl of sample was injected into ACQUITY UPLC system (Waters, UK) equipped with ACQUITY UPLC BEH C18 column (Waters, UK) (150 mm X 2.1 mm X 1.7 μm), A SYNAPT G2 QTOF (Waters, UK) and an electrospray ionization (ESI) source. The sample

analysis was run on positive mode by applying 3500 V capillary voltage and 30 L cone gas flow per hour. The source and desolvation glass flow was maintained at 1.8 and 800 L per h and the temperatures of source and desolvation were 150°C and 350°C respectively. The protein range was used from 50 Da to 150 Da. The trap and transfer collision energy was maintained constantly at 6 V and the ramp collision energy was set at 20 V and increased up to 45 V. The total acquisition time was 60 min and the solution flow rate was 300 nl/ min. The mobile phase consisted 0.1% formic acid in water (solvent A) and 0.1% formic acid in acetonitrile (solvent B). A linear 60 min gradient consisted: solvent A 98% and solvent B 2% for 1min, solvent A and B 50% for 29 min, solvent A 20% and solvent B 80% for 15 min, followed by 15 min solvent A 98% and solvent B 2%. Wash solution was used at the end of each program to reduce carry-over between samples.

Protein identification

The raw data acquired from the above analysis was processed using PLGS software 3.0.2 (Waters, India, identification and expression algorithm) within which data processing and database search was performed. The source of the sample being *Fabaceae* proteins for 2 samples sequence in FASTA format was downloaded from swiss-prot and used for searching peptides present in samples. On each run, sample was processed using the following search parameters in the software: peptide tolerance 50 ppm, fragment tolerance 100 ppm, min number of fragment matches for peptides 2, minimum number of fragment matches for proteins 5 and carbamidomethylation of cysteine and oxidation of methionine were selected as fixed and variable modifications respectively. Uniprot (*Fabaceae*, reviewed protein) was used as the database against which the search was done.

Gene ontology and bioinformatic analysis

The identified proteins in this study were annotated based on their molecular function, biological process and cellular component with Gene Ontology (GO) annotation by using Uniprot. Hierarchical cluster analysis was performed based on correlation values by using R statistical package. Network analysis was performed by using Cytoscape bioinformatics software version (3.7.2).

Identification of protein by nLC-MS/MS and GO analysis

Roots were harvested carefully from hydroponically grown control and salt (500 mM NaCl) treated plants after 4 days (Figure 1). A total of 1062 differentially expressed proteins (DEPs) were identified in both control and salt treated plants (Table 1). The DEPs of Pongamia showed sequence homology with *Glycine* sp. (22%), *Pisum* sp. (21%) and *Medicago* sp. (10%), followed by other Fabaceae family members (45%) and the sequence search similarity with Uniprot (Universal Protein Resource) database (Figure 2A). Based on relative expression, these proteins (1062 DEPs) were categorized into two groups: commonly expressed DEPs (proteins expressed in both control and salt treated plants; CDEPs) and specifically expressed proteins (unique to control and salt treated plants; SDEPs) (Table 1). Further, these CDEPs were categorized based on fold change (≤ 0.5 or ≥ 2.0 ($p \leq 0.05$)) into three groups: up-, down-regulated and unchanged proteins (Table 1). In Pongamia, most of the proteins belonged to unchanged protein category (82.4%) as their expression levels did not significantly change upon stress exposure, while the percentage of up- and down-regulated proteins were ~7.8 and ~9.8% respectively (Figure 2B). Based on biological and molecular functions (GO analysis), these DEPs were classified into 28 groups belonging to various metabolic pathways including carbohydrates, lipids, amino acids, fatty acids, secondary metabolism, pigment metabolism, seed storage protein, transport protein, photosynthesis, defense responsive proteins, cell cycle, signal transduction, cell wall synthesis, catalytic activity, DNA binding, carboxylic acid biosynthesis, mRNA processing, DNA repair, protease inhibitor, proteolysis, catalytic activity, chaperone, cytoskeleton, growth and developmental process, pathogenesis, replication, transcription and translation regulatory proteins (Table 1).

Primary metabolism

Pongamia roots accumulated a diverse number of proteins related to cell wall synthesis and energy metabolism including FUT1, RGP1, PDC2, isocitrate lyase 1, granule-bound starch synthase 2 (chloroplast origin), and malate dehydrogenase (chloroplast origin) (Figure 6). We observed significant decrease in protein expression levels of ribulose bisphosphate carboxylase large chain (RBL), malate dehydrogenase (MDHC), probable mannitol dehydrogenase (MTDH), sucrose synthase (SUS), glucose-1-phosphate adenylyltransferase small subunit (GLGS) 2, pectinesterase (PME) 3 and polygalacturonase inhibitor (PGIP) 1. The expression levels of 1,4-α-glucan-branching enzyme (GLGB) 1 (chloroplast origin), GLGB 2 (chloroplast origin), α-1,4 glucan phosphorylase-L-isozyme, α-amylase inhibitor (AMYA) 1, LEA2, α-glucan phosphorylase H isozyme, α-mannosidase, β-amylase (AMYB), cyanogenic β-glucosidase, galactinol-sucrose galactosyltransferase (RFS), GLGS 1 (chloroplast origin), glucose-6-phosphate dehydrogenase (G6PD), glyceraldehyde-3-phosphate dehydrogenase (G3P) A (chloroplast origin), G3PB (chloroplast origin), G3PC, glycerol-3-phosphate acyltransferase (PLSB) (chloroplast origin), glycogen synthase kinase-3 homolog (MSK) 1, MSK3, granule-bound starch synthase (SSG) 1, ACEA2, MDHP (chloroplast origin), MDHG (glyoxysomal origin), malate synthase (MAS) Y (glyoxysomal origin), mannan synthase (CSLA) 1, NADP-dependent malic enzyme (MAOX), phosphoenolpyruvate carboxylase (PEP) 1, PEP 2, phosphoglucomutase (PGMP) (chloroplast origin), PGM (mitochondrial origin), MTDH3, probable sucrose-phosphate synthase (SPSA), pyruvate kinase, RBL (isoform of RBL), ribulose bisphosphate carboxylase small chain (RBS) 4, ribulose bisphosphate carboxylase/ oxygenase activase (RCA), ribulose bisphosphate carboxylase/ oxygenase large subunit N-methyltransferase, RuBisCO large subunit-binding protein subunit

α, stachyose synthase, SUS (isoform of SUS), SUS2, UDP-glucose-4-epimerase, UDP-glucose 6-dehydrogenase 1, UDP-glycosyltransferase (UGT2) 2, UGT43, UDP-glycosyltransferase 79B30 (FG3H), UDP-sugar pyrophospharylase (USP) 1,β-fructofuranosidase (cell wall enzyme), β-xylosidase/ α-L-arabinofuranosidase (XYL) 1, XYL 2, bifunctional UDP-glucose-4-epimerase/ UDP-xylose 4-epimerase 1, digalactosyldiacylglycerol synthase 1 (chloroplast origin), PME (isoform of PME), PGIP2, PGIP3, probable ureide permease A3 and xyloglucan endotransglucosylase/ hydrolase 1 were not changed significantly under salinity stress conditions. However, UGT13, UDP-glucose 4-epimerase GEPI48, RBS 1, RUBB, RuBisCO-associated protein, fructose-1,6-bisphosphatase, isocitrate dehydrogenase (IDH) (chloroplast origin), inactive UDP-glycosyltransferase 79A6, IDH, UDP-glycosyltransferase 79A6, non-specific lipid-transfer protein (NLTP) 1, NLTP 2, CASP-like protein (CSPL 4) 2D1, CSPL 5 and digalactosyldiacylglycerol synthase 2 (chloroplast origin) showed significant increase only in roots of salt treated plants.

Proteins associated with amino acid metabolism such as S-adenosylmethionine synthase (METK) and glutamine synthetase were increased significantly, whereas γ-glutamyl hydrolase and adenosylhomocysteinase expression levels were significantly down-regulated under salt stress conditions (Figure 6). Aminomethyltransferase (mitochondria origin), asparagine synthetase [glutamine-hydrolyzing] (ASNS) 1, ASNS 2, δ-1-pyrroline-5-carboxylate synthase (P5CS), glutamate synthase [NADH] (amyloplast origin), glutamate-cysteine ligase (chloroplast origin), glutamine synthetase (GLNA) 1, GLNA 2 (chloroplast origin), GLNA 3, GLNA 4 (chloroplast origin), glycine dehydrogenase (mitochondria origin), methylcrotonoyl-CoA carboxylase subunit α (mitochondria origin), probable 2-isopropylmalate synthase, pyrroline-5-carboxylate reductase, METK (isoform of METK), METK 1, METK 2, serine hydroxymethyltransferase (mitochondria

origin) and threonine dehydratase (chloroplast origin) did not change significantly. Ketol-acid reductoisomerase (chloroplast origin), pyridoxal 5'-phosphate synthase subunit PDX1 (PDX 1), aspartate carbamoyltransferase 1 (chloroplast origin), arginine decarboxylase, isoaspartyl peptidase/ L-asparaginase (ASPG), glutamate-1-semialdehyde-2,1-aminomutase (chloroplast origin), aspartate aminotransferase 1, serine carboxypeptidase-like and ornithine carbamoyltransferase (chloroplast origin) were induced in roots of salt treated plants.

Secondary metabolism and seed storage proteins

Proteins of secondary metabolism such as chalcone synthase (CHS) and isoforms of CHS were significantly enhanced during stress, which include CHS1, CHS2, CHS3, CHS5, CHS6, CHS6-4, CHS7, CHS17/ Y and isoflavone reductase (IFR) (Figures 3 and 4A). There were several isoforms of CHS showing significant decrease included namely CHS1 (isoform of CHS1), CHS2 (isoform of CHS2), CHS4, CHS4-1, CHS5, CHS17/ Y (isoform of CHS17/ Y) and IFR (isoform of IFR) in roots of Pongamia under salt stress (Figure 3). The expression levels of several other chalcone synthases CHS1 (isoform of CHS1), CHS1A, CHS1B, CHS2 (isoform of CHS2), CHS3 (isoform of CHS3), CHS4 (isoform of CHS4), CHS4-2, CHS5 (isoform of CHS5), CHS6 (isoform of CHS6), CHS8, CHS9 and CHS17/ Y (isoform of CHS17/ Y) which remained unchanged during salinity. In addition, Pongamia induced expression of numerous proteins associated with secondary metabolism such as caffeic acid 3-O-methyltransferase (COMT), favin, phenylalanine ammonia lyase (PAL) class 3, NAD(P)H-dependent 6'-deoxychalcone synthase and trans-cinnamate 4-monooxygenase (TCMO) showing down regulation during salt stress. A diverse set of proteins involved in secondary metabolism including 6α-hydroxymaackiain 3-O-methyltransferase (M3OM) 1, M3OM2, 2-hydroxyisoflavanone dehydratase, 2-hydroxyisoflavanone synthase, 4-coumarate-CoA ligase 2, caffeoyl-CoA O-methyltransferase, chalcone-flavonone isomerase

Figure 1. Root morphology of hydroponically grown 30-days old *Pongamia pinnata* seedlings treated with 500 mM NaCl for 4 days (A–C) when compared to corresponding controls.

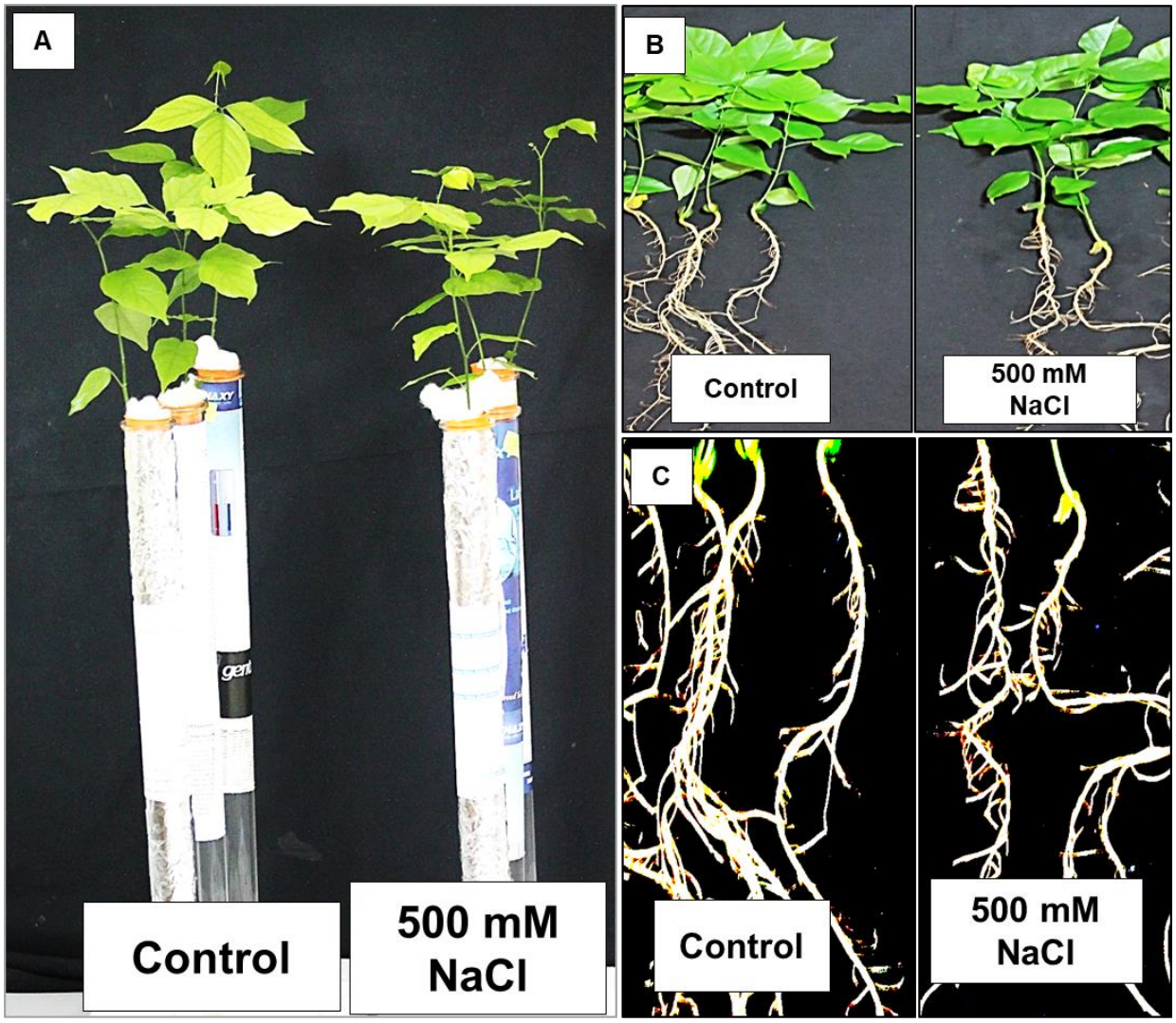
A
Control
500 mM NaCl
B
Control
500 mM NaCl
C
Control
500 mM NaCl

(CFI), CFI1, CFI1A, dihydroflavonol 4-reductase (DFRA), flavonoid 4'-O-methyltransferase, isoflavone 2'-hydroxylase, isoflavone 3'-hydroxylase, isoflavone 4'-O-methyltransferase, isoflavone 7-O-glucosyltransferase 1, IFR (isoform of IFR), isoflavonoid 7-O-beta-apiosyl-glucoside beta-glycosidase, isoliquiritigenin 2'-O-methyltransferase, lactoylglutathione lyase, phenylalanine ammonia lyase (PAL) Y, PAL1, PAL2, putative stilbene synthase 2, TCMO (isoform of TCMO), tricyclene synthase (TPS) 2 (chloroplast origin) and TPS4 (chloroplast origin) maintained expression levels equal to that of controls under salt stress. Isoflavone reductase homolog, naringenin 8-dimethylallyltransferase 2 (chloroplast origin), 2-hydroxyisoflavanone synthase and flavonoid 3-O-glucosyltransferase were significantly induced only in treated roots (abbreviations see in Table 1).

Significant expression of seed storage proteins such as vicilin, legumain, arachin, basic 7S globulin, legumin (LEG) B2, LEG B4, LEG B6, LEG B7, LEG K and LEG J was observed, whereas arcelin (ARC) 5A, ARC5B, and albumin (ALB) 2 expression levels were significantly decreased under salt stress (Figure 4B). Several other seed storage proteins namely ALB2 (isoform of ALB2), allergen Ara h 1 (ALL11), ALL12, β-conglycinin, canavalin, conglutin-β 1 (CONB) 1, CONB2, CONB3, CONB4, CONB5, CONB6, CONB7, convicilin (CVC) A, CVCB, glycinin (GLYG) 1, GLYG 4, GLYG 5, LEGB (isoform of LEGB), phaseolin-α-type, provicilin (VCL) A, VCLB, VCLC, seed biotin-containing protein (SBP65), and sucrose-binding proteins maintained their expression levels unchanged under salinity stress (Figure 5). Notably, proteins such as LEGA2, ALB1D, seed-agglutinin 2, ALB1, ARC1 and phaseolin-β-type showed significant increase only in roots of salt treated plants. Proteins related to saponin metabolism showed significant alterations (Figure 5). Notably, saponins β-amyrin 11-oxidase showed significant

Figure 2. (A) Percentage homology of Pongamia proteins with other related legume species and (B) percentage of differentially expressed proteins.

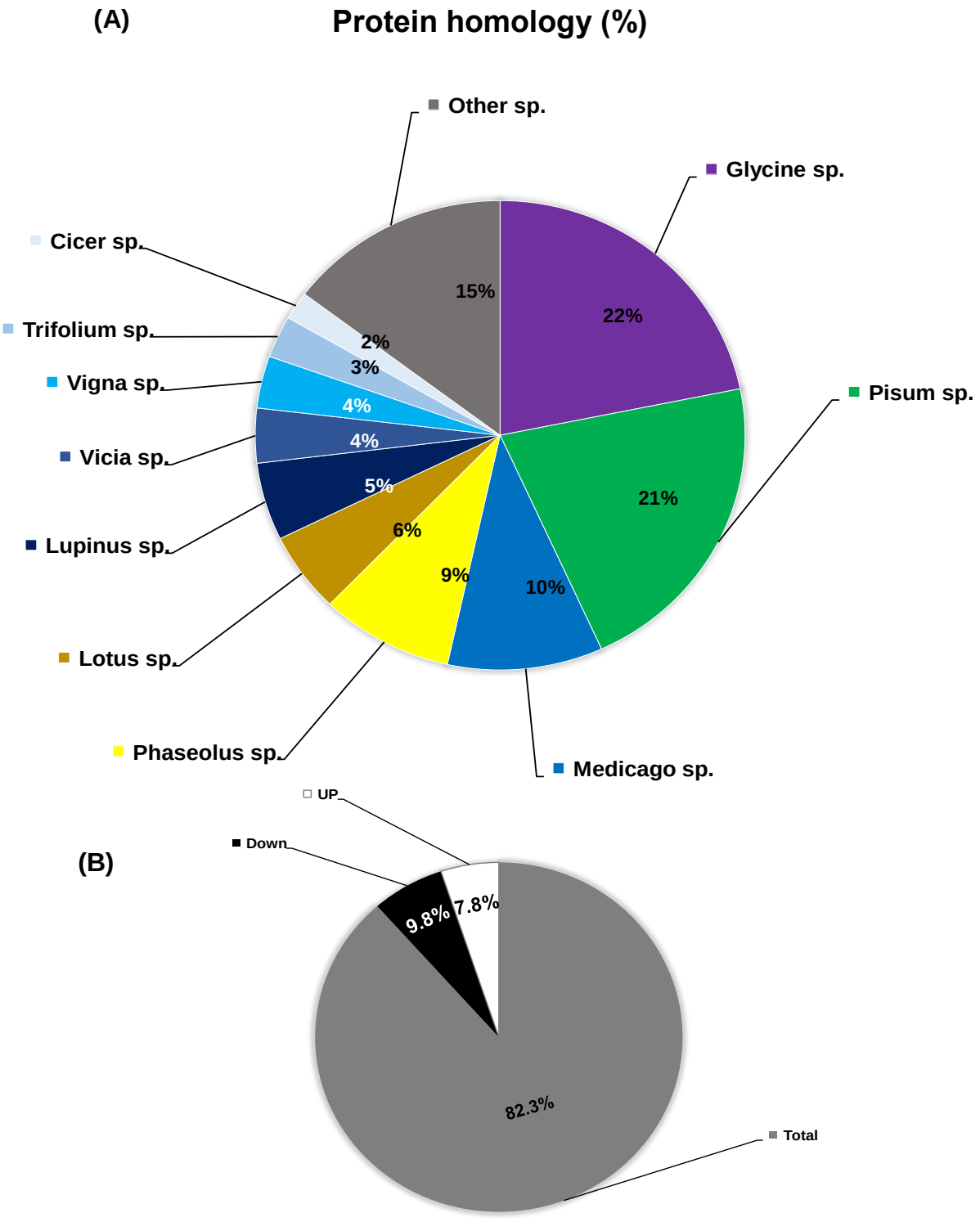
(A)
Protein homology (%)
Other sp.
Glycine sp.
Cicer sp.
Trifolium sp.
Vigna sp.
Vicia sp.
Lupinus sp.
Lotus sp.
Phaseolus sp.
Medicago sp.
Pisum sp.
15%
22%
2%
3%
4%
4%
5%
6%
9%
10%
21%
(B)
UP
Down
9.8%
7.8%
82.3%
Total

increase, whereas β-amyrin synthase (BAMS) and soyasaponin III rhamnosyltransferase decreased with unchanged levels of cycloartenol synthase, β-amyrin synthase (isoform of BAMS), mixed-amyrin synthase, 11-oxo-β-amyrin 30-oxidase (C7263) and soyasapogenol β-glucuronide galactosyltransferase. However, expression of 11-oxo-β-amyrin 30-oxidase (C7254) was significant in roots of salt treated plants.

Hormone metabolism and signal transduction

In response to salt stress, Pongamia enhanced expression levels of ABA-responsive protein (ABR) 18 and auxin-induced protein (IAA) 6 (Figure 7). A significant increase was observed in the levels of serine/ threonine-protein phosphatase catalytic subunit A (PP2A), calcium-dependent protein kinase SK5 and phytochrome-associated serine/ threonine protein phosphatase in roots of Pongamia under salt stress conditions. The expression levels of several proteins associated with hormone metabolism including carotenoid 9, 10 (9', 10') cleavage dioxygenase 1, G2OX1, G2OX2, abscisate β-glucosyltransferase, calmodulin (CALM) 2, guanine nucleotide-binding protein subunit β-like (GBLP) protein and Rac-like GTP-binding (RAC) protein 1 were decreased in roots of salt treated plants when compared to their controls. Conversely, several other proteins which did not change significantly during salt stress include: auxin-induced protein (AUX) 22, AUX 22A, AUX 28, cell division cycle protein 48 homolog (Figures 7 and 8), protein SCARECROW (SCR), OBERON-like protein, glutathione γ-glutamyl-cysteinyltransferase (PCS) 1, PCS 2, 9-cis-epoxycarotenoid dioxygenase NCED1 (chloroplast origin), G3OX, ent-copalyl diphosphate synthase (chloroplast origin), zeatin-O-glucosyltransferase, 1-aminocyclopropane-1-carboxylate synthase (1A1C), primary amine oxidase (AMO), 1-aminocyclopropane-1-carboxylate oxidase (ACCO), serine/ threonine phosphatase (PP1), calcium/ almodulin dependent serine/ threonine-protein kinase DMI-3 (CCAMK), serine/threonine receptor-like

Table 1. List of all proteins expressed in roots of 500 mM NaCl treated Pongamia at 4DAS.

S.No	Accession	Abbreviation	Description	Score	Fold change	P values	GO description
Down-regulated proteins							
1	Q41116	AR5B	Arcelin-5B	118.8	0.00	0.03	Seed storage protein
2	Q42460	AR5A	Arcelin-5A	77.9	0.00	0.04	Seed storage protein
3	Q8MCA4	RK16	50S ribosomal protein L16, chloroplastic	53.0	0.03	0.04	Translation
4	P28002	COMT1	Caffeic acid 3-O-methyltransferase	55.5	0.04	0.01	Secondary metabolism
5	Q5D1B9	MATK	Maturase K	16.9	0.05	0.01	mRNA processing
6	P48724	IF5	Eukaryotic translation initiation factor 5	57.6	0.05	0.02	Translation
7	Q85XY8	MATK	Maturase K	29.1	0.05	0.05	mRNA processing
8	P02237	LGC3	Leghemoglobin C3	8.3	0.09	0.02	Nodulation
9	O24035	PANC	Pantoate-β-alanine ligase	28.4	0.16	0.04	Cofactor biosynthesis
10	D4AEP7	ALB2	Albumin-2	115.3	0.16	0.04	Seed storage protein
11	Q2PMP8	RK16	50S ribosomal protein L16, chloroplastic	53.0	0.16	0.03	Translation
12	P46417	GSTX3	Glutathione S-transferase 3	26.8	0.18	0.01	Redox homeostasis
13	P26585	HMGL	HMG1/2-like protein	73.7	0.18	0.02	DNA binding
14	Q8LP17	CCD1	Carotenoid 9,10(9',10')-cleavage dioxygenase 1	110.2	0.19	0.05	Hormone metabolism
15	O23884	CHS5	Chalcone synthase 5	34.8	0.21	0.02	Secondary metabolism
16	Q10370	HMGYB	HMG-Y-related protein B (Fragment)	377.2	0.21	0.03	DNA binding
17	O23882	CHS4	Chalcone synthase 4	34.8	0.21	0.01	Secondary metabolism
18	P93164	GGH	γ-glutamyl hydrolase	71.9	0.21	0.02	Amino acid metabolism
19	P02235	LGC1	Leghemoglobin C1	8.3	0.22	0.01	Nodulation
20	P51084	CHS2	Chalcone synthase 2	34.8	0.22	0.05	Secondary metabolism
21	P02871	LEC	Favin	213.3	0.22	0.03	Secondary metabolism
22	P51077	CHS4-1	Chalcone synthase 4-1	34.8	0.23	0.04	Secondary metabolism
23	P49440	CHSY	Chalcone synthase 17	28.3	0.23	0.01	Secondary metabolism
24	O81971	C71D9	Cytochrome P450 71D9	22.5	0.23	0.01	Monooxygenase
25	Q9SML4	CHS1	Chalcone synthase 1	60.6	0.24	0.03	Secondary metabolism
26	P18663	RK2A	50S ribosomal protein L2-A	74.3	0.24	0.01	Translation
27	P30073	CHS1	Chalcone synthase 1	34.8	0.24	0.05	Secondary metabolism
28	Q00423	HMGYA	HMG-Y-related protein A	365.7	0.27	0.02	DNA binding
29	P52417	GLGS2	Glucose-1-phosphate adenylyltransferase small subunit 2	51.7	0.27	0.05	Carbohydrate metabolism
30	Q9B1H9	RK2	50S ribosomal protein L2	74.3	0.27	0.01	Translation
31	A4GGF8	RK2	50S ribosomal protein L2	135.7	0.27	0.02	Translation
32	Q8LVH2	RK2	50S ribosomal protein L2	143.8	0.28	0.03	Translation
33	O48905	MDHC	Malate dehydrogenase, cytoplasmic	45.8	0.29	0.03	Carbohydrate metabolism
34	Q01286	CHS1	Chalcone synthase 1	34.8	0.30	0.05	Secondary metabolism
35	P01071	ITRB	Trypsin inhibitor B	97.0	0.30	0.05	Protease inhibitor
36	Q96453	1433D	14-3-3-like protein D	62.2	0.31	0.01	Defense response
37	P51089	CHSY	Chalcone synthase	28.3	0.31	0.01	Secondary metabolism
38	O62964	RBL	Ribulose bisphosphate carboxylase large chain	6.8	0.32	0.04	Carbohydrate metabolism
39	A7VLV2	non-SGRW	Non-functional protein STAY-GREEN	126.5	0.33	0.03	Photosynthesis
40	Q2PMV0	ATPB	ATP synthase subunit β, chloroplastic	74.0	0.33	0.04	Electron transport
41	O20304	RBL	Ribulose bisphosphate carboxylase large chain (Fragment)	41.2	0.33	0.01	Carbohydrate metabolism
42	P42654	1433B	14-3-3-like protein B	59.6	0.34	0.03	Photosynthesis
43	A7VLV1	SGRW	Protein STAY-GREEN, chloroplastic	126.5	0.35	0.05	Saponin biosynthesis
44	D4Q9Z5	SGT3	Soyasaponin III rhamnosyltransferase	13.3	0.35	0.04	Defense response
45	Q96452	1433C	14-3-3-like protein C	88.0	0.36	0.03	Monooxygenase
46	P93149	C93B1	Licodione synthase	29.1	0.36	0.02	Secondary metabolism
47	P52576	IFR	Isoflavone reductase	69.3	0.37	0.04	Hormone metabolism
48	B5WWZ9	FAO2	Long-chain-alcohol oxidase FAO2	95.6	0.38	0.02	Hormone metabolism
49	Q9SQ80	G2OX1	Gibberellin 2-β-dioxygenase 1	103.9	0.39	0.04	Signal transduction
50	Q39836	GBLP	Guanine nucleotide-binding protein subunit β-like protein	139.7	0.40	0.01	Carbohydrate metabolism
51	A4GG89	RBL	Ribulose bisphosphate carboxylase large chain	32.5	0.40	0.05	Fatty acid metabolism
52	Q42783	BCCP	Biotin carboxyl carrier protein of acetyl-CoA carboxylase, chloroplastic	79.7	0.41	0.04	Electron transport
53	P28552	ATPG	ATP synthase γ chain, chloroplastic	24.2	0.41	0.05	Translation
54	Q2PMM3	RK2B	50S ribosomal protein L2-B, chloroplastic	75.8	0.41	0.04	Carbohydrate metabolism
55	O62943	RBL	Ribulose bisphosphate carboxylase large chain	56.8	0.42	0.04	Signal tranduction
56	P62163	CALM2	Calmodulin-2	33.6	0.42	0.03	Cell wall synthesis
57	Q43111	PME3	Pectinesterase 3	64.7	0.43	0.04	Fatty acid metabolism
58	Q8W3P8	AOG	Abscisate β-glucosyltransferase	214.1	0.44	0.02	Saponin biosynthesis
59	Q9LRH8	BAMS	β-Amyrin synthase	38.7	0.44	0.04	Secondary metabolism
60	P19143	PAL3	Phenylalanine ammonia-lyase class 3	102.3	0.44	0.04	Electron transport
61	A4GG90	ATPB	ATP synthase subunit β, chloroplastic	9.2	0.44	0.05	Secondary metabolism
62	P26690	6DCS	NAD(P)H-dependent 6'-deoxychalcone synthase	35.7	0.44	0.05	Cell wall synthesis
63	P35334	PGIP1	Polygalacturonase inhibitor 1	74.5	0.45	0.04	Electron transport
64	P05037	ATPB	ATP synthase subunit β, chloroplastic	15.2	0.45	0.02	Secondary metabolism
65	I1L3T1	708D1	UDP-glycosyltransferase 708D1	22.5	0.45	0.03	Hormone metabolism
66	Q9XHM5	G2OX2	Gibberellin 2-β-dioxygenase 2	43.7	0.46	0.05	Carbohydrate metabolism

67	O82515	MTDH	Probable mannitol dehydrogenase	102.9	0.46	0.03	Signal transduction
68	O04369	RAC1	Rac-like GTP-binding protein RAC1	22.0	0.48	0.05	Carbohydrate metabolism
69	Q01390	SUS	Sucrose synthase	57.4	0.48	0.01	Secondary metabolism
70	Q42797	TCMO	Trans-cinnamate 4-monooxygenase	44.2	0.48	0.02	Electron transport
71	Q9TKI7	ATPB	ATP synthase subunit β, chloroplastic	23.4	0.48	0.03	Amino acid metabolism
72	P50246	SAHH	Adenosylhomocysteinase	53.1	0.49	0.01	Nodulation
73	P10816	LGB3	Leghemoglobin 3	14.9	0.50	0.03	Transport
			Unchanged protein				
74	P04991	RBL	Ribulose bisphosphate carboxylase large chain	138.5	0.50	0.1	Carbohydrate metabolism
75	P49093	ASNS2	Asparagine synthetase [glutamine-hydrolyzing] 2	165.7	0.51	0.3	Amino acid metabolism
76	Q40357	NO10	Early nodulin-10	43.6	0.52	0.2	Nodulation
77	P49092	ASNS1	Asparagine synthetase [glutamine-hydrolyzing] 1	11.8	0.52	0.5	Amino acid metabolism
78	F5B8W1	CONB3	Conglutin β 3	95.6	0.52	0.5	Seed storage protein
79	Q9BBU1	RBL	Ribulose bisphosphate carboxylase large chain	36.6	0.53	0.3	Carbohydrate metabolism
80	A4GG84	RR3	30S ribosomal protein S3, chloroplastic	116.1	0.53	0.1	Translation
81	Q5QGZ8	NRL4A	Bifunctional nitrilase/nitrile hydratase NIT4A	52.8	0.54	0.4	Catalytic activity
82	P31926	SUS	Sucrose synthase	34.6	0.54	0.1	Carbohydrate metabolism
83	P29530	OLEO1	P24 oleosin isoform A	44.6	0.54	0.1	Growth and development
84	P09886	HS21C	Small heat shock protein, chloroplastic	202.5	0.54	0.2	Chaperone
85	P43237	ALL11	Allergen Ara h 1, clone P17	23.0	0.55	0.4	Seed storage protein
86	Q42808	TBP	TATA-box-binding protein	109.7	0.55	0.1	DNA binding
87	Q04672	SBP	Sucrose-binding protein	98.7	0.55	0.5	Seed storage protein
88	O63094	RBL	Ribulose bisphosphate carboxylase large chain	36.6	0.55	0.5	Carbohydrate metabolism
89	P02854	VCLB	Provicilin (Fragment)	63.3	0.55	0.2	Seed storage protein
90	Q9BBP6	NU5C	NAD(P)H-quinone oxidoreductase subunit 5, chloroplastic	102.0	0.55	0.4	Electron transport
91	A4GGB9	CYF	Cytochrome f	93.9	0.55	0.2	Electron transport
92	Q41121	NO30	Nodulin-30	217.3	0.55	0.4	Nodulation
93	Q5W915	USP	UDP-sugar pyrophospharylase	63.1	0.55	0.1	Carbohydrate metabolism
94	A0A109QYD3	RMS3	Strigolactone esterase RMS3	110.8	0.55	0.4	Defense response
95	P18823	ACCD	Acetyl-coenzyme A carboxylase carboxyl transferase subunit β, chloroplastic	55.3	0.57	0.2	Fatty acid biosynthesis
96	P48490	PP1	Serine/threonine-protein phosphatase PP1	19.2	0.57	0.2	Signal transduction
97	O48901	DPOD1	DNA polymerase δ catalytic subunit	112.0	0.57	0.3	Replication
98	P83594	IFXA	Factor Xa inhibitor BuXI	169.6	0.58	0.1	Protease inhibitor
99	Q6WNR0	C81E7	Isoflavone 2'-hydroxylase	69.1	0.59	0.4	Secondary metabolism
100	P27456	GSHRP	Glutathione reductase, chloroplastic/ mitochondrial	43.4	0.59	0.1	Redox homeostasis
101	Q40987	LECR	Nodule lectin	291.4	0.59	0.5	Nodulation
102	P11728	NO75	Early nodulin-75 (Fragment)	1382.1	0.59	0.1	Nodulation
103	Q5YJU6	MATK	Maturase K	23.6	0.59	0.4	mRNA processing
104	O49885	RL13A	60S ribosomal protein L13a	144.4	0.60	0.4	Translation
105	P25011	CCNB1	G2/mitotic-specific cyclin S13-6	116.6	0.60	0.4	Cell cycle
106	Q6E2Z6	REHY	1-Cys peroxiredoxin	51.0	0.61	0.1	Redox homeostasis
107	Q5H873	HLTT	13-hydroxylupanine O-tigloyltransferase	6.0	0.61	0.2	Alkaloid biosynthesis
108	A6BM07	I7GT1	Isoflavone 7-O-glucosyltransferase 1	157.4	0.61	0.5	Secondary metabolism
109	P37228	MDHG	Malate dehydrogenase, glyoxysomal	163.0	0.61	0.5	Carbohydrate metabolism
110	Q9BBR8	CYF	Cytochrome f	108.4	0.61	0.5	Electron transport
111	Q9AWB2	SIR	Sulfite reductase [ferredoxin], chloroplastic (Fragment)	66.2	0.61	0.2	Replication
112	Q8MCJ4	MATK	Maturase K	30.8	0.62	0.2	mRNA processing
113	Q9BBU0	ATPB	ATP synthase subunit β, chloroplastic	75.4	0.62	0.1	Transport
114	Q43715	TOC75	Protein TOC75, chloroplastic	60.7	0.63	0.4	Transport
115	Q5YK47	MATK	Maturase K	34.5	0.63	0.5	mRNA processing
116	P14594	LEGB	Legumin B (Fragment)	49.4	0.63	0.3	Seed storage protein
117	O81980	CFI1	Chalcone-flavonone isomerase 1 (Fragment)	7.1	0.63	0.1	Secondary metabolism
118	P25698	EF1A	Elongation factor 1-α	95.4	0.63	0.4	Translation
119	Q94IR2	CCD1	Carotenoid 9,10 (9',10')-cleavage dioxygenase 1	174.9	0.63	0.4	Secondary metabolism
120	P49347	CONB	Concanavalin B	58.2	0.64	0.2	Carbohydrate metabolism
121	P93471	COP1	E3 ubiquitin-protein ligase COP1	51.0	0.64	0.4	Protein modification
122	Q96423	TCMO	Trans-Cinnamate 4-monooxygenase	89.8	0.64	0.3	Secondary metabolism
123	Q9FZL4	MGDG	Probable monogalactosyldiacylglycerol synthase, chloroplastic	99.8	0.66	0.3	Lipid metabolism
124	P51139	MSK3	Glycogen synthase kinase-3 homolog MsK-3	186.1	0.66	0.5	Signal transduction
125	Q6J540	C79D4	Isoleucine N-monooxygenase 2	66.2	0.66	0.3	Secondary metabolism
126	Q07185	AOX1	Ubiquinol oxidase 1, mitochondrial	63.4	0.67	0.4	Electron transport
127	Q41266	AOX2	Ubiquinol oxidase 2, mitochondrial	48.0	0.67	0.1	Electron transport
128	O65015	AMYB	β-Amylase	122.3	0.67	0.5	Carbohydrate metabolism
129	F5B8W5	CONB7	Conglutin β 7	65.7	0.67	0.1	Seed storage protein
130	Q41008	ACCA	Acetyl-coenzyme A carboxylase carboxyl transferase subunit α, chloroplastic	47.4	0.67	0.4	Fatty acid biosynthesis
131	P58822	PGIP2	Polygalacturonase inhibitor 2	74.5	0.68	0.1	Cell wall synthesis
132	Q40316	VESTR	Vestitone reductase	110.0	0.68	0.5	Defense response
133	P58823	PGIP3	Polygalacturonase inhibitor 3	26.7	0.68	0.2	Cell wall synthesis
134	Q42919	G6PD	Glucose-6-phosphate 1-dehydrogenase, cytoplasmic isoform	40.4	0.68	0.5	Carbohydrate metabolism
135	P32646	COX2	Cytochrome c oxidase subunit 2, mitochondrial (Fragment)	89.6	0.68	0.2	Electron transport
136	Q1W376	PMM	Phosphomannomutase	41.3	0.68	0.1	Carbohydrate metabolism
137	P05311	PSAB	Photosystem I P700 chlorophyll a apoprotein A2	17.3	0.68	0.1	Photosynthesis
138	P27066	RBL	Ribulose bisphosphate carboxylase large chain	36.6	0.68	0.4	Carbohydrate metabolism
139	P02873	LEA1	α-Amylase inhibitor 1	18.7	0.68	0.4	Carbohydrate metabolism
140	Q2TE74	PCS2	Glutathione γ-glutamylcysteinyltransferase 2	35.4	0.69	0.5	Hormone metabolism
141	P12628	MAOX	NADP-dependent malic enzyme	25.9	0.69	0.5	Carbohydrate metabolism

142	Q43876	SPSA	Probable sucrose-phosphate synthase	73.5	0.69	0.2	Carbohydrate metabolism
143	P92397	RBL	Ribulose bisphosphate carboxylase large chain (Fragment)	115.1	0.69	0.4	Carbohydrate metabolism
144	Q8MCR7	MATK	Maturase K	26.3	0.70	0.3	mRNA processing
145	O04235	SSRP1	FACT complex subunit SSRP1	87.1	0.70	0.3	DNA Repair
146	P93324	CHOMT	Isoliquiritigenin 2'-O-methyltransferase	34.1	0.70	0.1	Secondary metabolism
147	Q43092	SSG1	Granule-bound starch synthase 1, chloroplastic/ amyloplastic	148.5	0.70	0.3	Carbohydrate metabolism
148	D2XNR0	FLOT3	Flotillin-like protein 3	48.1	0.70	0.4	Defense response
149	P19251	ASNS1	Asparagine synthetase, nodule [glutamine-hydrolyzing]	113.4	0.72	0.2	Amino acid metabolism
150	P69589	RBL	Ribulose bisphosphate carboxylase large chain (Fragment)	115.1	0.72	0.5	Carbohydrate metabolism
151	Q42798	C93A1	3,9-dihydroxypterocarpan 6α-monooxygenase	110.9	0.72	0.1	Defense response
152	O04862	FOLM	Folate synthesis bifunctional protein, mitochondrial	109.1	0.72	0.2	Nucleotide metabolism
153	Q6RET7	CCAMK	Calcium and calcium/ calmodulin-dependent serine/threonine-protein kinase DMI-3	55.4	0.73	0.1	Signal transduction
154	Q2TSC7	PCS1	Glutathione γ-glutamylcysteinyltransferase 1	6.2	0.73	0.4	Hormone metabolism
155	P13915	CVCA	Convicilin	57.2	0.73	0.1	Seed storage protein
156	Q8MCA5	RR3	30S ribosomal protein S3, chloroplastic	101.2	0.73	0.5	Translation
157	Q9BBN7	RR15	30S ribosomal protein S15, chloroplastic	67.5	0.73	0.5	Translation
158	Q0GXS4	NFP	Serine/threonine receptor-like kinase NFP	123.6	0.73	0.5	Signal transduction
159	P06669	CYF	Cytochrome f	291.8	0.73	0.2	Electron transport
160	P49161	CYF	Cytochrome f	24.0	0.74	0.4	Electron transport
161	B5LMP9	PSBB	Photosystem II CP47 reaction center protein	58.7	0.74	0.3	Photosynthesis
162	Q9TKP6	MATK	Maturase K	50.1	0.74	0.3	mRNA processing
163	O24301	SUS2	Sucrose synthase 2	93.3	0.75	0.5	Carbohydrate metabolism
164	Q2PMP7	RR3	30S ribosomal protein S3, chloroplastic	139.1	0.75	0.5	Translation
165	P69572	RBL	Ribulose bisphosphate carboxylase large chain (Fragment)	115.1	0.75	0.5	Carbohydrate metabolism
166	Q5YK03	MATK	Maturase K	23.8	0.75	0.1	mRNA processing
167	P46277	CCNB1	G2/ mitotic-specific cyclin-1	18.2	0.76	0.3	Cell cycle
168	P28553	CRTI	Phytoene dehydrogenase, chloroplastic/ chromoplastic	65.3	0.76	0.2	Pigment Metabolism
169	O24509	INVA	Acid β-fructofuranosidase	46.4	0.76	0.4	Carbohydrate metabolism
170	P69591	RBL	Ribulose bisphosphate carboxylase large chain (Fragment)	115.1	0.76	0.3	Carbohydrate metabolism
171	P13708	SUS	Sucrose synthase	50.7	0.76	0.3	Carbohydrate metabolism
172	Q42777	MCCA	Methylcrotonoyl-CoA carboxylase subunit α, mitochondrial	59.4	0.76	0.5	Amino acid metabolism
173	O81973	C93A3	Cytochrome P450 93A3	38.7	0.76	0.5	Monooxygenase
174	B3EWQ9	LECA2	Lectin α chain	231.2	0.76	0.3	Carbohydrate binding
175	Q8MCM4	MATK	Maturase K	68.6	0.76	0.2	mRNA processing
176	Q93XE6	CFI1A	Chalcone-flavonone isomerase 1A	112.3	0.76	0.5	Secondary metabolism
177	P10933	FENR	Ferredoxin--NADP reductase, leaf isozyme, chloroplastic	79.6	0.76	0.4	Photosynthesis
178	P30124	HEM2	δ-aminolevulinic acid dehydratase, chloroplastic (Fragment)	31.2	0.76	0.5	Pigment Metabolism
179	P34811	EFGC1	Elongation factor G-1, chloroplastic	80.2	0.76	0.3	Translation
180	P69584	RBL	Ribulose bisphosphate carboxylase large chain (Fragment)	115.1	0.76	0.3	Carbohydrate metabolism
181	Q42807	STAD	Stearoyl-[acyl-carrier-protein] 9-desaturase, chloroplastic	297.6	0.76	0.3	Lipid metabolism
182	P12859	G3PB	Glyceraldehyde-3-phosphate dehydrogenase B, chloroplastic	72.8	0.77	0.5	Carbohydrate metabolism
183	P41346	FENR	Ferredoxin-NADP reductase, chloroplastic	143.6	0.77	0.3	Photosynthesis
184	A4GGD1	PSBB	Photosystem II CP47 reaction center protein	34.5	0.77	0.2	Photosynthesis
185	Q5YK50	MATK	Maturase K	44.5	0.77	0.1	mRNA processing
186	Q4VYC8	NSP1	Nodulation-signaling pathway 1 protein	103.2	0.77	0.1	Nodulation
187	P04347	GLYG5	Glycinin	53.0	0.78	0.4	Seed storage protein
188	P29001	INVA	Acid β-fructofuranosidase	62.9	0.78	0.3	Carbohydrate metabolism
189	P45458	MASY	Malate synthase, glyoxysomal (Fragment)	42.1	0.78	0.1	Carbohydrate metabolism
190	Q9BBS1	ACCD	Acetyl-coenzyme A carboxylase carboxyl transferase subunit β, chloroplastic	83.6	0.78	0.5	Fatty acid biosynthesis
191	Q43067	TCMO	Trans-cinnamate 4-monooxygenase	46.5	0.78	0.1	Secondary metabolism
192	I1K0K6	EFGC2	Elongation factor G-2, chloroplastic	75.5	0.78	0.3	Translation
193	F5B8W3	CONB5	Conglutin β 5	67.6	0.78	0.5	Seed storage protein
194	Q5YK01	MATK	Maturase K	4.9	0.78	0.4	mRNA processing
195	A3RF67	BAGBG	Isoflavonoid 7-O-β-apiosyl-glucoside β-glycosidase	77.5	0.78	0.5	Secondary metabolism
196	Q2PMU3	PSAB	Photosystem I P700 chlorophyll a apoprotein A1	79.6	0.79	0.3	Photosynthesis
197	P93998	RBL	Ribulose bisphosphate carboxylase large chain (Fragment)	38.7	0.79	0.2	Carbohydrate metabolism
198	P24099	GLNA1	Glutamine synthetase cytosolic isozyme 1	20.9	0.79	0.2	Amino acid metabolism
199	P53536	PHSL	α-1,4 Glucan phosphorylase L isozyme, chloroplastic/ amyloplastic	120.6	0.79	0.1	Carbohydrate metabolism
200	A4GG97	PSAA	Photosystem I P700 chlorophyll a apoprotein A1	79.6	0.79	0.5	Photosynthesis
201	Q8MCR8	MATK	Maturase K	73.0	0.79	0.3	mRNA processing
202	P46280	EFTU2	Elongation factor Tu, chloroplastic	28.2	0.79	0.3	Translation
203	Q01861	PAL1	Phenylalanine ammonia-lyase 1	87.9	0.79	0.3	Secondary metabolism
204	P05310	PSAA	Photosystem I P700 chlorophyll a apoprotein A1	95.2	0.79	0.1	Photosynthesis
205	P08281	GLNA2	Glutamine synthetase leaf isozyme, chloroplastic	14.8	0.79	0.2	Amino acid metabolism
206	P69579	RBL	Ribulose bisphosphate carboxylase large chain (Fragment)	115.1	0.79	0.3	Carbohydrate metabolism
207	Q40983	SPP	Stromal processing peptidase, chloroplastic	63.4	0.79	0.3	Proteolysis
208	Q9MUK5	TOC64	Translocon at the outer membrane of chloroplasts 64	121.3	0.79	0.2	Transport
209	O04279	GPA2	Guanine nucleotide-binding protein α-2 subunit	43.2	0.79	0.1	Signal transduction
210	O65194	RBS	Ribulose bisphosphate carboxylase small chain, chloroplastic	23.1	0.80	0.5	Carbohydrate metabolism
211	P13918	VCLC	Vicilin	94.2	0.80	0.4	Seed storage protein
212	Q9SM60	PGMC	Phosphoglucomutase, cytoplasmic	131.3	0.80	0.5	Carbohydrate metabolism
213	Q9BBP8	RR3	30S ribosomal protein S3, chloroplastic	78.8	0.80	0.1	Translation
214	Q43056	CFI	Chalcone-flavonone isomerase	68.2	0.80	0.5	Secondary metabolism
215	O49817	LEA2	Late embryogenesis abundant protein 2	74.4	0.80	0.4	Defense response

216	P46258	ACT3	Actin-3	92.2	0.81	0.5	Cytoskeleton
217	P27480	LOXA	Linoleate 9S-lipoxygenase 1	31.9	0.81	0.5	Fatty acid biosynthesis
218	Q5YJX4	MATK	Maturase K	12.8	0.81	0.2	mRNA processing
219	P69580	RBL	Ribulose bisphosphate carboxylase large chain (Fragment)	115.1	0.81	0.1	Carbohydrate metabolism
220	P49364	GCST	Aminomethyltransferase, mitochondrial	76.5	0.81	0.5	Amino acid metabolism
221	P86349	EFGC	Elongation factor G, chloroplastic (Fragments)	56.0	0.81	0.5	Translation
222	O48921	C97B2	Cytochrome P450 97B2, chloroplastic	237.0	0.81	0.5	Monooxygenase
223	Q9SWB4	PARP3	Poly [ADP-ribose] polymerase 3	42.7	0.82	0.1	Transcription
224	Q8MCM9	MATK	Maturase K	24.9	0.82	0.3	mRNA processing
225	P19252	ASNS2	Asparagine synthetase, root [glutamine-hydrolyzing]	137.0	0.82	0.2	Amino acid metabolism
226	Q6TND0	MATK	Maturase K	110.6	0.82	0.1	mRNA processing
227	Q9BBS3	ATPA	ATP synthase subunit α, chloroplastic	38.3	0.82	0.4	Transport
228	Q9M6E8	NCED1	9-cis-epoxycarotenoid dioxygenase NCED1, chloroplastic	50.8	0.82	0.4	Hormone metabolism
229	P26205	BGLT	Cyanogenic β-glucosidase (Fragment)	38.9	0.82	0.5	Carbohydrate metabolism
230	P31163	RK2	50S ribosomal protein L2, chloroplastic	82.3	0.82	0.2	Translation
231	Q41062	SECA	Protein translocase subunit SecA, chloroplastic	78.4	0.82	0.2	Transport
232	Q41060	SBP65	Seed biotin-containing protein SBP65	96.9	0.82	0.1	Seed storage protein
233	Q8MCJ5	MATK	Maturase K	39.7	0.83	0.3	mRNA processing
234	Q9SM59	PGMP	Phosphoglucomutase, chloroplastic	203.4	0.83	0.5	Carbohydrate metabolism
235	A4GGA5	RPOB	DNA-directed RNA polymerase subunit β	82.3	0.83	0.4	Transcription
236	Q9M6E9	AGGL	Agglutinin-1	171.2	0.83	0.3	Carbohydrate binding
237	Q5YJX3	MATK	Maturase K	22.9	0.83	0.2	mRNA processing
238	P34922	G3PC	Glyceraldehyde-3-phosphate dehydrogenase, cytosolic	91.0	0.84	0.1	Carbohydrate metabolism
239	O48560	CATA3	Catalase-3	25.2	0.84	0.5	Redox homeostasis
240	Q9TK08	MATK	Maturase K	138.0	0.84	0.4	mRNA processing
241	C6L7U1	LIN1	Putative E3 ubiquitin-protein ligase LIN-1	123.8	0.84	0.5	Protein modification
242	P42348	PI3K2	Phosphatidylinositol 3-kinase, nodule isoform	88.7	0.84	0.3	Lipid metabolism
243	Q04903	FNTB	Protein farnesyltransferase subunit β	70.7	0.84	0.2	Lipid metabolism
244	O48665	LGB5	Leghemoglobin Lb120-29	191.8	0.84	0.3	Nodulation
245	P29756	CATA1	Catalase-1/2	23.5	0.84	0.2	Redox homeostasis
246	Q8MCN3	MATK	Maturase K	53.7	0.84	0.4	mRNA processing
247	Q2PMT9	PSBC	Photosystem II CP43 reaction center protein	66.1	0.84	0.1	Photosynthesis
248	P45457	ACEA2	Isocitrate lyase 2 (Fragment)	70.5	0.84	0.5	Carbohydrate metabolism
249	Q9TKP0	MATK	Maturase K	157.5	0.84	0.3	mRNA processing
250	Q75NZ0	SIR	Sulfite reductase [ferredoxin], chloroplastic	64.3	0.85	0.4	Replication
251	P93673	PHYA	Phytochrome type A	31.2	0.85	0.1	Signal transduction
252	Q5YJU0	MATK	Maturase K	43.0	0.85	0.4	mRNA processing
253	P04776	GLYG1	Glycinin G1	72.1	0.85	0.2	Seed storage protein
254	P13088	AUX22	Auxin-induced protein AUX22	87.8	0.85	0.1	Growth and development
255	Q8MCR6	MATK	Maturase K	28.5	0.86	0.4	mRNA processing
256	Q2PMQ9	PSBB	Photosystem II CP47 reaction center protein	84.6	0.86	0.4	Photosynthesis
257	Q02909	CAPP1	Phosphoenolpyruvate carboxylase, housekeeping isozyme	41.2	0.86	0.1	Carbohydrate metabolism
258	Q9AU12	CAPP	Phosphoenolpyruvate carboxylase	45.6	0.86	0.5	Carbohydrate metabolism
259	P00155	CYF	Cytochrome f	48.4	0.86	0.3	Electron transport
260	A0A0G4DBR5	FG3H	UDP-glycosyltransferase 79B30	12.2	0.87	0.5	Carbohydrate metabolism
261	P24459	ATPAM	ATP synthase subunit α, mitochondrial	103.9	0.87	0.4	Transport
262	Q672F7	TPS2	Tricyclene synthase EBOS, chloroplastic	25.1	0.87	0.2	Secondary metabolism
263	D1FP53	LIN	Putative E3 ubiquitin-protein ligase LIN	118.8	0.87	0.2	Protein modification
264	P37116	NCPR	NADPH-cytochrome P450 reductase	80.5	0.87	0.4	Electron transport
265	P15231	PHAM	Leucoagglutinating phytohemagglutinin	90.0	0.87	0.2	Defense response
266	Q9TKI5	MATK	Maturase K	23.5	0.87	0.4	mRNA processing
267	Q8MCR5	MATK	Maturase K	28.5	0.88	0.1	mRNA processing
268	O24648	G3OX	Gibberellin 3-β-dioxygenase 1	128.9	0.88	0.5	Hormone metabolism
269	P43238	ALL12	Allergen Ara h 1, clone P41B	9.7	0.88	0.4	Seed storage protein
270	Q9SPB1	LEGRE	Leghemoglobin reductase	41.0	0.88	0.1	Nodulation
271	K7LC65	DAT1C	Diacylglycerol O-acyltransferase 1C	30.9	0.88	0.1	Lipid metabolism
272	Q9BBT1	PSBC	Photosystem II CP43 reaction center protein	66.1	0.88	0.2	Photosynthesis
273	P55195	PUR6	Phosphoribosylaminoimidazole carboxylase, chloroplastic (Fragment)	53.3	0.88	0.4	Nucleotide metabolism
274	P13548	VATA	V-type proton ATPase catalytic subunit A	135.0	0.88	0.2	Transport
275	P37114	TCMO	Trans-cinnamate 4-monooxygenase	67.4	0.88	0.1	Secondary metabolism
276	P51061	CAPP2	Phosphoenolpyruvate carboxylase	38.4	0.88	0.4	Carbohydrate metabolism
277	Q5YJU7	MATK	Maturase K	47.1	0.88	0.3	mRNA processing
278	Q5YK53	MATK	Maturase K	22.9	0.88	0.2	mRNA processing
279	P34799	URIC2	Uricase-2 isozyme 2	15.5	0.88	0.5	Nodulation
280	P31165	RK15	50S ribosomal protein L15, chloroplastic (Fragment)	44.4	0.88	0.5	Translation
281	P06006	PSBD	Photosystem II D2 protein	512.7	0.88	0.2	Photosynthesis
282	Q6E4Q8	MATK	Maturase K	92.0	0.88	0.3	mRNA processing
283	Q9GI85	MATK	Maturase K	81.2	0.88	0.5	mRNA processing
284	A0A072VMJ3	CN15C	Protein CNGC15c	44.1	0.88	0.3	Transport
285	Q02028	HSP7S	Stromal 70 kDa heat shock-related protein, chloroplastic	58.3	0.89	0.2	Chaperone
286	Q9SMJ4	LEG	Legumin	88.8	0.89	0.1	Seed storage protein
287	O24303	TI110	Protein TIC110, chloroplastic	110.7	0.89	0.3	Transport
288	Q8MCL7	MATK	Maturase K	102.9	0.89	0.5	mRNA processing
289	P54774	CDC48	Cell division cycle protein 48 homolog	70.0	0.89	0.4	Growth and development
290	Q6Q7X3	MATK	Maturase K	95.8	0.89	0.3	mRNA processing
291	D1FP57	LIN2	Putative E3 ubiquitin-protein ligase LIN-2	74.5	0.89	0.4	Protein modification
292	A4GGA1	PSBC	Photosystem II CP43 reaction center protein	66.1	0.89	0.4	Photosynthesis
293	Q42899	GLNA1	Glutamine synthetase cytosolic isozyme	1.2	0.89	0.1	Amino acid metabolism

294	P23569	CHSY	Chalcone synthase	57.4	0.89	0.3	Secondary metabolism
295	I1N2Z5	SLE1	Protein SLE1	81.1	0.89	0.1	Signal transduction
296	P13089	AUX28	Auxin-induced protein AUX28	47.7	0.89	0.3	Growth and development
297	Q8MCL8	MATK	Maturase K	78.8	0.90	0.4	mRNA processing
298	A0A172J2D0	UGT2	UDP-glycosyltransferase 2	72.9	0.90	0.5	Carbohydrate metabolism
299	O80405	LGB3	Leghemoglobin Lb120-1	483.0	0.90	0.5	Nodulation
300	Q6TND4	MATK	Maturase K	110.6	0.90	0.1	mRNA processing
301	Q8HVY5	RPOB	DNA-directed RNA polymerase subunit β	85.0	0.90	0.3	Transcription
302	P42347	PI3K1	Phosphatidylinositol 3-kinase, root isoform	110.0	0.90	0.1	Lipid metabolism
303	B5LMM0	PSBC	Photosystem II CP43 reaction center protein	66.1	0.90	0.1	Photosynthesis
304	G7IBJ4	CN15A	Protein CNGC15a	29.3	0.90	0.1	Transport
305	Q8MCM1	MATK	Maturase K	82.5	0.90	0.5	mRNA processing
306	Q948P5	FRI4	Ferritin-4, chloroplastic	120.0	0.90	0.5	Photosynthesis
307	Q9SXV6	CAS1	Cycloartenol synthase	74.3	0.90	0.5	Saponin biosynthesis
308	Q5YJY5	MATK	Maturase K	62.1	0.90	0.1	mRNA processing
309	Q6EBC1	CONB2	Conglutin β 2	113.2	0.90	0.4	Seed storage protein
310	P29828	PDI	Protein disulfide-isomerase	61.9	0.90	0.4	Redox homeostasis
311	Q9SAZ0	LB120-34	Leghemoglobin Lb120-34	220.4	0.90	0.1	Nodulation
312	P38414	LOX1	Linoleate 9S-lipoxygenase	30.4	0.90	0.5	Fatty acid biosynthesis
313	P02858	GLYG4	Glycinin G4	57.1	0.90	0.1	Seed storage protein
314	Q9TKR9	MATK	Maturase K	37.1	0.90	0.1	mRNA processing
315	Q8MCS1	MATK	Maturase K	22.1	0.91	0.5	mRNA processing
316	O22437	CHLD	Magnesium-chelatase subunit ChlD, chloroplastic	22.2	0.91	0.3	Photosynthesis
317	Q8LKZ1	NORK	Nodulation receptor kinase	31.1	0.91	0.4	Nodulation
318	Q6RET6	CCAMK	Calcium and calcium/calmodulin-dependent serine/threonine-protein kinase (Fragment)	123.2	0.91	0.5	Signal transduction
319	O65026	SUS	Sucrose synthase	37.9	0.91	0.4	Carbohydrate metabolism
320	Q5YJV9	MATK	Maturase K	27.8	0.91	0.4	mRNA processing
321	B5LMM1	PBSD	Photosystem II D2 protein	512.7	0.91	0.1	Photosynthesis
322	O20346	RBL	Ribulose bisphosphate carboxylase large chain (Fragment)	36.6	0.91	0.4	Carbohydrate metabolism
323	Q8S3J3	HIUH	Hydroxyisourate hydrolase	225.7	0.91	0.3	Nucleotide metabolism
324	Q8MCP4	MATK	Maturase K	31.8	0.92	0.1	mRNA processing
325	Q8MCL9	MATK	Maturase K	115.0	0.92	0.1	mRNA processing
326	Q39846	SBP65	Seed biotin-containing protein SBP65	147.9	0.92	0.5	Seed storage protein
327	Q96450	1433A	14-3-3-like protein A	67.6	0.92	0.5	Defense response
328	P32290	CATA	Catalase	32.6	0.92	0.4	Redox homeostasis
329	P16149	RS16	40S ribosomal protein S16	334.8	0.92	0.1	Translation
330	A9UL14	RBR	Retinoblastoma-related protein	79.1	0.92	0.5	Cell cycle
331	C0HK20	LECC1	Mannose-specific lectin CML-2	27.1	0.92	0.3	Carbohydrate binding
332	Q9AVK4	SCR	Protein SCARECROW	33.6	0.92	0.5	Cell cycle
333	P35055	HEM6	Oxygen-dependent coproporphyrinogen-III oxidase, chloroplastic	79.7	0.93	0.2	Pigment Metabolism
334	P42499	PHYB	Phytochrome B	51.2	0.93	0.1	Signal transduction
335	Q02226	COXT	Cytochrome C oxidase subunit 2, mitochondrial (Fragment)	39.9	0.93	0.3	Electron transport
336	I1N462	SBT1	Subtilisin-like protease	272.8	0.93	0.4	Defense response
337	P48640	GSHRP	Glutathione reductase, chloroplastic	32.0	0.93	0.5	Redox homeostasis
338	P39870	NIA2	Inducible nitrate reductase [NADH] 2	90.9	0.93	0.3	Nodulation
339	Q9BBU2	MATK	Maturase K	87.4	0.94	0.5	mRNA processing
340	Q6PSE2	MATK	Maturase K	33.3	0.94	0.1	mRNA processing
341	Q8MCP5	MATK	Maturase K	31.8	0.95	0.2	mRNA processing
342	P48628	FAD6C	ω-6 fatty acid desaturase, chloroplastic	16.5	0.95	0.2	Fatty acid biosynthesis
343	Q8HVY3	RPOC2	DNA-directed RNA polymerase subunit β	89.0	0.95	0.1	Transcription
344	Q41014	FENR2	Ferredoxin-NADP reductase, root isozyme, chloroplastic	79.7	0.95	0.1	Photosynthesis
345	P93163	GPA2	Guanine nucleotide-binding proteinα-2 subunit	112.4	0.95	0.3	Signal transduction
346	O64981	RCA	Ribulose bisphosphate carboxylase/ oxygenase activase, chloroplastic	141.6	0.96	0.2	Carbohydrate metabolism
347	P09439	LOX2	Seed linoleate 9S-lipoxygenase-2	62.8	0.96	0.1	Lipid metabolism
348	Q6PSC4	MATK	Maturase K	48.0	0.96	0.2	mRNA processing
349	Q6UDF0	CSLA1	Mannan synthase 1	28.5	0.96	0.5	Carbohydrate metabolism
350	Q9MB42	BAMS	β-Amyrin synthase	19.8	0.96	0.1	Saponin biosynthesis
351	P25699	FRI	Ferritin, chloroplastic	151.2	0.96	0.3	Photosynthesis
352	Q8MCP6	MATK	Maturase K	23.5	0.97	0.5	mRNA processing
353	Q8MCN9	MATK	Maturase K	102.9	0.97	0.5	mRNA processing
354	P12227	RPOC2	DNA-directed RNA polymerase subunit β (Fragment)	29.3	0.97	0.2	Transcription
355	Q9BBS9	RPOB	DNA-directed RNA polymerase subunit β	87.2	0.97	0.5	Transcription
356	Q5H8A5	POLLU	Ion channel POLLUX	49.3	0.97	0.2	Transport
357	Q39821	SDLCA	Dynamin-related protein 12A	138.7	0.97	0.5	Growth and development
358	Q41114	LEA2	α-Amylase inhibitor 2	75.9	0.97	0.3	Carbohydrate metabolism
359	Q5YJV6	MATK	Maturase K	97.5	0.97	0.5	mRNA processing
360	P14298	CFI	Chalcone-flavonone isomerase	44.6	0.97	0.4	Secondary metabolism
361	P06004	PBSC	Photosystem II CP43 reaction center protein	66.1	0.97	0.2	Photosynthesis
362	P04770	GLNA1	Glutamine synthetase PR-1	64.1	0.97	0.2	Amino acid metabolism
363	P39869	NIA	Nitrate reductase [NADH]	74.5	0.97	0.5	Nodulation
364	Q8MCN8	MATK	Maturase K	109.3	0.98	0.4	mRNA processing
365	Q8MCN0	MATK	Maturase K	109.3	0.98	0.2	mRNA processing
366	Q8MCM3	MATK	Maturase K	103.1	0.98	0.5	mRNA processing
367	Q8MCK8	MATK	Maturase K	63.1	0.98	0.3	mRNA processing
368	Q9SLZ4	RBR1	Retinoblastoma-related protein 1	218.7	0.98	0.3	Cell cycle
369	Q9FVL0	HBL1	Non-symbiotic hemoglobin 1	79.3	0.98	0.1	Transport

370	Q43082	HEM3	Porphobilinogen deaminase, chloroplastic	103.5	0.98	0.4	Pigment Metabolism
371	A5JTQ3	XYL2	β-Xylosidase/α-L-arabinofuranosidase 2	48.8	0.98	0.5	Cell wall synthesis
372	P57997	IF2C	Translation initiation factor IF-2, chloroplastic	42.9	0.98	0.1	Translation
373	P69590	RBL	Ribulose bisphosphate carboxylase large chain (Fragment)	115.1	0.98	0.4	Carbohydrate metabolism
374	Q42805	PUR3	Phosphoribosylglycinamide formyltransferase, chloroplastic	80.3	0.98	0.3	Nucleotide metabolism
375	Q41058	GLGB1	1,4-α-glucan-branching enzyme 1, chloroplastic/ amyloplastic	58.8	0.98	0.2	Carbohydrate metabolism
376	Q6E4Q3	MATK	Maturase K	15.8	0.98	0.2	mRNA processing
377	Q6DW76	DGDG1	Digalactosyldiacylglycerol synthase 1, chloroplastic	99.8	0.98	0.3	Cell wall synthesis
378	P21616	AVP	Pyrophosphate-energized vacuolar membrane proton pump	40.8	0.98	0.2	Transport
379	Q70DJ5	LECC1	α-methyl-mannoside-specific lectin	108.9	0.98	0.1	Carbohydrate binding
380	I1KEV6	FG3H	UDP-glycosyltransferase 79B30	13.4	0.98	0.3	Carbohydrate metabolism
381	O04865	PLDA1	Phospholipase D α 1	47.7	0.98	0.3	Lipid metabolism
382	P11140	ABRA	Abrin-a	62.4	0.99	0.2	Defense response
383	Q8MCM8	MATK	Maturase K	61.7	0.99	0.1	mRNA processing
384	Q8MCM7	MATK	Maturase K	93.8	0.99	0.4	mRNA processing
385	Q8MCM2	MATK	Maturase K	109.7	0.99	0.1	mRNA processing
386	P13916	GLCA	β-conglycinin, α chain	0.0	0.99	0.1	Seed storage protein
387	A4GGF4	TI214	Protein TIC 214	87.8	0.99	0.4	Transport
388	Q8L4H4	NORK	Nodulation receptor kinase	24.2	0.99	0.4	Nodulation
389	P69575	RBL	Ribulose bisphosphate carboxylase large chain (Fragment)	115.1	0.99	0.3	Carbohydrate metabolism
390	Q5YK00	MATK	Maturase K	4.9	0.99	0.2	mRNA processing
391	Q53HY0	CONB1	Conglutin β 1	24.3	0.99	0.4	Seed storage protein
392	P31023	DLDH	Dihydrolipoyl dehydrogenase, mitochondrial	107.1	0.99	0.5	Catalytic activity
393	Q8MCN1	MATK	Maturase K	57.6	1.00	0.1	mRNA processing
394	P17067	CAHC	Carbonic anhydrase, chloroplastic	60.2	1.00	0.4	Catalytic activity
395	P51137	MSK1	Glycogen synthase kinase-3 homolog MsK-1	212.0	1.00	0.3	Signal transduction
396	Q5D1C1	MATK	Maturase K	34.9	1.00	0.2	mRNA processing
397	P37115	TCMO	Trans-cinnamate 4-monooxygenase	105.5	1.00	0.1	Secondary metabolism
398	Q33438	RBL	Ribulose bisphosphate carboxylase large chain (Fragment)	65.6	1.00	0.3	Carbohydrate metabolism
399	Q40224	GPA1	Guanine nucleotide-binding protein α-1 subunit	84.3	1.00	0.5	Signal transduction
400	Q9TKP8	MATK	Maturase K	31.7	1.00	0.3	mRNA processing
401	O81928	TCMO	Trans-cinnamate 4-monooxygenase	52.7	1.00	0.5	Secondary metabolism
402	Q8MCR9	MATK	Maturase K	113.7	1.01	0.5	mRNA processing
403	A4ULF8	METK	S-Adenosylmethionine synthase	28.5	1.01	0.4	Amino acid metabolism
404	Q8MCN2	MATK	Maturase K	102.9	1.01	0.2	mRNA processing
405	Q43078	C97B1	Cytochrome P450 97B1, chloroplastic	73.9	1.01	0.5	Monooxygenase
406	P69573	RBL	Ribulose bisphosphate carboxylase large chain (Fragment)	115.1	1.01	0.4	Carbohydrate metabolism
407	Q5YK05	MATK	Maturase K	17.6	1.01	0.1	mRNA processing
408	Q39469	THD1	Threonine dehydratase biosynthetic, chloroplastic	61.9	1.01	0.1	Amino acid metabolism
409	P39866	NIA2	Nitrate reductase [NADH] 2	41.6	1.01	0.3	Nodulation
410	Q6WNQ9	C81E9	Isoflavone 3'-hydroxylase (Fragment)	133.2	1.02	0.2	Secondary metabolism
411	P80366	PPAF	Fe(3+)-Zn(2+) purple acid phosphatase	49.2	1.02	0.4	Catalytic activity
412	Q9XHM1	EIF3C	Eukaryotic translation initiation factor 3 subunit C	59.2	1.02	0.5	Translation
413	Q9BBT0	PBSD	Photosystem II D2 protein	512.7	1.02	0.3	Photosynthesis
414	P26969	GCSP	Glycine dehydrogenase (decarboxylating), mitochondrial	24.4	1.02	0.4	Amino acid metabolism
415	P20077	THS2	Putative stilbene synthase 2 (Fragment)	40.6	1.02	0.3	Secondary metabolism
416	Q39891	LEU1	Probable 2-isopropylmalate synthase	102.5	1.02	0.5	Amino acid metabolism
417	P08283	H1	Histone H1	101.2	1.02	0.5	DNA binding
418	P69582	RBL	Ribulose bisphosphate carboxylase large chain (Fragment)	115.1	1.02	0.1	Carbohydrate metabolism
419	F5B8V9	CONB1	Conglutin β 1	64.2	1.02	0.5	Seed storage protein
420	P58310	PSAA	Photosystem I P700 chlorophyll a apoprotein A1	81.4	1.02	0.4	Photosynthesis
421	Q1SGF1	PARP3	Putative poly [ADP-ribose] polymerase 3	60.7	1.02	0.2	Transcription
422	P49613	METK	S-Adenosylmethionine synthase 2	28.5	1.02	0.4	Amino acid metabolism
423	Q6DW74	DGDG1	Digalactosyldiacylglycerol synthase 1,chloroplastic	99.1	1.02	0.4	Cell wall synthesis
424	Q9SWR5	C93C1	2-hydroxyisoflavanone synthase	23.5	1.02	0.5	Secondary metabolism
425	Q9TKS6	MATK	Maturase K	111.1	1.02	0.2	mRNA processing
426	Q8HUG7	MATK	Maturase K	48.3	1.03	0.2	mRNA processing
427	O24534	EF1A	Elongation factor 1-α	77.5	1.03	0.4	Translation
428	A4GGA7	RPOC2	DNA-directed RNA polymerase subunit β	40.4	1.03	0.5	Transcription
429	P39865	NIA1	Nitrate reductase [NADH] 1	50.7	1.03	0.4	Nodulation
430	Q9TKS1	MATK	Maturase K	37.3	1.03	0.1	mRNA processing
431	P50477	CANA	Canavalin	4.6	1.03	0.5	Seed storage protein
432	Q2PMU2	PSAB	Photosystem I P700 chlorophyll a apoprotein A2	40.8	1.04	0.4	Photosynthesis
433	Q43468	HSOP1	Hsp70-Hsp90 organizing protein 1	95.0	1.04	0.5	Chaperone
434	G7JND3	CN15B	Protein CNGC15b	63.3	1.04	0.2	Transport
435	A4GGA2	PSBD	Photosystem II D2 protein	512.7	1.04	0.1	Photosynthesis
436	P69581	RBL	Ribulose bisphosphate carboxylase large chain (Fragment)	115.1	1.04	0.2	Carbohydrate metabolism
437	P32296	P5CS	δ-1-pyrroline-5-carboxylate synthase	72.2	1.04	0.3	Amino acid metabolism
438	Q5YJU1	MATK	Maturase K	87.4	1.04	0.5	mRNA processing
439	Q04593	PAL2	Phenylalanine ammonia-lyase 2	90.2	1.04	0.1	Secondary metabolism
440	P42500	PHYA	Phytochrome A	51.8	1.04	0.3	Signal transduction
441	Q8MCM0	MATK	Maturase K	91.2	1.05	0.3	mRNA processing
442	P48406	CHS5	Chalcone synthase 5	18.9	1.05	0.4	Secondary metabolism
443	Q84KK6	I4OMT	Isoflavone 4'-O-methyltransferase	160.1	1.05	0.5	Secondary metabolism
444	P51109	DFRA	Dihydroflavonol 4-reductase (Fragment)	88.3	1.05	0.1	Secondary metabolism
445	O98997	RCA	Ribulose bisphosphate carboxylase/ oxygenase activase, chloroplastic	36.1	1.05	0.5	Carbohydrate metabolism
446	P10562	CANA	Canavalin	4.6	1.05	0.1	Seed storage protein
447	P69588	RBL	Ribulose bisphosphate carboxylase large chain (Fragment)	115.1	1.05	0.2	Carbohydrate metabolism

448	P08215	ATPA	ATP synthase subunit α, chloroplastic	40.3	1.05	0.2	Transport
449	O62970	RBL	Ribulose bisphosphate carboxylase large chain (Fragment)	36.6	1.05	0.3	Carbohydrate metabolism
450	B5WWZ8	FAO1	Long-chain-alcohol oxidase FAO1	105.3	1.05	0.1	Lipid metabolism
451	Q9TKP9	MATK	Maturase K	47.7	1.05	0.5	mRNA processing
452	Q03460	GLSN	Glutamate synthase [NADH], amyloplastic	40.1	1.06	0.2	Amino acid metabolism
453	Q8MCN7	MATK	Maturase K	104.2	1.06	0.3	mRNA processing
454	Q2PMS8	ATPA	ATP synthase subunit α, chloroplastic	126.4	1.06	0.4	Transport
455	P08926	RUBA	RuBisCO large subunit-binding protein subunit α, chloroplastic	33.6	1.06	0.1	Carbohydrate metabolism
456	P30706	PLSB	Glycerol-3-phosphate acyltransferase, chloroplastic	17.7	1.06	0.5	Carbohydrate metabolism
457	P69578	RBL	Ribulose bisphosphate carboxylase large chain (Fragment)	115.1	1.06	0.4	Carbohydrate metabolism
458	P69576	RBL	Ribulose bisphosphate carboxylase large chain (Fragment)	115.1	1.06	0.4	Carbohydrate metabolism
459	F5B8W2	CONB4	Conglutin β 4	106.6	1.06	0.1	Seed storage protein
460	P49612	METK1	S-Adenosylmethionine synthase 1 (Fragment)	76.5	1.06	0.2	Amino acid metabolism
461	Q02735	CAPP	Phosphoenolpyruvate carboxylase	52.3	1.06	0.3	Carbohydrate metabolism
462	P31687	4CL2	4-Coumarate-CoA ligase 2	48.9	1.07	0.5	Secondary metabolism
463	Q02920	NO70	Early nodulin-70	21.0	1.07	0.3	Nodulation
464	Q9BBQ8	PSBB	Photosystem II CP47 reaction center protein	24.5	1.07	0.5	Photosynthesis
465	P69587	RBL	Ribulose bisphosphate carboxylase large chain (Fragment)	115.1	1.07	0.5	Carbohydrate metabolism
466	P69585	RBL	Ribulose bisphosphate carboxylase large chain (Fragment)	115.1	1.07	0.5	Carbohydrate metabolism
467	Q01288	CHS6	Chalcone synthase 6	34.8	1.08	0.1	Secondary metabolism
468	Q96558	UGDH1	UDP-glucose 6-dehydrogenase 1	82.3	1.08	0.4	Carbohydrate metabolism
469	Q40106	TBB2	Tubulin β-2 chain	171.1	1.08	0.2	Cytoskeleton
470	Q8SKU2	TIC62	Protein TIC 62, chloroplastic	99.1	1.08	0.2	Transport
471	Q9BBN6	TI214	Protein TIC 214	83.5	1.08	0.4	Transport
472	Q39817	CALX	Calnexin homolog	85.5	1.08	0.2	Chaperone
473	C6TEX6	FEN1	Flap endonuclease 1	36.9	1.08	0.1	DNA Repair
474	P69586	RBL	Ribulose bisphosphate carboxylase large chain (Fragment)	115.1	1.08	0.1	Carbohydrate metabolism
475	P69577	RBL	Ribulose bisphosphate carboxylase large chain (Fragment)	115.1	1.08	0.1	Carbohydrate metabolism
476	F5B8W4	CONB6	Conglutin β 6	102.7	1.08	0.3	Seed storage protein
477	Q41706	UPSA3	Probable ureide permease A3 (Fragment)	158.3	1.08	0.3	Cell wall synthesis
478	P92407	RBL	Ribulose bisphosphate carboxylase large chain (Fragment)	115.1	1.08	0.5	Carbohydrate metabolism
479	P92401	RBL	Ribulose bisphosphate carboxylase large chain (Fragment)	115.1	1.08	0.1	Carbohydrate metabolism
480	Q9ZNX6	GSH1	Glutamate-cysteine ligase, chloroplastic	43.3	1.08	0.2	Amino acid metabolism
481	P24826	CHS1	Chalcone synthase 1	18.9	1.09	0.1	Secondary metabolism
482	Q84KK4	I4OMT	Isoflavone 4'-O-methyltransferase	219.5	1.09	0.2	Secondary metabolism
483	A0A172J2G3	UGT43	UDP-glycosyltransferase 43	68.4	1.09	0.3	Carbohydrate metabolism
484	Q41107	INO1	Inositol-3-phosphate synthase	46.0	1.09	0.2	Lipid metabolism
485	A4GG98	PSAB	Photosystem I P700 chlorophyll a apoprotein A2	11.6	1.09	0.4	Photosynthesis
486	Q40313	CAMT	Caffeoyl-CoA O-methyltransferase	57.8	1.09	0.2	Secondary metabolism
487	P92406	RBL	Ribulose bisphosphate carboxylase large chain (Fragment)	115.1	1.09	0.3	Carbohydrate metabolism
488	O64407	AMYB	β-Amylase	84.2	1.09	0.5	Carbohydrate metabolism
489	O04408	KSA	Ent-copalyl diphosphate synthase, chloroplastic	43.2	1.11	0.2	Hormone metabolism
490	P07218	PAL1	Phenylalanine ammonia-lyase class 1 (Fragment)	77.5	1.11	0.3	Secondary metabolism
491	B8R4B1	NU5C	NAD(P)H-quinone oxidoreductase subunit5C; chloroplastic	15.9	1.11	0.5	Electron transport
492	D2XNQ9	FLOT2	Flotillin-like protein 2	13.7	1.11	0.4	Defense response
493	P49082	GPA1	Guanine nucleotide-binding protein α-1 subunit	104.0	1.11	0.2	Signal transduction
494	Q5YK33	MATK	Maturase K	54.4	1.11	0.4	mRNA processing
495	Q42806	KPYC	Pyruvate kinase, cytosolic isozyme	94.4	1.11	0.2	Carbohydrate metabolism
496	P08863	NO26B	Nodulin-26B	36.0	1.11	0.2	Nodulation
497	P14856	LOX2	Seed linoleate 9S-lipoxygenase-2	75.1	1.11	0.5	Lipid metabolism
498	O22585	AMYB	β-Amylase	12.4	1.11	0.2	Carbohydrate metabolism
499	P08170	LOX1	Seed linoleate 13S-lipoxygenase-1	30.5	1.11	0.5	Lipid metabolism
500	P35100	CLPC	Chaperone protein ClpC, chloroplastic	170.8	1.11	0.4	Chaperone
501	P37900	HSP7M	Heat shock 70 kDa protein, mitochondrial	67.5	1.11	0.2	Chaperone
502	Q43460	NO20A	Nodulin-20a	124.7	1.12	0.5	Nodulation
503	Q9ZSK5	ZOG	Zeatin O-glucosyltransferase	35.0	1.12	0.2	Hormone metabolism
504	P98188	C94A2	Cytochrome P450 94A2	60.2	1.12	0.3	Monooxygenase
505	Q6PP79	MATK	Maturase K	4.0	1.12	0.3	mRNA processing
506	P49044	VPE	Vacuolar-processing enzyme	88.4	1.12	0.1	Seed storage protein
507	F5B8W0	CONB2	Conglutin β 2	117.7	1.12	0.3	Seed storage protein
508	Q2PMP0	TI214	Protein TIC 214	101.6	1.13	0.2	Transport
509	Q9BBS7	RPOC2	DNA-directed RNA polymerase subunit β	25.4	1.13	0.3	Transcription
510	Q43089	INV1	β-Fructofuranosidase, cell wall isozyme	14.6	1.13	0.1	Cell wall synthesis
511	D2XNQ8	FLOT1	Flotillin-like protein 1	184.9	1.13	0.4	Defense response
512	Q5YJX5	MATK	Maturase K	36.0	1.13	0.1	mRNA processing
513	Q09WE7	USP1	UDP-sugar pyrophosphorylase 1	68.6	1.13	0.3	Carbohydrate metabolism
514	Q5NUF4	HIDM	2-hydroxyisoflavanone dehydratase	15.0	1.13	0.3	Secondary metabolism
515	Q9LRH7	ABAMS	Mixed-amyrin synthase	100.5	1.14	0.5	Saponin biosynthesis
516	Q00016	IFR	Isoflavone reductase	61.9	1.14	0.5	Secondary metabolism
517	P48621	FAD3C	ω-3 Fatty acid desaturase, chloroplastic	348.5	1.14	0.4	Fatty acid biosynthesis
518	Q43621	GSHRC	Glutathione reductase, cytosolic	45.0	1.14	0.2	Redox homeostasis
519	P69583	RBL	Ribulose bisphosphate carboxylaselarge chain (Fragment)	115.1	1.14	0.3	Carbohydrate metabolism
520	P49084	GPA1	Guanine nucleotide-binding protein α-1 subunit	50.9	1.14	0.4	Signal transduction
521	P51062	CAPP	Phosphoenolpyruvate carboxylase	33.9	1.15	0.5	Carbohydrate metabolism
522	P32293	AX22A	Auxin-induced protein 22A	77.2	1.15	0.4	Growth and development
523	P69574	RBL	Ribulose bisphosphate carboxylase large chain (Fragment)	115.1	1.15	0.2	Carbohydrate metabolism
524	Q06215	PPO	Polyphenol oxidase A1, chloroplastic	34.8	1.15	0.4	Pigment Metabolism
525	Q9SAZ1	LGB4	Leghemoglobin Lb120-8	150.8	1.15	0.1	Nodulation
526	Q40353	MMK2	Mitogen-activated protein kinase homolog MMK2	138.0	1.16	0.2	Signal transduction

527	C6TAY1	SOMT2	Flavonoid 4'-O-methyltransferase	30.8	1.16	0.2	Secondary metabolism
528	Q01912	1A1C	1-Aminocyclopropane-1-carboxylate synthase (Fragment)	0.0	1.16	0.5	Hormone metabolism
529	P17957	CHS2	Chalcone synthase 2	18.9	1.17	0.3	Secondary metabolism
530	P09918	LOX3	Seed linoleate 9S-lipoxygenase-3	40.6	1.17	0.2	Lipid metabolism
531	P07374	UREA	Urease	39.6	1.17	0.5	Nodulation
532	P09186	LOX3	Seed linoleate 9S-lipoxygenase-3	67.5	1.19	0.5	Lipid metabolism
533	P08960	NO20A	Nodulin-20	5.4	1.19	0.4	Nodulation
534	Q43066	GLNA4	Glutamine synthetase root isozyme β	16.3	1.20	0.2	Amino acid metabolism
535	Q6RHR6	DMI1	Ion channel DMI1	53.2	1.20	0.5	Transport
536	O49816	LEA1	Late embryogenesis abundant protein 1	46.0	1.20	0.4	Defense response
537	P54233	NIA1	Inducible nitrate reductase [NADH] 1	31.1	1.20	0.3	Nodulation
538	P02855	VCLA	Provicilin (Fragment)	68.4	1.20	0.3	Seed storage protein
539	O24310	EFTU	Elongation factor Tu, chloroplastic	8.8	1.21	0.2	Translation
540	D2XNR1	FLOT4	Flotillin-like protein 4	26.4	1.21	0.4	Defense response
541	Q39828	SDL5A	Dynamin-related protein 5A	121.1	1.21	0.2	Growth and development
542	P19142	PAL2	Phenylalanine ammonia-lyase class 2	80.3	1.21	0.3	Secondary metabolism
543	P52423	PUR3	Phosphoribosylglycinamide formyltransferase, chloroplastic	4.8	1.21	0.1	Nucleotide metabolism
544	P27990	PALY	Phenylalanine ammonia-lyase	219.8	1.21	0.3	Secondary metabolism
545	Q9B133	RR12	30S ribosomal protein S12, chloroplastic	62.2	1.21	0.4	Translation
546	P05493	ATPAM	ATP synthase subunit α, mitochondrial	113.4	1.21	0.1	Transport
547	Q9SMK9	PAL2	Phenylalanine ammonia-lyase 2	19.8	1.22	0.3	Secondary metabolism
548	P25890	CATA	Catalase	29.5	1.22	0.4	Redox homeostasis
549	A4GGC9	RR12	30S ribosomal protein S12, chloroplastic	53.9	1.22	0.3	Translation
550	A4GGA6	RPOC1	DNA-directed RNA polymerase subunit β	48.7	1.22	0.1	Transcription
551	O49856	FTRC	Ferredoxin-thioredoxin reductase catalytic chain, chloroplastic	2.0	1.22	0.4	Photosynthesis
552	P38417	LOX4	Linoleate 9S-lipoxygenase-4	56.1	1.22	0.2	Fatty acid biosynthesis
553	P52780	SYQ	Glutamine-tRNA ligase	31.7	1.23	0.3	Translation
554	P27481	LOXB	Linoleate 9S-lipoxygenase (Fragment)	85.4	1.25	0.5	Fatty acid biosynthesis
555	Q84N37	PVIP	OBERON-like protein (Fragment)	128.5	1.25	0.2	Growth and development
556	Q8HVY4	RPOC1	DNA-directed RNA polymerasesubunit β	44.6	1.25	0.4	Transcription
557	P24095	LOXX	Seed linoleate 9S-lipoxygenase	45.9	1.26	0.3	Lipid metabolism
558	P52416	GLGS1	Glucose-1-phosphate adenylyltransferase small subunit 1, chloroplastic	103.9	1.26	0.3	Carbohydrate metabolism
559	P07134	RR12	30S ribosomal protein S12, chloroplastic	59.9	1.26	0.5	Translation
560	P11827	GLCAP	β-Conglycinin, α chain	36.2	1.26	0.1	Seed storage protein
561	Q01899	HSP7M	Heat shock 70 kDa protein, mitochondrial	44.6	1.27	0.4	Chaperone
562	O49931	TIC55	Protein TIC 55, chloroplastic	153.3	1.27	0.1	Transport
563	Q9BBS8	RPOC1	DNA-directed RNA polymerase subunit β	63.5	1.27	0.4	Transcription
564	Q43088	RBCMT	Ribulose-1,5 bisphosphate carboxylase/oxygenase large subunit N-methyltransferase, chloroplastic	81.6	1.27	0.1	Carbohydrate metabolism
565	P22895	P34	P34 probable thiol protease	67.3	1.27	0.5	Proteolysis
566	P15001	PHYA	Phytochrome A	33.5	1.27	0.1	Signal transduction
567	Q69F95	C85A	Cytochrome P450 85A	95.4	1.27	0.5	Monooxygenase
568	O24304	FNTA	Protein farnesyltransferase/ geranylgeranyltransferase type-1 subunit α	40.7	1.28	0.1	Lipid metabolism
569	D2XNR2	FLOT6	Flotillin-like protein 6	99.1	1.28	0.1	Defense response
570	P29502	TBB3	Tubulin β-3 chain (Fragment)	3.8	1.28	0.4	Cytoskeleton
571	O49818	LGUL	Lactoylglutathione lyase	67.3	1.28	0.4	Secondary metabolism
572	P30080	CHS6	Chalcone synthase 6	18.9	1.28	0.3	Secondary metabolism
573	P37392	TBB1	Tubulin β-1 chain	3.8	1.28	0.4	Cytoskeleton
574	Q8W3Y4	METK	S-Adenosylmethionine synthase	131.0	1.28	0.2	Amino acid metabolism
575	Q93XK2	STSYN	Stachyose synthase	58.5	1.30	0.2	Carbohydrate metabolism
576	O24308	TOP2	DNA topoisomerase 2	115.3	1.30	0.1	Replication
577	P28551	TBB3	Tubulin β chain (Fragment)	3.8	1.30	0.3	Cytoskeleton
578	P30164	ACT1	Actin-1	40.4	1.30	0.2	Cytoskeleton
579	Q41651	CYPB	Peptidyl-prolyl cis-trans isomerase, chloroplastic	89.6	1.30	0.3	Protein modification
580	P07694	GLNA3	Glutamine synthetase root isozyme A	34.1	1.30	0.2	Amino acid metabolism
581	P29450	TRXF	Thioredoxin F-type, chloroplastic	37.5	1.31	0.5	Electron transport
582	P13919	CVCB	Convicilin (Fragment)	85.9	1.32	0.1	Seed storage protein
583	P45732	PALY	Phenylalanine ammonia-lyase	78.1	1.32	0.2	Secondary metabolism
584	P53537	PHSH	α-Glucan phosphorylase, H isozyme	44.9	1.32	0.1	Carbohydrate metabolism
585	Q41011	EF1A	Elongation factor 1-α	83.0	1.32	0.2	Translation
586	P53392	SUT2	High affinity sulfate transporter 2	150.1	1.34	0.2	Transport
587	Q5H8A6	CASTO	Ion channel CASTOR	20.0	1.34	0.4	Transport
588	H1A981	C7263	11-Oxo-β-amyrin 30-oxidase	62.8	1.34	0.1	Saponin biosynthesis
589	Q8VWN6	RFS	Galactinol-sucrose galactosyltransferase	22.1	1.34	0.1	Carbohydrate metabolism
590	Q6PSB9	MATK	Maturase K	41.3	1.34	0.1	mRNA processing
591	Q6PP78	MATK	Maturase K	35.8	1.34	0.1	mRNA processing
592	G1CWH1	CYC2	Cliotide T2	194.9	1.34	0.2	Defense response
593	P27991	PAL1	Phenylalanine ammonia-lyase 1	144.0	1.35	0.4	Secondary metabolism
594	P34798	URIC1	Uricase-2 isozyme 1	35.0	1.35	0.2	Nodulation
595	P53391	SUT1	High affinity sulfate transporter 1	204.0	1.36	0.4	Transport
596	Q43077	AMO	Primary amine oxidase	9.0	1.36	0.4	Hormone metabolism
597	Q5NUF3	HIDH	2-hydroxyisoflavanone dehydratase	50.4	1.36	0.1	Secondary metabolism
598	P13911	RPOA	DNA-directed RNA polymerase subunit α	236.1	1.38	0.2	Transcription
599	Q8GT66	TIC40	Protein TIC 40, chloroplastic	204.6	1.39	0.5	Transport
600	Q6J541	C79D3	Isoleucine N-monooxygenase 1	43.2	1.39	0.5	Secondary metabolism
601	D4Q9Z4	SGT2	Soyasapogenol β glucuronide galactosyltransferase	56.3	1.39	0.3	Saponin biosynthesis

602	Q39857	XTH1	Xyloglucan endotransglucosylase/hydrolase 1	53.6	1.39	0.1	Cell wall synthesis
603	P10538	AMYB	β-Amylase	59.0	1.39	0.1	Carbohydrate metabolism
604	P32289	GLNA	Glutamine synthetase nodule isozyme	40.8	1.39	0.4	Nodulation
605	Q9BAE0	FTSH	ATP-dependent zinc metalloprotease FTSH, chloroplastic	56.1	1.39	0.3	Proteolysis
606	P08438	VCL	Vicilin	77.9	1.39	0.3	Seed storage protein
607	P30165	ACT2	Actin-2	51.7	1.40	0.1	Cytoskeleton
608	Q43467	EFTU1	Elongation factor Tu, chloroplastic	62.9	1.42	0.3	Translation
609	P29531	OLEO2	P24 oleosin isoform B	107.3	1.42	0.3	Growth and development
610	P45734	PALY	Phenylalanine ammonia-lyase	86.9	1.43	0.5	Secondary metabolism
611	Q948P6	FRI3	Ferritin-3, chloroplastic	108.8	1.43	0.5	Photosynthesis
612	A5JTQ2	XYL1	β-Xylosidase/ α-L-Arabinofuranosidase 1 (Fragment)	49.2	1.43	0.3	Cell wall synthesis
613	O48922	C98A2	Cytochrome P450 98A2	77.6	1.43	0.3	Monooxygenase
614	P08688	ALB2	Albumin-2	50.7	1.45	0.3	Seed storage protein
615	O04278	GPA1	Guanine nucleotide-binding protein α-1 subunit	70.1	1.45	0.3	Signal transduction
616	P12886	ADH1	Alcohol dehydrogenase 1	17.5	1.46	0.5	Catalytic activity
617	P31531	1A1C	1-Aminocyclopropane-1-carboxylate synthase	2.3	1.46	0.2	Hormone metabolism
618	P12468	RBS4	Ribulose bisphosphate carboxylase small chain 4, chloroplastic	102.0	1.46	0.4	Carbohydrate metabolism
619	Q94G16	TATB	Sec-independent protein translocase protein TATB, chloroplastic	85.7	1.46	0.5	Transport
620	P34899	GLYM	Serine hydroxymethyltransferase, mitochondrial	92.3	1.48	0.5	Amino acid metabolism
621	P52418	PUR1	Amidophosphoribosyltransferase, chloroplastic	43.1	1.48	0.2	Nucleotide metabolism
622	C0HJB3	MANA	α-Mannosidase	38.2	1.48	0.1	Carbohydrate metabolism
623	Q43138	MTDH3	Probable mannitol dehydrogenase 3	122.0	1.49	0.5	Carbohydrate metabolism
624	Q5UB07	TPS4	Tricyclene synthase TPS4, chloroplastic	112.5	1.49	0.1	Secondary metabolism
625	P51082	CHSB	Chalcone synthase 1B	24.0	1.49	0.2	Secondary metabolism
626	P42353	RRL16	50S ribosomal protein L16; chloroplastic (Fragment)	53.0	1.49	0.1	Translation
627	P58385	PSAB	Photosystem I P700 chlorophyll a apoprotein A2	31.8	1.51	0.3	Photosynthesis
628	P26413	HSP70	Heat shock 70 kDa protein	67.3	1.51	0.5	Chaperone
629	P0DH60	M3OM2	(+)-6a-hydroxymaackiain 3-O-methyltransferase 2	61.7	1.52	0.1	Secondary metabolism
630	P15102	GLNA4	Glutamine synthetase leaf isozyme, chloroplastic	16.4	1.52	0.3	Amino acid metabolism
631	B5LMN4	ACCD	Acetyl-coenzyme A carboxylase carboxyl transferase subunit β, chloroplastic	227.5	1.52	0.1	Fatty acid biosynthesis
632	Q9BBT4	YCF3	Photosystem I assembly protein Ycf3	4.4	1.54	0.4	Photosynthesis
633	O49859	C82A4	Cytochrome P450 82A4	101.4	1.54	0.4	Monooxygenase
634	P48631	FD6E2	ω-6 fatty acid desaturase, endoplasmic reticulum isozyme 2	39.7	1.55	0.3	Fatty acid biosynthesis
635	Q6EJ97	ISPS	Isoprene synthase, chloroplastic	58.4	1.57	0.4	Lipid metabolism
636	Q2PMQ0	RR8	30S ribosomal protein S8, chloroplastic	210.7	1.57	0.5	Translation
637	Q9BBQ4	RPOA	DNA-directed RNA polymerase subunit α	173.8	1.57	0.4	Transcription
638	Q9BBP9	RK16	50S ribosomal protein L16, chloroplastic	119.0	1.57	0.4	Translation
639	P20178	THS1	Stilbene synthase 1	0.0	1.58	0.5	Defense response
640	Q2PMN8	NDHH	NAD(P)H-quinone oxidoreductase subunit H, cloroplastic	15.9	1.58	0.2	Electron transport
641	Q04708	P5CR	Pyrroline-5-carboxylate reductase	251.3	1.58	0.4	Amino acid metabolism
642	P93472	DIM	δ(24)-sterol reductase	75.0	1.58	0.1	Steroid biosynthesis
643	Q2HVD6	MTA70	Putative N6-adenosine-methyltransferase MT-70-like	90.1	1.60	0.2	Nucleotide metabolism
644	P08241	RR2	30S ribosomal protein S2, chloroplastic	85.7	1.60	0.1	Translation
645	Q764T8	LUPS	Lupeol synthase	31.2	1.62	0.5	Saponin biosynthesis
646	Q6RVV4	TIC32	Short-chain dehydrogenase TIC 32, chloroplastic	153.9	1.62	0.1	Redox homeostasis
647	P40620	HMGL	HMG1/2-like protein	137.4	1.63	0.2	DNA binding
648	Q42920	PME	Pectinesterase/pectinesterase inhibitor	45.6	1.65	0.3	Cell wall synthesis
649	P31239	ACCO	1-Aminocyclopropane-1-carboxylate oxidase	178.9	1.65	0.5	Hormone metabolism
650	A4GG85	RRL16	50S ribosomal protein L16, chloroplastic	31.5	1.65	0.3	Translation
651	Q42823	RBS	Ribulose bisphosphate carboxylase small chain, chloroplastic	99.4	1.65	0.2	Carbohydrate metabolism
652	O81972	C82A2	Cytochrome P450 82A2	43.0	1.65	0.2	Monooxygenase
653	Q01289	POR	Protochlorophyllide reductase, chloroplastic	106.7	1.67	0.5	Pigment Metabolism
654	O24305	M3OM1	(+)-6a-hydroxymaackiain 3-O-methyltransferase 1	74.7	1.67	0.1	Secondary metabolism
655	P51069	THS3	Stilbene synthase 3	0.0	1.67	0.2	Defense response
656	Q41059	GLGB2	1,4-α-glucan-branching enzyme 1, chloroplastic/amyloplastic (Fragment)	150.8	1.67	0.1	Carbohydrate metabolism
657	P02580	ACT3	Actin-3	64.7	1.70	0.3	Cytoskeleton
658	P25012	CCNB2	G2/ mitotic-specific cyclin S13-7 (Fragment)	19.8	1.70	0.4	Cell cycle
659	O48928	C77A3	Cytochrome P450 77A3	49.5	1.70	0.5	Monooxygenase
660	P51080	CHS	Chalcone synthase (Fragment)	43.8	1.72	0.3	Secondary metabolism
661	Q43822	PLSB	Glycerol-3-phosphate acyltransferase, chloroplastic	78.7	1.72	0.1	Carbohydrate metabolism
662	O48902	MDHP	Malate dehydrogenase [NADP], chloroplastic	144.0	1.72	0.1	Carbohydrate metabolism
663	Q4VY51	SYM8	Probable ion channel SYM8	26.3	1.73	0.5	Transport
664	Q84XA3	IMDH	Inosine-5'-monophosphate dehydrogenase	53.8	1.73	0.5	Nucleotide metabolism
665	P12858	G3PA	Glyceraldehyde-3-phosphate dehydrogenase A, chloroplastic	190.9	1.73	0.3	Carbohydrate metabolism
666	P15792	KPK1	Protein kinase PVPK-1	34.9	1.75	0.1	Signal transduction
667	O03376	AOX3	Alternative oxidase 3, mitochondrial	12.4	1.77	0.4	Electron transport
668	O65729	RL18	60S ribosomal protein L18 (Fragment)	90.5	1.77	0.5	Translation
669	P93328	NO16	Early nodulin-16	36.9	1.80	0.5	Nodulation
670	P30077	CHS9	Chalcone synthase 9	34.8	1.80	0.2	Secondary metabolism
671	Q9SC88	GCP4	γ-Tubulin complex component 4 homolog	89.1	1.82	0.2	Cytoskeleton
672	Q29U70	I4OMT	Isoflavone 4'-O-methyltransferase	80.4	1.84	0.3	Secondary metabolism
673	P07219	PHSA	Phaseolin, α-type	30.2	1.86	0.2	Seed storage protein
674	P51081	CHSA	Chalcone synthase 1A	6.1	1.88	0.1	Secondary metabolism
675	Q43070	GALE1	UDP-glucose 4-epimerase	27.9	1.90	0.4	Carbohydrate metabolism

676	P51078	CHS5	Chalcone synthase 4-2	34.8	1.90	0.4	Secondary metabolism
677	P51086	CHS4	Chalcone synthase 4 (Fragment)	34.8	1.92	0.5	Secondary metabolism
678	P30075	CHS4	Chalcone synthase 4	34.8	1.92	0.1	Secondary metabolism
679	P30076	CHS8	Chalcone synthase 8	34.8	1.93	0.5	Secondary metabolism
680	B0M3E8	UGE1	Bifunctional UDP-glucose 4-epimerase and UDP-xylose 4-epimerase 1	27.9	1.93	0.4	Cell wall synthesis
681	O48559	UNI	Protein UNIFOLIATA	43.1	1.97	0.4	DNA binding
682	P51085	CHS3	Chalcone synthase 3	34.8	1.97	0.3	Secondary metabolism
683	O49858	C82A3	Cytochrome P450 82A3	33.2	1.97	0.1	Monooxygenase
684	P19168	CHS3	Chalcone synthase 3	18.9	1.99	0.3	Secondary metabolism
			Up-regulated proteins				
685	P36875	2AAA	Protein phosphatase PP2A regulatory subunit A (Fragment)	56.1	2.01	0.04	Signal transduction
686	Q9BBN8	NDHH	NAD(P)H-quinone oxidoreductase subunit H, chloroplastic	15.9	2.05	0.05	electron transport
687	P30074	CHS2	Chalcone synthase 2	34.8	2.05	0.01	Secondary metabolism
688	Q01915	ATPAM	ATP synthase subunit α, mitochondrial	101.9	2.05	0.05	Transport
689	O23883	CHS3	Chalcone synthase 3	34.8	2.10	0.01	Secondary metabolism
690	P52575	IFR	Isoflavone reductase	66.2	2.10	0.05	Secondary metabolism
691	O22307	C71DB	Cytochrome P450 71D11 (Fragment)	34.2	2.10	0.03	Monooxygenase
692	P02856	VCL1	Vicilin, 14 kDa component	39.5	2.12	0.03	Seed storage protein
693	P49046	LEGU	Legumain	86.0	2.14	0.02	Seed storage protein
694	P53393	SUT3	Low affinity sulfate transporter 3	66.9	2.16	0.01	Transport
695	O82709	CALX	Calnexin homolog	157.8	2.16	0.04	Chaperone
696	P51087	CHS5	Chalcone synthase 5	34.8	2.20	0.05	Secondary metabolism
697	P51083	CHS1	Chalcone synthase 1	34.8	2.20	0.01	Secondary metabolism
698	P51079	CHS6-4	Chalcone synthase 6-4	24.9	2.20	0.04	Secondary metabolism
699	P51088	CHS6	Chalcone synthase 6	34.8	2.23	0.01	Secondary metabolism
700	Q01287	CHS2	Chalcone synthase 2	34.8	2.25	0.05	Secondary metabolism
701	Q43785	GLNA3	Glutamine synthetase nodule isozyme	5.8	2.25	0.01	Nodulation
702	O24326	VPE2	Vacuolar-processing enzyme	41.3	2.27	0.03	Seed storage protein
703	P30081	CHS7	Chalcone synthase 7	24.9	2.29	0.03	Secondary metabolism
704	A4GGB2	ATPA	ATP synthase subunit α, chloroplastic	33.6	2.34	0.03	electron transport
705	O22586	CHSY	Chalcone synthase	34.8	2.36	0.05	Secondary metabolism
706	P20780	ARA1	Arachin 21 kDa protein	161.3	2.51	0.02	Seed storage protein
707	P21528	MDHP	Malate dehydrogenase [NADP], chloroplastic	54.1	2.56	0.01	Carbohydrate metabolism
708	P46259	TBA1	Tubulin α-1 chain	142.3	2.61	0.03	Cell cycle
709	P28583	TBA1	Calcium-dependent protein kinase SK5	87.1	2.69	0.01	Signal transduction
710	O48561	CATA4	Catalase-4	48.6	2.75	0.05	Redox homeostasis
711	Q43068	C82A1	Cytochrome P450 82A1 (Fragment)	20.8	2.86	0.03	Monooxygenase
712	Q43093	SSG2	Granule-bound starch synthase 2, chloroplastic/ amyloplastic	26.2	3.00	0.04	Carbohydrate metabolism
713	A4PU48	METK	S-Adenosylmethionine synthase	19.2	3.10	0.04	Amino acid metabolism
714	P49680	IAA6	Auxin-induced protein IAA6	28.1	3.19	0.03	Growth and development
715	Q9M5Q1	FUT1	Galactoside 2-α-L-fucosyltransferase	22.8	3.25	0.01	Cell wall synthesis
716	P93484	VSR1	Vacuolar-sorting receptor 1	40.4	3.25	0.05	Transport
717	Q2PMU9	ATPE	ATP synthase ε chain, chloroplastic	78.5	3.29	0.04	electron transport
718	O81117	C94A1	Cytochrome P450 94A1	51.5	3.39	0.05	Monooxygenase
719	O04300	RGP1	Probable UDP-arabinopyranose mutase 1	32.5	3.46	0.05	Cell wall synthesis
720	P00965	GLNA3	Glutamine synthetase N-1	7.4	3.67	0.05	Amino acid metabolism
721	P28590	ABRC	Abrin-c OS	160.2	3.74	0.04	Defense response
722	P25700	IT2	Trypsin inhibitor 2	237.8	4.18	0.02	Protease inhibitor
723	P51851	PDC2	Pyruvate decarboxylase 2 (Fragment)	189.4	4.57	0.01	Carbohydrate metabolism
724	P13917	7SB1	Basic 7S globulin	117.1	5.10	0.02	Seed storage protein
725	Q06009	PP2A	Serine/ threonine-protein phosphatase PP2A catalytic subunit	32.0	6.55	0.03	Signal transduction
726	O82134	PCNA	Proliferating cell nuclear antigen	129.0	7.17	0.02	Replication
727	P81007	ENT	Cytolytic protein enterolobin	199.0	7.32	0.03	Pathogenesis
728	O65743	RL24	60S ribosomal protein L24	28.8	7.92	0.01	Translation
729	Q06930	ABR18	ABA-responsive protein ABR18	23.6	8.41	0.03	Growth and development
730	B5BSX1	BAMO	β-Amyrin 11-oxidase	17.9	8.85	0.01	Saponin biosynthesis
731	P45456	ACEA1	Isocitrate lyase 1 (Fragment)	53.2	12.55	0.05	Carbohydrate metabolism
732	P05190	LEGB4	Legumin type B	14.7	13.20	0.01	Seed storage protein
733	P01070	ITRA	Trypsin inhibitor A	347.1	17.99	0.02	Protease inhibitor
734	P05693	LEGK	Legumin K (Fragment)	79.0	19.89	0.04	Seed storage protein
735	Q6PSC6	MATK	Maturase K	15.1	23.81	0.04	mRNA processing
736	O48923	C71DA	Cytochrome P450 71D10	35.9	26.31	0.01	Monooxygenase
737	Q9TKS4	MATK	Maturase K	17.1	27.66	0.02	mRNA processing
738	Q8LSN3	FYPP	Phytochrome-associated serine/threonine-protein phosphatase	192.3	31.50	0.05	Signal transduction
739	P16080	LEGB7	Legumin type B (Fragment)	14.7	41.68	0.03	Seed storage protein
740	P16078	LEGB2	Legumin type B (Fragment)	14.7	42.95	0.01	Seed storage protein
741	P05692	LEGJ	Legumin J	52.9	43.38	0.01	Seed storage protein
742	P16079	LEGB6	Legumin type B (Fragment)	32.1	46.53	0.05	Seed storage protein
			Control-specific proteins				
743	Q53B75	CF1B1	Chalcone-flavonone isomerase 1β-1	233.8	Control		Secondary metabolism
744	P51820	DRTS	Bifunctional dihydrofolate reductase-thymidylate synthase	57.0	Control		Nucleotide metabolism
745	P83311	IBB	Bowman-Birk type proteinase inhibitor	103.9	Control		Protease inhibitor
746	Q03467	E13B	Glucan endo-1,3-β-glucosidase	96.4	Control		Cell wall synthesis
747	P52904	ODPB	Pyruvate dehydrogenase E1 component subunit β, mitochondrial	70.6	Control		Carbohydrate metabolism
748	P52902	ODPA	Pyruvate dehydrogenase E1 component subunit α, mitochondrial	62.6	Control		Carbohydrate metabolism

749	P83304	LEC	Mannose/glucose-specific lectin (Fragment)	4.1	Control		Carbohydrate binding
750	O49046	ARGI	Arginase	48.7	Control		Amino acid metabolism
751	P46298	RS13	40S ribosomal protein S13	66.7	Control		Translation
752	Q6WNQ8	C81E8	Cytochrome P450 81E8	88.5	Control		Monooxygenase
753	Q8GTE3	RS3A	40S ribosomal protein S3a	58.2	Control		Translation
754	P31656	CADH	Probable cinnamyl alcohol dehydrogenase	22.2	Control		Secondary metabolism
755	P46275	F16P1	Fructose-1,6-bisphosphatase, chloroplastic	112.0	Control		Carbohydrate metabolism
756	P32733	ID5A	Kunitz-type trypsin inhibitor α chain	80.5	Control		Protease inhibitor
757	P46256	ALF1	Fructose-bisphosphate aldolase, cytoplasmic isozyme 1	70.8	Control		Carbohydrate metabolism
758	P14749	AGAL	α-Galactosidase	62.0	Control		Carbohydrate metabolism
759	P04670	URIC1	Uricase-2 isozyme 1	35.7	Control		Nodulation
760	P81406	GAPN	NADP-dependent glyceraldehyde-3-phosphate dehydrogenase	114.4	Control		Carbohydrate metabolism
761	Q2PMU5	RR4	30S ribosomal protein S4, chloroplastic	111.8	Control		Translation
762	P53385	HUTU	Urocanate hydratase	45.3	Control		Nodulation
763	P22973	LEC2	Anti-H(O) lectin 2	82.7	Control		Carbohydrate binding
764	Q564G7	GMGT1	Galactomannan galactosyltransferase 1	60.2	Control		Cell wall synthesis
765	P38661	PDIA6	Probable protein disulfide-isomerase A6	102.1	Control		Redox homeostasis
766	Q2PMR0	CLPP	ATP-dependent Clp protease proteolytic subunit	1.6	Control		Proteolysis
767	P13603	ADH1	Alcohol dehydrogenase 1	4.5	Control		Catalytic activity
768	P81726	ICI2	Subtilisin inhibitor CLSI-II	46.0	Control		Defense response
769	Q2PMQ3	RPOA	DNA-directed RNA polymerase subunit α	224.3	Control		Transcription
770	Q01516	ALFC1	Fructose-bisphosphate aldolase 1, chloroplastic (Fragment)	38.3	Control		Carbohydrate metabolism
771	C6T0L2	SLE3	Protein SLE3	18.2	Control		Signal transduction
772	P19594	2SS	2S albumin	15.5	Control		Seed storage protein
773	Q9ZST8	TIC20	Protein TIC 20, chloroplastic	118.7	Control		Transport
774	P41089	CFI	Chalcone-flavonone isomerase	119.0	Control		Secondary metabolism
775	P46519	LEA14	Desiccation protectant protein Lea14 homolog	47.5	Control		Defense response
776	P85172	IBB1	Bowman-Birk type proteinase inhibitor	69.2	Control		Protease inhibitor
777	P55844	RL14	Probable 60S ribosomal protein L14	31.3	Control		Translation
778	O65751	RSSA	40S ribosomal protein SA	53.6	Control		Translation
779	Q9XHC6	C93E1	β-Amyrin 24-hydroxylase	88.8	Control		Saponin biosynthesis
780	Q41219	LEGRE	Leghemoglobin reductase	31.0	Control		Nodulation
781	Q5NE24	NSP2	Nodulation-signaling pathway 2 protein	32.5	Control		Nodulation
782	C6SXZ3	CSPL8	CASP-like protein 1D1	23.4	Control		Cell wall synthesis
783	O65731	RS5	40S ribosomal protein S5 (Fragment)	47.7	Control		Translation
784	P35694	XTH2	Xyloglucan endotransglucosylase/ hydrolase 2	14.0	Control		Cell wall synthesis
785	Q8LNZ5	XTHB	Probable xyloglucan endotransglucosylase/ hydrolase protein B	8.9	Control		Cell wall synthesis
786	Q07463	PUR7	Phosphoribosylaminoimidazole-succinocarboxamide synthase, chloroplastic (Fragment)	58.7	Control		Nucleotide metabolism
787	Q01807	LEC2	Truncated lectin 2	69.9	Control		DNA binding
788	P47905	RS27A	Ubiquitin-40S ribosomal protein S27a	163.7	Control		Signal transduction
789	P50346	RLA0	60S acidic ribosomal protein P0	134.6	Control		Translation
790	P05088	PHAE	Erythroagglutinating phytohemagglutinin	138.5	Control		Carbohydrate binding
791	P05087	PHAL	Leucoagglutinating phytohemagglutinin	378.3	Control		Defense response
792	Q9SM57	OEP21	Outer envelope pore protein 21, chloroplastic	48.3	Control		Transport
793	P93332	NOD3	Bidirectional sugar transporter N3	61.8	Control		Transport
794	A0AAR7	CCAMK	Calcium and calcium/calmodulin-dependent serine/threonine-protein kinase	107.1	Control		Signal transduction
795	P17673	RBS	Ribulose bisphosphate carboxylase small chain, chloroplastic	38.1	Control		Carbohydrate metabolism
796	P49163	RK22	50S ribosomal protein L22, chloroplastic	16.7	Control		Translation
797	Q8MC99	RPOA	DNA-directed RNA polymerase subunit α	110.3	Control		Transcription
798	P26987	SAM22	Stress-induced protein SAM22	129.0	Control		Defense response
799	Q9BBU3	PSBA	Photosystem II protein D1	26.7	Control		Photosynthesis
800	P40590	RL34	60S ribosomal protein L34	58.5	Control		Translation
801	O24296	GPX1	Phospholipid hydroperoxide glutathione peroxidase, chloroplastic	97.4	Control		Redox homeostasis
802	P05046	LEC	Lectin	47.1	Control		Carbohydrate binding
803	P05045	LEC1	Seed lectin subunit I	73.6	Control		Carbohydrate binding
804	Q9BBR1	RR18	30S ribosomal protein S18, chloroplastic	71.8	Control		Translation
805	Q9XH46	TATA	Sec-independent protein translocase protein TATA, chloroplastic	316.3	Control		Transport
806	Q6PSU2	CONG7	Conglutin-7	54.0	Control		Seed storage protein
807	Q9BBQ1	RR8	30S ribosomal protein S8, chloroplastic	44.7	Control		Translation
808	Q9SP37	SAHH	Adenosylhomocysteinase	98.5	Control		Amino acid metabolism
809	P81371	LECS	Seed lectin	107.0	Control		Carbohydrate binding
810	P13240	DR206	Disease resistance response protein 206	25.9	Control		Secondary metabolism
811	Q9S9E3	IBB	Horsegram inhibitor 1	140.8	Control		Protease inhibitor
812	Q39527	LECR	Lectin-related protein (Fragment)	273.1	Control		Carbohydrate binding
813	Q43064	PYRB3	Aspartate carbamoyltransferase 3, chloroplastic	90.0	Control		Amino acid metabolism
814	P17928	CALM	Calmodulin	248.4	Control		Signal transduction
815	Q3LSN4	LIAS1	Lipoyl synthase 1, mitochondrial	37.7	Control		Carbohydrate metabolism
816	P31893	OAT	Ornithine aminotransferase	40.2	Control		Amino acid metabolism
817	P25804	CYSP	Cysteine proteinase 15A	55.3	Control		Proteolysis
818	Q96451	1433B	14-3-3-like protein B (Fragment)	186.9	Control		Defense response
819	A4GGF3	RR15	30S ribosomal protein S15, chloroplastic	365.8	Control		Translation
820	P12459	TBB1	Tubulin β-1 chain	95.6	Control		Cytoskeleton
821	A4GGE3	NU5C	NAD(P)H-quinone oxidoreductase subunit 5, chloroplastic	13.0	Control		Electron transport
822	Q4LDF9	OEP37	Outer envelope pore protein 37, chloroplastic	25.9	Control		Transport

823	P22503	GUN	Endoglucanase	137.8	Control		Cell wall synthesis
824	P12786	COX1	Cytochrome c oxidase subunit 1	115.2	Control		Electron transport
825	P42088	LEC	Lectin OS	124.2	Control		Carbohydrate binding
826	P36361	CHI5	Endochitinase CH5B	87.9	Control		Defense response
827	O22308	7OMT6	Isoflavone-7-O-methyltransferase 6	92.3	Control		Secondary metabolism
828	P26291	UCRIA	Cytochrome b6-f complex iron-sulfur subunit, chloroplastic	31.1	Control		Electron transport
829	P09059	SVF30	Unknown seed protein 30.1	103.8	Control		Seed storage protein
830	P42054	VDAC	Outer plastidial membrane protein porin	96.6	Control		Transport
831	C6TBN2	AKR1	Probable aldo-keto reductase 1	68.9	Control		Redox homeostasis
832	Q41112	SRP	Stress-related protein	66.1	Control		Defense response
833	Q9ZS21	LGUL	Lactoylglutathione lyase	57.9	Control		Secondary metabolism
834	Q2HU68	H2A1	Probable histone H2A.1	282.1	Control		DNA binding
835	P0CC62	NU2C1	NAD(P)H-quinone oxidoreductase subunit 2 A, chloroplastic	151.7	Control		Electron transport
836	Q40359	ALFIN	PHD finger protein Alfin1	68.7	Control		Transcription
837	P11964	SODCP	Superoxide dismutase [Cu-Zn], chloroplastic	62.6	Control		Redox homeostasis
838	A4GG96	YCF3	Photosystem I assembly protein Ycf3	52.4	Control		Photosynthesis
839	A4GG95	RR4	30S ribosomal protein S4, chloroplastic	41.0	Control		Translation
840	P32291	FAD3E	ω-3 fatty acid desaturase, endoplasmic reticulum	140.8	Control		Fatty acid biosynthesis
841	P16148	PLZ12	Protein PPLZ12	77.3	Control		Cell cycle
842	P52419	PUR1	Amidophosphoribosyltransferase, chloroplastic (Fragment)	118.3	Control		Nucleotide metabolism
843	P26204	BGLS	Non-cyanogenic β-glucosidase	111.7	Control		Carbohydrate metabolism
844	P26563	AATM	Aspartate aminotransferase P2, mitochondrial (Fragment)	22.4	Control		Amino acid metabolism
845	P52766	NDHK	NAD(P)H-quinone oxidoreductase subunit K, chloroplastic	19.4	Control		Electron transport
846	A2Q1V6	ATG4	Cysteine protease ATG4	37.5	Control		Proteolysis
847	P16121	HSP70	Heat shock 70 kDa protein (Fragment)	98.2	Control		Chaperone
848	Q8H0G2	CFI1	Chalcone-flavonone isomerase 1	14.5	Control		Secondary metabolism
849	P31175	NDHK	NAD(P)H-quinone oxidoreductase subunit K, chloroplastic	41.9	Control		Electron transport
850	P31174	NDHJ	NAD(P)H-quinone oxidoreductase subunit J, chloroplastic	113.5	Control		Electron transport
851	P22196	PER2	Cationic peroxidase 2	164.4	Control		Cell wall synthesis
852	P10821	IT1A	Trypsin inhibitor 1A	38.0	Control		Protease inhibitor
853	O50044	KDSA	2-dehydro-3-deoxyphosphooctonate aldolase	113.4	Control		Carbohydrate metabolism
854	Q9XG83	G2OX	Gibberellin 2-β-dioxygenase	15.7	Control		Hormone metabolism
855	Q3LRV4	NRL4B	Bifunctional nitrilase/ nitrile hydratase NIT4B	18.8	Control		Catalytic activity
856	Q8LPW2	RT13	Small ribosomal subunit protein S13, mitochondrial	47.0	Control		Translation
857	P22177	PCNA	Proliferating cell nuclear antigen (Fragment)	196.1	Control		Replication
858	Q9LKG7	UGPA	UTP-glucose-1-phosphate uridylyltransferase	91.9	Control		Carbohydrate metabolism
859	Q42800	DAPA	4-hydroxy-tetrahydrodipicolinate synthase, chloroplastic	151.2	Control		Amino acid metabolism
860	P23233	NO16	Nodulin-16	93.4	Control		Nodulation
861	Q41701	NO12	Early nodulin-12	235.2	Control		Nodulation
862	C0HJX1	LECC1	Mannose/ glucose-specific lectin	48.3	Control		Carbohydrate binding
863	Q39445	TBB	Tubulin β chain	179.5	Control		Cytoskeleton
864	C0HJW7	MANA	α-Mannosidase (Fragments)	441.9	Control		Carbohydrate metabolism
865	P49351	FPPS1	Farnesyl pyrophosphate synthase 1	17.0	Control		Lipid metabolism
866	C0HK81	LECA	Lectin	118.7	Control		Carbohydrate binding
867	P14226	PSBO	Oxygen-evolving enhancer protein 1, chloroplastic	92.3	Control		Photosynthesis
868	Q03227	COX3	Cytochrome c oxidase subunit 3	201.3	Control		Electron transport
869	P23558	LEC1	Lectin 1	162.1	Control		Carbohydrate binding
870	P04149	ARA5	Arachin 25 kDa protein	79.8	Control		Seed storage protein
871	P04144	NO23	Nodulin-23	140.3	Control		Nodulation
872	P23535	E13B	Glucan endo-1,3-β-glucosidase, basic isoform	111.4	Control		Cell wall synthesis
873	P04122	LECB	Lectin β-1 and β-2 chains	365.8	Control		Carbohydrate binding
874	P80463	PHS1	Phaseolin	86.6	Control		Seed storage protein
875	P24924	ITRY	Trypsin inhibitor	189.7	Control		Protease inhibitor
876	B5LMS0	NDHH	NAD(P)H-quinone oxidoreductase subunit H, chloroplastic	48.5	Control		Electron transport
877	P48513	TF2B	Transcription initiation factor IIB	112.2	Control		Transcription
878	P02240	LGB2	Leghemoglobin-2	92.4	Control		Nodulation
879	Q9SQL2	CB24	Chlorophyll a-b binding protein P4, chloroplastic	100.2	Control		Photosynthesis
880	P39882	NIA	Nitrate reductase [NADH] (Fragment)	19.3	Control		Nodulation
881	P02238	LGBA	Leghemoglobin A	75.3	Control		Nodulation
882	P02233	LGB1	Leghemoglobin-1	110.3	Control		Nodulation
883	P02232	LGB1	Leghemoglobin-1	25.0	Control		Nodulation
884	Q6DW73	DGDG2	Digalactosyldiacylglycerol synthase 2, chloroplastic	117.4	Control		Cell wall synthesis
885	Q41015	PIP21	Kunitz-type trypsin inhibitor-like 1 protein	17.0	Control		Protease inhibitor
886	P56707	SMTA	Selenocysteine methyltransferase	28.6	Control		Amino acid metabolism
887	O22518	RSSA	40S ribosomal protein SA	59.7	Control		Translation
888	Q35639	NU5M	NADH-ubiquinone oxidoreductase chain 5 (Fragment)	81.3	Control		Electron transport
889	Q42799	C93A2	Cytochrome P450 93A2	49.4	Control		Monooxygenase
890	Q42796	F16P1	Fructose-1,6-bisphosphatase, chloroplastic	104.4	Control		Carbohydrate metabolism
891	Q647H2	AHY3	Arachin Ahy-3	79.0	Control		Seed storage protein
892	P93162	CHLI	Magnesium-chelatase subunit ChlI, chloroplastic	43.6	Control		Photosynthesis
893	Q84V83	LAR	Leucoanthocyanidin reductase	63.9	Control		Secondary metabolism
894	P02870	LEC	Lectin	192.3	Control		Carbohydrate binding
895	P35450	EFGC	Elongation factor G, chloroplastic (Fragment)	30.5	Control		Translation
896	Q43857	INVA	Acid β-fructofuranosidase	104.3	Control		Carbohydrate metabolism
897	P53763	URIC	Uricase-2	37.0	Control		Nodulation

898	P28640	DHN2	Dehydrin DHN2	181.4	Control		Defense response
899	Q9ZTR1	SPD1	Spermidine synthase 1	46.5	Control		Amino acid metabolism
900	Q9ZTR0	SPD2	Spermidine synthase 2	58.5	Control		Amino acid metabolism
901	P02866	CONA	Concanavalin-A	43.8	Control		Carbohydrate metabolism
902	P28639	DHN1	Dehydrin DHN1	226.7	Control		Defense response
903	P10743	VSPB	Stem 31 kDa glycoprotein	52.3	Control		Seed storage protein
904	O81970	C71A9	Cytochrome P450 71A9	58.7	Control		Monooxygenase
905	Q94G17	TATC	Sec-independent protein translocase protein TATC, chloroplastic	66.6	Control		Transport
906	P83052	BBKI	Kunitz-type serine Protease inhibitor BbKI	219.6	Control		Protease inhibitor
907	P83051	BBCI	Kunitz-type proteinase inhibitor BbCI	179.4	Control		Protease inhibitor
908	Q43820	DCAM	S-ASdenosylmethionine decarboxylase proenzyme	65.7	Control		Amino acid metabolism
909	Q41649	FKB15	FK506-binding protein 2	115.6	Control		Defense response
910	Q41640	RAB7	Ras-related protein Rab7	121.2	Control		Signal transduction
911	Q41638	XTHA	Xyloglucan endotransglucosylase/hydrolase protein A	23.0	Control		Cell wall synthesis
912	P83036	ITRY	Trypsin inhibitor	158.6	Control		Protease inhibitor
913	O48920	ARF	ADP-ribosylation factor	44.8	Control		Transport
914	P07371	CB22	Chlorophyll a-b binding protein AB80, chloroplastic	40.7	Control		Photosynthesis
915	O24076	GBLP	Guanine nucleotide-binding protein subunit β-like protein	139.7	Control		Signal transduction
916	P86993	LECT	Lectin	81.4	Control		Carbohydrate binding
917	P32110	GSTX6	Probable glutathione S-transferase	168.0	Control		Redox homeostasis
918	P86624	LECA	Lectin α chain	111.2	Control		Carbohydrate binding
919	P51850	PDC1	Pyruvate decarboxylase 1	104.2	Control		Carbohydrate metabolism
920	Q9M4T8	PSA5	Proteasome subunit α type-5	13.8	Control		Protein Modification
921	A2SY66	VICHY	Vicianin hydrolase (Fragment)	63.9	Control		Carbohydrate metabolism
922	A7ISP6	CFI3	Chalcone-flavonone isomerase 3	6.8	Control		Secondary metabolism
923	P06585	PSBA	Photosystem II protein D1	19.6	Control		Photosynthesis
924	C6SZ04	CSPL3	CASP-like protein 2C1	40.9	Control		Cell wall synthesis
			Treated-specific proteins				
925	P20150	CEMA	Chloroplast envelope membrane protein	86.1	Treated		Transport
926	O82043	ILV5	Ketol-acid reductoisomerase, chloroplastic	95.3	Treated		Amino acid metabolism
927	Q9ZTA9	FRIL	Flt3 receptor-interacting lectin	107.0	Treated		Carbohydrate binding
928	O24325	VPE1	Vacuolar-processing enzyme	85.7	Treated		Seed storage protein
929	P56331	IF1A	Eukaryotic translation initiation factor 1α	188.1	Treated		Translation
930	Q2N2K1	PHYK1	Probable phytol kinase 1, chloroplastic	131.7	Treated		Pigment Metabolism
931	Q2N2K0	PHYK3	Probable phytol kinase 3, chloroplastic	23.3	Treated		Pigment Metabolism
932	P46266	1433	14-3-3-like protein	167.2	Treated		Defense response
933	A0A067YBQ3	UGT13	UDP-glycosyltransferase 13	66.0	Treated		Carbohydrate metabolism
934	P15838	LEGA2	Legumin A2	6.2	Treated		Seed storage protein
935	P01066	IBB1	Bowman-Birk type proteinase inhibitor A-II	258.1	Treated		Protease inhibitor
936	P01057	IBB3	Bowman-Birk type proteinase inhibitor DE-3	188.0	Treated		Protease inhibitor
937	Q94IC4	FRI2	Ferritin-2, chloroplastic	25.4	Treated		Photosynthesis
938	Q1S9I9	H2B1	Probable histone H2B.1	33.5	Treated		DNA binding
939	K7LFJ0	PP890	Protein PROPEP890	587.9	Treated		Cell cycle
940	Q42372	LCB2	Bark agglutinin I polypeptide β	61.6	Treated		Carbohydrate binding
941	Q2QKL5	PCS3	Glutathione γ-glutamylcysteinyltransferase 3	78.7	Treated		Hormone metabolism
942	Q40193	RB11C	Ras-related protein Rab11C	225.8	Treated		Signal transduction
943	Q40191	RB11A	Ras-related protein Rab11A	142.2	Treated		Signal transduction
944	Q07176	MMK1	Mitogen-activated protein kinase homolog MMK1	46.5	Treated		Signal transduction
945	P05718	CYB	Cytochrome b	85.0	Treated		Electron transport
946	Q2PMQ5	CYB6	Cytochrome b6	21.7	Treated		Electron transport
947	Q06076	ABRD	Abrin-d	38.4	Treated		Defense response
948	O65781	GALE2	UDP-glucose 4-epimerase GEPI48	99.9	Treated		Carbohydrate metabolism
949	A0A161AT60	NLTP1	Non-specific lipid-transfer protein 1	1034.5	Treated		Cell wall synthesis
950	P10322	NO25	Nodulin-25	140.8	Treated		Nodulation
951	Q2PMN2	NU4C	NAD(P)H-quinone oxidoreductase chain 4, chloroplastic	110.5	Treated		Electron transport
952	P52581	IFRH	Isoflavone reductase homolog	60.1	Treated		Secondary metabolism
953	Q2PMM9	NU5C	NAD(P)H-quinone oxidoreductase subunit 5, chloroplastic	101.3	Treated		Electron transport
954	P25273	KTI2	Kunitz-type trypsin inhibitor KTI2	190.7	Treated		Protease inhibitor
955	B1B5P4	N8DT2	Naringenin 8-dimethylallyltransferase 2, chloroplastic	20.2	Treated		Secondary metabolism
956	P47923	NDK2	Nucleoside diphosphate kinase 2, chloroplastic	25.7	Treated		Nucleotide metabolism
957	Q9FT25	PDX1	Pyridoxal 5'-phosphate synthase subunit PDX1	18.6	Treated		Amino acid metabolism
958	O49929	OEP24	Outer envelope pore protein 24, chloroplastic	156.9	Treated		Transport
959	P24146	LEC4	Lectin-4	123.7	Treated		Carbohydrate binding
960	P50345	RLA0	60S acidic ribosomal protein P0	63.9	Treated		Translation
961	P51428	RT10	Ribosomal protein S10, mitochondrial	57.1	Treated		Translation
962	P58155	CEMA	Chloroplast envelope membrane protein	74.3	Treated		Transport
963	P86893	LECS	Seed lectin	16.9	Treated		Carbohydrate binding
964	P62929	ALB1D	Albumin-1 D	48.4	Treated		Seed storage protein
965	P49158	ACCD	Acetyl-coenzyme A carboxylase carboxyl transferase subunit β, chloroplastic	111.3	Treated		Fatty acid biosynthesis
966	P00865	RBS1	Ribulose bisphosphate carboxylase small chain 1, chloroplastic	188.6	Treated		Carbohydrate metabolism
967	Q9BBR0	RK20	50S ribosomal protein L20, chloroplastic	176.0	Treated		Translation
968	Q9BBQ9	CLPP	ATP-dependent Clp protease proteolytic subunit	15.8	Treated		Proteolysis
969	Q43086	PYRB1	Aspartate carbamoyltransferase 1, chloroplastic	151.8	Treated		Amino acid metabolism
970	Q43075	SPE1	Arginine decarboxylase	56.6	Treated		Amino acid metabolism
971	Q43072	HIS7	Imidazoleglycerol-phosphate dehydratase	70.2	Treated		Nucleotide metabolism
972	Q39528	LEC1	Agglutinin-1	48.1	Treated		Carbohydrate binding

973	H1A988	C7254	11-oxo-β-amyrin 30-oxidase	80.4	Treated		Saponin biosynthesis
974	P08927	RUBB	RuBisCO large subunit-binding protein subunit β, chloroplastic	82.7	Treated		Carbohydrate metabolism
975	O24542	AX22D	Auxin-induced protein 22D	158.2	Treated		Growth and development
976	O24541	AX22C	Auxin-induced protein 22C	115.7	Treated		Growth and development
977	P29257	LEC2	2-Acetamido-2-deoxy-D-galactose-binding seed lectin 2	41.6	Treated		Carbohydrate binding
978	A4GGF2	NDHH	NAD(P)H-quinone oxidoreductase subunit H, chloroplastic	86.4	Treated		Electron transport
979	A4GGE6	NU4C	NAD(P)H-quinone oxidoreductase chain 4, chloroplastic	25.4	Treated		Electron transport
980	P80572	ADHX	Alcohol dehydrogenase class-3	41.5	Treated		Catalytic activity
981	Q39818	HS22M	Heat shock 22 kDa protein, mitochondrial	127.7	Treated		Chaperone
982	P39657	RUAP	RuBisCO-associated protein	62.0	Treated		Carbohydrate metabolism
983	P48630	FD6E1	ω-6 fatty acid desaturase,endoplasmic reticulum isozyme 1	160.6	Treated		Fatty acid biosynthesis
984	P27047	DRR4	Disease resistance response protein DRRG49-C	45.1	Treated		Secondary metabolism
985	A4GGB8	CEMA	Chloroplast envelope membrane protein	80.1	Treated		Transport
986	Q41161	LCS2	Seed agglutinin 2	61.7	Treated		Seed storage protein
987	Q41160	LCB3	Putative bark agglutinin LECRPA3 (Fragment)	213.1	Treated		Defense response
988	Q01417	PM1	18 kDa seed maturation protein	72.4	Treated		Growth and development
989	Q03943	IM30	Membrane-associated 30 kDa protein, chloroplastic	264.8	Treated		Transport
990	Q41159	LCB1	Bark agglutinin I polypeptide A	516.7	Treated		Carbohydrate binding
991	Q9FRT8	ALB1	Albumin-1 (Fragment)	60.5	Treated		Seed storage protein
992	Q8H0P8	RBP1	RNA-binding protein 1	14.4	Treated		mRNA processing
993	Q944T2	TCTP	Translationally-controlled tumor protein homolog	159.8	Treated		Cell cycle
994	P0CC88	NU2C1	NAD(P)H-quinone oxidoreductase subunit 2 A, chloroplastic	118.5	Treated		Electron transport
995	Q1SU99	H2B3	Probable histone H2B.3	33.5	Treated		DNA binding
996	Q8RW99	F16P2	Fructose-1,6-bisphosphatase, cytosolic	10.5	Treated		Carbohydrate metabolism
997	Q9SXS3	C93C2	2-hydroxy-isoflavanone synthase	45.6	Treated		Secondary metabolism
998	P50288	ASPG	Isoaspartyl peptidase/L-asparaginase	136.5	Treated		Amino acid metabolism
999	P29501	TBB2	Tubulin β-2 chain (Fragment)	95.0	Treated		Cytoskeleton
1000	A4GG99	RR14	30S ribosomal protein S14, chloroplastic	100.9	Treated		Translation
1001	C6T2J5	CSPL4	CASP-like protein 2D1	44.2	Treated		Cell wall synthesis
1002	P45621	GSA	Glutamate-1-semialdehyde 2,1-aminomutase, chloroplastic	129.7	Treated		Amino acid metabolism
1003	Q40345	IDHP	Isocitrate dehydrogenase [NADP], chloroplastic (Fragment)	176.1	Treated		Carbohydrate metabolism
1004	P52424	PUR5	Phosphoribosylformylglycinamidine cyclo-ligase, chloroplastic/ mitochondrial	64.6	Treated		Nucleotide metabolism
1005	E4NKF8	PUB1	U-box domain-containing protein 1	43.1	Treated		Nodulation
1006	E3SXU4	BHLHW	Basic helix-loop-helix protein A	149.0	Treated		Secondary metabolism
1007	P49045	VPE	Vacuolar-processing enzyme	85.8	Treated		Seed storage protein
1008	Q42822	RBS	Ribulose bisphosphate carboxylase small chain, chloroplastic	34.4	Treated		Carbohydrate metabolism
1009	Q05462	RL27	60S ribosomal protein L27	273.9	Treated		Translation
1010	P25795	AL7A1	Aldehyde dehydrogenase family 7 member A1	21.2	Treated		Catalytic activity
1011	P68430	H32	Histone H3.2	106.0	Treated		DNA binding
1012	P42653	1433A	14-3-3-like protein A	165.0	Treated		Defense response
1013	P68427	H32	Histone H3.2	106.0	Treated		DNA binding
1014	A0AT30	NLTP3	Non-specific lipid-transfer protein 3	764.0	Treated		Cell wall synthesis
1015	Q40977	MDAR	Monodehydroascorbate reductase	68.2	Treated		Redox homeostasis
1016	Q9FEL7	LAX2	Auxin transporter-like protein 2	148.3	Treated		Growth and development
1017	Q9FEL6	LAX3	Auxin transporter-like protein 3	108.4	Treated		Growth and development
1018	U3THC0	FG2KI	Inactive UDP-glycosyltransferase 79A6	49.1	Treated		Carbohydrate metabolism
1019	Q9FY06	PPF1	Inner membrane protein PPF-1, chloroplastic	67.4	Treated		Transport
1020	C6SZP8	CSPL5	CASP-like protein 1E2	25.7	Treated		Cell wall synthesis
1021	P30364	ASPG	Isoaspartyl peptidase/L-asparaginase	159.8	Treated		Amino acid metabolism
1022	P30362	ASPG	Isoaspartyl peptidase/L-asparaginase (Fragment)	30.6	Treated		Amino acid metabolism
1023	K7K424	DAT2D	Diacylglycerol O-acyltransferase 2D	47.7	Treated		Lipid metabolism
1024	Q04655	YMA6	Uncharacterized mitochondrial protein ORF154	107.3	Treated		Uncharacterized
1025	P15958	NU5C	NAD(P)H-quinone oxidoreductase subunit 5, chloroplastic	68.5	Treated		Electron transport
1026	P48534	APX1	L-Ascorbate peroxidase, cytosolic	53.3	Treated		Redox homeostasis
1027	P04793	HSP13	17.5 kDa class I heat shock protein	155.2	Treated		Chaperone
1028	P14848	LGB2	Leghemoglobin 2	413.5	Treated		Nodulation
1029	Q09134	GRPA	Abscisic acid and environmental stress-inducible protein	26.8	Treated		Defense response
1030	Q09131	PPAF	Purple acid phosphatase	57.8	Treated		Signal transduction
1031	Q41050	OEP16	Outer envelope pore protein 16, chloroplastic	111.2	Treated		Transport
1032	P28011	AAT1	Aspartate aminotransferase 1	52.3	Treated		Amino acid metabolism
1033	P28010	LGB4	Leghemoglobin	174.5	Treated		Nodulation
1034	P02236	LGB2	Leghemoglobin C2	35.4	Treated		Nodulation
1035	Q6DW75	DGDG2	Digalactosyldiacylglycerol synthase 2, chloroplastic	18.3	Treated		Cell wall synthesis
1036	P25096	P21	Protein P21	12.8	Treated		Cell cycle
1037	Q43560	PR1	Class-10 pathogenesis-related protein 1	212.1	Treated		Pathogenesis
1038	P52389	CDC2	Cell division control protein 2 homolog	80.9	Treated		Growth and development
1039	Q06197	IDHC	Isocitrate dehydrogenase [NADP]	71.9	Treated		Carbohydrate metabolism
1040	P11894	RK9	50S ribosomal protein L9, chloroplastic	210.0	Treated		Translation
1041	P11893	RK24	50S ribosomal protein L24, chloroplastic	52.5	Treated		Translation
1042	Q6UD73	LYK3	LysM domain receptor-like kinase 3	69.3	Treated		Defense response
1043	Q41009	TOC34	Translocase of chloroplast 34	169.3	Treated		Transport
1044	Q41005	CBPX	Serine carboxypeptidase-like (Fragment)	29.2	Treated		Secondary metabolism
1045	Q35638	RHO1	Rac-like GTP-binding protein RHO1	87.0	Treated		Signal transduction

1046	O65874	MTF1	MADS-box transcription factor 1	91.8	Treated		DNA binding
1047	P19329	ARC1	Arcelin-1	152.9	Treated		Seed storage protein
1048	P16064	ICI1	Subtilisin inhibitor 1	860.5	Treated		Defense response
1049	P16059	PSBP	Oxygen-evolving enhancer protein 2, chloroplastic	68.6	Treated		Photosynthesis
1050	P02853	PHSB	Phaseolin, β-type	18.0	Treated		Seed storage protein
1051	O81974	C71D8	Cytochrome P450 71D8	11.2	Treated		Monooxygenase
1052	Q41669	MT1A	Metallothionein-like protein 1A	76.7	Treated		Defense response
1053	A6XNC6	UGFGT	Flavonoid 3-O-glucosyltransferaseαα	129.6	Treated		Secondary metabolism
1054	P27880	HSP12	18.2 kDa class I heat shock protein	206.4	Treated		Chaperone
1055	Q43814	OTC	Ornithine carbamoyltransferase, chloroplastic	139.6	Treated		Amino acid metabolism
1056	P16002	PLAS	Plastocyanin, chloroplastic	26.7	Treated		Photosynthesis
1057	Q8W171	CYP1	Peptidyl-prolyl cis-trans isomerase 1	127.7	Treated		Protein modification
1058	Q06445	CYTI	Cysteine proteinase inhibitor	103.3	Treated		Protease inhibitor
1059	I1LCI8	FG2KO	UDP-glycosyltransferase 79A6	49.1	Treated		Carbohydrate metabolism
1060	Q9SWF9	ZFNL	Zinc finger CCCH domain-containing protein ZFN-like	29.8	Treated		DNA binding
1061	P49252	AMO	Primary amine oxidase (Fragment)	66.0	Treated		Hormone metabolism
1062	P25985	PR1	Pathogenesis-related protein 1	118.3	Treated		Pathogenesis

Figure 3. Schematic representation of secondary metabolic pathway. Relative expression of proteins in roots of Pongamia related to phenylproponoid pathway.

Colour key represents fold expression and number indicates number of identified peptides; red colour: up-regulated proteins, green colour: down-regulated proteins, blue colour: unchanged proteins, yellow colour: control specific proteins, and violet colour: treated specific proteins. CHS: chalcone synthase, PAL: phenylalanine ammonia lyase. For protein abbreviations see in table 1.

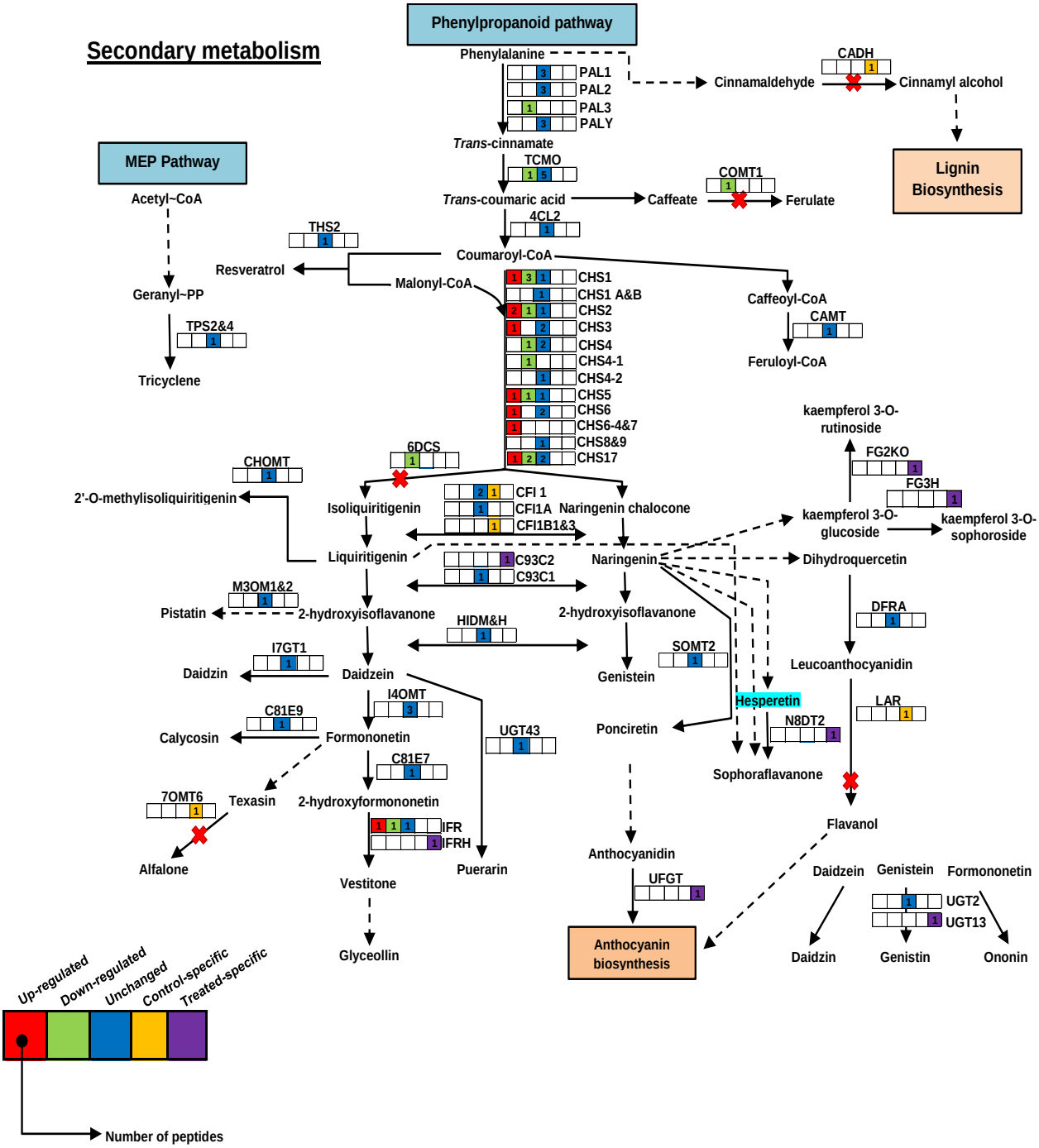
Secondary metabolism
Phenylpropanoid pathway
Phenylalanine
PAL1
PAL2
PAL3
PALY
Cinnamaldehyde
CADH
Cinnamyl alcohol
Lignin Biosynthesis
Trans-cinnamate
TCMO
Trans-coumaric acid
Caffeate
COMT1
Ferulate
MEP Pathway
Acetyl~CoA
4CL2
Coumaroyl-CoA
THS2
Resveratrol
Malonyl-CoA
Geranyl~PP
TPS2&4
Tricyclene
CHS1
CHS1 A&B
CHS2
CHS3
CHS4
CHS4-1
CHS4-2
CHS5
CHS6
CHS6-4&7
CHS8&9
CHS17
Caffeoyl-CoA
CAMT
Feruloyl-CoA
kaempferol 3-O-rutinoside
FG2KO
FG3H
kaempferol 3-O-glucoside
kaempferol 3-O-sophoroside
CHOMT
2'-O-methylisoliquiritigenin
6DCS
Isoliquiritigenin
CFI 1
CFI1A
CFI1B1&3
Naringenin chalcone
Liquiritigenin
C93C2
C93C1
Naringenin
Dihydroquercetin
M3OM1&2
Pistatin
2-hydroxyisoflavanone
HIDM&H
2-hydroxyisoflavanone
DFRA
Leucoanthocyanidin
I7GT1
Daidzin
Daidzein
SOMT2
Genistein
Hesperetin
LAR
I4OMT
C81E9
Calycosin
Formononetin
UGT43
Ponciretin
N8DT2
Sophoraflavanone
C81E7
7OMT6
Texasin
2-hydroxyformononetin
IFR
IFRH
Flavanol
Alfalone
Vestitone
Puerarin
Anthocyanidin
UFGT
Daidzein
Genistein
Formononetin
UGT2
UGT13
Glyceollin
Anthocyanin biosynthesis
Daidzin
Genistin
Ononin
Up-regulated
Down-regulated
Unchanged
Control-specific
Treated-specific
Number of peptides

Figure 4. (A) Relative fold expression of chalcone synthase proteins and (B) isoforms of seed storage proteins. For protein abbreviations see in table 1.

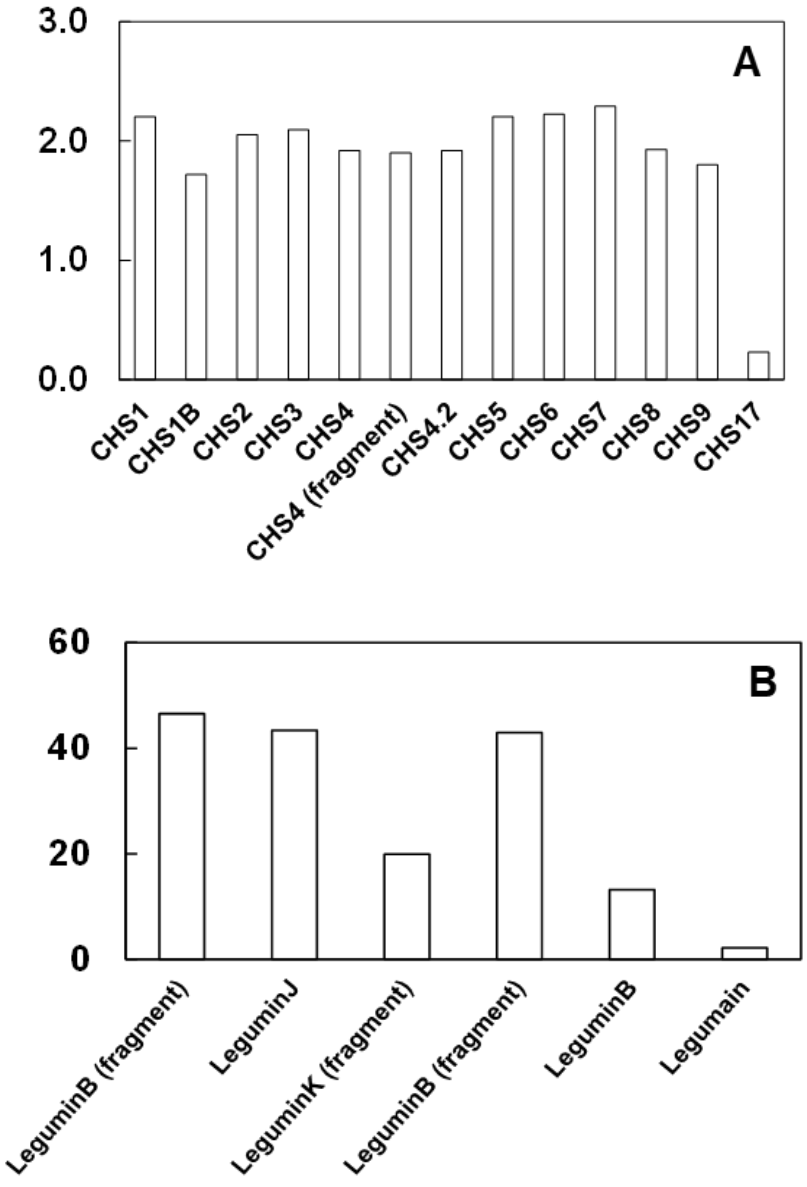
3.0
2.0
1.0
0.0
A
CHS1
CHS1B
CHS2
CHS3
CHS4
CHS4 (fragment)
CHS4.2
CHS5
CHS6
CHS7
CHS8
CHS9
CHS17
60
40
20
0
B
LeguminB (fragment)
LeguminJ
LeguminK (fragment)
LeguminB (fragment)
LeguminB
Legumain

Figure 5. Relative fold expression of DEPs belongs to various metabolic pathways.

Colour key represents fold expression and number indicates number of identified peptides; red colour: up-regulated proteins, green colour: down-regulated proteins, blue colour: unchanged proteins, yellow colour: control specific proteins, and violet colour: treated specific proteins. For protein abbreviations see in table 1.

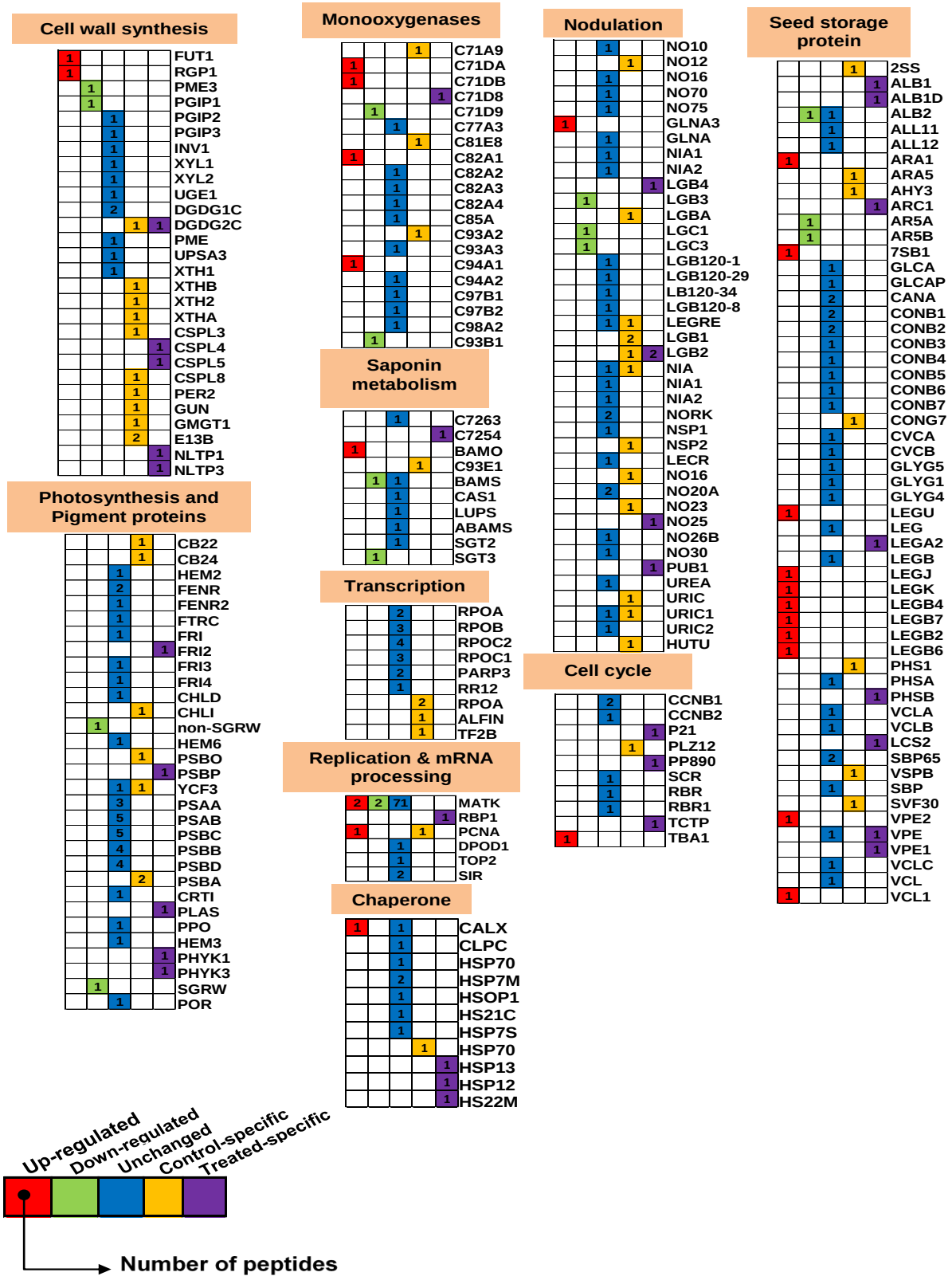
Cell wall synthesis
FUT1
RGP1
PME3
PGIP1
PGIP2
PGIP3
INV1
XYL1
XYL2
UGE1
DGDG1C
DGDG2C
PME
UPSA3
XTH1
XTHB
XTH2
XTHA
CSPL3
CSPL4
CSPL5
CSPL8
PER2
GUN
GMGT1
E13B
NLTP1
NLTP3
Photosynthesis and Pigment proteins
CB22
CB24
HEM2
FENR
FENR2
FTRC
FRI
FRI2
FRI3
FRI4
CHLD
CHLI
non-SGRW
HEM6
PSBO
PSBP
YCF3
PSAA
PSAB
PSBC
PSBB
PSBD
PSBA
CRTI
PLAS
PPO
HEM3
PHYK1
PHYK3
SGRW
POR
Monooxygenases
C71A9
C71DA
C71DB
C71D8
C71D9
C77A3
C81E8
C82A1
C82A2
C82A3
C82A4
C85A
C93A2
C93A3
C94A1
C94A2
C97B1
C97B2
C98A2
C93B1
Saponin metabolism
C7263
C7254
BAMO
C93E1
BAMS
CAS1
LUPS
ABAMS
SGT2
SGT3
Transcription
RPOA
RPOB
RPOC2
RPOC1
PARP3
RR12
RPOA
ALFIN
TF2B
Replication & mRNA processing
MATK
RBP1
PCNA
DPOD1
TOP2
SIR
Chaperone
CALX
CLPC
HSP70
HSP7M
HSOP1
HS21C
HSP7S
HSP70
HSP13
HSP12
HS22M
Nodulation
NO10
NO12
NO16
NO70
NO75
GLNA3
GLNA
NIA1
NIA2
LGB4
LGB3
LGBA
LGC1
LGC3
LGB120-1
LGB120-29
LB120-34
LGB120-8
LEGRE
LGB1
LGB2
NIA
NIA1
NIA2
NORK
NSP1
NSP2
LECR
NO16
NO20A
NO23
NO25
NO26B
NO30
PUB1
UREA
URIC
URIC1
URIC2
HUTU
Cell cycle
CCNB1
CCNB2
P21
PLZ12
PP890
SCR
RBR
RBR1
TCTP
TBA1
Seed storage protein
2SS
ALB1
ALB1D
ALB2
ALL11
ALL12
ARA1
ARA5
AHY3
ARC1
AR5A
AR5B
7SB1
GLCA
GLCAP
CANA
CONB1
CONB2
CONB3
CONB4
CONB5
CONB6
CONB7
CONG7
CVCA
CVCB
GLYG5
GLYG1
GLYG4
LEGU
LEG
LEGA2
LEGB
LEGJ
LEGK
LEGB4
LEGB7
LEGB2
LEGB6
PHS1
PHSA
PHSB
VCLA
VCLB
LCS2
SBP65
VSPB
SBP
SVF30
VPE2
VPE
VPE1
VCLC
VCL
VCL1
Up-regulated
Down-regulated
Unchanged
Control-specific
Treated-specific
Number of peptides

kinase (NFP), guanine nucleotide-binding protein α-2 subunit (GPA1), GPA 2, phytochrome type (PHY) A, PHY B, mitogen-activated protein kinase homolog (MMK) 2 and protein kinase PVPK-1. Notably, proteins AUX 22C, AUX 22D, LAX 2, LAX 3, PCS 3, AMO (isoform of AMO), Ras-related protein Rab 11A, Rab 11C, MMK 1 (isoform of MMK 1), purple acid phosphatase, and Rac-like GTP-binding protein (RHO1) only induced in salt treated plants.

Antioxidant enzymes and electron transport chain components

CATA4 showed significant up-regulation under salt stress (Figure 9). Two antioxidant enzymes monodehydroascorbate reductase and L-ascorbate peroxidase increased significantly in roots of salt treated plants. Electron transport chain proteins such as NAD(P)H-quinone oxidoreductase (NDHH) subunit H (chloroplast origin), ATP synthase subunit α (mitochondrial origin), ATPA (chloroplast origin) and ATP E (chloroplast origin) significantly increased under salt stress (Figure 9). However, the expression levels of proteins glutathione S-transferase (GSTX) 3, ATP B (chloroplast origin) and ATP G (chloroplast origin) decreased significantly in treated roots of Pongamia. CATA 1, CATA 2, CATA 3, NAD(P)H-quinone oxidoreductase (NU) subunit 5 (chloroplast origin), cytochrome f (CYF), ubiquinol oxidase (AOX) 1 (mitochondria origin), cytochrome c oxidase subunit (COX) 2 (mitochondria origin), NADPH-cytochrome P450 reductase, thioredoxin F-type (chloroplast origin), NDHH (isoform of NDHH), alternative oxidase (AOX) 3 (mitochondria origin), ATP B (chloroplast origin) (isoform of ATP B), ATP A (chloroplast origin) (isoform of ATP A) and ATP A (mitochondria origin) (isoform of ATP A). Proteins such as CYB, CYB6, NU2A, NU4 (chloroplast origin), NU5 (chloroplast origin) (isoform of NU5) and NDHH (chloroplast origin) (isoform of NDHH) were induced significantly in roots of treated plants.

Other DEPs

Trypsin protease inhibitors (IT) such as IT2 and ITRA showed significant increase, while ITRB was decreased in roots of salt treated plants (Table 1). Proteinase inhibitors bowman-Birk type proteinase inhibitor A-II (IBB1), IBB3, kunitz-type trypsin inhibitor KTI2, cysteine proteinase inhibitor, peptidyl-prolyl cis-trans isomerase 1 and ATP-dependent Clp protease proteolytic subunit were significantly up-regulated in roots of treated plants. Proteins belonging to monooxygenase family, cytochrome P450 71D10 (C71DA), C71DB, cytochrome P450 82A1 and cytochrome P450 94A1, showed significant induction, while cytochrome P450 71D9 showed significant decrease in roots of salt treated plants (Figure 10). Several other proteins namely calnexin homolog, maturase (MATK) K, proliferating cell nuclear antigen (PCNA), vacuolar-sorting receptor 1, low affinity sulfate transporter 3, abrin-c OS, tubulin alpha-1 chain, cytolytic protein enterolobin, and glutamine synthetase nodule isozyme increased under salt stress (Figure 11). Conversely, we also observed that isoforms of MATK showed some increase or unchanged during salt stress. Translation proteins such as 60S ribosomal protein (RL) L24 showed significant increase, while 50S ribosomal protein (RK16) L16 (chloroplast origin), eukaryotic translation initiation factor 5, RK2A, RK2B and RK2 showed significant decrease in roots of salt treated plants. Proteins such as eukaryotic translation initiation factor 1A, 60S acidic ribosomal protein (RL) P0, RL27, ribosomal protein S10 (mitochondria origin), RK20, RK14, RK9 and RK24 showed significant increase in only roots of salt treated plants. However, carbohydrate binding proteins such as Flt3 receptor-interacting lectin, bark agglutinin I polypeptide (LC) B1, lectin-4, seed lectin (LEC) 1, agglutinin-1, LEC2, LCB2 and LCB3 showed an increase in roots of treated plants.

Figure 6. Schematic representation of carbohydrate metabolic pathway.

The relative expression of proteins in the roots of Pongamia related to carbohydrate metabolism. Colour key represents fold expression and number indicates number of identified peptides; red colour: up-regulated proteins, green colour: down-regulated proteins, blue colour: unchanged proteins, yellow colour: control specific proteins, and violet colour: treated specific proteins. G6P: glucose-6-phosphatase, MTDH: mannitol dehydrogenase. For protein abbreviations see in table 1.

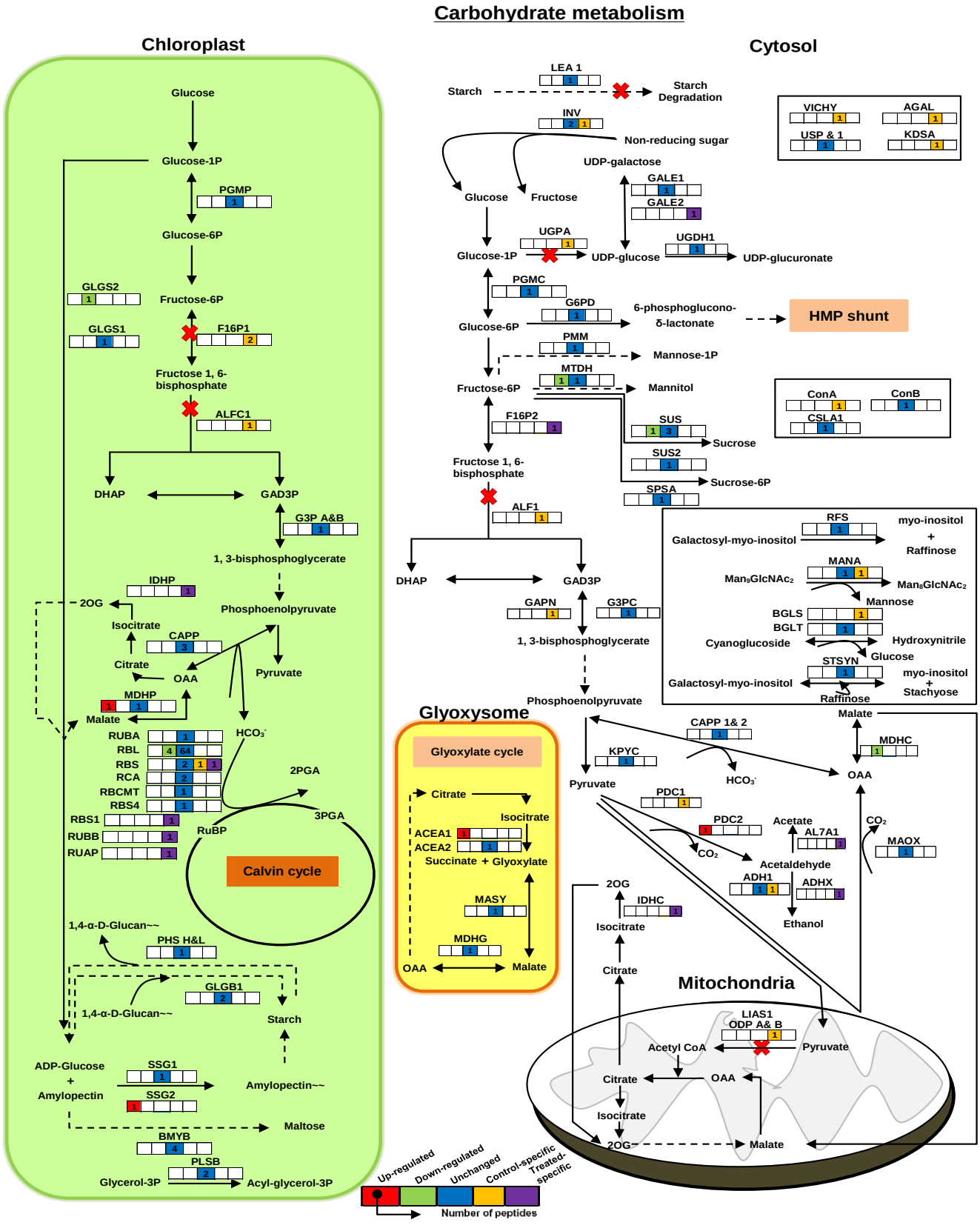
Carbohydrate metabolism
Chloroplast
Cytosol
Glyoxysome
Mitochondria
Glucose
Glucose-1P
PGMP
Glucose-6P
GLGS2
Fructose-6P
GLGS1
F16P1
Fructose 1, 6-bisphosphate
ALFC1
DHAP
GAD3P
G3P A&B
1, 3-bisphosphoglycerate
IDHP
2OG
Isocitrate
Phosphoenolpyruvate
CAPP
Citrate
OAA
Pyruvate
MDHP
Malate
RUBA
RBL
RBS
RCA
RBCMT
RBS4
RBS1
RUBB
RUAP
HCO3-
2PGA
3PGA
RuBP
Calvin cycle
1,4-α-D-Glucan~~
PHS H&L
GLGB1
Starch
ADP-Glucose + Amylopectin
SSG1
SSG2
Amylopectin~~
Maltose
BMYB
PLSB
Glycerol-3P
Acyl-glycerol-3P
LEA 1
Starch
Starch Degradation
INV
Non-reducing sugar
UDP-galactose
GALE1
GALE2
Glucose
Fructose
UGPA
UDP-glucose
UGDH1
UDP-glucuronate
PGMC
G6PD
6-phosphoglucono-δ-lactonate
HMP shunt
PMM
Mannose-1P
MTDH
Mannitol
F16P2
SUS
Sucrose
SUS2
Sucrose-6P
SPSA
ALF1
GAPN
G3PC
VICHY
AGAL
USP & 1
KDSA
ConA
ConB
CSLA1
RFS
Galactosyl-myo-inositol
myo-inositol + Raffinose
MANA
Man9GlcNAc2
Man8GlcNAc2
Mannose
BGLS
BGLT
Cyanoglucoside
Hydroxynitrile
Glucose
STSYN
Galactosyl-myo-inositol
myo-inositol + Stachyose
Raffinose
Glyoxylate cycle
Citrate
Isocitrate
ACEA1
ACEA2
Succinate + Glyoxylate
MASY
MDHG
OAA
Malate
KPYC
CAPP 1& 2
PDC1
PDC2
Acetate
AL7A1
CO2
MAOX
Acetaldehyde
ADH1
ADHX
Ethanol
IDHC
LIAS1
ODP A& B
Acetyl CoA
Pyruvate
Up-regulated
Down-regulated
Unchanged
Control-specific
Treated-specific
Number of peptides

Figure 7. Relative fold expression of DEPs belongs to various metabolic pathways.
Colour key represents fold expression and number indicates number of identified peptides; red colour: up-regulated proteins, green colour: down-regulated proteins, blue colour: unchanged proteins, yellow colour: control specific proteins, and violet colour: treated specific proteins. For protein abbreviations see in table 1.

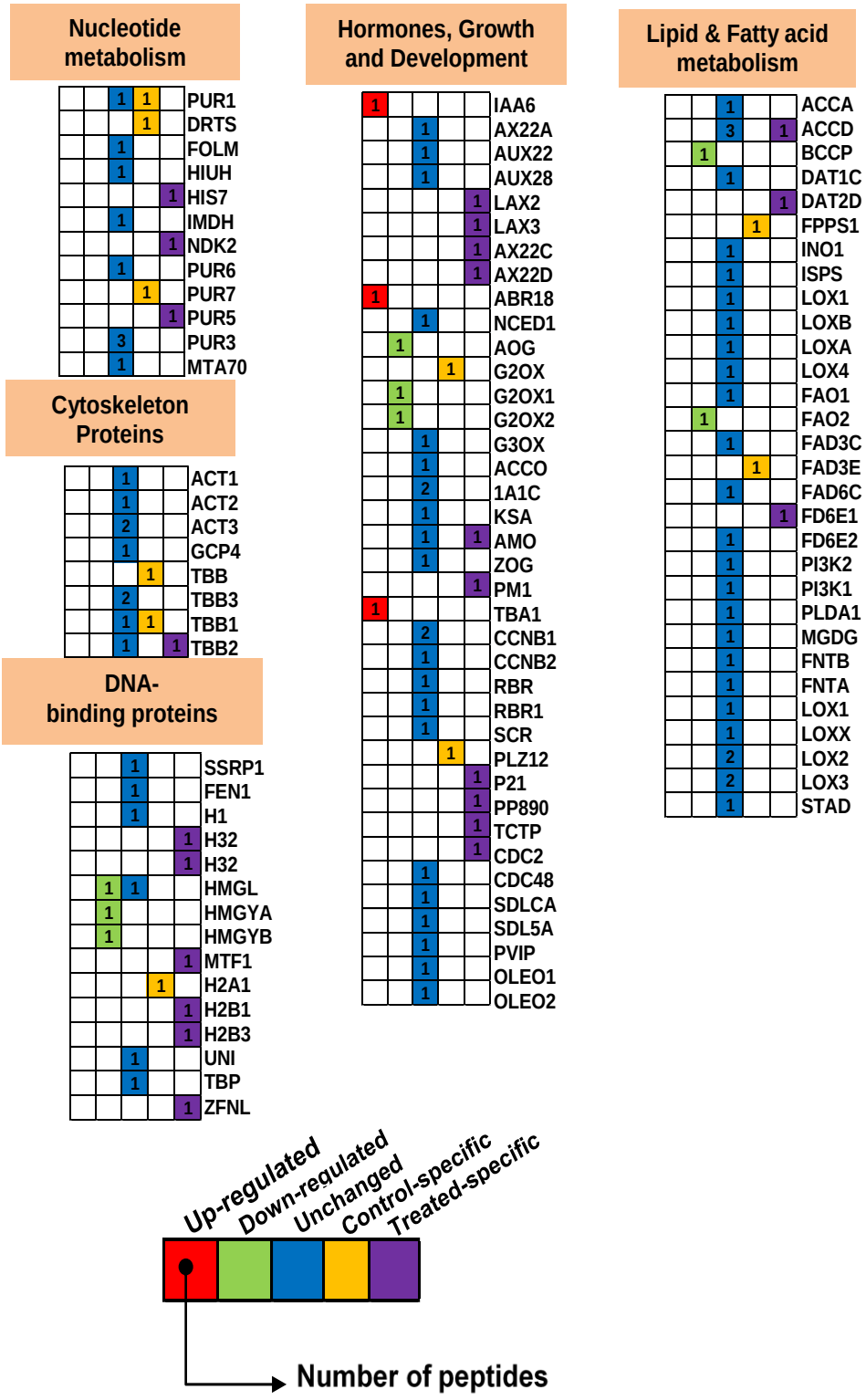
Nucleotide metabolism
PUR1
DRTS
FOLM
HIUH
HIS7
IMDH
NDK2
PUR6
PUR7
PUR5
PUR3
MTA70
Cytoskeleton Proteins
ACT1
ACT2
ACT3
GCP4
TBB
TBB3
TBB1
TBB2
DNA-binding proteins
SSRP1
FEN1
H1
H32
H32
HMGL
HMGYA
HMGYB
MTF1
H2A1
H2B1
H2B3
UNI
TBP
ZFNL
Hormones, Growth and Development
IAA6
AX22A
AUX22
AUX28
LAX2
LAX3
AX22C
AX22D
ABR18
NCED1
AOG
G2OX
G2OX1
G2OX2
G3OX
ACCO
1A1C
KSA
AMO
ZOG
PM1
TBA1
CCNB1
CCNB2
RBR
RBR1
SCR
PLZ12
P21
PP890
TCTP
CDC2
CDC48
SDLCA
SDL5A
PVIP
OLEO1
OLEO2
Lipid & Fatty acid metabolism
ACCA
ACCD
BCCP
DAT1C
DAT2D
FPPS1
INO1
ISPS
LOX1
LOXB
LOXA
LOX4
FAO1
FAO2
FAD3C
FAD3E
FAD6C
FD6E1
FD6E2
PI3K2
PI3K1
PLDA1
MGDG
FNTB
FNTA
LOX1
LOXX
LOX2
LOX3
STAD
Up-regulated
Down-regulated
Unchanged
Control-specific
Treated-specific
Number of peptides

Figure 8. Our proposed model for signalling transcription factors associate with salinity tolerance in *Pongamia pinnata*.

Colour key represents fold expression and number indicates number of identified peptides; red colour: up-regulated proteins, green colour: down-regulated proteins, blue colour: unchanged proteins, yellow colour: control specific proteins, and violet colour: treated specific proteins. For protein abbreviations see in table 1.

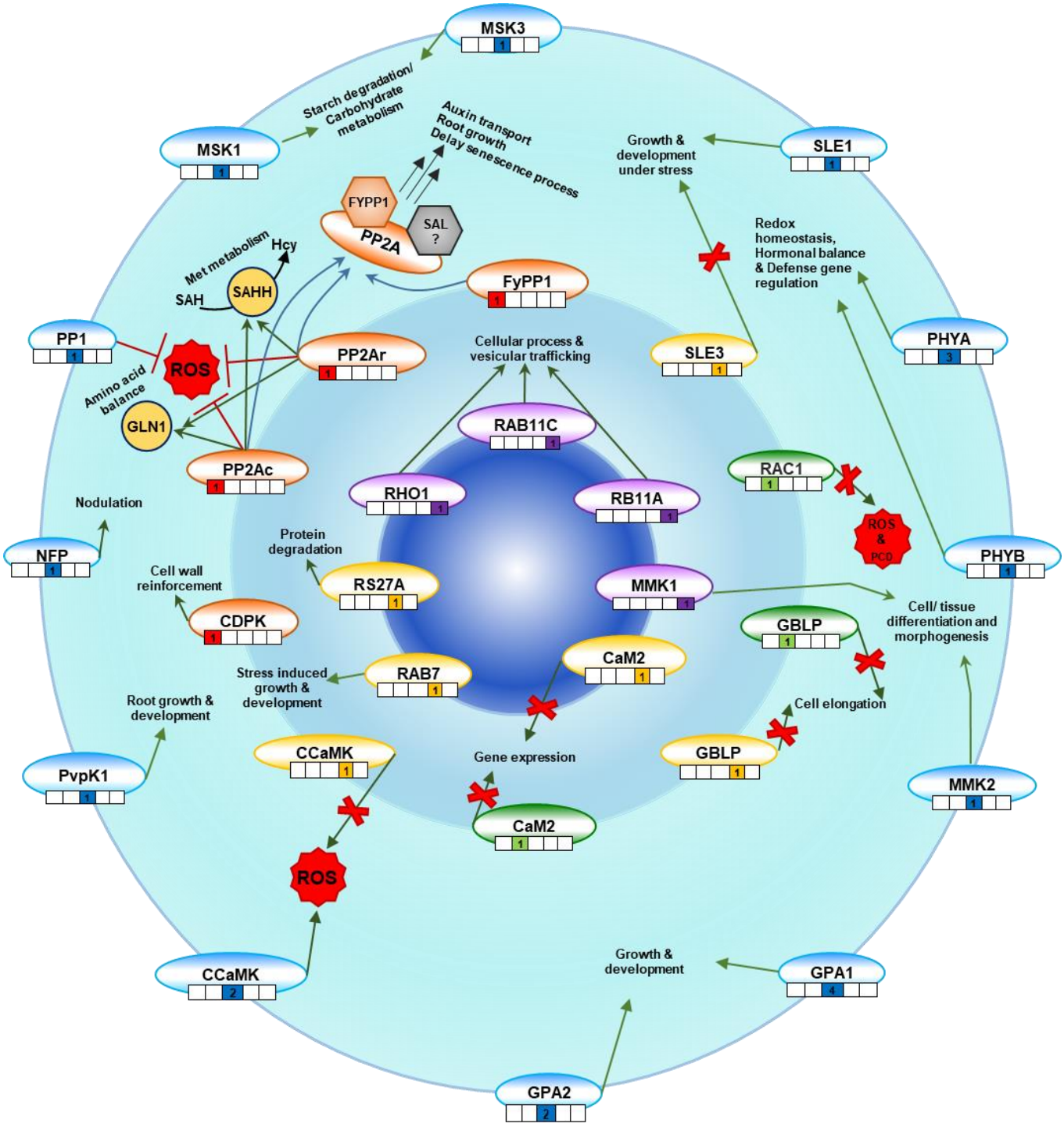
MSK3
MSK1
Starch degradation/ Carbohydrate metabolism
Auxin transport
Root growth
Delay senescence process
FYPP1
PP2A
SAL ?
Met metabolism
Hcy
SAH
SAHH
FyPP1
Growth & development under stress
SLE1
Redox homeostasis, Hormonal balance & Defense gene regulation
PHYA
PP1
ROS
Amino acid balance
GLN1
PP2Ar
PP2Ac
Cellular process & vesicular trafficking
SLE3
RAB11C
RHO1
RB11A
RAC1
ROS & PCD
PHYB
Nodulation
NFP
Protein degradation
RS27A
MMK1
Cell wall reinforcement
CDPK
GBLP
Cell/ tissue differentiation and morphogenesis
CaM2
Stress induced growth & development
RAB7
Root growth & development
Cell elongation
CCaMK
Gene expression
GBLP
PvpK1
MMK2
CaM2
ROS
CCaMK
Growth & development
GPA1
GPA2

Figure 9. Relative fold expression of DEPs belong to various metabolic pathways in *Pongamia pinnata*.

Colour key represents fold expression and number indicates number of identified peptides; red colour: up-regulated proteins, green colour: down-regulated proteins, blue colour: unchanged proteins, yellow colour: control specific proteins, and violet colour: treated specific proteins. For protein abbreviations see in table 1.

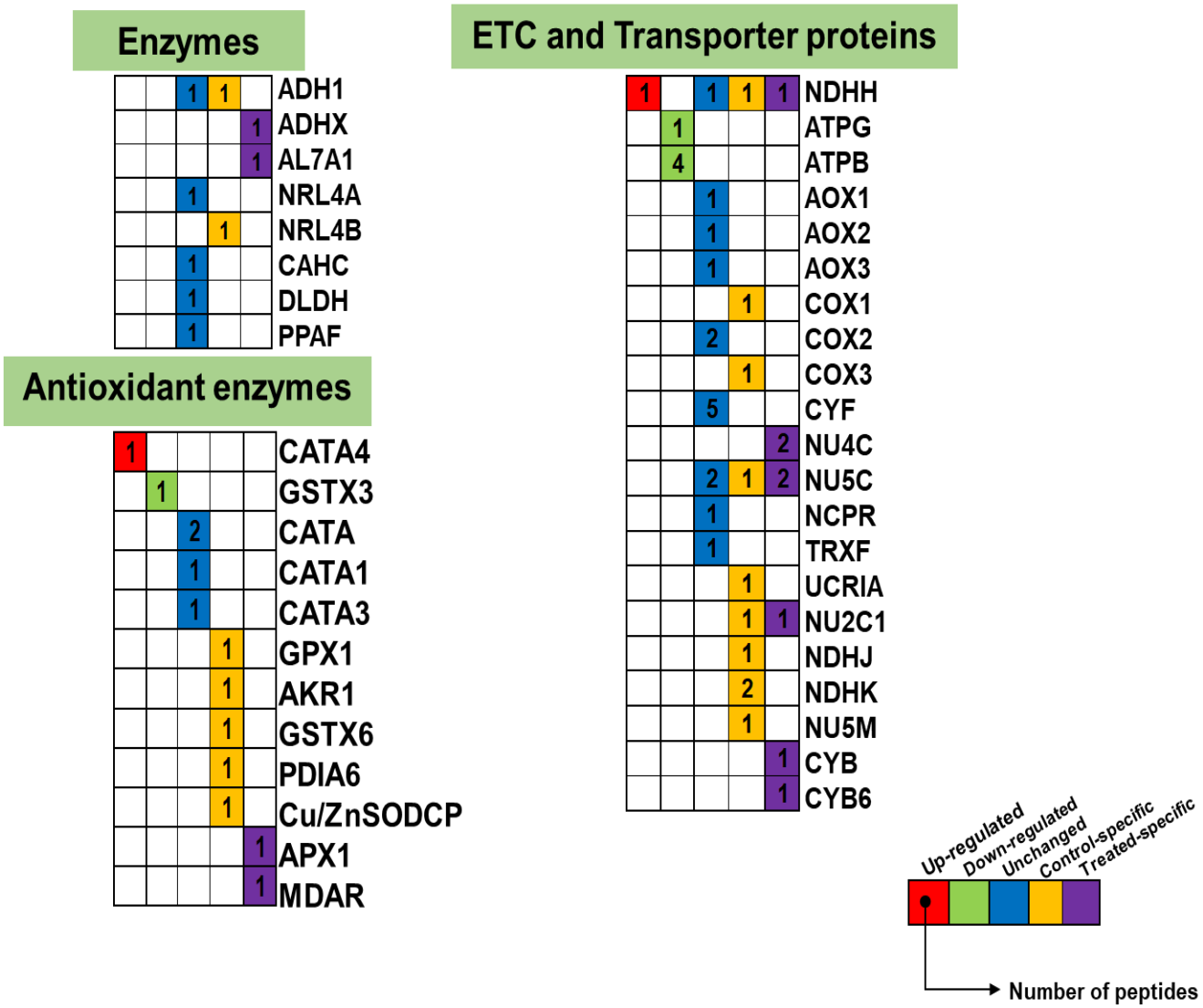
Enzymes
ADH1
ADHX
AL7A1
NRL4A
NRL4B
CAHC
DLDH
PPAF
Antioxidant enzymes
CATA4
GSTX3
CATA
CATA1
CATA3
GPX1
AKR1
GSTX6
PDIA6
Cu/ZnSODCP
APX1
MDAR
ETC and Transporter proteins
NDHH
ATPG
ATPB
AOX1
AOX2
AOX3
COX1
COX2
COX3
CYF
NU4C
NU5C
NCPR
TRXF
UCRIA
NU2C1
NDHJ
NDHK
NU5M
CYB
CYB6
Up-regulated
Down-regulated
Unchanged
Control-specific
Treated-specific
Number of peptides

Figure 10. Relative fold expression of CYP450 family proteins in the root tissue of *Pongamia pinnata.*

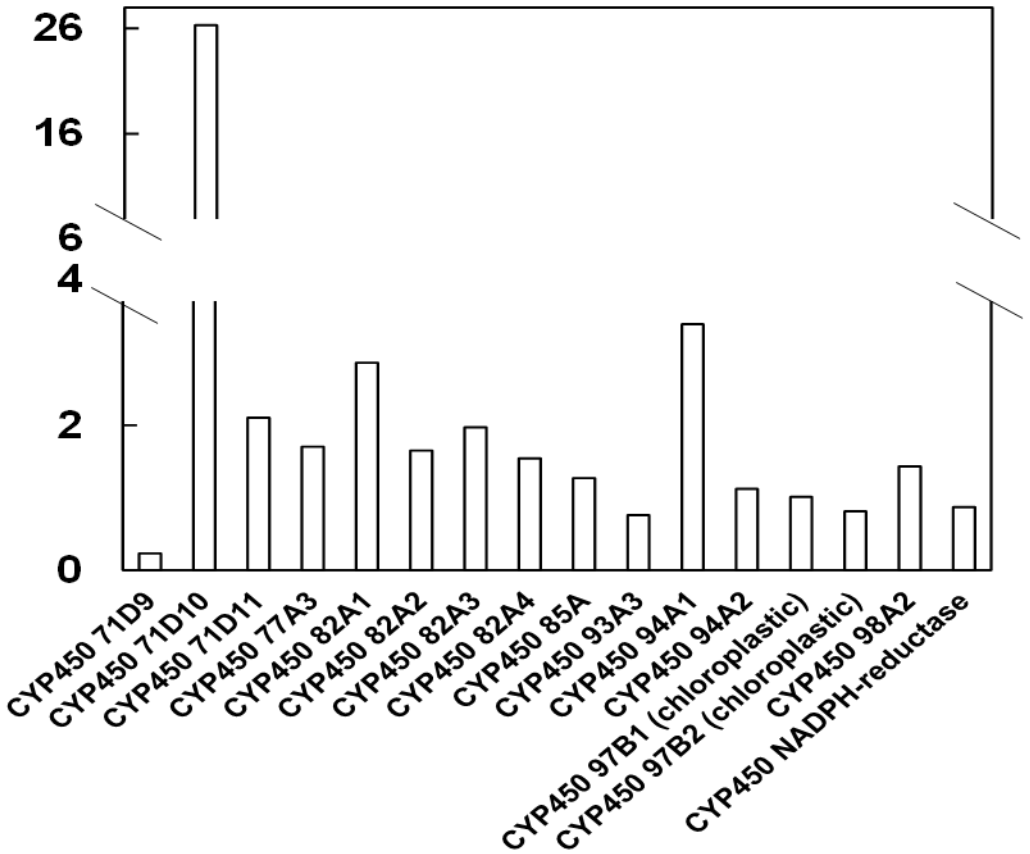
26
16
6
4
2
0
CYP450 71D9
CYP450 71D10
CYP450 71D11
CYP450 77A3
CYP450 82A1
CYP450 82A2
CYP450 82A3
CYP450 82A4
CYP450 85A
CYP450 93A3
CYP450 94A1
CYP450 94A2
CYP450 97B1 (chloroplastic)
CYP450 97B2 (chloroplastic)
CYP450 98A2
CYP450 NADPH-reductase

Figure 11. Relative fold expression of DEPs.

Colour key represents fold expression and number indicates number of identified peptides; red colour: up-regulated proteins, green colour: down-regulated proteins, blue colour: unchanged proteins, yellow colour: control specific proteins, and violet colour: treated specific proteins. For protein abbreviations see in table 1.

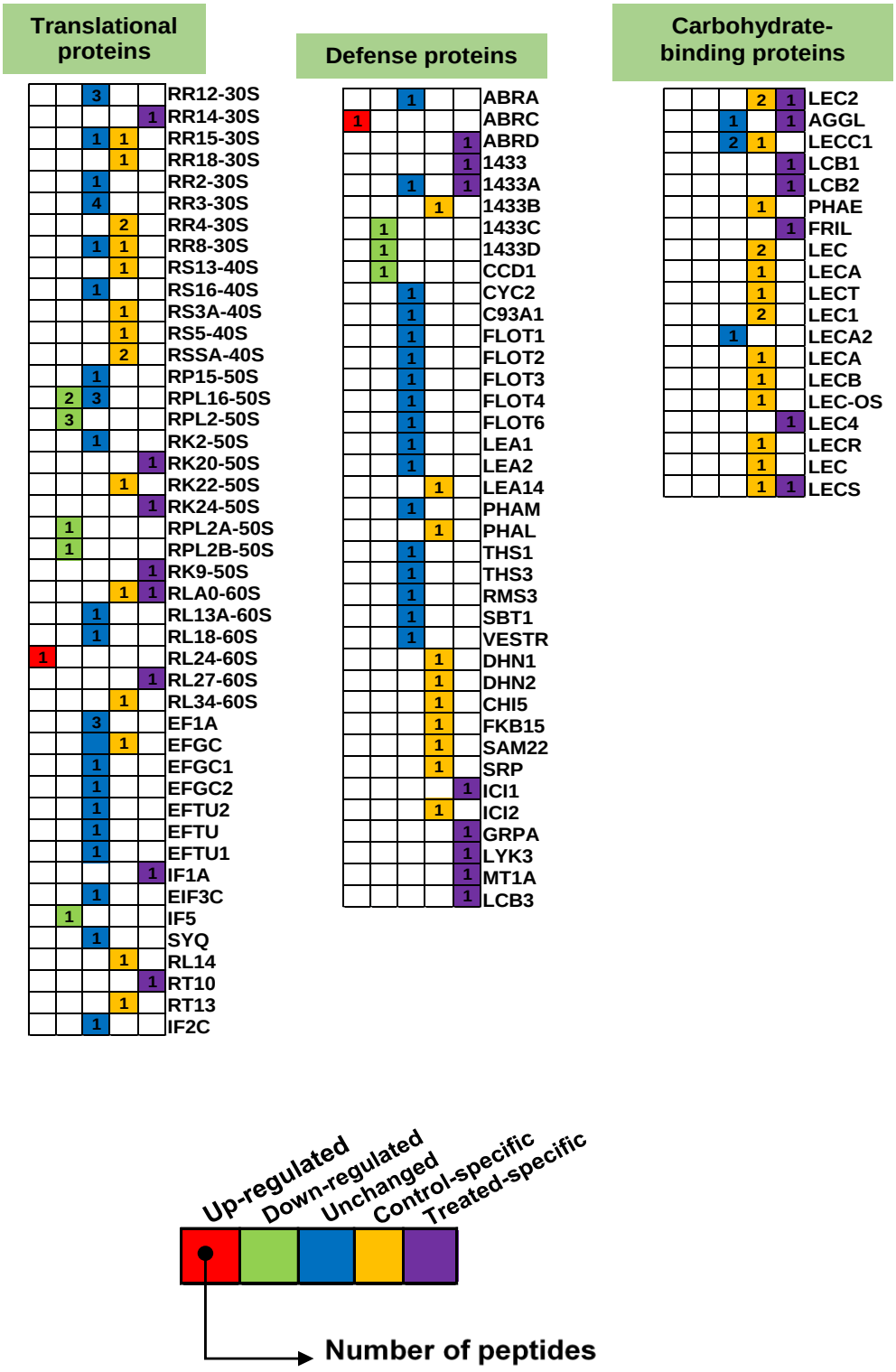
Translational proteins
RR12-30S
RR14-30S
RR15-30S
RR18-30S
RR2-30S
RR3-30S
RR4-30S
RR8-30S
RS13-40S
RS16-40S
RS3A-40S
RS5-40S
RSSA-40S
RP15-50S
RPL16-50S
RPL2-50S
RK2-50S
RK20-50S
RK22-50S
RK24-50S
RPL2A-50S
RPL2B-50S
RK9-50S
RLA0-60S
RL13A-60S
RL18-60S
RL24-60S
RL27-60S
RL34-60S
EF1A
EFGC
EFGC1
EFGC2
EFTU2
EFTU
EFTU1
IF1A
EIF3C
IF5
SYQ
RL14
RT10
RT13
IF2C
Defense proteins
ABRA
ABRC
ABRD
1433
1433A
1433B
1433C
1433D
CCD1
CYC2
C93A1
FLOT1
FLOT2
FLOT3
FLOT4
FLOT6
LEA1
LEA2
LEA14
PHAM
PHAL
THS1
THS3
RMS3
SBT1
VESTR
DHN1
DHN2
CHI5
FKB15
SAM22
SRP
ICI1
ICI2
GRPA
LYK3
MT1A
LCB3
Carbohydrate-binding proteins
LEC2
AGGL
LECC1
LCB1
LCB2
PHAE
FRIL
LEC
LECA
LECT
LEC1
LECA2
LECA
LECB
LEC-OS
LEC4
LECR
LEC
LECS
Up-regulated
Down-regulated
Unchanged
Control-specific
Treated-specific
Number of peptides

Figure 12. The distribution pattern of the chloroplasts across the root section. The bright-filed illumination of chloroplasts across the roots (green in colour) (A-D). The auto fluorescence of chloroplasts (Red in colour) (E-J). False colour was given to chloroplasts violet (G). The chloroplast auto fluorescence was excited with a blue argon laser (488 nm), and emitted light was collected from 660 to 731 nm. Red and White circles were drawn to show the chloroplasts.

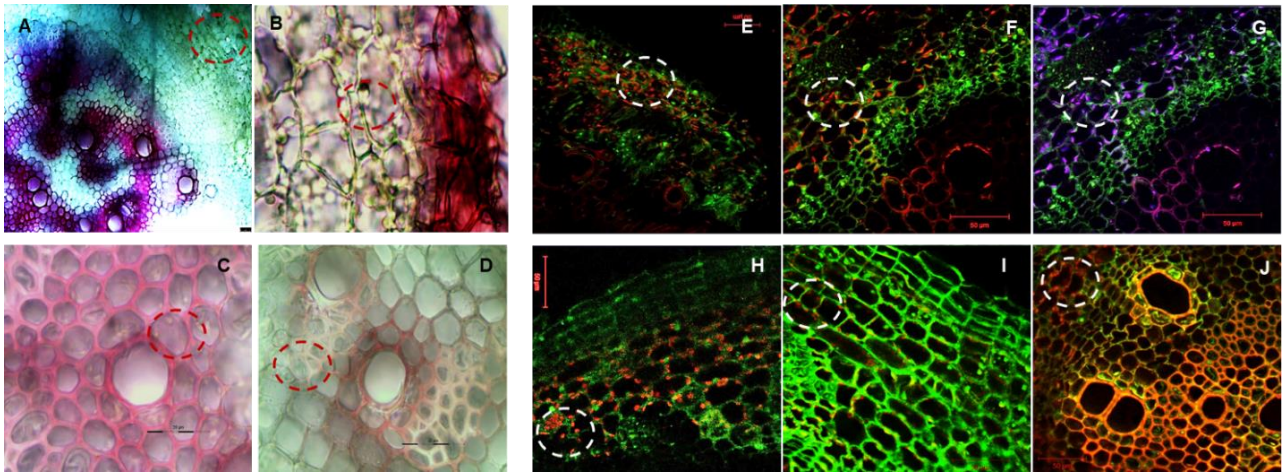
A
B
E
F
G
C
D
H
I
J

Figure 13. Hierarchical cluster heat maps of up-regulated proteins and protein-protein correlations in roots of 500 mM NaCl treated *P. pinnata* at 4DAS.

Each correlation value (based on Pearson correlation coefficient) corresponds to average of six biological replicates. HAC analysis was performed among the up-regulated proteins at 4DAS. Boxes were drawn to represent individual groups of DEPs. The colour key and histogram show degree of correlation. For protein abbreviations see in table 1.

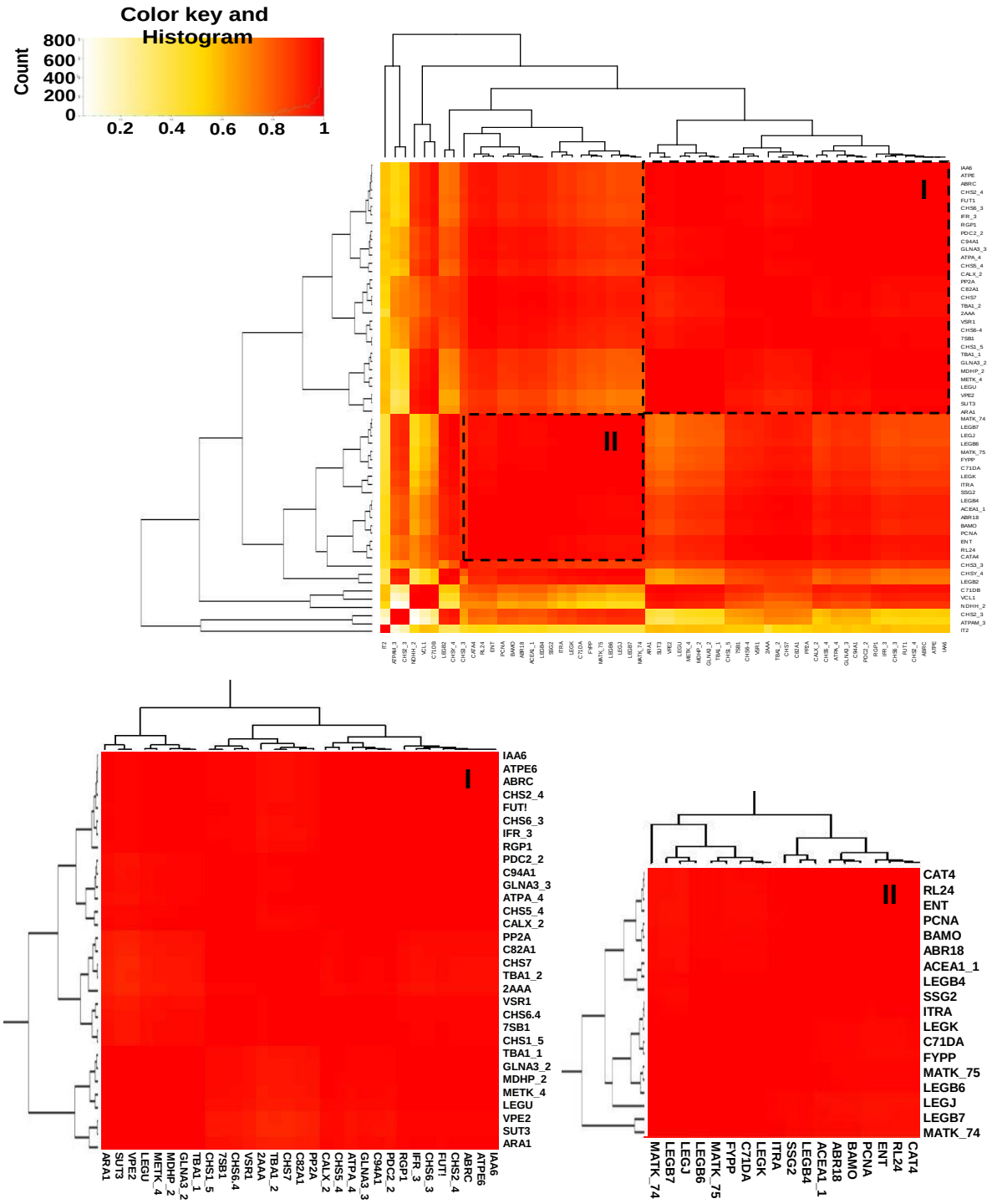
Color key and Histogram
Count
800
600
400
200
0
0.2
0.4
0.6
0.8
1
I
II
IAA6
ATPE6
ABRC
CHS2_4
FUT1
CHS6_3
IFR_3
RGP1
PDC2_2
C94A1
GLNA3_3
ATPA_4
CHS5_4
CALX_2
PP2A
C82A1
CHS7
TBA1_2
2AAA
VSR1
CHS6.4
7SB1
CHS1_5
TBA1_1
GLNA3_2
MDHP_2
METK_4
LEGU
VPE2
SUT3
ARA1
CAT4
RL24
ENT
PCNA
BAMO
ABR18
ACEA1_1
LEGB4
SSG2
ITRA
LEGK
C71DA
FYPP
MATK_75
LEGB6
LEGJ
LEGB7
MATK_74

Figure 14. Hierarchical cluster heat maps of down-regulated proteins and protein-protein correlations in roots of 500 mM NaCl treated *P. pinnata* at 4DAS.

Each correlation value (based on Pearson correlation coefficient) corresponds to average of six biological replicates. HAC analysis was performed among the down-regulated proteins at 4DAS. Boxes were drawn to represent individual groups of DEPs. The colour key and histogram show degree of correlation. For protein abbreviations see in table 1.

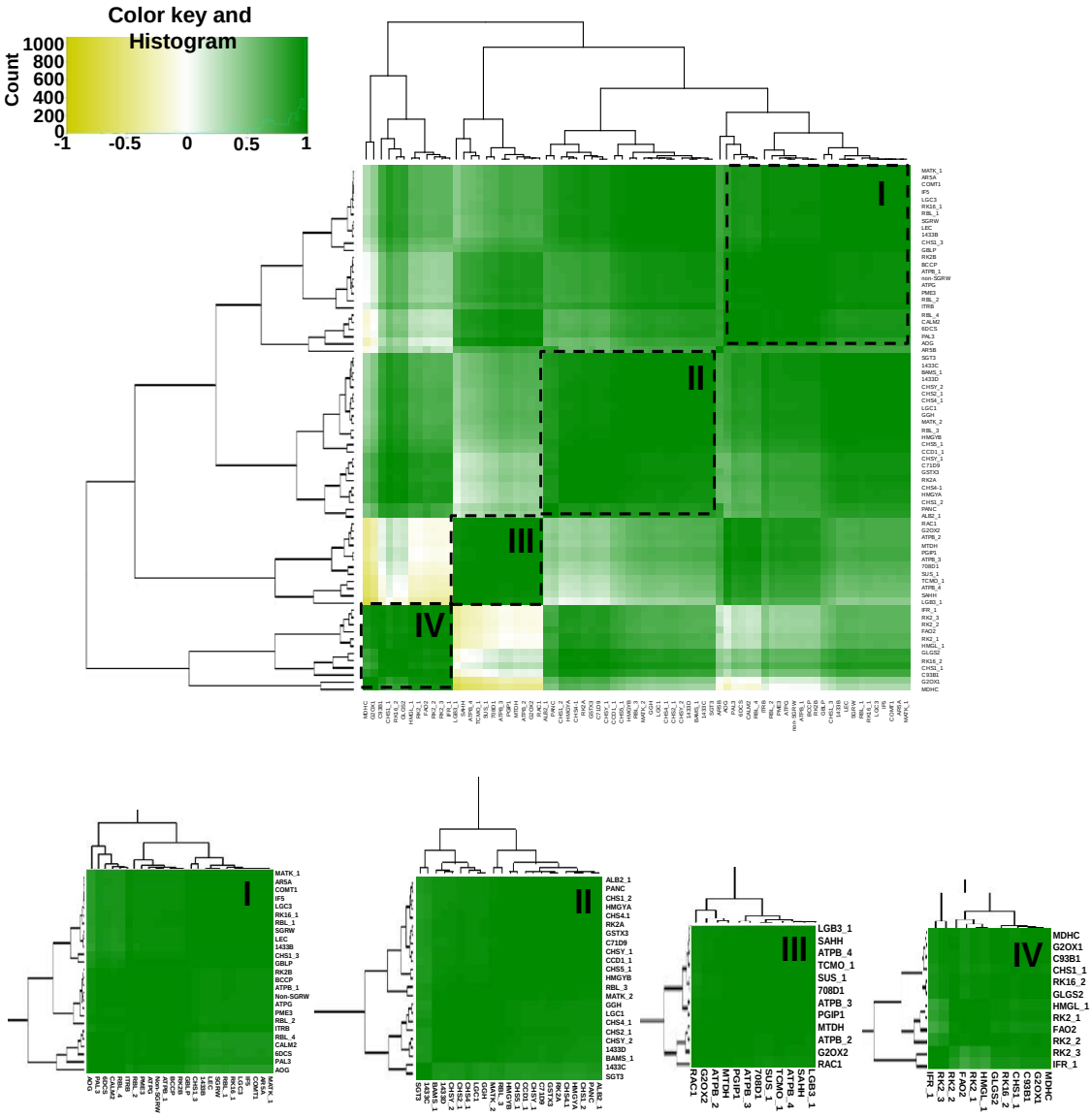
Color key and Histogram
Count
1000
800
600
400
200
0
-1
-0.5
0
0.5
1
I
II
III
IV
MATK_1
ARSA
COMT1
IFS
LGC3
RK16_1
RBL_1
SGRW
LEC
1433B
CHS1_3
GBLP
RK2B
BCCP
ATPB_1
Non-SGRW
ATPG
PME3
RBL_2
ITRB
RBL_4
CALM2
6DCS
PAL3
AOG
ALB2_1
PANC
CHS1_2
HMGYA
CHS4.1
RK2A
GSTX3
C71D9
CHSY_1
CCD1_1
CHS5_1
HMGYB
RBL_3
MATK_2
GGH
LGC1
CHS4_1
CHS2_1
CHSY_2
1433D
BAMS_1
1433C
SGT3
LGB3_1
SAHH
ATPB_4
TCMO_1
SUS_1
708D1
ATPB_3
PGIP1
MTDH
ATPB_2
G2OX2
RAC1
MDHC
G2OX1
C93B1
CHS1_1
RK16_2
GLGS2
HMGL_1
RK2_1
FAO2
RK2_2
RK2_3
IFR_1

Correlation analysis

Hierarchical cluster (HAC) analysis was performed to explore the relationship among the proteins in Pongamia. As shown in the Figures 13 and 14, HAC matrix was constructed based on Pearson correlation coefficients for each DEP pair. For better understanding, the correlations among proteins, both up- and down-regulated proteins were analyzed individually. There were 58 up-regulated proteins and 72 down-regulated proteins. A total of 3,364 correlation values were generated for 58 up-regulated proteins and clustered into matrix form. There were several DEPs involved in various metabolic pathways, which include mainly seed storage proteins (11), secondary metabolism (10), carbohydrate metabolism (4), signal transduction proteins (4), monooxygenases (4), ETC protein (3), transport proteins (3), amino acid metabolism (2), cell wall synthesis proteins (2), hormone metabolism (2), protease inhibitor proteins (2) and other metabolism (9) related proteins. Based on correlation values these DEPs were grouped into two individual clusters (cluster I and cluster II) (Figure 5). In cluster I, a strong correlation was observed among proteins related to amino acid metabolism (METK, GLNA3), carbohydrate metabolism (MDHP, PDC2), cell wall synthesis (FUT1, RGP1), secondary metabolism (CHS1, CHS2, CHS5, CHS6, CHS6-4, CHS7, IFR), seed storage proteins (LEGU, VPE2, ARA1, 7SB1), signal transduction (PP2A, CDPK-SK5), ETC proteins (ATPA, ATPE (chloroplast origin)), transport (SUT3,VSR1), tubulin α1, calnexin homolog, abrin-c and IAA6. We also observed a strong association between proteins of carbohydrate metabolism (SSG2, ACEA1), seed storage proteins (LEGB4, LEGK, LEGB7, LEGJ, LEGB6), ABR18, MATK, ITRA, CATA4, PCNA, BAMO, FYPP and RL24.

Similarly, HAC analysis was also performed on down-regulated proteins. A total of 5,184 correlation values were generated for 72 down-regulated proteins and clustered in the form of matrix. Several DEPs were involved in various metabolic pathways which include secondary metabolism (16), carbohydrate metabolism (8), translation proteins (8), ETC protein (5), hormone metabolism (4), DNA-binding proteins (3), seed storage proteins (3), signal transduction proteins (3), fatty acid metabolism (2), monooxygenases (2), amino acid metabolism (2), cell wall synthesis proteins (2), photosynthesis proteins (2), saponin metabolism (2) and others (10). Based on correlation values these DEPs were grouped into four individual clusters (cluster I, cluster II, cluster III, and cluster IV) (Figure. 6). In cluster I, a positive correlation was observed among proteins related to secondary metabolism (COMT1, CHS1, favin, 6DCS, PAL3), signal transduction protein (CALM2, GBLP), translational proteins (RKL16, RKL2B, IF5), photosynthesis proteins (non-SGRW, SGRW), ETC proteins (ATPG, ATPB (chloroplast origin)) RBL, PME3, 1433B, BCCP, AOG, MATK, ITRB, LGC3, and AR5A. In cluster II, a strong association was observed between proteins of secondary metabolism (CHSY, CHS1 (isoform), CHS2, CHS4, CHS4.1, CHS5), saponin biosynthesis (BAMS, SGT3) GGH, RBL (isoform), PANC, 1433C, 1433D, CCD1, HMGYA, HMGYB, C71D9, MATK (isoform), LGC1, GSTX3, ALB2 and RKL2A. In cluster III, a strong interaction was reported between proteins secondary metabolism (TCMO, 708D1), SAHH, SUS, PGIP1, ATPB (isoform), G2OX2, LGB3 and RAC1. In cluster IV, a strong interaction between proteins MDHC, HMGL, FAO2, G2OX1, C93B1, CHS1 (isoform), IFR (isoform), AR5B, GLGS2, RKL16 (isoform) and RKL2 (isoform).

Protein network studies

To elucidate protein-protein interaction networks, we employed Pearson's correlation coefficient (*r*) on selected fold values of ≤ 0.5 (down-regulated) and ≥ 2.0 (up-regulated) data points. The correlation network was generated at the $P < 0.99$ significance threshold and at $P \leq 0.05$ statistical significance. We analyzed the network as an undirected with combined paired edges.

For up-regulated protein correlation network, each data point was considered as a node and a total of 58 nodes formed 1350 edges (neighboring interactions) on an average each node shared 47 edges with neighboring nodes (clustering coefficient of 0.92) (Figures 15A and B). In order to simplify the correlation network, the nodes were represented in circles with three colours (yellow, blue and green) based on degree of interactions. The number of interactions range from ~15 to ~55, yellow circles ranges from ~15 to ~40, blue circles ranges from ~45 to ~50, and green ranges from ~50 to ~55; Notably, green nodes consists a dense network containing on average of ~50 interaction edges (closeness centrality < 0.90) with neighboring nodes. These correspond to proteins related to secondary metabolism (CHS1, CHS2, CHS5, CHS6, CHS6-4, CHS7, IFR), carbohydrate metabolism (ACEA1, SSG2), cell wall synthesis (FUT1, RGP1, PDC2), hormone metabolism (ABR18, IAA6), ETC proteins (ATPE, ATPA), seed storage proteins (7SB1, LEGB4, LEGK), CATA4, CALX, PP2A, GLNA3, C94A1, VSR1, C82A1, TBA1, ITRA, BAMO, RL24, ENT, PCNA and ABRC.

Similarly, 72 nodes were formed a dense interaction network with 1414 edges for down-regulated correlation network. Each node shared its interaction network on an average of 39 neighboring nodes (clustering coefficient of 0.84) (Figure 15C and D). To simplify correlation matrix, each node was represented with specific colour (yellow, blue, red) based on degree of

Figure 15. **Correlation networks of DEPs.**

(A) Up-regulated correlation network based on Pearson correlation coefficient with probability threshold $P < 0.0001$. Each node was represented with different colour based on degree of interaction. The order of interaction was green colour node > blue colour node > yellow colour node respectively.

(B) Correlation network of the 53 proteins in cluster; box was drawn to represent zoom-in of the most highly interconnected core of proteins.

(C) Down-regulated correlation network based on Pearson correlation coefficient with probability threshold $P < 0.0001$. Each node was represented with different colour based on degree of interaction. The order of interaction was red colour node > blue colour node > yellow colour node respectively.

(D) Correlation network of the 72 proteins in cluster; box was drawn to represent zoom-in of the most highly interconnected core of proteins. For protein abbreviations see in table 1.

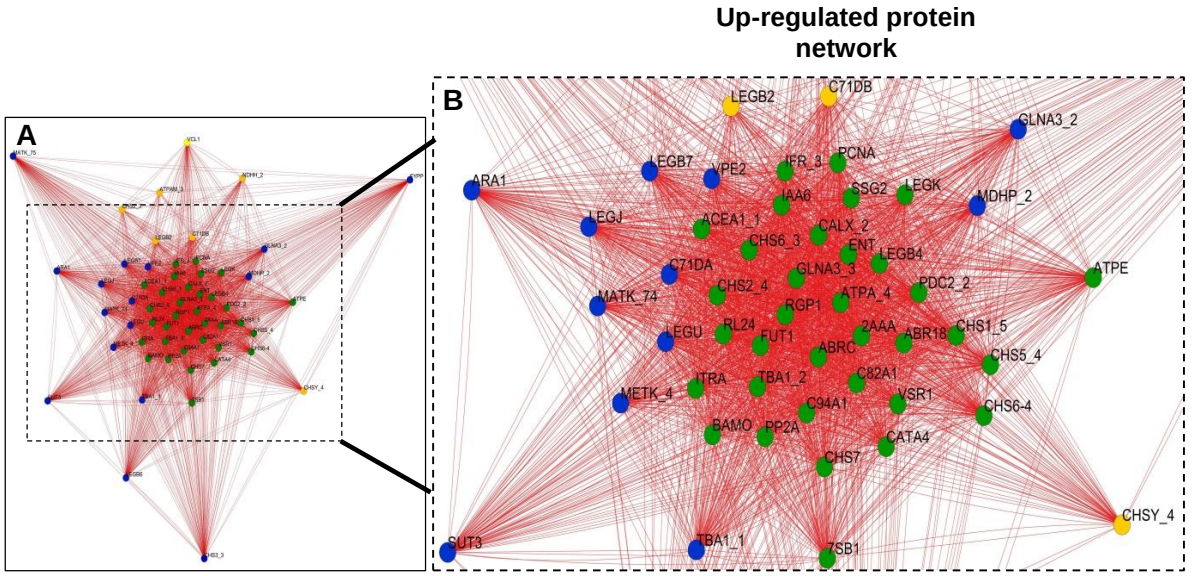
Up-regulated protein network
A
B
LEGB2
C71DB
GLNA3_2
LEGB7
VPE2
IFR_3
PCNA
ARA1
SSG2
LEGK
IAA6
MDHP_2
LEGJ
ACEA1_1
CALX_2
CHS6_3
ENT
LEGB4
C71DA
GLNA3_3
ATPE
CHS2_4
ATPA_4
PDC2_2
MATK_74
RGP1
LEGU
RL24
FUT1
2AAA
ABR18
CHS1_5
ABRC
CHS5_4
C82A1
METK_4
ITRA
TBA1_2
VSR1
C94A1
CHS6-4
BAMO
PP2A
CATA4
CHS7
CHSY_4
SUT3
TBA1_1
7SB1

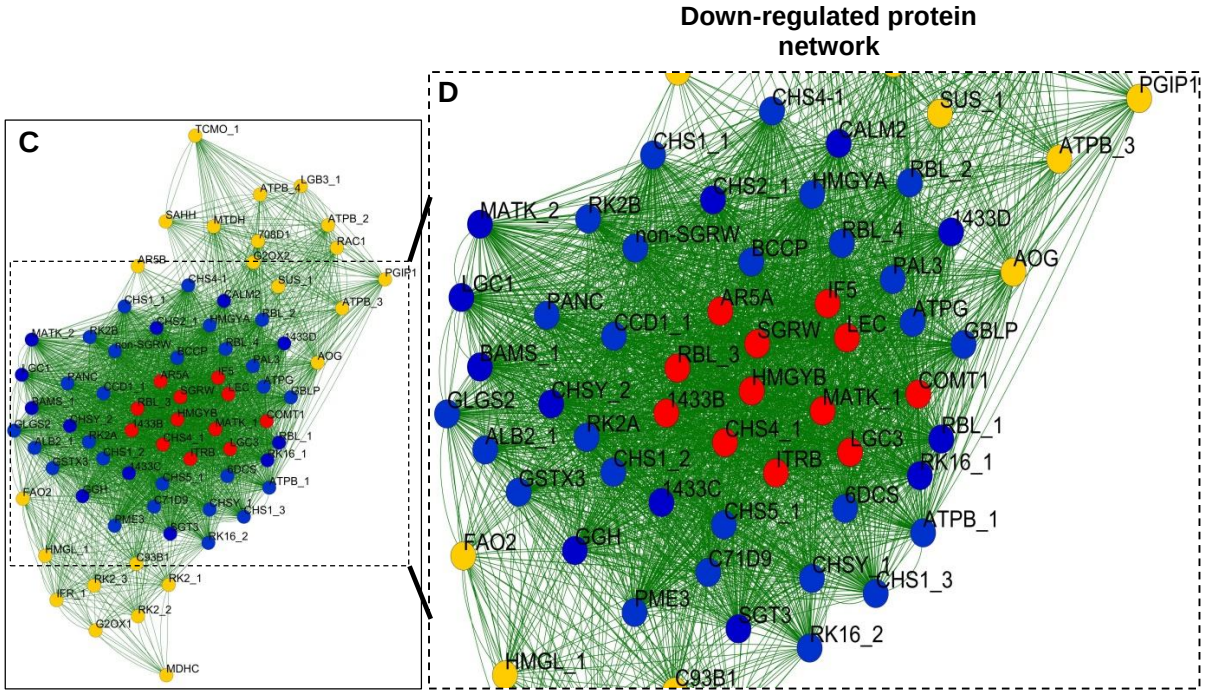
Down-regulated protein network
C
D
TCMO_1
LGB3_1
ATPB_4
SAHH
MTDH
ATPB_2
708D1
RAC1
92QX2
AR5B
PGIP1
CHS4-1
SUS_1
CHS1_1
CALM2
ATPB_3
MATK_2
RK2B
CHS2_1
HMGYA
RBL_2
non-SGRW
BCCP
RBL_4
1433D
AOG
LGC1
PANC
AR5A
IF5
PAL3
CCD1_1
SGRW
ATPG
LEC
GBLP
BAMS_1
RBL_3
HMGYB
COMT1
GLGS2
CHSY_2
1433B
MATK_1
ALB2_1
RK2A
CHS4_1
LGC3
RBL_1
CHS1_2
ITRB
RK16_1
GSTX3
1433C
6DCS
CHS5_1
ATPB_1
FAO2
GGH
C71D9
CHSY_1
CHS1_3
PME3
SGT3
RK16_2
HMGL_1
C93B1
RK2_3
RK2_1
IFR_1
RK2_2
G2OX1
MDHC

interaction (Figure 15C and D). The number of interactions range from ~10 to ~55; yellow circles ranges from ~10 to ~40, blue circles ranges from ~40 to ~50, and red ranges from ~50 to ~55.Further, red and blue nodes formed a dense network containing on an average of ~50 interaction edges (closeness centrality < 0.75) with neighboring nodes, corresponding to proteins related to secondary metabolism (CHS2 (isoform), CHS4, CHSY, COMT, LEC), saponin metabolism (BAMS, SGT3), defense response proteins (1433B, C and D), ITRB, RBL (isofom), LGC1, GGH, MATK (isoform), RK16, CALM2, SGRW, HMGYB, LGC3, IF5, and AR5A.

Figure 16. Our proposed model of high salinity tolerance in *Pongamia pinnata*.

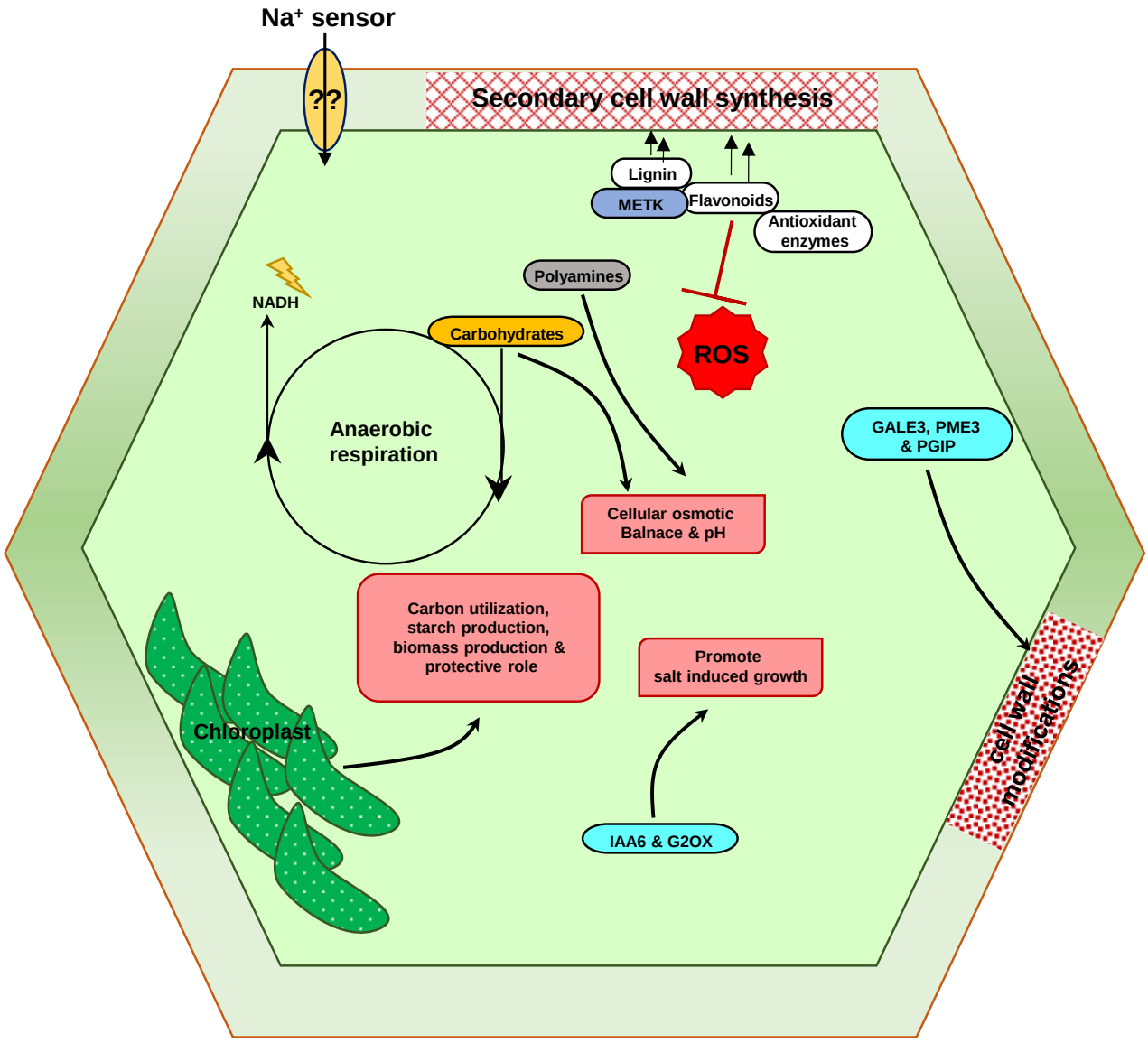
Na⁺ sensor
??
Secondary cell wall synthesis
Lignin
METK
Flavonoids
Antioxidant enzymes
Polyamines
NADH
Carbohydrates
ROS
Anaerobic respiration
GALE3, PME3 & PGIP
Cellular osmotic Balnace & pH
Carbon utilization, starch production, biomass production & protective role
Promote salt induced growth
Chloroplast
cell wall modifications
IAA6 & G2OX

Chapter 5 Discussion

In present study, plants were treated with 500 mM NaCl (3% NaCl; equivalent to sea saline concentration) for 4DAS and root proteome analysis was carried out by using nLC-MS. To our knowledge, this is the first report on Pongamia root proteome. A total of 1062 proteins were identified through label free shot-gun proteome analysis in roots of Pongamia. Additionally, we used computational platforms (R-program and cytoscape network analysis) and GO based analysis to explore more knowledge on global proteome change in Pongamia as well as to further simplify the complex data into visual graphical and network forms. Based on above analysis, the protein homology appears to confirm the relatedness of Pongamia with other *Fabaceae* members (Kazakoff et al., 2012; Sreeharsha et al., 2016). However, our protein homology studies revealed that Pongamia showed relatedness with two legume members *Pisum* and *Glycine* with 21% protein homology (Figure 1A). Upon stress, Pongamia showed 7.8, 82.3 and 9.8% higher, unchanged and lower abundance of proteins related to various metabolic and cellular pathways respectively. Most of the proteins were unchanged in response to salt stress suggesting the dynamic nature root cell proteome, which is essentially important to preserve the cellular processes and may provide resilience to changing environmental cues. In this study, we identified proteins related to various metabolic processes including primary metabolism, secondary metabolism, ion transport, signal transduction and other cellular processes. Furthermore, correlation studies and network analysis provided an extensive comprehensive insights into the mechanisms of tolerance in Pongamia. A total of 130 DEPs, detected during salt stress, demonstrates that global changes in protein expression determines the plant growth during stress. However, system based approaches, correlation studies and integrated network analysis are needed to understand such complex

processes. For better understanding, we constructed two co-regulation networks, one for up-regulated DEPs and the other for down regulated proteins.

In response to stress, Pongamia roots expressed numerous proteins related to secondary metabolism including phenylpropanoid pathway (Figure 3). The unchanged expression of PALs, TCMO (rate-limiting enzyme) and 4CL2 may replenish the phenylpropanoid pathway intermediates (*trans*-cinnamate, *trans*-coumaric acid and coumaroyl-CoA), which are crucial for synthesis of naringenin chalocone. Our study focuses interactive co-regulation networks of each protein group to elucidate pathways responsible for tolerance in Pongamia. For example, correlation among the proteins belonging to same pathways was observed for flavonoid synthesis from CHSs, IFR and IFRH, indicating the branched pathway is an important target for studying the salt tolerance mechanism in *P. pinnata* (Jia et al., 2017; Xiong et al., 2017; Wang et al., 2018; Wu et al., 2020). In addition, correlation network also revealed several node proteins closely linked with other. CHS1 found to be a network node containing highest number of interactions with other proteins. CHS catalyses the synthesis of naringenin chalocone which is a branch point for synthesis of flavanones, flavonols and anthocyanins (Kang et al., 2014; Chen et al., 2019; Zhang et al., 2020). The increased levels of CHSs might help in biosynthesis of flavonoids to scavenge the ROS generated during salt stress and is a potential target to study salt tolerance mechanism (Chen et al., 2019). Expression of CADH, COMT, THS2, and CAMT indicates use of phenylpropanoid pathway intermediates to produce crucial secondary metabolites such as cinnamaldehyde, caffeate, resveratrol and feruloyl-CoA respectively which are involved in defense role against ROS and in maintaining the cell wall integrity under saline conditions (Le-Gall et al., 2015; Liu et al., 2018; Souid et al., 2019). The present study also shows the expression of several proteins of flavonoid

synthesis including isoflavanone synthase (IFS), naringenin-8-dimethylallyltransferase 2, UGT13, FG3H, FG2KO and (flavonoid-3-O-glucosyltransferase) UFGT which were associated with biosynthesis of 2-hydroxyflavanone, sophoraflavanone, daidzin, genistin, ononin, kaempferol-3-O-sophoroside, kaempferol-3-O-rutinoside (nicotiflorin) and other anthocynanins respectively in response to salt stress. Further, up-regulation of glycosyltransferases (FG3H and FG2KO) may induce the accumulation of flavonoids such as kaempferol-3-O-sophoroside and kaempferol-3-O-rutinoside to play defense role in plants during salt stress (Martinez et al., 2016; Li et al., 2017). The significant increase in the expression of UFGT levels may result in enhanced accumulation of anthocyanins for exceptionally high ROS scavenging activity (Sakamoto and Suzuki, 2019). The present study demonstrates that Pongamia is a rich source of chemically diverse secondary metabolites possessing high antioxidant activity to defend ROS damage and its root growth during high salinity conditions.

Pongamia also accumulated numerous amino acids in roots upon salt stress to mitigate its negative effects. Enhanced expression of cytoplasmic glutamine synthetase (GLNA) and ASPG may induce the production of glutamate and aspartate respectively to increase the availability of nitrogen for newly synthesizing proteins involved, in cellular processes and salt adaptive signalling. Glutamate was found to act as a second messenger involved in carrying long distance signalling under various biotic and abiotic stress conditions including salinity (Qiu et al., 2020). The increased availability of free amino acids may also help in maintaining osmotic balance within the cell (Credali et al., 2012). Significant increase in the S-adenosylmethionine synthetase (METK) would enhance the formation of adenosyl-methionine (AdoMet), which is the principle methyl group donor involved in numerous cellular reactions including polyamine and lignin biosynthesis.

Further, the decreased expression of SPD1 and 2 clearly suggest that AdoMet contribution was significantly reduced in biosynthesis of polyamines such as spermine and spermidine. The induction of ADC might increase the synthesis of putrescine, while concomitant decrease in the expression of SPD1 and 2 may lead to the availability of putrescine either in free or conjugate form in the cell. The perennial plants might use the conjugated putrescine to stabilize the membrane potential and cellular pH balance under saline conditions, albeit the free form of putrescine which is toxic to the cell (Yamamoto et al., 2017). The correlation between METK and lignin precursor synthesizing enzymes CHSs and IFR may help in reorganising the root vasculature in response to saline environment. This hypothesis justified our previous findings where root xylem tracheary elements were lignified to improve cell-to-cell water and ion transport pathway. Very few studies have reported the functional role of plastids inside root cells and its importance in non-photosynthetic tissues (Kobayashi et al., 2017). Pongamia roots showed high abundance of chloroplasts inside the root cells (Figure 4). Additionally, we also observed significant increase in the expression of chloroplast localized proteins OTC, ILV5, GSA and PYRB1 which are involved in synthesis of polyamines, branched chain amino acids, chlorophyll pigments, and nucleotide synthesis to modulate root growth under to saline condition (Damaris et al., 2016; Nounjan et al., 2018; Dong et al., 2019).

Expression of INV indicates that constant supply of carbohydrates (glucose and fructose) to downstream pathways including glycolysis and HMP shunt. The rise in F16P2 expression levels might favour accumulation of fructose-6-phoshate, which is a substrate for numerous metabolic pathways including sucrose and osmolyte biosynthesis (Dikilitas et al., 2019; Stein and Granot, 2019). The steady state levels of F6P catalysing enzymes SUS/ SUS2, SPSA, PMM and MTDH

should help the plant to synthesize modified sugar moieties such as sucrose-6p, mannose-1p and mannitol to retain celluar osmotic potential and cell turgor (Dong et al., 2018). The decreased levels of MDHC and expression of CAPP1 & 2, MAOX may enhance the PEP levels, which will be further converted into pyruvate by KPYC. Notably, with induction of PDC2, ADHX and AL7A1 expression, pyruvate undergoes into anaerobic process with the production of reduced energy equivalents, NAD(P)H (Luo et al., 2017). Therefore, driving the anaerobic process is beneficial for the plant to quickly restore the cellular energy needs under adverse conditions. In addition, increased levels of isocitrate dehydrogenases IDHC (cytosol), and IDHP (chloroplast) might enable the plant to produce NADH by converting isocitrate to α-ketoglutarate, which plays a crucial role in energy metabolism. During salt stress, Pongamia showed root glyoxylate cycle fluxes. Both glyoxylate and succinate are involved in the production of NADH, $FADH_2$ and other TCA cycle intermediates to provide carbon redox energy source for other cellular metabolic process (Yuenyong et al., 2019). Interaction between ACEA1 and PDC2 divert the carbohydrate pool to anaerobic respiration towards acetate and ethanol formation to replenish reducing energy equivalents rather than channelizing the carbohydrate pool towards TCA cycle (Figure 16). We also observed significant increase in the expression of chloroplast localized RBS, RBS1, RUBA, RUBB, and SSG2 suggesting fixation of CO_2 and synthesis of carbohydrates including starch and amylopectin. However, the enhanced expression proteins related to chloroplast CO_2 fixation and amylopectin biosynthesises in roots and their role in salt stress needs further investigation. Significant increase in the chloroplast localized proteins (NDHH, NU4C, NU5C, NU2C1, CYB, CYB6, FRI2, PSBP, PLAS, PHYK1 and PHYK3) involved in both linear and cyclic electron transport of photosynthesis are recorded suggesting that the increased expression of these proteins

may help in maintaining cellular redox energy status and also involved in protecting cellular organelles from oxidative stress damage under adverse environmental conditions (Wang et al., 2014; Spicher et al., 2017; Yang et al., 2017; Wu et al., 2020). Thus, we hypothesize that the viability of chloroplast within the roots of Pongamia may be crucial in protecting the roots under saline conditions.

The induction of auxin responsive proteins IAA6, LAX2, and LAX3 might be involved in regulation of salt-induced root growth (Péret e al., 2012). We also observed a significant decrease in G2OX expression. Decreased G2OX expression leading to increased active gibberellin levels to promote root growth under salt stress (Wang et al., 2019). Pongamia induced numerous proteins related to cell wall synthesis including FUT1, RGP1, CSPL4, CSPL5, NLTP1 and NLTP3 which are involved in the glycosylation and acylation processes in the cell to stabilize the membranes in response to the changing environmental cues (Tryfona et al., 2014; Liu et al., 2015; Yang et al., 2015; D'Agostino et al., 2019; Saqib et al., 2019). In order to protect cellular components, Pongamia also induced expression of numerous chaperon proteins CALX, HSP13, HSP12 and HS22M in roots under salt stress. The up-regulation of these chaperons might prevent miss-fold and aggregation of proteins caused under salinity stress (Haq et al., 2019). Antioxidant enzymes including APX1, CAT4, and MDAR showed significant up-regulation in Pongamia roots under salt stress to reduce ROS production inside the cell under salt stress (Li et al., 2015; Sofo et al., 2015). In response to salinity, Pongamia also accumulated several defense related proteins including carbohydrate binding proteins (CYP450 family proteins, ABRC, ABRD, 1433, GRPA, LYK3, MT1A and LCB3) in order to adapt extreme salinity conditions (Paparella et al., 2014; Yang and Guo, 2018; Mekawy et al., 2020). Induction of proteins related to transcription and

translation localized in both chloroplast and cytosol may be beneficial for the plant growth and development (Kosová et al., 2013; Xu et al., 2016). Further, a significant increase in PDX1, which is involved in the synthesis of cofactor vitamer, pyridoxal 5'-phosphate (vitamin B6) was recorded. Vitamin B6 acts as an efficient quencher of ROS in addition to its cofactor function for numerous cellular reactions (Czégény et al., 2019). Previous studies suggest lack of PDX1 showed a differential impairment in root growth and viability under abiotic stresses (Boycheva et al., 2015).

Signal transduction or signal sensing molecules play crucial role in plant defense, metabolism, growth and development (Dikilitas et al., 2019). Up-regulation of both PP2A and FyPP1 expression, and positive interaction between PP2A and FyPP1 leads to the formation of PP2A-FyPP1 complex, which might regulate salt-induced root growth and auxin transport across the plant (Dai et al., 2013). ABA negatively regulates both PP2A and FyPP1 functions (Dai et al., 2013). Induction of both PP2Ac and PP2Ar might regulate amino acid balance by controlling both SAHH and GLN1 expression (Lillo et al., 2014). In addition to PP2A expression, increased or decreased expression of PP1, RAC1, CCaMK might help in ROS regulation, which plays crucial role in plant survival and under high salinity stress conditions (Choudhary et al., 2020). Pongamia roots also induced numerous proteins of small G family (RHO1, RAB11A, RAB11C, RS27A, GAP1, GAP2, GBLP, and RAB7), SLE1, SLE3, PHYA, PHYB, MSK1, MSK3, CaM2, CDPK, MMK1 and MMK2. Altered expression of these proteins may contribute to plant growth by promoting cell wall reinforcement, salt-induced root growth, cell and tissue morphogenesis under salt stress (Cheval et al., 2013; Zeng et al., 2015; Liu et al., 2018; Yang et al., 2018).

In conclusion, the extensive root proteome analysis in Pongamia as shown in this study proposed new insights into salt tolerance mechanisms in a tree species, *P. pinnata*, which would be beneficial for tree important programs.

Chapter 6

Summary and Conclusions

Pongamia with full of pods at our germplasm site, Tree Oils India Limited (TOIL), Zaheerabad, Telangana, India

Chapter 6 Summary and Conclusions

Summary

Pongamia pinnata is a medium sized leguminous tree belong to Fabaceae family. Despite of using whole plant as a crude drug in Indian ayurvedic medicines, Pongamia seed oil has 50% oleic acid and can be used as a potential feed stock for biofuel. Further, with the nitrogen fixing ability, Pongamia can fix huge amounts of nitrogen even under normal field conditions. Although, there are several reports on growth and development of Pongamia even under most unfavourable environmental conditions, the precise regulatory events associated with physiology and biochemistry at the whole plant level under such stressful conditions are little known. Saline lands and salinized arable lands are inadequate for plant growth and propagation. Cultivation of tree species such as Pongamia as a rehabilitate tree species in these lands would have high economic gain as it is a well-known tree species for biofuel production.

Soil salinity is gradually becoming a threat to the global economy by affecting agricultural productivity worldwide. Here, we analyze the salinity tolerance of *Pongamia pinnata* with an insight into the underlying physiological and molecular responses. Despite a reduction in net photosynthetic rate, *P. pinnata* efficiently maintained its leaf water potentials even at 500 mM NaCl for 15 days and displayed no visible stress symptoms. Na^+ localization analysis using CoroNa-Green AM revealed effective Na^+ sequestration in the roots when compared to leaves. Elemental analysis demonstrated that roots accumulated more of Na^+ while K^+ content was higher in leaves. At the molecular level, salt stress significantly induced the expression levels of salt overly sensitive1 (SOS1), SOS2, SOS3, high affinity K^+ transporter (HKT1), ABA biosynthetic and receptor genes (NCED and PYL4), guaiacol peroxidase (POD) exclusively in roots while tonoplast localized Na^+/H^+ exchanger (NHX1) was significantly enhanced in leaves.

Chapter 6 Summary and Conclusions

Without display of salt-induced morphological symptoms in plants grown 500 mM NaCl (3% NaCl; sea saline equivalent) for 30 days, the plants showed strong adaptive mechanisms operating under the extreme saline environment. Pongamia showed reduced gas exchange characteristics (net photosynthesis (A_{sat}), transpiration (E), and stomatal conductance (g_s)) to about 50% at 15 DAS (day after salt-treatment) and maintained these levels for 30 days. Similar results were obtained in A_{sat}/Ci and A_{sat}/Q analysis. Analysis of polyphasic chl *a* fluorescence kinetics revealed well maintained structural and functional integrity of PSII. The characteristic negative L-band (which denotes grouping or connectivity among PSII units) was observed in both 300 and 500 mM NaCl treated plants at 30 DAS. A negative bell shaped K-band was also recorded at 300 μs time interval in salt treated plants at 30 DAS. The JIP-test analysis and phenomenological fluxes showed salt induced photoacclimation responses including reduced electron transport and enhanced thermal dissipation of light energy from PSII. Proline levels were slightly increased in 300 and 500 mM salt treated plants at 30 DAS.

Hydroponically grown 30 days old seedlings of Pongamia were treated with two different salt concentrations (300 and 500 mM NaCl) for 8 days and analysed at regular intervals of 1, 4 and 8 days after salt exposure. Physiological parameters were recorded using infrared gas analyser and portable mini-PAM. Ion (Na^+, K^+, Cl^-, and Ca^{2+}) accumulation in leaves and roots were analysed through atomic absorption spectroscopy and Na^+ localization was tracked through confocal laser scanning microscopy. Histochemical detection of lignin and suberin depositions in leaves and roots were carried out. Pongamia roots act as ultra-filters/strong barriers to avoid accumulation of excess Na^+ levels in the leaves. The Na^+ probe fluorescence analysis demonstrated effective vacuolar

sequestration of Na^+ in the roots. Formation of suberized multiseriate exodermis in the roots, along with extensive lignification maximized water permeability in both leaves and the roots.

The present investigation further describes alterations in hormonal and metabolic responses in correlation with physiological and molecular variations in leaves and roots of Pongamia at sea salinity level (3% NaCl) for 8days. At physiological level, salinity induced adjustments in plant morphology and leaf gas exchange patterns were observed. Our study also revealed that phytohormones including JAs and ABA play crucial role in promoting the salt adaptive strategies in Pongamia. Correlation studies demonstrated that hormones including ABA, JAs and SA showed a positive interaction with selective compatible metabolites (sugars, polyols and organic acids) to aid in maintaining osmotic balance and conferring salt tolerance in Pongamia. At the molecular level, our data showed that differential expression of transporter genes as well as antioxidant genes regulate the ionic and ROS homeostasis in Pongamia. These data shed new insights on an integrated physiological, structural, molecular and metabolic adaptations conferring salinity tolerance to Pongamia.

Fresh roots were harvested for protein extraction and whole proteome was quantified by using free labelled nanoLC-MS/MS technique. A total number of 1062 proteins were identified with 130 differentially expressed proteins (DEPs). Protein homology studies have shown Pongamia sharing ~22% sequence similarity with *Glycine* and *Pisum*. Most of the DEPs belonged to flavonoid biosynthesis, CYP450 family proteins, seed storage proteins and carbohydrate metabolism. Interestingly, we recorded a significant increase in the chloroplast protective as well as glyoxylate cycle proteins. Our correlation network studies also clearly demonstrated a cross link between carbohydrate metabolism and amino acid metabolism. Our data on whole root proteome have

explored novel insights into the salt tolerance mechanisms in *Pongamia pinnata* which are crucial to improve certain tree species to adapt for the fast changing and unfavourable climate regimes.

Conclusions

1. For the first time, our data explored novel insights into underlying mechanisms which are responsible for unchanged leaf morphology characteristics in *Pongamia pinnata* under high saline environment.
2. Our results clearly demonstrate that leaves and roots of Pongamia exhibit differential responses under salt stress, although roots are more efficient in sequestering the Na^+ ions.
3. The Na^+ probe fluorescence analysis demonstrated effective vacuolar sequestration of Na^+ in the roots.
4. Formation of suberized multiseriate exodermis in the roots, along with extensive lignification, maximized water permeability in both leaves and the roots of Pongamia.
5. Correlation studies demonstrated that hormones including ABA, JAs and SA showed a positive interaction with selective compatible metabolites including sugars, polyols and organic acids in order to aid in maintaining osmotic balance and conferring salt tolerance in Pongamia.
6. For the first time, our data on whole root proteome have explored novel insights into the salt tolerance mechanisms in *Pongamia pinnata* which are crucial to improve certain tree species to adapt for the fast changing and unfavourable climate regimes.

Collectively, the present study provides crucial inputs and shed new insights on an integrated physiological, structural, molecular and metabolic adaptations conferring salinity tolerance in *Pongamia pinnata,* a potential biofuel tree species.

Chapter 7

Literature cited

Chapter 7 Literature cited

Abdallaha, M.M.S., Abdelgawad, Z.A., El-Bassiounya, H.M.S., (2016). Alleviation of the adverse effects of salinity stress using trehalose in two rice varieties. S. Afr. J. Bot. 103, 275-282.

AbdElgawad, H., Zinta, G., Hegab, M.M., Pandey, R., Asard, H., Abuelsoud, W., (2016). High salinity induces different oxidative stress and antioxidant responses in maize plants organs. Front. Plant Sci. 7, 276.

Abebe, T., Guenzi, A.C., Martin, B., Cushman, J.C., (2003). Tolerance of mannitol accumulating transgenic wheat to water stress and salinity. Plant Physiol. 131, 1748-1755.

Abogadallah, G.M., (2010). Antioxidative defense under salt stress. Plant Signal. Behav. 5, 369-374.

Adolfa, V.I., Jacobsen, S.E., Shabala, S., (2013). Salt tolerance mechanisms in quinoa (*Chenopodium quinoa* Willd.). Environ. Exp. Bot. 92, 43-54.

AlHassan, M., Chaura, J., Donat-Torres, M.P., Boscaiu, M., Vicente, O., (2017). Antioxidant responses under salinity and drought in three closely related wild monocots with different ecological optima. AoB Plants 9, plx009.

Ali, A., Raddatz, N., Aman, R., Kim, S., Park, H.C., Jan, M., Bressan, R.A., (2016). A single amino acid substitution in the sodium transporter HKT1 associated with plant salt tolerance. Plant Physiol. 171, 2112-2126.

Ali, M.F., Baek, K.H., (2020). Jasmonic acid signaling pathway in response to abiotic stresses in plants. Int. J. Mol. Sci. 21, 621.

Al-Kharusi, L., Al-Yahyai, R., Yaish, M.W., (2019). Antioxidant response to salinity in salt-tolerant and salt-susceptible cultivars of date palm. Agric. 9, 8.

An, D., Chen, J.G., Gao, Y.Q., Li, X., Chao, Z.F., Chen, Z.R., Li, Q.Q., Han, M.L., Wang, Y.L., Wang, Y.F., Chao, D.Y., (2017). AtHKT1 drives adaptation of Arabidopsis thaliana to salinity by reducing floral sodium content. PloS Genet. 13, e1007086.

Anower, M.R., Peel, M.D., Mott, I.W., Wu, Y., (2017). Physiological process associated with salinity tolerance in an alfalfa half-sib family. J. Agron. Crop Sci. 203, 506-518.

Chapter 7 Literature cited

Arbelet-Bonnin, D., Blasselle, C., Palm, E.R., Redwan, M., Ponnaiah, M., Laurenti, P., Meimoun, P., Gilard, F., Gakière, B., Mancuso, S., El-Maarouf-Bouteau, H., Bouteau, F., (2020). Metabolism regulation during salt exposure in the halophyte *Cakile maritime*. Environ. Exp. Bot. 104075.

Arnon, D., (1949). Copper enzymes isolated chloroplasts, polyphenoloxidase in *Beta vulgaris*. Plant Physiol. 24, 1-15.

Arpiwi, N.L., Yan, G., Barbour, E.L., Plummer, J.A., (2013). Genetic diversity, seed traits and salinity tolerance of *Millettia pinnata* (L.) panigraphi (syn. *Pongamia pinnata*), a biodiesel tree. Genet. Resour. Crop. Evol. 60, 677-692.

Assaha, D.V., Ueda, A., Saneoka, H., Al-Yahyai, R., Yaish, M.W., (2017). The role of Na^+ and K^+ transporters in salt stress adaptation in glycophytes. Front. Physiol. 8, 509.

Atikij, T., Syaputri, Y., Iwahashi, H., Praneenararat, T., Sirisattha, S., Kageyama, H., Sirisattha, R.W., (2019). Enhanced lipid production and molecular dynamics under salinity stress in green microalga *Chlamydomonas reinhardtii* (137C). Mar. Drugs 17, 484.

Bahieldin, A., Sabir, J.S.M., Ramadan, A., Alzohairy, A.M., Younis, R.A., Shokry, A.M., Gadalla, N.O., Edris, S., Hassan, S.M., Al-Kordy, M.A., Kamal, K.B.H., Rabah, S., Abuzinadah, O.A., El-Domyati, F.M., (2013). Control of glycerol biosynthesis under high salt stress in Arabidopsis. Funct. Plant Biol. 41, 87.

Bassil, E., Zhang, S., Gong, H., Tajima, H., Blumwald, E., (2018). Cation specificity of vacuolar NHX-type cation/H^+ antiporters. Plant Physiol. 179, 616-629.

Benito, B., Haro, R., Amtmann, A., Cuin, T., Dreyer, I., (2014). The twins K^+ and Na^+ in plants. J. Plant Physiol. 171, 723-731.

Biswas, S., Biswas, A.K., De, B., (2018). Metabolomics analysis of *Cajanus cajan* L. seedlings unravelled amelioration of stress induced responses to salinity after halopriming of seeds. Plant Signal. Behav. 13, e1489670.

Chapter 7 Literature cited

Böhm, J., Messerer, M., Müller, H.M., Scholz-Starke, J., Gradogna, A., Scherzer, S., Maierhofer, T., Bazihizina, N., Zhang, H., Stigloher, C., Ache, P., Al-Rasheid, K.A.S., Mayer, K.F.X., Shabala, S., Carpaneto, A., Haberer, G., Zhu, J.K., Hedrich, R., (2018). Understanding the molecular basis of salt sequestration in epidermal bladder cells of *Chenopodium quinoa*. Curr. Biol. 28, 3075-3085.

Boycheva, S., Dominguez, A., Rolcik, J., Boller, T., Fitzpatrick, T.B., (2015). Consequences of a deficit in vitamin B6 biosynthesis *denovo* for hormone homeostasis and root development in Arabidopsis. Plant Physiol. 167, 102-117.

Boyle, P.C., Schwizer, S., Hind, S.R., Kraus, C.M., De la Torre-Diaz, S., He, B., Martin, G.B., (2016). Detecting N-myristoylation and S-acylation of host and pathogen proteins in plants using click chemistry. Plant Methods 12, 38.

Byrt, C.S., Munns, R., Burton, R.A., Gilliham, M., Wege, S., (2018). Root cell wall solutions for crop plants in saline soils. Plant Sci. 269, 47-55.

Cai, Q., Yuan, Z., Chen, M., Yin, C., Luo, Z., Zhao, X., Liang, W., Hu, J., Zhang, D., (2014). Jasmonic acid regulates spikelet development in rice. Nat. Commun. 5, 3476.

Cai, Z.Q., Gao, Q., (2020). Comparative physiological and biochemical mechanisms of salt tolerance in five contrasting highland quinoa cultivars. BMC Plant Biol. 20, 70.

Cao, D., Lutz, A., Hill, C.B., Callahan, D.L., Roessner, U., (2017). A quantitative profiling method of phytohormones and other metabolites applied to barley roots subjected to salinity stress. Front. Plant Sci. 7, 2070.

Cao, J., Li, M., Chen, J., Liu, P., Li, Z., (2016). Effects of MeJA on Arabidopsis metabolome under endogenous JA deficiency. Sci. Rep. 6, 37674.

Chaitanya, B.S.K., Kumar, S., Kaki, S.S., Balakrishna, M., Karuna, M.S.L., Prasad, R.B.N., Sastry, P.S., Reddy, A.R., (2015). Stage-specific fatty acid fluxes play a regulatory role in glycerolipid metabolism during seed development in *Jatropha curcas* L. Agric. Food Chem. 63, 10811-10821.

Chen, C.L., van der Schoot, H., Dehghan, S., Alvim-Kamei, C.L., Schwarz, K.U., Meyer, H., Visser, R.G.F., van der Linden, G.C., (2017). Genetic diversity of salt tolerance in Miscanthus. Front. Plant Sci. 8, 187.

Chen, J., Xiao, Q., Wu, F., Dong, X., He, J., Pei, Z., Zheng, H., Näsholm, T., (2010). Nitric oxide enhances salt secretion and Na^+ sequestration in a mangrove plant, *Avicennia marina*, through increasing the expression of H^+-ATPase and Na^+/H^+ antiporter under high salinity. Tree Physiol. 30, 1570-1585.

Chen, S., Polle, A., (2010). Salinity tolerance of Populus. Plant Biol. 12, 317-333.

Chen, S., Wu, F., Li, Y., Qian, Y., Pan, X., Li, F., Wang, Y., Wu, Z., Fu, C., Lin, H., Yang, A., (2019). *NtMYB4* and *NtCHS1* are critical factors in the regulation of flavonoid biosynthesis and are involved in salinity responsiveness. Front. Plant Sci. 10, 178.

Chen, X., Wang, H., Li, X., Ma, K., Zhan, Y., Zeng, F., (2019). Molecular cloning and functional analysis of 4-coumarate:CoA ligase 4 (4CL-like 1) from *Fraxinus mandshurica* and its role in abiotic stress tolerance and cell wall synthesis. BMC Plant Biol. 19, 231.

Cheng, H., Inyang, A., Li, C.D., Fei, J., Zhou, Y.W., Wang, Y.S., (2020). Salt tolerance and exclusion in the mangrove plant *Avicennia marinaina* relation to root apoplastic barriers. Ecotoxicol. https://doi.org/10.1007/s10646-020-02203-6.

Che-Othman, M.H., Jacoby, R.P., Millar, A.H., Taylor, N.L., (2019). Wheat mitochondrial respiration shifts from the TCA cycle to the GABA shunt under salt stress. New Phytol. 225, 1166-1180.

Cheval, C., Aldon, D., Galaud, J.P., Ranty, B., (2013). Calcium/calmodulin-mediated regulation of plant immunity. Bioch. Biophys. Acta 1833, 1766-1771.

Chhetri, A.B., Tango, M.S., Budge, S.M., Watts, K.C., Islam, M.R., (2008). Non-edible plant oils as new sources for biodiesel production. Int. J. Mol. Sci. 9, 169-180.

Choudhary, A., Kumar, A., Kaur, N., (2020). ROS and oxidative burst: Roots in plant development. Plant Divers. 42, 33-43.

Chowdhury, M.A.H., Bhuyia, M.S.R., Shah-e-Alam, M., Azad, M.A.K., (2018). Low Ca^{2+} content and Ca^{2+}/Na^+ ratio in leaf tissues determine salinity tolerance in spanish type groundnut (*Arachishypogeal* L.). J. Agr. Sci. Tech. B 8, 71-84.

Conde, A., Regalado, A., Rodrigues, D., Costa, J.M., Blumwald, E., Chaves, M.M., (2015). Polyols in grape berry: transport and metabolic adjustments as a physiological strategy for water-deficit stress tolerance in grapevine. J. Exp. Bot. 66, 889-906.

Corso, M., Doccula, F.G., de Melo, J.R.F., Costa, A., Verbruggen, N., (2018). Endoplasmic reticulum-localized CCX2 is required for osmotolerance by regulating ER and cytosolic Ca^{2+} dynamics in Arabidopsis. Proc. Natl. Acad. Sci. USA 115, 3966-3971.

Credali, A., García-Calderón, M., Dam, S., Perry, J., Díaz-Quintana, A., Parniske, M., Wang, T.L., Stougaard, J., Vega, J.M., Márquez, A.J., (2012). The K^+-dependent asparaginase, NSE1, is crucial for plant growth and seed production in *Lotus japonicas*. Plant Cell Physiol. 54, 107-118.

Czégény, G., Kőrösi, L., Strid, Å., Hideg, E., (2019). Multiple roles for vitamin B6 in plant acclimation to UV-B. Sci. Rep. 9, 1259.

D'Agostino, N., Buonanno, M., Ayoub, J., Barone, A., Monti, S.M., Rigano, M.M., (2019). Identification of non-specific lipid transfer protein gene family members in *Solanum lycopersicum* and insights into the features of Sola l 3 protein. Sci. Rep. 9, 1607.

Dai, M., Xue, Q., Mccray, T., Margavage, K., Chen, F., Lee, J.H., Nezames, C.D., Guo, L., Terzaghi, W., Wan, J., Deng, X.W., Wang, H., (2013). The PP6 phosphatase regulates ABI5 phosphorylation and abscisic acid signaling in Arabidopsis. Plant Cell 25, 517-534.

Damaris, R.N., Li, M., Liu, Y., Chen, X., Murage, H., Yang, P., (2016). A proteomic analysis of salt stress response in seedlings of two African rice cultivars. Biochim. Biophys. Acta 1864, 1570-1578.

Davenport, R.J., Muñoz-Mayor, A., Jha, D., Essah, P.A., Rus, A., Tester, M., (2007). The Na^+ transporter AtHKT1;1 controls retrieval of Na^+ from the xylem in Arabidopsis. Plant Cell Environ. 30, 497-507.

Devinar, G., Llanes, A., Masciarelli, O., Luna, V., (2013). Different relative humidity conditions combined with chloride and sulfate salinity treatments modify abscisic acid and salicylic acid levels in the halophyte *Prosopis strombulifera*. Plant Growth Regul. 70, 247-256.

Diallo, A.O., Agharbaoui, Z., Badawi, M.A., Ali-Benali, M.A., Moheb, A., Houde, M., Sarhan, F., (2014). Transcriptome analysis of an mvp mutant reveals important changes in global gene expression and a role for methyl jasmonate in vernalization and flowering in wheat. J. Exp. Bot. 65, 2271-2286.

Dikilitas, M., Simsek, E., Karakas, S., (2019). *Plant signaling molecules role and regulation under stressful environments*. Eds: M.I.R. Khan., P.S. Reddy, A. Ferrante., N.A. Khan., Woodhead, United Kingdom, pp19-42.

Divakara, B.N., Alur, A.S., Tripati, S., (2010). Genetic variability and relationship of pod and seed traits in *Pongamia pinnata* (L.) pierre, a potential agroforestry tree. Int. J. Plant Prod. 4, 129-141.

Dong, H., Bai, L., Zhang, Yu., Zhang, G., Mao, Y., Min, L., Xiang, F., Qian, D., Zhu, X., Song, C.P., (2018). Modulation of guard cell turgor and drought tolerance by a peroxisomal acetate-malate shunt. Mol. Plant 11, 1278-1291.

Dong, Q., Zhang, Y.X., Quan, Z., Liu, Q.E, Chen, D.B., Wang, H., Cheng, S.H., Cao, L. Y., Shen, X.H., (2019). UMP kinase regulates chloroplast development and cold response in rice. Int. J. Mol. Sci. 20, 2107.

Dragwidge, J.M., Ford, B.A., Ashnest, J.R., Das, P., Gendall, A.R., (2018). Two endosomal NHX-type Na^+/H^+ antiporters are involved in auxin mediated development in *Arabidopsis thaliana*. Plant Cell Physiol. 59, 1660-1669.

Dumschott, K., Dechorgnat, J., Merchant, A., (2019). Water deficit elicits a transcriptional response of genes governing D-pinitol biosynthesis in soybean (*Glycine max*). Int. J. Mol. Sci. 20, 2411.

Escalante-Pérez, M., Lautner, S., Nehls, U., Selle, A., Teuber, M., Schnitzler, J.P., Teichmann, T., Fayyaz, P., Hartung, W., Polle, A., Fromm, J., Hedrich, R., Ache, P., (2009). Salt stress affects xylem differentiation of grey poplar (*Populus* X *Canescens*). Planta 229, 299-309.

Fahad, S., Nie, L., Chen, Y., Wu, C., Xiong, D., Saud, S., Hongyan, L., Cui, K., Huang, J., (2015). Crop plant hormones and environmental stress. Sustain. Agric. Rev. 15, 371-400.

Falhof, J., Pedersen, J.T., Fuglsang, A.T., Palmgren, M., (2016). Plasma membrane H^+-ATPase regulation in the center of plant physiology. Mol. Plant 9, 323-337.

Fattorini, L., Hause, B., Gutierrez, L., Veloccia, A., Rovere, F.D., Piacentini, D., Falasca, G., Altamura, M.M., (2018). Jasmonate promotes auxin-induced adventitious rooting in dark-grown *Arabidopsis thaliana* plants and stem thin cell layers by a cross-talk with ethylene signaling and a modulation of xylogenesis. BMC Plant Biol. 18, 182.

Felle, H.H., Hermann, A., Hückelhoven, R., Kogel, K.H., (2005). Root-to-shoot signalling: apoplastic alkalinization, a general stress response and defence factor in barley (*Hordeum vulgare*). Protoplasma 227, 17-24.

Feng, X., Xu, S., Li, J., Yang, Y., Chen, Q., Lyu, H., Zhong, C., He, Z., Shi, S., (2020). Molecular adaptation to salinity fluctuation in tropical intertidal environments of a mangrove tree *Sonneratia alba*. BMC Plant Biol. 20, 178.

Formentin, E., Barizza, E., Stevanato, P., Falda, M., Massa, F., Tarkowskà, D., Novak, O., Lo Schiavo, F., (2018). Fast regulation of hormone metabolism contributes to salt tolerance in rice (*Oryzasativa* spp. Japonica, L.) by inducing specific morpho-physiological responses. Plants (Basel) 7, 75.

Fu, Y., Yang, Y., Chen, S., Ning, N., Hu, H., (2019). Arabidopsis IAR4 modulates primary root growth under salt stress through ROS-mediated modulation of auxin distribution. Front. Plant Sci. 10, 522.

Fukuda, A., Tanaka, Y., (2006). Effects of ABA, auxin, and gibberellin on the expression of genes for vacuolar H^+-inorganic pyrophosphatase, H^+-ATPase subunit A, and Na^+/H^+ antiporter in barley. Plant Physiol. Biochem. 44, 351-358.

Furtado, B.U., Nagy, I., Asp, T., Tyburski, J., Skorupa, M., Gołębiewski, M., Hulisz, P., Hrynkiewicz, K., (2019). Transcriptome profiling and environmental linkage to salinity across *Salicornia europaea* vegetation. BMC Plant Biol. 19, 427.

Gao, R., Duan, K., Guo, G., Du, Z., Chen, Z., Li, L., He, T., Lu, R., Huang, J., (2013). Comparative transcriptional profiling of two contrasting barley genotypes under salinity stress during the seedling stage. Int. J. Genomics 139, 822-835.

Geilfus, C.M., Tenhaken, R., Carpentier, S.C., (2017). Transient alkalinization of the leaf apoplast stiffens the cell wall during onset of chloride-salinity in corn leaves. J. Biol. Chem. 292, 18800-18813.

Genc, Y., Taylor, J., Lyons, G., Li, Y., Cheong, J., Appelbee, M., Oldach, K., Sutton, T., (2019). Bread wheat with high salinity and sodicity tolerance. Front. Plant Sci. 10, 1280.

Gharbi, E., Lutts, S., Dailly, H., Quinet, M., (2018). Comparison between the impacts of two different modes of salicylic acid application on tomato (*Solanum lycopersicum*) responses to salinity. Plant Signal. Behav. 13, e146936.

Gharsallah, C., Fakhfakh, H., Grubb, D., Gorsane, F., (2016). Effect of salt stress on ion concentration, proline content, antioxidant enzyme activities and gene expression in tomato cultivars. AoB Plants 8, plw055.

Gilbert, L., Alhagdow, M., Nunes-Nesi, A., Quemener, B., Guillon, F., Bouchet, B., Faurobert, M., Gouble, B., Page, D., Garcia, V., Petit, J., Stevens, R., Causse, M., Fernie, A.R., Lahaye, M., Gill, S.S., Tuteja, N., (2010). Reactive oxygen species and antioxidant machinery in abiotic stress tolerance in crop plants. Plant Physiol. Biochem. 48, 909-930.

Golan, Y., Shirron, N., Avni, A., Shmoish, M., Gepstein, S., (2016). Cytokinins induce transcriptional reprograming and improve Arabidopsis plant performance under drought and salt stress conditions. Front. Environ. Sci. 4, 63.

Gonzalez, P., Syvertsen, J.P., Etxeberria, E., (2012). Sodium distribution in salt-stressed citrus root stock plants. Hort. Sci. 47, 1504-1511.

Graus, D., Konrad, K.R., Bemm, F., Patir-Nebioglu, M.G., Lorey, C., Duscha, K., Güthoff, T., Herrmann, J., Ferjani, A., Cuin, T.A., Roelfsema, M.R.G., Schumacher, K., Neuhaus, H.E., Marten, I., Hedrich, R., (2018). High V-PPase activity is beneficial under high salt loads, but detrimental without salinity. New Phytol. 219, 1421-1432.

Guan, Q., Tan, B., Kelley, T.M., Tian, J., Chen, S., (2020). Physiological changes in *Mesembryanthemum crystallinum* during the C3 to CAM transition induced by salt stress. Front. Plant Sci. 11:283.

Guan, R., Qu, Y., Guo, Y., Yu, L., Liu, Y., Jiang, J., Chen, J., Ren, Y., Liu, G., Tian, L., Jin, L., Liu, Z., Hong, H., Chang, R., Gilliham, M., Qiu, L., (2014). Salinity tolerance in soybean is modulated by natural variation in *GmSALT3*. Plant J. 80, 937-950.

Guo, H., Zhang, L., Cui, Y.N., Wang, S.M., Bao, AK., (2019). Identification of candidate genes related tosalt tolerance of the secretohalophyteAtriplex canescensby transcriptomicanalysis. BMC Plant Biol. 19, 213.

Guo, M., Lu, J.P., Zhai, Y.F., Chai, W.G., Gong, Z.H., Lu, M.H., (2015). Genome-wide analysis, expression profile of heat shock factor gene family (CaHsfs) and characterization of CaHsfA2 in pepper (*Capsicum annuum* L.). BMC Plant Biol. 15, 151.

Gupta, A., Hisano, H., Hojo, Y., Matsuura, T., Ikeda, Y., Mori, I. C., Senthil-Kumar, M., (2017). Global profiling of phytohormone dynamics during combined drought and pathogen stress in *Arabidopsis thaliana* reveals ABA and JA as major regulators. Sci. Rep. 7, 4017.

Gupta, B., Huang, B., (2014). Mechanism of salinity tolerance in plants: Physiological, biochemical, and molecular characterization. Int. J. Genome 1-18.

Hadi, M.R., Karimi, N., (2012). The role of calcium in plants' salt tolerance. J. Plant Nutr. 35, 2037-2054.

Hanin, M., Ebel, C., Ngom, M., Laplaze, L., Masmoudi, K., (2016). New insights on plant salt tolerance mechanisms and their potential use for breeding. Front. Plant Sci. 7, 1787.

Haq, S.U., Khan, A., Ali, M., Khattak, A.M., Gai, W.X., Zhang, H.X., Wei, A.M., Gong, Z.H., (2019). Heat shock proteins: Dynamic biomolecules to counter plant biotic and abiotic stresses. Int. J. Mol. Sci. 20, 5321.

Harfouche, A., Meilan, R., Altman, A., (2014). Molecular and physiological responses to abiotic stress in forest trees and their relevance to tree improvement. Tree Physiol. 34, 1181-1198.

Hasanuzzaman, M., Bhuyan, M.H.M.B., Nahar, K., Hossain, M.S., Mahmud, J.A., Hossen, M.S., Masud, A.A.C., Moumita., Fujita, M., (2018). Potassium: A vital regulator of plant responses and tolerance to abiotic stresses. Agron. 8, 1-29.

Hasegawa, P.M., (2013). Sodium (Na^+) homeostasis and salt tolerance of plants. Environ. Exp. Bot. 92, 19-31.

Hassan, S., Sarwar, M.B., Sadique, S., Rashid, B., Aftab, B., Mohamed, B.B., Husnain, T., (2014). Growth, physiological and molecular responses of cotton (*Gossypium arboreum* L.) under NaCl stress. Am. J. Plant Sci. 5, 605-614.

He, Y., Zhu, Z., Yang, J., Ni, X., Zhu, B., (2009). Grafting increases the salt tolerance of tomato by improvement of photosynthesis and enhancement of antioxidant enzymes activity. Environ. Exp. Bot. 66, 270-278.

Hill, C.B., Jha, D., Bacic, A., Tester, M., Roessner, U., (2013). Characterization of ion contents and metabolic responses to salt stress of different Arabidopsis AtHKT1;1 genotypes and their parental strains. Mol. Plant 6, 350-368.

Horie, T., Karahara, I., Katsuhara, M., (2012). Salinity tolerance mechanisms in glycophytes: An overview with the central focus on rice plants. Rice 5, 11.

Hossain, M.S., Persicke, M., ElSayed, A.I., Kalinowski, J., Dietz, K.J., (2017). Metabolite profiling at the cellular and subcellular level reveals metabolites associated with salinity tolerance in carbohydrate beet. J. Exp. Bot. 68, 5961-5976.

Huang, J., Lu, X., Yan, H., Chen, S., Zhang, W., Huang, R., Zheng, Y., (2012). Transcriptome characterization and sequencing-based identification of salt responsive genes in *Millettia pinnata*, a semi-mangrove plant. DNA Res. 19, 195-207.

Husen, A., Iqbal, M., Sohrab, S.S., Ansari, M.K.A., (2018). Salicylic acid alleviates salinity caused damage to foliar functions, plant growth and antioxidant system in Ethiopian mustard (*Brassica carinataa*. Br.). Agri. Food Secur. 7, 44.

Igamberdiev, A.U., Kleczkowski, L.A., (2018). The glycerate and phosphorylated pathways of serine synthesis in plants: the branches of plant glycolysis linking carbon and nitrogen metabolism. Front. Plant Sci. 9, 318.

Ishimaru, Y., Hayashi, K., Suzuki, T., Fukaki, H., Prusinska, J., Meester, C., Quareshy, M., Egoshi, S., Matsuura, H., Takahashi, K., Kato, N., Kombrink, E., Napier, R.M., Hayashi, K.I., Uedaa, M., (2018). Jasmonic acid inhibits auxin-induced lateral rooting independently of the CORONATINE INSENSITIVE1 receptor. Plant Physiol. 177, 1704-1716.

Ismail, A.M., Horie, T., (2017). Genomics, physiology, and molecular breeding approaches for improving salt tolerance. Annu. Rev. Plant Biol. 19, 33.

Jamil, A., Riaz, S., Ashraf, M., Foolad, M.R., (2011). Gene expression profiling of plants under salt stress. Crit. Rev. Plant Sci. 30, 435-458.

Jang, G., Chang, S.H., Um, T.Y., Lee, S., Kim, J.K., Do Choi, Y., (2017). Antagonistic interaction between jasmonic acid and cytokinin in xylem development. Sci. Rep. 7, 10212.

Jayakannan, M., Bose, J., Babourina, O., Rengel, Z., Shabala, S., (2013). Salicylic acid improves salinity tolerance in Arabidopsis by restoring membrane potential and preventing salt-induced K^+ loss via a GORK channel. J. Exp. Bot. 64, 2255-2268.

Jia, T., An, J., Liu, Z., Yu, B., Chen, J., (2017). Salt stress induced soybean *GmIFS1* expression and isoflavone accumulation and salt tolerance in transgenic soybean cotyledon hairy roots and tobacco. *Plant Cell Tiss. Org.* 128, 469-477.

Jiang, G.F., Goodale, U.M., Liu, Y.Y., Hao, G.Y., Cao, K.F., (2017). Salt management strategy defines the stem and leaf hydraulic characteristics of six mangrove tree species. Tree Physiol. 37, 389-401.

Jones, M.B., Finnan, J., Hodkinson, T.R., (2014). Morphological and physiological traits for higher biomass production in perennial rhizomatous grasses grown on marginal land. Glob. Change Biol. Bioen. 7, 375-385.

Julkowska, M.M., Hoefsloot, H.C.J., Mol, S., Richard, F., Boer, G.J.D., Haring, M.A., Testerink, C., (2014). Capturing *Arabidopsis* root architecture dynamics with ROOT-FIT reveals diversity in responses to salinity. Plant Physiol. 166, 1387-1402.

Kamboj, A., Ziemann, M., Bhave, M., (2015). Identification of salt-tolerant barley varieties by a consolidatedphysiological and molecular approach. Acta Physiol. Plant 37, 1716.

Kang, D.J., Seo, Y.J., Lee, J.D., Ishii, R., Kim, K.U., Shin, D.H., Park, S.K., Jang, S.W., Lee, I.J., (2005). Jasmonic acid differentially affects growth, ion uptake and abscisic acid concentration in salt-tolerant and salt-sensitive rice cultivars. J. Agron. Crop Sci. 191, 273-282.

Kang, J.H., McRoberts, J., Shi, F., Moreno, J.E., Jones, A.D., Howe, G.A., (2014). The flavonoid biosynthetic enzyme chalcone isomerase modulates terpenoid production in glandular trichomes of tomato. Plant Physiol. 164, 1161-1174.

Kaur, R., Grewal, S.K., Singh, S., Kaur, J., Bhardwaj, R.D., (2020). Desi and kabuli chickpea cultivars had differential behaviour towards salinity stress tolerance. Biol. Future https://doi.org/10.1007/s42977-020-00004-w.

Kaur, R., Nayyar, H., (2014). *Ascorbic acid: A potent defender against environmental stresses; Oxidative damage to plants-antioxidant networks and signaling*. Eds: P. Ahmad, Academic press, San Diego, USA, pp235-287.

Kazakoff, S.H., Imelfort. M., Edwards, D., Koehorst, J., Biswas, B., Batley, J., Scott, P.T., Gresshoff, M.P., (2012). Capturing the biofuel well head and powerhouse: the chloroplast and mitochondrial genomes of the leguminous feed stock tree *Pongamia pinnata*. PLoS One 2, e5168.

Kesari, V., Rangan, L., (2010). Development of Pongamia pinnata as an alternative biofuel crop-current status and scope of plantations in India. J. Crop Sci. Biotech. 13, 127-137.

Kim, B.H., Kim, S.Y., Nam, K.H., (2012). Genes encoding plant-specific class III peroxidases are responsible for increased cold tolerance of the brassinosteroid-insensitive 1 mutant. Mol. Cells 34, 539-548.

Kim, J.I., Baek, D., Park, H.C., Chun, H.J., Oh, D.H., Lee, M.K., Cha, J.Y., Kim, W.Y., Kim, M.C., Chung, W.S., Bohnert, H.J., Lee, S.Y., Bressan, R.A., Lee, S.W., Yun, D.J., (2012). Overexpression of Arabidopsis *YUCCA6* in potato results in high auxin developmental phenotypes and enhanced resistance to water deficit. Mol. Plant 6, 337-349.

Kobayashi, K., Ohnishi, A., Sasaki, D., Fujii, S., Iwase, A., Sugimoto, K., Masuda, T., Wada, H., (2017). Shoot removal induces chloroplast development in roots via cytokinin signalling. Plant Physiol. 173, 2340-2355.

Koksal, N., Alkan-Torun, A., Kulahlioglu, I., Ertargin, E., Karalar, E., (2016). Ion uptake of marigold under saline growth conditions. Springer Plus 5, 139.

Korkmaz, D., (2001). Precipitation titration: “determination of chloride by the Mohr method”. Methods 2, 4.

Kosová, K., Vitamvas, P., Urban, M.O., Prasil, I.T., Renaut, J., (2018). Plant abiotic stress proteomics: The major factors determining alterations in cellular proteome. Front. Plant Sci. 9, 122.

Kosová, K., Prášil, I.T., Vítámvás, P., (2013). Protein contribution to plant salinity response and tolerance acquisition. Int. J. Mol. Sci.14, 6757-6789.

Krishnamurthy, K.V., (1999). Light microscopic cytochemistry: Methods in cell wall cytochemistry. Florida, CRC Press.

Krishnamurthy, P., Jyothi-Prakash, P.A., Qin, L., He, J., Lin, Q., Loh, C.S., Kumar, P.P., (2014). Role of root hydrophobic barriers in salt exclusion of a mangrove plant *Avicennia officinalis*. Plant Cell Environ. 37, 1656-1671.

Kumar, S., Beena, A.S., Awana, M., Singh, A., (2017). Physiological, biochemical, epigenetic and molecular analyses of wheat (*Triticum aestivum*) genotypes with contrasting salt tolerance. Front. Plant Sci. 8, 1151.

Kürsteiner, O., Dupuis, I., Kuhlemeier, C., (2003). The *pyruvate decarboxylase1* gene of Arabidopsis is required during anoxia but not other environmental stresses. Plant Physiol. 132, 968-978.

Lee, B.R., Kim, K.Y., Jung, W.J., Avice, J.C., Ourry, A., Kim, T.H., (2007). Peroxidases and lignification in relation to the intensity of water-deficit stress in white clover (*Trifoliumrepens* L.). J. Exp. Bot. 58, 1271-1271.

Le-Gall, H., Philippe, F., Domon, J.M., Gillet, F., Pelloux, J., Rayon, C., (2015). Cell wall metabolism in response to abiotic stress. Plants 4, 112-166.

Li, H., Chang, J., Chen, H., Wang, Z., Gu, X., Wei, C., Zhang, Y., Ma, J., Yang, J., Zhang, X., (2017). Exogenous melatonin confers salt stress tolerance to watermelon by improving photosynthesis and redox homeostasis. Front. Plant Sci. 8, 295.

Li, P., Li, Y.J., Zhang, F.J., Zhang, G.Z., Jiang, X.Y., Yu, H.M., Hou, B.K., (2017). The Arabidopsis UDP-glycosyltransferases UGT79B2 and UGT79B3, contribute to cold, salt and drought stress tolerance via modulating anthocyanin accumulation. Plant J. 89, 85-103.

Li, Q., Zheng, J., Li, S., Huang, G., Skilling, S.J., Wang, L., Li, L., Li, M., Yuan, L., Liu, P., (2017). Transporter-mediated nuclear entry of jasmonoyl-isoleucine is essential for jasmonate signalling. Mol. Plant 10, 695-708.

Li, W., Zhao, F., Fang, W., Xie, D., Hou, J., Yang, X., Zhao, Y., Tang, Z., Nie, L., Lv, S., (2015). Identification of early salt stress responsive proteins in seedling roots of upland cotton (*Gossypium hirsutum* L.) employing iTRAQ-based proteomic technique. Front. Plant Sci. 6, 732.

Li, Z., Wang, X., Chen, J., Gao, J., Zhou, X., Kuai, B., (2016). CCX1, a putative Cation/Ca^{2+} exchanger, participates in regulation of reactive oxygen species homeostasis and leaf senescence. Plant Cell Physiol. 57, 2611-2619.

Lillo, C., Kataya, A.R.A., Heidari, B., Creighton, M.T., Nemie-Eissa, D., Ginbot, Z., Jonassen, E.M., (2014). Protein phosphatases PP2A, PP4 and PP6: mediators and regulators in development and responses to environmental cues. Plant Cell Environ. 37, 2631-2648.

Liu, C., Chen, K., Zhao, X., Wang, X., Shen, C., Zhu, Y., Dai, M., Qiu, X., Yang, R., Xing, D., Pang, Y., Xu, J., (2019). Identification of genes for salt tolerance and yield-related traits in rice plants grown hydroponically and under saline field conditions by genome-wide association study. Rice 12, 88.

Liu, F., Zhang, X., Lu, C., Zeng, X., Li, Y., Fu, D., Wu, G., (2015). Non-specific lipid transfer proteins in plants: presenting new advances and an integrated functional analysis. J. Exp. Bot. 66, 5663-5681.

Liu, J., Gao, F., Ren, J., Lu, X., Ren, G., Wang, R., (2017). A novel AP2/ERF transcription factor CR1 regulates the accumulation of vindoline and serpentine in *Catharanthus roseus*. Front. Plant Sci. 8, 2082.

Liu, Q., Luo, L., Zheng, L., (2018). Lignins: Biosynthesis and biological functions in plants. Int. J. Mol. Sci. 19, 335.

Liu, Y.D., Yin, Z.J., Yu, J.W., LI, J., Wei, H.L., Han, X.L., Shen, F.F., (2012). Improved salt tolerance and delayed leaf senescence in transgenic cotton expressing the *Agrobacterium IPT* gene. Biol. Plant. 56, 237-246.

Livak, K.J., Schmittgen, T.D., (2001). Analysis of relative gene expression data using real-time 1202 quantitative PCR and the $2^{-\Delta\Delta C}{}_{T}$ method. Methods 25, 402-408.

Lombardo, V.A., Osorio, S., Borsani, J., Lauxmann, M.A., Bustamante, C.A., Budde, C.O., Andreo, C.S., Lara, M.V., Fernie, A.R., Drincovich, M.F., (2011). Metabolic profiling during peach fruit development and ripening reveals the metabolic networks that underpin each developmental stage. Plant Physiol. 157, 1969-1710.

Luo, H.T., Zhang, J.Y., Wang, G., Jia, Z.H., Huang, S.N., Wang, T., Guo, Z.R., (2017). Functional characterization of waterlogging and heat stresses tolerance gene pyruvate decarboxylase2 from *Actinidia deliciosa*. Int. J. Mol. Sci. 8, 2377.

Ma, T., Wang, J., Zhou, G., Yue, Z., Hu, Q., Chen, Y., Liu, B., Qiu, Q., Wang, Z., Zhang, J., Wang, K., Jiang, D., Gou, C., Yu, L., Zhan, D., Zhou, R., Luo, W., Ma, H., Yang, Y., Pan, S., Fang, D., Luo, Y., Wang, X., Wang, G., Wang, J., Wang, Q., Lu, X., Chen, Z., Liu, J., Lu, Y., Yin, Y., Yang, H., Abbott, R.J., Wu, Y., Wan, D., Li, J., Yin, T., Lascoux, M., DiFazio, S.P., Tuskan, G.A., Wamg, J., Liu, J., (2014). Genomic insights into salt adaptation in a desert poplar. Nat. Commun. 4, 2797.

Majeran, W., Le Caer, J.P., Ponnala, L., Meinnel, T., Giglione, C., (2018). Targeted profiling of Arabidopsis thaliana sub-proteomes illuminates co- and post-translationally N-Terminal myristoylated proteins. Plant Cell 30, 543-562.

Marriboina, S., Attipalli, R.R., (2020a). Hydrophobic cell-wall barriers and vacuolar sequestration of Na^{+} ions are the key mechanisms conferring high salinity tolerance in a biofuel tree species *Pongamia pinnata* L. pierre. Environ. Exp. Bot. 171, 103949.

Marriboina, S., Attipalli, R.R., (2020b). Optimization of hydroponic growth system and Na^{+}-fluorescence measurements for tree species *Pongamia pinnata* (L.) pierre. *MethodsX* **7,** 100809.

Marriboina, S., Sengupta, D., Kumar, S., Attipalli, R.R., (2017). Physiological and molecular insights into the high salinity tolerance of *Pongamia pinnata* (L.) pierre, a potential biofuel tree species. Plant Sci. 258, 102-111.

Marriboina, S., Sharma, K., Sengupta, D., Yadavalli, A.D., Sharma, R.P., Reddy, A.R., (2020c). Systematic hormone-metabolite network provides insights of high salinity tolerance in *Pongamia pinnata* (L.) pierre. *bioRxiv*. doi: https://doi.org/10.1101/2020.04.28.066050.

Martinez, V., Mestre, T.C., Rubio, F., Vilaplana, A.G., Moreno, D.A., Mittler, R., Rivero, R.M., (2016). Accumulation of flavonols over hydroxycinnamic acids favors oxidative damage protection under abiotic stress. Front. Plant Sci. 7, 838.

Mathur, A., Vyas, D.K., (2013). Socio-ecological issues eco-economic and sustainability status. J. Ecol. Environ. Sci. 4, 87-90.

Maury, S., Sow, M.D., Le Gac, A.L., Genitoni, J., Lafon-Placette, C., Mozgova, I., (2019). Phytohormone and chromatin crosstalk: The missing link for developmental plasticity?. Front. Plant Sci. 10, 395.

Maxwell, K., Johnson, G.N., (2000). Chlorophyll fluorescence-a practical guide. J. Exp. Bot. 51, 659-668.

Md-Hossain, S., (2019). Present scenario of global salt affected soils, its management and importance of salinity research. Int. Res. J. Biol. Sci. 1, 1-3.

Mekawy, A.M.M., Assaha, D.V.M., Ueda, A., (2020). Constitutive overexpression of rice metallothionein-like gene OsMT-3a enhances growth and tolerance of Arabidopsis plants to a combination of various abiotic stresses. J. Plant Res. 133, 429-440.

Melchiorre, M., Quero, G.E., Parola, R., Racca, R., Trippi, V.S., Lascano, R., (2009). Physiological characterization of four model Lotus diploid genotypes: L. japonicus (MG20 and Gifu), L. filicaulis, and L. burttii under salt stress. Plant Sci. 177, 618-628.

Melo, Y.L., Dantas, C.V.S., Melo, Y.L., Maia, J.M., De-Macêdo, C.E.C., (2016). Changes in osmotic and ionic indicators in *Ananascomosus* (L.) cv. MD gold pre-treated with phytohormones and submitted to saline medium. Rev. Bras. Frutic. 39, e-155.

Méndez-Alonzo, R., López-Portillo, J., Moctezuma, C., Bartlett, M.K., Sack, L., (2016). Osmotic and hydraulic adjustment of mangrove saplingsto extreme salinity. Tree Physiol. 36, 1562-1572.

Meyer, C.J., Peterson, C.A., Steudle, E., (2011). Permeability of Iris germanica's multiseriate exodermis to water, NaCl, and ethanol. J. Exp. Bot. 62, 1911-1926.

Mitra, S., Baldwin, I.T., (2014). RuBPCase activase (RCA) mediates growth-defense trade-offs: silencing RCA redirects jasmonic acid (JA) flux from JA-isoleucine to methyl jasmonate (MeJA) to attenuate induced defense responses in *Nicotiana attenuata*. New Phytol. 201, 1385-1395.

Mohamed, I.H., Latif, H.H., (2017). Improvement of drought tolerance of soybean plants by using methyl jasmonate. Physiol. Mol. Biol. Plants 23, 545-556.

Moing, A., Aharoni, A., Biais, B., Rogachev, I., Meir, S., Brodsky, L., Allwood, J.W., Erban, A., Dunn, W.B., Kay, L., de-Koning, S., de-Vos, R.C., Jonker, H., Mumm, R., Deborde, C., Maucourt, M., Bernillon, S., Gibon, Y., Hansen, T.H., Husted, S., Goodacre, R., Kopka, J., Schjoerring, J.K., Rolin, D., Hall, R.D., (2011). Extensive metabolic cross-talk in melon fruit revealed by spatial and developmental combinatorial metabolomics. New Phytol. 190, 683-696.

Moradi, F., Ismail, A.M. (2007). Responses of photosynthesis, chlorophyll fluorescence and ROS-scavenging systems to salt stress during seedling and reproductive stages in rice. Ann. Bot. 99, 1161-1173.

Morton, M.J.L., Awlia, M., Al-Tamimi, N., Saade, S., Pailles, Y., Negrão, S., Tester, M., (2019). Salt stress under the scalpel-dissecting the genetics of salt tolerance. Plant J. 97, 148-163.

Mudalkar, S., Golla, R., Ghatty, S., Reddy, A.R., (2014). De novo transcriptome analysis of an imminent biofuel crop, *Camelina sativa* L. using Illumina GAIIX sequencing platform and identification of SSR markers. Plant Mol. Biol. 84, 159-171.

Munemasa, S., Hossain, M.A., Nakamura, Y., Mori, I.C., Murata, Y., (2011). The Arabidopsis calcium-dependent protein kinase, CPK6, functions as a positive regulator of methyl jasmonate signaling in guard cells. Plant Physiol. 155, 553-561.

Munns, R., Gilliham, M., (2015). Salinity tolerance of crops-what is the cost?. New Phytol. 208, 668-673.

Munns, R., James, R.A., Xu, B., Athman, A., Conn, S.J., Jordans, C., Byrt, C.S., Hare R.A., Tyerman, S.D., Tester, M., Plett, D., Gilliham, M., (2012). Wheat grain yield on saline soils is improved by an ancestral Na^+ transporter gene. Nat. Biotechnol. 30, 360-364.

Munns, R., Tester, M., (2008). Mechanisms of salinity tolerance. Annu. Rev. Plant Biol. 59, 651-681.

Munns, R., Wallace, P.A., Teakle, N.L., Colmer, T.D., (2010). *Measuring soluble ion concentrations (Na^+, K^+, Cl^-) in salt-treated plants*. Eds: R. Sunkar., Plant stress tolerance. Methods in molecular biology. Springer protocols, Berlin, Humana Press, pp371-382.

Naik, M., Meher, L.C., Naik, S.N., Das, L.M., (2008). Production of biodiesel from high free fatty acid Karanja (*Pongamia pinnata*) oil. Biomass Bioenerg. 32, 354-357.

Naliwajski, M.R., Skłodowska. M., (2018). The relationship between carbon and nitrogen metabolism in cucumber leaves acclimated to salt stress. PeerJ 6, e6043.

Nasir, F.A., Batarseh, M., Abdel-Ghani, A.H., Jiries, A., (2010). Free amino acids content in some halophytes under salinity stress in arid environment, Jordan. Clean Soil Air Water 38, 592-600.

Negrão, S., Schmöckel, S.M., Tester, M., (2017). Evaluating physiological responses of plants to salinity stress. Ann. Bot. 119, 1-11.

Netondo, G.W., Onyango, J.C., Beck, E., (2004). Sorghum and salinity: II. Gas exchange and chlorophyll fluorescence of sorghum under salt stress. Crop Sci. 44, 806-811.

Neves, G.Y.S., Marchiosi, R., Ferrarese, M.L.L., Siqueira-Soares, R.C., Ferrarese-Filho, O., (2010). Root growth inhibition and lignification induced by salt stress in soybean. J. Agron. Crop Sci. 196, 467-473.

Nishiyama, R., Watanabe, Y., Fujita, Y., Le, D.T., Kojima, M., Werner, T., Vankova, R., Yamaguchi-Shinozaki, K., Shinozaki, K., Kakimoto, T., Sakakibara, H., Schmülling, T., Tran, L.S.P., (2011). Analysis of cytokinin mutants and regulation of cytokinin metabolic genes reveals important regulatory roles of cytokinins in drought, salt and abscisic acid responses, and abscisic acid biosynthesis. Plant Cell 23, 2169-2183.

Nitschke, S., Cortleven, A., Iven, T., Feussner, I., Havaux, M., Riefler, M., Schmulling, T., (2016). Circadian stress regimes affect the circadian clock and cause jasmonic acid-dependent cell death in cytokinin-deficient Arabidopsis plants. Plant Cell 28, 1616-1639.

Nounjan, N., Chansongkrow, P., Charoensawan, V., Siangliw, J.L., Toojinda, T., Chadchawan, S., Theerakulpisut, P., (2018). High performance of photosynthesis and osmotic adjustment are associated with salt tolerance ability in rice carrying drought tolerance QTL: physiological and co-expression network analysis. Front. Plant Sci. 9, 1135.

Oh, D.H., Dassanayake, M., Bohnert, H.J., Cheeseman, J.M., (2012). Life at the extreme: Lessons from the genome. Genome Biol. 13, 241.

Oh, D.H., Lee, S.Y., Bressan, R.A., Yun, D.J., Bohnert, H.J., (2010). Intracellular consequences of SOS1 deficiency during salt stress. J. Exp. Bot. 61, 1205-1213.

Oh, D.H., Leidi, E., Zhang, Q., Hwang, S.M., Li, Y., Quintero, F.J., Jiang, X., D´Urzo, M.P., Lee, S.Y., Zhao, Y., Bahk, J.D., Bressan, R.A., Yun, D.J., Pardo, J.M., Bohnert, H.J., (2009). Loss of halophytism by interference with SOS1 expression. Plant Physiol. 151, 210-222.

Olfatmiri, H., Alemzadeh, A., Zakipour, Z., (2014). Up-regulation of plasma membrane H^+-ATPase under salt stress may enable *Aeluropus littoralis* to cope with stress. Mol. Biol. Res. Commun. 3, 67-75.

Pan, X., Welti, R., Wang, X., (2010). Quantitative analysis of major plant hormones in crude plant extracts by high-performance liquid chromatography-mass spectrometry. Nat. Protoc. 5, 986-992.

Pandolfi, C., Bazihizina, N., Giordano, C., Mancuso, S., Azzarello, E., (2016). Salt acclimation process: a comparison between a sensitive and a tolerant *Olea europaea* cultivar. Tree Physiol. 37, 380-388.

Paparella, C., Savatin, D.V., Marti, L., DeLorenzo, G., Ferrari, S., (2014). The Arabidopsis LYSIN MOTIF-CONTAININGRECEPTOR-LIKE KINASE3 regulates the cross talk between immunity and abscisic acid responses. Plant Physiol. 165, 262-276.

Papazian, S., Khaling, E., Bonnet, C., Lassueur, S., Reymond, P., Moritz, T., Blande, J.D., Albrectsen, B.R., (2016). Central metabolic responses to ozone and herbivory affect photosynthesis and stomatal closure. Plant Physiol. 172, 2057-2078.

Parida, A.K., Jha, B., (2010). Salt tolerance mechanisms in mangroves: A review. Trees 24, 199-217.

Péret, B., Swarup, K., Ferguson, A., Seth, M., Yang, Y., Dhondt, S., James, N., Casimiro, I., Perry, P., Syed, A., Yang, H., Reemmer, J., Venison, E., Howells, C., Perez-Amador, M.A., Yun, J., Alonso, J., Beemster, G.T.S., Laplaze, L., Murphy, A., Bennett, M.J., Nielsen, E., Swarup, R., (2012). AUX/LAXGenes encode a family of auxin influx transporters that perform distinct functions during Arabidopsis development. Plant Cell 24, 2874-2885.

Pi, E., Qu, L., Hu, J., Huang, Y., Qiu, L., Lu, H., Jiang, B., Liu, C., Peng, T., Zhao, Y., Wang, H., Tsai, S.N., Ngai, S., Du, L., (2016). Mechanisms of soybean roots' tolerances to salinity revealed by proteomic and phosphoproteomic comparisons between two cultivars, Mol. Cell. Proteom. 15, 266-288.

Polle, A., Chen, S., (2015). On the salty side of life: Molecular, physiological and anatomical adaptation and acclimation of trees to extreme habitats. Plant Cell Environ. 38, 1794.

Qi, X., Li, M.W., Xie, M., Liu, X., Ni, M., Shao, G., Song, C., Yim, A.K.Y., Tao, Y., Wong, F.L., Isobe, S., Wong, C.F., Wong, K.S., Xu, C., Li, C., Wang, Y., Guan, R., Sun, F., Fan, G., Xiao, Z., Zhou, F., Phang, T.H., Liu, X., Tong, S.W., Chan, T.F., Yiu, S.M., Tabata, S., Wang, J., Xu, X., Lam, H.M., (2014). Identification of a novel salt tolerance gene in wild soybean by whole-genome sequencing. Nat. Commun. 5, 4340.

Qiu, X.M., Sun, Y.Y., Ye, X.Y., Li, Z.G., (2020). Signaling role of glutamate in plants. Front. Plant Sci. 10, 1743.

Quan, R., Wang, J., Hui, J., Bai, H., Lyu, X., Zhu, Y., Zhang, H., Zhang, Z., Li, S., Huang, R., (2017). Improvement of salt tolerance using wild rice genes. Front. Plant Sci. 8, 2269.

Quinn, L.D., Straker, K.C., Guo, J., Kim, S., Santanu, T., Kling, G., Lee, D.K., Voigt, T.B., (2015). Stress-tolerant feedstocks for sustainable bioenergy production on marginal land. Bioenerg. Res. 8, 1081-1100.

Rady, M.M., (2012). A novel organo-mineral fertilizer can mitigate salinity stress effects for tomato production on reclaimed saline soil. S. Afr. J. Bot. 81, 8-14.

Raza, A., Razzaq, A., Mehmood, S.S., Zou, X., Zhang, X., Lv, Y., Xu, J., (2019). Impact of climate change on crops adaptation and strategies to tackle its outcome: A review. Plants 8, 39.

Reddy, A.R., Chaitanya, K.V., Vivekanandan, M., (2004). Drought induced responses of photosynthesis and antioxidant metabolism in higher plants. J. Plant Physiol. 61, 1189-1202.

Roessner, U., Wagner, C., Kopka, J., Trethewey, R.N., Willmitzer, L., (2000). Simultaneous analysis of metabolites in potato tuber by gas chromatography-mass spectrometry. Plant J. 23, 131-142.

Rossatto, T., do Amaral, M.N., Benitez, L.C., Vighi, I.L., Braga, E.J.B., de Magalhães Jr, A.M., Maia, M.A.C., da Silva Pinto, L., (2017). Gene expression and activity of antioxidant enzymes in rice plants, cv. BRS AG, under saline stress. Physiol. Mol. Biol. Plants 23, 865-875.

Saand, M.A., Xu, Y.P., Munyampundu, J.P., Li, W., Zhang, X.R., Cai, X.Z., (2015). Phylogeny and evolution of plant cyclic nucleotide-gated ion channel (CNGC) gene family and functional analyses of tomato CNGCs. DNA Res. 22, 471-483.

Sahoo, R. K., Ansari, M. W., Tuteja, R., Tuteja, N., (2014). *OsSUV3* transgenic rice maintains higher endogenous levels of plant hormones that mitigates adverse effects of salinity and sustains crop productivity. Rice 7, 17.

Sakamoto, M., Suzuki, T., (2019). Methyljasmonate and salinity increase anthocyanin accumulation in radish sprouts. Hortic. 5, 62.

Sakamoto, T., Murata, N., (2002). Regulation of the desaturation of fatty acids and its role in tolerance to cold and salt stress. Curr. Opin. Microbiol. 5, 208-210.

Samuel, S., Scott, P.T., Gresshoff, P.M., (2013). Nodulation in the legume biofuel feedstock tree *Pongamia pinnata*. Agric. Res. 2, 207-214.

Sánchez-Aguayo, I., Rodríguez-Galán, J.M., Torreblanca, R.G.J., Pardo, J.M., (2004). Salt stress enhances xylem development and expression of S-adenosyl-L-methionine synthase in lignifying tissues of tomato plants. Planta 220, 278-285.

Sandhu, D., Cornacchione, M.V., Ferreira, J.F.S. Suarez, D.L., (2017). Variable salinity responses of 12 alfalfa genotypes and comparative expression analyses of salt-response genes. Sci. Rep. 7, 42958.

Sangwan, S., Rao, D.V., Sharma, R.A., (2010). A review on *Pongamia pinnata* (L.) pierre: A great versatile leguminous plant. Nat. Sci. 8, 11.

Santos, R.W., Schmidt, É.C., Vieira, I.C., Costa, G.B., Rover, T., Simioni, C., Barufi, J.B., Soares, C.H.L., Bouzon, Z.L., (2015). The effect of different concentrations of copper and lead on the morphology and physiology of *Hypnea musciformis* cultivated in vitro: A comparative analysis. Protoplasma 252, 1203-1215.

Saqib, A., Scheller, H.V., Fredslund, F., Welner, D.H., (2019). Molecular characteristics of plant UDP-arabinopyranose mutases. Glycobiol. 29, 839-846.

Saravanan, R.S., Rose, J.K., (2004). A critical evaluation of sample extraction techniques for enhanced proteomic analysis of recalcitrant plant tissues. Proteomics 4, 2522-2532.

Scott, P.T., Pregelj, L., Chen, N., Hadler, J.S., Djordjevic, M.A., Gresshoff, P.M., (2008). *Pongamia pinnata*: An untapped resource for the biofuels industry of the future. Bioenerg. Res. 1, 2-11.

Seifikalhor, M., Aliniaeifard, S., Hassani, B., Niknam, V., Lastochkina, O., (2019). Diverse role of γ-aminobutyric acid in dynamic plant cell responses. Plant Cell Rep. 38, 847-867.

Shabala, S., Demidchik, V., Shabala, L., Cuin, T.A., Smith, S.J., Miller, A.J., Davies, J.M., Newman, I.A., (2006). Extracellular Ca^{2+} ameliorates NaCl-induced K^+ loss from Arabidopsis root and leaf cells by controlling plasma membrane K^+-permeable channels. Plant Physiol. 141, 1653-1665.

Shabala, L., Mackay, A., Tian, Y., Jacobsen, S.E., Zhou, D.W., Shabala, S., (2012). Oxidative stress protection and stomatal patterning as components of salinity tolerance mechanism in quinoa (*Chenopodium quinoa*), Physiol. Plant. 146, 26-38.

Shabala, L., Zhang, J., Pottosin, I., Bose, J., Zhu, M., Fuglsang, A.T., Buendia, A.V., Massart, A., Hill, C.B., Roessner, U., Bacic, A., Wu, H., Azzarello, E., Pandolfi, C., Zhou, M., Poschenrieder, C., Mancuso, S., Shabala S., (2016). Cell-type-specific H^+-ATPase activity in root tissues enables K^+ retention and mediates acclimation of barley (*Hordeum vulgare*) to salinity stress. Plant Physiol. 172, 2445-2458.

Shabala, S., (2013). Learning from halophytes: physiological basis and strategies to improve abiotic stress tolerance in crops. Ann. Bot. 112, 1209-1221.

Shabala, S., Cuin, T.A., Pottosin, I., (2007). Polyamines prevent NaCl-induced K^+ efflux from pea mesophyll by blocking nonselective cation channels. FEBS Lett. 581, 1993-1999.

Shabala, S., Mackay, A., (2011). Ion transport in halophytes. Adv. Bot. Res. 57, 151-199.

Shahid, M.A., Pervez, M.A., Balal, R.M., Abbas, T., Ayyub, C.M., Mattson, N.S., Riaz, A., Iqbal, Z., (2012). Screening of pea (*Pisum sativum* L.) genotypes for salt tolerance based on early growth stage attributes and leaf inorganic osmolytes. Aust. J. Crop Sci. 6, 1324-1331.

Shahid, S.A., Zaman, M., Heng, L., (2018). *Soil salinity: Historical perspectives and a world overview of the problem. In guideline for salinity assessment, mitigation and adaptation using nuclear and related techniques*. Eds: M. Zaman., S.A. Shahid., L. Heng., Springer, Cham, Switzerland, pp43-53.

Shahzad, R., Waqas, M., Khan, A.L., Hamayun, M., Kang, S.M., Lee, I.J., (2015). Foliar application of methyljasmonate induced physio-hormonal changes in *Pisum sativum* under diverse temperature regimes. Plant Physiol. Biochem. 96, 406-416.

Shaki, F., Maboud, H.E., Niknam, V., (2019). Effects of salicylic acid on hormonal cross talk, fatty acids profile, and ions homeostasis from salt-stressed safflower. J. Plant Interact. 14, 340-346.

Sharma, A., Kumar, V., Yuan, H., Kanwar, M.K., Bhardwaj, R., Thukral, A.K., Zheng, B., (2018). Jasmonic acid observed treatment stimulates insecticide detoxification in *Brassica juncea* L. Front. Plant Sci. 9, 1609.

Sharma, R., Wungrampha, S., Singh, V., Pareek, A., Sharma, M.K., (2016). Halophytes as bioenergy crops. Front. Plant Sci. 7, 1372.

Shi, L., Guo, M.M., Ye, N.H., Liu, Y.G., Liu, R., Xia, Y.J., Cui, S.X., Zhang, J.H., (2015). Reduced ABA accumulation in the root system is caused by ABA exudation in upland rice (*Oryza sativa* L. var. Gaoshan 1) and this enhanced drought adaptation. Plant Cell Physiol. 56, 951-964.

Shinozaki, K., Yamaguchi-Shinozaki, K., (1997). Gene expression and signal transduction in water-stress response. Plant Physiol. 115, 327-334.

Shrivastava, P., Kumar, R., (2015). Soil salinity: A serious environmental issueand plant growth promoting bacteria as oneof the tools for its alleviation. Saudi J. Biol. Sci. 22, 123-131.

Shu, S., Yuan, Y., Chen, J., Sun, J., Zhang, W., Tang, Y., Zhong, M., Guo, S., (2015). The role of putrescine in the regulation of proteins and fatty acids of thylakoid membranes under salt stress. Sci. Rep. 5, 14390.

Siddiqi, K.S., Husen, A., (2019). Plant response to jasmonates: current developments and their role in changing environment. Bull. Natl. Res. Cent. 43, 153.

Singha, K.T., Sreeharsha, R.V., Marriboina, S., Attipalli, R.R., (2019). Dynamics of metabolites and key regulatory proteins in the developing seeds of *Pongamia pinnata*, a potential biofuel tree species. Ind. Crops Prod. 140, 111621.

Skorupa, M., Gołębiewski, M., Kurnik, K., Niedojadło, J., Kęsy, J., Klamkowski, K., Wójcik, K., Treder, W., Tretyn, A., Tyburski, J., (2019). Salt stress vs. salt shock the case of carbohydrate beet and its halophytic ancestor. BMC Plant Biol. 19, 57.

Slama, I., Abdell, C., Bouchereau, A., Flowers, T., Savoure, A., (2015). Diversity, distribution and roles of osmoprotective compounds accumulated in halophytes under abiotic stress. Ann. Bot. 115, 433-447.

Soares, A.L.C., Geilfus, C.M., Carpentier, S.C., (2018). Genotype-specific growth and proteomic responses of maize toward salt stress. Front. Plant Sci. 9, 661.

Sofo, A., Scopa, A., Nuzzaci, M., Vitti, A., (2015). Ascorbate peroxidase and catalase cctivities and their genetic regulation in plants subjected to drought and salinity stresses. Int. J. Mol. Sci.16, 13561-13578.

Souid, I., Toumi, I., Hermosín-Gutiérrez, I., Nasri, S., Mliki, A., Ghorbel, A., (2019). The effect of salt stress on resveratrol and piceid accumulation in two *Vitis vinifera* L. Cultivars. Physiol. Mol. Biol. Plants 25, 625-635.

Spicher, L., Almeida, J., Gutbrod, K., Pipitone, R., Dörmann, P., Glauser, G., Rossi, M., Kessler, F., (2017). Essential role for phytol kinase and tocopherol in tolerance to combined light and temperature stress in tomato. J. Exp. Bot. 68, 5845-5856.

Spiess, G.M., Hausman, A., Yu, P., Cohen, J.D., Rampey, R.A., Zolman. K., (2014). Auxin input pathway disruptions are mitigated by changes in auxin biosynthetic gene expression in Arabidopsis. Plant Physiol. 165, 1092-1104.

Sreeharsha, R.V., Shalini, M., Singha, K.T., Attipalli, R.R., (2016). Unravelling molecular mechanisms from floral initiation to lipid biosynthesis in a promising biofuel tree species, *Pongamia pinnata* using transcriptome analysis. Sci. Rep. 6, 34315.

Stein, O., Granot, D., (2019). An overview of sucrose synthases in plants. Front. Plant Sci. 10, 95.

Sun, J., He, L., Li, T., (2019). Response of seedling growth and physiology *of Sorghum bicolor* (L.) Moench to saline-alkali stress. PLoS One 14, e0220340.

Taha, R., Mills, D., Heimer, Y., Tal, M., (2000). The relation between low K^+/Na^+ ratio and salt tolerance in the wild tomato species *Lycopersicon pennellii*. J. Plant Physiol. 157, 59-64.

Taher, M., Beyaz, R., Javani, M., Gürsoy, M., Yildiz, M., (2018). Morphological and biochemical changes in response to salinity in sunflower (*Helianthus annus* L.) cultivars. Ital. J. Agron. 13, 1096.

Taïbi, K., Taïbi, F., Abderrahim, L.A., Ennajah, A., Belkhodja, M., Mulet, J.M., (2016). Effect of salt stress on growth, chlorophyll content, lipid peroxidation and antioxidant defence systems in *Phaseolus vulgaris* L. S. Afr. J. Bot. 105, 306-312.

Tavallali, V., Karimi, S., (2019). Methyl jasmonate enhances salt tolerance of almond rootstocks by regulating endogenous phytohormones, antioxidant activity and gas exchange. J. Plant Physiol. 234-235, 98-105.

Thor, K., (2019). Calcium-nutrient and messenger. Front. Plant Sci. 10, 440.

Tognetti, V.B., Aken, O.V., Morreel, K., Vandenbroucke, K., van de Cotte, B., De Clercq, I., Chiwocha, S., Fenske, R., Prinsen, E., Boerjan, W., Genty, B., Stubbs, K.A., Inzé, D., Breusegem F.V., (2010). Perturbation of indole-3-butyric acid homeostasis by the UDP-glucosyltransferase UGT74E2 modulates Arabidopsis architecture and water stress tolerance. Plant Cell 22, 2660-2679.

Tran, D.Q., Konishi, A., Morokuma, M., Toyota, M., Agarie, S., (2020). NaCl-stimulated ATP synthesis in mitochondria of a halophyte *Mesembryanthemum crystallinum* L. Plant Prod. Sci. 23, 129-135.

Tryfona, T., Theys, T.E., Wagner, T., Stott, K., Keegstra, K., Dupree, P., (2014). Characterisation of FUT4 and FUT6a-(1R2)-fucosyltransferases reveals that absence of root arabinogalactan fucosylation increases Arabidopsis root growth salt sensitivity. PLoS One 9, e93291.

Tsai, C.J., Harding, S.A., Cooke, J.E.K., (2018). Branching out: a new era of investigating physiological processes in forest trees using genomic tools. Tree Physiol. 38, 303-310.

Tuteja, N., (2007). Abscisic acid and abiotic stress signaling. Plant Signal. Behav. 2, 135-138.

Uddin, M.R., Thwe, A.A., Kim, Y.B., Park, W.T., Chae, S.C., Park, S.U., (2013). Effects of jasmonates on sorgoleone accumulation and expression of genes for sorgoleone biosynthesis in sorghum roots. J. Chem. Ecol. 39, 712-722.

Ueda, J., Kato, J., (1982). Inhibition of cytokinin-induced plant growth by jasmonic acid and its methylester. Physiol. Plant. 54, 249-252.

Wang, F., Guo, Z., Li, H., Wang, M., Onac, E., Zhou, J., Xia, X., Shi, K., Yu, J., Zhou, Y., (2016). Phytochrome A and B function antagonistically to regulate cold tolerance via abscisic acid-dependent jasmonate signaling. Plant Physiol. 170, 459-471.

Wang, H., Hu, T., Huang, J., Lu, X., Huang, B., Zheng, Y., (2013). The expression of *Millettia pinnata* chalcone isomerase in *Saccharomyces cerevisiae* salt-sensitive mutants enhances salt-tolerance. Int. J. Mol. Sci. 14, 8775-8786.

Wang, J., Meng, Y., Li, B., Ma, X., Lai, Y., Si, E., Yang, K., Xu, X., Shang, X., Wang, H., Wang, D., (2015). Physiological and proteomic analyses of salt stress response in the halophyte *Halogeton glomeratus*. Plant Cell Environ. 38, 655-669.

Wang, L., Liu, X., Liang, M., Tan, F., Liang, W., Chen, Y., Lin, Y., Huang, L., Xing, J., Chen, W., (2014). Proteomic analysis of salt-responsive proteins in the leaves of mangrove *Kandelia candel* during short-term stress. PLoS One 9, e83141.

Wang, L., Mu, M., Li, X., Lin, P., Wang, W., (2011). Differentiation between true mangroves and mangrove associates based on leaf traits and salt contents. J. Plant Ecol. 4, 292-301.

Wang, W., Xu, L., You, S., Liu, C., Wang, M., (2020). Daily salinity fluctuation alleviates salt stress on seedlings of the mangrove *Bruguiera gymnorhiza*. Hydrol. Process. 34, 2466-2476.

Wang, X., Chang, L., Wang, B., Wang, D., Li, P., Wang, L., Yi, X., Huang, Q., Peng, M., Guo, A., (2013). Comparative proteomics of *Thellungiella halophila* leaves from plants subjected to salinity reveals the importance of chloroplastic starch and soluble sugarsin halophyte salt tolerance. Mol. Cell. Proteom. 12, 2174-2195.

Wang, X., Chen, X., Wang, Q., Chen, M., Liu, X., Gao, D., Li, D., Li, L., (2019). MdBZR1 and MdBZR1-2like transcription factors improves salt tolerance by regulating gibberellin biosynthesis in apple. Front. Plant Sci. 10, 1473.

Wang, Y.F., Munemasa, S., Nishimura, N., Ren, H.M., Robert, N., Han, M., Puzorjova, I., Kollist, H., Lee, S., Mori, I., Schroeder, J.I., (2013). Identification of cyclic GMP-activated nonselective Ca^{2+} permeable cation channels and associated CNGC5 and CNGC6 genes in Arabidopsis guard cells. Plant Physiol. 163, 578-590.

Wang, Z., Yu, Q., Shen, W., El-Mohtar, C.A., Zhao, X., Gmitter-Jr, F.G., (2018). Functional study of CHS gene family members in citrus revealed a novel CHS gene affecting the production of flavonoids. BMC Plant Biol. 18, 189.

Wang, Z.Q., Xu, X.Y., Gong, Q.Q., Xie, C., Fan, W., Yang, J.L., Lin, Q.S., Zheng, S.J., (2014). Root proteome of rice studied by iTRAQ provides integrated insight into aluminum stress tolerance mechanisms in plants. J. Proteomics 98, 189-205.

Wei, P., Wang, L., Liu, A., Yu, B., Lam, H.M., (2016). *GmCLC1* confers enhanced salt tolerance through regulating chloride accumulation in soybean. Front. Plant Sci. 25, 1082.

Wu, H., Shabala, L., Azzarello, E., Huang, Y., Jones, C., Su, N., Wu, Q., Cai, S., Bazihizina, N., Wang, L., Zhou, M., Mancuso, S., Chen, Z., Shabala, S., (2018). Na^+ extrusion from the cytosol and tissue-specific Na^+ sequestration in roots confer differential salt stress tolerance between durum and bread wheat. J. Exp. Bot. 69, 3987-4001.

Wu, X., He, J., Chen, J., Yang, S., Zha, D., (2014). Alleviation of exogenous 6-benzyladenine on two genotypes of eggplant (*Solanum melongena* Mill.) growth under salt stress. Protoplasma 251, 169-176.

Wu, X., Zhang, S., Liu, X., Shang, J., Zhang, A., Zhu, Z., Zha, D., (2020). Chalcone synthase (CHS) family members analysis from eggplant (*Solanummelongena* L.) in the flavonoid biosynthetic pathway and expression patterns in response to heat stress. PLoS One 15, e0226537.

Xie, X., He, Z., Chen, N., Tang, Z., Wang, Q., Cai, Y., (2019). The roles of environmental factors in regulation of oxidative stress in plant. BioMed. Res. Int. 2019, 9732325.

Xiong, J., Sun, Y., Yang, Q., Tian, H., Zhang, H., Liu, Y., Chen, M., (2017). Proteomic analysis of early salt stress responsive proteins in alfalfa roots and shoots. Proteome Sci. 15, 19.

Xu, L., Zhao, H., Ruan, W., Deng, M., Wang, F., Peng, J., Luo, J., Chen, Z., Yi, K., (2017). ABNORMAL INFLORESCENCE MERISTEM1 functions in salicylic acid biosynthesis to maintain proper reactive oxygen species levels for root meristem activity in rice. Plant Cell 29, 560-574.

Xu, W., Lv, H., Zhao, M., Li, Y., Qi, Y., Peng, Z., Xia, G., Wang, M., (2016). Proteomic comparison reveals the contribution of chloroplast to salt tolerance of a wheat introgression line. Sci. Rep. 6, 32384.

Yamamoto, A., Shim, I.S., Fujihara, S., (2017). Inhibition of putrescine biosynthesis enhanced salt stress sensitivity and decreased spermidine content in rice seedlings. Biol. Plant. 61, 385-388.

Yang, C.Y., Liang, Y.B., Qiu, D.W., Zeng, H.M., Yuan, J.J., Yang, X.F., (2018). Lignin metabolism involves Botrytis cinerea BcG1-induced defense response in tomato. BMC Plant Biol. 18, 103.

Yang, J., Ding, C., Xu, B., Chen, C., Narsai, R., Whelan, J., Hu, Z., Zhang, M., (2015). A casparian strip domain-like gene, CASPL, negatively alters growth and cold tolerance. Sci. Rep. 5, 14299.

Yang, J., Xie, X., Yang, M., Dixon, R., Wang, Y.P., (2017). Modular electron-transport chains from eukaryotic organelles function to support nitrogenase activity. Proc. Natl. Acad. Sci. USA 114, E2460-E2465.

Yang, T., Lv, R., Li, J., Lin, H., Xi, D., (2018). Phytochrome A and B negatively regulate salt stress tolerance of Nicotiana tobacum via ABA-jasmonic acid synergistic cross-talk. Plant Cell Physiol. 59, 2381-2393.

Yang, Y., Qi, M., Me, C., (2004). Endogenous salicylic acid protects rice plants from oxidative damage caused by aging as well as biotic and abiotic stress. Plant J. 40, 909-919.

Yang, Y., Guo, Y., (2018). Elucidating the molecular mechanisms mediating plant salt-stress responses. New Phytol. 217, 523-539.

Yao, Y., Zhang, X., Wang, N., Cui, Y., Zhang, L., Fan, S., (2020). Transcriptome analysis of salt stress response in halophyte *Atriplex centralasiatica* leaves. Acta Physiol. Plant. 42, 3.

Yong, H.Y., Zou, Z., Kok, E.P., Kwan, B.H., Chow, K., Nasu, S., Nanzyo, M., Kitashiba, H., Nishio, T., (2014). Comparative transcriptome analysis of leaves and roots in response to sudden increase in salinity in Brassica napus by RNA-seq. Biomed. Res. Int. 467395.

Younesi-Melerdi, E., Nematzadeh, G.A., Pakdin-parizi, A., Bakhtiarizadeh M.R., Motahari, S.A., (2020). De *novo* RNA sequencing analysis of *Aeluropus littoralis* halophyte plant under salinity stress. Sci. Rep. 10, 9148.

Yuan, F., Guo, J., Shabala, S., Wang, B., (2019). Reproductive physiology of halophytes: Current standing. Front. Plant Sci. 9, 1954.

Yuenyong, W., Sirikantaramas, S., Qu, L.J., Buaboocha, T., (2019). Isocitrate lyase plays important roles in plant salt tolerance. BMC Plant Biol. 19, 472.

Zelm, E.V., Zhang, Y., Testerink, C., (2020). Salt tolerance mechanisms of plants. Ann. Rev. Plant Biol. 71, 24.1-24.31.

Zeng, H., Xu, L., Singh, A., Wang, H., Du, L., Poovaiah, B.W., (2015). Involvement of calmodulin and calmodulin-like proteins in plant responses to abiotic stresses. Front. Plant Sci. 6, 600.

Zhang, H., Zhang, Z., Li, S., Huang, R., (2018). Improvement of salt tolerance using wild rice genes. Front. Plant Sci. 8, 2269.

Zhang, H., Zhao, X., Sun, Q., Yan, C., Wang, J., Yuan, C., Li, C., Shan, S., Liu, F., (2020). Comparative transcriptome analysis reveals molecular defensive mechanism of *Arachis hypogaea* in response to salt stress. Int. J. Genomics 2020, 13.

Zhang, J., Zhang, Y., Du, Y., Chen, S., Tang, H., (2011). Dynamic metabonomic responses of tobacco (*Nicotiana tabacum*) plants to salt stress. J. Proteome Res. 10, 1904-1914.

Zhang, M., Cao, Y., Wang, Z., Wang, Z.Q., Shi, J., Liang, X., Song, W., Chen, Q., Lai, J., Jiang, C., (2018). A retrotransposon in an HKT1 family sodium transporter causes variation of leaf Na^+ exclusion and salt tolerance in maize. New Phytol. 217, 1161-1176.

Zhang, X., Yao, Y., Li, X., Zhang, L., Fan, S., (2020). Transcriptomic analysis identifies novel genes and pathways for salt stress responses in *Suaeda salsa* leaves. Sci. Rep. 10, 4236.

Zhang, Z., Mao, C., Shi, Z., Kou, X., (2017). The amino acid metabolic and carbohydrate metabolic pathway play important roles during salt-stress response in tomato. Front. Plant Sci. 8, 1231.

Zhao, C., Zayed, O., Zeng, F., Liu, C., Zhang, L., Zhu, P., Hsu, C.C., Tuncil, Y.E., Tao, W.A., Carpita, N.C., Zhu, J.K., (2019). Arabinose biosynthesis is critical for salt stress tolerance in Arabidopsis. New Phytol. 224, 274-290.

Zhao, Q., Tobimatsu, Y., Zhou, R., Pattathil, S., Gallego-Giraldo, L., Fu, C., Jackson, L.A., Hahn, M.G., Kim, H., Chen, F., Ralph, J., Dixon, R.A., (2013). Loss of function of cinnamyl alcohol dehydrogenase 1 leads to unconventional lignin and a temperature-sensitive growth defect in *Medicago truncatula*. Proc. Natl. Acad. Sci. USA 110, 13660-13665.

Zhou, J., Zhang, Z., Zhang, Y., Wei, Y., Jiang, Z., (2018). Effects of lead stress on the growth, physiology, and cellular structure of privet seedlings. PLoS One 13, e0191139.

Zhu, J., Fan, Y., Shabala, S., Li, C., Lv, C., Guo, B., Xu, R., Zhou, M., (2020). Understanding mechanisms of salinity tolerance in barley by proteomic and biochemical analysis of near-isogenic lines. Int. J. Mol. Sci. 21, 1516.

Zörb, C., Geilfus, C.M., Dietz, K.J., (2018). Salinity and crop yield. Plant Biol. 21, 31-38.

Plant Science 258 (2017) 102–111

Contents lists available at ScienceDirect

Plant Science

journal homepage: www.elsevier.com/locate/plantsci

Physiological and molecular insights into the high salinity tolerance of *Pongamia pinnata* (L.) pierre, a potential biofuel tree species

Sureshbabu Marriboina, Debashree Sengupta, Sumit Kumar, Attipalli R. Reddy*

Photosynthesis and Stress Biology Laboratory, Department of Plant Sciences, University of Hyderabad, Hyderabad 500046, India

ARTICLE INFO

Article history:
Received 7 November 2016
Received in revised form 15 February 2017
Accepted 21 February 2017
Available online 24 February 2017

Keywords:
Na^+ localization
Photosynthetic performance
Pongamia pinnata
Roots
Salt tolerance
SOS pathway

ABSTRACT

Soil salinity is gradually becoming a threat to the global economy by affecting agricultural productivity worldwide. Here, we analyze the salinity tolerance of *Pongamia pinnata* with an insight into the underlying physiological and molecular responses. Despite a reduction in net photosynthetic rate, *P. pinnata* efficiently maintained its leaf water potentials even at 500 mM NaCl for 15 days and displayed no visible stress symptoms. Na^+ localization analysis using CoroNa-Green AM revealed effective Na^+ sequestration in the roots when compared to leaves. Elemental analysis demonstrated that roots accumulated more of Na^+ while K^+ content was higher in leaves. At the molecular level, salt stress significantly induced the expression levels of salt overly sensitive1 (SOS1), SOS2, SOS3, high affinity K^+ transporter (HKT1), ABA biosynthetic and receptor genes (NCED and PYL4), guaiacol peroxidase (POD) exclusively in roots while tonoplast localized Na^+/H^+ exchanger (NHX1) was significantly enhanced in leaves. Our results clearly demonstrate that leaves and roots of *Pongamia* exhibit differential responses under salt stress although roots are more efficient in sequestering the Na^+ ions. The present study provides crucial inputs for understanding salt tolerance in a tree species which can be further utilized for developing salt tolerance in higher plants.

1. Introduction

Continuous salinization of arable lands at an annual rate of 10% forecasts the possibility of approximately 50% of the total cultivated land area to be salinized by the year 2050 worldwide [1]. Thus, demands for initiating cultivation of economically important tree species in salinized lands, which are otherwise unfit for agricultural productivity is increasing in many parts of the world, as a potential alternative for optimum economic sustainability [2]. A recent review on salt tolerance ability of trees discussed the wide variations in salinity tolerance among tree species which can thrive at soil salinities ranging from 200 to 450 mM [3]. Despite having considerable reports on salt tolerance of trees, the underlying genetic, physiological and molecular basis for the trait is still superficial and limited mostly to poplars [4–6] and mangroves [7].

In general, salinity affects plant growth and development by decreasing the water potential of the soil leading to reduced water uptake by roots. Thus, both salinity and drought stress induces a set of common responses in plants owing to the osmotic stress signal [8]. However, in addition to osmotic changes salinity leads to uptake of Na^+ and Cl^- ions along with water. Thus, long term salinity and/or absence of efficient extrusion/sequestering mechanisms in plants result in accumulation of high concentrations of Na^+ and Cl^- in the cytosol causing ion homeostasis imbalance at cellular level. Salinity-induced decline in photosynthetic rates due to stomatal closure is an adaptive response [9]. However, excessive accumulation of Na^+ ions within photosynthetic tissues leads to toxicity and damage to the photosynthetic machinery which is detrimental to the plant. Thus in order to survive, plants need to limit Na^+ transport into the shoot tissue by compartmentalizing the Na^+ into the root stele and vacuoles [10–12].

In order to withstand the Na^+ toxicity, salt-tolerant plant species develop certain morphological, physiological and biochemical mechanisms which include initiation of lateral roots, ion compartmentalization, biosynthesis of osmo-protectants and activation of salt exclusion and/or sequestering pathways [13]. Before

Abbreviations: A_{sat}, light saturated net photosynthetic rate; C_T, cycle threshold; E, transpiration rate; FESEM-EDX, field emission scanning electron microscopy coupled with energy dispersive X-ray spectroscopy; F_v/F_m, maximum quantum yield of photo system II; g_s, stomatal conductance to water vapour; HKT1, high affinity K^+ transporter1; NCED, 9-cis epoxycarotenoid dioxygenase; NHX1, tonoplast localized sodium/proton exchanger1; PAR, photosynthetically active radiation; POD, peroxidase; PYL4, PYR1-like 4; ROS, reactive oxygen species; RWC, relative water content; SOS, salt overly sensitive; SP, saturation pulse; TOIL, tree oil India ltd; WUE, water use efficiency.

* Corresponding author.
E-mail address: attipalli.reddy@gmail.com (A.R. Reddy).

http://dx.doi.org/10.1016/j.plantsci.2017.02.008
0168-9452/

responding to salinity stress, plants need to first perceive the stress signal and then transfer it through a series of signaling components to the final response *i.e.* expression of salt-responsive genes. The phytohormone abscisic acid (ABA) is a well known cellular signal for mediating the expressions of salt and drought responsive genes and reported to be induced rapidly in roots [14]. Further, antioxidative defense system has been reported to play a key role in some members of both C3 and C4 plants, to neutralize the effect of stress-induced toxic levels of reactive oxygen species (ROS). As ROS production is a continuous process, most of the antioxidative enzymes are constitutively expressed. Salt stress is known to induce expressions of certain key enzymes including guaiacol peroxidase (POD), glutathione reductase (GR) and ascorbate peroxidase (APX) which are considered as fine regulators of ROS and are required to maintain the ROS levels within physiological levels [15]. Apart from these, the most important mechanism for salt-tolerance in plants is through the salt overly sensitive (SOS) pathway, wherein following salt stress perception by a salinity receptor (unknown), Ca^{2+} spikes (enhanced Ca^{2+} levels) gets generated within the cytoplasm acting as secondary signals for activating the SOS pathway components. Increase in cytosolic Ca^{2+} is perceived by SOS3 (a myristoylated calcium-binding protein) which gets activated and in turn binds and activate the serine/threonine protein kinase SOS2. Following SOS2 activation it goes and activate SOS1 through phosphorylation (a plasma membrane localized Na^+/H^+ antiporter) which brings about the extrusion of excess Na^+ ions from the cytosol to the apoplast [16,17].

Most of the available information regarding salt tolerance mechanisms at physiological and molecular levels is limited to crops while only few reports are available for trees [6,3]. At present, mangroves are the only known plant community that can tolerate up to 500 mM NaCl, which is equivalent to seawater salt levels [18,19]. Ironically, in spite of being an excellent model for understanding high salinity tolerance in trees, mangroves are unsuitable for cultivation in salinized terrestrial lands [2] and hence identification of new tree species having high economic potential and salinity endurance as well as understanding the physiological and molecular responses in tree species is highly crucial. On the other hand, due to the dwindling fossil fuel resources, a parallel strong demand has arisen for identification of certain tree species acting as potential sources for high quality biofuel production [20]. This demand has recently led to the unravelling of a fast-growing leguminous tree *Pongamia pinnata* (Linn.) Pierre (Synonym: *Millettia pinnata*), indigenous to India and Southeast Asia, whose non-edible seed oil was recognized worldwide as a potential feedstock for biodiesel production [21,22]. Biodiesel production was reported from *Pongamia* seed oil through the consecutive acid and base-catalyzed dual step transesterification method [23]. Apart from the seed oil, all other parts of the plant have also been implemented as crude drugs in Indian traditional medicine as well as for application as animal fodder and timber [22].

Fortunately, *P. pinnata* was found to display semi-mangrove characteristics, capable of operating both glycophytic and halophytic mechanisms, preferentially, for adaptation to salinity [24]. Unlike mangroves, *Pongamia* does not exhibit physiological and anatomical adaptations to exclude Na^+ in order to endure salinity stress [25]. Previous studies have shown partial salinity tolerance in *Pongamia* [26–28]. More recently, Huang et al. [29] used salt-responsive transcriptome to demonstrate that *Pongamia* can overcome salt stress within 8 h after treatment. On the other hand, another report by Arpiwi et al. [30] showed that some varieties of *P. pinnata*, collected from Kununurra, Western Australia and some parts of India did not tolerate salinity stress beyond 250 mM. However, an integrated knowledge regarding the physiological and molecular responses of *P. pinnata* under salt stress is still at its incipient stage and needs proper characterization. However, a comprehensive analysis on the leaf and root responses as well as Na^+ localization patterns under different salt concentrations at both physiological and molecular level is not yet elucidated.

In the present study, we aim to analyze the salt tolerance of one month old *P. pinnata* plants under two different salt concentrations (300 and 500 mM NaCl) by targeting the underlying physiological and molecular responses in both leaves and roots. Nevertheless, the high tolerance of *P. pinnata* to soil salinity makes it an ideal target for cultivation in the marginal or degraded lands which are otherwise not suitable for food production.

2. Materials and methods

2.1. Plant material and experimental condition

Seeds of *P. pinnata* accession TOIL12 were obtained from Tree Oils India Limited (TOIL), Zaheerabad, Telangana, India. The experimental plants were grown under greenhouse conditions at the University of Hyderabad (Hyderabad, Telangana, India). Oven dried seeds (40 °C overnight) were initially germinated in trays containing soilrite (mixture of expanded perlite, Irish Peat moss and exfoliated vermiculite in 1/3:1/3:1/3 w/w) under controlled temperature of 23 °C for 2 weeks. Later, healthy and uniform seedlings were selected and transplanted one each in 20-L capacity pots filled with mixture of soil and sand (3:1w/w) to be grown under greenhouse conditions (temperature 25 ± 1 °C, relative humidity 60–70%, and natural photoperiod). The pot water holding capacity (PC) was measured according to Ennahli and Earl [31] before performing any experiment. The PC was found to be approximately 1L. Plants were allowed to grow under regular and optimum watering condition till the production of four mature tripartite leaves (30 days). After 30 days, plants were randomly selected and divided into two groups: well-watered (WW) and salinity-stressed (SS). WW plants were regularly maintained at 100% PC (as control) for 15 days, whereas SS plants were further subjected to two different salinity treatments: 300 mM (moderate salinity) and 500 mM NaCl (sea water equivalent) for 15 days. Each treatment group comprised 9 plants. Salt treatment was given according to Mudalkar et al. [32], with small modifications. Each individual plant was watered with 1L of 300 mM and 500 mM NaCl solution separately to each respective treatment pot ensuring that soil in the pot was completely moist with salt water. Control plants were treated with the same amount of distilled water. The treatment was repeated at an interval of 7 days and samples were collected 15 days after the first NaCl application.

2.2. Photosynthetic leaf gas exchange measurements

Leaf gas exchange measurements were performed by using a portable infra-red gas analyzer (IRGA, LCpro-32070, ADC Bioscientific Ltd., UK). All measurements were performed on fully expanded 2nd and 3rd leaves of the plant. Throughout the measurement, the following conditions were maintained: a saturating photosynthetically active radiation (PAR) of 1600 $\mu mol\ m^{-2}\ s^{-1}$ supplied by a LED light source (LCpro Lamp 32070–Broad, ADC Bioscientific Ltd., UK) attached to leaf chamber, air temperature of 25–26 °C and relative humidity of 55–60%. Light saturated net photosynthetic rate (A_{sat}), stomatal conductance (g_s), and transpiration rate (E) were measured in leaves of control and treated plants during 10.00–11.00 h. Leaf water use efficiency (WUE) was calculated as A_{sat}/E.

2.3. Measurement of photosystem-II (PSII) efficiency

To determine changes in maximum quantum yield (F_v/F_m), Chl *a* fluorescence measurements were performed by using a portable

Handy PEA (Plant Efficiency Analyzer-2126) fluorometer (Hansatech Instruments Ltd., Kings Lynn Norfolk, UK) on the same leaves used for photosynthetic leaf gas exchange measurements. Fully expanded third leaves of control and treated plants were dark-adapted for 30 min using leaf-clips and the fluorescence intensities were recorded after illuminating with a saturating light intensity of 3000 $\mu mol\ m^{-2}\ s^{-1}$ (an excitation intensity sufficient to ensure closure of all PSII reaction centers), of 650 nm peak wave length provided by an array of three light emitting diodes, for 1 s. Data presented are average of three independent replicates.

2.4. Leaf relative water status

Fully expanded third leaves of control and treated plants were collected, immediately weighed and recorded as fresh weight (fw). The leaf samples were rehydrated by immersing in distilled water in plastic trays sealed with plastic bag for 24 h at 4 °C in dark and then weighed after removing the moisture superficially on leaf surface with blotting paper (turgid weight, tw). After turgid weight measurement, the samples were oven-dried at 60 °C for 72 h and weighed (dry weight, dw). The leaf relative water content (LRWC) was calculated using the following formula: $100 \times [(fw - dw)/(tw - dw)]$ [33].

2.5. Electrolyte leakage assays

Fresh leaves of control and treated plants were harvested and uniform leaf discs of 1 cm diameter were punched out. Equal quantity (100 mg) of leaf disc samples were taken and immersed into 20 ml of deionized water taken in a falcon tube and kept for shaking in a rotary shaker at room temperature for 2 h. The initial electrical conductivity (C_1) of the solution was recorded using a conductivity meter (Digisun Electronics, Hyderabad, India). Further, the leaf discs were boiled in deionized water at 100 °C for 20 min in order to facilitate complete release of electrolytes from the tissue followed by cooling the samples to room temperature. Then the final electrical conductivity (C_2) of the solution was measured and the percentage of electrolyte leakage was calculated according to the formula: $(C_1/C_2) \times 100$ [34].

2.6. Chlorophyll measurements

Fresh leaves from control and salt-treated plants were collected, washed in distilled water and homogenized with 80% (v/v) ice cold acetone solution. Chlorophyll content was measured according to Arnon [35].

2.7. Visualization of Na^+ ions through confocal laser scanning microscopy

Leaves and roots harvested from control and treated plants were used for Na^+ ions visualization using a Na^+ specific probe CoroNa-Green AM in a laser scanning confocal microscopy (Leica TCS SP2 with AOBS, Heidelberg, GmbH, Germany). All measurements were performed as described by Oh et al. [36] with some minor modifications. Roots and leaves were incubated in 2.5% glutaraldehyde fixative solution overnight at room temperature. Thin free-hand sections of leaves and roots were stained with 20 μM CoroNa-Green AM (Invitrogen) in the presence of a final concentration of 0.02% (w/v) pluronic acid (Invitrogen) for 3 h. The sections were further incubated with 2.5 μM propidium iodide (Invitrogen) for ~10–20 min before visualization under microscope.

2.8. Quantification of Na^+ and K^+ ions

The measurement of Na^+ and K^+ contents in both roots and leaves of control and treated plants was performed through flame photometer. The leaves and roots from both control and treated plants were harvested, washed with deionized water and oven-dried at 60 °C for 72 h. The dried leaves and roots were powdered for further analysis. Powdered leaves and roots from control and treated plants (0.1 g each) were then extracted with 10 ml of tri acid mixture (TAM) (which is a mixture of nitric acid, sulfuric acid and perchloric acid in the ratio of 10:5:4) for 60 min at 95 °C. The resulting solution diluted appropriately, and analyzed for Na^+ and K^+ concentrations with a flame photometer (Khera-391, Khera Instruments, New Delhi, India) in emission mode (Na – 589 nm, K – 766 nm) against a standard curve of 0–400 $mg\ ml^{-1}$ concentration range for both ions [37].

2.9. Field emission scanning electron microscopy-Energy dispersive X-ray spectroscopy (FESEM-EDX) analysis

FESEM-EDX was used on dehydrated sections of leaves and roots harvested from 4 week-old soil grown plants for the measurement of Na^+ and K^+ ions. The tissue sections were incubated in 2.5% glutaraldehyde solution for overnight at room temperature and then dehydrated with gradient solutions of ethanol (30%, 50%, 70%, 90% and 100%) for 15 min [36]. The dried sections were mounted on copper stubs using double stick cellophane tape and the mounted samples were coated with gold in a sputter coater for 2 min prior to visualization under scanning electron microscope (Carl-Zeiss MERLIN Compact, S. No. 6027, Germany). Samples were analyzed with an ATW detector interfaced with a link ISIS analyzer (Oxford Instruments) under the following conditions: accelerating voltage, 15 kV; working distance between sample and detector, 9.9 mm; X-ray exposure time, 60 s.

2.10. Quantitative RT-PCR analysis

Indirect primers were designed for four of the targeted genes (*SOS1, SOS2, SOS3* and *HKT1*) based on the available gene sequences of *Glycine max* from SoyKB (www.soykb.org) database since the transcriptome as well as plastome sequence analysis indicated that *P. pinnata* is closely related to *G. max* [38,39], while direct primers were used for the genes NCED, PYL, NHX1 and POD based on the salt-responsive *P. pinnata* transcriptome sequence given by Huang et al. [29] to amplify approx. 200 bp products for qPCR analysis (details of primers given in Supplementary Table S1). All genes were PCR amplified using *P. pinnata* cDNA, the products were gel purified and the amplicons obtained via the indirect *G. max* primers were sequenced for confirming the identity of the amplified target gene from *P. pinnata*. Quantitative PCR analysis was performed using KAPA SYBR FAST [Mastermix (2×) Universal; KAPA Biosystems] real-time PCR kit following the manufacturer's instructions in an Eppendorf Realplex MasterCycler (Eppendorf, Germany). For the relative quantification, equal quantities (500 ng) of total RNA extracted from control and salt-treated *Pongamia* leaf and root tissues using Sigma Spectrum™ Plant Total RNA kit (Sigma, USA) and were used for preparing cDNA using Reverse Aid cDNA synthesis kit (ThermoScientific). Target genes were amplified using the following program: 1 cycle at 95 °C for 2 min, followed by 40 cycles of 30 s at 95 °C for template denaturation, 30 s at 60 °C and 20 s at 72 °C, followed by the dissociation (melting) curve. Fluorescence was detected using the Realplex software (Eppendorf, Germany). Each reaction was carried out in triplicate with 50 ng of cDNA as template. Templates (cDNAs) were used from three biological replicate, wherein for each biological replicate cDNAs from 3 individual plants were pooled up. The relative fold difference was determined

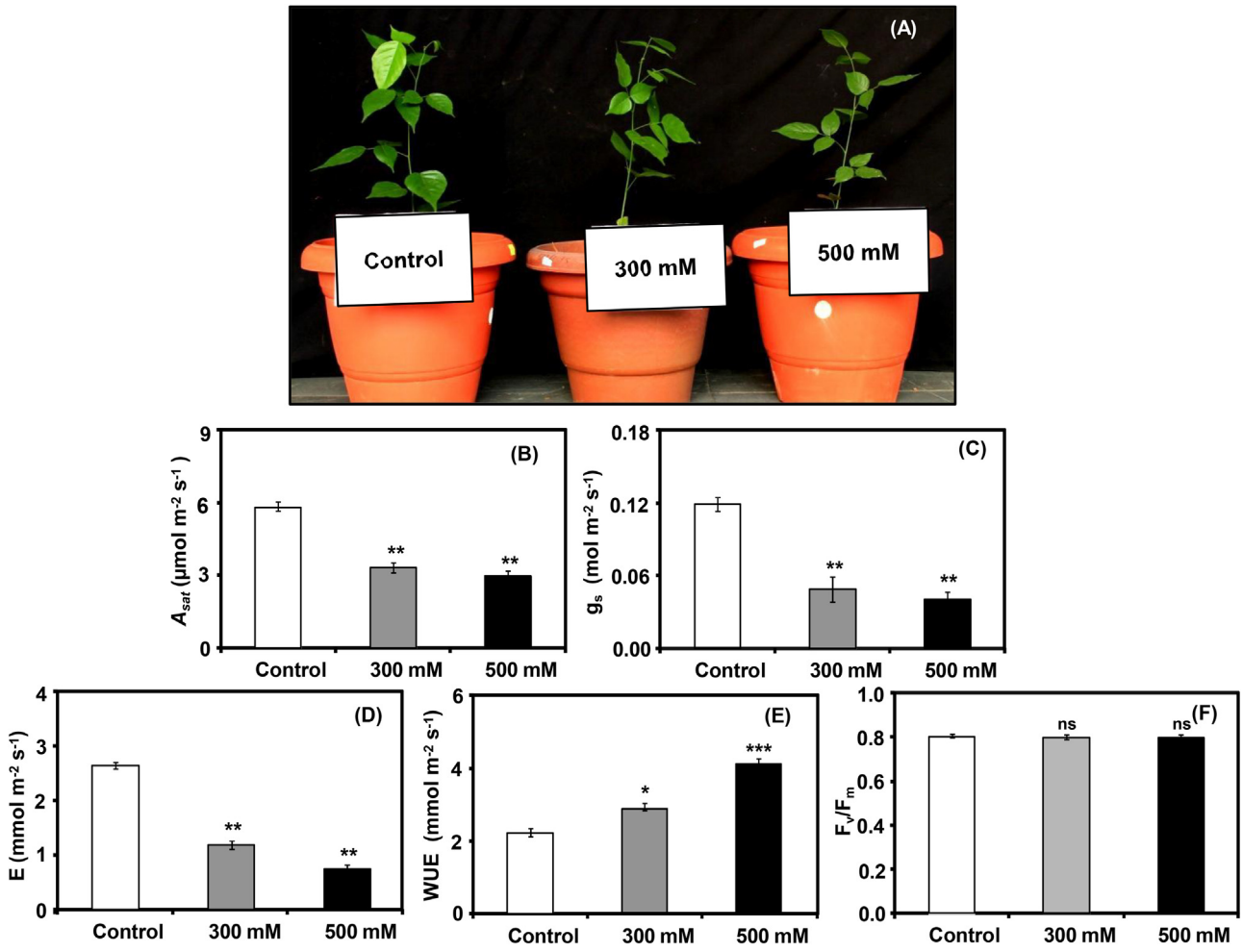

Fig. 1. Effect of salinity stress on plant morphology and photosynthetic performance of *Pongamia pinnata*. (A) Shoot morphology of 1 month old soil-grown *P. pinnata* plants after 15 days treatment with 0 (Control), 300 and 500 mM NaCl. (B) Variations in light saturated net photosynthetic rate (A_{sat}) (µmol m^{-2} s^{-1}), (C) stomatal conductance (g_s) (mol m^{-2} s^{-1}), (D) transpiration rate (E) (mmol m^{-2} s^{-1}), (E) water use efficiency (WUE) (mmol m^{-2} s^{-1}) and maximum quantum yield of PSII (F_v/F_m) (F), in *P. pinnata* grown under control and salt treatment. Error bars represent the mean ± SD (n = 4).

using the $2^{-\Delta\Delta C}{}_T$ formula [40]. We checked the efficiency of the target and reference as per the Applied Biosystems User Bulletin No. 2 (P/N 4303859) to ensure that both the genes amplify with approximately equal efficiency. The 18SrRNA was used as the reference gene after confirming its stability under salt stress.

2.11. Statistical analysis

All physiological and biochemical parameters were represented as mean ± SD (n = 3). Three individual plants were taken for each treatment under each biological replicate and the final results represents the data obtained from 3 biological replicates. The significance of the differences between mean values of control and salinity-treated plants was determined using Student's *t* test. For qPCR analysis, three independent RNA samples were used for each sample, and each reaction was run in triplicate for both control and salinity stressed samples of each time point.

3. Results

3.1. Comparative morphology and photosynthetic performance of *P. pinnata*

To identify the level of salt-tolerance in the biofuel tree *P. pinnata*, 1 month old plants were subjected to 300 and 500 mM NaCl treatment continuously for 15 days. Salt-treated *P. pinnata* seedlings displayed no stress-induced symptoms till 15 days treatment (Fig. 1A). The leaves of treated seedlings were healthy and green similar to leaves of control plants. This was corroborated by our findings on relative water content (RWC) of leaves, electrolyte leakage as well as leaf chlorophyll and carotenoid contents which did not show any significant variations in both 300 and 500 mM NaCl treated plants (Table 1).

Photosynthesis being the major biochemical process getting affected under stress conditions, we measured A_{sat}, E, g_s and WUE of control and salt-treated seedlings of *P. pinnata*. Significant variations were recorded for gas exchange characteristics of *Pongamia* grown in salinity conditions. The A_{sat} of both 300 and 500 mM NaCl treated *Pongamia* plants significantly declined by ~50% in comparison to control plants and was recorded to be ~3 µmolm^{-2} s^{-1} while it was ~6 µmolm^{-2} s^{-1} for control plants after 15 days of growth ($p < 0.01$; Fig. 1B). Similarly, significant reduction of ~58% (300 mM) and ~67% (500 mM) was observed in gs and ~67% (both 300 and 500 mM) in E, respectively for treated plants in comparison to control plants ($p < 0.01$; Fig. 1C and D). Transpiration rate is inversely proportional to WUE and in the present study also, with a gradual decline in E under salt stress, the corresponding WUE showed significant increase of ~27% (300 mM; $p < 0.05$) and ~82% (500 mM; $p < 0.001$) respectively, in comparison to control plants (Fig. 1E). We also analyzed the PSII efficiency in salt-treated *P. pinnata* through

Table 1
Modulations in leaf relative water content (RWC), electrolyte leakage, chlorophyll and carotenoid contents in 1 month old *P. pinnata* leaves after 15 days salt treatment. Values represent mean ± standard deviations (n = 3).

Parameters	Control	300 mM NaCl	500 mM NaCl
RWC (%)	85.55 ± 2.80(ns)	90.34 ± 3.90(ns)	94.98 ± 2.10(ns)
Electrolyte leakage (%)	71.27 ± 0.73(ns)	73.73 ± 0.19(ns)	74.21 ± 1.14(ns)
Chl *a* (mg g^{-1} FW)	2.55 ± 0.01(ns)	2.54 ± 0.02(ns)	2.55 ± 0.01(ns)
Chl *b* (mg g^{-1} FW)	1.05 ± 0.05(ns)	1.05 ± 0.04(ns)	1.08 ± 0.02(ns)
Chl *a*/*b* (mg g^{-1} FW)	2.39 ± 0.04(ns)	2.41 ± 0.04(ns)	2.34 ± 0.02(ns)
Total Chl (mg g^{-1} FW)	3.95 ± 0.05(ns)	3.94 ± 0.06(ns)	4.00 ± 0.03(ns)
Total carotenoids (mg g^{-1} FW)	0.68 ± 0.02(ns)	0.69 ± 0.03(ns)	0.69 ± 0.02(ns)

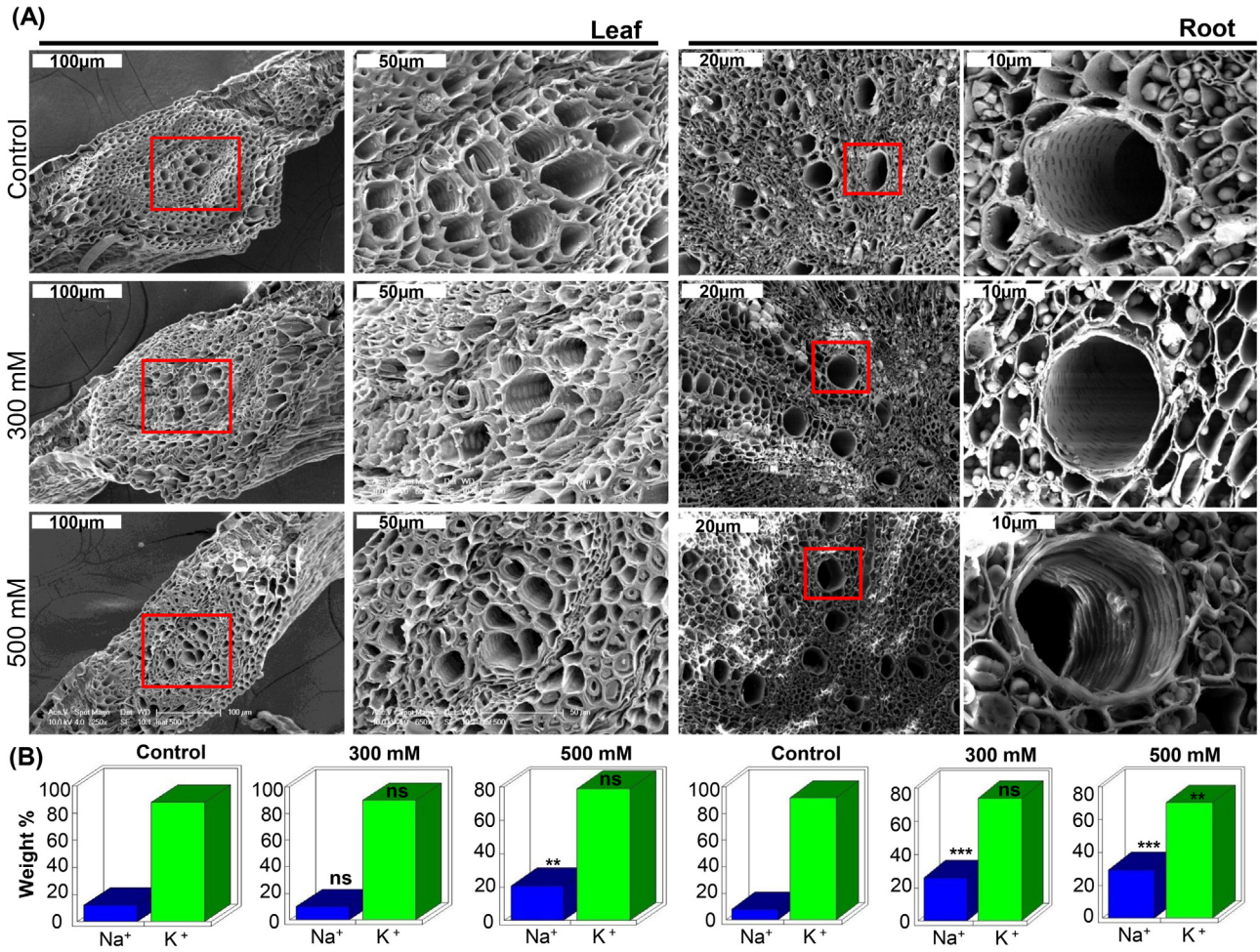

Fig. 2. FESEM-EDX analysis for tissue integrity and ion measurement in leaves and roots of salt-treated *P. pinnata*. (A) Cross section of leaves of control, (C) 300 mM NaCl and (E) 500 mM NaCl treated *P. pinnata* and (B, D, F) magnified view of the vascular bundle region enclosed in red border where ion measurements were performed in all three treatments. Similarly, (G) cross section of roots of control, (I) 300 mM NaCl and (K) 500 mM NaCl treated *P. pinnata* and (H, J and L) magnified view of the vascular bundle region enclosed in red border where ion measurements were performed in all three treatments. Graphical representation and comparison of Na^+ and K^+ contents from both leaves (M) and roots (N). Samples from both control and treated processed simultaneously and ion measurements were performed on four to six cells from each tissue. Values are represented as percentage of relative weight. The white bar in each micrograph represents the scale of measurement. (For interpretation of the references to colour in this figure legend, the reader is referred to the web version of this article.)

Handy PEA fluorometer. Our results demonstrated that the maximum quantum yield of PSII (F_v/F_m) of treated plants remained similar to that of controls even after 15 days of treatment and was recorded to be ~0.8 (Fig. 1F).

3.2. Anatomical variations and Na^+ and K^+ content in leaves and roots of salt treated P. pinnata

At the anatomical level, FESEM-EDX analysis revealed that the cellular integrity of both leaves (Fig. 2A–F) and roots (Fig. 2G–L) of 300 and 500 mM NaCl treated plants remained similar to that of the controls. The vascular bundles in both leaves and roots of the treated plants did not shrivel and were similar to the vascular bundles of the control plants. There were no significant variations in K^+ content in the vascular bundles of leaves of treated plants in comparison to control plants as demonstrated by EDX analysis (Fig. 2M). However, the K^+ content in roots decreased significantly in 300 and 500 mM treated plants by ~19% and ~23% respectively, when compared to control plants ($p < 0.05$; Fig. 2N). Interestingly, we recorded a significant variation in accumulation pattern of Na^+ with increasing salt concentrations in both leaves and roots of treated plants. There was a non-significant decrease of ~17% in the Na^+ content

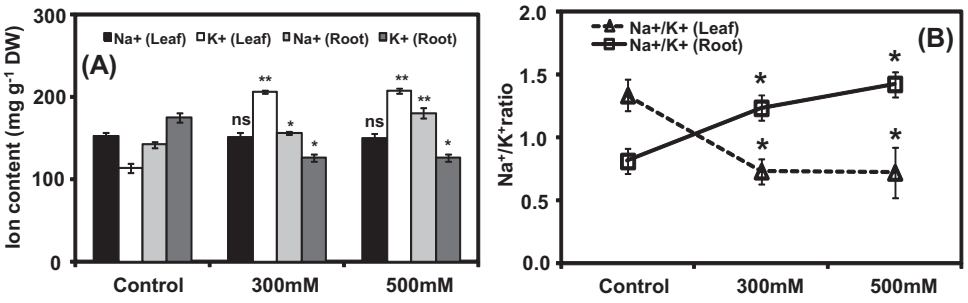

Fig. 3. Sodium and potassium concentrations in the leaves and roots of salt-treated *P. pinnata*. (A) Flame photometer based quantification of the Na^+ and K^+ content in leaves and roots of salt-treated *P. pinnata*. (B) Variations in the Na^+/K^+ ratios in the leaves and roots of control and salt treated plants.

in the leaves of 300 mM treated plants while a significant ($p < 0.01$) increase of ~70% in 500 mM was recorded when compared to control plants (Fig. 2M). Further, a significant ($p < 0.001$) increase of ~218% and ~260% for 300 and 500 mM treated plants respectively was recorded for Na^+ content in roots when compared to control plants (Fig. 2N). The Na^+ and K^+ quantification in vascular bundles indicated accumulation of Na^+ ions was higher in roots while K^+ in leaves in the salt treated plants.

3.3. Na^+ sequestration capacity in leaves and roots of salt treated *P. pinnata*

Flame photometric based quantification of Na^+ and K^+ contents in the whole leaf and root displayed the same trend as FSEM–EDX that accumulation of Na^+ ions was higher in roots, while K^+ accumulated more in the leaves. There was no significant variation in Na^+ content recorded in the leaves of both control and salt treated *Pongamia* plants (Fig. 3A). However the K^+ content significantly ($p < 0.01$) increased by ~82% in leaves of both 300 and 500 mM treated plants in comparison to leaves of control plants (Fig. 3A). The Na^+ content in roots increased significantly by ~10% ($p < 0.05$) and ~27% ($p < 0.01$) in 300 and 500 mM treated plants respectively when compared to roots in control plants (Fig. 3A). However, K^+ content decreased significantly by ~27% in the roots of both 300 and 500 mM treated plants ($p < 0.05$; Fig. 3A). When taken as Na^+/K^+ ratios as a whole, roots showed a significant ($p < 0.05$) dose-dependent increase in the Na^+/K^+ ratios, while the Na^+/K^+ ratios declined significantly ($p < 0.05$) with increasing salt concentrations in leaves (Fig. 3B).

To gain further insight into the Na^+ dynamics within tissues, we studied the Na^+ localization patterns in control and salt-treated *P. pinnata* roots as well leaves by using a cell permeable fluorescent Na^+ probe CoroNa-Green AM (Fig. 4A–L). In the present study, the transverse section of leaves showed a consistent high intensity staining of the central vascular bundle region in both control and salt-treated plants (Fig. 4A–F). Apart from the central pith, cell walls (apoplasmic region) also showed green fluorescence in both control (Fig. 4A and B) and salt-treated leaves of *P. pinnata* (Fig. 4C–F). Though leaf tissues of *P. pinnata* did not show significant accumulation of Na^+ within photosynthesizing cells (symplasm) in the salt-treated plants when compared based on the fluorescence intensities of symplasmic and apoplasmic regions of six replicate images ($p < 0.05$, $n = 6$), we observed high intensity fluorescent spots in 500 mM NaCl treated leaf sections (Fig. 4F arrows). On the other hand, root tissues showed a completely different Na^+ localization pattern. Most of the green fluorescence was visible in the symplasmic region and control plants (Fig. 4G and H) showed minimal fluorescence intensities in most of the cells while the intensity increased gradually in 300 and 500 mM salt-treated roots (Fig. 4I–L). Further, in 300 and 500 mM NaCl treatment, vacuolar sequestration of Na^+ is clearly visible (Fig. 4J and L arrows).

3.4. Differential expression of salt-responsive genes in the leaves and roots of salt treated *P. pinnata*

We monitored the gene expression levels of some of the key salt-responsive genes including the SOS pathway components. The sequence obtained for the PCR amplified gene products from *G. max* based indirect primers confirmed the identity of the target genes (details given in Supplementary Fig. S1). In the present study, high affinity potassium transporter 1 (HKT1) was significantly up-regulated by ~4 fold under both 300 and 500 mM NaCl treated roots, while in leaves only 300 mM NaCl induced significant expression of HKT1 by ~3 fold (Fig. 5A). Interestingly, NHX1 showed significant induction only in the leaves of 300 and 500 mM NaCl treated plants by ~2 fold, while in roots the NHX1 gene expression remained unchanged (Fig. 5B). SOS1 expression was significantly upregulated by ~2 fold in both 300 and 500 mM NaCl treatment (Fig. 5C). However, in leaves significant up-regulation of ~2 fold was recorded only in 300 mM NaCl treatment (Fig. 5C). SOS2 kinase showed significant up-regulation by ~60 and ~25 fold in the leaves during 300 mM and 500 mM NaCl treated plants, respectively. While ~26 fold up-regulation was observed in the roots of only 300 mM NaCl treated plants, which declined to near control levels during 500 mM salt treatment (Fig. 5D). SOS3 was significantly upregulated in leaves by ~2 fold in both 300 and 500 mM NaCl treated plants while in roots it was significantly induced by ~2 and ~29 fold in 300 and 500 mM treated plants respectively (Fig. 5E). Further, the salt-responsive peroxidase (POD) gene also showed high up-regulation in the roots of 300 and 500 mM NaCl treated plants by ~9 and ~7 fold respectively, while in the leaves, the expression levels remained unchanged (Fig. 5F). NCED (9-cis epoxy-carotenoid dioxygenase) and PYL4 (PYR1-like4) showed ~3 and ~2 fold up-regulation respectively in the roots of 300 mM NaCl treated plants and gets strongly induced by ~14 and ~229 fold respectively in 500 mM NaCl treated-roots (Fig. 5G and H). However, the expression levels of both NCED and PYL4 remain unchanged in the leaves (Fig. 5G and H).

4. Discussion

In the present study, the key molecular and physiological responses of a particular accession (Toil 12) of *P. pinnata* were analyzed under high salinity conditions. The seed oil being a potential feedstock for biofuels, *P. pinnata* plantations are currently in high demand worldwide [21]. Thus, an integrated insight into the salt-induced responses of *Pongamia* will create a *win-win* situation for the present need of utilizing salinized land areas towards economic gains from trees. Moreover, being native to India [41] availability of a range of accessions of *P. pinnata* makes it a boon for stress biologists to screen and select the comparatively best accessions suited for a particular environmental constraint, for example soil salinity.

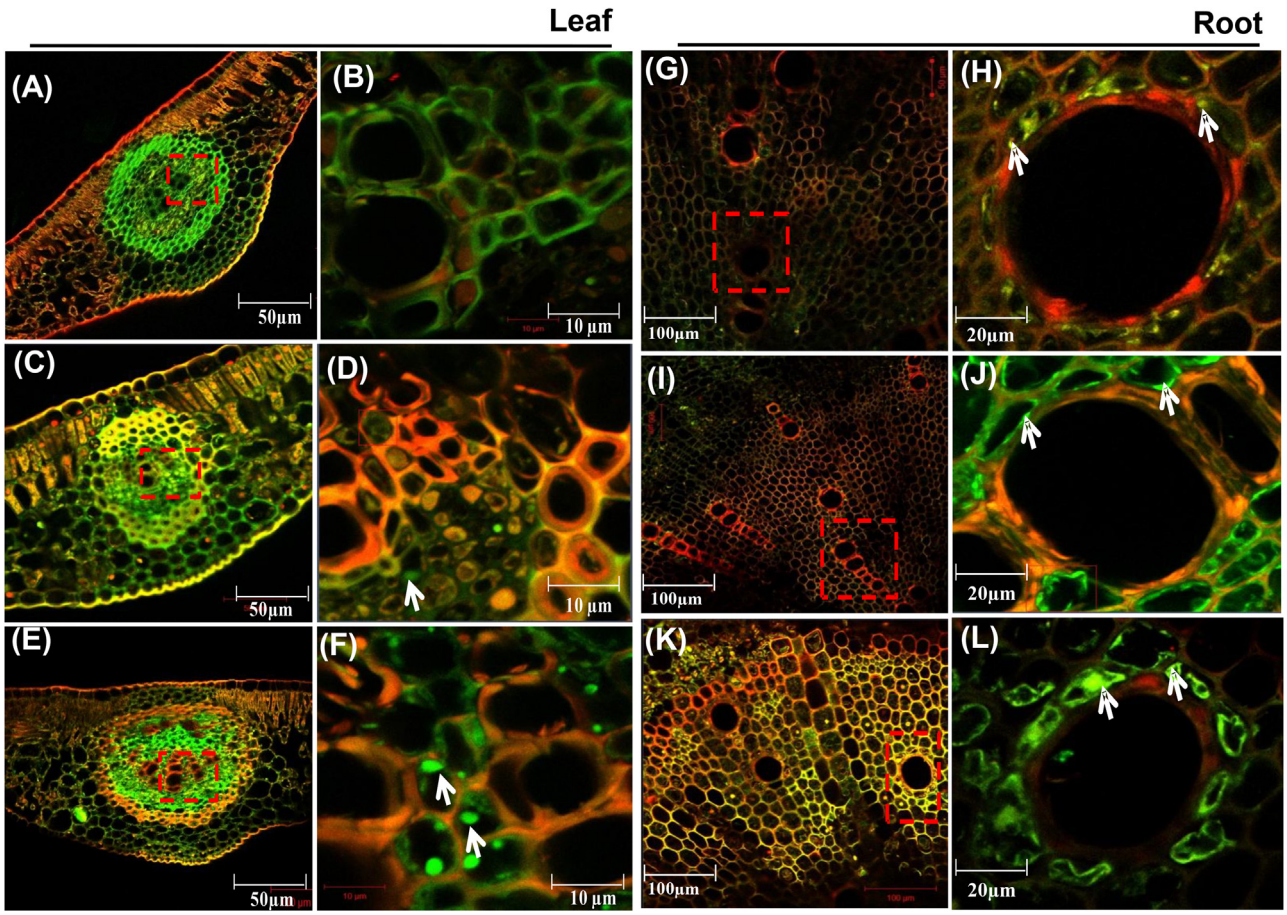

Fig. 4. Visualization of Na^+ in fluorescent CoroNa-Green AM stained leaves and roots of control and salt-treated *P. pinnata* through confocal microscope. (A and G) Cross section of leaves and roots of control, (C and I) 300 mM NaCl and (E and K) 500 mM NaCl treated *P. pinnata* and magnified view of the vascular bundles enclosed in red border in leaves (B, D and F) and (H, J and L) roots where Na^+ localization was visualized around xylem vessels respectively in all three treatments. The white arrows indicate the regions of high Na^+ localization in the vacuoles. (For interpretation of the references to colour in this figure legend, the reader is referred to the web version of this article.)

Salt-treated *P. pinnata* seedlings displayed no stress-induced symptoms till 15 days treatment, which indicate the existence of strong adaptive mechanisms effectively ameliorating the impact of salt-induced osmotic imbalance and ion-induced toxicity that is comparable to that of known halophytes [42,43]. *Pongamia* is considered as a semi-mangrove i.e. a transitional species having intermediate characteristics between glycophytes and halophytes and is known to tolerate a broad range of soil salinity without possessing specialized morphological and physiological traits like true halophytes [29]. Thus, it was interesting to understand the physiological, biochemical and molecular responses of *P. pinnata* under salinity stress. We observed a significant decline in A_{sat}, g_s and E in 300 and 500 mM salt-treated plants when compared to controls. Salinity decreases the soil water potential and reduces water uptake by roots. Hence, the first physiological response is to avoid water loss through transpiration, which is achieved *via* stomatal closure leading to decline in g_s values [44]. As a consequence of reduced stomatal conductivity, E and A_{sat} also showed a concomitant decline. The observed decline in photosynthetic gas exchange parameters could either be an adaptive response of *P. pinnata* to tolerate the salinity-induced osmotic imbalance and is reversible upon providing optimum conditions or it could be the result of salt-induced toxicity and irreversible damage to the photosynthetic machinery. As no morphological stress symptoms were observed in the salt treated seedlings, it was unlikely that the photosynthetic machinery were damaged. The gas exchange and Chl *a* fluorescence results clearly demonstrate that the photosynthetic machinery was not affected under salt stress indicating that *P. pinnata* effectively restricted the entry as well as accumulation of Na^+ ions to toxic levels in leaves which is detrimental to the plant. Further, there was no significant reductions in the leaf relative water contents, electrolyte leakage as well as leaf chlorophyll and carotenoid contents in both 300 and 500 mM NaCl treated plants. Moreover at the anatomical level also, the cellular integrity of both leaves and roots of 300 and 500 mM NaCl treated plants remained similar to that of the controls despite a gradual accumulation of Na^+ with increasing salt concentrations. Taken together, it can be hypothesized that the decline in the photosynthetic performance under salt stress is an adaptive response of *P. pinnata*. Similar level of salinity tolerance in other accessions of *P. pinnata* was also reported by Huang et al. [29], though the treatments were given on a short-term (hourly) basis. Our results are in slight contradiction with those of Arpiwi et al. [30], which showed moderate salinity tolerance in some selected genotypes of *Pongamia* (upto 250 mM NaCl). As different genotypes of *P. pinnata* are sporadically reported to possess tolerance against a wide range of salt concentrations, such differences in the salt tolerance capacity in *Pongamia* could be attributed to the genotypic variations as well as developmental stage and the mode of application of salt-treatment.

Flame photometric based quantification of Na^+ and K^+ as well as FSEM–EDX data revealed that accumulation of Na^+ ions was higher in roots, while K^+ accumulated more in the leaves. Salt-tolerant plants were reported to show Na^+ sequestration in roots in order to restrict Na^+ entry into leaf tissues [45,46]. Based on the observed

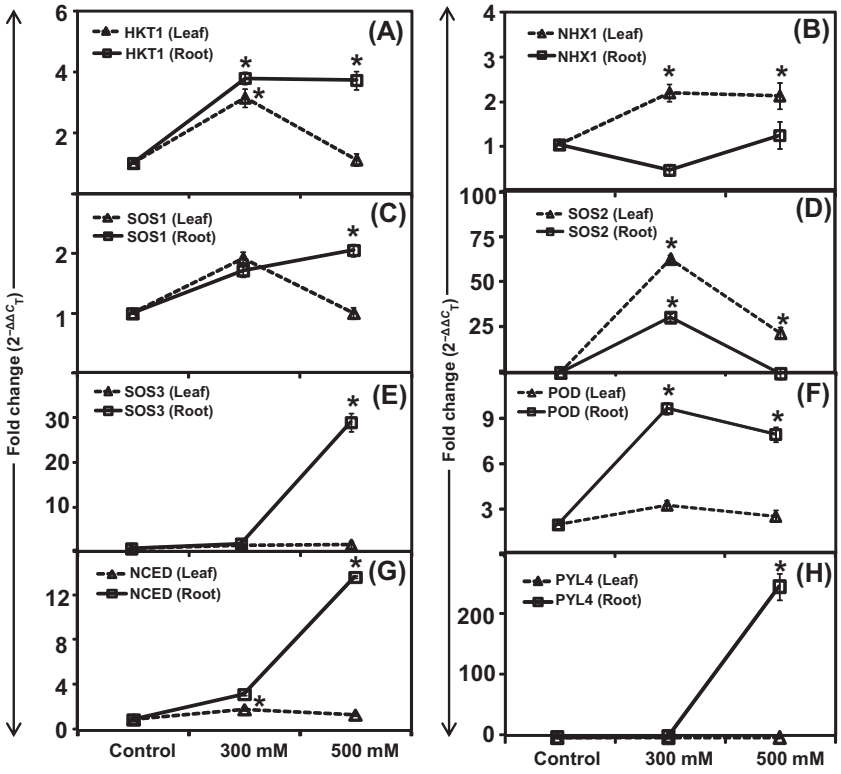

Fig. 5. Relative mRNA expression levels of salt-responsive genes in salt-treated *Pongamia*. The effect of NaCl treatment (0, 300, 500 mM) for 15 days on the expression profile of (A) HKT1, (B) NHX1, (C) SOS1, (D) SOS2, (E) SOS3, (F) POD, (G) NCED and (H) PYL4 in both roots and leaves. Results are the mean ± SD (n = 3).

Na^+ accumulation pattern, it can be inferred that a similar mechanism is possibly operating in the roots of *P. pinnata* to inhibit excessive accumulation of Na^+ in the leaf tissues, which is essential to protect the photosynthetic machinery from ion toxicity. It has been reported that accumulation of K^+ in guard cells regulates stomatal behavior and in turn the photosynthetic gas exchange and transpiration patterns in plants [47]. Thus, it is crucial to modulate K^+ homeostasis under high salinity conditions to ensure optimum water potential, cell turgidity as well as photosynthesis. Previous studies have shown that maintenance of low Na^+/K^+ ratio as well as high K^+ levels in cytoplasm is crucial for conferring salt tolerance in plants [48,49]. Also, it has been recently reported that K^+ retention ability plays a major role in salinity tolerance [50]. In case of *Pongamia*, we observed that salt-treated leaves accumulate more K^+ than Na^+, which could be either due to enhanced K^+ uptake or reduced efflux of K^+. Previous studies have reported the role played by high affinity K^+ transporters including HAK5, CHX17 and KUP1 in increasing K^+ uptake and maintaining ion homeostasis under nutrient deficiency and salinity stress [51,50]. In the present study, we observed high expression of HKT1 gene which might also be involved in contributing to K^+ uptake under salt stress along with other K^+ transporters. Based on our results, we can predict that enhanced K^+ content in leaves under salinity stress is one of the major factors responsible for conferring high salinity tolerance to *Pongamia*.

In the present study, the leaves showed a consistent high intensity staining of the central vascular bundle region in both control and salt-treated plants which is possibly due to the pre-existing salts (including NaCl as well as other salts present in the soil). Similar high intensity staining pattern in the stellar region has been reported in citrus leaf sections also [52]. Apart from the central pith, cell walls (apoplasmic region) also showed green fluorescence in both control and salt-treated leaves of *P. pinnata* which is due to the inherent nature of apoplast to act as cation-binding matrix and probably retains the Na^+ ions in these regions [53]. The observed high intensity fluorescent spots in 500 mM NaCl treated leaf sections were in congruence with similar studies performed on different plants. Exactly similar 2–6 μm fluorescent spots have been observed through CoroNa-Green staining in salt-treated citrus leaves by Gonzalez et al. [52], which they described as membrane bound cytosolic organelle-like structures and assumed that Na^+ initially gets sequestered within these spots and then into vacuoles. In the present analysis the authentication of such membrane bound organelle-like structure were carried out, but based on the exact similarity in the appearance of the fluorescent spots, it is likely the small amount of Na^+ which escaped the root barriers and reached the leaves of the 500 mM salt-treated plants, is sequestered within these 2–6 μm structures. The pattern of Na^+ accumulation in root tissues corresponded well with the observed dry weight based ion contents. In general, tolerance against salinity is achieved through reduction in Na^+ uptake by the root system, sequestering the Na^+ ions within root tissues, restricting xylem loading of Na^+ and finally through the increased ability to sequester Na^+ in intercellular compartments of leaves [52,54]. Further, vacuolar sequestration of Na^+ ions is a highly crucial and complementary mechanism which not only ameliorates the toxic effects of Na^+ in the cytosol but also provides additional protection by enhancing osmoticum levels for continued water uptake and turgor maintenance under long term salinity conditions [55]. A recent study analyzed the Na^+ localization pattern using CoroNa-Green probe in wheat varieties under salinity stress. It was demonstrated that the meristematic regions of the root apex could probably act as salt sensors and the pattern of Na^+ sequestration ability in the mature zones correlated with the observed salt tolerance [56]. In case of *Pongamia*, the CoroNa-Green AM sodium probe study demonstrated that there is significant compartmentalization of Na^+ into the vacuoles in roots.

Salinity tolerance is known to be a highly complex trait, wherein plants experience both osmotic limitations as well as toxicity due

to gradual accumulation of ions in the cytosol during long term salinity exposures [57]. High salt concentrations in the soil leads to gradient based passive uptake of Na^+ into the cytosol. However, majority of the accumulated Na^+ in the roots gets expelled back to the soil by the active efflux mechanism of a highly conserved plasma membrane localized Na^+/H^+exchanger or salt overly sensitive 1 (SOS1) [45,16]. Though SOS1 actively extrudes excess Na^+ into the soil, long term high salinity conditions will inevitably cause accumulation of Na^+ in the cytosol due to the passive uptake of Na^+ through various potassium channels or non-specific cation channels (NSCC) [58]. In order to have a picture of the high salt-tolerance of *P. pinnata*, we monitored the gene expression levels of some of the key salt-responsive genes including the SOS pathway components.

Role of HKT1 genes in conferring salinity tolerance to plants have been well documented [59]. In general, HKT1 takes part in removal of Na^+ from the xylem into the neighboring parenchyma cells and thus inhibiting Na^+ translocation to the shoots and protects leaves from Na^+-induced toxicity [60,61]. Based on the present observations of the expression patterns of HKT1, we can hypothesize that the HKT1 homologue is responsible for the observed low Na^+ levels in leaves of *Pongamia* by reducing Na^+ loading into the xylem. However, exact confirmation of the role played by HKT1 requires *in-situ* localization studies under salt stress conditions, as based on localization only, we can predict that whether the HKT1 is playing a role in Na^+ uptake in the roots along with NSCCs [13,62] or in Na^+ unloading from the xylem [45]. Tonoplast-localized NHX1 and NHX2 are known to facilitate K^+ uptake in vacuoles to regulate stomatal behavior and cell turgidity as in Arabidopsis [63]. In the present study, the K^+ accumulation pattern shows a positive correlation with the NHX1 gene expression pattern in both leaves and roots. Thus, it can be assumed that the particular isoform of NHX1 analyzed in the present study is possibly mediating an active K^+ uptake in the leaves, which could be responsible for maintaining the cellular water potential under high salinity conditions. However, more experimentation is required to authenticate the assumptions. The NHX1 isoform targeted in the present study was found to correlate more with vacuolar K^+ uptake rather than Na^+ and hence, some other NHX isoform might operate for mediating vacuolar Na^+ uptake in *Pongamia*. Alternatively, it is also possible that SOS2 kinase mediated post-translational activation of the existing NHX1 proteins [64] is responsible for the observed vacuolar sequestration of Na^+ and hence, the NHX1 mRNA levels did not correlate with the Na^+ localization data in the roots. The differential expression data of SOS1, SOS2 and SOS3 provides an indication for effective activation of the SOS pathway in the both roots and leaves of salt-treated *P. pinnata*. As the proteins for the above genes are known to be post-translationally regulated, further analysis in terms of protein activity is required for understanding the role of SOS pathway in *Pongamia* under salinity stress. Moreover, apart from acting as a Na^+ ion extruder SOS1 is also known to be involved in indirect uptake of K^+ [65] as well as the stele-localized isoform of SOS1 performs either loading or unloading of Na^+ from the stele depending of external Na^+ condition [66,67]. Hence, in-situ localization studies are required for confirming the actual role played by SOS1 under salt stress.

Enhanced expression of POD gene in roots indicates a strong ROS modulating mechanism operative within the roots of *P. pinnata* under salinity conditions. The regulatory enzyme of ABA biosynthetic pathway, NCED (9-cis epoxycarotenoid dioxygenase) and the ABA receptor PYL4 (PYR1-like4) showed more than two fold up-regulation in the roots of 300 mM NaCl treated plants and gets strongly induced in 500 mM NaCl treated roots. In the case of *Pongamia*, significant up-regulation of the homologues of both ABA biosynthetic gene NCED as well as ABA receptor PYL4 was observed in the salt-treated roots. Similar to previous studies [68,69], we can postulate that the high ABA biosynthesis and receptor gene expressions might be contributing towards the observed high salinity tolerance in *Pongamia*.

5. Conclusion

Based on the overall salt stress mediated adaptive responses in this study, it can be concluded that roots play a key role in conferring salt-tolerance in *P. pinnata*. Further, vacuolar sequestration of Na^+ in roots minimizes Na^+ translocation to the shoot system. Uptake of K^+ in the leaves might contribute in maintaining leaf water potential and photosynthetic efficiency. At the molecular level, SOS pathway components as well as other crucial salt responsive genes including ABA biosynthesis/receptor and POD effectively operate in the roots and contribute towards the high salinity tolerance of *P. pinnata*.

Acknowledgements

This research was supported by the project grant (BT/PR-12024/BCE/8/1097/2014) from Department of Biotechnology, Govt. of India. We gratefully acknowledge Tree Oil India Ltd. (TOIL), Zaheerabad, Telangana State, India for providing *Pongamia* seed (TOIL12). We also acknowledge Mr. Poli Yugandhar, Indian Institute of Rice Research, Rajendranagar, Hyderabad, Telangana, India. Mr. K Madhana Sekhar help is also acknowledged in analyzing leaf gas exchange results. DS acknowledges the fellowship from the Young Scientist start up grant scheme (YSS/2015/000635) from Department of Science and Technology, Govt. of India. S.M and S.K acknowledges University Grant Commission, New Delhi, India for fellowships.

Appendix A. Supplementary data

Supplementary data associated with this article can be found, in the online version, at http://dx.doi.org/10.1016/j.plantsci.2017.02.008.

References

[1] A. Jamil, S. Riaz, M. Ashraf, M.R. Foolad, Gene expression profiling of plants under salt stress, Crit. Rev. Plant Sci. 30 (2011) 435–458.
[2] D.H. Oh, M. Dassanayake, H.J. Bohnert, J.M. Cheeseman, Life at the extreme: lessons from the genome, Genome Biol. 13 (2012) 241.
[3] A. Polle, S. Chen, On the salty side of life: molecular, physiological and anatomical adaptation and acclimation of trees to extreme habitats, Plant Cell Environ. 38 (2015) 1794.
[4] S. Chen, A. Polle, Salinity tolerance of populus, Plant Biol. 12 (2010) 317–333.
[5] A. Harfouche, R. Meilan, A. Altman, Molecular and physiological responses to abiotic stress in forest trees and their relevance to tree improvement, Tree Physiol. 34 (2014) 1181–1198.
[6] T. Ma, J. Wang, G. Zhou, Z. Yue, Q. Hu, Y. Chen, B. Liu, Q. Qiu, Z. Wang, J. Zhang, K. Wang, D. Jiang, C. Gou, L. Yu, D. Zhan, R. Zhou, W. Luo, H. Ma, Y. Yang, S. Pan, D. Fang, Y. Luo, X. Wang, G. Wang, J. wang, Q. Wang, X. Lu, Z. Chen, J. Liu, Y. Lu, Y. Yin, H. Yang, R.J. Abbott, Y. Wu, D. Wan, J. Li, T. Yin, M. Lascoux, S.P. DiFazio, G.A. Tuskan, J. Wamg, J. Liu, Genomic insights into salt adaptation in a desert poplar, Nat. Commun. 4 (2014) 2797.
[7] J. Chen, Q. Xiao, F. Wu, X. Dong, J. He, Z. Pei, H. Zheng, T. Näsholm, Nitric oxide enhances salt secretion and Na^+ sequestration in a mangrove plant, *Avicennia marina*, through increasing the expression of H^+-ATPase and Na^+/H^+ antiporter under high salinity, Tree Physiol. 30 (2010) 1570–1585.
[8] K. Shinozaki, K. Yamaguchi-Shinozaki, Gene expression and signal transduction in water-stress response, Plant Physiol. 115 (1997) 327–334.
[9] L. Shabala, A. Mackay, Y. Tian, S.E. Jacobsen, D.W. Zhou, S. Shabala, Oxidative stress protection and stomatal patterning as components of salinity tolerance mechanism in quinoa (*Chenopodium quinoa*), Physiol. Plant. 146 (2012) 26–38.
[10] P.M. Hasegawa, Sodium (Na^+) homeostasis and salt tolerance of plants, Environ. Exp. Bot. 92 (2013) 19–31.
[11] B. Benito, R. Haro, A. Amtmann, T. Cuin, I. Dreyer, The twins K^+ and Na^+ in plants, J. Plant Physiol. 171 (2014) 723–731.
[12] M.M. Julkowska, H.C.J. Hoefsloot, S. Mol, F. Richard, G.J.D. Boer, M.A. Haring, C. Testerink, Capturing *Arabidopsis* root architecture dynamics with ROOT-FIT reveals diversity in responses to salinity, Plant Physiol. 166 (2014) 1387–1402.

[13] R. Munns, M. Tester, Mechanisms of salinity tolerance, Annu. Rev. Plant Biol. 59 (2008) 651–681.
[14] W. Jia, Y. Wang, S. Zhang, J. Zhang, Salt-stress-induced ABA accumulation is more sensitively triggered in roots than in shoots, J. Exp. Bot. 53 (2002) 2201–2206.
[15] G.M. Abogadallah, Antioxidative defense under salt stress, Plant Signal. Behav. 5 (2010) 369–374.
[16] H. Ji, J.M. Pardo, G. Batelli, M.J. Van Oosten, R.A. Bressan, X. Li, The salt overly sensitive (SOS) pathway: established and emerging roles, Mol. Plant 6 (2013) 275–286.
[17] Q. Yang, Z.Z. Chen, X.F. Zhou, H.B. Yin, X. Li, X.F. Xin, X.H. Hong, Z.K. Zhu, Z. Gong, Overexpression of SOS (Salt Overly Sensitive) genes increases the salt tolerance in transgenic *Arabidopsis*, Mol. Plant 2 (2009) 22–31.
[18] H.W. Harvey, The chemistry and fertility of sea waters, J. Mar. Biol. Assoc. UK 35 (1956) 289.
[19] M.C. Ball, Ecophysiology of mangroves, Trees 2 (1988) 129–142.
[20] A. Mathur, D.K. Vyas, Socio-ecological issues-eco-economic and sustainability status, J. Ecol. Environ. Sci. 4 (2013) 87–90.
[21] P.T. Scott, L. Pregelj, N. Chen, J.S. Hadler, M.A. Djordjevic, P.M. Gresshoff, *Pongamia pinnata*: An untapped resource for the biofuels industry of the future, Bioenerg. Res. 1 (2008) 2–11.
[22] S. Sangwan, D.V. Rao, R.A. Sharma, A review on *Pongamia pinnata* (L.) pierre: a great versatile leguminous plant, Nat. Sci. 8 (2010) 11.
[23] M. Naik, L.C. Meher, S.N. Naik, L.M. Das, Production of biodiesel from high free fatty acid Karanja (*Pongamia pinnata*) oil, Biomass Bioenerg. 32 (2008) 354–357.
[24] L.M. Wang, M.R. Mu, X.F. Li, P. Lin, W.Q. Wang, Differentiation between true mangroves and mangrove associates based on leaf traits and salt contents, J. Plant Ecol. 4 (2010) 292–301.
[25] K. Singh, Effect of soil salinity and sodicity on seedling growth and mineral composition of *Pongamia pinnata* and *Araucaria cunninghamii*, Trop. Ecol. 31 (1990) 124–130.
[26] B.N. Divakara, A.S. Alur, S. Tripati, Genetic variability and relationship of pod and seed traits in *Pongamia pinnata* (L.) Pierre, a potential agroforestry tree, Int. J. Plant Prod. 4 (2010) 129–141.
[27] V. Kesari, L. Rangan, Development of *Pongamia pinnata* as an alternative biofuel crop-current status and scope of plantations in India, J. Crop Sci. Biotech. 13 (2010) 127–137.
[28] H. Wang, T. Hu, J. Huang, X. Lu, B. Huang, Y. Zheng, The expression of *Millettia pinnata* chalcone isomerase in *Saccharomyces cerevisiae* salt-sensitive mutants enhances salt-tolerance, Int. J. Mol. Sci. 14 (2013) 8775–8786.
[29] J. Huang, X. Lu, H. Yan, S. Chen, W. Zhang, R. Huang, Y. Zheng, Transcriptome characterization and sequencing-based identification of salt responsive genes in *Millettia pinnata*, a semi-mangrove plant, DNA Res. 19 (2012) 195–207.
[30] N.L. Arpiwi, G. Yan, E.L. Barbour, J.A. Plummer, Genetic diversity, seed traits and salinity tolerance of *Millettia pinnata* (L.) Panigraphi (syn. *Pongamia pinnata*), a biodiesel tree, Genet. Resour. Crop. Evol. 60 (2013) 677–692.
[31] S. Ennahli, H.J. Earl, Physiological limitations to photosynthetic carbon assimilation in cotton under water stress, Crop Sci. 45 (2005) 2374–2382.
[32] S. Mudalkar, R.V. Sreeharsha, A.R. Reddy, A novel aldo-keto reductase from *Jatropha curcas* L. (JcAKR) plays a crucial role in the detoxification of methylglyoxal, a potent electrophile, J. Plant Physiol. 195 (2016) 39–49.
[33] H. Barrs, P. Weatherley, A re-examination of the relative turgidity technique for estimating water deficits in leaves, Aust. J. Biol. Sci. 15 (1962) 413–428.
[34] W.H. Cao, J. Liu, X.J. He, R.L. Mu, H.L. Zhou, S.Y. Chen, J.S. Zhang, Modulation of ethylene responses affects plant salt-stress responses, Plant Physiol. 143 (2007) 707–719.
[35] D.I. Arnon, Copper enzymes in isolated chloroplasts. ploy phenoloxidase in *Beta vulgaris*, Plant Physiol. 24 (1949) 1–15.
[36] D.H. Oh, E. Leidi, Q. Zhang, S.M. Hwang, Y. Li, F.J. Quintero, X. Jiang, M.P. DíUrzo, S.Y. Lee, Y. Zhao, J.D. Bahk, R.A. Bressan, D.J. Yun, J.M. Pardo, H.J. Bohnert, Loss of halophytism by interference with SOS1 expression, Plant Physiol. 151 (2009) 210–222.
[37] R. Munns, P.A. Wallace, N.L. Teakle, T.D. Colmer, Measuring soluble ion concentrations (Na^+, K^+, Cl^-) in salt-treated plants, in: R. Sunkar (Ed.), Plant Stress Tolerance: Methods and Protocols, Humana Press, Springer, New York, 2010, pp. 371–382.
[38] S. Sherman-Broyles, A. Bombarely, J. Grimwood, J. Schmutz, J. Doyle, Complete plastome sequences from *Glycine syndetika* and six additional perennial wild relatives of soybean, G3 (Bethesda) 4 (2014) 2023–2033.
[39] R.V. Sreeharsha, S. Mudalkar, K.T. Singha, A.R. Reddy, Unravelling molecular mechanisms from floral initiation to lipid biosynthesis in a promising biofuel tree species, *Pongamia pinnata* using transcriptome analysis, Sci. Rep. 6 (2016) 34315.
[40] K.J. Livak, T.D. Schmittgen, Analysis of relative gene expression data using real-time quantitative PCR and the $2^{-\Delta\Delta C_T}$ method, Methods 25 (2001) 402–408.
[41] V. Lakshmikanthan, Tree Borne Oil Seeds. Directorate of Nonedible Oils and Soap Industry, Khadi and Village Industries Commission, Mumbai, India, 1978, pp. 10.
[42] S. Shabala, A. Mackay, Ion transport in halophytes, Advan. Bot. Res. 57 (2011) 151–187.
[43] I. Slama, C. Abdelly, A. Bouchereau, T. Flowers, A. Savoure, Diversity distribution and roles of osmoprotective compounds accumulated in halophytes under abiotic stress, Ann. Bot. 115 (2015) 433–447.
[44] F. Tardieu, W.J. Davies, Stomatal response to abscisic acid is a function of current plant water status, Plant Physiol. 98 (1993) 540–545.
[45] M.P. Apse, E. Blumwald, Na^+ transport in plants, FEBS Lett. 581 (2007) 2247–2254.
[46] I. Møller, M. Gilliham, D. Jha, G. Mayo, S.J. Roy, J. Coates, J. Haseloff, M. Tester, Salinity tolerance engineered by cell type specific over-expression of a Na^+ transporter in the Arabidopsis root, Plant Cell 21 (2009) 2163–2178.
[47] Z. Andres, J. Perez-Hormaeche, E.O. Leidi, K. Schlücking, L. Steinhorst, D.H. McLachlan, K. Schumacher, A.M. Hetherington, J. Kudla, B. Cubero, Control of vacuolar dynamics and regulation of stomatal apertaure by tonoplast potassium uptake, Proc. Natl. Acad. Sci. U. S. A. 111 (2014) 1806–1814.
[48] Y. Hu, W. Fricke, U. Schmidhalter, Salinity and the growth of non-halophytic grass leaves: the role of mineral nutrient distribution, Funct. Plant. Biol. 32 (2005) 973–985.
[49] F.J.M. Maathuis, A. Amtmann, K^+ nutrition and Na^+ toxicity: the basis of cellular K^+/Na^+ ratios, Ann. Bot. 84 (1999) 123–133.
[50] Y. Sun, X. Kong, C. Li, Y. Liu, Z. Ding, Potassium retention under salt stress is associated with natural variation in salinity tolerance among *Arabidopsis* accessions, PLoS One 10 (2015) e0124032.
[51] P. Gonzalez, J.P. Syvertsen, E. Etxeberria, Sodium distribution in salt-stressed citrus rootstock seedlings, HortScience 1504 (2012) 1511.
[52] Etxeberria, sodium distribution in salt-stressed citrus rootstock seedlingsP. Gonzalez, J.P. Syvertsen (Eds.), Hort. Sci. 47 (2012) 1504–1511.
[53] D.C. Plett, I.S. Møller, Na^+ transport in glycophytic plants: what we know and would like to know, Plant Cell Environ. 33 (2010) 612–626.
[54] N. Tester, R. Davenport, Na^+ tolerance and Na^+ transport in higher plants, Ann. Bot. 91 (2003) 1–25.
[55] M.P. Apse, G.S. Aharon, W.A. Snedden, E. Blumwald, Salt tolerance conferred by overexpression of a vacuolar Na^+/H^+ antiport in *Arabidopsis*, Science 285 (1999) 1256–1258.
[56] H. Wu, L. Shabala, X. Liu, E. Azzarello, M. Zhou, C. Pandolfi, Z.H. Chen, J. Bose, S. Mancuso, S. Shabala, Linking salinity stress tolerance with tissue-specific Na^+ sequestration in wheat roots, Front. Plant Sci. 6 (2015) 71.
[57] J.K. Zhu, Genetic analysis of plant salt tolerance using Arabidopsis, Plant Physiol. 124 (2000) 941–948.
[58] E. Blumwald, G.S. Aharon, M.P. Apse, Sodium transport in plant cells, BBA – Biomembranes 1465 (2001) 140–151.
[59] U. Deinlein, A.B. Stephan, T. Horie, W. Luo, G. Xu, J.I. Schroeder, Plant salt-tolerance mechanisms, Trends Plant Sci. 19 (2014) 371–379.
[60] T. Horie, R. Horie, W.Y. Chan, H.Y. Leung, J.I. Schroeder, Calcium regulation of sodium hypersensitivities of *sos3* and *athkt1* mutants, Plant Cell Physiol. 47 (2006) 622–633.
[61] R.J. Davenport, A. Munoz-Mayor, D. Jha, P.A. Essah, A. Rus, M. Tester, The Na^+ transporter AtHKT1 controls xylem retrieval of Na^+ in Arabidopsis, Plant Cell Environ. 30 (2007) 497–507.
[62] T. Horie, F. Hauser, J.I. Schroeder, HKT transporter-mediated salinity resistance mechanisms in *Arabidopsis* and monocot crop plants, Trends Plant Sci. 14 (2009) 660–668.
[63] V. Barragán, E.O. Leidi, Z. Andrés, L. Rubio, A.D. Luca, J.A. Fernández, B. Cubero, J.M. Pardo, Ion exchangers NHX1 and NHX2 mediate active potassium uptake into vacuoles to regulate cell turgor and stomatal function in *Arabidopsis*, Plant Cell 24 (2012) 1127–1142.
[64] Q.S. Qiu, Y. Guo, F.J. Quintero, J.M. Pardo, K.S. Schumaker, J.K. Zhu, Regulation of vacuolar Na^+/H^+ exchange in *Arabidopsis thaliana* by the SOS pathway, J. Biol. Chem. 279 (2004) 207–215.
[65] S.J. Wu, D. Lei, J.K. Zhu, SOS1, a genetic locus essential for salt tolerance and potassium acquisition, Plant Cell 8 (1996) 617–627.
[66] H.Z. Shi, F.J. Quintero, J.M. Pardo, J.K. Zhu, The putative plasma membrane Na^+/H^+ antiporter SOS1 controls long-distance Na^+ transport in plants, Plant Cell 14 (2002) 465–477.
[67] M. Zhu, M. Zhou, L. Shabala, S. Shabala, Physiological and molecular mechanisms mediating xylem Na^+ loading in barley in the context of salinity stress tolerance, Plant Cell Environ. (2016), http://dx.doi.org/10.1111/pce.12727.
[68] S. Chen, J. Li, S. Wang, A. Hüttermann, A. Altman, Salt, nutrient uptake and transport, and ABA of *Populus euphratica*; a hybrid in response to increasing soil NaCl, Trees 15 (2001) 186–194.
[69] S. Chen, J. Li, T. Wang, S. Wang, A. Polle, A. Hüttermann, Osmotic stress and ion-specific effects on xylem abscisic acid and the relevance to salinity tolerance in poplar, J. Plant Growth Regul. 21 (2002) 224–233.

Environmental and Experimental Botany 171 (2020) 103949

Contents lists available at ScienceDirect

Environmental and Experimental Botany

journal homepage: www.elsevier.com/locate/envexpbot

Hydrophobic cell-wall barriers and vacuolar sequestration of Na^+ ions are among the key mechanisms conferring high salinity tolerance in a biofuel tree species, *Pongamia pinnata* L. pierre

Sureshbabu Marriboina[a], Attipalli Ramachandra Reddy[a,b,*]

[a] Department of Plant Sciences, School of Life Sciences, University of Hyderabad, Hyderabad, 500046, India
[b] Yogi Vemana University, Kadapa, 516003, Andhra Pradesh, India

ARTICLE INFO

Keywords:
Biseriate exodermis
Lignin
Multiseriate exodermis
Na^+ localization
Photosynthetic performance
Pongamia pinnata
Salt tolerance
Suberin lamellae

ABSTRACT

Gradual soil-salinization is enhancing the proportion of non-arable salinized land areas. Developing strategies to utilize salinized lands for balanced economical productivity are highly desirable. Salt-tolerating *Pongamia pinnata* has gained significant attraction as a potential biofuel tree species and hence, could act as an efficient energy- crop alternative for cultivation in salinized lands. However, mechanisms conferring salt-tolerance to Pongamia are not yet demonstrated. It is highly crucial to understand the tolerance mechanisms for future breeding purposes for enhanced productivity under saline conditions. Hydroponically grown 30 days old seedlings of Pongamia are treated with two different salt concentrations (300 and 500 mM NaCl) for 8 days and analysed at regular intervals of 1, 4 and 8 days after salt exposure. Physiological parameters were recorded using infrared gas analyser and portable mini-PAM. Ion (Na^+, K^+, Cl^-, and Ca^{2+}) accumulation in leaves and roots were analysed through atomic absorption spectroscopy and Na^+ localization was tracked through confocal laser scanning microscopy. Histochemical detection of lignin and suberin depositions in leaves and roots were carried out. Pongamia roots act as ultra-filters/strong barriers to avoid accumulation of excess Na^+ levels in the leaves. The Na^+ probe fluorescence analysis demonstrated effective vacuolar sequestration of Na^+ in the roots. Formation of suberized multiseriate exodermis in the roots, along with extensive lignification maximized water permeability in both leaves and the roots. The present study clearly demonstrates the key cellular mechanisms conferring salinity tolerance in *P. pinnata*, which can be sustainably grown in salinized marginal lands as a potential biofuel tree species.

1. Introduction

Salinity is one of the major environmental constraints limiting plant growth and productivity and is becoming more extensive in the arid and semi-arid areas (Munns and Gilliham, 2015). Global climate change, inadequate water supply, and excessive irrigation are further expanding the marginalization of arable lands and thereby limiting their availability for crop production (Sharma et al., 2016; Quinn et al., 2015; Shabala, 2013). To date, attempts to extend the crop productivity on saline lands have had limited success, due to the failures in determining plant's responses to this stress owing to the high physiological and genetic diversity among various plant species and spatio-temporal heterogeneity of soil salinity (Shabala et al., 2016; Pandolfi et al., 2016). Indeed, salt tolerance is a complex trait governed by multiple genes intertwining with various physiological and biochemical mechanisms. A comparative understanding of physiological and morphological adaptive mechanisms evoked interest among researchers worldwide over the past few decades, to sustain crop productivity on marginal lands (Jones et al., 2014). However, it is also essential to understand the detailed anatomic and molecular level mechanisms leading to salinity tolerance in plants.

Plants growing in saline soils, restrains the root cell wall expansion through increased deposition of lignin and suberin on the root cell walls to prevent excessive flow of toxic Na^+ ions through the apoplastic pathway and increase water retention in the roots (Shabala and Mackay, 2011). According to Krishnamurthy et al. (2014) and Meyer et al. (2011) plants such as *Bruguiera* and *Iris germanica* possess layers of suberin and lignin coated exodermis (BEX and MEX) in roots, as well vascular tissues in leaves to enhance the water permeability under salt stress. In addition, the increased number of lignified tracheary elements in the vascular tissues under salt stress also enhances the water permeability and greater selectivity for ion uptake in crops such as soybean

* Corresponding author at: Department of Plant Sciences School of Life Sciences, University of Hyderabad, Hyderabad, 500046, Telangana, India.
E-mail address: attipalli.reddy@gmail.com (R.R. Attipalli).

https://doi.org/10.1016/j.envexpbot.2019.103949
Received 23 May 2019; Received in revised form 22 October 2019; Accepted 9 November 2019
Available online 11 November 2019
0098-8472/

and tomato (Neves et al., 2010). Based on their survival strategies, halophytes are broadly classified as salt-secretors which excrete the salt through specialized glands on the leaves, and non-secretors exclude out the salt through specialized barriers in the roots (Jiang et al., 2017; Wang et al., 2011; Parida and Jha, 2010). However, the tolerance of all halophytes to salinity relies on controlled uptake and compartmentalization of Na^+, K^+, and Cl^- and the synthesis of organic 'compatible' solutes, even where salt glands are operative.

Also, during salt stress reduced water uptake may limit the intercellular CO_2 concentration in the leaf due to stomatal closure. In addition, excessive Na^+ decreases the synthesis of photosynthetic pigments and net photosynthesis which leads to an imbalance between absorption and utilization of the energy during carbon fixation, resulting in excessive accumulation of reactive oxygen species (ROS) and disruption of the cellular redox homeostasis (Li et al., 2017). The accumulation of high amounts of Na^+ ions in the plants can also create ionic imbalance leading to osmotic stress, ion toxicity, and oxidative stress. To mitigate the effect of osmotic and ionic toxicity, plants are known to accumulate various compatible inorganic ions (K^+ and Ca^{2+}) and organic osmolytes (valine, glucose, fructose, sucrose, mannitol, pinitol, glycerol, and myo-inositol) (Gharsallah et al., 2016; Papazian et al., 2016). However, an integrated analysis to demonstrate the co-existing adaptive and defensive mechanisms for conferring overall tolerance under salinity stress is essential for gaining a thorough understanding of a specific plant's salt stress responses.

Oil seed-producing perennial halophytes are now gaining importance as a renewable energy resource (Chhetri et al., 2008). Growing salt-tolerant perennial halophytes for sustainable bioenergy production on marginal lands, will efficiently manage the energy and land use competition without interfering with productive arable land areas (Quinn et al., 2015). Interestingly, Pongamia can serve as a good alternative for the utilization of marginal saline lands associated with economic gain. Although Pongamia does not possess salt adaptive characters such as leaf salt bladders, succulence and trichomes like mangroves, it can still endure up to sea saline concentration (3% NaCl). Based on its physiological and molecular characteristics under salt stress Pongamia is classified as a translation species (intermittent species between glycophytes and halophytes), semi-mangrove or mangrove associate (Jiang et al., 2017; Wang et al., 2013). In our previous study, we demonstrated the varied physiological and molecular responses of leaves and roots of Pongamia to high salinity in soil-grown plants in pots (Marriboina et al., 2017). However, for in-depth analysis, a systematic and accurate salt exposure under non-limiting root proliferation conditions are essential to understand the mechanism of stress tolerance, specifically salinity stress in Pongamia.

In the present study, we aimed to analyse the physiological, biochemical, anatomical as well as molecular adaptive and defensive responses of Pongamia pinnata under medium and severe salinity stress conditions both in terms of concentration as well as duration of exposure by utilizing a hydroponic growth system consisting of specialized elongated glass tubes, with periodic replacement of nutrient medium. The present outcomes proposed a possible model of salt management strategy in leaves and roots of Pongamia pinnata, which can be highly useful for further studies on yield improvement of Pongamia under saline conditions.

2. Materials and methods

2.1. Plant material, growth conditions, and salinity treatment

Seeds of *P. pinnata* accession TOIL 12 were obtained from Tree Oil India Limited (TOIL), Zaheerabad, Hyderabad, Telangana and were germinated on moist cotton for 10 days at 25 °C in the dark. The germinated seedlings were grown in a long cylindrical glass tube (5 cm diameter X60 cm length) filled with full-strength Hoagland No. 2 basal salt mixture (Himedia) solution adjusted to pH 5.75 ± 0.02 for 30 days. The solution was replenished every day. The hydroponic experiment was carried out in a plant culture room maintained at 24 °C with a 16 h photoperiod and relative humidity maintained approximately at 60%. For salinity treatment, 30 days old plants (n = 20–30) were selected and subjected to 300 and 500 mM NaCl concentrations with an increment of 100 mM NaCl per day (Chen et al., 2017). Control plants were maintained with fresh Hoagland nutrient solution. Plants were harvested at an interval of 1 day after stress treatment (1 DAS), 4 and 8 DAS. Fresh weights of leaf and root were measured immediately after harvest. Dry weights of control and treated plants were determined after drying at 70 °C for 3 days. Control and treated samples were harvested at each time intervals, flash frozen in liquid nitrogen and stored at −80 °C prior to analysis.

2.2. Leaf gas exchange and chlorophyll fluorescence parameters

Leaf gas exchange measurements were performed by using an infrared gas exchange system (LI-6400/LI-6400XT, LI-COR Inc., Lincoln, NE, USA). All measurements were performed on fully expended 2nd and 3rd leaves of the plant between 10:00 and 13:00 h. Gas exchange parameters such as light saturated net photosynthetic rate (A_{sat}), stomatal conductance (g_s) and transpiration rate (E) were measured in leaves of control and salt-treated plants at 1, 4 and 8 DAS. Leaf water use efficiency was calculated as A_{sat}/E.

Chl*a* fluorescence measurements were performed with a portable mini-PAM chlorophyll fluorometer (Walz, Germany). Whole plants were adapted in dark for 30 min prior to the analysis. Photosynthetic induction and light responsive curves were measured with the intensities of measuring light (< 0.1 μmol photons m^{-2} s^{-1}), saturating pulse (3000 μmol photons m^{-2} s^{-1}), actinic light (170 μmol photons m^{-2} s^{-1}) and far-red light (7 μmol photons m^{-2} s^{-1}) respectively. The duration of actinic light and saturation pulses were 0.8 and 30 s. Induction curve measurements were taken at ~780 PAR about 5 min to complete with 0.8 and 30 s between saturating and actinic flashes of light and the light curve measurements were taken about 88 s to complete with increasing intensities actinic light (~190 PAR to ~3000 PAR). Concentration of chlorophyll *a* and *b* was calculated by using Arnon (1949).

2.3. Histochemical detection of lignin and suberin depositions in leaves and roots

Freshly collected leaves and roots of control and salt-treated plant samples were incubated in 2.5% glutaraldehyde solution in 0.1 M MOPS overnight at 4 °C and quickly cut into small thin sections. To check for lignin deposition, both leaf and root cross section were stained with phloroglucinol-HCl for 15 min. To check for suberin deposition, both leaf and root cross section were stained for overnight with sudan III stain. Stained leave and root cross-sections are examined with Leica DM6B (GmbH, Germany) light microscope (Krishnamurthy, 1999). Total five biological replicates were used and ~12 cross sections from each replicate were used for the examination.

2.4. Quantification of Na^+, K^+, Ca^{2+} and Cl^- ions

Accumulation of Na^+, K^+, Ca^{2+} and Cl^- in leaf and root tissues was determined as described in Munns et al. (2010) with some minor modifications. The collected samples were oven dried at 70 °C for 3 days. Ions (Na^+, K^+, and Ca^{2+}) were extracted in 5 ml of Aqua Regia at 95 °C for 60 min. The resulting solution was diluted and analysed for ions with an atomic absorption spectroscopy (GBC 932, Braeside, Australia). Chloride ion concentration was determined by titrimetric method.

2.5. Visualization of intracellular Na^+ ions through confocal laser scanning microscopy

Leaves and roots collected from and salt-treated plants were segmented into 1 cm sections and incubated with 2.5% glutaraldehyde solution in 0.1 M MOPS buffer overnight at 4 °C. For sodium illumination, tissues were stained with 5 µm Na^+ specific probe CoroNa-Green AM (Invitrogen) in the presence of 0.02% pluronic acid in 50 mM MOPS (pH 7.0) for overnight at room temperature. Samples were thoroughly washed with 50 mM MOPS (pH 7.0) several times, sectioned and immediately immersed in propidium iodide (Invitrogen) for 15 min. Cross sections of leaves and roots were examined under a laser scanning confocal microscopy (Leica TCS SP2, Heidelberg, GmbH, Germany) as described by Oh et al. (2009) with some minor modifications. The cytosolic and vacuolar Na^+ fluorescence was calculated by LCS software (Heidelberg, GmbH, Germany).

2.6. Statistical analyses

Significant differences at $P < 0.001$, $P < 0.01$ and $P < 0.05$ in various parameters estimated between control and salt-treated plants were calculated by using one-way ANOVA. All the statistical and linear regression analyses were performed using the statistical package Sigma Plot 11.0.

3. Results

3.1. Morphology and physiology of P. pinnata under salt stress

After 8 DAS, leaves of 300 mM NaCl treated plants were healthy and green as that of control. However, leaves of 500 mM NaCl treated plants exhibited minor senescence symptoms after 8 DAS (Fig. 1D). The A_{sat} significantly declined by ~25, ~11, and ~10%, in 300 mM NaCl treated plants and ~54, ~72, and ~63% in 500 mM NaCl treated plants at 1, 4 and 8 DAS, respectively when compared to controls (Fig. 2A). A significant reduction of ~50% (300 mM NaCl) and ~75% (500 mM NaCl) was observed in g_s (Fig. 2B) as well as ~50% (300 mM NaCl) and ~83% (500 mM NaCl) decline was recorded in E, respectively with respect to control plants (Fig. 2C) at 1 DAS, which showed no gradual declining trend with increasing exposure times at 4 and 8 DAS. However, WUE showed significant increase by ~1.3, ~1.7 and ~1.5-fold in 300 mM NaCl treated plants as well as ~2.0, ~1.1 and ~1.6-fold increase in 500 mM NaCl treated plants at 1, 4 and 8 DAS, respectively (Fig. 2D). In 300 mM NaCl treated plants, the leaf relative water content (LRWC) did not change significantly at 1, 4 and 8 DAS when compared to controls, whereas 500 mM NaCl treatment showed significant decline in LRWC at 4 and 8 DAS (Fig. 2E). Root relative water content (RRWC %) remained unchanged in both the salt treatments throughout the exposure period (Fig. 2F).

There was no significant difference in the maximum quantum yield of PSII (Fv/Fm) of 300 mM NaCl treated plants at 1, 4 and 8 DAS (Fig. 2G). In 500 mM NaCl treated plants, Fv/Fm significantly decreased at 4 and 8 DAS, while these levels remained similar to that of control at 1 DAS. Further, the quantum yields of non-photochemical quenching (YNPQ) and constitutive heat dissipation (YNO) were significantly varied in control and salt-treated plants. In 500 mM NaCl treated plants, YNO was significantly increased, while YNPQ values decreased significantly at 1, 4 and 8 DAS (Fig. 2H). However, YNO and YNPQ did not change significantly in 300 mM NaCl treated leaves at 1, 4 and 8 DAS. Our results demonstrated that the chlorophyll contents (Chl *a*, Chl *b* and Chl *a/b*) were not changed much in both control and salt-treated plants (Fig. 2I).

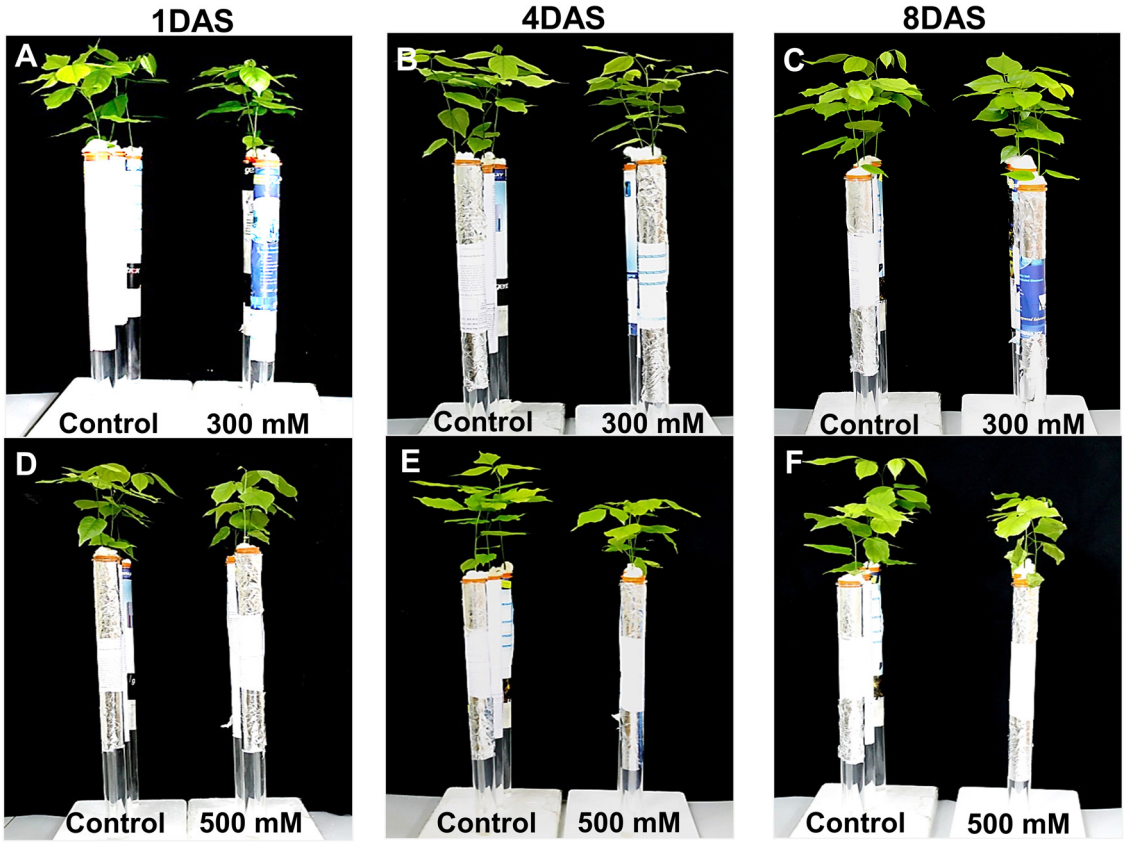

Fig. 1. Shoot and root morphology of hydroponically grown 30-days old *P. pinnata* treated with 300 mM NaCl (A–C) and 500 mM NaCl (D–F) for 1, 4 and 8 DAS, respectively when compared to corresponding controls.

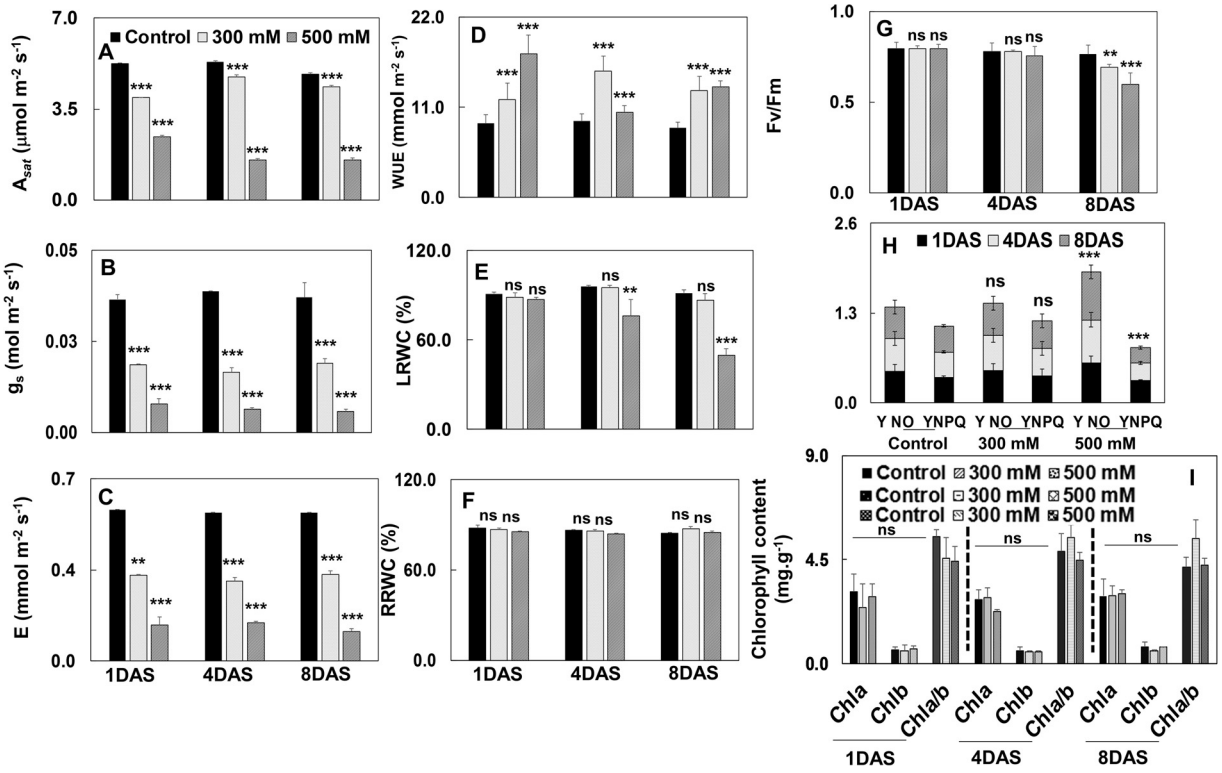

Fig. 2. Physiological parameters of *P. pinnata* under salt stress conditions. (A) light-saturated net photosynthetic rate (A_{sat}) (µmol m^{-2} s^{-1}). (B) Stomatal conductance (g_s) (mol m^{-2} s^{-1}). (C) Transpiration rate (E) (mmol m^{-2} s^{-1}). (D) Water use efficiency (WUE) (mmol m^{-2} s^{-1}). (E) Leaf relative water content (LRWC). (F) Root relative water content (RRWC). (G) Changes in maximal photochemical efficiency of PSII (Fv/Fm). (H) Changes in effective quantum yields of regulated (YNPQ) and non-regulated heat dissipation (YNPQ) of PSII. (I) chlorophyll content. Error bars represent the mean ± SD (n = 5).

3.2. Salinity-induced Na^+, K^+, Ca^{2+} and Cl^- ion homeostasis in leaves and roots of P. Pinnata

In leaves, Na^+ and Ca^{2+} levels increased gradually in both 300 and 500 mM NaCl treated plants at 1, 4 and 8 DAS. However, K^+ levels remained unchanged during 1 DAS of both 300 and 500 mM NaCl treatment but got slightly enhanced at 4 and 8 DAS of 300 mM salt stress and at 8 DAS of 500 mM salt treatment. Correspondingly, the Cl^- ion content was significantly enhanced at 1 DAS of only 500 mM salt-treated plants and 4 and 8 DAS of both 300 and 500 mM NaCl treated plants (Fig. 3A–C).

Interestingly, in roots Na^+ and Cl^- ion content showed similar pattern of gradual accumulation in 300 and 500 mM salt-treated plants at 1, 4 and 8 DAS. However, Ca^{2+} levels were only slightly enhanced at 1 DAS under 300 mM salt treatment and remained similar to controls during 4 and 8 DAS, while 500 mM salt-treated plants showed significant gradual increase in the Ca^{2+} content from 1 to 8 DAS. Further, K^+ content also increased slightly in 300 mM NaCl treatment, which showed a gradual increase from 1 to 8 DAS, however, in 500 mM salt-treated plants, K^+ levels were enhanced only till 4 DAS and declined again to control levels at 8 DAS (Fig. 3D–F). Also, K^+/Na^+ ratio declined significantly and consistently when compared to control in both leaves and roots under 300 and 500 mM salt-treatment during all time points. However, leaf K^+/Na^+ ratio remained slightly higher than roots at all points except 8 DAS of 500 mM NaCl treatment (Fig. 3G). A similar trend was observed for Ca^{2+}/Na^+ ratios, wherein it declined significantly under both 300 and 500 mM salt treatment across all time points, but the leaf Ca^{2+}/Na^+ ratio was maintained at higher levels than roots across all the time points (Fig. 3H). In contrast, the Na^+/Cl^- ratio increased when compared to control plants in both leaves and roots under 300 and 500 mM salt treatments across all time points. Here also, in the overall trend leaf ratios were higher than root Na^+/Cl^- ratios during all points, except at 1 DAS of 300 mM NaCl treatment when both are same. Also, at 8 DAS of 300 mM salt treatment, leaf Na^+/Cl^- showed unusually high values when compared to controls, which appeared like an outlier for the overall trend of gradual increase (Fig. 3I).

3.3. Visualization of Na^+ ion sequestration and salinity induced hydrophobic barrier (suberin and lignin) formation in leaves and roots of P. pinnata

Significantly higher green fluorescence was observed in the symplasmic regions of 300 mM and 500 mM NaCl treated leaf sections at 1, 4 and 8 DAS, when compared to the corresponding control sections (Fig. 4A–I). Further, significant fluorescence intensity was also observed in the apoplasmic regions of 500 mM NaCl treated leaves at 4 and 8 DAS (Fig. 4H, I). Further, the vacuolar and cytosolic Na^+ intensity was also measured in control and salt-treated plants. The cytosolic Na^+ intensity did not change significantly in 300 and 500 mM NaCl treated leaves, however, the vacuolar Na^+ intensity was increased consistently in 300 and 500 mM NaCl treated laves at 1, 4 and 8 DAS (Fig. 4J).

On other hand, root tissue exhibited a completely different pattern of sodium compartmentalization in salt-treated plants. The Na^+ fluorescence intensity was significantly increased in 300 and 500 mM NaCl treated roots at 1, 4 and 8 DAS with respect to the controls (Fig. 4K–S). Surprisingly, high intensity of sodium specific fluorescence was observed in the vacuolar region of salt-treated plants. The profile distribution of Na^+ between cytosol and vacuole in roots of control and salt-treated plants was shown in Fig. 4T. The cytosolic Na^+ intensity was slightly changed in the 300 and 500 mM NaCl treated roots. However, the vacuolar Na^+ intensity was significantly increased in 300 and 500 mM NaCl treated roots at 1, 4 and 8 DAS.

Characteristic magenta-pink color of lignin from phloroglucinol-HCl was observed across all cross-sections of leaves and roots of control and

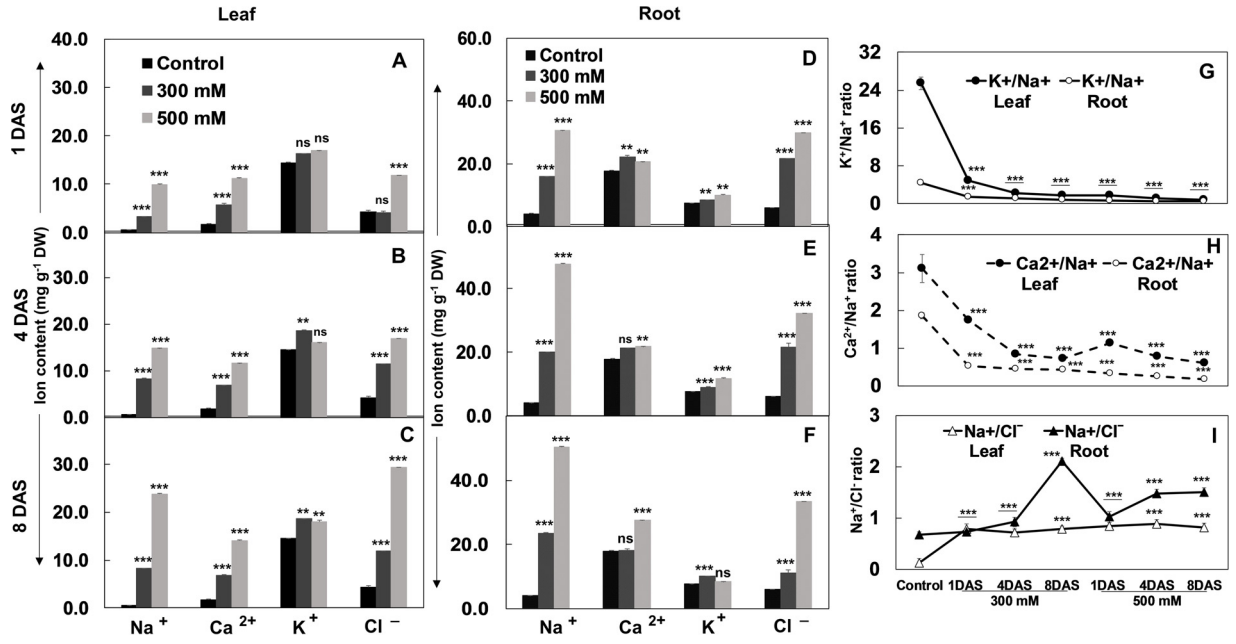

Fig. 3. Sodium, calcium, potassium and chloride ion content in leaves of 0 (control), 300 and 500 mM NaCl treated plants at (A) 1 DAS, (B) 4 DAS and (C) 8 DAS and in roots of 0 (control), 300 and 500 mM NaCl treated plants at (D) 1 DAS, (E) 4 DAS and (F) 8 DAS respectively. Variations in the ratios of K^+/Na^+, Ca^{2+}/Na^+ and Na^+/Cl–in the leaves and roots of control and salt-treated plants (G–I). Error bar represents the mean ± SD (n = 6).

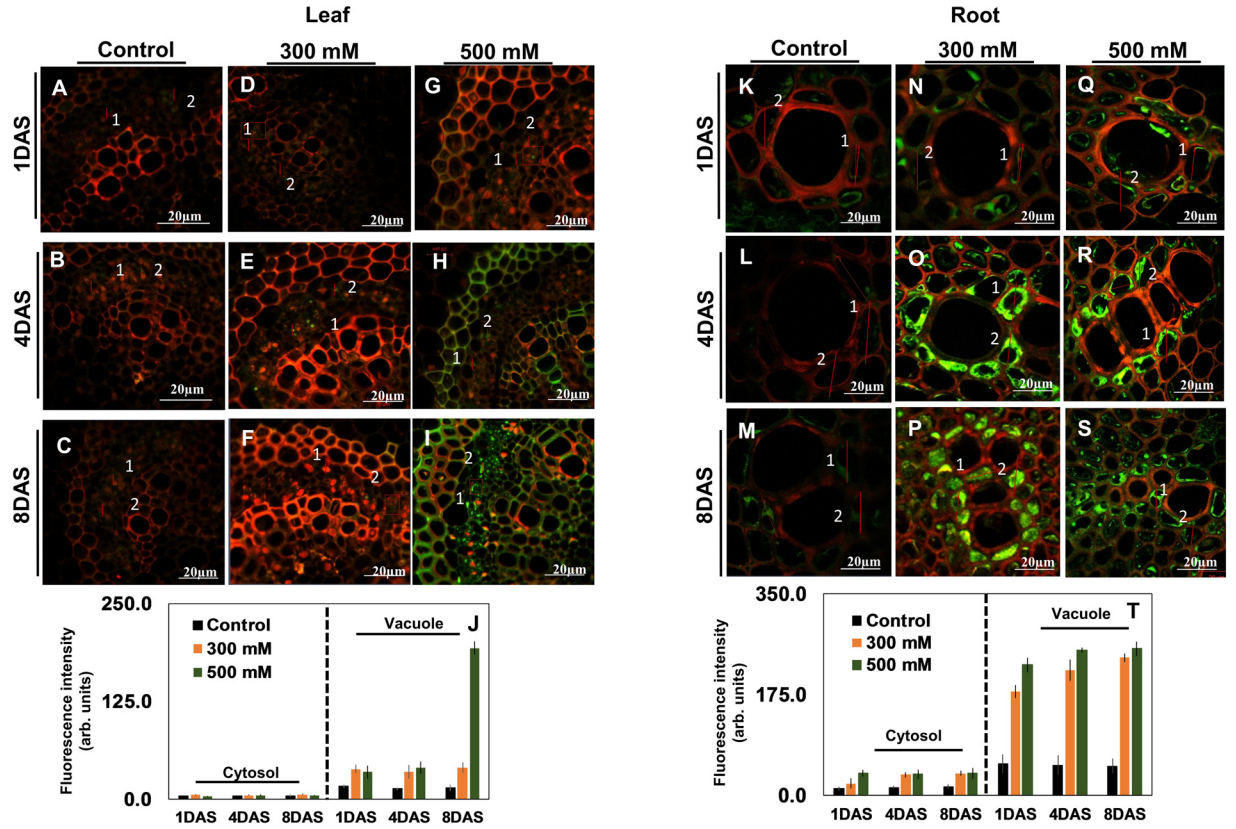

Fig. 4. CLSM localization of Na^+ ions using Na^+ specific Coro Na-Green AM (green) and cell-wall binding propidium iodide (red) stains. Leaf sections from control plants (A–C), 300 mM NaCl (D–F) and 500 mM NaCl treated plants (G–I) at 1, 4 and 8 DAS. Intensity of CoroNa-Green AM fluorescence in cytosolic and vacuolar compartments in the leaf sections (J). Root sections of control plants (K–M), 300 mM NaCl (N–P) and 500 mM NaCl treated plants (Q–S) 1, 4 and 8DAS. Intensity of CoroNa-Green AM fluorescence in cytosolic and vacuolar compartments in the root sections (T). Red lines were drawn to measure Na^+ fluorescence intensity. For quantification of Na^+ fluorescence intensity more than 20 images were pooled from five biological replicates in control and salt-treated plants. Error bar represents the mean ± SD (n = 20).

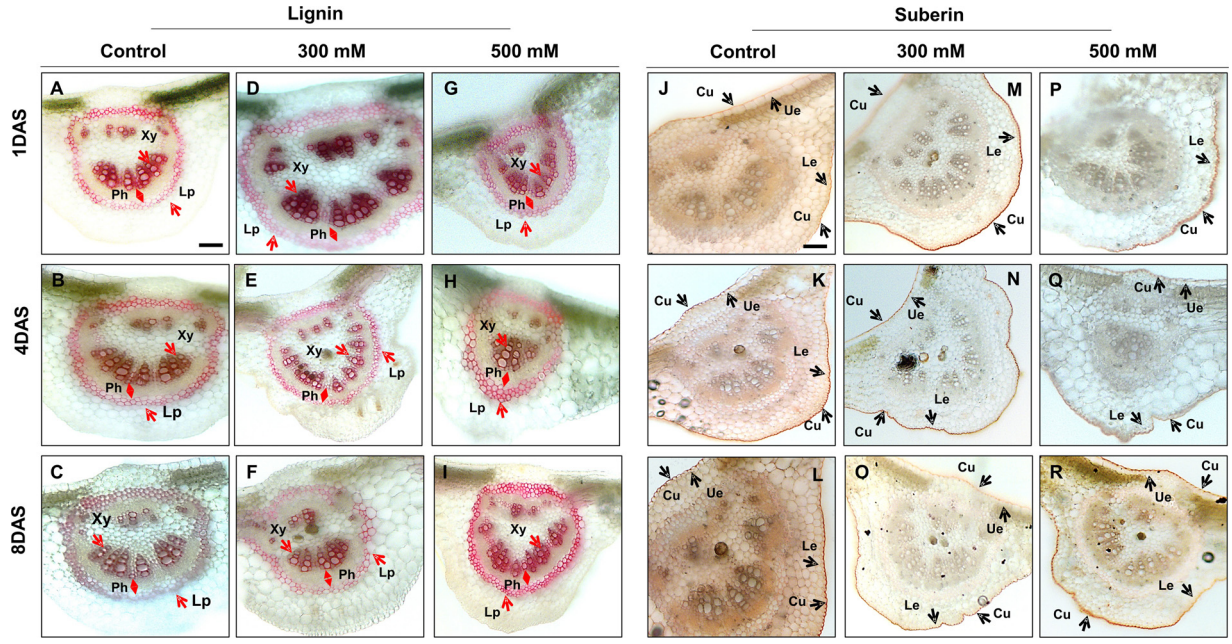

Fig. 5. Histochemical detection of lignin and suberin content in leaves of *P. pinnata*. For lignin visualization, sections were stained with HCl-phloroglucinol. Leaf sections of control (A–C) 300 mM (D–F) and 500 mM NaCl (G–I) treated plants at 1, 4 and 8 DAS, respectively. For suberin visualization, sections were stained with Sudan III. Leaf sections of control (J–L), 300 mM (M–O) and 500 mM NaCl (P–R) treated plants at 1, 4 and 8 DAS. Red arrows indicate lignin deposition and black arrows indicate suberin deposition. Cu: cuticle, Ue: upper epidermis, Xy: xylem, Ph: phloem, Lp: lignified parenchyma, Le: lower epidermis. Scale bars =100 μm.

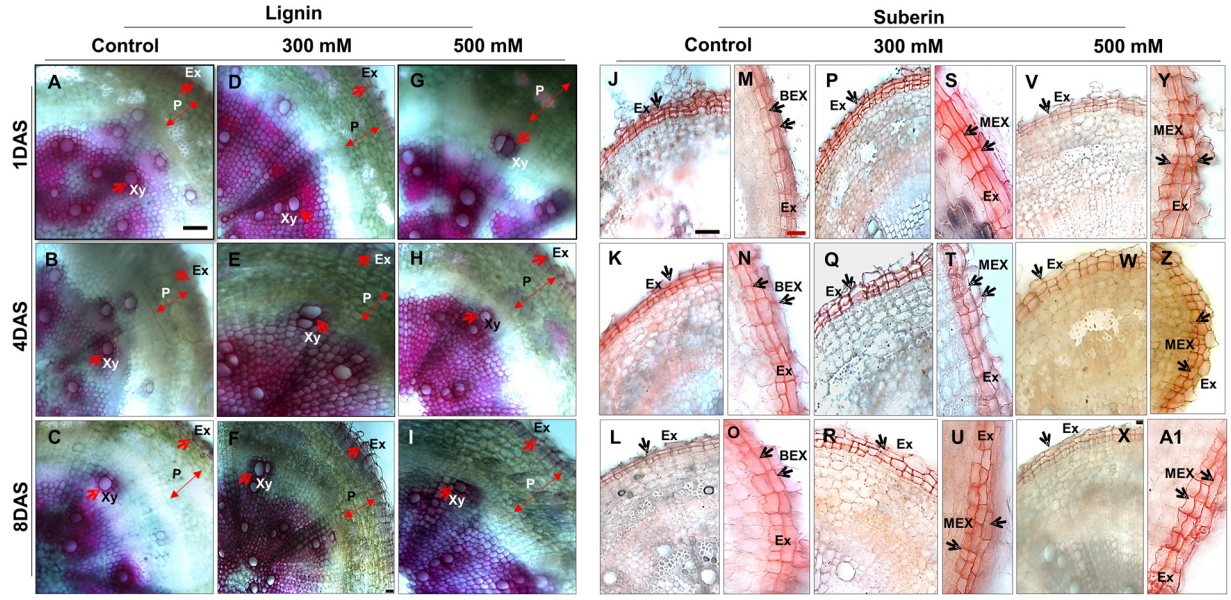

Fig. 6. Histochemical detection of lignin and suberin content in roots *P. pinnata*. Staining was done similar to leaf sections explained previously. Lignin visualization in the root sections of control (A–C) 300 mM (D–F) and 500 mM NaCl (G–I) treated plants at 1, 4 and 8 DAS, respectively. Suberin visualization in the root sections of control (J–O), 300 mM (P–U) and 500 mM NaCl (V-A1) treated plants at 1, 4 and 8 DAS. Red arrows indicate lignin deposition and black arrows indicate suberin deposition. Ex: exodermis, P: phloem-enriched fraction, Xy: xylem, BEX: biseriate exodermis, MEX: multiseriate exodermis. Bars: black bars equivalent to 100 μm and red bars equivalent to 50 μm.

salt-treated plants (Figs. 5 and 6). In leaves, under control conditions lignin deposition was faint in both lipid-parenchyma and xylem vessels of the vascular tissue at 1, 4 and 8 DAS (Fig. 5A–C). In treated leaves, lignification of xylem cells was slightly increased in 300 and 500 mM NaCl treatment at 1, 4 and 8 DAS. Further, a lignified layer of lipid-parenchyma cells increased across the leaf axis in both 300 and 500 mM NaCl treatment at 1, 4 and 8 DAS (Fig. 5D–I). Sudan III staining was used to detect the suberin deposition across the cross-sections of leaves and roots of control and salt-treated plants. Similar pattern of suberin deposition was observed in control and salt-treated leaves at 1, 4 and 8 DAS (Fig. 5J–R).

In roots, under control and salt-treated conditions magenta-pink color staining was detected in the cortical cells or xylem cells of 300 and 500 mM NaCl treatment at 1, 4 and 8 DAS (Fig. 6A–I). However, lignification gradually increased in the cortical cells or xylem cells of 300 and 500 mM NaCl treated roots at 1, 4 and 8 DAS (Fig. 6D–I). Also, a thin uniform suberized bilayer exodermis (biseriate exodermis (BEX)) was seen at 1, 4 and 8 DAS (Fig. 6J–O). Interestingly, a continuous band of suberized exodermis (multiseriate exodermis (MEX)) in salt-treated plants was recorded. The cells of BEX and MEX showed thick layer of

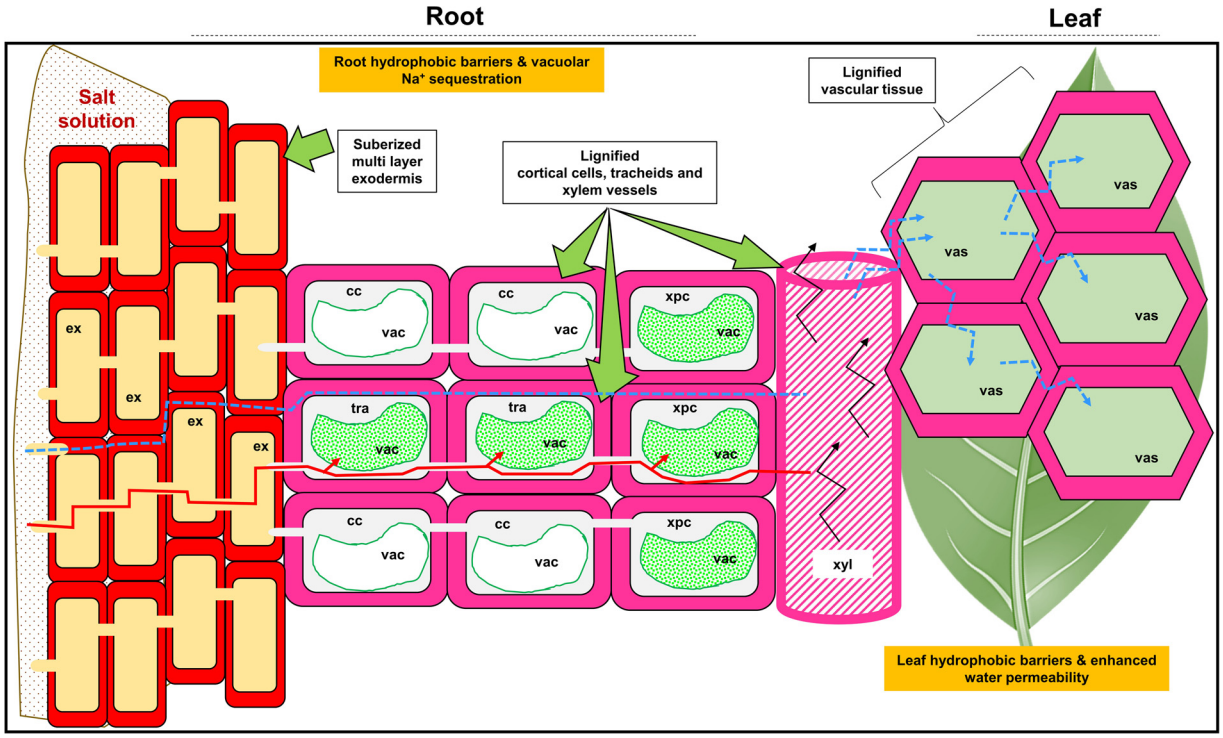

Fig. 7. Our proposed model based to show the mechanism of high salinity tolerance in *Pongamia pinnata*. Suberized multiseriate exodermis and lignified walls of xylem vessels, cortical cells, tracheids of root and lignified vascular tissues of leaf are represented. Red line and red arrows: symplastic water and Na^+ transport through cytosol to enhance the Na^+ ion sequestration into the vacuoles of tracheids and xylem parenchyma cells; blue dashed lines: apoplastic water and Na^+ transport through suberized and lignified cell walls to reduce the excess deposition of Na^+ ions in the cytosol of leaf and root cells. Black arrows: water and solute transport though xylem vessels. Red color: suberin lamellae; pink color: cells with lignin deposition; green spots: vacuoles with Na^+ ions; white region with green border: empty vacuole. Abbreviations: vac, vacuole; ex, exodermis; cc, cortical cells; tra, tracheids; xyl, xylem vessel; xpc, xylem parenchyma cells; vas, vascular tissues.

suberin deposition in 300 (Fig. 6P–U) and 500 mM NaCl treated plants at 1, 4 and 8 DAS (Fig. 7V–A1).

4. Discussion

4.1. Pongamia adapts to high salinity conditions through physiological adjustments

Pongamia exhibited a remarkable tolerance to salinity stress which is comparable with other established halophytes. Salt-treated hydroponically grown Pongamia seedlings displayed no salt-stress induced symptoms such as wilting, yellowed leaves, leaf tip burning, chlorosis or necrosis in leaves till 8 days treatment indicating a strong adaptive mechanism to combat salinity induced oxidative stress and ionic imbalance (Shabala and Mackay, 2011) (Fig. 1). Exposure of Pongamia to high salinity resulted in a significant decrease stomatal conductance (g_s), photosynthetic rate at saturating light conditions (A_{sat}), and transpiration rates (E) (Fig. 2). The pattern of gas exchange rates was similar to our previously reported ones on soil grown Pongamia (Marriboina et al., 2017). Salinity can cause osmotic stress and minimize water uptake by roots resulting reduced A_{sat} and E. Water use efficiency (WUE) increased substantially in salt-treated Pongamia seedlings (Fig. 1D). The higher WUE improves the level of salt tolerance since high WUE can reduce the salt uptake by roots and substantiate the water deficiency caused by salinity (He et al., 2009). Plants have developed various mechanisms to improve the RWC in order to withstand ion and osmotic imbalance caused by osmotic stress (Shabala, 2013). The reduced RWC as shown in this study is relatively a rapid adaptive strategy, which might allow the plants to accumulate the selective cations and compatible solutes to maintain cell or tissue turgor under high salinity stress (Negrão et al., 2017).

The Fv/Fm levels were not changed significantly in 300 mM NaCl treated leaves (Fig. 2G) which results suggest that photoinhibition was not triggered. Although the maximum quantum yields of PSII did not change significantly, the ETR and qP levels in 300 mM NaCl treated leaves were progressively decreased as the time of salt exposure increased (Supplementary Fig. S1). The observed increase in the quantum yields of non-photochemical energy loss of PSII (NPQ and qN) might protect the photosynthetic apparatus against photodamage (Moradi and Ismail, 2007; Netondo et al., 2004). However, the leaves of 500 mM NaCl treatment showed a significant reduction in Fv/Fm at 4 and 8DAS, but these levels remained unchanged at 1DAS. After prolonged exposure of 500 mM NaCl stress YII, NPQ, and YNPQ levels also showed a concomitant decline. In addition, decreased levels of Fv/Fm led to the gradual decrease in the efficiency of photochemical quenching (qP) and relative electron transport rate (ETR). Similar results were reported by Zhou et al. (2018) in privet seedlings were treated with lead. The observed decline in chl*a* fluorescence parameters and increased levels of YNO could be the result of salt-induced irreversible damage to photosynthetic machinery (Maxwell and Johnson, 2000). As seedlings showed no morphological and as well as well-maintained chlorophyll pigments (Fig. 2I), it was unlikely that the photosynthetic machinery was damaged (Marriboina et al., 2017; Santos et al., 2015). Further, the increased levels of qN may substantiate the photo-damage caused by non-regulated energy dissipation (YNO) through a lutein dependent process (Santos et al., 2015).

4.2. Salinity induced increase in Ca^{2+} and K^+ ions in roots of salt-treated P. pinnata effectively retained Na^+ and Cl^- ions in root tissues and restricted their entry into leaf tissues

Atomic emission spectroscopy and titrimetric based quantification

of Na^+, K^+, Ca^{2+}, and Cl^- reveals that salt treated leaves and roots of *P. pinnata* showed different pattern of ion accumulation across all time points. The Na^+ and Cl^- contents were significantly increased in both leaves and roots of salt-treated plants (Fig. 3A–F). Our results showed that the levels of Na^+ and Cl– were significantly higher in roots than in leaves as well as maintenance of high Na^+/Cl^- ratio in roots than in leaves (Fig. 3I), suggesting that roots were actively involved in the ion sequestration in order to reduce the salt-induced toxic effect on areal parts of the plant (Wu et al., 2018; Marriboina et al., 2017). Initial exposure of 300 mM NaCl treatment did not induce the K^+ content significantly in the leaves, while these levels significantly increased at 4 and 8DAS. In contrast, 500 mM NaCl treated leaves showed significant increase only at 8DAS. Further, content in roots K^+ showed significant increase in 500 mM NaCl treatment across all time points as well as in 300 mM NaCl treated roots at 1DAS. In general, high level of Na^+ inhibits the uptake of K^+ ion which results in growth impairment and may even lead to death of the plant (Gupta and Huang, 2014). The observed increase in K^+ content with an accompanying increase in Na^+ content in both leaves and roots enhances salt tolerance in *P. pinnata*. In addition, the steady-state increase of K^+ content in 500 mM NaCl treated roots with treatment time could be either due to increased magnitude of the NaCl-induced K^+ influx or decreased efflux of K^+ across cell and vacuolar membranes (Shabala et al., 2007). The results suggest that the increase in the K^+ level may be crucial to maintain osmoregulation caused by excess accumulation of Na^+ in the vacuole which in turn regulates cytosolic enzyme activity and protein stability under high salinity conditions (Hasanuzzaman et al., 2018). Low K^+/Na^+ ratio under salt stress indicates low selectivity for K^+ in the presence of high NaCl concentration (Fig. 3G) (Taha et al., 2000). The fact that K^+ is essential for the growth and survival of the plant raises, the question how *P. pinnata* and other salt-tolerant plant species cope along with low K^+/Na^+ and maintain ion balance under high salinity stress. A possible way to answer is possible existence of strong adaptive mechanisms to compensate the low retention of K^+ in both leaves and roots under high salinity stress. In addition, the accumulation and compartmentation of Na^+ in the vacuole is energetically more efficient as compared with K^+ accumulation to maintain high K^+/Na^+ in the plant tissues under high salinity condition (Taha et al., 2000; Yeo, 1983). Similarly, Ca^{2+} levels were significantly increased in both leaves and roots of salt-treated plants across all time points, while these levels did not show any significant change in 500 mM NaCl treated roots at 8DAS. Calcium is well known for its role in maintaining structural and functional integrity plant cell membranes, stabilizes cell wall and cellular structures regulates ion transport across cell membrane and act as an intracellular second messenger under salt stress condition (Hadi and Karimi, 2012; Shabala et al., 2006). Further, the enhanced uptake of Na^+ into the vacuole conceals the significant increase in the Ca^{2+} levels resulting low Ca^{2+}/Na^+ ratio in both leaves and roots of Pongamia (Chowdhury et al., 2018; Koksal et al., 2016). However, the plants with low Ca^{2+}/Na^+ ratio showed no morphological stress symptoms with respect to the controls (Fig. 3H) and it was unlikely that the cellular integrity and cell wall structures were damaged. Further, the transient increase in Ca^{2+} levels of salt-treated plants might help the plant activating its salinity adaptive signaling pathways as well as the oxidative stress protective enzymes under salinity conditions (Hadi and Karimi, 2012).

4.3. Roots of salt treated P. pinnata effectively sequestered Na^+ ions

Similar to our previous results (Marriboina et al., 2017), the salt-treated Pongamia leaves showed a consistent high intensity staining of the central vascular bundle region, while control leaves did not change in its Na^+ specific fluorescence across all time points (Fig. 4A–C). In addition, a high intensity of green fluorescence was observed in the cell walls (apoplastic region) of 500 mM NaCl treated leaves of Pongamia at 4 and 8DAS, which is due to increased accumulation of Na^+ ions in the apoplast. The results suggest that the higher accumulation of Na^+ ions may increase the availability of cation-binding groups in the cell wall matrix to enhance the apoplastic based Na^+ sequestration, which may act as an additional barrier to existing vacuolar Na^+ sequestration in order to protect the plant cellular integrity from Na^+ toxicity (Byrt et al., 2018). In this study, we investigated the distribution of Na^+ between the cytosol and the vacuole in control and salt-treated leaves of *P. pinnata* at 1, 4 and 8DAS. Interestingly, we could observe high vacuolar Na^+ intensity in 500 mM NaCl treated leaves only at 8DAS, while cytosolic Na^+ intensity did not change significantly in both 300 and 500 mM NaCl treated leaves across all time points (Fig. 4J). From the above observation, we infer that the small amount of sodium which escaped root barrier and reached salt-treated leaves, is actively sequestered into the vacuole and cell wall matrix (apoplastic region) to attain structural and functional integrity of photosynthetic machinery under high salinity (Marriboina et al., 2017). The CoroNa-Green intensity increased with increasing salt concentration in both 300 and 500 mM NaCl treated roots (Fig. 4N–S). Further, the xylem companion cells which are surrounded by xylem vessel exhibited high levels of Na^+ specific fluorescence across the cross sections of both 300 and 500 mM NaCl treated roots, while the Na^+ specific fluorescence intensity level of adjacent cortical cells remain similar to that of controls. The data suggest that the xylem parenchyma cells (XPCs) might act as Na^+ ion specific filter barrier which restricts the entry of excess Na^+ ions (transported across the root either by symplastic or apoplastic origin) to the aerial parts of the plant. These very well corresponded with the observed dry weight-based Na^+ ion content that the roots accumulated more Na^+ than leaves. Further, intracellular Na^+ ion distribution pattern of Na^+ ions was investigated in the XPCs of both control and salt-treated roots. The vacuolar Na^+ intensity of XPCs was significantly higher in roots of both 300 and 500 mM NaCl treated plants, while the cytosolic Na^+ intensity was remained unchanged (Fig. 4T). The Na^+ vacuolar sequestration and low cytosolic Na^+ content in the XPCs might favor the uptake of Na^+ ions from the xylem vessel, as the observation showed that the vacuolar Na^+ intensity increased with salt treatment time. The absence of propidium iodide-stained cells across the cross-sections of leaves and roots of salt-treated plants suggest that the structural and functional integrity of cell and cellular components were well maintained even under high salt condition (Oh et al., 2010).

4.4. Salinity induced multiseriate exodermis/hydrophobic barrier formation in the roots of P. pinnata effectively enhanced the leaf and root water permeability and vacuolar Na^+ sequestration

Lack of morphological salt-induced stress symptoms, low Na^+ content in the salt-treated leaves and unchanged root relative water content led us to examine the development of hydrophobic barriers in leaves and roots, which have been shown to restrict the ion uptake and water transport in some plants (Krishnamurthy et al., 2014). In this study, the structural development of exodermal layers of leaves and roots in *P. pinnata* were recorded. In roots, we could observe increased pattern of suberization in both 300 and 500 mM NaCl treated roots across all time points (Fig. 6J–A1). Suberin is a complex biopolymer with a polyaliphatic domain that forms hydrophobic barriers in exodermis and endodermis, which mediates the symplastic transportation by regulating the unregulated apoplastic by flow of water and solutes. Enhanced deposition of suberin in the exodermis as evidenced in the roots result decreased uptake of Na^+ into shoot and increased retention of water in root under salinity stress. The results also corresponded with unchanged RWC content of root and low Na^+ ion content in leaves of 300 and 500 mM NaCl treatment. Interestingly, a third suberized multiseriate or multilayer exodermis (MEX) was formed periclinally to the existing biseriate or bilayer exodermis (BEX) in the salt-treated roots of *P. pinnata* across all time points, while control roots did not exhibit MEX across all time points. Such multiseriate exodermis formation was reported in *Iris germanica* in response to varying environmental

conditions, which restrict water and solute transport through apoplasmic route (Meyer et al., 2011). To the best our knowledge, this is the first study reporting on the identification of salt-induced multilayered exoderm in this species. Moreover, at anatomical level, though we could not observe significant changes in suberization pattern between the cross sections of control and salt-treated leaves (Fig. 5J–R), the cellular integrity of both 300 and 500 mM NaCl treated leaves was well maintained as similar to that of respective controls.

Histological cross sections of leaves and roots showed that salt-treated plants showed high lignification of xylem vessels, XPCs and cortical cells with respect to controls across all time points. Increased salinity also resulted in number of lignified cells in xylem vessels, XPCs, and tracheids in the roots of Pongamia at all-time points (Fig. 6A–I). Presumably, this increased in the number lignified tracheids, xylem vessels and its XPCs is an adaptive strategy to high salinity stress aiming to restrict the Na^+ uptake through apoplastic flow as well as enhance the cell-to-cell pathway for water transport (Neves et al., 2010; Sánchez-Aguayo et al., 2004). Further, the numbers of tracheary elements in the vascular bundle of NaCl treated leaves were increased with increasing treatment time. Under salinity stress, the occurrence of high lignin content in the cell wall not only decreased the excess ion accumulation in the plant but also reduced the water uptake by several folds. The abundance of lignified xylem vessels may compensate for the salt-induced reduction in water uptake (Sánchez-Aguayo et al., 2004).

In conclusion, the absence of salt-induced symptoms on leaves, decline in the leaf photosynthetic parameters and continuous increase in the regulated heat dissipation of PSII confer salinity adaptive mechanisms in *P. pinnata*. Further, increased Ca^{2+} and K^+ minimizes the salt-induced damage in leaves and roots. Higher Na^+ content in the roots than leaves also revealed that Pongamia roots act as ultra-filters/strong barriers to protect the leaves from Na^+ toxicity. The Na^+ probe fluorescence data reveals the existence of vacuolar Na^+ sequestration mechanism in the root and the confinement of Na^+ specific fluorescence to certain cells such as tracheid cells and xylem parenchyma showing the strong salinity tolerance mechanisms effectively operating in the roots of *P. pinnata*. At the anatomical level, formation of salt-induced suberized multiseriate exodermis in the roots and a greater deposition of lignin maximize the water permeability leaves and roots (in Fig. 7 Our proposed model). In addition, suberin and lignin synthesis effectively operate in the roots and leaves to contribute towards the high salinity tolerance of *P. pinnata*. Our results highlight the key mechanisms conferring high salt tolerance in Pongamia, which can be highly crucial for further research to develop Pongamia as a tolerant and sustainable biofuel tree crop.

Funding

This work is supported by the Department of Biotechnology [BT/PR12024/BCE/8/1097/2014], India.

Author statement

In the present study, we have carried out an extensive experimental analysis on the mechanisms conferring high salinity tolerance in *Pongamia pinnata*, a potential biofuel tree species. A combination of physiological, biochemical, anatomical and molecular level analyses was carried out on hydroponically grown 30-day old *P. pinnata* seedlings, which were treated with two different salt concentrations (300 mM NaCl and 500 mM NaCl) and investigated systematically at regular time intervals after salt exposure. Our data clearly highlighted that the formation of hydrophobic cell wall barriers and effective vacuolar sequestration of Na^+ ions in the roots are among the key mechanisms conferring high salinity tolerance in Pongamia.

Declaration of Competing Interest

Authors have no conflicts of interest to declare.

Acknowledgment

This research was supported by the project grant (BT/PR-12024/BCE/8/1097/2014) from Department of Biotechnology, Govt. of India. We gratefully acknowledge Tree Oil India Ltd. (TOIL), Zaheerabad, Telangana State, India for providing Pongamia seed (TOIL12). We thank Dr. Debashree Sengupta, for helpful discussions. SM acknowledges University Grant Commission (UGC), New Delhi, India for fellowships.

Appendix A. Supplementary data

Supplementary material related to this article can be found, in the online version, at doi:https://doi.org/10.1016/j.envexpbot.2019.103949.

References

Arnon, D., 1949. Copper enzymes isolated chloroplasts, polyphenoloxidase in Beta vulgaris. Plant Physiol. 24, 1–15.
Byrt, C.S., Munns, R., Burton, R.A., Gilliham, M., Wege, S., 2018. Root cell wall solutions for crop plants in saline soils. Plant Sci. 269, 47–55.
Chen, C.L., van der Schoot, H., Dehghan, S., Alvim Kamei, C.L., Schwarz, K.U., Meyer, H., Visser, R.G.F., van der Linden, G.C., 2017. Genetic diversity of salt tolerance in Miscanthus. Front. Plant Sci. 8, 187.
Chhetri, A.B., Tango, M.S., Budge, S.M., Watts, K.C., Islam, M.R., 2008. Non-edible plant oils as new sources for biodiesel production. Int. J. Mol. Sci. 9, 169–180.
Chowdhury, M.A.H., Bhuyia, M.S.R., Shah-e-Alam, M., Azad, M.A.K., 2018. Low Ca^{2+} content and Ca^{2+}/Na^+ ratio in leaf tissues determine salinity tolerance in spanish type groundnut (*Arachishypogeal* L.). J. Agr. Sci. Tech. B 8, 71–84.
Gharsallah, C., Fakhfakh, H., Grubb, D., Gorsane, F., 2016. Effect of salt stress on ion concentration, proline content, antioxidant enzyme activities and gene expression in tomato cultivars. AoB Plants 8, plw055.
Gupta, B., Huang, B., 2014. Mechanism of salinity tolerance in plants: physiological, biochemical, and molecular characterization. Int. J. Genome 1–18.
Hadi, M.R., Karimi, N., 2012. The role of calcium in plants' salt tolerance. J. Plant Nutr. 35, 2037–2054.
Hasanuzzaman, M., Bhuyan, H.M., Nahar, K., Hossain, S.M., Mahmud, A.J., Hossen, S.M., Masud, A.A.C., Moumita, Fujita, M., 2018. Potassium: a vital regulator of plant responses and tolerance to abiotic stresses. Agronomy 8, 1–29.
He, Y., Zhu, Z., Yang, J., Ni, X., Zhu, B., 2009. Grafting increases the salt tolerance of tomato by improvement of photosynthesis and enhancement of antioxidant enzymes activity. Environ. Exp. Bot. 66, 270–278.
Jiang, G.F., Goodale, U.M., Liu, Y.Y., Hao, G.Y., Cao, K.F., 2017. Salt management strategy defines the stem and leaf hydraulic characteristics of six mangrove tree species. Tree Physiol. 37, 389–401.
Jones, M.B., Finnan, J., Hodkinson, T.R., 2014. Morphological and physiological traits for higher biomass production in perennial rhizomatous grasses grown on marginal land. Glob. Change Biol. Bioen. 7, 375–385.
Koksal, N., Alkan-Torun, A., Kulahlioglu, I., Ertargin, E., Karalar, E., 2016. Ion uptake of marigold under saline growth conditions. SpringerPlus 5, 139.
Krishnamurthy, K.V., 1999. Light Microscopic Cytochemistry: Methods in Cell Wall Cytochemistry. CRC Press, Florida.
Krishnamurthy, P., Jyothi-Prakash, P.A., Qin, L., He, J., Lin, Q., Loh, C.S., Kumar, P.P., 2014. Role of root hydrophobic barriers in salt exclusion of a mangrove plant Avicennia officinalis. Plant Cell Environ. 37, 1656–1671.
Li, H., Chang, J., Chen, H., Wang, Z., Gu, X., Wei, C., Zhang, Y., Ma, J., Yang, J., Zhang, X., 2017. Exogenous melatonin confers salt stress tolerance to watermelon by improving photosynthesis and redox homeostasis. Front. Plant Sci. 8, 295.
Marriboina, S., Sengupta, D., Kumar, S., Reddy, A.R., 2017. Physiological and molecular insights into the high salinity tolerance of *Pongamia pinnata* (L.) Pierre, a potential biofuel tree species. Plant Sci. 258, 102–111.
Maxwell, K., Johnson, G.N., 2000. Chlorophyll fluorescence-a practical guide. J. Exp. Bot. 51, 659–668.
Meyer, C.J., Peterson, C.A., Steudle, E., 2011. Permeability of *Iris germanica*'s multiseriate exodermis to water, NaCl, and ethanol. J. Exp. Bot. 62, 1911–1926.
Moradi, F., Ismail, A.M., 2007. Responses of photosynthesis, chlorophyll fluorescence and ROS-scavenging systems to salt stress during seedling and reproductive stages in rice. Ann. Bot. 99, 1161–1173.
Munns, R., Gilliham, M., 2015. Salinity tolerance of crops–what is the cost? New Phytol. 208, 668–673.
Munns, R., Wallace, P.A., Teakle, N.L., Colmer, T.D., 2010. Measuring Soluble Ion Concentrations (Na+, K+, Cl−) in Salt-treated Plants. Plant Stress Tolerance: Methods in Molecular Biology (Methods and Protocols). Humana Press, U. S. A.
Negrão, S., Schmöckel, S.M., Tester, M., 2017. Evaluating physiological responses of

plants to salinity stress. Ann. Bot. 119, 1–11.
Netondo, G.W., Onyango, J.C., Beck, E., 2004. Sorghum and salinity: II. Gas exchange and chlorophyll fluorescence of sorghum under salt stress. Crop Sci. 44, 806–811.
Neves, G.Y.S., Marchiosi, R., Ferrarese, M.L.L., Siqueira-Soares, R.C., Ferrarese-Filho, O., 2010. Root growth inhibition and lignification induced by salt stress in soybean. J. Agron. Crop Sci. 196, 467–473.
Oh, D.H., Lee, S.Y., Bressan, R.A., Yun, D.J., Bohnert, H.J., 2010. Intracellular consequences of SOS1 deficiency during salt stress. J. Exp. Bot. 61, 1205–1213.
Oh, D.H., Leidi, E., Zhang, Q., Hwang, S.M., Li, Y.Z., Quintero, F.J., Jiang, X., D´Urzo, M.P., Lee, S.Y., Zhao, Y., Bahk, J.D., Bressan, R.A., Yun, D.J., Pardo, J.M., Bohnert, H.J., 2009. Loss of halophytism by interference with SOS1 expression. Plant Physiol. 151, 210–222.
Pandolfi, C., Bazihizina, N., Giordano, C., Mancuso, S., Azzarello, E., 2016. Salt acclimation process: a comparison between a sensitive and a tolerant *Olea europaea* cultivar. Tree Physiol. 37, 380–388.
Papazian, S., Khaling, E., Bonnet, C., Lassueur, S., Reymond, P., Moritz, T., Blande, J.D., Albrectsen, B.R., 2016. Central metabolic responses to ozone and herbivory affect photosynthesis and stomatal closure. Plant Physiol. 172, 2057–2078.
Parida, A.K., Jha, B., 2010. Salt tolerance mechanisms in mangroves: a review. Trees 24, 199–217.
Quinn, L.D., Straker, K.C., Guo, J., Kim, S., Thapa, S., Kling, G., Lee, D.K., Voigt, T.B., 2015. Stress tolerant fee stocks for sustainable bioenergy production on marginal land. Bioenergy Res. 8, 1081–1100.
Sánchez-Aguayo, I., Rodriguez-Galan, J.M., García, R., Torreblanca, J., Pardo, J.M., 2004. Salt stress enhances xylem development and expression of S-adenosyl-methionine synthase in lignifying tissues of tomato plants. Planta 220, 278–285.
Santos, R.W., Schmidt, É.C., Vieira, I.C., Costa, G.B., Rover, T., Simioni, C., Barufi, J.B., Soares, C.H.L., Bouzon, Z.L., 2015. The effect of different concentrations of copper and lead on the morphology and physiology of *Hypnea musciformis* cultivated in vitro: a comparative analysis. Protoplasma 252, 1203–1215.
Shabala, L., Zhang, J., Pottosin, I., Bose, J., Zhu, M., Fuglsang, A.T., Buendia, A.V., Massart, A., Hill, C.B., Roessner, U., Bacic, A., Wu, H., Azzarello, E., Pandolfi, C., Zhou, M., Poschenrieder, C., Mancuso, S., Shabala, S., 2016. Cell-type-specific H^+-ATPase activity in root tissues enables K^+ retention and mediates acclimation of barley (*Hordeum vulgare*) to salinity stress. Plant Physiol. 172, 2445–2458.
Shabala, S., 2013. Learning from halophytes: physiological basis and strategies to improve abiotic stress tolerance in crops. Ann. Bot. 112, 1209–1221.
Shabala, S., Mackay, A., 2011. Ion transport in halophytes. Adv. Bot. Res. 57, 151–199.
Shabala, S., Cuin, T.A., Pottosin, I., 2007. Polyamines prevent NaCl-induced K^+ efflux from pea mesophyll by blocking nonselective cation channels. FEBS Lett. 581, 1993–1999.
Shabala, S., Demidchik, V., Shabala, L., Cuin, T.A., Smith, S.J., Miller, A.J., Davies, J.M., Newman, I.A., 2006. Extracellular Ca^{2+} ameliorates NaCl-induced K^+ loss from *Arabidopsis* root and leaf cells by controlling plasma membrane K^+-permeable channels. Plant Physiol. 141, 1653–1665.
Sharma, R., Wungrampha, S., Singh, V., Pareek, A., Sharma, M.K., 2016. Halophytes as bioenergy crops. Front. Plant Sci. 7, 1372.
Taha, R., Mills, D., Heimer, Y., Tal, M., 2000. The relation between low K^+/Na^+ ratio and salt tolerance in the wild tomato species *Lycopersicon pennellii*. J. Plant Physiol. 157, 59–64.
Wang, H., Hu, T., Huang, J., Lu, X., Huang, B., Zheng, Y., 2013. The expression of *Millettia pinnata* chalcone isomerase in *Saccharomyces cerevisiae* salt-sensitive mutants enhances salt-tolerance. Int. J. Mol. Sci. 14, 8775–8786.
Wang, L., Mu, M., Li, X., Lin, P., Wang, W., 2011. Differentiation between true mangroves and mangrove associates based on leaf traits and salt contents. J. Plant Ecol. 4, 292–301.
Wu, H., Shabala, L., Azzarello, E., Huang, Y., Pandolfi, C., Su, N., Wu, Q., Cai, S., Bazihizina, N., Zhou, L.W.M., Mancuso, S., Chen, Z., Shabala, S., 2018. Na^+ extrusion from the cytosol and tissue-specific Na^+ sequestration in roots confer differential salt stress tolerance between durum and bread wheat. J. Exp. Bot. 69, 3987–4001.
Yeo, A.R., 1983. Salinity resistance: physiologies and prices. Physiol. Plant. 58, 214–222. https://doi.org/10.1111/j.1399-3054.1983.tb04172.x.
Zhou, J., Zhang, Z., Zhang, Y., Wei, Y., Jiang, Z., 2018. Effects of lead stress on the growth, physiology, and cellular structure of privet seedlings. PLoS One 13, e0191139.

MethodsX 7 (2020) 100809

Contents lists available at ScienceDirect

MethodsX

journal homepage: www.elsevier.com/locate/mex

Method Article

Optimization of hydroponic growth system and Na^+-fluorescence measurements for tree species *Pongamia pinnata* (L.) pierre

Sureshbabu Marriboina, Ramachandra Reddy Attipalli*

Department of Plant Sciences, School of Life Sciences, University of Hyderabad, Hyderabad 500046, Telangana, India

A B S T R A C T

Domestication and cultivation of tree species, such as *Pongamia pinnata* is quite important because of its biofuel properties. Seedlings grown in modified hydroponic culture were morphologically similar to that of soil grown seedlings. Further, seedlings were allowed to grow without root limitation. Comparatively, our modified hydroponic growth system can be performed with minimal resources. Prior incubated root segments with CoroNa-Green AM dye retained maximum amount of dye when compared to CoroNa-Green AM dye incubated sections. Our modified protocol provides quantitative analysis of 2D and 3D imaging process at cellular and sub-cellular level.

- Our protocol is customized to study individual plant behavior.
- Additionally, it is customized for growing tap rooted trees species hydroponically. Changing the nutrient solution with regular intervals provides continuous supply of nutrients to the plants.
- Prior incubation of root segments with Na^+ probe (CoroNa-Green AM) provides better resolution in imaging process. Additionally, both 2D and 3D imaging provides a means to acquire and analyze entirety of the sample.

A R T I C L E I N F O

Method name: Hydroponic cultivation of tree species *Pongamia pinnata* (L.) pierre and Na^+-fluorescence measurements
Keywords: CoroNa-Green AM dye, Na^+ fluorescence intensity, Plant growth, Propidium iodide, Salt stress, Z-stack
Article history: Received 16 December 2019; Accepted 29 January 2020; Available online 20 February 2020

DOI of original article: 10.1016/j.envexpbot.2019.103949

* Corresponding author.
E-mail address: arrsl@uohyd.ernet.in (R.R. Attipalli).

https://doi.org/10.1016/j.mex.2020.100809

Specification Table

Subject Area:	Environmental Science
More specific subject area:	Hydroponic system and Na^+-fluorescence measurements
Method name:	Hydroponic cultivation of tree species *Pongamia pinnata* (L.) pierre and Na^+-fluorescence measurements
Name and reference of original method:	Our method is a modified version of Khan et al. [2] hydroponic system; Oh et al. [8] and Wu et al. [9] Na^+ probe visualization protocol.
Resource availability:	n/a [2]

Method details

Background

Plant growth and optimization of hydroponic system

Hydroponic growth system is a versatile platform to study plant behavior under controlled conditions. It is a convenient system for not only controlling the plant nutrition but also provides an excellent model for researchers to study root system and its responses under different environmental conditions [1,7]. Certain hydroponic systems have been developed for Arabidopsis and other crop species to study their behavior under various environmental stress conditions [2–4]. To our best knowledge, only few studies were available on trees species which were grown hydroponically under controlled environment [5]. Based on existing knowledge, we have modified/ customized hydroponic system for Pongamia seedlings. Pongamia is known to possess elongated tap root (about 50 cm long roots in 30 days old seedlings) and lateral root system [7]. To accommodate Pongamia tap root system and without facing the root inhibiting effect, we have designed new experimental system. Our method was uniquely designed to perform tree species stress studies with minimal resources.

Pods of *P. pinnata* accession TOIL 12 were obtained from Tree Oil India Limited (TOIL), Zaheerabad, Hyderabad, Telangana. Freshly collected pods were kept in incubator (Orbitek) for drying at 37 °C for three days. Seeds were removed carefully from the dried pods with the help of pruning secateurs (Falcon). Uniform sized seeds were selected for the experiment. The seeds were sterilized with 1% (*v*/v) hypochlorite solution for 5 min and washed thoroughly with sterilized double distilled water for 3 h. The sterilized seeds were transferred on a sterile moist cotton bed in an air tight container kept in dark for 10 days. After 10 days of dark incubation, radicle emergence was observed. Synchronously germinated seeds were used for experimentation. For hydroponic culture experiment, full strength Hoagland's No. 2 basal salt mixture (Himedia) solution was used. The solution was sterilized under 121 °C and 16 lbs pressure for 30 min after adjusting the pH 5.75 ± 0.02. Nevertheless, we were discouraged with our results when plants grown in full strength Murashige and Skoog (MS) media (Himedia), and 10 X Yoshida solutions (Himedia). In addition, plants grown in MS solution were showed stunt in growth, while 10 X Yoshida solution was formed a white color precipitate at the bottom of the culture tube after 7days of plant growth. The germinated seeds were placed just above the nutrient medium level with help of parafilm in 50 ml falcon tubes (Genaxy) for 10 days. At this stage, seedling with primary root length was ~10.0 cm long. Careful measures were taken that the tip of primary root was not allowed to touch the bottom of the culture tube. According to Bengough et al. [11], root limitation imposes a direct effect on plant growth and development. Further, the seedlings were transferred to 300 ml glass tubes (5 cm diameter X 30 cm length) and kept for 15 days. At this stage, length of primary root was increased ~25.0 cm long. Finally, the seedlings were transferred to 1000 ml glass tubes (5 cm diameter X 60 cm length) before root tip touch the bottom of the culture tube and kept for 15 days (Fig. 1A–C) (Table 1). The culture medium was renewed every day. Each tube was designed to maintain only a single seedling. These tubes were fitted with a rubber stopper with sterile non-adsorbent cotton to support the seedlings. Further, the tubes were covered with black paper to protect the roots from photo-oxidative damage. Changing the culture media on a regular basis may save the energy consumption on maintaining the air filtration system and also prevent the anoxia condition [6,7]. The following culture conditions were maintained throughout the experiment; plant culture room maintained 24 °C room temperature, 16 h light and 8 h dark

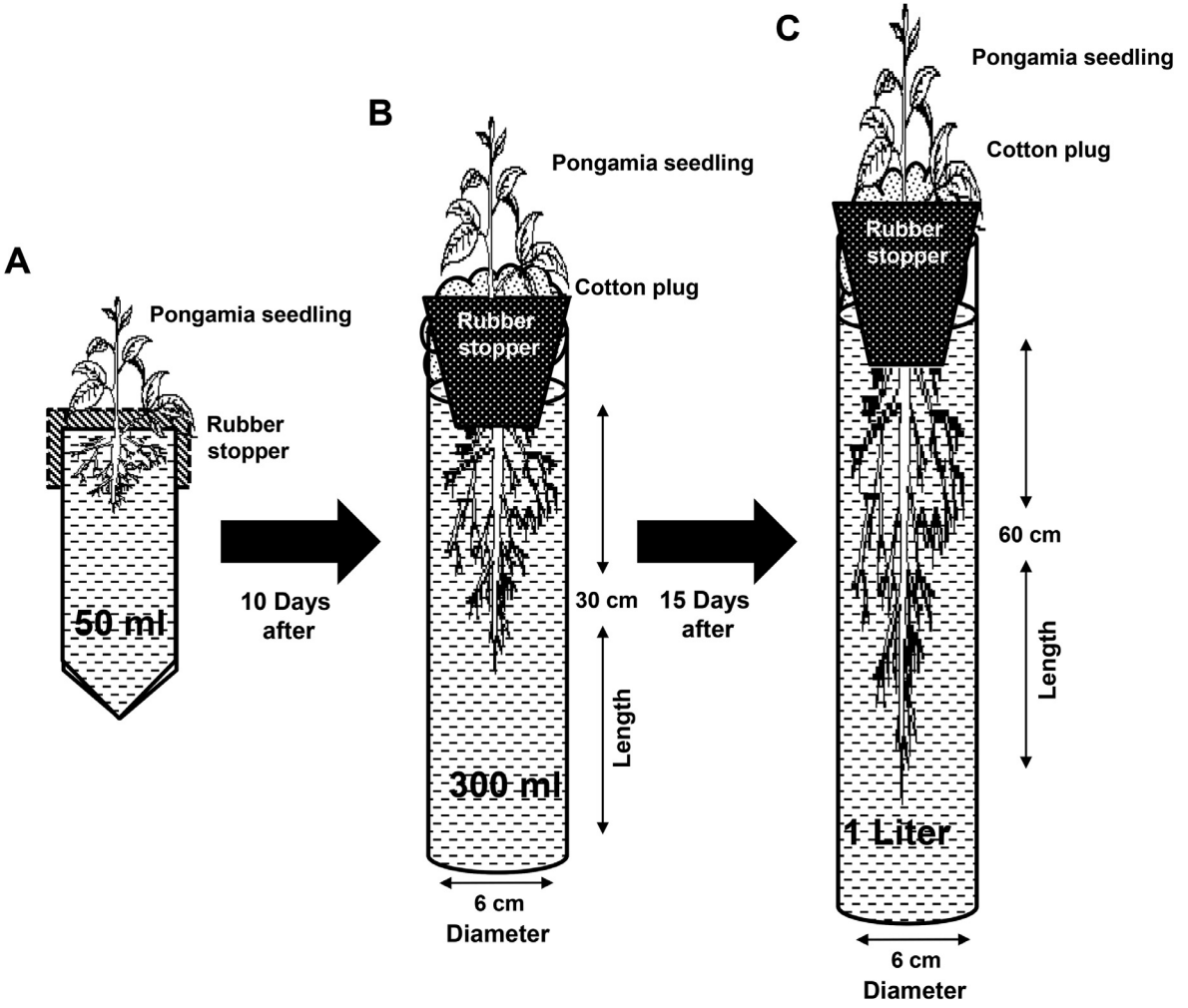

Fig. 1. Optimized plant hydroponic culture system for *P. pinnata* seedlings. (A) Plants were grown in 50 ml falcon tubes for 10 days, (B) in 300 ml vertical glass tubes for 15 days and (C) in 1liter vertical glass tubes for 20 days.

Table 1
Comparison of new modified method to the old methods of hydroponic culture system.

Components	Old method	New method
Apparatus		
Culture media reservoir	Plastic tanks, plastic trays	Customized glass tubes
Culture media circulating system	Nutrient pumps, drip system	-n/a-
Air pumping system	Submerged pumps, air pumps, air stones	Changing the nutrient solutions on regular basis
Root supporting/ holding material	Peat moss, expanded clay, coco coir, rock wool, Sand, perlite, vermiculate, etc.,	Non-absorbent cotton
Culture media		
Nutrient solution	Murashige and Skoog, Hoagland, Yoshida, etc., with carbon and vitamin supplements	Hoagland's No. 2 basal salt mixture

photoperiod and humidity were maintained approximately at 60%. Moreover, we compared both soil grown and hydroponically grown plants (Supplementary Fig. 1A and B). Interestingly, hydroponically grown plants were morphologically similar to that of soil grown plants. For salt stress treatment, 30 days old plants ($n = 20 \pm 30$) were subjected to 300 and 500 mM NaCl treatment with an increment of 100 mM NaCl per day to avoid sudden osmotic shock [12]. Acclimatizing the plants with lower salt concentrations and attaining desired concentrations of salt stress produces accurate effect of stress. Sudden exposure of 300 and 500 mM NaCl salt stress may impose lethal effects on plants.

Visualization of intracellular Na^+ ions by using CoroNa-Green dye through confocal laser scanning microscopy

CoroNa-Green AM (Invitrogen) is a cell permeant Na^+ specific fluorescent dye that exhibits a characteristic increase in green fluorescence upon binding to Na^+ ions, with little shifts in its absorption/ emission maxima at ~492/516 nm wavelength. It has a wide application in cell physiology studies to visualize the Na^+ homeostasis mechanisms in both plant and animal cells [8–10].

In the current study, Oh et al. [8] and Wu et al. [9] protocol was optimized to investigate Na^+ ion localization in higher plants/ tree species (Fig. 2). Freshly harvested Pongamia roots were cut into 1 cm long placed in fixative solution (2.5% glutardehyde solution in 0.1 M MOPS buffer, pH 7.5) for overnight at 4 °C. Notably, Pongamia roots were hard to performing the sections. However, the fixative solution was helped to soften tissue. The segments were washed thoroughly with 50 mM MOPS buffer solution 2–3 times. Further, the segments were incubated in 5 µM Na^+ specific probe CoroNa-Green AM (Invitrogen) and 0.02% pluronic acid in 50 mM MOPS (pH 7.0) for overnight at room temperature. The segments were washed thoroughly with 50 mM MOPS buffer solution 2–3 times before performing sections. The sections were immersed in propidium iodide solution (Invitrogen) (2 µM in 50 mM MOPS buffer) for 15 min before visualizing under confocal microscope. We were discouraged with our results when the sections were directly incubated with CoroNa-Green AM dye (Supplementary Fig. 2A). However, prior incubation of root segments with CoroNa-Green AM dye produced good results for Na^+ imaging and quantification (Supplementary Fig. 2B).

We followed two methods for Na^+ ion intensity measurements: first is 2D approach-sections were observed under confocal microscopy (Leica TCS SP2, Heidelberg, GmbH, Germany) and images captured on 2D plane (Fig. 3A). The cytosolic and vacuolar Na^+ fluorescence was calculated by LCS software (Heidelberg, GmbH, Germany) (Fig. 3B). Selective regions were taken in the sections and lines or boxes were drawn to measure Na^+ fluorescence by using LCS software. The observed intensity of Na^+ specific fluorescence was ~250 arb. units. Similarly, in second method (3D approach), sections were observed under confocal microscopy and images captured on 3D plane by using Z-stacking (Fig. 3C). Each section was thoroughly scanned, made optical sections at distance of 0.48 µm and 3D images were constructed (Supplementary Fig. 3). This approach provides a means to acquire and analyze entirety of the sample to measure Na^+ fluorescence in salt treated plants (Fig. 3D).

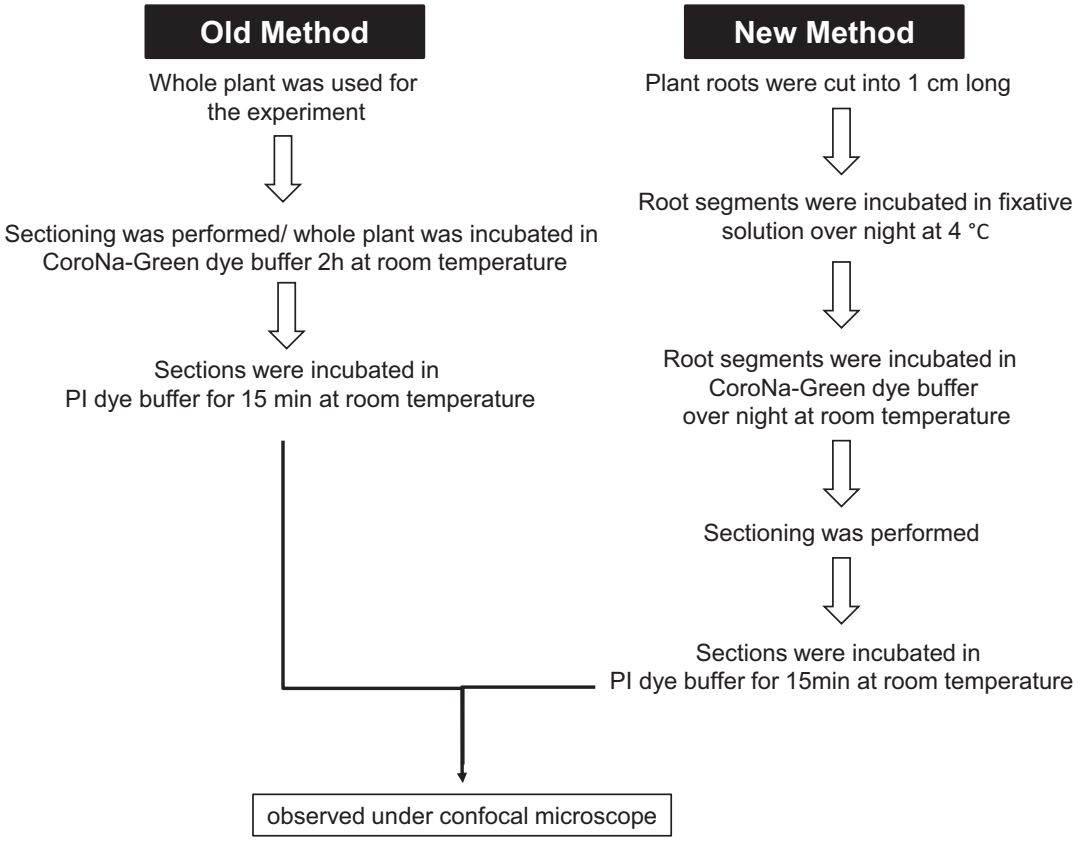

Fig. 2. Comparison of the modified method and the old method of Na^+ localization and Na^+ fluorescence intensity measurements.

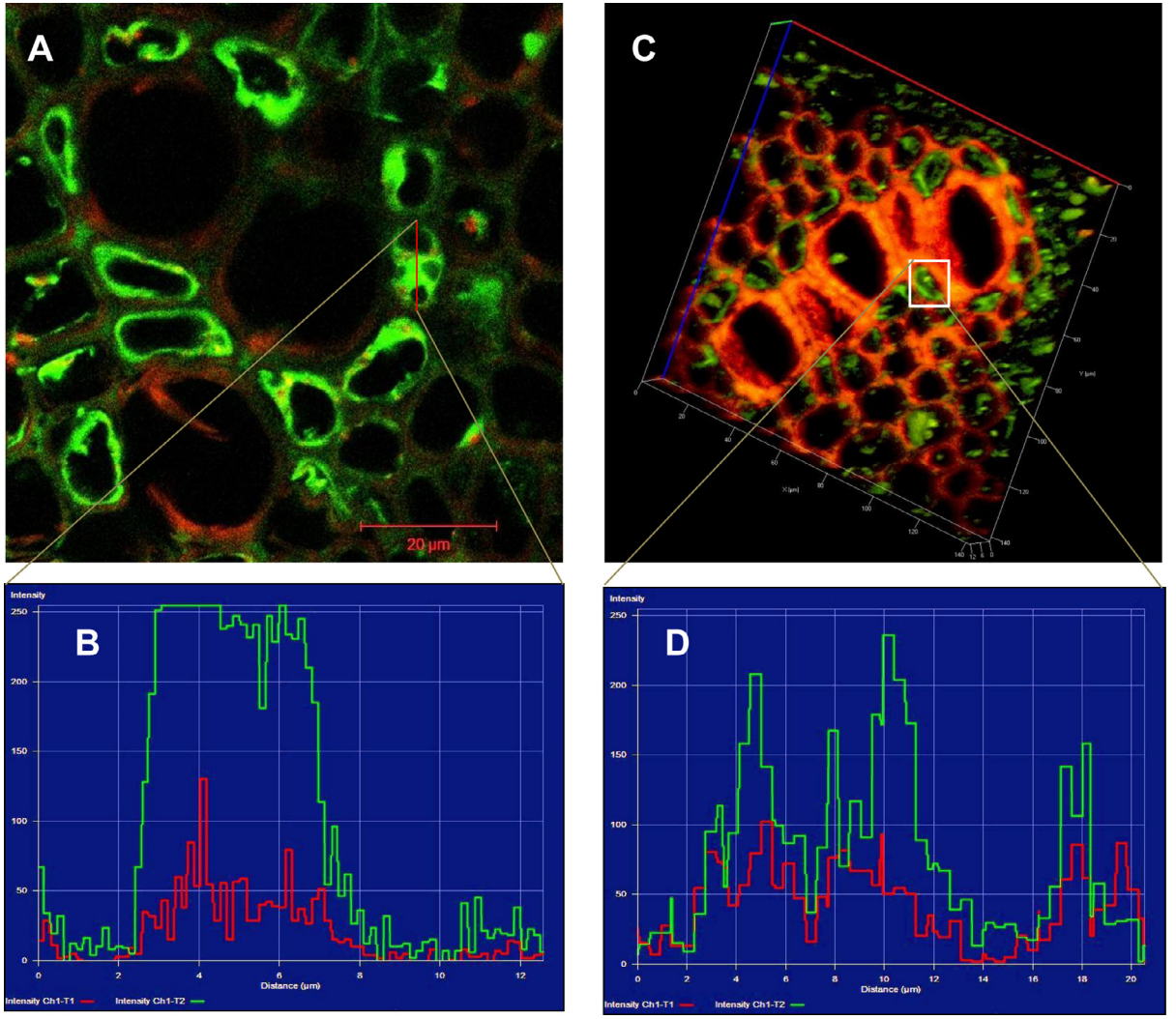

Fig. 3. Intensity of CoroNa-Green AM fluorescence in cytosolic and vacuolar compartments in the root sections. Red lines were drawn to measure Na^+ fluorescence intensity. (A) 2D view of the root sections and (B) red lines were drawn to measure Na^+ fluorescence intensity represented in graph. (C) 3D view of the root sections and (D) white box was drawn to measure Na^+ fluorescence intensity was represented in graph. (For interpretation of the references to color in this figure, the reader is referred to the web version of this article.)

Conclusion

In this study, we demonstrated that Pongamia seedlings exhibited similar morphological pattern as compared to soil grown seedlings with the modified hydroponic system. Apparatus designed on basis of root growth and morphology permits to conduct extensive studies on root/ rhizosphere studies. The method was modified to study individual plant responses to environmental cues. Our modified hydroponic growth system could be a promisive and reliable resource one can be able to perform hydroponic studies on tree species with minimal resources. Further, our method can be executable with low cost and power consumption. Our modified Na^+ fluorescence imaging protocol can ideally be used to produce high quality Na^+ fluorescence images in the roots of tree species. Our modified protocol also provides quantitative analysis of 2D and 3D imaging process at cellular and sub-cellular level.

Funding

This work is supported by funding from the Department of Biotechnology, Govt. of India [to A.R.R].

Acknowledgments

This research was supported by a Grant (BT/PR-12024/BCE/8/1097/2014) from Department of Biotechnology, Govt. of India. We gratefully acknowledge Tree Oil India Ltd. (TOIL), Zaheerabad, Telangana State, India for providing Pongamia seeds (TOIL12). Ms. Manthapuram Nalini's help in analyzing the confocal microscopy results are acknowledged. SM acknowledges University Grant Commission (UGC), New Delhi, India for fellowship.

Declaration of Competing Interest

Authors have no conflicts of interest to declare.

Supplementary materials

Supplementary material associated with this article can be found, in the online version, at doi:10.1016/j.mex.2020.100809.

References

[1] S. Marriboina, D. Sengupta, S. Kumar, A.R. Reddy, Physiological and molecular insights into the high salinity tolerance of *Pongamia pinnata* (L.) pierre, a potential biofuel tree species, Plant Sci. 258 (2017) 102–111.
[2] M.A. Khan, N.A. Castro-Guerrero, S.A. McInturf, N.T. Nguyen, A.N. Dame, J. Wang, R.K. Bindbeutel, T. Joshi, S.S. Jurisson, D.A. Nusinow, D.G. Mendoza-Cozatl, Changes in iron availability in arabidopsis are rapidly sensed in the leaf vasculature and impaired sensing leads to opposite transcriptional programs in leaves and roots, Plant Cell Environ. 41 (2018) 2263–2276.
[3] R.M. Mansuri, Z.S. Shobbar, N.B. Jelodar, M.R. Ghaffari, G.A. Nematzadeh, S. Asari, Dissecting molecular mechanisms underlying salt tolerance in rice: a comparative transcriptional profiling of the contrasting genotypes, Rice 12 (2019) 13.
[4] H.Y. Lee, Z. Chan, C. Zhang, G.M. Yoon, Editing of the osacs locus alters phosphate deficiency-induced adaptive responses in rice seedlings, J. Exp. Bot. 70 (2016) 1927–1940.
[5] H. Wan, J. Du, J. He, D. Lyu, H. Li, Copper accumulation, subcellular partitioning and physiological and molecular responses in relation to different copper tolerance in apple rootstocks, Tree Physiol. 39 (2019) 1215–1234.
[6] A. Lenzi, A. Baldi, R. Tesi, Growing spinach in a floating system with different volumes of aerated or non-aerated nutrient solution, Adv. Hort. Sci. 25 (2011) 21–25.
[7] S. Marriboina, A.R. Reddy, Hydrophobic cell-wall barriers and vacuolar sequestration of Na^+ ions are the key mechanisms conferring high salinity tolerance in a biofuel tree species *Pongamia pinnata* L. pierre, Environ. Exp. Bot. 171 (2020) 103949.
[8] D.H. Oh, E. Leidi, Q. Zhang, S.M. Hwang, Y.Z. Li, F.J. Quintero, X. Jiang, M.P. DÚrzo, S.Y. Lee, Y. Zhao, J.D. Bahk, R.A. Bressan, D.J. Yun, J.M. Pardo, H.J. Bohnert, Loss of halophytism by interference with SOS1 expression, Plant Physiol. 151 (2009) 210–222.
[9] H. Wu, L. Shabala, X. Liu, E. Azzarello, M. Zhou, C. Pandolfi, Z.H. Chen, J. Bose, S. Mancuso, S. Shabala, Linking salinity stress tolerance with tissue-specific Na^+ sequestration in wheat roots, Front. Plant Sci. 6 (2015) 71.
[10] S.D. Meier, Y. Kovalchuk, C.R. Rose, Properties of the new fluorescent Na^+ indicator CoroNa-Green: comparison with SBFI and confocal Na^+ imaging, J. Neuro. Sci. Methods 155 (2006) 251–259.

[11] A.G. Bengough, M.F. Bransby, J. Hans, S.J. McKenna, T.M. Roberts, T.A. Valentine, root responses to soil physical conditions; growth dynamics from field to cell, J. Exp. Bot. 57 (2006) 437–447.
[12] C.-L. Chen, H. van der Schoot, S. Dehghan, C.L. Alvim Kamei, K.U. Schwarz, H. Meyer, R.G.F. Visser, G.C. van der Linden, Genetic diversity of salt tolerance in *Miscanthus*, Frontiers in Plant Sciences 8 (187) (2017) 1–14.

Industrial Crops & Products 140 (2019) 111621

Contents lists available at ScienceDirect

Industrial Crops & Products

journal homepage: www.elsevier.com/locate/indcrop

Dynamics of metabolites and key regulatory proteins in the developing seeds of *Pongamia pinnata*, a potential biofuel tree species

Kambam Tamna Singha[a], Rachapudi Venkata Sreeharsha[a], Sureshbabu Mariboina[a], Attipalli Ramachandra Reddy[a,b,*]

[a] Dept. of Plant Sciences, School of Life Sciences, University of Hyderabad, Hyderabad, 500046, India
[b] Yogi Vemana University, Kadapa, Andhra Pradesh, India

ARTICLE INFO

Keywords:
Pongamia pinnata
Seed development
Metabolome
Proteome
Triacylglycerols
Oil body

ABSTRACT

The present study analyzed the dynamic changes in metabolites and key proteins during the seed development of *Pongamia pinnata* L. (Family: Fabaceae) with a particular focus on lipid biosynthesis and oil accumulation. The developing seeds were collected at four different stages: 120 (stage 1), 180 (stage 2), 240 (stage 3) and 300 (stage 4) days after flowering (DAF), representing S1, S2, S3 and S4 respectively. The analysis of seed pigments and mRNA expression patterns of key photosynthetic genes confirmed the photo-autotrophic behavior of *P. pinnata* seed during the initial stages of development. The metabolite profiling of developing *P. pinnata* seeds also revealed differentially expressed sugars, amino acids, free fatty acids and organic acids. Proteins related to development, energy metabolism, lipid accumulation as well as stress responses were documented through MALDI-TOF-MS/MS analysis. The structure and pattern of oil body accumulation at each stage of seed development were determined by electron and confocal microscopy of the cotyledonary sections. The thin layer chromatogram of *P. pinnata* oil revealed higher amount of Triacylglycerides and the fatty acid profile of extracted triacylglycerides showed a rapid increase in oleic acid (C18:1) at S3 and S4. The outcomes reveal new insights into the complex oleogenic metabolism during *P. pinnata* seed development at macro level.

1. Introduction

Plant oils have a potential to replace petroleum based fuels by acting as feedstock for the oleochemical and biofuel industries. Understanding the regulatory networks of seed oil biosynthesis has been a target of agronomists and metabolic engineers for decades in order to enhance the oil production. The current knowledge on regulation of seed development and oil accumulation is limited to food crops and other model plants. While, very limited reports are available for biofuel plants including *Pongamia pinnata, Jaropha curcus, Camelina sativa* (Mudalkar et al., 2014; Chaitanya et al., 2015; Kumar et al., 2017). In general, the seed development bears a complex regulatory network of metabolic and developmental machinery which include signaling elements associated with accumulation of storage compounds (Baud et al., 2008; Atabani et al., 2013). Further, the seed storage-compound synthesis overlays the developmental progression of embryogenesis and is to an extent governed by the metabolite and hormonal signals inside the embryo (Borisjuk et al., 2003). The proportional distribution of seed storage products into carbohydrates, oils and proteins will depend on the influx of metabolic pathways during the development and can vary between species (Schiltz et al., 2005; Ekman et al., 2008; Chaitanya et al., 2015). For oil development, carbon is delivered to fatty acid synthesis in seed plastids via glycolysis with hexose and triose as the predominant carbohydrates entering the plastid. Previous reports signified the role of sucrose import into embryo and its metabolism in the cytosol and plastids in the formation of starch and oil (Luthra et al., 1991; Eastmond and Rawsthorne, 2000). It is well established in several model legumes that the dynamic changes of hexose/sucrose ratios play a key role in the commencement of storage product synthesis as the seed development progressed. On the

Abbreviations: ACP, acyl carrier proteins; BSA, bovine serum albumin; DAF, days after flowering; DAGs, diacylglycerides; DGAT, acyl-coA: diglyceride acyltransferase; DTT, dithiothreitol; DW, dry weight; EGTA, ethylene glycol-bis(β-aminoethyl ether)-N,N,N′,N′-tetraacetic acid; FAMEs, fatty acid methyl esters; FFA, Free Fatty acids; FW, fresh weight; NADGA, N-acetyl- D-glucosamine; PBS, phosphate buffer saline; PCA, Principle component analysis; PDAT, phospholipid:diacylglycerol acyltransferase; PL, Phospholipids; PMSF, phenylmethylsulfonyl fluoride; TAGs, triacylglycerides; TCA, tricarboxylic acid; TLC, thin layer chromatography

* Corresponding author.
E-mail address: arrsl@uohyd.ernet.in (A.R. Reddy).

https://doi.org/10.1016/j.indcrop.2019.111621
Received 10 December 2018; Received in revised form 15 June 2019; Accepted 27 July 2019

other hand, the primary metabolism inside the seed which includes major pathways of glycolysis and TCA link the biosynthesis of carbohydrates, amino acids and fatty acids which also provide energy balance inside the developing seeds (Rolletschek et al., 2005; Schwender et al., 2015). Hence, the precise understanding of changes in these regulatory metabolites will provide insights into the seed development and oil composition in non-model legume tree species, specifically *P. pinnata*.

The oilseeds can be photo-autotrophic or heterotrophic depending on the presence of chloroplast and light plays an important role in regulating the green oil seed development. It was reported in certain crop plants that the seed carries out photosynthesis during embryogenesis which provides energy for FA biosynthesis and also helps in refixing the respiratory CO_2 release (Schwender et al., 2004). Though the absence of seed photosynthesis will not affect the overall FA biosynthesis, it will be considered as an important factor in promoting carbon storage, energy flux and lipid biosynthesis in oilseeds. The dynamic shift in the expression patterns of photosystem related proteins along with FA biosynthesis enzymes during the seed development of *Arabidopsis* and *Glycine max* support the active role of seed photosynthesis. Hence, studying the pigments and associated protein expression patterns in large seeds with long developmental cycles will provide more insights into the role of seed photosystems in synthesizing storage compounds.

The cultivation of *P. pinnata* is suitable in diverse tropical and subtropical environments. The oil content of *P. pinnata* seeds ranges from 35 to 40% of seed dry weight and 55–65 % of the total lipid has been reported as oleic acid which is the ideal fatty acid for biodiesel production (Sreeharsha et al., 2016; Xiong et al., 2018). Due to the accumulation of high levels of poly unsaturated fatty acids in the *P. pinnata* seed oil, it is considered as a potential biofuel feedstock with an optimized efficiency to use as a biodiesel for diesel engines (Singh et al., 2018; Jain et al., 2018). Moreover, not only the *P. pinnata* oil, but also the seed waste after oil extraction have recently been used to produce bio-ethanol (Muktham et al., 2016). The biochemical characteristics and protein profiling during seed development has been investigated in *P. pinnata* (Kesari and Rangan, 2011; Pavithra et al., 2014). The proximal chemical composition of mature *P. pinnata* seed along with fatty acid composition were also reported earlier (Bala et al., 2011; Sharma et al., 2011; Pavithra et al., 2012). However, in depth analysis of metabolite and proteomic profiles throughout the lengthy developmental period of *P. pinnata* seed have not yet been reported. It is crucial to study the metabolome and proteome of the developing seed to understand the complex association between various metabolites and FA biosynthesis to oil body formation. The objective of the current study is to decipher the metabolome and identification of key regulatory proteins in different developing stages of *P. pinnata* seed and their role in FA accumulation. In addition, the photosynthetic behavior of the *P. pinnata* seed also have been identified which will help in understanding the carbon influx to FA biosynthesis. Our results will deepen the knowledge on metabolic regulation of *P. pinnata* seed development and oil accumulation which is important for further metabolic engineering of this potential biofuel feedstock for different industrial and agricultural applications.

2. Materials and methods

2.1. Plant material and study site description

Ten year old *P. pinnata* plantation, established in the experimental farm of Tree Oils India Limited (TOIL) Zaheerabad, Medak district, Telangana state, India (latitude 17°36′; longitude 77°31′E; 622 m MSL) was selected for the present study. The study site has a tropical, hot-steppe agroclimate with the summer months between March to May having maximum temperature up to ~42 °C and an average temperature of 22–23 °C in the winter months of September to February, monsoon starts during June to October with average rainfall ranging from 700 to 1500 mm. Plants were maintained under natural photoperiod with uniform 2 m spacing between as well as within the rows. The recorded range of light intensity in the region on a normal sunny day ranged between 1200–2000 μmol/m^2/s during 10.00–14.00 h solar time. The plants were regularly watered during hot summer months with alternate watering during winter months and no watering during monsoon season. Nitrogen was provided by applying cow dung mixed with vermicompost as farmyard manure at the rate of 12 kg/year twice in equal splits during growth. Trees had a circular canopy with 15–20 tertiary branches. The flowering and fruiting seasonal events were recorded periodically for further experimental analyses. Flowering initiated in the month of March with visible inflorescence which continued until April. Natural pollination resulted in formation of pods with first visible appearance recorded at 80–90 days after the flowering started. Seed development and maturation was completed by nearly 300 days (~10 months) from the first visible appearance of flowers. The appearance of flower buds in each tertiary branches was considered as 0 days after flowering (DAF). Individual flowers were tagged randomly and the development of pod and seed was monitored regularly in the tagged trees. The tagged pods were collected at 120, 180, 240 and 300 DAF to study the seed morphology and stored at –80 °C for further biochemical and molecular analyses. The pod contained very tiny seeds with negligible dry mass during first initial stages of development (30 to 100 DAF). Therefore the experiments were carried out when the seeds reached 120 DAF till maturation. Seeds inside 120, 180, 240 and 300 DAF old pods were considered as stage1 (S1), stage2 (S2), stage3 (S3) and stage4 (S4) respectively. The study was performed for two successive flowering seasons of *P. pinnata* (for two consecutive years, March 2016 to February 2017 and March 2017 to February 2018).

2.2. Seed morphology and biochemical analysis

Fresh seeds were initially weighed and dried for 12 h at 65–70 °C in a ventilated hot air oven. The weight of seed coat and cotyledon were measured gravimetrically and percentage was calculated using the formula: (weight of cotyledon / weight of total seed) ×100; (weight of seed coat / weight of total seed) ×100, respectively. The seed dry mass was recorded and seed moisture content (%) was calculated according to the formula: (FW–DW/FW) ×100.

Chlorophyll content in the seed samples was estimated according to the method reported by Hiscox and Israelstam (1979). Fresh seeds (100 mg) were ground and refluxed for 1 h in 10 mL of DMSO, extracted liquid was collected and absorbance was measured at 645 and 663 nm using a UV–vis spectrophotometer (Eppendorf, Germany) and chlorophyll contents were calculated according to Arnon (1949) using the formula: chlorophyll *a* (g/L) = 0.0127 × A_{663}– 0.00269 × A_{645}; chlorophyll *b* (g/L) = 0.0229 × A_{645} – 0.00468 × A_{663}; the results were expressed as mg/g FW (where A_{663}, A_{645} represents the absorbance measured at 663 and 645 nm respectively).

Total carbohydrates and starch content in the seeds were estimated according to Anthrone method as described by Hedge and Hofreiter (1962), where 100 mg of fresh seed tissue was refluxed with 5 mL of 2.5 N HCl followed by neutralizing with NaOH. The mixture was centrifuged for 10 min at 6000 × g. An aliquot of supernatant (1 mL) was taken and added with 4 mL of Anthrone reagent. After heating at 80–90 °C for 8 min in a water bath, the solution was allowed to cool rapidly and the absorbance was measured at 630 nm. Spectrometric readings were quantified using glucose standards and represented in mg/g FW of the seed.

For starch estimation, 100 mg of fresh seed tissue was first ground with hot 80% ethanol. The supernatant of this mixture was removed after centrifugation. The residue was washed repeatedly with 80% hot ethanol till the washings did not give green color with Anthrone reagent. The dried residue was mixed with 5 mL of water and 6.5 mL of 52% perchloric acid. The mixture was kept at 0 °C for 20 min and

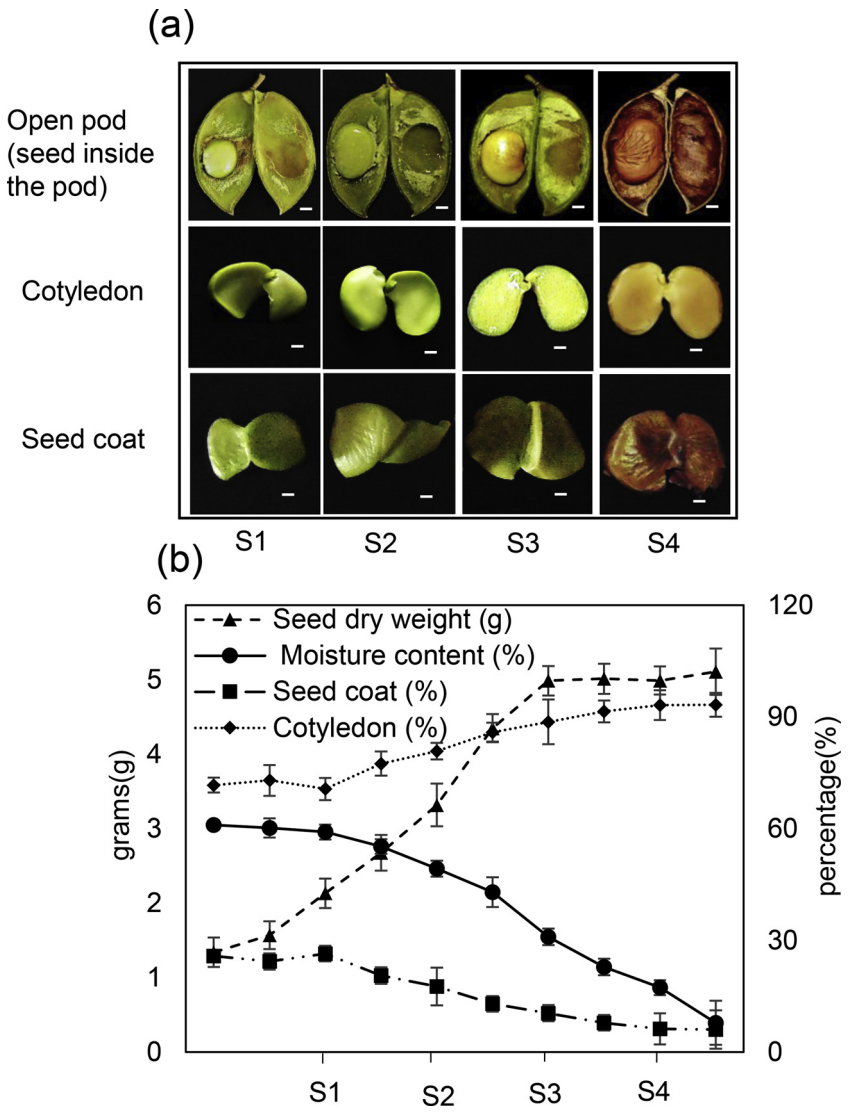

Fig. 1. Position of seed inside the pod and cotyledons separated from seed coat at each developmental stage **(a)**. Morphological and biochemical analysis of developing *P. pinnata* seeds. Changes in seed dry weight, moisture content, % cotyledon and seed coat throughout development **(b)**. Values are mean ± SD, (n = 40); the scale is presented by white bar with the length of 0.3 cm.

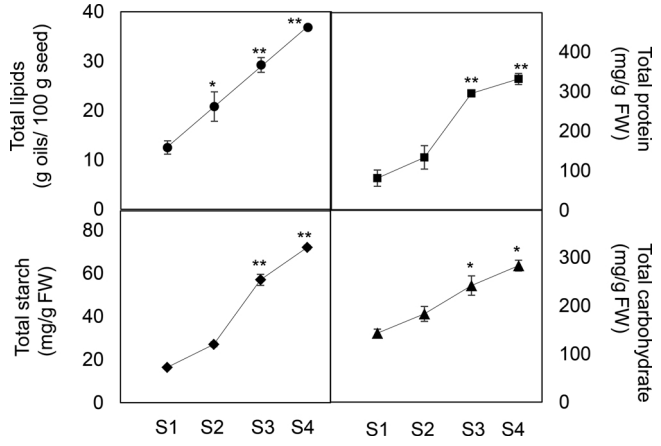

Fig. 2. Pattern of increasing storage products (lipid, protein, total carbohydrate and starch) with development. Values are mean ± SD (n = 3). Data are given as means ± SD; (n = 3). *, ** represents significant differences within the stages analyzed by one-way ANOVA, $P < 0.05$; $P < 0.01$ respectively.

centrifuged at 8000 × g for 5 min, supernatant was collected and the extraction was repeated twice. The collected supernatant (1 mL) was mixed with 4 mL of Anthrone reagent and starch was estimated by the method used in estimation of carbohydrates.

For total protein quantification, fresh tissue (100 mg) was ground with liquid nitrogen and mixed with 2 mL of protein extraction buffer consisting of 25 mM Tris − HCl (pH 7.2), 15 mM $MgCl_2$, 15 mM EGTA, 75 mM NaCl, 2 mM DTT, 1 mM NaF, 1 mM PMSF with 0.1% Nonidet, followed by centrifugation at 12,000 × g for 5 min at 4 °C. Supernatant was collected and protein was estimated according to Bradford (1976). Quantification of total protein was achieved by using BSA as the protein standard and represented as mg/g FW.

Total lipids were extracted by using the method described by Bligh and Dyer (1959) with slight modifications. Fresh seeds were ground with $CHCl_3$:MeOH:H_2O (2:2:1.8) v/v and the mixture was centrifuged at 10,000 × g for 15 min. The lower $CHCl_3$ layer was collected and the extraction was repeated three times. The chloroform was separated by a Rotary evaporator (Heidolph, Germany) and total lipid was estimated gravimetrically and represented as g oils/100 *g* seed. All of the chemical reagents used for biochemical analysis were purchased from Sigma Aldrich, USA.

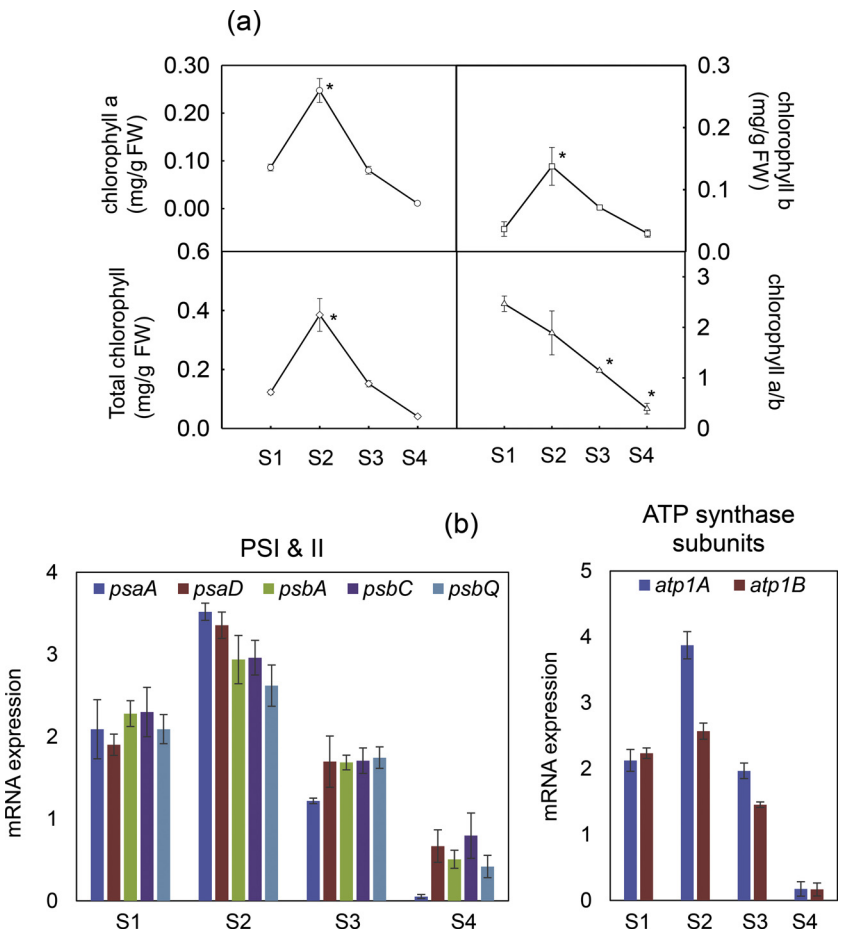

Fig. 3. Changes in the chlorophyll *a*, b, total chlorophyll and chlorophyll *a*/b **(a).** Expression patterns of key regulatory genes represented in fold change related to photosynthesis **(b).** Fold change > 2 is considered as upregulation. Values are mean ± SD (n = 3). Data are given as means ± SD; (n = 3). *, ** represents significant differences within the stages analyzed by one-way ANOVA, P < 0.05; P < 0.01 respectively.

2.3. Gene expression analysis by real time PCR

Total RNA was isolated from developing fresh seeds using Plant total RNA extraction kit by following manufacturer's instructions (Sigma Aldrich, USA). Primers for the required genes were designed from available *P. pinnata* transcriptome sequences (Sreeharsha et al., 2016). First strand cDNA was synthesized with 1 µg of RNA using Revert aid first strand cDNA synthesis kit (Thermo-Fischer Scientific, USA). Expression analysis of selected genes were carried out on Realplex thermal cycler (Eppendorf, Germany) using SYBR FAST qPCR universal master mix (2X) (KAPA Biosystems, USA) with 50 ng of cDNA as template and following the program: 2 min at 95 °C, followed by 40 cycles of 15 s at 95 °C, 30 s at 55 °C annealing temperature and 20 s at 72 °C, followed by the dissociation (melting) curve. The mRNA expression level was calculated according to the $2^{-\Delta\Delta Ct}$ formula (Livak and Schmittgen, 2001). For the internal control, 18 s ribosomal RNA gene was used.

2.4. Metabolite profiling

P. pinnata seeds at different developing stages were ground into fine powder in liquid nitrogen. 100 mg of the seed powder was homogenized with 1.4 mL precooled methanol by vortexing for 10 s and 60 µL of ribitol (0.2 mg/mL) was added to the mixture as internal standard followed by 10 s of vortexing. This solution was ultra-sonicated for 10 min, followed by centrifugation at 11,000 × g for 10 min. The supernatant was transferred to a new tube and mixed with 750 µL of precooled chloroform and 1.5 mL of precooled water. The mixture was then centrifuged at 2200 × g for 15 min. 150 µL of extraction solution from upper phase was dried under vacuum and stored at –80 °C until derivatization. The extract was methoxyaminated, silylated and the dried extract was dissolved in 20 µL of methoxy amine hydrochloride pyridine solution (40 mg/mL) which was incubated at 30 °C with vigorous shaking for 90 min. Then 80 µL of N-methyl-N-(trimethylsilyl) trifluoro-acetamide-solution was added to the sample followed by 30 min incubation at 37 °C with vigorous shaking. The derivatized sample was centrifuged at 20,000 × g for 8 min. The supernatant was then transferred to vials for measurement. Samples were measured with gas chromatography coupled with LECO Pegasus R 4D GC GC–TOF spectrometry (GC-TOF-MS) (Agilent 6890, USA). Each sample was injected under both split less and split 25 times mode for better quantification of candidates with a wide capacity range. Candidates were manually annotated by comparing their retention times (RTs) and mass spectra to those of standards in GMD database (Kopka et al., 2005) with a minimum match factor of 700. The peak areas of the same metabolite with different derived groups were merged and normalized to internal standard of ribitol. The concentration of the metabolites was calculated with respect to the known concentration of ribitol and represented as µg/g FW. The differential analysis at developing stages were analyzed using MetaboAnalyst Version 4.0 [Software] (available from http://www.metaboanalyst.ca/MetaboAnalyst/faces/home.xhtml).

2.5. 2-D protein profiling and identification using MALDI TOF MS/MS analysis

Gel based 2D proteome was carried out according to the method described by Sengupta et al. (2011). Protein extracted earlier (200 µL) was precipitated using 800 µL of 0.1% ammonium acetate in methanol and kept at –20 °C for 8–12 h. The mixture was centrifuged at 10,000 × g for 10 min at 4 °C and the precipitate was washed with fresh methanol for 3 times followed by 2 times wash with acetone. The

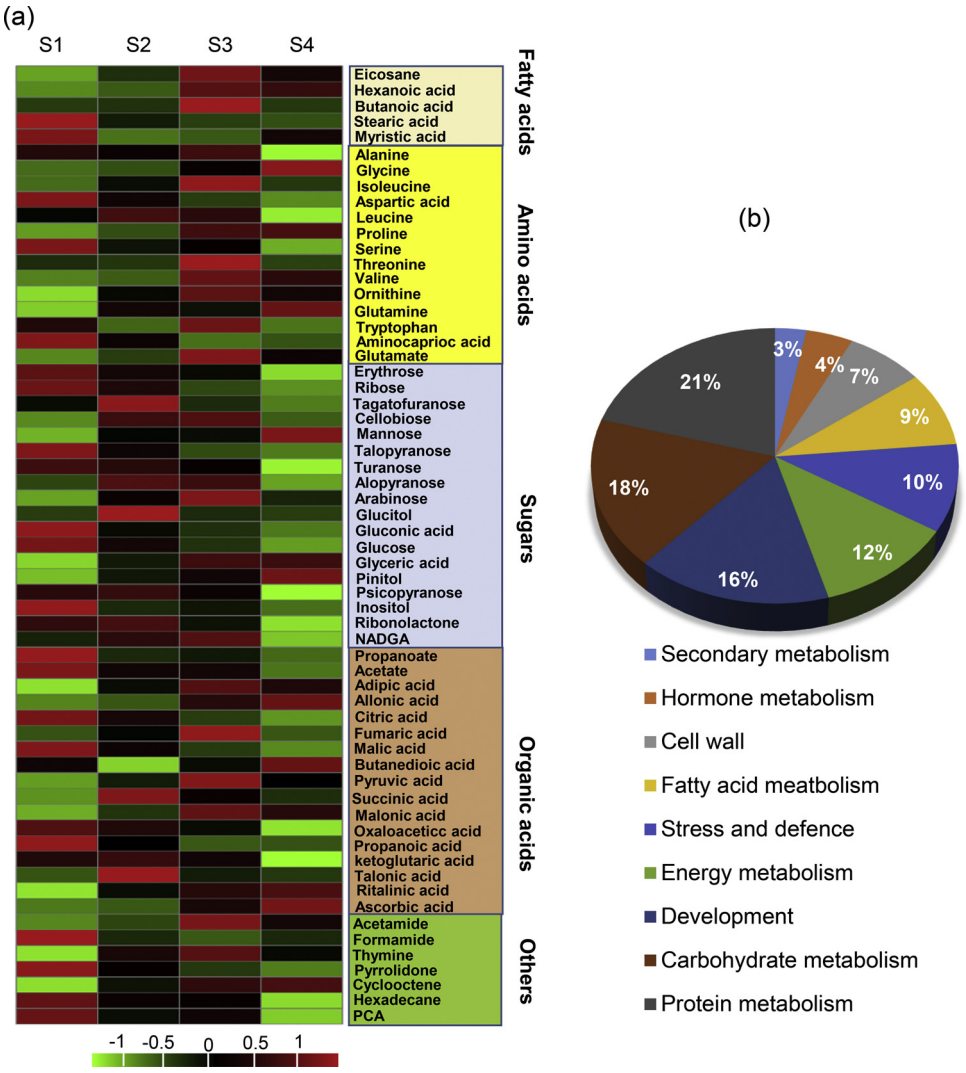

Fig. 4. Heat map based on the fold change in concentration of metabolites (μg/g FW) at S1, S2, S3 and S4 **(a)**. Pie chart representing functional classification of metabolites detected in all the developing stages **(b)**.

isolated protein sample (900 μg) was then solubilized in rehydration buffer followed by isoelectric focusing using pH 4–7 isoelectric focusing strips (18 cm, 4–7 pH linear gradient; GE Healthcare, USA) for 12 h at 50 V for first separation. Rehydration and focusing was carried out in Ettan IPGphor II (GE Healthcare, USA) at 20 °C, using the following program: 30 min at 500 V, 3 h to increase from 500 to 10,000 V and 6 h at 10,000 V (a total of 60,000 Vh). The IEF strips were then placed over 12% acrylamide gel for the second separation through SDS PAGE at 300–500 V using standard protocol. After staining, the gels were scanned and the gel image obtained was analyzed though Image Master 2-D Platinum version 6 image analysis software (GE Healthcare, USA).

For the identification of proteins, MALDI TOF MS/MS was carried out through in-gel trypsin digestion and database searches (PMF and MS/MS) using MASCOT program [Software] (available from http://www.matrixscience.com). The similarity search for mass values was done with existing digests and sequence information from NCBInr and Swiss Prot database. The taxonomic category was set to Viridiplantae (green plants). The other search parameters were: fixed modification of carbamidomethyl (C), variable modification of oxidation (M), enzyme trypsin, peptide charge of 1+ and monoisotopic. Out of top ten most significantly identified proteins, results having highest score, peptide match, and similarity of molecular weights were considered.

2.6. Microscopic studies of P. Pinnata seeds

Fresh seeds were made into thin sections and fixed in 2.5% glutaraldehyde for 8–12 h followed by re-fixing again in 0.2% osmium tetra oxide for 2–3 h. After washing with 0.1% PBS and series of ethanol dehydration, thin sections were embedded in epoxy resin (Araldite 502). Ultrathin sections were made using ultra microtome (LEICA EM UC6, Germany) and observed under Scanning electron microscope (TESCAN S8000, Czech Republic). For TEM, ultrathin sections were fixed in grids and stained with uranyl acetate and lead citrate which was observed later in TEM (FEI Model, Tecnai G2S Twin, Spain) (200 kV). Nile red staining was performed by following the method reported by Greenspan et al. (1985) with slight modifications. Prefixed thin sections of the fresh tissues were infiltrated with the working concentration of 2 μg/mL Nile red solution in 0.1% HEPES buffer for 1–2 h under dark. After washing for 4–5 times with HEPES buffer, the sections were visualized under confocal microscope (LIECA TCS SP2 AOBS, Heidelberg, Germany) under excitation of 488 nm and emission range of 530–650 nm. All images were obtained with 10% laser power.

2.7. Thin layer chromatography for lipid profiles

Total lipid (5 mg) extracted from all the samples were dissolved in chloroform and spotted on the TLC Silica gel 60 F254 (Merck,

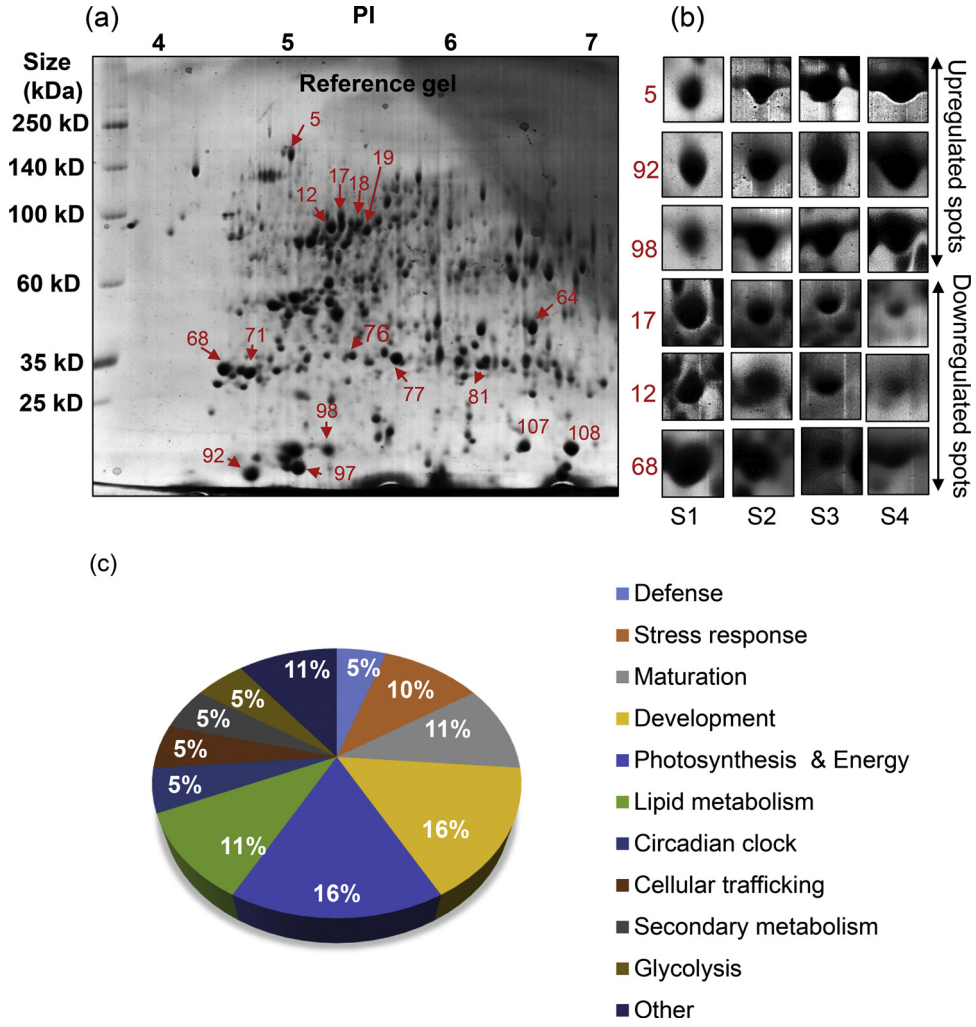

Fig. 5. 2D reference gel image where the identified spots were indicated by spot ids in red mark **(a)**, some of the upregulated and downregulated spots were presented as separated images at each stage **(b)**. Functional classification of identified proteins in pie chart **(c).**

Germany). The separation was carried out with hexane and ethyl acetate (9:1 v/v) as the mobile phase and silica gel bonded with aluminum sheet as the stationary phase. The TLC plates were air dried and exposed to iodine vapor. Iodine stained spots were compared with the standards of phospholipids, DAGs and TAGs separated in TLC plates with the same mobile phase.

The TAGs from the multiple TLC plates were scrapped carefully and extracted using chloroform. Further, chloroform was separated from the extracted TAGs with the help of rotary evaporator (Heidolph, Germany). The fatty acid profiling and quantification was carried by following the methods reported by Coetzee et al. (2008) and Sun et al. (2017) with slight modifications. FAMEs were prepared by refluxing 50 mg of the TAGs extracted with 5% H_2SO_4 in methanol (w/v) for 6 h on a hot plate. Prepared esters were analyzed through gas chromatography (GC-TOF-MS) (Agilent 6890, USA) with DB225 column (inner diameter = 0.25 mm, length = 37 m, thickness = 0.25 µm; Agilent, USA). The injector and flame ionization detectors were set at 250 °C and 270 °C, respectively. The oven temperature was set at 160 °C for 2 min and then increased to 230 °C at a rate of 5 °C/min. Nitrogen was used as the carrier gas at a flow rate of 1 mL/min. Fatty acids were confirmed by comparing with standard FAMEs mix (C14 – C22, Supelco, Sigma Aldrich, USA) analyzed at different concentrations. Quantification of fatty acids was carried out using area normalization method with percentage area of each peak corresponding to the identified fatty acid.

2.8. Statistical analysis

Each seed collected at various stages was considered as one unit (n = 40), where n is the number of seeds for the verification of difference in its morphological and physiological measurements. All the experiments were carried out in triplicates for the developing stages. PCA and heat map analysis was carried out for metabolome data using MetaboAnalyst online tool version 4.0 [Software] (available from http://www.metaboanalyst.ca/MetaboAnalyst/faces/home.xhtml). The mean values were compared and analysis of significance ($P < 0.05$) was determined by student's *t*-test and one way ANOVA using Sigma plot 11.0.

3. Results

3.1. Seed morphological characteristics and storage biochemistry during development

A single pod of *P. pinnata* generally houses either one or two seeds with 3–4 seeds occasionally/rarely observed. All the four different stages of *P. pinnata* seed with developmental progressing of pod, cotyledon and seed coat are shown in Fig. 1. The young seeds are green in color initially, which turned completely brown upon maturation (Fig. 1a). There was a gradual decrease in the seed moisture content from S1 to S4 whereas, the seed dry weight increased till S3 and got stabilized by maturation (Fig. 1b). Seed coat percentage decreased

Table 1
The list of protein spots identified with their % spot volume and MASCOT search results at four stages of development. Values are mean ± S.D, (n = 3), level of significant difference was analyzed by one-way-ANOVA with reference to S1. Note - *, P < 0.05; **, P < 0.01.

Sp. ID	Spot intensities	Protein identified	MW observed in gel	MW from literature	Known Function	Organism related to	Accession no.	MS/MS Score	Peptide sequences matched
5	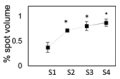	Acetyl coA carboxylase	200kD	226 kD	Fatty acid biosynthesis	*Sesamum indicum*	XP011083400.1	98	DEGRGPMR EDAFFQAVTEVACAQK ASQLLEQTK(Total matched peptides-29)
12	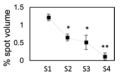	Midasin	95kD	116kD	Female gamete and seed development	*Arabidopsis thaliana*	MDN1_ARANTH	94	WMYLESIFVGSDDIRHQLPAEAK KSFEMVSLAVSQK (Total matched peptides - 34)
17	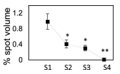	AP2 Complex subunit alpha 1	91kD	112kD	Vesicular transport and development	*Arabidopsis thaliana*	AP2A1_ARATH	94	FAPDLSWYVDVILQLIDK LVLFMGWK (Total matched peptides - 12)
18	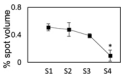	Phosphoenol pyruvate carboxykinase	95kD	73.7kD	Photosynthesis carbon fixation and energy metabolism	*Zea maize*	PCKA_MAIZE	64	GLFGVMHYLMPK AQTIDELHSL QR(Total matched peptides - 12)
19	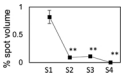	Probable disease resistance protein	100kD	104.5kD	Defence and disease resistance	*Arabidopsis thaliana*	PX24L_ARATH	108	VLGGLLAAKYTLHDWKR ERKDEIQNMK(Total matched peptides - 31)
64	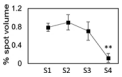	Glyceraldehyde-3-phosphate dehydrogenase	45kD	36.5kD	Glycolysis and energy metabolism	*Oryza sativa*	G3PC1_ORYSJ	278	AASFNIIPSSTGAAK LKGIIGYVEEDLVSTOFVGD SR(Total matched peptides - 7)
68	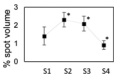	ATP synthase subunit beta	35kD	53.3kD	Photosynthesis electron transport and energy	*Brimeura amethystina*	ATPB_BRIAM	68	AVAMSATDGLTR EGNDLYMEKESGVINEK(Total matched peptides - 8)
71	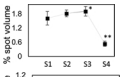	Ent-copalyl diphosphate synthase 1	35kD	99kD	Secondary metabolism	*Oryza sativa*	CPS1_ORYSJ	88	ARNFSYEFLR EIEQNMDYVNR(Total matched peptides - 8)
76	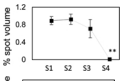	1-cys peroxiredoxin B	35kD	24.4kD	Vitamins	*Oryza sativa*	REHYB_ORYSI	67	DTAGGELPNR VVIPPGVSDEEAK(Total matched peptides - 8)
77	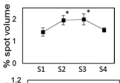	GTP Binding protein SARB1	30 kD	22.02kD	Vesicular transport of storage bodies	*Arabidopsis thaliana*	SAR1B_ARATH	74	VWKDYYAK YHLGLTNFTTGKG (Total matched peptides - 9)
81	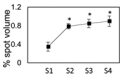	Heat stress transcription factor c-1b	30kD	27.4 kD	Abiotic stress regulator	*Oryza sativa*	HFC1B_ORYSJ	97	NFASFVR QLNTYGFR(Total matched peptides - 17)
92	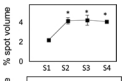	Lipid transfer like protein VAS	10kD	17kD	Lipid transfer metabolism	*Arabidopsis thaliana*	VAS_ARATH	90	WSSQAER EVPQVCCNPLK(Total matched peptides - 8)
98	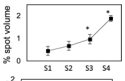	Integrin linked protein kinase 1	25kD	52.4kD	Signal transduction (Plant defence response)	*Cucurbita maxima*	XP_022970695.1	101	TNPGSRSFSK WGSTPLADAIYYK(Total matched peptides - 6)
107	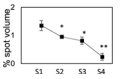	Class I heat shock protein	10.5kD	17.7kD	Heat shock and stress	*Solanum pennelli*	XP_015078018.1	88	FRLPENAK VEVEEDRVLQISGER(Total matched peptides - 7)
108	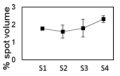	Class I heat shock protein	10.3kD	17.8kD	Heat shock and stress	*Solanum lycopersicum*	HSP11_SOLLC	66	FRLPENAK VEVEEDRVLQISGER(Total matched peptides - 6)
97	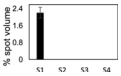	Protein ELF 4 Like	15kD	14.07kD	Circadian clock	*Arabidopsis thaliana*	EF4LT_ARATH	58	DGDTTTTTTGSS NVGLINEINISQVMEIYSDLSLNFAK (Total matched peptides - 2)
N17	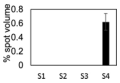	Allergen LEN	90kD	47.7kD	Allergen protein in non-edible plants	*Lens culineris*	CAD87730.1	112	IFENLQNYR KSVSSESESEPFNLR(Total matched peptides - 8)

gradually while the percentage of cotyledon increased as the seed matured (Fig. 1b). Accumulation of all the storage products including starch, protein and lipids increased gradually, reaching the highest levels during S4 (Fig. 2). Protein and lipid contents were similar at younger stages (S1–S2), while the lipid content reached up to 37% of total 100 g of seeds (~36.8 g oil/100 g seed), whereas protein content reached to 33% (~331 mg/g FW) by the end of the development. Similarly, the total carbohydrate content in the mature seeds (S4) was ~298 mg/g FW (1.9 folds higher when compared to S1), out of which the content of starch was only ~80 mg/g FW (4.3 folds higher when compared to S1) (Fig. 2). Chlorophyll *a*, chlorophyll b and total chlorophyll concentrations showed a distinct pattern when the seeds were green where their contents increased from S1 to S2 with a further decrease thereon at S3 and S4, during which the seeds started to develop brown color (Fig. 3a). Similarly, chlorophyll *a*/b ratio also consistently decreased with the progression of seed development (Fig. 3a). Relative gene expression of some of the key photosynthetic genes were analyzed at different stages of development by considering S1 as reference (Fig. 3b). All genes related to Photosystem I and II major subunits (*psaA, psaD psbA, psbC, psbQ*) and ATP synthase subunit (*atp1A* and *atp1B*) were upregulated at S2 which subsequently decreased from S3 to S4 (Fig. 3b).

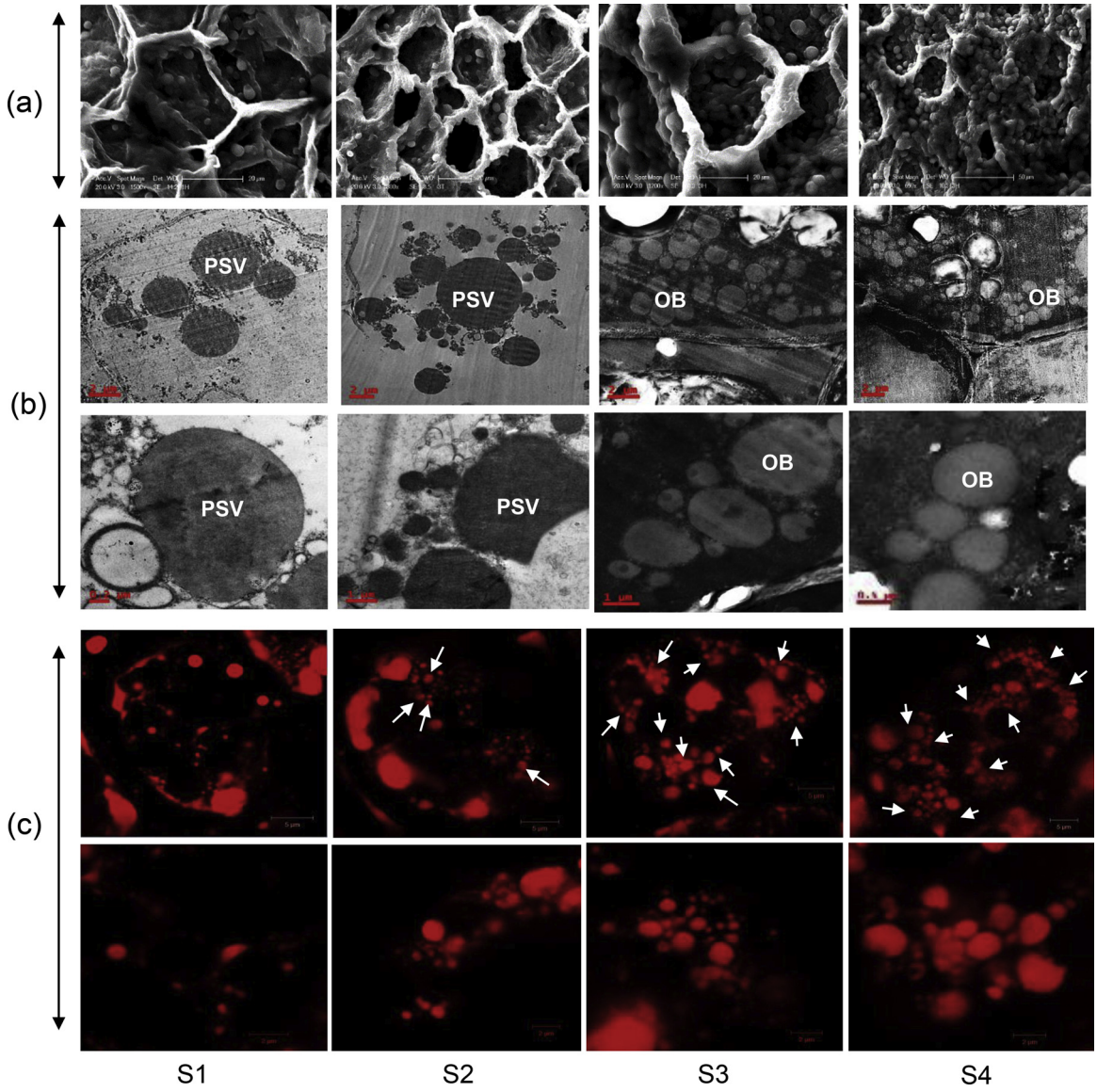

Fig. 6. *P. pinnata* seed cross section under SEM **(a)** (20–50 μ) and TEM **(b)** (2–0.2 μ). Nile red staining of *P. pinnata* seed sections observed under confocal microscope, oil bodies are marked by white arrows **(c)** (5–2 μ). PSV- protein storage vacuole; OB- oil body.

3.2. Complete metabolome analysis of developmental stages of P. Pinnata seed

In all the four stages, 61 metabolites were identified with the help of GCMS analysis (Supplementary data 1). Metabolites were classified based on their chemical structure (Fig. 4a) and biological functions (Fig. 4b). The variation among distinctive profile of metabolites was observed through PCA analysis where there was overall 71.7% separation among the developing stages (Supplementary data 3). Separation or variation of seed metabolites among S2 and S3 was less when compared to S1 and S4. Majority of the metabolites detected were functionally related to protein metabolism (21%), carbohydrate metabolism (18%) and development (16%). Rest of the metabolites belonged to energy (12%), stress and defense (10%), fatty acids (9%), cell wall formation (7%), hormonal responses (4%) and secondary metabolism (3%) (Fig. 4b). The dynamics of the metabolites were determined by their concentration during the 4 developing stages analyzed through heat map using Pearson's test in MetaboAnalyst online software. Metabolites were classified as fatty acids, amino acids, sugars and organic acids depending on their respective chemical characteristics (Fig. 4a). Among the sugars, ribose, glucose, erythrose, gluconic acid, inositol and ribonolactone had higher concentrations at S1 which gradually decreased with the maturation. Glyceric acid, pinitol and mannose were abundant at S4 whereas sugars like cellobiose, arabinose and NADGA were higher during S1 to S2. In contrast to the sugars, most of the amino acids and organic acids were abundant during S3 and S4 (Fig. 4a). Leucine, threonine, alanine, tryptophan, valine, glutamate and some organic acids including keto-glutaric acid, fumaric acid, succinic acid, pyruvic acid and malonic acid were abundant in S3 and S4. The concentrations of glycine, proline and glutamine were higher in S4. Similarly, adipic acid and allonic acids were higher during S3 and S4 respectively (Fig. 4a). In contrast, few organic acids including propionic acid, acetate, malic acid, citric acid, oxalic acid and certain amino acid such as aspartic acid were more at S1, which gradually decreased to the lowest levels at S4. Fatty acids which were abundant in S1 were stearic acid and myristic acid, hexanoic acid was abundant in S3, while others including butanoic acid, and eicosane were more in S4 (Fig. 4a).

3.3. 2D- proteomic profile of developing P. Pinnata seed

The seed protein expression patterns were quantified at different

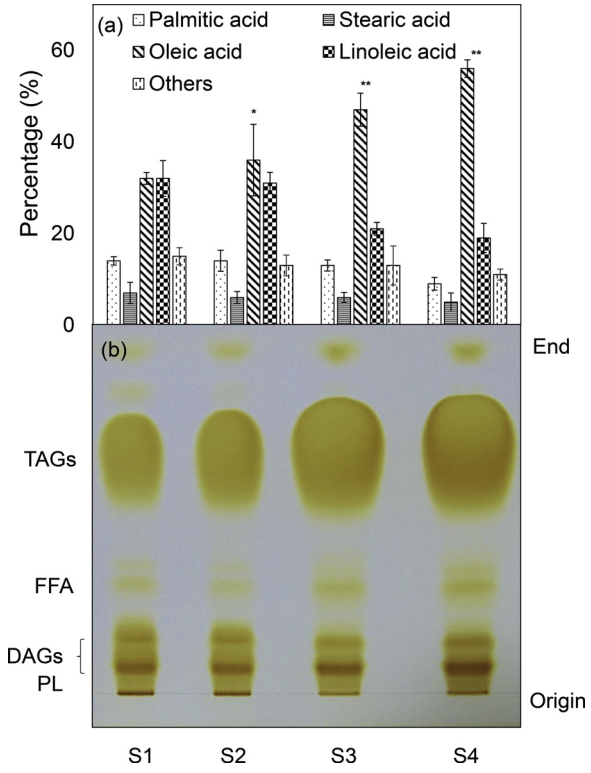

Fig. 7. Percentage of fatty acids accumulated in the TAGs at different developing stages **(a)**. Total lipid profiling through TLC **(b)**. Values are mean ± SD (n = 3). *, ** represents significance difference (P < 0.05, P < 0.01) between the fatty acid content with respect to 120 DAA, analyzed by *t*-test.

developing stages of *P. pinnata* seed. More than 300 spots were reproducibly detected in all the gels with Image Master 2D Platinum software and 125 spots matched in all the four stages (Fig. 5a). Based on the percent spot volume in the S1 stage, we have determined the significantly upregulated, unchanged or downregulated spots throughout developing stages. Some of the spots were selected and successfully identified using MALDI MSMS (Table 1). Rest of the spots which did not give any significant match in the MASCOT search were not considered. All of the differentially regulated spots were represented as gel picture in the supplementary data 2, and the changes in some of the spots among the different stages were represented along with the reference gel in Fig. 5a,b. The spot distribution and intensity at each stage were analyzed through PCA analysis which illustrated the variation in the form of percentage separation (Supplementary data 4). There was overall 64.4% separation among the stages and the graph clearly showed the protein profile of S4 was different compared to the younger stages (120–240 DAF). The profiles of S2 and S3 were more similar with least separation (Supplementary data 4). The functions of the identified spots were classified based on the available literature (Fig. 5c). The upregulated spots from S1 to S4 were identified as Accase, lipid transfer like protein VAS, ATP synthase subunit β and GTP binding protein SAR1b. The unchanged spots were identified as PEP carboxykinase and G3PD. Two of the downregulated spots included Midasin and ap2 complex subunit alpha1 (Table 1). The protein spot identified as ELF 4 was observed only in S1 whereas, Allergen Len was observed only in S4 (Table 1).

3.4. Visualization of storage granules and oil bodies in developing P. Pinnata seeds

The surface morphology of *P. pinnata* cotyledonary cross sections analyzed by SEM at various stages showed an increase in storage granules from S1 to S4 (Fig. 6a). Further the biochemical nature of these storage granules were studied through TEM analysis and identified large protein vacuoles at S1 which further increased during S2. The appearance of a large amount of oil body accumulation was observed in S3 and S4, where the lipid droplets were located at cellular periphery (Fig. 6b). For more clarification of the accumulation of oil bodies in developing stages, Nile red fluorescent staining was performed which specifically stains only the lipid containing substances. Oil body accumulation was very low at S1 and S2, but showed rapid increase at S3 to S4 (Fig. 6b, c). Moreover, the oil bodies were localized near the periphery of the cell with sizes varying from 1 to 2 μ while the protein storage vacuoles have unusually large diameter (~2–5 μ) and situated mostly in the central region (Fig. 6).

3.5. Fatty acid profiling of the TAGs

The separation of phospholipids, DAGs and TAGs during developing stages were compared by the intensities on the TLC plates which have been loaded with equal quantity and separated with the same mobile phase. There was a visible change in the TAGs accumulation where it progressively increased as the seeds reached maturity (Fig. 7b). The fatty acid profile of the accumulated TAGs was examined with the help of GCMS analysis and compared with the FAMEs standards, based on which the percentage was also determined. The major fatty acids during initial stages of development (S1 and S2) were oleic and linoleic acid which were present in equal amounts (Fig. 7a). In later stages of development, oleic acid gradually increased with a significant ($P < 0.05$) decrease in linoleic acid (Fig. 7a). Furthermore, palmitic acid also decreased gradually from S1 to S4 (Fig. 7a) while there was no change in stearic acid content in all the stages.

4. Discussion

The basic seed morphology and biochemistry of developing *P. pinnata* seed share certain similar developmental regulatory processes with other legumes where, the pods were nearly flat in younger stages with a tiny developing seed inside and the pod thickness increased as the seed developed, finally filling the pod (Wright and Lenssen, 2013). The duration of seed development in *P. pinnata* is a prolonged process making it complex to understand the seed filling and oil accumulation patterns in this imminent biofuel tree species. Thus, knowledge on physiological and molecular dynamics of this lengthy seed development will boost the attempts to improve the seed productivity towards potential biofuel feedstock. The current study thoroughly examined the seed developmental processes of *P. pinnata* and deduced the physiological, biochemical and molecular changes through metabolomics and proteomic approaches. Our present studies also provide insights into the photo-autotrophic nature of *P. pinnata* seed.

Legume seed development and differentiation is characterized by three rapid growth phases separated by two lag phases (Weber et al., 2005). Majorly, the growth phases are marked by the development of endosperm, seed coat and embryo associated with maturation and cell expansion. The differentiation of processes during seed development is a sequential process which involves active mitotic cell division, sucrose uptake, cell expansion, greening and gaining of photosynthetic activity as well as accumulation of storage products (Baud et al., 2002). For oil seeds, the differentiation phase is of special interest because during this stage a regulatory network initiates the accumulation of storage products. The developing seeds of *P. pinnata* are green in color at younger stages (S1-S2) which turned brown during maturation with a gradual increase in seed weight, storage products and lipid content but decrease in moisture content as well as the weight of seed coat. The importance of maternal seed coat in providing the necessary sources of filial cotyledons for development and controlling germination is well known in legumes (Weber et al., 2005). Seed coat percentage in terms of its structural weight is high during younger stages of development which indicated its active role in maintaining seed development. During

natural seed maturation process, there is a gradual increase in seed desiccation, wherein the water content declined significantly, (Angelovici et al., 2010). In general, chlorophyll content and the ratio of chlorophyll *a*/b ratio play a significant role in developing green seeds and are directly related to the photosynthetic efficiency of the green seeds (Eastmond and Kolacna, 1996). In the current study, initial stages of *P. pinnata* seed showed higher chlorophyll *a*/b ratio (> 1), which declined gradually with maturation. This clearly indicated the active photosynthesis in *P. pinnata* developing seeds during S1 and S2. To support our results, we have also analyzed the gene expression of some of the key photosynthetic electron transport genes. PS I and PS II related gene expression was reported in many green and oil yielding seeds and it is also considered to be an important factor for embryo development and fatty acid biosynthesis (Niu et al., 2009; Allorent et al., 2015). The expression of photosynthetic genes in *P. pinnata* was higher till S2 after which there was a steady decline in expression levels indicating very active photosynthetic process during the initial stages of seed development. The temporal induction of ATP synthase subunit gene (atp1A) could have also contributed for substantial production of ATP which is needed for the energy productions and fatty acid biosynthesis. The seed photosynthesis may provide energy for the fatty acid biosynthesis during subsequent stages and also helps in re-fixing the respiratory CO_2 release. The release of O_2 through the photosynthesis can aid in reducing NO:O_2 ratio, thereby preventing anoxia in seeds during development (Borisjuk and Rolletschek, 2009). Active photosynthesis might also contribute for significant accumulation of storage products including protein, starch and other carbohydrates which was evident in this study with *P. pinnata* seeds.

Metabolites are considered as very robust and sensitive as they maintain the seed physiology and storage biochemistry (Weselake et al., 2009). Understanding the dynamics of metabolic profile among various stages of development might give new insights into the mechanism of seed oil biosynthesis with respect to quantity and quality of lipids in this potential biofuel crop. The stage dependent metabolite changes of various crops including *Oryza sativa*, *Glycine max* and *Brassica napus* were recently reported which had enlightened the role of metabolites in regulating oil biosynthesis, cellular morphology, seed filling and maturity (Tan et al., 2015; Hu et al., 2016; Gupta et al., 2017). We have detected sugars, organic acids, free fatty acids and amino acids through our metabolite analysis in developing *P. pinnata* seed. Sugars and organic acids take part in energy metabolism thus providing reducing compounds as well as precursors for fatty acid biosynthesis, cell division and differentiation. Among the detected sugars, glucose is utilized as a signal for cellular multiplication and differentiation while other sugars like ribose and erythrose take part in nucleotide formation and energy metabolism such as Calvin cycle. Interestingly, sugars related to cell wall formation and cell division were higher in S2-S3, for example NADGA, cellobiose, pyranose and arabinose indicating that the active stages of cellular division and differentiation are from S1 to S3. Sugars such as mannose were most abundant in the mature stage S4 and it may contribute to the production of bioethanol from remaining seed residue after the extraction of oil. The major organic acid components of TCA cycle were also detected in the metabolites where, the stage wise quantitative changes were observed in *P. pinnata* seeds. The presence of a flux mode for respiratory energy synthesis through TCA may be the reason of expression of these metabolites in higher concentration during initial stages (S1-S3), which in turn can aid the fatty acid biosynthesis. Amino acids in the developing seeds contribute in various metabolic activities including storage protein accumulation, germination, stress responses and in respiratory catabolic processes to maintain optimum energy status inside the developing seeds (Miranda et al., 2001; Galili et al., 2014). Most of the amino acids were abundant in S2-S3, while glycine and proline which are having stress responsive characteristics were abundant during S4 providing clues for stress tolerance nature of *P. pinnata* seed as the development progressed (Hayat et al., 2012; Czolpinska and Rurek, 2018). The other important amino acids such as glutamate, aspartate, glutamine were also detected which play a central role in the synthesis of other amino acids during seed development (Brian et al., 2007; Jander and Joshi, 2009).

Total seed storage protein profile analyzed through 2D gel electrophoresis gave the overall picture of stage wise variation in protein expression and regulation, where some key regulatory proteins have been successfully identified. The proteins, related specifically to seed development are Midasin and ap2 complex subunit alpha which take part in the development of female gametophyte as well as the cotyledonary development (Chantha et al., 2010). On the other hand, glyceraldehyde-3-phosphate dehydrogenase, a glycolytic enzyme showed higher expression during younger stages which decreased significantly at S4 indicating an active cellular mechanism such as glycolysis at younger stages S1-S2 which gradually decreased with maturation. ATPase subunit beta of photosynthetic electron transport and PEP carboxykinase of carbon assimilation metabolism were upregulated at S2-S3. Our data infers that photosynthesis in *P. pinnata* seed plays a critical role in carbon recycling and energy metabolism which is crucial for fatty acid biosynthesis. Significantly upregulated spots from S1 to S4 included acetyl CoA carboxylase (Accase), the first catalyzing enzyme of fatty acid biosynthesis and lipid transfer like proteins (LTPs). The LTPs are low molecular weight (9–10 kD) proteins and have a significant role in plant development such as transporting lipids for membrane biosynthesis, defense responses and vesicular transports (Liu et al., 2015). A subcellular localization study in seeds also showed the involvement of LTPs with protein as well as lipid bodies (De O. Carvalho et al., 2004). In addition, GTP binding protein SAR1b, which is well known for taking part in vesicular protein traffic from Endoplasmic reticulum to Golgi leading to storage body formation was detected in *P. pinnata* seeds (Memon, 2004). Moreover, recently in liver cells, phosphorylation of SAR1b had been proven to be an important step for release of lipid chylomicrons (Siddiqi and Mansbach., 2012). However, in plants particularly the high oil yielding species like *P. pinnata*, it still remains a question to whether this protein carries a role in the synthesis of lipid bodies.

The accelerating accumulation of oil bodies in developing seeds could help in determining the best harvest time of *P. pinnata* seeds. However, the size and pattern of oil body accumulation during seed development is important for understanding the dynamics of molecular regulation behind this process. It was evident from our data that TAG levels were increased gradually as the seed development progressed and the fate of most of the TAGs accumulated is to ultimately form oil bodies (Hills, 2004). The increasing number of oil bodies with maturation suggest that majority of storage product observed were lipids in *P. pinnata* seed. The FAMEs composition of biofuel and its blend can determine its efficiency for fuel capacity (Sbihi et al., 2018; Xiong et al., 2018). In *P. pinnata*, the fatty acid composition of accumulated TAGs at each stage had shown that oleic acid was predominantly incorporated only after S3 making the seed oil of *P. pinnata* rich with unsaturated fatty acids and making it a valuable source of biodiesel which meets all the standard criteria for biodiesel production (Karmee and Chadha, 2005).

5. Conclusion

Present study highlights the active role of metabolites and some key proteins in the stage specific regulation of *P. pinnata* seed development. The pattern of gene expressions along with metabolites and the proteome data can contribute to possible regulatory networks of cellular metabolism responsible for synthesis and accumulation of oil in Pongamia seeds during different developmental stages. Major metabolites and proteins of each stage belonging to various pathways are identified and their profiles reveal that energy metabolism and cell division are major processes in S1 and S2 which is followed by rapid increase in storage products along with oil bodies from S3 to S4. The TAGs are the major form of lipids in Pongamia oil and we confirmed

that in mature seeds they contribute to the highest content of oleic acid, which also concur with high content of unsaturated fatty acid in *P. pinnata* making it desirable for biofuel production. These results will possibly lay the foundation for metabolic engineering of oilseed crops for improving the quality and quantity of seed oil as a potential feedstock in the biofuel industry.

Declaration of Competing Interest

Authors declare to have no conflict of interest.

Acknowledgements

The present study was supported by a grant from Department of Biotechnology (DBT), Govt. of India (BT/PR12024/BCE/8/1097/2014). Authors like to thank Tree Oils India Limited for providing access to the farm for sample collection and experimental setup. KTS thanks DBT, New Delhi and RVS, SM thanks UGC, New Delhi for fellowship.

Appendix A. Supplementary data

Supplementary material related to this article can be found, in the online version, at doi:https://doi.org/10.1016/j.indcrop.2019.111621.

References

Allorent, G., Osorio, S., et al., 2015. Adjustments of embryonic photosynthetic activity modulate seed fitness in Arabidopsis thaliana. New Phytol. 205, 707–719.
Angelovici, R., Galili, G., et al., 2010. Seed desiccation: a bridge between maturation and germination. Trends Plant Sci. 15, 211–218.
Arnon, D., 1949. Copper enzymes isolated chloroplasts, polyphenoloxidase in Beta vulgaris. Plant Physiol. 24, 1–15.
Atabani, A.E., Silitonga, A.S., et al., 2013. Non-edible vegetable oils: a critical evaluation of oil extraction, fatty acid compositions, biodiesel production, characteristics, engine performance and emissions. Renew Sust Energ Rev. 18, 211–245.
Bala, M., Nag, T.N., et al., 2011. Proximate composition and fatty acid profile of *Pongamia pinnata*, a potential biodiesel crop. J. Am. Oil Chem. Soc. 88, 559–562.
Baud, S., Boutin, J., et al., 2002. An integrated overview of seed development in *Arabidopsis thaliana* ecotype WS. Plant Physiol. Biochem. 40 (2), 151–160.
Baud, S., Dubreucq, B., et al., 2008. Storage reserve accumulation in *Arabidopsis*: metabolic and developmental control of seed filling. Arabidopsis. Book. 6, e0113.
Bligh, E.G., Dyer, W.J., 1959. A rapid method of total lipid extraction and purification. Can. J. Biochem. Physiol. 37, 911–917.
Borisjuk, L., Rolletschek, H., 2009. The oxygen status of the developing seed. New Phytol. 182, 17–30.
Borisjuk, L., Rolletschek, H., et al., 2003. Differentiation of legume cotyledons as related to metabolic gradients and assimilate transport into seeds. J. Exp. Bot. 54 (382), 503–512.
Bradford, M.M., 1976. A Rapid and sensitive method for the quantitation of microgram quantities of protein utilizing the principle of protein-dye binding. Anal. Biochem. 72, 248–254.
Chaitanya, B.S.K., Kumar, S., et al., 2015. Pivotal role of sugar fluxes between the inner integument and endosperm in lipid synthesis during seed ontogeny in *Jatropha curcas* L. Ind. Crops Prod. 76, 1106–1113.
Chantha, S.C., Gray-Mitsumune, M., et al., 2010. The MIDASIN and NOTCHLESS genes are essential for female gametophyte development in Arabidopsis thaliana. Physiol. Mol. Biol. Plants 16 (1), 3–18.
Coetzee, R., Labuschagne, M.T., et al., 2008. Fatty acid and oil variation in seed from kenaf (Hibiscus cannabinus L.). Ind. Crops Prod. 27 (1), 104–109.
Czolpinska, M., Rurek, M., 2018. Plant glycine-rich proteins in stress response: an emerging, still prospective story. Front. Plant Sci. 9, 302.
De O. Carvalho, A., De S. Teodoro, C.E., et al., 2004. Intracellular localization of a lipid transfer protein in *Vigna unguiculata* seeds. Physiol. Plant. 122, 328–336.
Eastmond, P.J., Kolacna, L., 1996. Photosynthesis by developing embryos of oilseed rape Brassica napus. J. Exp. Bot. 47, 1763–1769.
Eastmond, P.J., Rawsthorne, S., 2000. Coordinate changes in carbon partitioning and plastidial metabolism during the development of oilseed rape embryos. Plant Physiol. 122 (3), 767–774.
Ekman, A., Hayden, D.M., et al., 2008. Carbon partitioning between oil and carbohydrates in developing oat (*Avena sativa* L.) seeds. J. Exp. Bot. 59 (15), 4247–4257.
Galili, G., Avin-Wittenberg, T., et al., 2014. The role of photosynthesis and amino acid metabolism in the energy status during seed development. Front. Plant Sci. 5, 447.
Greenspan, P., Mayer, E.P., et al., 1985. Nile red: a selective fluorescent stain for intracellular lipid droplets. J. Cell Biol. 100 (3), 965–973.
Gupta, M., Bhaskar, P.B., et al., 2017. Integration of omics approaches to understand oil/protein content during seed development in oilseed crops. Plant Cell Rep. 36 (5), 637–652.
Hayat, S., Hayat, Q., et al., 2012. Role of proline under changing environments: a review. Plant Signal. Behav. 7 (11), 1456–1466.
Hedge, J.E., Hofreiter, B.T., 1962. In: Whistler, R.L., Be Miller, J.N. (Eds.), Methods in Carbohydrate Chemistry 17. Academic Press, New York.
Hills, M.J., 2004. Control of storage-product synthesis in seeds. Curr. Opin. Plant Biol. 7, 302–308.
Hiscox, J.D., Israelstam, G.F., 1979. A method for the extraction of chlorophyll from leaf tissue without maceration. Can. J. Bot. 57, 1332–1334.
Hu, C., Tohge, T., et al., 2016. Identification of conserved and diverse metabolic shifts during rice grain development. Sci. Rep. 6, 20942. https://doi.org/10.1038/srep20942.
Jander, G., Joshi, V., 2009. Aspartate-derived amino acid biosynthesis in Arabidopsis thaliana. Arabidopsis Book 7, e0121.
Karmee, S.K., Chadha, A., 2005. Preparation of biodiesel from crude oil of Pongamia pinnata. Bioresour. Technol. 13, 1425–1429.
Kesari, V., Rangan, L., 2011. Coordinated changes in storage proteins during development and germination of elite seeds of *Pongamia pinnata* a, a versatile biodiesel legume. AoB Plants 2011 (2011), plr026.
Kopka, J., Schauer, N., et al., 2005. GMD @ CSB. DB: the golm metabolome database. Bioinformatics 21, 1635–1638.
Kumar, S., Sreeharsha, R.V., et al., 2017. Molecular insights into photosynthesis and carbohydrate metabolism in Jatropha curcas grown under elevated CO2 using transcriptome sequencing and assembly. Sci. Rep. 7, 11066.
Liu, F., Zhang, X., et al., 2015. Non-specific lipid transfer proteins in plants: presenting new advances and an integrated functional analysis, J. Exp. Bot. 66 (19), 5663–5681.
Livak, K.J., Schmittgen, T.D., 2001. Analysis of relative gene expression data using real time quantitative PCR and the $2-\Delta\Delta CT$ method. Methods 25, 402–408.
Luthra, R., Munshi, S.K., et al., 1991. Elationship of carbohydrate metabolism with lipid biosynthesis in developing sunflower (*Helianthus annuus* L.) seeds. J. Plant Physiol. 137 (3), 312–318.
Memon, A.R., 2004. The role of ADP-ribosylation factor and SAR1 in vesicular trafficking in plants. Biochim. Biophys. Acta 1664 (1), 9–30.
Miranda, M., Borisjuk, L., et al., 2001. Amino acid permeases in developing seeds of *Vicia faba* L.: expression precedes storage protein synthesis and is regulated by amino acid supply. Plant J. 28, 61–71.
Mudalkar, S., Golla, R., et al., 2014. De novo transcriptome analysis of an imminent biofuel crop, Camelina sativa L. Using Illumina GAIIX sequencing platform and identification of SSR markers. Plant Mol. Biol. 84, 159–171.
Muktham, R., Ball, A.S., et al., 2016. Bioethanol production from non-edible de-oiled *Pongamia pinnata* seed residue-optimization of acid hydrolysis followed by fermentation. Ind. Crops Prod. 94, 490–497.
Niu, Y., Wu, G.Z., et al., 2009. Global analysis of gene expression profiles in *Brassica napus* developing seeds reveals a conserved lipid metabolism regulation with *Arabidopsis thaliana*. Mol. Plant 2, 1107–1122.
Pavithra, H.R., Gowda, B., et al., 2012. Oil, fatty acid profile and karanjin contentin developing *Pongamia pinnata* (L.) Pierre seeds. J. Am. Oil Chem. Soc. 89, 2237–2244.
Pavithra, H.R., Gowda, B., et al., 2014. Biochemical changes in the composition of developing seeds of *Pongamia pinnata* (L.) Pierre. Ind Crops Pro6d 53, 199–208.
Rolletschek, H., Radchuk, R., et al., 2005. Evidence of a key role for photosynthetic oxygen release in oil storage in developing soybean seeds. New Phytol. 167, 777–786.
Sbihi, H.M., Nehdi, I.A., et al., 2018. Study of oxidative stability and cold flow properties of Citrillus colocynthis oil and *Camelus dromedaries* fat biodiesel blends. Ind. Crops Prod. 122, 133–141.
Schiltz, S., Munier-Jolain, N., et al., 2005. Dynamics of exogenous nitrogen partitioning and nitrogen remobilization from vegetative organs in pea revealed by 15N in Vivo labeling throughout seed filling. Plant Physiol. 137 (4), 1463–1473.
Schwender, J., Goffman, F., et al., 2004. Rubisco without the Calvin cycle improves the carbon efficiency of developing green seeds. Nature 432, 779–782.
Schwender, J., Hebbelmann, I., et al., 2015. Quantitative multilevel analysis of central metabolism in developing oilseeds of oilseed rape during in vitro culture. Plant Physiol. 168 (3), 828–848.
Sengupta, D., Kannan, M., et al., 2011. A root proteomics-based insight reveals dynamic regulation of root proteins under progressive drought stress and recovery in *Vigna radiata* (L.) Wilczek. Planta 233 (6), 1111–1127.
Sharma, S., Guleria, S., et al., 2011. Lipid accumulation in developing soybean: influence of seed position on stem axis. Genet. Plant Physiol. 1, 56–67.
Siddiqi, S., Mansbach, C.M., 2012. Phosphorylation of Sar1b protein releases liver fatty acid-binding protein from multiprotein complex in intestinal cytosol enabling it to bind to endoplasmic reticulum (er) and bud the pre-chylomicron transport vesicle. J. Biol. Chem. 287 (13), 10178–10188.
Singh, Y., Sharma, A., et al., 2018. Optimization of performance and emission parameters of direct injection diesel engine fuelled with Pongamia methyl esters-response surface methodology approach. Ind. Crops Prod. 126, 218–226.
Sreeharsha, R.V., Mudalkar, S., et al., 2016. Unravelling molecular mechanisms from floral initiation to lipid biosynthesis in a promising biofuel tree species, *Pongamia pinnata* using transcriptome analysis. Sci. Rep. 6, 34315.
Sun, C., Jia, L., et al., 2017. Natural variation in fatty acid composition of *Sapindus spp*. Seed oils. Ind. Crops Prod. 102, 97–104.
Tan, H., Xie, Q., et al., 2015. Dynamic metabolic profiles and tissue-specific source effects on the metabolome of developing seeds of Brassica napus. PLoS One 10 (4), e0124794.
Weber, H., Borisjuk, L., et al., 2005. Molecular physiology of legume seed development. Annu. Rev. Plant Biol. 56, 253–279.
Weselake, R.J., Taylor, D.C., et al., 2009. Increasing the flow of carbon into seed oil. Biotechnol. Adv. 27 (6), 866–878.
Wright, D., Lenssen, A.W., 2013. Staging soybean development. Agri.Environ.Exten. Pub. 191.
Xiong, B., Zhang, Z., et al., 2018. Biodiesel from *Lindera glauca* oil, a potential non-food feedstock in Southern China. Ind. Crops Prod. 122, 107–113.

Research Article

Received: 1 August 2018 Revised: 25 October 2018 Accepted article published: 29 October 2018 Published online in Wiley Online Library: 27 December 2018

(wileyonlinelibrary.com) DOI 10.1002/jsfa.9457

Pod-wall proteomics provide novel insights into soybean seed-filling process under chemical-induced terminal drought stress

Debashree Sengupta,[a] Divya Kariyat,[a] Sureshbabu Marriboina[a] and Attipalli R Reddy[a,b]*

Abstract

BACKGROUND: Drought is very detrimental when it occurs during the reproductive phase of soybeans, leading to considerable yield loss due to the disproportionate allocation of photo-assimilates to competing sinks. As pod walls are known to play a crucial role in regulating carbon partitioning during seed filling under stress conditions, the present study aims to analyze the stage-specific carbon allocation pattern during potassium iodide (KI)-simulated terminal drought, and to provide an insight into the pod-wall proteome responses during drought onset.

RESULTS: A comparative proteomics approach was adopted to visualize the differential protein expression in soybean pod-wall at stage R5 (seed initiation). Sugar status was analyzed using high-performance liquid chromatography (HPLC) and biochemical methods. Potassium iodide-simulated terminal drought during reproductive stages 4, 5 and 6 (R4, R5, and R6) caused a significant decline in starch, total carbohydrate, and reducing sugar in the leaves; however, the pod-wall and seeds showed a reduction only in the total carbohydrate content, whereas starch and reducing sugar levels remained unchanged. A pod-wall proteome at stage R5 showed immediate induction of proteins belonging to stress signaling / regulation, protein folding / stabilization, redox-homeostasis, cellular energy, and carbon utilization and down-regulation of negative regulators of drought stress and protein degradation-related proteins.

CONCLUSIONS: A KI spray effectively simulated terminal drought stress and caused around 50% yield loss when compared to controls. Our results indicate that, at the very onset of desiccation stress, the pod wall (stage R5) activates strong protective responses to maintain the carbon allocation to the surviving seeds.

Supporting information may be found in the online version of this article.

Keywords: carbon allocation; chemical desiccation; *Glycine max*; pod wall; seed filling; terminal drought

INTRODUCTION

The productivity of most economically important crops is often compromised due to adverse environmental conditions, such as drought, high / low temperatures and soil salinity.[1] In general, to ensure survival under water-limiting conditions, plants channel most of the assimilates towards root maintenance, while reproductive structures are deprived, leading to early embryo abortion, reduced seed numbers / weight, and a considerable decrease in the final yield.[2] Analyzing drought stress responses has become the highest priority for agricultural research, and it is making use of the latest information regarding complex drought-induced regulatory mechanisms.[3,4] Among various droughts, agricultural drought, which results from insufficient rainfall, is of particular interest for plant scientists as it has a major effect on plant growth and productivity. Moreover, in India, rainfall patterns are highly erratic and unpredictable leading to droughts and floods, which result in huge crop losses every year.[5] If water deprivation occurs during crucial reproductive growth stages, e.g seed-filling, it results in a massive reduction in the crop yield. Most of the drought-based research focuses on understanding the key defense responses of plants under water-limiting regimes of varying intensities including low, medium, and high levels of stress.[6,7] Studies have also investigated and compared the effect of drought on plant responses at seedling, vegetative, and reproductive stages.[2,8] Such extensive research on drought response in plants has facilitated the current understanding of the complex drought-response mechanism at physiological, biochemical, and molecular levels. Development of drought-tolerant crop varieties through modernized crop improvement programs such as precision breeding and *cis*-genics approaches are gradually materializing.[9,10] Despite the present scientific understanding of drought responses, there is still quite a limited understanding of

* *Correspondence to: AR Reddy, Vice Chancellor, Yogi Vemana University, Kadapa-516005, Andhra Pradesh, India. E-mail: attipalli.reddy@gmail.com*

a *Department of Plant Sciences, School of Life Sciences, University of Hyderabad, Prof. CR Rao Road, Hyderabad, India*

b *Yogi Vemana University, Kadapa, Andhra Pradesh, India*

the immediate molecular responses of the plant for regulating resource allocation to developing reproductive structures. On the other hand, chemical-induced desiccation was reported to simulate terminal drought effects and has been used in several plants including wheat, pearl millet, and soybean for rapid screening purposes.[11–13] To gain an insight into specific regulatory mechanisms, it is crucial to have an in-depth analysis of the KI-induced terminal drought response at the very onset – i.e within a day after spraying (DASP). The outcomes of such an analysis could provide new concepts for understanding the drought-induced regulation of plant physiological and metabolic plasticity.

Soybean (*Glycine max* L. Merril) is a highly important crop legume serving as a rich source of protein and oil because of its high protein (40%) and oil (20%) content. The importance of soybean is evident from the extensive research leading to whole genome sequencing and development of herbicide-tolerant transgenic soybean for commercial cultivation.[14,15] India has lower soybean productivity than other developed countries. One of the major reasons for this is the rainfed cultivation system, with uneven and erratic rainfall patterns. This often causes terminal drought stress, i.e. water deprivation during the key reproductive stages of soybeans, which substantially hampers the final grain yield.[16] At present, extensive research is being diverted towards soybean crop development in terms of yield and disease resistance through breeding and many new hybrid varieties have been developed and released for cultivation. However, the quest for developing significant terminal drought tolerant soybean varieties is still continuing and, hence, an increasing amount of research is being directed towards the analysis of terminal drought tolerance strategies in soybean.

Recent reviews have indicated that the pod walls of leguminous crops are not merely protecting structures but also play a crucial role in regulating carbon partitioning to the developing seed under various adverse environmental conditions.[17] Photosynthetically active (green) pod walls act as additional source for nutrients to the developing seeds and simultaneously perform the action of active sinks, which are capable of storing remobilized carbon and nitrogen from senescing leaves or stems under terminal drought conditions.[18] Studies on developmental stage-specific transcriptional profiling of the pod wall showed that the pod's anatomical changes, along with chlorophyll concentrations, correlated significantly with transcription factor expression patterns.[17,19] Due to the strong interrelationship between pod development and seed size, pod length was even considered as a phenotypic marker for crop yield.[20] Thus, an insight into the pod wall-based molecular mechanisms in response to terminal drought conditions during seed-filling stages will provide very useful information regarding the regulation of seed filling under drought conditions. In the present study, we aim to understand the proteome responses of soybean pod walls, occurring within 24 h (or 1 day after spraying) of potassium iodide-induced desiccation, simulating the initial onset of drought conditions. As far as the authors are aware, this is the first report analyzing the immediate effect of KI-induced desiccation on soybean pod wall proteome and its impact on the final carbon allocation patterns. We believe that the outcomes of the present study will be crucial for an understanding of the initial regulatory aspects of seed filling in soybean under terminal drought conditions and will also facilitate further research for developing terminal drought-tolerant soybean varieties.

MATERIALS AND METHODS

Plant material and experimental design

Gycine max (L.) Merril var. JS335 (Jawahar Soybean-335), a semi-determinate and early maturing (99 days) soybean variety, was used for the present study. The study was carried out in the greenhouse of University of Hyderabad Telangana state, Hyderabad, India (17.3° 10′ N, 78° 23′ E, at an altitude of 542.6 m above mean sea level). The greenhouse conditions were as follows: photosynthetic photon flux density (PPFD) ranged from 900–1200 $\mu molm^{-2}\ s^{-1}$, air temperature 24 ± 1 °C (~5:00–6:00 h) to 36 ± 4 °C (~12:00–14:00 h) and relative humidity 36 ± 5%–48 ± 2%. Seeds were germinated in 2 L capacity pots, filled with a mixture of red soil and manure. Commercial *Bradyrhizobium japonicum* in powdered form (Rhizo powder, AgriLife Pvt Ltd, Medak Dist., Hyderabad, India) was mixed with the seeds before sowing. Plants were maintained until the initiation of the reproductive stage (ca. 45 days) under regular watering regimes in which the pot water holding capacity (PC) was maintained at approximately 80–90%.[21] After stage R1 (initial flowering), plants were monitored daily to calculate the days post-anthesis (dpa), and were recorded until stage R8 (supporting information, Table S1).

For the present study, seed-filling stages, i.e. R4 (pod-elongation), R5 (seed initiation), and R6 (complete seed filling) were selected for carbon allocation analysis while only stage R5 was used for proteomics and other molecular analysis. Terminal drought was simulated by using 0.1% potassium iodide (KI) as foliar spray, and 100 mL of 0.1% KI was sprayed uniformly per plant, individually at each stage. Spray treatment was given to three individual plants at each stage. Controls were sprayed with equal amount of double distilled water. The present study was divided into three phases. The first phase was for the confirmation of KI acting as a terminal drought simulator. The second phase analyzed the final impact of stage-specific KI-spray on the H/S ratio, carbohydrates, and yield parameters. The final phase marked the major experimental analysis to gain an understanding of the immediate proteome response of the soybean pod wall to KI spray. The entire experimental strategy is schematically represented in the supporting information, Fig. S1.

It has been well documented that KI simulates terminal drought conditions very effectively and that the development of the stress effect (in the form of senescence) is gradual.[22] For clarity purposes, our experimental design is depicted in three phases. In phase I, randomly selected plants (n = 6), which all belonged to stage R5 (seed initiation), were sprayed with 0.1% KI (100 mL), and another group of stage R5 plants (n = 6) was sprayed with equal amounts of distilled water, and this group served as controls. Then, the morpho-physiological effects of KI-spray at 1 and 9 days after spraying (DASP) were monitored and parameters such as leaf relative water content (LRWC %), total chlorophyll, and carotenoids were estimated during the two time points (1 and 9 DASP) apart from recording the visual leaf pod and seed morphologies. In phase II, a separate group of plants (20 plants at each of stages R4, R5, and R6) were maintained for final yield analysis. Ten plants from each stage were sprayed with 0.1% KI, while the remaining ten were maintained as controls. Potassium iodide-sprayed plants from each stage were allowed to grow until stage R8 (or complete senescence) and seeds, pods, roots, and shoots were harvested, oven dried at 80 °C for 48–72 h and the dry weights were recorded along with the total number of pods and seeds. The same

samples were utilized for reducing sugar, starch, and total carbohydrate analysis, and high-performance liquid chromatography (HPLC)-based estimation of glucose, fructose and sucrose.

As we were interested in identifying key regulatory mechanisms acting immediately in response to terminal drought, in phase III, all experiments were performed during 1 DASP of KI-spray treatment at stage R5 (n = 6) to obtain information on the immediate stress response during the seed-filling stages. Hence, samples were collected at 1 DASP and either submerged in fixative solutions (for further microscopic analysis) or frozen in liquid nitrogen and stored in −80 °C. In phase III, comparative pod wall proteomics and scanning electron microscopy were performed.

Physiological measurements

To identify the immediate impact of KI-induced stress in soybean during seed filling, we analyzed some of the key physiological parameters, at both 1 DASP and 9 DASP of KI (sprayed during 22 dpa). Plant water status was determined by measuring the leaf relative water content (LRWC %) calculated as: LRWC (%) = [(FW-DW)/(TW-DW)] × 100, where FW is leaf fresh weight, TW is the turgid weight (mass after rehydration obtained by storing leaf samples for 24 h in distilled water) and DW is oven-dried weight (105 °C) of leaves.[23] Leaf pigments were extracted using the dimethyl sulfoxide (DMSO) method according to Hiscox and Israelstam.[24] Absorbance of the extract was recorded at 663.2, 646.8, and 470 nm and the amount of Chl *a*, *b* and total carotenoids were calculated according to the following formula: Chl *a* (μg mL^{-1}): $12.25 \times A_{663.2} - 2.79 \times A_{646.8}$; Chl *b* (μg mL^{-1}): $21.5 \times A_{646.8} - 5.1 \times A_{663.2}$; total carotenoids (μg mL^{-1}):$1000 \times A_{470}$-1.82 × Chl *a*-85.02 × Chl *b*.[25]

Sugars (glucose, fructose, and sucrose) were extracted by following the method of Giannoccaro *et al.*[26] with minor modifications. Briefly, 100 mg of dried and powdered samples was extracted in 1 mL (1:10 w/v) of milliQ water for 15 min in a rotospin. The extracted sample was then centrifuged at 13 000 rpm for 10 min at room temperature and 500 μL of the clear supernatant was transferred to a fresh Eppendorf. This sample aliquot (500 μL) was then purified by adding 1.5 mL of 95% Acetonitrile and mixed for 30 min in the rotospin. The sample was then centrifuged at 13 000 rpm for 10 min at room temperature. The supernatant was collected in a fresh tube and was evaporated completely in a drybath set to 95 °C. The residue was redissolved in 1 mL of milliQ water and filtered through 0.22 μm filter paper (Millipore, Merck) using syringe filters. Sugars were separated isocratically through reverse-phase HPLC using an NH2 column (Shodex-Asahipak NH2P-50-4E) with acetonitrile : water (70:30 v/v) as the mobile phase. Flow rate was set to 1 mL min^{-1} and the absorbance was detected at 190 nm (UV) using a photodiode array (PDA) detector. Glucose, fructose, and sucrose peaks were identified through spiking with standards and the concentrations were calculated using an external standard calibration method. Calibration curves for glucose, fructose, and sucrose were made using 0.5, 1, 2, 5, 10, 15, and 20 mg mL^{-1} concentrations and straight line equations were used for calculating the concentrations from the 'area' of the HPLC peaks of the respective sugars.

To identify the KI spray's effect on the ultimate yield in terms of carbon status of the plant, we analyzed the reducing sugars, starch, and total carbohydrates after stage R8, from each individual KI-sprayed stage (R4, R5, and R6). The total reducing sugars were estimated using a dinitro-salicylic acid (DNS) method following Miller.[27] Total carbohydrate and starch was estimated following Hedge and Hofreiter[28] using Anthrone reagent.

Scanning electron microscopy (SEM)

Anatomical changes were observed using SEM by following the method of Guha *et al.*[29] Freshly harvested pods (stage R5) samples from control and KI-treated (1 DASP) plants were separated into pod-wall, funiculus, and seeds. The pod wall is cut into smaller pieces and fixed in FAA (formaldehyde acetic acid ethanol) solution, along with funiculus and seed tissues, and stored at 4 °C overnight in 50 mL glass vials. Before SEM analysis, fixed pod-wall tissues were sectioned (immersed in pre-cooled fixative solution) longitudinally to obtain 3 × 3 mm inner wall surface. Similarly, the funiculus tissues were also sectioned longitudinally (horizontal surface attached to the seeds), and the seed coats were excised into 3 × 3 mm pieces. All sectioned samples were stored in fresh fixative at 4 °C and then subjected to postfixation in 2% osmium tetroxide for 2 h followed by dehydration in graded ethanol series. Following critical point drying, samples were mounted horizontally in copper stubs using double stick cellophane tape to observe the pod-wall inner surface, funiculus surface, and seed-coat inner surface. The mounted samples were gold-coated in a Polaron sputter coater (Quorum Technologies, UK).Observation and photography were made with a transmission electron microscope (JEOL, Tokyo, Japan) fitted with a scanning attachment (Hitachi S-570, Japan) at 20 kV.

Protein extraction and two-dimensional electrophoresis (2-DE)

Pod walls from both control and KI-sprayed pods were collected at 1 DASP, immediately frozen in liquid nitrogen, and stored at −80 °C until protein extraction. Proteins were extracted as described previously.[6] In brief, 6 g of pod wall tissue was ground to fine powder in liquid nitrogen and suspended in 24 mL of the extraction buffer consisting of 0.5 mol L^{-1} tris–HCl (pH 7.5), 0.7 mol L^{-1} sucrose, 0.1 mol L^{-1} KCl, 50 mmol L^{-1} EDTA, 2% β mercaptoethanol and 1 mmol L^{-1} PMSF. Equal volumes (24 mL) of phenol saturated with tris–HCl (pH 7.5) were added, mixed for 30 min at 4 °C, and centrifuged at 5000 g for 30 min at 4 °C. The upper phenolic phase was collected, and an equal volume of extraction buffer was added to it. The above step was repeated, and the upper phenolic phase was re-extracted. Four volumes of 0.1 M ammonium acetate in methanol was added to the collected phenolic phase and kept overnight at −20 °C for protein precipitation. The samples were then centrifuged at 10 000×*g* at 4 °C for 30 min and the precipitate was washed three times in ice-cold methanol and twice in ice-cold acetone and air dried. The final pellet was solubilized in 200 μL of the rehydration solution (8 M (w/v) urea, 2 M (w/v) thiourea, 4% (w/v), CHAPS, 30 mmol L^{-1} Dithiothreitol (DTT), 0.8% (v/v) Immobilized pH gradient (IPG) buffer pH range 4–7 (GE Healthcare)), and the protein concentration was determined.

Aliquots of 800 μg protein were mixed with rehydration solution (8 mol L^{-1} urea, 2 mol L^{-1} thiourea, 4% (3-((3-cholamidopropyl) dimethylammonio)-1-propanesulfonate) (CHAPS), 30 mmol L^{-1} DTT, 0.8% IPG buffer pH range 4–7% and 0.004% bromophenol blue) to a final volume of 320 μL and used for 2-DE. Active rehydration of protein (800 μg) was carried out on immobilized pH gradient (IPG) strips (18 cm, 4–7 pH linear gradient; Amersham, GE Healthcare (Chicago, United States) for 12 h at 50 V. Rehydration and focusing was carried out in Ettan IPGphor II GE Healthcare at

20 °C, using the following program: 30 min at 500 V, 3 h to increase from 500 to 10 000 V and 6 h at 10 000 V (a total of 60 000 Vh). After isoelectric focussing (IEF), strips were equilibrated twice for 30 min with gentle rocking at room temperature (25 ± 2 °C) in equilibration buffers. The first equilibration was performed in a solution containing 6 mol L^{-1} urea, 50 mmol L^{-1} Tris-HCl buffer (pH 8.8), 30% (w/v) glycerol, 2% (w/v) SDS and 2% DTT and the second equilibration was performed by using 2.5% (w/v) iodoacetamide instead of DTT. The proteins were separated in the second dimension SDS-PAGE (12% vertical polyacrylamide slab gels) using an EttanDalt6 chamber (GE Healthcare). The gels were stained with modified colloidal Coomassie staining.[30] Protein patterns in the gels were recorded as digitized images using a calibrated densitometric scanner (GE Healthcare) and analyzed (spot cropping, correlation among triplicate gels within control and treated groups, correlation between control and treated groups, statistical analysis using ANOVA), using Image Master 2-D Platinum version 7 (IMP7) image analysis software (GE Healthcare).

In gel digestion and mass spectrometry (MS)

In gel digestion and matrix-assisted laser desorption / ionization time of flight mass spectrometric (MALDI-TOF MS) analysis was conducted with a MALDI- TOF/TOF mass spectrometer (Bruker Autoflex III smartbeam, Bruker Daltonics, Germany) according to the method described by Shevchenko *et al.*[31] with slight modifications. Colloidal Coomassie-stained protein spots were manually excised from three reproducible gels. The excised gel pieces were destained with 100 µL of 50% acetonitrile (ACN) in 25 mmol L^{-1} ammonium bicarbonate (NH_4HCO_3) for five times. Thereafter, the gel pieces were treated with 10 mmol L^{-1} DTT in 25 mmol L^{-1} NH_4HCO_3 and incubated at 56 °C for 1 h. This is followed by treatment with 55 mmol L^{-1} iodoacetamide in 25 mmol L^{-1} NH_4HCO_3 for 45 min at room temperature (25 ± 2 °C), washed with 25 mmol L^{-1} $NH4HCO_3$ and ACN, dried in speed vac and rehydrated in 20 µL of 25 mmol L^{-1} NH_4HCO_3 solution containing 12.5 ng μL^{-1} trypsin (sequencing grade, Promega). The above mixture was incubated on ice for 10 min and kept overnight for digestion at 37 °C. After digestion, it was spun for 10 min and the supernatant was collected in a fresh Eppendorf tube. The gel pieces were re-extracted with 50 µL of 0.1% trifluoroacetic acid (TFA) and ACN (1:1) for 15 min with frequent vortexing. The supernatants were pooled together and dried using speed vac and were reconstituted in 5 µL of 1:1 ACN and 0.1% TFA. Two microliter of the above sample was mixed with 2 µL of freshly prepared α-cyano-4-hydroxycinnamic acid (CHCA) matrix in 50% ACN and 1% TFA (1:1) and 1 µL was spotted on target plate.

MS/MS analysis

Protein identification was performed by database searches (MS/MS) using MASCOT program (http://www.matrixscience.com) employing biotools software (Bruker Daltonics, Germany). The similarity search for mass values was done with existing digests and sequence information from NCBIprot and the Swiss Prot database. The taxonomic category was set to Viridiplantae (green plants) / other green plants. The other search parameters were fixed modification of carbamidomethyl (C), variable modification of oxidation (M), enzyme trypsin, peptide charge of 1+, and monoisotropic. According to the MASCOT probability analysis ($P < 0.05$), only significant hits were accepted for protein identification. Functional categorization of identified proteins was based on the UniProt database (www.uniprot.org).

Statistical analysis

Results of the physiological parameters were represented as mean ± standard deviations (n = 10). The significance of the differences between mean values of control and KI-sprayed plants was determined using Student's *t*-test. All the statistical analyses were performed using the statistical package Sigma Plot 11.0. For proteomic analysis, the 'pooled sample' method was followed to reduce the biological variance and obtain an average sample, in which six randomly selected plant samples were pooled to one for each control and KI-sprayed groups.[32] Further, from each group, triplicate gels were run and each gel within the control as well as treated groups was matched carefully by using IMP7 software, so that the minimum correlation coefficient (R^2) among the gels within or between groups was > 0.8. A one-way ANOVA ($P < 0.05$) was performed by the IMP7 software, which gives a cumulative ANOVA table and only those spots were selected where $P < 0.05$. Further, using the central spot intensity of each spot, we calculated the respective induction factor (relative fold expression) as a ratio of central spot intensity of a particular protein under KI treatment / central spot intensity of that protein under control conditions; > 1.5 fold was considered significant up-regulation, < 0.75 as significant down-regulation.

RESULTS

KI-spray effectively simulates terminal drought stress during seed filling stages of *G. max* JS335

Morphologically, KI-spray during stage R5 of soybean development caused only minimal senescing symptoms within 1 DASP, which gradually increased, and significant yellowing of the leaves was observed at 9 DASP (Fig. 1(a)–(e)). Seed filling was severely affected by KI spray, so that at 9 DASP the seed size remained similar to the initial seed size at the stage R5 with no further development (Fig. 1(f)).The KI-induced desiccation effect on seed filling is similar to terminal drought conditions.[33] Drought simulation was also evident from the LRWC values, which declined by 20% at 1 DASP and around 40% at 9 DASP (Fig. 1(g)). As KI-induced desiccation leads to early senescence, we observed a significant decline in the total chlorophyll content in the leaves at 9 DASP. However, the total chlorophyll content was found to be initially enhanced at 1 DASP (Fig. 1(h)). Total carotenoid content was also significantly increased during 1 DASP, but no significant change was observed at 9 DASP (Fig. 1(i)).

Effect of stage-specific KI spray on pattern of carbohydrate accumulation and hexose-to-sucrose ratios

Significantly less total carbohydrate (TC) accumulated in the leaves of KI-sprayed plants at stages R4, R5, and R6 when compared to the control. Specifically, 32%, 28%, and 21% less TC content was observed in stages R4, R5, and R6 KI-treated plants, respectively. Similarly, 51%, 24%, and 23% lesser starch accumulated in the leaves of KI treated plants at stages R4, R5, and R6, respectively. However, reducing sugars (RS %) were found to be significantly enhanced in the R5 and R6 stage KI-treated plants when compared to controls, while the RS % remained unchanged in plants treated with KI at stage R4 (Fig. 2(a)). In the pod wall, TC declined significantly ($P < 0.05$) by 25%, 40%, and 30% in stages R4, R5, and R6 KI-treated plants, respectively when compared with control plants. However, the changes observed in starch and reducing sugar content were not found to be statistically significant when compared to controls (Fig. 2(b)). Similarly, in the seeds too, the TC levels

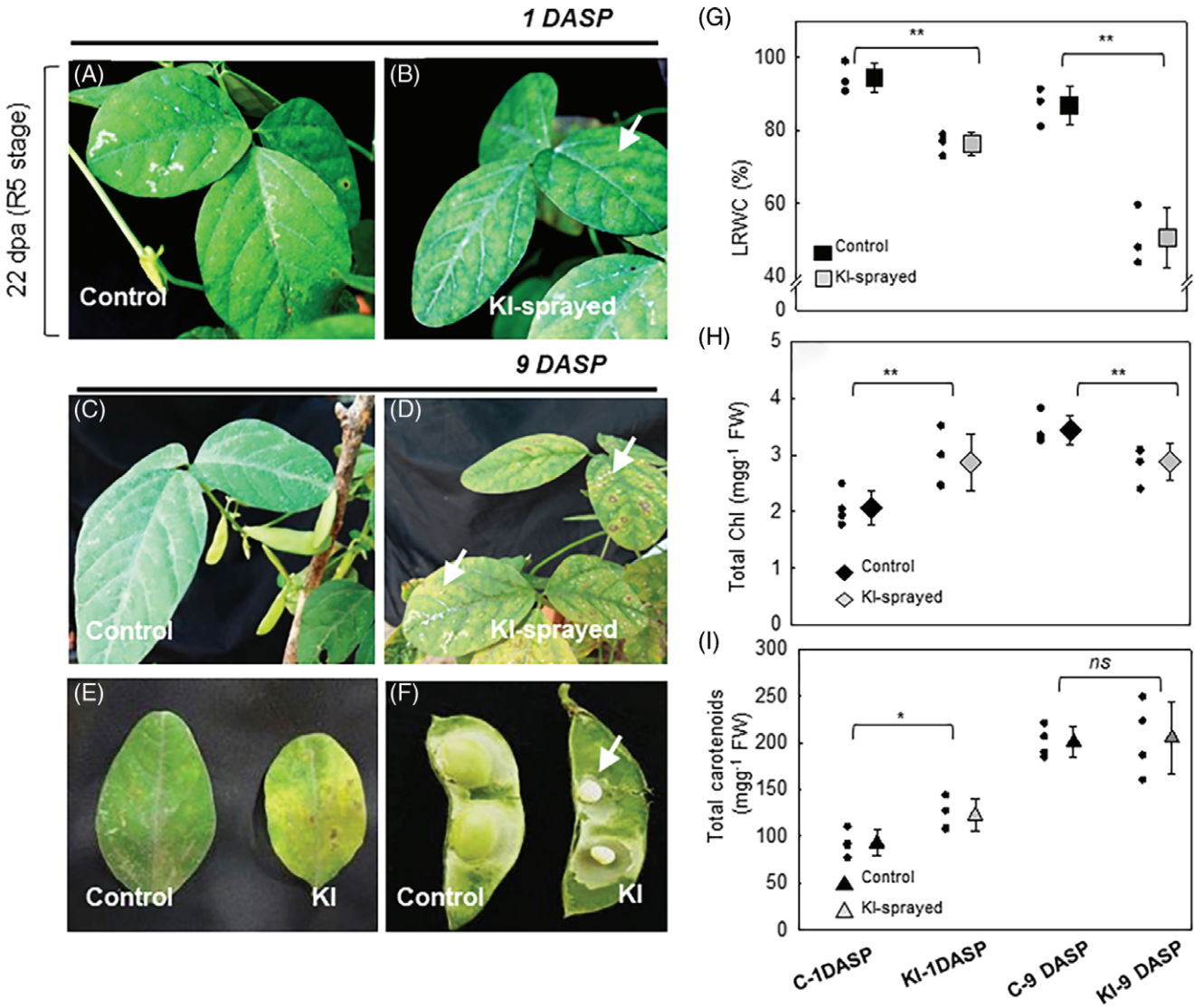

Figure 1. Morpho-physiological parameters of soybean treated with KI spray during 25 dpa and sampled after 1 and 10 DASP to evaluate immediate and prolonged KI-induced desiccation effects, respectively. (a) Soybean leaf morphology at 22 dpa under regular watering conditions. (b) Potassium iodide-sprayed soybean leaf morphology sampled at 1 DASP, showing only slight yellowing (arrow head) at the intravenous space of the leaf lamina and dark green pigmentation in the rest of the spaces. (c) Control leaf morphology at 9 DASP. (d) Potassium iodide-sprayed (during 22 dpa) leaves, sampled at 9 DASP, showing severe senescence symptoms (arrow head). (e) Comparison of single leaf morphology between control and KI-sprayed leaves, sampled at 9 DASP. (f) Seed growth comparison between control and KI-sprayed (during 22 dpa) pods, sampled at 9 DASP, showing complete seed-growth arrest in the KI-sprayed pods. (g) Leaf relative water content. (h) Total chlorophyll. (i) Total carotenoid content in control and KI-sprayed plants at 1 and 9 DASP. Values represent means ± SE (n = 3 or 4) and ***$P < 0.001$, **$P < 0.01$, and *$P < 0.05$.

declined significantly by 32%, 28%, and 28% with respect to controls in stages R4, R5, and R6 KI-treated plants, respectively, but the starch and reducing sugar levels remained statistically unchanged in comparison to control plants (Fig. 2(c)).

We have also analyzed the glucose (G), fructose (F) and sucrose (S) levels individually through HPLC. For maintaining the figure clarity, the statistical significance results for Fig. 2(d), (e) and (f) are presented in Table 1. We observed that the hexose (F + G) to sucrose ratio (H/S) was not significantly changed in the leaves of soybean plant when treated with KI at stages R4 and R5 but was significantly enhanced with KI treatment during stage R6. Similarly, fructose and glucose levels were significantly enhanced in the leaves of stage R4 and R5 KI-treated plants; however, the change in the sucrose levels with KI treatment in the corresponding stage of development remained insignificant. KI treatment during stage R6 resulted in a significant increase in the H/S ratio and a corresponding increase in glucose and decrease in sucrose content, while no significant change was observed in fructose levels (Fig. 2(d) and Table 1). In the pod wall, glucose, fructose, sucrose content and also the H/S ratios were found to be significantly enhanced with KI treatment at all the stages (R4, R5, R6) when compared to control plants (Fig. 2(e) and Table 1). Interestingly, in the seeds, the H/S ratio was found to be significantly less than control seeds. Correspondingly, the sucrose content was found to be significantly enhanced with KI treatment at each stage. Fructose content declined in the seeds when the plants were KI sprayed at stage R4 of development but remained unchanged with KI treatment at stages R5 or R6. Glucose content also declined significantly in seeds on KI treatment of the plants at stages R4 and R5 but remained statistically similar to controls sprayed at stage

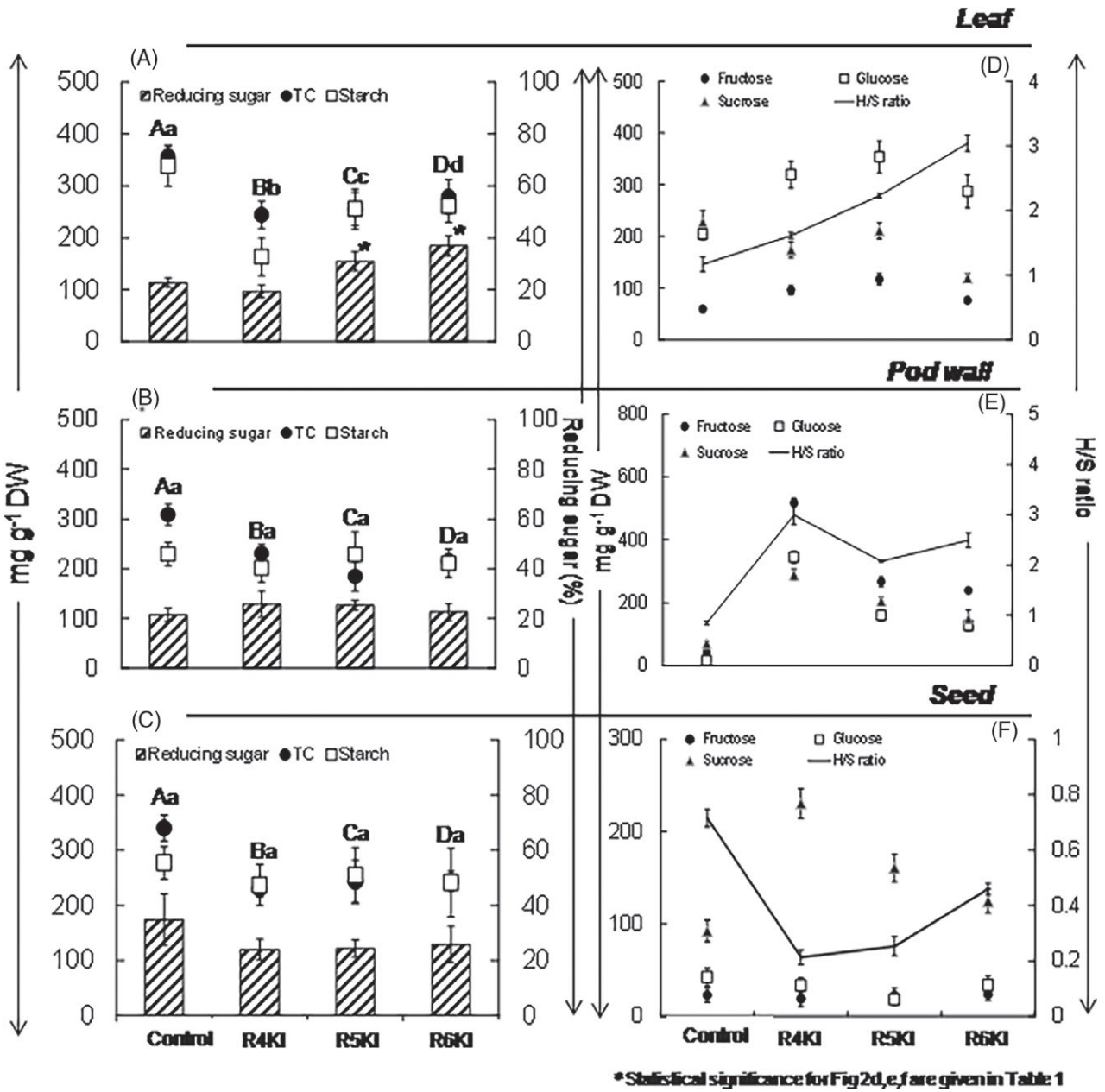

Figure 2. Sugar and carbohydrate alterations with stage-specific KI treatment on *G. max* JS335, analyzed at the end of stage R8. Total carbohydrate, starch (mg g^{-1} DW) and reducing sugar (%) content in the leaves (a), pods (b), and seeds (c) of the control (without treatment), R4 KI-sprayed, R5 KI-sprayed, and R6-KI sprayed plants. Fructose, glucose, sucrose, and hexose (fructose + glucose) to sucrose ratios in leaves (d), pods (e), and seeds (f) of control (without treatment), R4 KI-sprayed, R5 KI-sprayed, and R6 KI-sprayed plants. Values are represented as means of three replicates ± SD, each replicate consisting of samples pooled from three different plants. In (a), (b), and (c), statistical significance was analyzed by one-way ANOVAs and different capital and small letters indicate statistically significant difference in TC and starch, respectively, whereas * indicates the statistically significant difference in reducing sugar with respect to controls (n = 3, $P < 0.05$).

R6 (Fig. 2(f) and Table 1).Yield parameters (Table 2) showed that KI-induced drought stress at stage R5 (seed initiation) resulted in maximum yield loss.

Immediate response of pod-wall proteome to KI-induced desiccation

The entire 2D protein profile of the control soybean pod wall at stage R5 reproducibly detected around 800 protein spots, which matched significantly in all the three replicate gel (correlation coefficient > 0.8), while the 2D gels from KI-sprayed pod wall at 1 DASP reproducibly detected around 600 distinct protein spots, which correlated significantly in the three replicates (correlation coefficient > 0.8) (Fig. 3(a), (b) and supporting information, Fig. S2). Considering one of the control gels as the reference, all three replicate KI-treated gels were matched, which resulted in a significant correlation (correlation coefficient > 0.8) of around 500 protein spots from each gel (supporting information, Fig. S3). Among the matched protein spots, only those were taken for calculating induction factor that showed significant ANOVA results ($P < 0.05$). Among the reproducible protein spots, 20 significantly up-regulated proteins (IF >1.5 fold), seven down-regulated proteins, and six unchanged proteins

Table 1. Student's *t*-test statistical analysis showing significant difference with respect to controls for the fructose, glucose, and sucrose content and H/S ratios in the leaves, pod wall, and seeds of control and stage-specific KI-treated soybean plants (analyzed after stage R8)

Stage of KI treatment	Leaf			
	Fructose	Glucose	Sucrose	H/S ratio
R4	↑**	↑**	ns	ns
R5	↑***	↑↑***	ns	ns
R6	ns	*	↓***	↑**
Stage of KI treatment	Pod wall			
	Fructose	Glucose	Sucrose	H/S ratio
R4	↑***	↑***	↑***	↑***
R5	↑***	↑***	↑***	↑***
R6	↑***	↑***	↑**	↑***
Stage of KI treatment	Seed			
	Fructose	Glucose	Sucrose	H/S ratio
R4	↓*	↓*	↑***	↓***
R5	ns	↓**	↑***	↓***
R6	ns	ns	↑**	↓***

*$P < 0.05$, **$P < 0.01$, ***$P < 0.001$ (n = 3).

were selected for MALDI-TOF-TOF analysis. Among the 33 protein spots, 27 spots showed significant hits ($P < 0.05$) in the MS/MS analysis (Mascot search). Protein profile from representative 2D protein profile of soybean pod wall indicating the position of all the 27 identified proteins is given in Fig. 4(a) and the details of each identified protein is provided in Table 3. Significantly up-regulated, down-regulated, and unchanged proteins in the soybean pod wall within 1 DASP of KI spray were categorized into five, three, and two major functional groups, respectively. Up-regulated proteins include signaling / regulatory, cellular energy, redox-homeostasis, carbon utilization, and protein folding / stabilization-related proteins, whereas protein degradation and ABA responsive negative stress regulator proteins were found to be down-regulated. Nutrient storage and cytoskeleton-related proteins remained consistently unchanged (Fig. 4(b), (c)).

Immediate alterations in pod ultrastructure to KI-induced desiccation

To observe the immediate effect of KI spray on the ultra-structural components in the carbon allocation pathway from pod to seed, we observed the longitudinal sections of the pod wall (stage R5) inner surface, funiculus, and the seed coat inner surface through scanning electron microscopy. Significant anatomical alterations in the form of starch granule disruption were observed within 1 DASP of KI spray in the pod-wall inner surface and funiculus when compared to control plants (Fig. 5(a) – (d)). The funiculus cells also showed shrinkage when compared to controls. However, no significant difference could be observed in the inner surface of the seed coats from control and KI-treated plants within 1 DASP (Fig. 5(e), (f)).

DISCUSSION

Terminal drought stress leads to significant loss in soybean yield due to seed and pod abortion.[34] The role of the pod wall as a crucial regulator of reserve accumulation in developing seeds has been evidenced through various studies.[17,35] In the present study, a chemical desiccation-based simulation of terminal drought effects was created to carry out a systematic stage-specific study of soybean. Potassium iodide (KI), as a foliar spray for simulating terminal drought stress in soybean had been standardized previously.[13] In the present study it was observed that KI treatment during stages R4 (pod elongation), R5 (seed-initiation), and R6 (complete seed fill) significantly reduced the pod weight as well as pod and seed number, which closely simulates the terminal drought stress effects leading to pod and seed abortions.[33] The total carbohydrate and starch content in the leaves significantly reduced upon KI treatment during all three stages stage, which clearly indicates photosynthetic inhibition due to KI induced senescence and oxidative stress.[36] However, reducing sugar levels were found to be increased upon KI treatment during R5 and R6. This could be attributed to desiccation-induced osmotic adjustment in the leaf tissues[37,38] and / or enhanced starch degradation.[39]

On the other hand, the pod wall and seeds of KI-treated plants during all three stages showed reductions in total carbohydrates but the starch and reducing-sugar levels remained similar to those of control plants. This could be due to effective stem reserve remobilization or to pod photosynthesis.[17] Terminal drought / KI is also known to induce early senescence symptoms in the plants.[33] It is postulated that senescence is an 'altruistic' behavior, as nutrients are remobilized from senescing leaves to newly developing structures.[40] Thus, the observed maintenance of starch and reducing sugars in pod walls and seeds in the present study could be the result of a combined effect of resource allocation from senescing leaves and osmotic response to dehydration stress. Apart from acting as osmoticum and nutrient sources, soluble sugars – specifically hexoses and sucrose – are also known to be involved in metabolic signaling in the form of hexose-to-sucrose ratios (H/S), to regulate various plant developmental processes.[41,42] However, analysis of H/S ratio patterns during the final yield could provide information regarding the overall stress defense responses of the plant, with respect to a particular tissue. In the present study, the H/S ratios of leaves, pod-walls, and seeds were compared among control and KI-treated plants after stage R8 (after harvest). The

Table 2. Effect of stage-specific KI-spray on *G. max* JS335 yield component grown under greenhouse condition in 1 L capacity pots, values represent mean ± SD *$P < 0.05$, **$P < 0.01$, ***$P < 0.001$, ns, not significant (n = 10 for plants, n = 40 for seeds)

Yield component	Stages of KI spray treatment			
	Control(without KI spray)	R4	R5	R6
Shoot weight (mg plant$^{-1)}$	588.3 ± 47.3	443.8 ± 132.5*	243.6 ± 48.7***	363.5 ± 73.8***
Root weight (mg plant^{-1})	116.8 ± 16.2	90 ± 24.6^{ns}	25.3 ± 10.6***	50.2 ± 6.3***
Pod weight (mg pod^{-1})	84.6 ± 8.4	30.7 ± 4.2***	23.7 ± 9.8***	51.5 ± 9.5***
Seed weight (mg seed^{-1})	78.7 ± 5.0	39.3 ± 11.1***	26.4 ± 10.7***	44.9 ± 19.4***

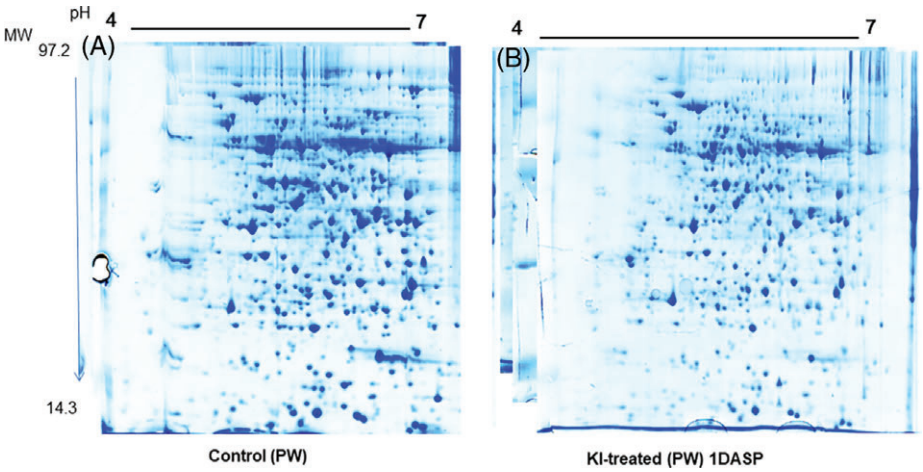

Figure 3. Two-dimensional protein profile of soybean pod wall at stage R5 under control (a) and KI-treated (1 DASP) conditions (b).

H/S ratio was higher than controls in the leaves and the pod wall of KI-treated plants but significantly lower in seeds. This could be due to higher starch degradation, reduced sucrose biosynthesis or enhanced sucrose translocation from the leaves.[43] In case of the pod wall, although sucrose levels were also found to increase, the corresponding rate of increase in hexoses was much higher and, hence, an elevated H/S ratio was observed on KI-induced desiccation. As starch levels were maintained, the observed high accumulation of hexoses could be attributed to enhanced rate of sucrolysis.[44] Now, a higher H/S ratio during harvest in stressed plants, could possibly act as an indicator of effective hexose-mediated osmotic adjustment in these tissues. In seeds, a very low H/S ratio was observed in KI-desiccated plants, which was the result of low hexose and high sucrose accumulation under dehydration stress. This could be due to inhibition of seed-coat associated cell wall invertase or down-regulation of hexose transporters.[45] Moreover, sucrose accumulation is known to be an effective drought response in developing seeds.[46,47]

To investigate the initial regulatory responses of the pod-wall upon KI-simulated terminal drought stress, we carried out a comparative proteomic analysis on stage R5 (seed initiation) KI treated plants within 1 DASP. Identified proteins were classified into the following functional groups:

- Signaling / regulatory proteins. Among the significantly induced proteins, the majority were signaling / regulatory proteins. The most important protein was the 14-3-3 protein, which is a family of serine / threonine binding proteins and acts as regulator of multiple stress-signaling pathways through protein–protein interaction.[48,49] The soybean 14-3-3 protein family was reported to regulate ABA sensitivity in Arabidopsis.[50] Our results are consistent with previous studies, which showed that 14-3-3 protein (GSGF140) was strongly induced during drought stress.[51] In plants, the MAP kinase cascade-based signaling mechanism for transducing extracellular signals to appropriate cellular response is well established.[52] Recently, it was reported that MAP kinase 3 regulates stomatal response and root growth in cotton, leading to drought tolerance.[53] We observed significant induction of MAP kinase 3 proteins in soybean within 1 DASP of KI spray in the pod wall at stage R5.
- Carbon utilization / metabolism and protein folding / stabilization. Rubisco activase (RCA) is an important regulator of photosynthesis as it helps in enhancing the activity of the Rubisco enzyme by removing the inhibitory sugar phosphates from the enzyme's catalytic site and also acts as a chaperonic protein under various stress conditions.[54] Rubisco activase was reported to be down-regulated in the leaves, hypocotyl and roots of soybean under saline stress.[55] However, in the present study we observed an enhanced expression of the protein with KI-induced desiccation stress in the soybean pod wall within 1 DASP. Higher expression of RCA in the silique wall of *Brassica napus*, leading to better silique wall photosynthesis was reported to influence seed oil content in a positive way.[35] Further, both isoforms of RCA proteins were found to be up-regulated under various abiotic stress conditions in rice leaves.[54] The observed up-regulation of RCA in soybean pod-wall could be attributed to its chaperonic function under desiccation stress and also for maintaining the pod-wall photosynthesis. Protein stabilizing / refolding proteins and photosynthesis-optimizing proteins, including HSP-70, Rubisco large subunit binding proteins, Kunitz-type trypsin inhibitor, and carbonic anhydrase were also significantly induced in the soybean pod wall within 24 h of KI treatment. This indicates that soybean pod-wall responds to KI-induced desiccation as early as 1 DASP by activating its drought-responsive signaling pathways and oxidative stress-protective enzymes.
- Redox-homeostasis and cellular energy related proteins. Another interesting protein that was induced in the pod wall of soybean is ferritin. Ferritin is an iron (Fe)-chelating protein that plays a crucial role under oxidative stress through rapid removal of freely available Fe in the cell, which otherwise takes part in the Fenton's reaction for producing highly reactive hydroxyl radicals.[56] Our results are consistent with previous studies where ferritin protein was found to be induced significantly in various organs of soybean under drought stress.[57] Involvement of various GSTs in the abiotic stress responses of plants for maintaining redox homeostasis is well documented.[58] In Arabidopsis, the GST protein (U17) was reported to be a negative regulator of the drought response, in which repression of the above gene leads to drought tolerance in the plant.[59] On the other hand, a recent study showed that overexpression of tomato GST (U2) in Arabidopsis confers tolerance against salt and osmotic stress and the maximum expression of the transcript was observed in flowers and roots.[60] Such differences could be attributed to variation in stress intensity, developmental stage

Table 3. Identified pod wall proteins of *Glycine max* JS335, differentially expressed and unchanged reproducibly when compared to control within 1 DASP of 0.1% KI spray treatment

Groups	S No	MatchID.	Protein identified	Peptide sequences matched	Mr/ pI	Accession no.	S C (%)[a]	Reference organism	MS / MS score
Up-regulated	1	2	14–3-3 protein 2	K.LAEQAERYEEMVQFMEK.V K.VSTSLGSEELTVEERNLLSVAYK.N R.NLLSVAYKNVIGAR.R R.NLLSVAYKNVIGAR.R R.LGLALNFSVFYYEILNSPDR.A	29/4.72	P93208	25	*Solanum lycopersicum*	199
	2	365	ATP synthase subunit β	R.LVLEVAQHLGEGVVR.T K.AHGGFSVFAGVGER.T R.IPSAVGYQPTLSTDLGALQER.I	60/5.8	XP_003536650.1	8	*Glycine max*	250
	3	137	Glutathione S-transferase	R.VPPLTSTSEPPSLFDGTTR.L R.LYISYICPYAQR.V	27/5.5	NP_001304567.1	13	*Glycine max*	139
	4	316	Rubisco activase 1	R.VPIIVTGNDFSTLYAPLIR.D K.LVDTFPGQSIDFFGALR.A	52/6.3	Q7X9A0.1	7	*Larrea tridentata*	141
	5	356	ATP synthase β subunit	K.GRDNSGQEINVTCEVQQLLGNNR.V R.IFNVLGEPIDNLGPVDTR.T	50/5.35	CAB90076	8	*Elaeagnus sp. Chase 2414*	150
	6	430	Heat shock 70 kda protein	R.TTPSYVAFTDTERLIGDAAK.N K.NAVVTVPAYFNDSQR.Q K.EQVFSTYSDNQPGVLIQVYEGER.A	70/5.2	P11143	8	*Zea mays*	274
	7	243	Adenosine kinase 2	K.VNYYEIDNTPTGTCAVCVVGGER.S K.VLPYMDYVFGNETEAR.T R.AGCYAANVIIQRPGCTYPPTPDFH	38/5.3	KHN48251	18	*Glycine soja*	237
	8	423	Carbonic anhydrase	K.EAVNVSLQNLLTYPFVK.E R.VCPSVTLGLEPGEAFTIR.N	35.7/8.9	CAHC_HORVU	10	*Hordeum vulgare*	55
	9	9	Endoglucanase13	R.QEGNPNVIMGALVGGPDRR.D K.FGLPMAFAVTMLSWSIIK.F	69/5.6	XP_010935663.1	5	*Elaeis guineensis*	70
	10	117	Ferritin-1(Chloroplastic)	R.VGKGHGVWHFDQR.L K.GHGVWHFDQR.L	28/5.7	FRI1_SOYBN	5	*Glycine max*	124
	11	167	14–3-3 protein 2	K.LAEQAERYEEMVQFMEK.V R.YLAEFKTGAER.K	29/4.7	14332_SOLLC	11	*Solanum lycopersicum*	90
	12	60	Kunitz type trypsin inhibitor	K.LTGYDNTVPGEFKIEK.A K.CGHIGIHFDDDGNR.R	23/5.5	XP_003532236.1	16	*Glycine max*	83
	13	133[a]	hypothetical protein KK1_033456	K.AIREKPQGKQDQGQATDI.-	22/7.0	KYP44995.1	9	*Cajanas cajan*	80
	14	121	mitogen-activated protein kinase kinase kinase Raf34.1	K.EPVMVIVTELLQGGTLRK.Y K.VDAYSFAIVLWELLHN.K	39.8/8.0	AGA37226.1	12	*Brassica napus*	94
	15	378	Endochitinase	R.ETFNQMLLHR.N R.GFYTYDAFIAAA.R	35.6/6.28	CHI1_GOSHI	5	*Gossypium hirsutum*	69
	16	400	Rubisco large subunit binding protein subunit β	K.AAVEEGIVVGGGCTLLR.L K.VVAAGANPVLIT.R	62/6.5	RUBB_BRANA	5	*Brassica napus*	73
	17	424	Probable nucleoredoxin1	R.DLVSLYGADAYPFTEER.I K.SFGSCSDFTPKLVEVYE.K	64/4.86	XP_003532006.1	6	*Glycine max*	84
	18	425[b]	Probable nucleoredoxin1	R.DLVSLYGADAYPFTEER.I	65/4.8	XP_003532006.1	2	*Glycine max*	65
	19	326	Eukaryotic initiation factor 4A-15	R.GIYAYGFEKPSAIQQR.G R.VLITTDLLA.R	47/5.4	KHN06630.1	7	*Glycine max*	69
Unchanged	20	26	Actin deplymeri-zing factor like	K.LGEPAQGYEDFTASLPADECR.Y R.YAVYDFEYLTEGNVPK.S R.IFFIAWSPDTSR.V	16/6.15	XP_006586815	35	*Glycine max*	298
	21	220	13S globulin seed storage protein 2	K.TLTEQDFPFIGDVGLSVIR.V K.APSYPINPTVQLIYIAR.G	33/5.16	XP_003531302.1	11	*Glycine max*	275
	22	296	Actin-52	K.TSSSVEKSYELPDGQVITIGSER.F K.SYELPDGQVITIGSER.F	37/5.4	Q96484	6	*Solanum lycopersicum*	79
	23	211	Annexin	K.VPAQLPSPLEDSEQLRK.A K.IAEKAYNDEDLIR.I	35/6.0	NP_001239752.1	9	*Glycine max*	149
Down-regulated	24	721	WPP domain associated protein (fragment)	K.HMSKDEMVTYFNNIMTK.M R.MVSDSVIKGIVSAVEQEAAER.L	96/5.07	WAP_SOLLC	4	*Solanum lycopersicum*	83
	25	746	Actin, partial	R.AVFPSIVGRPR.H K.LSYIALDYEQELETAR.T	37/5.6	AAB40082	8	*Glycine max*	95
	26	652	Arginine decrboxylase	K.SSGGLGLQLPLIVR.F K.VTGPKSSGGLGLQLPLIVR.F	78/5.1	SPE2_ARATH	2	*Arabidopsis thaliana*	69
	27	131	20S Proteasome subunit α	R.LYKEPIPVTQLVR.E EGFEGQISGTNIEIGIIGAD.K	28.3/5.5	BAU02938.1	13	*Vigna angularis*	78

[a] SC, Sequence coverage.
[b] Only one peptide match found (hypothetical protein was excluded from discussion, while spot 425 was considered similar to 424 based on the common peptide match).

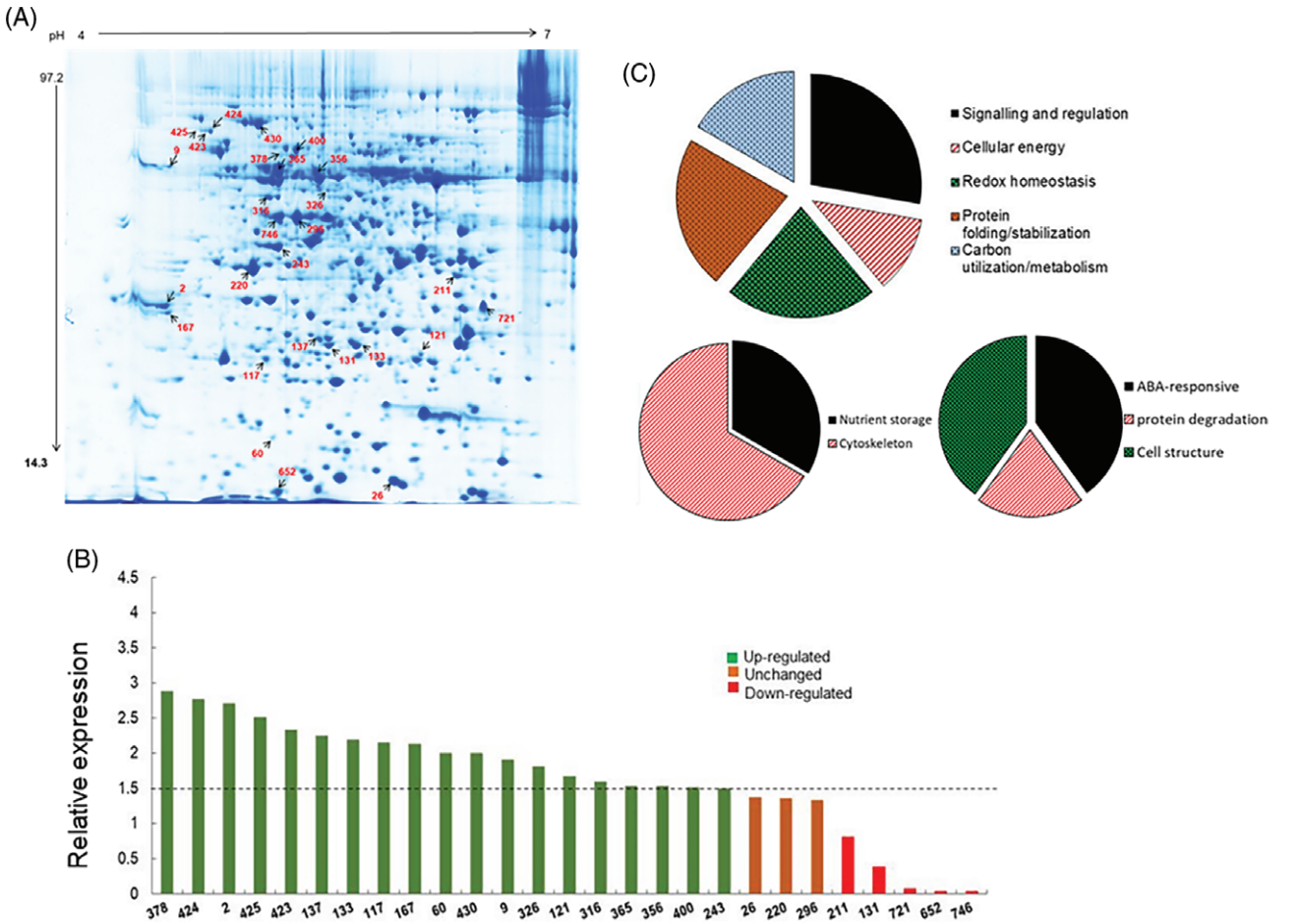

Figure 4. (a) Colloidal Coomassie-stained representative two-dimensional electrophoresis gels showing the protein profile of soybean pod wall at stage R5. Arrows indicate the reproducibly up-regulated, down-regulated, and unchanged proteins identified through MALDI-TOF-TOF. Numbering of the proteins in the gels correspond to the match ID numbers given in Table 2. (b) Induction factors (fold change) for the 27 identified proteins. (c) Functional categorization of the up-regulated, down-regulated, and unchanged proteins of soybean pod-wall in response to KI-induced desiccation stress within 1 DASP.

of the plant and / or protein isoform differences. In our study, a GST protein was found to be significantly up-regulated in the pod-wall of soybean within 24 h of KI-simulated drought conditions, which clearly indicates its involvement in mitigating the KI-induced oxidative imbalance. Apart from GST, two spots corresponding to soybean nucleoredoxins were also found to be induced in the present study. These proteins belong to the redoxin superfamily of oxidoreductases, which functions in reduction of oxidized proteins under high cellular reactive oxygen species (ROS) conditions. Recently, it was shown that nucleoredoxin activity is required to maintain the integrity of antioxidative enzyme systems under redox dis-balance.[61] Thus, our data demonstrates that soybean pod-wall immediately triggers the oxidative stress tolerance machinery under KI-simulated terminal drought onset. In addition to protective and redox-balancing protein systems, soybean pod walls also showed rapid activation of proteins related to cellular energy. Enhanced expression of the ATP synthase β subunit in response to drought and salinity stress has been observed consistently in all stress response studies, and they help the plant to meet the stress-induced energy demands.[6,62,63]

- Protein degradation and nutrient storage related proteins. The protein-degrading-machinery-related protein 20S proteasome subunit α, ABA-responsive negative regulator of drought stress (WPP domain associated protein), and arginine decarboxylase (involved in polyamine synthesis under drought stress) were among the significantly down-regulated protein in the soybean pod wall at stage R5 within 24 h of KI-simulated terminal drought. Seed storage protein globulin and annexin proteins remained consistently unchanged in the pod wall at stage R5 within 1 DASP of KI-induced desiccation.

Thus, overall the proteomics-based analysis revealed that, during seed initiation, soybean pod wall responds rapidly to KI-simulated terminal drought stress at the very onset (within 24 h) and triggers strong drought-tolerance mechanisms. Despite reduction in pod and seed numbers, the observed maintenance of starch and reducing sugar levels in the existing pods / seeds of stressed plants could be attributed the strong and rapid induction of defense / protective responses in the pod-wall. Though starch granule disruption was observed within 1 DASP of KI treatment, in the inner pod-wall sections upon SEM analysis, the difference in the final starch accumulation in pod-wall and seeds (after stage R8) when compared to controls was found to be insignificant. This could be attributed to remobilization of carbon reserves at later stages of KI-induced desiccation from senescing leaves or stems. A schematic model depicting the overall observations regarding the

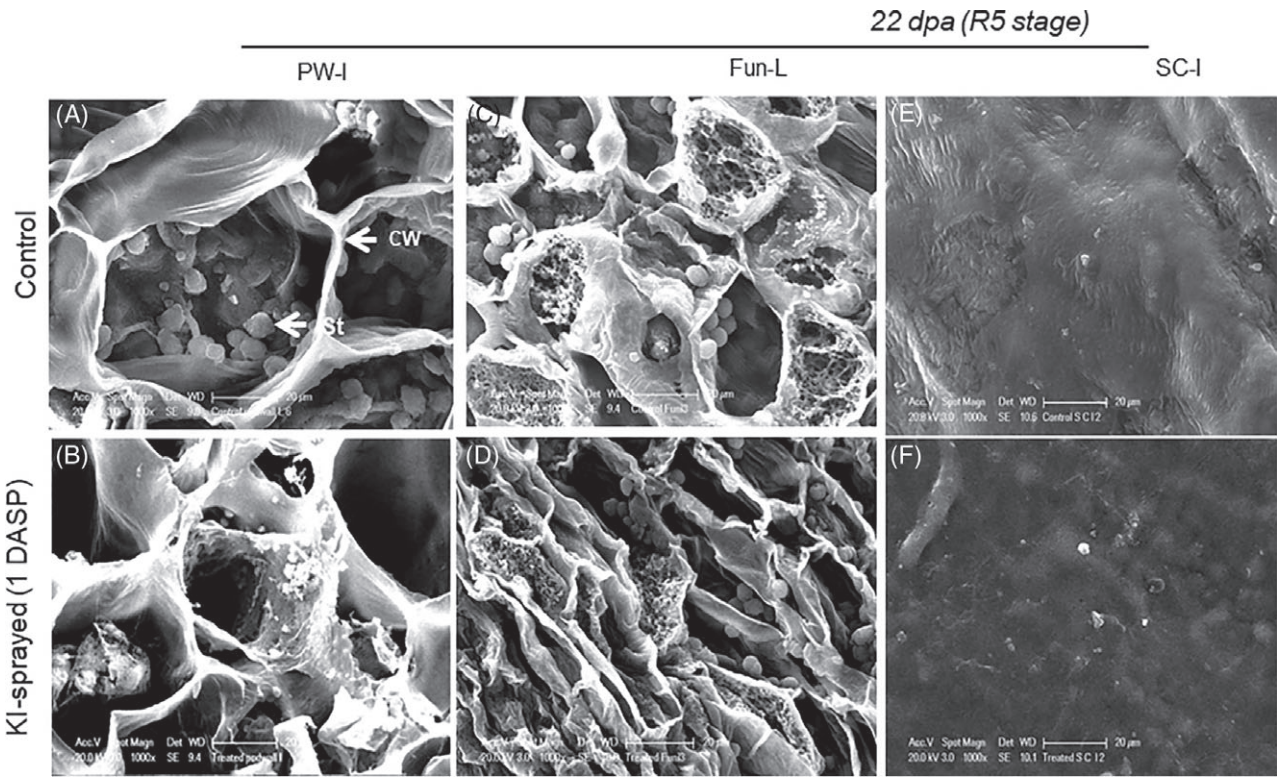

Figure 5. Scanning electron microscopic (SEM) analysis of the ultra-structural variations in the (a) pod-wall inner surface, (b) funiculus longitudinal section, (c) seed-coat inner surface, in control and 1 DASP KI-sprayed samples during stage R5 of development. A bar represents 20 μm in all the images. PW-I, pod-wall inner surface; Fun-L, funiculus longitudinal section; SC-I, seed coat inner surface.

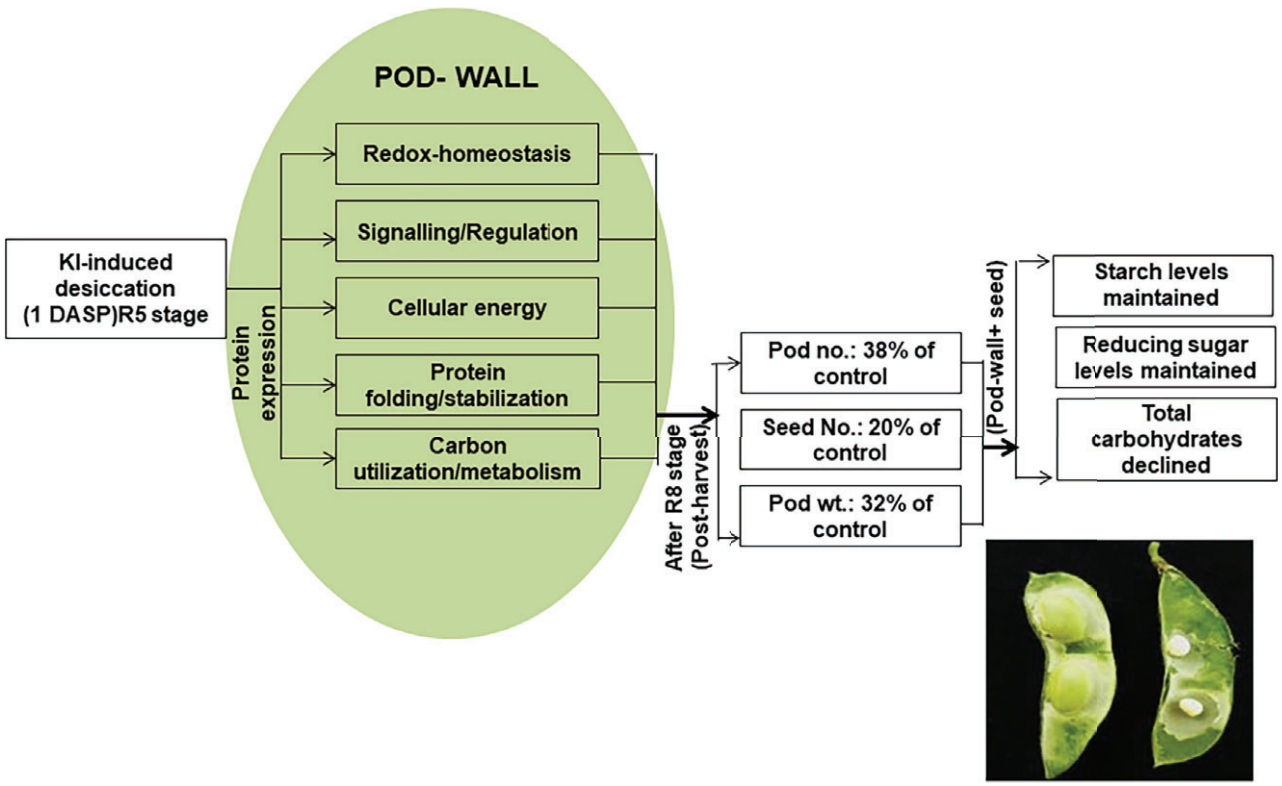

Figure 6. Schematic representation of the pod-wall-based molecular mechanisms triggered within 1 DASP of KI spray-induced desiccation, based on proteomics and gene expression data and their implications for the carbon allocation patterns in the developing seeds of soybean.

pod-wall-based molecular mechanisms and corresponding carbon allocation pattern during the seed initiation stage of soybeans under KI-simulated terminal drought is summarized in Fig. 6.

CONCLUSIONS

In conclusion, the present study revealed the immediate molecular responses of soybean pod-wall during the very onset of terminal drought stress with a parallel insight into the stage-specific postharvest carbon allocation and yield parameters in response to KI-induced desiccation. This provides key inputs for understanding the initial regulatory mechanisms under terminal drought stress, which ultimately affect the storage reserve and yield of soybean and hence would be useful for developing terminal drought-tolerant soybean cultivars.

ACKNOWLEDGEMENTS

The present work is supported by the Young Scientist Start-Up grant to Dr Debashree Sengupta (File no.: YSS/2015/000635) from the Science and Engineering Research Board (SERB), a statutory body of the Department of Science and Technology (DST), Government of India. We thank the Proteomics Facility of School of Life Sciences, University of Hyderabad, and Sandors Life Sciences Pvt Ltd for the MALDI-TOF-TOF analysis. We also thank the Central Instrumentation Facility (CIL), University of Hyderabad, for the SEM analysis. SBM acknowledges the junior and senior research fellowship from University Grant Commission (UGC), New Delhi, Government of India.

CONFLICT OF INTEREST

Authors declare no conflict of interest.

SUPPORTING INFORMATION

Supporting information may be found in the online version of this article.

REFERENCES

1 Cramer GR, Urano K, Delrot S, Pezzotti M and Shinozaki K, Effects of abiotic stress on plants: a systems biology perspective. *BMC Plant Biol* **11**:163 (2011).
2 Eziz A, Yan Z, Tian D, Han W and Tang Z, Drought effect on plant biomass allocation: a meta-analysis. *Ecology Evol* **7**:11002–11010 (2017).
3 Joshi R, Wani SH, Singh B, Bohra A, Dar ZA, Lone AA *et al.*, Transcription factors and plants response to drought Stress: current understanding and future directions. *Front Plant Sci* **7**:1029 (2016).
4 Kaur G and Asthir B, Molecular responses to drought stress in plants. *Biol Plant* **61**:201–209 (2017).
5 Verulkar SB, Mandal NP, Dwivedi JL, Singh BN, Sinha PK, Mahato RN *et al.*, Breeding resilient and productive genotypes adapted to drought-prone rainfed ecosystem of India. *Field Crops Res* **117**:197–208 (2010).
6 Sengupta D, Kannan M and Reddy AR, A root proteomics-based insight reveals dynamic regulation of root proteins under progressive drought stress and recovery in *Vignaradiata* (L.) Wilczek. *Planta* **233**:1111–1127 (2011).
7 Seminario A, Song L, Zulet A, Nguyen HT, González EM and Larrainzar E, Drought stress causes a reduction in the biosynthesis of ascorbic acid in soybean plants. *Front Plant Sci* **8**:1042 (2017).
8 Chaves MM, Flexas J and Pinheiro C, Photosynthesis under drought and salt stress: regulation mechanisms from whole plant to cell. *Ann Bot* **103**:551–560 (2009).
9 Swamy BP and Kumar A, Genomics-based precision breeding approaches to improve drought tolerance in rice. *Biotechnol Adv* **31**:1308–1318 (2013).
10 Hou H, Atlihan N and Lu ZX, New biotechnology enhances the application of cisgenesis in plant breeding. *Front Plant Sci* **5**:389 (2014).
11 Regan KL, Whan BR and Turner NC, Evaluation of chemical desiccant as a selection technique for drought resistance in a dry land wheat breeding programme. *Aust J Agric Res* **44**:1683–1691 (1993).
12 Royo C and Blanco R, Use of potassium iodide to mimic drought stress in triticale. *Field Crops Res* **59**:201–212 (1998).
13 Bhatia VS, Jumrani K and Pandey JP, Evaluation of the usefulness of senescing agent potassium iodide (KI) as a screening tool for tolerance to terminal drought in soybean. *Plant Know J* **3**:23–30 (2014).
14 Schmutz J, Cannon SB, Schlueter J, Ma J, Mitros T, Nelson W *et al.*, Genome sequence of the palaeopolyploid soybean. *Nature* **463**:178–183 (2010).
15 Padgette SR, Kolacz KH, Delannay X, Re DB, LaVallee BJ, Tinius CN *et al.*, Development, identification, and characterization of a glyphosate-tolerant soybean line. *Crop Sci* **35**:1451–1461 (1995).
16 Daryanto S, Wang L and Jacinthe PA, Global synthesis of drought effects on food legume production. *PLoS One* **10**:e0127401 (2015).
17 Bennett EM, Roberts JA and Wagstaff C, The role of the pod in seed development: strategies for manipulating yield. *New Phytol* **190**:838–853 (2011).
18 Schiltz S, Munier-Jolain N, Jeudy C, Burstin J and Salon C, Dynamics of exogenous nitrogen partitioning and nitrogen remobilization from vegetative organs in pea revealed by 15 N *in vivo* labeling throughout seed filling. *Plant Physiol* **137**:1463–1473 (2005).
19 Wagstaff C, Yang TJ, Stead AD, Buchanan-Wollaston V and Roberts JA, A molecular and structural characterization of senescing Arabidopsis siliques and comparison of transcriptional profiles with senescing petals and leaves. *Plant J* **57**:690–705 (2009).
20 Diepenbrock W, Yield analysis of winter oilseed rape (*Brassica napus*L.): a review. *Field Crops Res* **67**:35–49 (2000).
21 Ennahli S and Earl HJ, Physiological limitations to photosynthetic carbon assimilation in cotton under water stress. *Crop Sci* **45**:2374–2382 (2005).
22 Sawhney V and Singh DP, Effect of chemical desiccation at the post-anthesis stage on some physiological and biochemical changes in the flag leaf of contrasting wheat genotypes. *Field Crops Res* **77**:1–6 (2002).
23 Castillo FJ, Antioxidative protection in the in the inducible CAM plant *Sedum album* L. following the imposition of severe water stress and recovery. *Oecologia* **107**:469–477 (1996).
24 Hiscox JD and Israelstam GF, A method for the extraction of chlorophyll from leaf tissue without maceration. *Can J Bot* **57**:1332–1334 (1979).
25 Lichtenthaler HK, Chlorophylls and carotenoids: pigments of photosynthetic biomembranes. *Methods Enzymol* **148**:350–382 (1987).
26 Giannoccaro E, Wang YJ and Chen P, Effects of solvent, temperature, time, solvent-to-sample ratio, sample size, and defatting on the extraction of soluble sugars in soybean. *J Food Sci* **71**:59–64 (2006).
27 Miller JL, Use of dinitrosalicylic acid reagent for determination of reducing sugar. *Anal Chem* **31**:426–428 (1959).
28 Hedge JE and Hofreiter BT, in *Methods in Carbohydrate Chemistry*, Vol. **17**, ed. by Whistler RL and BeMiller JN. Academic Press, New York, p. 420 (1962).
29 Guha A, Sengupta D, Rasineni GK and Reddy AR, An integrated diagnostic approach to understand drought tolerance in mulberry (*Morusindica* L.). *Flora* **205**:144–151 (2010).
30 Wang X, Li X and Li Y, A modified commassie brilliant blue staining method at nanogram sensitivity compatible with proteomic analysis. *Biotechnol Lett* **29**:1599–1603 (2007).
31 Shevchenko A, Wilm A, Vorm O and Mann M, Mass spectrometric sequencing of protein from silver-stained polyacrylamide gels. *Anal Chem* **68**:850–858 (1996).
32 Diz AP, truebano M and Skibinski DOF, The consequences of sample pooling in proteomics: an empirical study. *Electrophoresis* **30**:2967–2975 (2009).
33 Manavalan LP, Guttikonda SK, Tran LSP and Nguyen HT, Physiological and molecular approaches to improve drought resistance in soybean. *Plant Cell Physiol.* **50**:1260–1276 (2009).
34 Liu F, Jensen CR and Andersen MN, Drought stress effect on carbohydrate concentration in soybean leaves and pods during early reproductive development: its implication in altering pod set. *Field Crops Res* **86**:1–13 (2004).
35 Hua W, Li RJ, Zhan GM, Liu J, Li J, Wang XF *et al.*, Maternal control of seed oil content in Brassica napus: the role of silique wall photosynthesis. *Plant J* **69**:432–444 (2012).

36 Gilbert ME, Zwieniecki MA and Holbrook NM, Independent variation in photosynthetic capacity and stomatal conductance leads to differences in intrinsic water use efficiency in 11 soybean genotypes before and during mild drought. *J Exp Bot* **62**:2875–2887 (2011).
37 Sánchez FJ, Manzanares M, de Andres EF, Tenorio JL and Ayerbe L, Turgor maintenance, osmotic adjustment and soluble sugar and proline accumulation in 49 pea cultivars in response to water stress. *Field Crops Res* **59**:225–235 (1998).
38 Solařová E, Holková L, Bradáčová M and Smutná P, Osmotic adjustment and activity of stress-related genes in wheats of different origin exposed to water stress. *Russ J Plant Physiol* **63**:532–541 (2016).
39 Thalmann M, Pazmino D, Seung D, Horrer D, Nigro A, Meier T *et al.*, Regulation of leaf starch degradation by abscisic acid is important for osmotic stress tolerance in plants. *Plant Cell* **28**:1860–1878 (2016).
40 Munné-Bosch S and Alegre L, Die and let live: leaf senescence contributes to plant survival under drought stress. *Funct Plant Biol* **31**:203–216 (2004).
41 Ruan YL, Jin Y, Yang YJ, Li GJ and Boyer JS, Sugar input, metabolism, and signalling mediated by invertase: roles in development, yield potential, and response to drought and heat. *Mol Plant* **3**:942–955 (2010).
42 Ruan YL, Signalling role of sucrose metabolism in development. *Mol Plant* **5**:763–765 (2012).
43 Liu F, Andersen MN and Jensen CR, Loss of pod set caused by drought stress is associated with water status and ABA content of reproductive structures in soybean. *Funct Plant Biol.* **30**:271–280 (2003).
44 Koch K, Sucrose metabolism: regulatory mechanisms and pivotal roles in sugar sensing and plant development. *Curr Opin Plant Biol* **7**:235–246 (2004).
45 Weschke W, Panitz R, Gubatz S, Wang Q, Radchuk R, Weber H *et al.*, The role of invertases and hexose transporters in controlling sugar ratios in maternal and filial tissues of barley caryopses during early development. *Plant J* **33**:395–411 (2003).
46 Gill PK, Sharma AD, Singh P and Bhullar SS, Effect of various abiotic stresses on the growth soluble sugars and water relations of sorghum seedlings grown in light and darkness. *Bulg J Plant Physiol* **27**:72–84 (2001).
47 Rosa M, Prado C, Podazza G, Interdonato R, Gonzalez JA, Hilal M *et al.*, Soluble sugars – Metabolism, sensing and abiotic stress. *Plant Signal Behav* **4**:388–393 (2009).
48 Roberts MR, 14-3-3 Proteins find new partners in plant cell signalling. *Trends Plant Sci* **8**:218–223 (2003).
49 Ferl RJ, 14-3-3 proteins: regulation of signal-induced events. *Physiol Plant* **120**:173–178 (2004).
50 Sun X, Sun M, Jia B, Chen C, Qin Z, Yang K *et al.*, A 14-3-3 family protein from wild soybean (*Glycine Soja*) regulates ABA sensitivity in Arabidopsis. *PLoS One* **10**:e0146163 (2015).
51 Sun X, Luo X, Sun M, Chen C, Ding X, Wang X *et al.*, A *Glycine soja* 14-3-3 protein GsGF14o participates in stomatal and root hair development and drought tolerance in Arabidopsis thaliana. *Plant Cell Physiol* **55**:99–118 (2014).
52 Sinha AK, Jaggi M, Raghuram B and Tuteja N, Mitogen-activated protein kinase signalling in plants under abiotic stress. *Plant Signal Behav* **6**:196–203 (2011).
53 Wang C, Lu W, He X, Wang F, Zhou Y, Guo X *et al.*, The cotton mitogen-activated protein kinase kinase 3 functions in drought tolerance by regulating stomatal responses and root growth. *Plant Cell Physiol* **57**:1629–1642 (2016).
54 Chen Y, Wang XM, Zhou L, He Y, Wang D, Qi YH *et al.*, Rubisco activase is also a multiple responder to abiotic stresses in rice. *PLoS One* **10**:e0140934 (2015).
55 Sobhanian H, Razavizadeh R, Nanjo Y, Ehsanpour AA, Jazii FR, Motamed N *et al.*, Proteome analysis of soybean leaves, hypocotyls and roots under salt stress. *Proteome Sci* **8**:19 (2010).
56 Kang Y and Udvardi M, Global regulation of reactive oxygen species scavenging genes in alfalfa root and shoot under gradual drought stress and recovery. *Plant Signal Behav* **7**:539–543 (2012).
57 Alam I, Sharmin SA, Kim KH, Yang JK, Choi MS and Lee BH, Proteome analysis of soybean roots subjected to short-term drought stress. *Plant Soil* **333**:491–505 (2010).
58 Dixon DP, Davis BG and Edwards R, Functional divergence in the glutathione transferase superfamily in plants – Identification of two classes with putative functions in redox homeostasis in *Arabidopsis thaliana*. *J Biol Chem* **2778**:30859–30869 (2002).
59 Chen JH, Jiang HW, Hsieh EJ, Chen HY, Chien CT, Hsieh HL *et al.*, Drought and salt stress tolerance of an Arabidopsis glutathione S-transferase U17 knockout mutant are attributed to the combined effect of glutathione and abscisic acid. *Plant Physiol* **158**:340–351 (2012).
60 Xu J, Xing XJ, Tian YS, Peng RH, Xue Y, Zhao W *et al.*, Transgenic Arabidopsis plants expressing tomato glutathione S-transferase showed enhanced resistance to salt and drought Stress. *PLoS One* **10**:e0136960 (2015).
61 Kneeshaw S, Keyani R, Delorme-Hinoux V, Imrie L, Loake GJ, Bihan TL *et al.*, Nucleoredoxin guards against oxidative stress by protecting antioxidant enzymes. *Proc Natl Acad Sci USA* **11**:8414–8419 (2017).
62 Marriboina S, Sengupta D, Kumar S and Reddy AR, Physiological and molecular insights into the high salinity tolerance of *Pongamia pinnata* (L.) pierre, a potential biofuel tree species. *Plant Sci* **258**:102–111 (2017).
63 Cao Y, Luo Q, Tian Y and Meng F, Physiological and proteomic analyses of the drought stress response in *Amygdalus Mira* (Koehne) Yüet Lu roots. *BMC Plant Biol* **17**:53 (2017).

DOI: 10.32615/ps.2019.060 PHOTOSYNTHETICA 57 (2): 458-469, 2019

Photosynthetic performance and sugar variations during key reproductive stages of soybean under potassium iodide-simulated terminal drought

D. SENGUPTA[*], S. MARRIBOINA[*], D. K. UNNIKRISHNAN[*], and A.R. REDDY[*,**,+]

Department of Plant Sciences, School of Life Sciences, University of Hyderabad, 500046 Hyderabad, India[*]
Yogi Vemana University, 516003 Kadapa, Andhra Pradesh, India[**]

Abstract

Importance of utilizing chemical desiccants to simulate terminal drought effects is gradually increasing. In the present study, a potassium iodide (KI)-simulated terminal drought stress was imposed during the full bloom (R2), pod elongation (R4), and seed initiation (R5) stages of soybean; the KI-induced desiccation effects were assessed at 1, 3, and 5 d after spraying (DASP). Plants responded to KI-simulated terminal drought stress within 1 DASP of KI-treatment, in terms of photosynthetic and transpiration rates. Seed initiation stage was found to be comparatively tolerant to KI-induced desiccation, with respect to chlorophyll degradation and PSII efficiency, which correlated well with the high hexose accumulation during this period. The present study provides a basic understanding regarding the stage-specific responses of soybean towards KI-simulated terminal drought, with respect to photosynthetic performance and sugar status and a correlation between the two traits, which could be useful for developing terminal drought-tolerant varieties.

Additional key words: chemical desiccation; *Glycine max*; hexose to sucrose ratio; linear regression; photosynthetic carbon exchange rate.

Introduction

Being the major source of edible oil, animal feed and other industrial products, soybean [*Glycine max* (L.) Merril] has become one of the most important grain legumes worldwide (Pagano and Miransari 2016). In India, soybean cultivation area increased from 0.03 Mha in 1970 to 11.67 Mha in 2016, with a corresponding increase in yield from 426 to 737 kg ha^{-1} (Agricultural Statistics at a Glance 2016). One of the major limitations to soybean productivity is the rain-fed cultivation system, with highly erratic monsoon patterns. Drastic spatio-temporal variations in rainfall often cause terminal drought stress, *i.e.*, water deprivation during the key reproductive stages, which substantially hampers the final grain yield (Daryanto *et al*. 2015). Physiologically, terminal drought effects include decreased photosynthetic carbon exchange rates (CER), early leaf senescence and maturity, and a reduced seed yield (Manavalan *et al*. 2009). Hence, the ability to remobilize stem carbohydrates towards developing pods/seeds is the key trait, which determines terminal drought tolerance in soybean. Screening and selection of cultivars with effective stem reserve mobilization marks the first step for subsequent breeding strategies for terminal drought tolerance. However, due to variation in soil moisture, field screening for terminal drought is quite difficult due to lack of uniformity and reproducibility of plant responses to the stress factor (Tuberosa 2012, Bhatia *et al*. 2014). Thus, to mimic terminal drought stress effects, chemical desiccants, such as potassium iodide (KI) were used (Regan *et al*. 1993, Royo and Blaco 1998, Bhatia *et al.* 2014). KI was reported to act as a contact desiccant and rapidly inhibits photosynthesis without showing any direct toxic effect to grain filling from the translocated carbohydrates (Nicolas and Turner 1993). The possible mechanism behind KI-induced desiccation is the interference with plant water relations. Hygroscopicity of the salt solution was also included as one of the major factors causing 'hydraulic activation of stomata' (HAS), which affects the stomatal conductance, transpiration rates, and ultimately photosynthesis (Burkhardt 2010). Also, desiccation leads to osmotic stress and triggers osmotic stress-inducible gene expression (Shapiguzov *et al*. 2005). Detailed physiochemical responses of soybean to KI-induced desiccation, with respect to specific reproductive growth stage, are not yet reported. Moreover, for wide

Received 28 May 2018, *accepted* 14 November 2018.
[+]Corresponding author; phone:+91 4023134508, fax: +91 4023010120, e-mail: attipalli.reddy@gmail.com
Abbreviations: CER – carbon exchange rate; Chl – chlorophyll; DASP – days after spraying; DMSO – dimethyl sulfoxide; H/S – hexose to sucrose ratio; Kn – nonphotochemical deexcitation rate constant; Kp –photochemical deexcitation rate constant; PDA – photodiode array; ΔV_{OJ} – kinetic difference of variable fluorescence between phase O and J with respect to 1 day control; ΔV_{OK} – kinetic difference of variable fluorescence between phase O and K with respect to 1 day control; $\delta_{(Ro)}$ – reduction efficiency/electron transport; $\Phi_{(Po)}$ – trapping/absorbance; $\psi_{(Eo)}$ – electron transport/trapping.
Acknowledgements: The present work is supported by the Young Scientist Start-Up grant to Dr. Debashree Sengupta (YSS/2015/000635) from Science and Engineering Research Board (SERB), a statutory body of Department of Science and Technology (DST), Govt. of India. Sureshbabu Marriboina acknowledges the fellowship from University Grant Commission (UGC), Govt. of India.

scale adoption of the technique, it is necessary to analyse and experimentally validate the plant responses to KI-simulated drought, at both physiological and biochemical levels.

As the primary plant metabolic process, photosynthesis is the 'hub', which controls all other metabolic and regulatory functions of the plant system under optimal as well as adverse environmental conditions (Lawlor and Cornic 2002, Reddy *et al*. 2004, Ashraf and Harris 2013, Flexas *et al*. 2014). During terminal drought, along with reduction in CER, leaf senescence is also triggered (Samarah *et al.* 2009, Saeidi and Abdoli 2015). It is reported that senescence itself is highly regulated and can contribute towards stress tolerance (Munné-Bosch and Alegre 2004, Jagadish *et al*. 2015). Further, sink strength variations from flowering (R1–R2) to complete seed fill (R5) also regulates the source photosynthetic capacity. Hence, KI-based terminal drought stress responses need to be analysed carefully with respect to growth stages, taking into consideration possible interactions between leaf senescence and sink strength. Apart from the actual CER, photosynthetic performance of plant is also characterized by the PSII efficiency, which is monitored *via* the chlorophyll (Chl) *a* fluorescence transients (Govindjee 2004, Boureima *et al*. 2012, Brestic *et al*. 2015). In fact, monitoring Chl *a* fluorescence has become one of the crucial nondestructive techniques for screening drought tolerance in plants, and is used extensively for screening purposes (Oukkaroum *et al*. 2007). Systematic analysis of fast kinetics of Chl *a* fluorescence provides information on quantum yield efficiency of PSII, electron transport from PSII to PSI, reduction of the end electron acceptor, photochemical and nonphotochemical quenching along with energy connectivity among PSII units, and stability of the oxygen-evolving complex (Strasser *et al*. 2004, Papageorgiou *et al*. 2007, Stirbet *et al.* 2018). For a complete understanding of the physiological responses of soybean to KI-simulated drought stress, it is necessary to evaluate the modulations in Chl *a* fluorescence patterns along with CER. Moreover, detailed stage-specific analysis of KI-desiccation effects on Chl *a* fluorescence kinetics in soybean has not been reported yet.

In general, drought stress inhibits photosynthetic rate and also disrupts carbohydrate metabolism in leaves, which together results in reduced availability of photosynthates for sink-translocation and hence, leads to seed abortion and yield loss (Nguyen *et al*. 2010, Lemoine *et al*. 2013, Osorio *et al*. 2014). As terminal drought tolerance primarily deals with reserve mobilization, either from stem or from senescing leaves, it is inevitable to analyse sugar accumulation patterns under KI-simulated drought stress. Also, it is evidenced that a sugar status plays a regulatory role in determining plant's metabolic responses under various adverse environmental conditions (Rosa *et al*. 2009, Smeekens and Hellmann 2014). Abiotic stress-induced changes in soluble sugars contents are the result of alteration in CO_2 assimilation, source-to-sink carbon partitioning, activity of sugar-metabolizing enzymes or expression of specific genes (Gupta and Kaur 2005, Baena-González *et al*. 2007). Hexose (mainly glucose and fructose) and sucrose concentrations plays crucial signalling roles for regulating metabolic processes in both source and sink tissues (Ruan 2012, Lemoine *et al*. 2013, Griffiths *et al*. 2016). Further, hexose to sucrose ratio (H/S) is also implicated as a key signalling factor regulating various aspects of plant growth and development, where high H/S ratio was reported to favour cell division and the low H/S to induce cellular differentiation (Weber *et al*. 1998, Koch 2004, Ruan *et al*. 2010, Eveland and Jackson 2012). The absolute concentration of leaf sucrose is governed by a number of concurrent factors including the rate of photosynthesis, photosynthetic carbon partitioning between starch and sucrose, sucrose hydrolysis, sucrose export rates, and drought-induced disproportions in any of the above factors will cause a change in the H/S ratio. Hence, it is important to have an insight into the pattern of hexose, sucrose, as well as H/S ratio upon KI-simulated terminal drought stress during specific reproductive stages of soybean. Previous studies have reported that under drought conditions, sucrose is accumulated due to the reduced activity of sucrose-cleaving enzyme, acid invertase. Though hexose concentrations were also reported to be enhanced under water deprivation, the amount of sucrose accumulation was comparatively higher and as a result, the H/S ratios were found to be lower under drought conditions (Zinselmeier *et al*. 1999, Andersen *et al*. 2002). KI-induced desiccation causes early senescence along with photosynthetic inhibition and it is known that during senescence reduced photosynthesis triggers metabolic reprogramming to maintain sugar homeostasis (Biswal and Pandey 2018). Hence, it is important to understand the stage-specific modulations in hexose and sucrose contents under KI-simulated terminal drought.

In the present study, we aimed to analyse the stage-specific responses of soybean to KI-simulated terminal drought stress from full bloom to seed initiation. Soybean response was analysed through modulations in the photosynthetic CER, transpiration rate, pigment composition, and various PSII efficiency parameters, along with the stage-specific sugar accumulation patterns. We also aimed to deduce a statistical correlation between the sugar status in terms of H/S ratio and the photosynthetic efficiency. Outcomes from the present study can provide a basic understanding of the usefulness of KI as a terminal drought simulator and the stage-specific variations in terminal drought response of soybean with respect to photosynthetic efficiency and sugar dynamics.

Materials and methods

Plant material and experimental conditions: The experimental material used, *Glycine max* (L.) Merril var. JS335 (Jawahar Soybean-335) is a semi-determinate and early maturing (~ 99 d) soybean variety, which is widely cultivated in India. The study was carried out in the greenhouse of University of Hyderabad, Telangana state, India (17.3°10'N and 78°23'E at an altitude of 542.6 m above mean sea level). The greenhouse conditions were as follows: PPFD ranged from 900–1,200 µmol(photon) m^{-2} s^{-1}, air temperature of 24 ± 1°C (~ 5:00–6:00 h) to

36 ± 4°C (~ 12:00–14:00 h), and relative humidity of 36 (± 5)–48 (± 2)%. Seeds were germinated in 2-L pots, filled with a mixture of red soil and manure. Commercial *Bradyrhizobium japonicum* in the powdered form (*Rhizopowder*, *AgriLife Pvt Ltd.*, India) was mixed with the seeds before sowing. Plants were maintained under regular watering regimes till flowering (*ca.* 45 d). For the present study, reproductive stages, *i.e.*, R2 (full bloom), R4 (pod elongation), and R5 (seed initiation) were selected for the 0.1% potassium iodide (KI) spray treatment, which simulates drought stress. Spray treatment (100 mL of 0.1% KI per plant) was given to three individual plants at the starting of each reproductive stage (R2, R4, and R5) and subsequent readings as well as sample collections were performed at 1, 3, and 5 DASP for each growth stage. Controls were sprayed with equal amount of double distilled water and are considered as initial or 0 DASP.

Leaf relative water content (RWC): Fresh mass (FM) of leaf samples were recorded immediately after sample collection from three different plants of control and treated groups. Leaf samples are then rehydrated in distilled water at 4°C for 24 h in order to obtain the corresponding turgid mass (TM). After recording the TM, leaves were oven-dried for 24 h to get the dry mass (DM) values. Leaf relative water content was calculated using the formula RWC [%] = [(FM) – (DM)/(TM) – (DM)] ×100.

Photosynthetic CER and transpiration rates (*E*): CER and *E* were measured using *Q-Box CO650* CO_2 exchange measurement system (*Qubit Systems Inc.*, Canada). Measurements were taken on fully expanded, mature leaves of three different plants, after applying a light intensity (white light) of 1,200 µmol(photon) m^{-2} s^{-1} for 2 min. All measurements were taken under atmospheric CO_2 conditions. Photosynthetic CO_2-fixation rate (or the carbon-exchange rate) expressed as µmol(CO_2) m^{-2} s^{-1} was calculated by the *LoggerPro* software (*Qubit Systems Inc.*, Canada) by using the differential CO_2 concentration, which is the difference between the influx and efflux CO_2 (dif. CO_2) following light exposure and the molecular flow (MF) rate. Following formulas were used for calculation:

MF = Flow rate/[22.4 × (273 + Tair)/273]/60 × 10,000/ leaf area,

CER = dif. CO_2 × MF

Transpiration rate (*E*) was also calculated automatically by the software by using the values of reference and analytical relative humidity (RH) values.

Chl *a* fluorescence transients and flux ratios: Three leaves from three different plants were dark-adapted for 30 min using leaf clips and the fluorescence intensities were recorded using a portable *Handy PEA* (*Plant Efficiency Analyzer-2126*, *Hansatech Instruments Ltd.*, Kings Lynn Norfolk, UK). Dark-adapted leaves were illuminated with a saturating light impulse of 3,000 µmol(photon) m^{-2} s^{-1}, provided by an array of three light emitting diodes, for 1 s which is sufficient to ensure closure of all PSII reaction centres. The *Handy PEA* data were analysed using the *Biolyzer* software. Three key PSII flux ratios or quantum yield parameters, *i.e.*, (*1*) TR/ABS (trapping/absorbance), which is also denoted as $\Phi_{(Po)}$ and calculated as $1 - F_0/F_m$, (*2*) ET/TR (electron transport/trapping) also denoted as $\psi_{(Eo)}$, calculated as $1 - V_j$, and (*3*) RE/ET (reduction efficiency/electron transport) or $\delta_{(Ro)}$ was calculated as $(1 - V_j)(1 - V_i)$, were selected for the present analysis which illustrates the PSII efficiency from photon capture to the reduction of the end electron acceptor in the thylakoid membrane. Further, patterns of nonphotochemical and photochemical quenching were also investigated using the deexcitation constants Kn and Kp values, respectively, which are obtained directly from the *Biolyzer* software. Analysis of Chl *a* fluorescence transients for O–K and O–J phases was performed by normalizing the variable fluorescence between O and K, as well as O and J phases of the OJIP curve [F1 (50µs) and F3 (300µs) for O–K; F1 (50µs) to F4 (2 ms) for O–J] by using the *Biolyzer* software. Theoretically, $V_{OK} = [(F_t - F_O)/(F_K - F_O)]$ and $V_{OJ} = [(F_t - F_O)/(F_J - F_O)]$, while the corresponding kinetic differences, ΔV_{OK} and ΔV_{OJ} were calculated from the normalized data by subtracting the '1 DASP control' values from the fluorescence values of each of the subsequent DASP of control and KI-treated groups, to get the L (in ΔV_{OK}) and K-bands (ΔV_{OJ}), respectively. Data presented are average of three independent replicates.

Chl pigments: Leaf samples (50 mg) were used for extraction of pigments by following dimethyl sulfoxide (DMSO) method described by Hiscox and Israelstam (1979) with minor modifications. Each leaf disc was kept in an Eppendorf tube and 2 mL of DMSO was added to each vial. Eppendorfs were kept at room temperature under dark conditions for 2 d. Then supernatant was removed through centrifugation. Absorbance of the supernatant was measured at 663.2 and 646.8 nm using *UV-Visible 160A* spectrophotometer (*Shimadzu*, Tokyo, Japan) and Chl contents were calculated using the following formula: Chl *a*: $12.25 \times A_{663.2} - 2.79 \times A_{646.8}$; Chl *b*: $21.5 \times A_{646.8} - 5.1 \times A_{663.2}$ and the results were expressed as mg g^{-1}(FM).

HPLC-based sugar estimation: Sugars (glucose, fructose, and sucrose) were extracted by following the method of Giannoccaro *et al.* (2006) with minor modifications. Briefly, 100 mg of dried and powdered sample was extracted in 1 mL (1:10, w/v) of milliQ water for 15 min in a rotospin. The extracted sample was then centrifuged at 13,000 rpm for 10 min at room temperature and 500 µL of the clear supernatant was transferred to a fresh Eppendorf tube. This sample aliquot (500 µL) was then purified by adding 1.5 mL of 95% acetonitrile and mixed for 30 min in the rotospin. Sample was then centrifuged at 13,000 rpm for 10 min at room temperature. The supernatant was collected in a fresh tube and evaporated completely by keeping in a dry bath at 95°C. Residue was redissolved in 1 mL of milliQ water and filtered through 0.22-µm filter paper (*Millipore*, *Merck*) using syringe filters. Sugars were separated isocratically through reverse phase HPLC using a NH_2 column (*Shodex-Asahipak NH2P-50-4E*) with acetonitrile:water (70:30, v/v) as a mobile phase. Flow rate was set to 1 ml min^{-1} and the absorbance was

detected at 190 nm (UV) using a photodiode array (PDA) detector. Glucose, fructose, and sucrose peaks were identified through spiking with internal standards and the concentrations were calculated using external standard calibration method. Calibration curves for glucose, fructose, and sucrose were made using 0.5, 1, 2, 5, 10, 15, and 20 mg mL^{-1} concentrations and respective slope and intercepts from the straight line equations were used for calculating the concentrations from the 'area' of the HPLC peaks of the respective sugars.

Statistical analysis and linear regression modelling: All physiological measurements and biochemical estimations were performed in triplicates**.** Statistical significance between control and treated groups at each sampling time of individual reproductive stage were analysed through *Student*'s *t*-test using *SigmaPlot 11.0* and significant difference having **p*<0.05 were considered. Linear regression models were generated using the average values of 1, 3, and 5 DASP from control and treated groups for each of the three growth stages (n = 18) for the response variable CER, *E*, and H/S using *SigmaPlot 11.0*.

Results

KI-simulated terminal drought impact on leaf RWC, photosynthetic CER, and transpiration rate (*E*): As KI is known to induce gradual desiccation (Sawhney and Singh 2002), we monitored the leaf RWC at 1, 3, and 5 DASP and correspondingly checked the photosynthetic CER and *E*. In the present study, leaf RWC declined gradually from 1 to 5 DASP upon KI spray, for each individual stage (R2 to R5), however, the statistically significant difference was observed from 3 DASP onwards during R2 (Fig. 1*A*) and at 5 DASP in R4 (Fig. 1*B*) and R5 stages (Fig. 1*C*). The corresponding CER values were significantly reduced to almost 50% of the control during 1 DASP of KI spray with no further progressive decline in the subsequent DASP, upon KI treatment in all three stages (Fig. 1*D–F*). A similar pattern was observed in *E*, which also declined considerably during 1 DASP and did not show any progressive decline in all the three stages (Fig. 1*G–I*).

Effect of chemical desiccation on pigment composition: Similar to natural drought conditions, KI treatment also enhanced the Chl *a*/*b* ratios consistently during 3 and 5 DASP of KI treatment at R2 and R4 stages (Fig. 2*A*,*B*), while in the R5 stage, the ratio was significantly higher than that of controls from 1 DASP onwards (Fig. 2*C*). Total Chl content declined gradually from 1 to 5 DASP of KI spray during R2, R4, and R5 stages of soybean development, however, when compared to respective controls, it was observed that at 1 DASP, total Chl content was slightly higher, but then declined during 3 and 5 DASP (Fig. 2*D–F*). To have further insight into the pigment system efficiency upon KI-induced drought stress, we analysed the PSII flux ratios or the quantum yields. The TR/ABS or $\Phi_{(Po)}$, also known as the PSII quantum yield, was found to decline at 5 DASP upon KI spray during R2 and R5 stages and at 3 and 5 DASP during R4 stage (Fig. 2*G–I*).

Effects of KI spray on quantum yield efficiencies and Chl *a* fluorescence transients: The flux ratio ET/TR (calculated as 1 – Vj) denotes the quantum yield of electron transport from PSII to PSI and is also denoted as

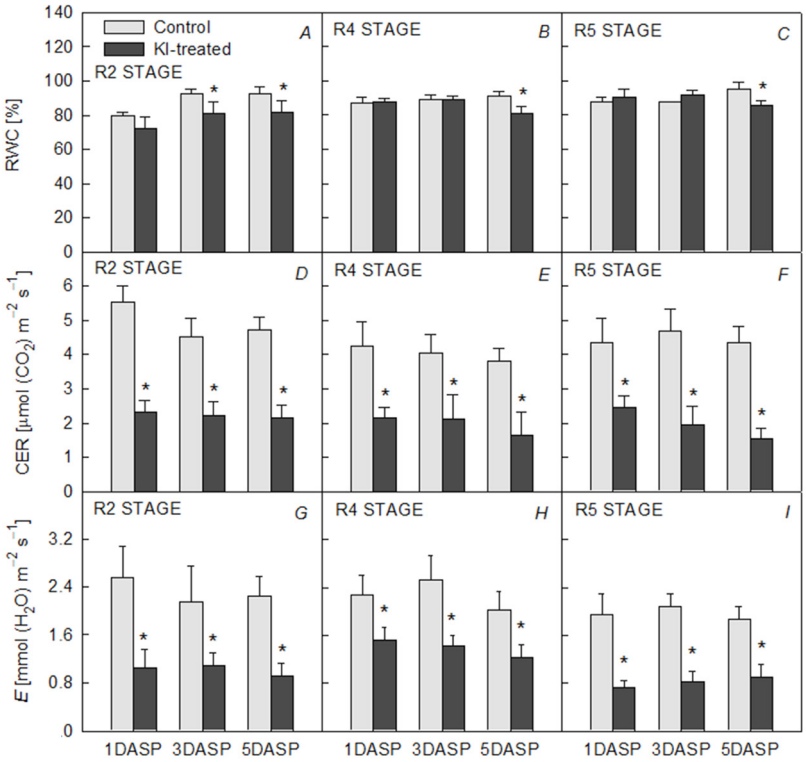

Fig. 1. Changes in the leaf relative water content (RWC) (*A–C*), photosynthetic carbon-exchange rate (CER) (*D–F*), and transpiration rate (*E*) (*G–I*) during 1, 3, and 5 d after spraying (DASP) of soybean plants with KI spray at full bloom (R2), pod elongation (R4), and seed initiation (R5) stage. Values are means ± SD (n = 3). * means significant difference with respect to control. **p*<0.05.

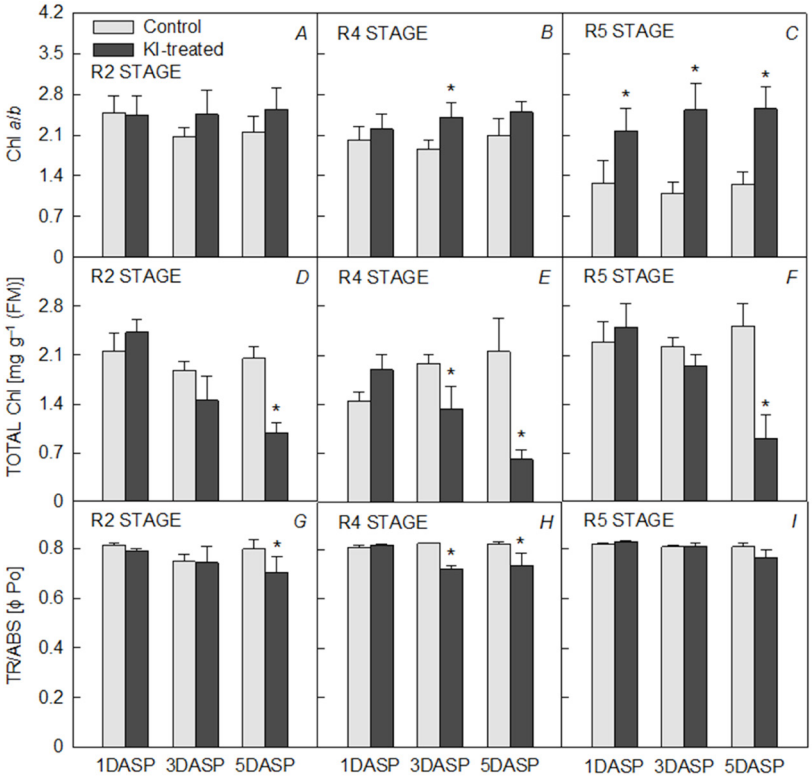

Fig. 2. Chlorophyll (Chl) *a*/*b* ratio (*A*–*C*), total chlorophyll content (*D*–*F*), and quantum yield of trapping ($\Phi_{(Po)}$) (*G*–*I*) during 1, 3, and 5 d after spraying (DASP) of soybean plants with KI spray at full bloom (R2), pod elongation (R4), and seed initiation (R5) stage. Values are means ± SD (n = 3). * p<0.05

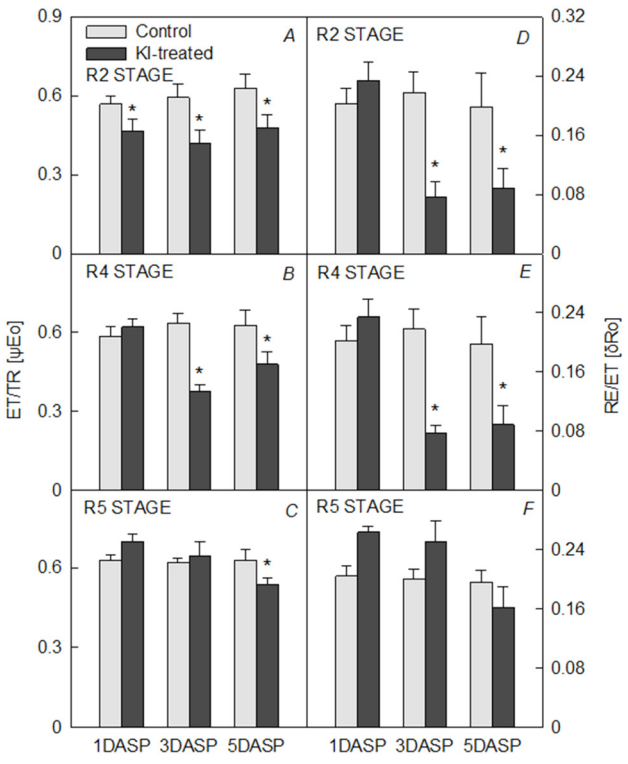

Fig. 3. Effect of KI-simulated drought stress on the quantum yield of electron transport from PSII to PSI (ET/TR, ψ_{Eo}) (*A*–*C*) and quantum yield for the reduction efficiency of the end electron acceptor (RE/ET, δ_{Ro}) (*D*–*F*) during 1, 3, and 5 d after spraying (DASP) of soybean plants with KI spray at full bloom (R2), pod elongation (R4), and seed initiation (R5) stage. Values represent mean ± SD (n = 3). * p<0.05

$\psi_{(Eo)}$. It was observed that $\psi_{(Eo)}$ declined significantly from 1 DASP onwards upon KI spray during R2 stage, after 3 and 5 DASP during R4 stage, and only at 5 DASP during R5 stage (Fig. 3*A*–*C*). The efficiency of the reduction of the end electron acceptor was indicated by the quantum yield for reduction efficiency, RE/ET or $\delta_{(Ro)}$. Here, we observed that $\delta_{(Ro)}$ decreased significantly during 3 and 5 DASP of KI treatment in both R2 and R4 stages of development (Fig. 3*D*,*E*). However, $\delta_{(Ro)}$ declined only marginally at 5 DASP of KI spray during R5 stage (Fig. 3*F*). The photochemical and nonphotochemical deexcitation rate constants (Kp and Kn) showed antagonistic response upon KI treatment. During R2 and R4 stages, Kp declined significantly from 3 DASP onwards when compared to controls. On the other hand, Kn was found to be enhanced, when compared to respective controls from 3 DASP onwards upon KI spray during R2 stage. However, during R4, Kn increased significantly during 3 and 5 DASP (Fig. 4*A*–*C*). Upon KI treatment during R5 stage, Kp showed a slight decline during 5 DASP and Kn enhanced at the same time (Fig. 4*D*–*F*).

The double normalized variable fluorescence transients between O to K phase $[(F_t - F_O)/(F_K - F_O)]$ and the corresponding kinetic difference ΔV_{OK} (Fig. 5*A*–*C*) with respect to 1 DASP control as a reference point, showed L-band during 3 and 5 DASP of KI treatment at R2 and R4 growth stages, while KI spray at R5 stage showed a significant L-band only after 5 DASP. Moreover, during

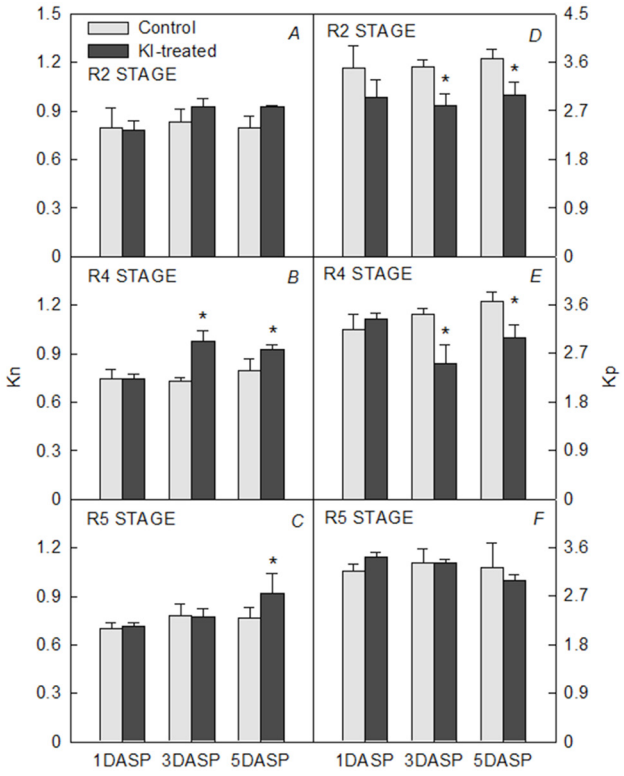

Fig. 4. The nonphotochemical (Kn) (*A–C*) and photochemical (Kp) (*D–F*) deexcitation rate constants during 1, 3, and 5 d after spraying (DASP) of soybean plants with KI spray at full bloom (R2), pod elongation (R4), and seed initiation (R5) stage. Values are mean +- S.D. *p<0.05

R2 stage, L-band at 5 DASP had higher amplitude than that at 3 DASP, while during R4 stage, the L-band amplitude was higher at 3 DASP. Similarly through O–J double normalization $[(F_t - F_O)/(F_J - F_O)]$ and corresponding kinetic difference, ΔV_{OJ}, positive K-bands were observed with gradually increasing amplitudes from 1 to 5 DASP of KI spray at R2 stage. During R4 stage, KI treatment showed positive K-band at 3 and 5 DASP, wherein the amplitude for 3 DASP was higher than that of 5 DASP, while at R5 stage, a positive K-band was observed only at 5 DASP of KI-induced drought stress (Fig. 5*D–F*).

KI effect on stage-specific sugar accumulation and H/S ratio patterns: Sugar accumulation was represented in terms of hexoses, which indicates the cumulative glucose (G) and fructose (F) content, sucrose contents, and the corresponding hexose to sucrose ratios (H/S) for each reproductive stage under KI-simulated terminal drought stress (Table 1). It was observed that hexose contents gradually declined with plant development from R2 to R5 stage under control conditions, however, under KI-simulated drought conditions, this trend was not followed. Further, KI-treatment resulted in higher hexose accumulation in all stages. Similar to hexoses, sucrose contents also progressively declined with reproductive development of soybean from R2 to R5 stages under non-stress conditions, but not under KI treatment. Also, enhanced sucrose accumulation was observed upon KI treatment during all stages, however, R2 stage showed significantly lesser increment in sucrose contents when compared to R4 and R5 stages. Under control conditions, the H/S ratio remained more or less stable during reproductive development from R2 to R5 stage during

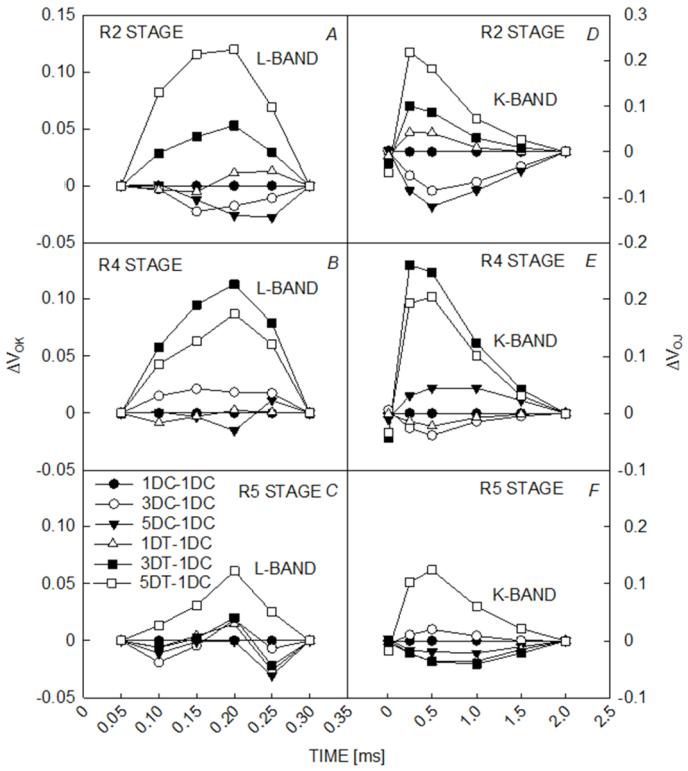

Fig. 5. Chl *a* fluorescence transients for O–K and O–J phase in soybean leaves upon KI-simulated drought stress during full bloom (R2), pod elongation (R4), and seed initiation (R5) stages. Kinetic difference of V_{OK} (ΔV_{OK}) with respect to 1 day after spraying (DASP) control (1 DC) as reference, showing prominent L-band (*A–C*). Kinetic difference of V_{OJ} (ΔV_{OJ}) with respect to 1 DASP control (1 DC) as reference, showing prominent K-band (*D–F*). Values are average of three independent replicates.

Table 1. Pattern of hexose, sucrose accumulation, and hexose to sucrose ratio (H/S) upon KI-simulated terminal drought stress at full bloom (R2), pod elongation (R4), and seed initiation (R5) stages of soybean development. Values are means ± SD (n = 3).* indicates significance at p<0.05, ns – not significant, DASP – days after spraying. [a]H/S ratio is represented as the mean(hexose)/mean(sucrose) and hence SD and statistical significance are not included.

Parameter	Growth stage	1 DASP		3 DASP		5 DASP	
		Control	KI-treated	Control	KI-treated	Control	KI-treated
Hexose [mg g^{-1}(DM)]	R2	71.6 ± 6.7	99.1 ± 7.5*	78.4 ± 3.6	96.2 ± 5.8*	75.7 ± 8.1	91.5 ± 4.9*
	R4	43.5 ± 3.7	45.3 ± 5.1ns	41.7 ± 2.2	55.7 ± 3.6*	47.7 ± 3.4	66.8 ± 4.8*
	R5	32.9 ± 2.8	106.5 ± 10.4*	35.0 ± 5.4	106.1 ± 5.7*	30.6 ± 7.3	98.2 ± 3.2*
Sucrose [mg g^{-1}(DM)]	R2	9.5 ± 1.1	9.7 ± 0.9ns	9.9 ± 0.6	12.1 ± 0.8*	9.1 ± 1.1	14.0 ± 1.7*
	R4	5.0 ± 1.6	34.4 ± 2.3*	5.2 ± 1.5	35.1 ± 3.7*	6.1 ± 2.1	70.4 ± 8.2*
	R5	3.4 ± 2.9	41.8 ± 5.8*	4.2 ± 3.1	44.0 ± 1.9*	3.8 ± 3.9	31.5 ± 7.4*
H/S ratio[a]	R2	7.5	10.1	7.9	7.9	8.2	6.5
	R4	8.6	1.3	8.0	1.6	7.8	0.9
	R5	9.7	2.5	8.2	2.4	7.9	3.1

all observation points. Upon KI-induced desiccation, H/S ratio declined significantly in R4 and R5 stages during all DASP observed, when compared to respective controls. However, at R2 stage, the ratio was higher in comparison to controls at 1 DASP, similar at 3 DASP, and slightly lower at 5 DASP.

Overall stage-specific sugar accumulation, pigment efficiency, and carbon assimilation patterns: Since sugar accumulation pattern did not follow any specific pattern with progressing DASP of KI spray treatment, we analysed the overall (an average of the 3 observations points, *i.e.*, 1, 3, and 5 DASP) pattern of sugar accumulation and H/S ratio for each individual stage of reproductive development. To get a comprehensive overview, along with sugar accumulation, we also analysed the pigment efficiency in terms of the overall stage-specific total Chl content, functional reaction centres (RC/CS_o) and the quantum yield of energy trapping (TR/ABS) as well as the carbon-assimilation efficiency defined with respect to quantum yield of electron transport from PSII to PSI (ET/TR), reduction efficiency for the final electron acceptor (RE/ET), and the actual carbon exchange rates (CER) in response to KI-induced drought stress. In the present study, we observed that hexose (G+F) concentrations showed a more or less gradual decline with stage progression from R2 to R5 under control conditions. Upon KI treatment, hexose contents were enhanced in all stages (Fig. 6*A*). Sucrose contents also declined gradually from R2 to R5 stage under control conditions. But, with KI-induced drought stress, sucrose accumulation increased and was found to be significantly higher than that of controls at R4 and R5 stages of development (Fig. 6*B*). On the other hand, hexose to sucrose ratios (H/S) were significantly lower than that of controls during R4 and R5 stage, remained similar to controls at R2 stage (Fig. 6*D*). Overall, the total Chl content declined upon KI treatment during R2 and R4 but remained similar to controls during R5 stage (Fig. 6*E*). Similarly, the overall RC/CS_o declined with KI treatment during R2 and R4 but remained stable during R5 stage (Fig. 6*C*). On average, the yield determining the light capturing efficiency, TR/ABS, remained stable in response to KI-induced drought in all growth stages except R2, which showed a slight decline (Fig. 6*G*). Both ET/TR and RE/ET declined significantly with KI treatment during R2 and R4 stages but remained unchanged during R5 stage (Fig. 6*H*,*I*). The photosynthetic CER showed an overall decrease upon KI treatment during all the growth stages when compared to controls (Fig. 6*F*).

Linear regression model for correlating H/S ratio with photosynthetic efficiency: In order to deduce a possible inter-relationship between the photosynthetic CER, stomatal conductance, and leaf H/S ratio, we considered the average values for each of the three observation points (1, 3, and 5 DASP) under control and KI-treated plants, at a particular reproductive growth stage (R2, R4, and R5) as dataset (n = 18) and carried out three linear regression modelling: (*1*) between CER and *E*, (*2*) CER and H/S, and (*3*) *E* and H/S using *SigmaPlot 11.0*. The regression analysis depicted that CER *vs*. *E* had the highest R^2 value (0.808), followed by CER *vs.* H/S (0.473), while *E vs.* H/S showed the minimum R^2 value (0.302). All the statistical details including correlation coefficients for the regression analyses are provided in Table S1 (*supplement*). The linear regression analyses are depicted graphically in Fig. 7*A–C*.

Discussion

Dependency on seasonal rains for cultivation of major crops, including soybean, often imposes the risk of encountering terminal drought stress, which results in huge decline in crop productivity (Sadras 2002, Samarah *et al*. 2009). Developing terminal drought tolerant varieties through breeding or genetic engineering approach requires extensive screening for terminal drought tolerance traits among cultivars/wild relatives and a proper understanding of the underlying physiological, biochemical, and molecular mechanisms. At the onset of grain filling, chemical desiccation of plant canopies

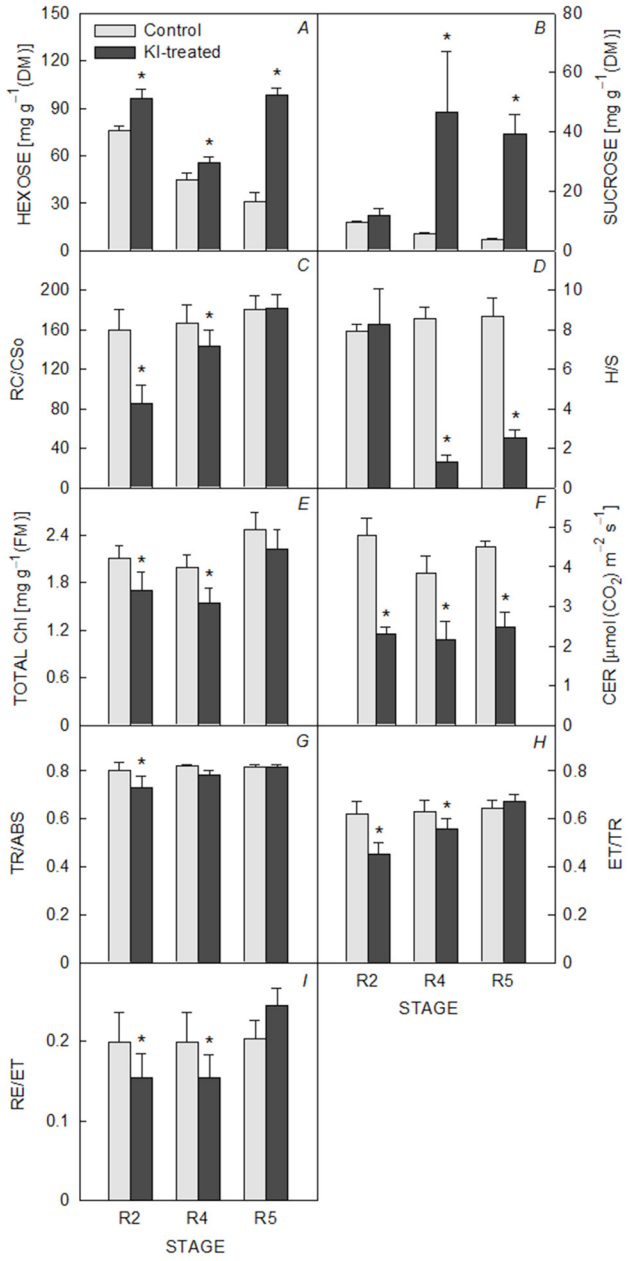

Fig. 6. Stage-specific accumulation patterns of hexose (*A*), sucrose (*B*), number of functional reaction centres per cross section area (RC/CS_o) (*C*), hexose to sucrose ratio (H/S) (*D*), total chlorophyll content (*E*), carbon-exchange rate (CER) (*F*), quantum yield efficiency of PSII (TR/ABS) (*G*), quantum yield of electron transport from PSII to PSI (ET/TR) (*H*), and reduction efficiency of the final electron acceptor (RE/ET) (*I*) in soybean plants with KI spray at full bloom (R2), pod elongation (R4), and seed initiation (R5) stage. Values represent mean ± SD ($n = 3$). *$p<0.05$

was long suggested as a tool for analysing genotypic differences in stem reserve-mediated grain filling, when current photosynthesis is limited (Blum *et al.* 1983) and KI was reported to act as a contact desiccant (Tyagi *et al*. 2000). Previous studies reported that KI-induced desiccation leads to a decreased Chl content, stomatal conductance, transpiration, photosynthetic rates, and induces early senescence and maturity (Royo and Blanco 1998, Sawhney and Singh 2002, Bhatia *et al*. 2014), which closely simulates terminal drought stress symptoms and hence, is proposed as a potential tool for screening terminal drought tolerance in field crops (Nezhad *et al*. 2012, Ongom *et al*. 2016). Also, drying initiates several major alterations in the carbohydrate metabolism, which might directly or indirectly correlate with desiccation tolerance. Present study involved a detailed stage-specific analysis of KI-simulated terminal drought responses in soybean with respect to photosynthetic physiology and sugar status.

Soybean is known to be most susceptible to water-deficit conditions during germination and reproductive stages (Liu *et al*. 2004, Angra *et al*. 2010). Occurrence of drought during full bloom and pod initiation (R2 and R4) stages of soybean induces flower/pod abortion causing significant decline in seed number and the effect is irreversible upon return of normal water conditions (Ruan *et al*. 2010), whereas water limitation during seed-filling stage (R5) results in seed abortion or low seed mass due to reduced photosynthate transfer to these structures (Borrás *et al*. 2004). Usefulness of KI, as a simulator of drought stress during reproductive stages, is established in rice, wheat, and recently in soybean as well (Singh *et al*. 2012, Kordenaeej *et al*. 2013, Bhatia *et al*. 2014). However, most of the studies characterizing the use of KI-simulated terminal drought stress concentrated on KI impact at a final yield stage or 6 to 7 d after spray with a few reports examining the plant responses within 1 DASP (Sawhney and Singh 2002). No reports have come up till date on detailed physiological and biochemical characterization of KI-simulated terminal drought responses in soybean.

In the present study, we observed that photosynthetic CER and *E* declined significantly within 1 DASP of KI-spray treatment, even though the total Chl content quantum yield (TR/ABS), Chl *a*/*b* ratio, and RC/CS_o remained unaffected (statistically insignificant) at 1 DASP for all the growth stages. As hygroscopicity of chemical desiccants, such as KI, was postulated to interfere with plant water relations and also the fact that cuticular and stomatal pathway for salt entry into plants is possible (Burkhardt 2010), we can hypothesize that physical deposition of KI on leaf surface interfered with stomatal conductance. This could be the reason behind the significant decline in CER and *E* after 1 DASP, when the corresponding RWC did not decline significantly. This hypothesis is also supported by the correlation coefficient analysis from the regression between CER and *E*, CER and H/S, and *E* and H/S, where the correlation coefficient as well as significance was maximal for regression between CER and *E*, followed by CER and H/S, while the correlation coefficient between *E* and H/S was the lowest. This supports the hypothesis that KI deposition on leaf surface caused closing of stomata leading to decrease in CER. At the same time, hexose and sucrose contents were also enhanced within 1 DASP of KI-spray during R2, R4 as well as R5 stages. Accumulation of hexoses under drought stress is a well-known plant osmotic regulation to withstand the decreasing water potential in the tissues (Hare *et al*. 1998,

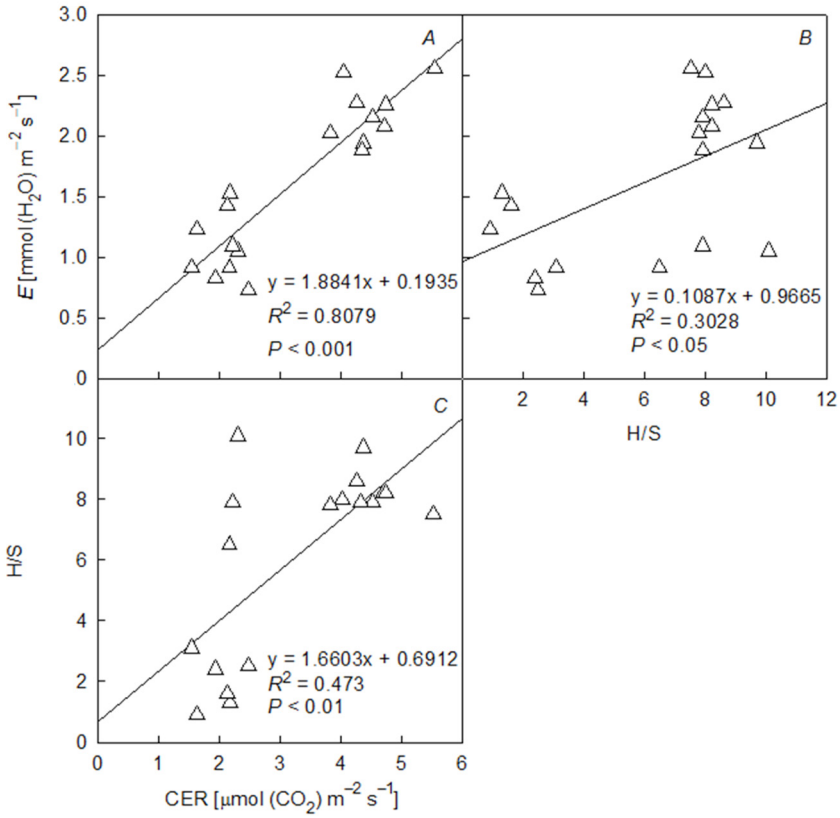

Fig. 7. Scatter plot for the linear regression analysis between carbon-exchange rate (CER) and transpiration rate (*E*) (*A*), hexose to sucrose ratio (H/S) and *E* (*B*), and CER and H/S (*C*).

Liu *et al*. 2004, Wang *et al.* 2016), which could be the result of higher invertase activity (Andersen *et al*. 2002, Fu *et al*. 2010) or enhanced starch degradation (Pelleschi *et al*. 1997, Lemoine *et al*. 2013). Previous studies on impact of drought stress on carbohydrate composition in soybean showed a significant decline in leaf sucrose content (Liu *et al*. 2004). However, in the present study, upon KI-induced desiccation, a significant increase in the sucrose content was observed. Higher sucrose accumulation with KI-simulated drought stress was also reported in wheat (Sawhney and Singh 2002), which can be attributed to a number of factors including higher partitioning of photosynthates towards sucrose rather than starch, impaired translocation of assimilated sucrose to sink tissues or utilizing the osmoregulatory functions of sucrose under desiccation stress. Also, irritation-induced electrical signals were reported to inactivate H^+-sucrose symporters, which reduces sucrose transport from leaves to phloem cells (Sukhov 2016). We can hypothesize that a similar mechanism operates under KI-induced desiccation resulting in a higher sucrose accumulation. In fact, the lowered photosynthetic CER within 1 DASP of KI spray, observed in the present study, could be due to the high hexose and sucrose accumulation in leaves, which is known to suppress photosynthesis through Rubisco inhibition (Goldschmidt and Huber 1992).

When compared to hexose contents, sucrose accumulation was found to be higher under KI-simulated drought stress during R4 and R5 stages, resulting in low H/S ratio when compared to controls. However, R2 stage showed a relatively lesser increase in sucrose leading to a higher H/S ratio at 1 DASP, similar at 3 DASP, and slightly lower ratio at 5 DASP with respect to controls. Comparatively lower sucrose accumulation at R2 stage can be attributed to rapid sucrose translocation to newly developed flowers at full-bloom stage, which upon gradual abortion showed progressive decline in the H/S ratio. It has been reported that the water demand in soybean during the flowering stage is the highest (Liu *et al*. 2003, Rosolem 2005) and leaf carbohydrate status is implicated in regulating the process of flower or pod abortion under natural drought conditions (Liu *et al*. 2004). It has been shown that H/S ratio plays a key role in regulating reproductive development of plants (Weber *et al*. 1998). A higher H/S ratio favors cell division during early stages of reproductive development, while a lower H/S ratio (or high sucrose content) is suggested to induce maturity and differentiation during later stages (Wang and Ruan 2013). Drought stress is reported to cause a decline in H/S ratio in pod and flowers of soybean, which was assumed to be one of the factors for pod/flower abortion due to reduced cell division (Liu *et al*. 2004). Importance of H/S ratio in leaf apoplasm has been described for mediating hormone-regulated leaf senescence, wherein a decreased H/S ratio due to lower cell wall invertase (CWIN) activity in the leaf apoplasm was hypothesized to trigger abscisic acid-mediated leaf senescence along with induction of cysteine protease genes (Ruan *et al*. 2010). As KI-simulated terminal drought stress is known to induce early senescence symptoms in plants, our results support the above hypothesis. In order to analyse whether H/S ratio correlates with photosynthetic CER during reproductive

development of soybean, we made a simple regression analysis using H/S ratio as the independent and CER as the dependent variable. A highly significant positive correlation was observed between the two parameters. Though the R^2 for the regression was only 0.473, it was highly significant as the P value was 0.002, *i.e.*, $P<0.01$. Sugar signals, especially hexose and sucrose, and/or H/S ratio-based are constantly found to be involved in modulating various photosynthesis-related parameters (Goldschmidt and Huber 1992, Iglesias *et al*. 2002, Lemoine *et al*. 2013). The actual concentrations of independent total hexose (glucose + fructose) and sucrose also correlated significantly with CER, just as H/S ratio. However, as the main objective of the present study was to show the role of H/S ratio, only the H/S and CER regression analysis is shown here. Hence, the present statistical correlation and modelling of H/S-based regulation of CER indicates that H/S ratio along with actual concentrations of hexose and sucrose plays a role in modulating photosynthetic performance of plants under terminal drought. Further validation of the model will require large-scale experimental inputs in this regard.

A strong inter-relationship exists between sink demand and source supply, which regulates the overall photosynthetic performance of plants during various growth stages (Paul and Foyer 2001). For a careful investigation of the KI-simulated terminal drought stress on stage-specific photosynthetic responses, Chl *a* fluorescence transients and quantum yield (flux ratios) were monitored simultaneously with CER and sugar status dynamics. The KI-induced senescence effects were evidenced in the present study by the observed gradual decrease in total Chl content. Lower energy connectivity among PSII units (higher L-band) and disrupted oxygen-evolving complex (higher K-band) were previously implicated as severe drought stress effects (Sengupta *et al*. 2013, Kalaji *et al*. 2016, Falqueto *et al*. 2017) and in the present study positive L and K-bands were observed during 3 and 5 DASP of KI spray at R2 and R4 stages, while only at 5 DASP (with comparatively lower amplitude) during R5 stage. Also, the quantum yield for electron transport from PSII to PSI, efficiency of reduction of the end electron acceptor and PSII quantum yield were significantly affected during KI-simulated terminal drought stress at R2 and R4 stages, but not R5 stage. Similar results were reported in wheat leaves in response to salt stress (Mehta *et al.* 2010). Our data demonstrates that KI-induced desiccation created a progressive damage to PSII stability during all the three stages, however, R5 stage exhibited relative tolerance. The observed maintenance in PSII efficiencies in R5 stage during 1 and 3 DASP of KI treatments correlated with the comparatively higher hexose accumulation during this period, which might act as osmoticum for tolerating the KI-induced desiccation damage at R5.

In conclusion, the present study demonstrated that soybean responded to KI-simulated terminal drought stress within 24 h of treatment, however, the desiccation impact was progressive in nature. Also, the H/S ratio could act as a key predictor of photosynthetic CER during reproductive stages of soybean under terminal drought stress. Further, seed initiation stage (R5) was found to be comparatively tolerant to KI-induced terminal drought stress with respect to Chl degradation and PSII efficiency, which correlated well with high hexose accumulation during this period. Outcomes from the present study not only elaborated the usefulness of utilizing KI spray as an agent for simulating terminal drought stress in soybean but also provided information on stage-specific response of soybean to terminal drought stress and highlighted the importance of the H/S ratio in predicting photosynthetic efficiency during terminal drought stress. However, future research is required to establish the molecular mechanisms underlying such physiological responses to KI-simulated terminal drought stress.

References

Agricultural Statistics at a Glance 2016. Available at eands.dacnet.nic.in/PDF/Glance-2016.pdf, 2016.

Andersen M.N., Asch F., Wu Y. *et al.*: Soluble invertase expression is an early target of drought stress during the critical, abortion-sensitive phase of young ovary development in maize. – Plant Physiol. **130**: 591-604, 2002.

Angra S., Kaur S., Singh K. *et al.*: Water-deficit stress during seed filling in contrasting soybean genotypes: Association of stress sensitivity with profiles of osmolytes and antioxidants. – Int. J. Agr. Res. **5**: 328-345, 2010.

Ashraf M., Harris P.J.C.: Photosynthesis under stressful environments: An overview. – Photosynthetica **51**: 163-190, 2013.

Baena-González E., Rolland F., Thevelein J.M. *et al.*: A central integrator of transcription networks in plant stress and energy signalling. – Nature **448**: 938-942, 2007.

Bhatia V.S., Jumrani K., Pandey J.P.: Evaluation of the usefulness of senescing agent potassium iodide (KI) as a screening tool for tolerance to terminal drought in soybean. – Plant Know. J. **3**: 23-30, 2014.

Biswal B., Pandey J.K.: Loss of photosynthesis signals a metabolic reprogramming to sustain sugar homeostasis during senescence of green leaves: Role of cell wall hydrolases. – Photosynthetica **56**: 404-410, 2018.

Blum A., Poyarkova H., Golan G., Mayer J.: Chemical desiccation of wheat plants as a simulator of post-anthesis stress. I. Effects on translocation and kernel growth. – Field Crop. Res. **6**: 51-58, 1983.

Borrás L., Slafer G.A., Otegui M.A.: Seed dry mass response to source-sink manipulations in wheat, maize and soybean: a quantitative reappraisal. – Field Crop. Res. **86**: 131-146, 2004.

Boureima S., Oukkaroum A., Diouf M. *et al.*: Screening for drought tolerance in mutant germplasm of sesame (*Sesamum indicum*) probing by chlorophyll *a* fluorescence. – Environ. Exp. Bot. **81**: 37-43, 2012.

Brestic M., Zivcak M., Kunderlikova K. *et al.*: Low PSI content limits the photoprotection of PSI and PSII in early growth stages of chlorophyll *b*-deficient wheat mutant lines. – Photosynth. Res. **125**: 151-166, 2015.

Burkhardt J.: Hygroscopic particles on leaves: nutrients or desiccants? – Ecol. Monogr. **80**: 369-399, 2010.

Daryanto S., Wang L., Jacinthe P.-A.: Global synthesis of drought effects on food legume production. – PLoS ONE **10**: doi: 10.1371/journal.pone.0127401, 2015.

Eveland A.L., Jackson D.P.: Sugars, signalling and plant development. – J. Exp. Bot. **63**: 3367-3377, 2012.

Falqueto A.R., da Silva Júnior R.A., Gomes M.T.G. *et al.*: Effects of drought stress on chlorophyll *a* fluorescence in two rubber tree clones. – Sci. Hortic.-Amsterdam **224**: 238-243, 2017.

Flexas J.A., Diaz-Espejo A., Gago J. *et al*.: Photosynthetic limitations in Mediterranean plants: A review. – Environ. Exp. Bot. **103**: 12-23, 2014.

Fu J., Huang B., Fry J.: Osmotic potential, sucrose level, and activity of sucrose metabolic enzymes in tall fescue in response to deficit irrigation. – J. Am. Soc. Hortic. Sci. **135**: 506-510, 2010.

Giannoccaro E., Wang Y.-J., Chen P.: Effects of solvent, temperature, time, solvent to sample ratio, sample size, and defatting on the extraction of soluble sugars in soybean. – J. Food Sci. **71**: 59-64, 2006.

Goldschmidt E.E., Huber S.C.: Regulation of photosynthesis by end-product accumulation in leaves of plants storing starch, sucrose, and hexose sugars. – Plant Physiol. **99**: 1443-1448, 1992.

Govindjee: Chlorophyll *a* fluorescence: A bit of basics and history. – In: Papageorgiou G.C., Govindjee (ed.): Chlorophyll *a* Fluorescence: A Signature of Photosynthesis. Pp. 1-42. Kluwer Academic, Dordrecht 2004.

Griffiths C.A., Paul M.J., Foyer C.H.: Metabolite transport and associated sugar signalling systems underpinning source/sink interactions. – Biochim. Biophys. Acta **1857**: 1715-1725, 2016.

Gupta A.K., Kaur N.: Sugar signalling and gene expression in relation to carbohydrate metabolism under abiotic stresses in plants. – J. Biosciences **30**: 761-776, 2005.

Hare P.D., Cress W.A., Van Staden J.A.: Dissecting the roles of osmolyte accumulation during stress. – Plant Cell Environ. **21**: 535-553, 1998.

Hiscox J.D., Israelstam G.F.: A method for the extraction of chlorophyll from leaf tissue without maceration. – Can. J. Botany **57**: 1332-1334, 1979.

Iglesias D.J., Lliso I., Tadeo F.R., Talon M.: Regulation of photosynthesis through source: sink imbalance in citrus is mediated by carbohydrate content in leaves. – Physiol. Plantarum **116**: 563-572, 2002.

Jagadish K.S.V., Kishor P.B.K., Bahuguna R.N. *et al*.: Staying alive or going to die during terminal senescence: An enigma surrounding yield stability. – Front. Plant Sci. **6**: doi: 10.3389/fpls.2015.01070, 2015.

Kalaji H.M., Jajoo A., Oukarroum A. *et al*.: Chlorophyll *a* fluorescence as a tool to monitor physiological status of plants under abiotic stress conditions. – Acta Physiol. Plant. **38**: doi: 10.1007/s11738-016-2113-y, 2016.

Koch K.: Sucrose metabolism: regulatory mechanisms and pivotal roles in sugar sensing and plant development. – Curr. Opin. Plant Biol. **7**: 235-246, 2004.

Kordenaeej A., Nejad A.A.N., Shojaeian A.A. *et al*.: Simulating the effect of terminal drought stress by potassium iodide and its use in mapping QTLs for yield and yield components in bread wheat. – Int. J. Agr. Plant Prod. **4**: 659-663, 2013.

Lawlor D.W., Cornic G.: Photosynthetic carbon assimilation and associated metabolism in relation to water deficits in higher plants. – Plant Cell Environ. **2**: 275-294, 2002.

Lemoine R., La Camera S., Atanassova R. *et al*.: Source to sink transport of sugar and regulation by environmental factors. – Front. Plant Sci. **4**: doi: 10.3389/fpls.2013.00272, 2013.

Liu F., Andersen M.N., Jensen C.R.: Loss of pod set caused by drought stress is associated with water status and ABA content of reproductive structures in soybean. – Funct. Plant Biol. **30**: 271-280, 2003.

Liu F., Jensen C.R., Andersen M.N.: Drought stress effect on carbohydrate concentration in soybean leaves and pods during early reproductive development: its implication in altering pod set. – Field Crop. Res. **86**: 1-13, 2004.

Manavalan L.P., Guttikonda S.K., Tran L.S.P. *et al*.: Physiological and molecular approaches to improve drought resistance in soybean. – Plant Cell Physiol. **50**: 1260-1276, 2009.

Mehta P., Allakhverdiev S.I., Jajoo A.: Characterization of photosystem II heterogeneity in response to high salt stress in wheat leaves (*Triticum aestivum*). – Photosynth. Res. **105**: 249-255, 2010.

Munné-Bosch S., Alegre L.: Die and let live: leaf senescence contributes to plant survival under drought stress. – Funct. Plant Biol. **31**: 203-216, 2004.

Nezhad K.Z., Weber W.E., Röder M.S. *et al*.: QTL analysis for thousand-grain weight under terminal drought stress in bread wheat (*Triticum aestivum* L.). – Euphytica **186**: 127-138, 2012.

Nguyen G.N., Hailstones D.L., Wilkes M. *et al*: Drought stress: Role of carbohydrate metabolism in drought-induced male sterility in rice anthers. – J. Agron. Crop Sci. **196**: 346-357, 2010.

Nicolas M.E., Turner N.C.: Use of chemical desiccants and senescing agents to select wheat lines maintaining stable grain size during post-anthesis drought. – Field Crop. Res. **31**: 155-171, 1993.

Ongom P.O., Volenec J.J., Ejeta G.: Selection for drought tolerance in sorghum using desiccants to simulate post-anthesis drought stress. – Field Crop. Res. **198**: 312-321, 2016.

Osorio S., Ruan Y.L., Fernie A.R.: An update on source-to-sink carbon partitioning in tomato. – Front. Plant Sci. **5**: doi: 10.3389/fpls.2014.00516, 2014.

Oukkaroum, A., Madidi, S.E., Schansker, G., Strasser, R.J.: Probing the responses of barley cultivars (*Hordeum vulgare* L.) by chlorophyll *a* fluorescence OLKJIP under drought stress and re-watering. – Environ. Exp. Bot. **60**: 438-446, 2007.

Pagano, M.C., Miransari, M.: The importance of soybean production worldwide. – In: Miransari, M. (ed.): Abiotic and Biotic Stresses in Soybean Production. Pp. 1-26. Academic Press, Amsterdam 2016.

Papageorgiou G.C., Tsimilli-Michael M., Stamatakis S.: The fast and slow kinetics of chlorophyll *a* fluorescence induction in plants, algae and cyanobacteria: a viewpoint. – Photosynth. Res. **94**: 275-290, 2007.

Paul M.J., Foyer C.H.: Sink regulation of photosynthesis. – J. Exp. Bot. **52**: 1383-1400, 2001.

Pelleschi S., Rocher J.P., Prioul, J.L.: Effect of water restriction on carbohydrate metabolism and photosynthesis in mature maize leaves. – Plant Cell Environ. **20**: 493-503, 1997.

Reddy A.R., Chaitanya K.V., Vivekanandan M.: Drought-induced responses of photosynthesis and antioxidant metabolism in higher plants. – J. Plant Physiol. **161**: 1189-1202, 2004.

Regan K.L., Whan B.R., Turner N.C.: Evaluation of chemical desiccant as a selection technique for drought resistance in a dry land wheat breeding programme. – Aust. J. Agr. Res. **44**: 1683-1691, 1993.

Rosa M., Prado C., Podazza G. *et al*.: Soluble sugars – metabolism, sensing and abiotic stress, a complex network in the life of plants. – Plant Signal. Behav. **4**: 388-393, 2009.

Rosolem C.A.: {Role of Brazil in fighting hunger in the World.] – In: Suzuki S., Yuyama, M.M., Camacho, S.A.: [Bulletin of Soybean Research.] Pp. 95-102. Fundação MT, Mato Grosso, Brazil 2005. [In Portuguese]

Royo C., Blanco R.: Use of potassium iodide to mimic drought stress in triticale. – Field Crop. Res. **59**: 201-212, 1998.

Ruan Y.L., Jin Y., Yang Y.J. *et al*.: Sugar input, metabolism, and signalling mediated by invertase: Roles in development, yield potential, and response to drought and heat. – Mol. Plant **3**: 942-955, 2010.

Ruan Y.L.: Signalling role of sucrose metabolism in development.

– Mol. Plant **5**: 763-765, 2012.
Sadras V.: Interaction between rainfall and nitrogen fertilisation of wheat in environments prone to terminal drought: economic and environmental risk analysis. – Field Crop. Res. **77**: 201-215, 2002.
Saeidi M., Abdoli M.: Effect of drought stress during grain filling on yield and its components, gas exchange variables, and some physiological traits of wheat cultivars. – J. Agr. Sci. Tech.-Iran **17**: 885-898, 2015.
Samarah N.H., Alqudah A.M., Amayreh J.A. *et al*.: The effect of late-terminal drought stress on yield components of four barley cultivars. – J. Agron. Crop Sci. **195**: 427-441, 2009.
Sawhney V., Singh D.P.: Effect of chemical desiccation at the post-anthesis stage on some physiological and biochemical changes in the flag leaf of contrasting wheat genotypes. – Field Crop. Res. **77**: 1-6, 2002.
Sengupta D., Guha A., Reddy A.R.: Interdependence of plant water status with photosynthetic performance and root defense responses in *Vigna radiata* (L.) Wilczek under progressive drought stress and recovery. – J. Photochem. Photobiol. **127**: 170-181, 2013.
Shapiguzov A., Lyukevich A.A., Allakhverdiev S.I. *et al*.: Osmotic shrinkage of cells of *Synechocystis* sp. PCC 6803 by water efflux *via* aquaporins regulates osmostress-inducible gene expression. – Microbiology **151**: 447-455, 2005.
Singh A.K., Singh A., Singh A.K. *et al*.: Application of potassium iodide as a new agent for screening of drought tolerance upland rice genotypes at flowering stage. – Plant Know. J. **1**: 25-32, 2012.
Smeekens S., Hellmann H.J.: Sugar sensing and signalling in plants. – Front. Plant Sci. **5**: doi: 10.3389/fpls.2014.00113, 2014.
Stirbet A., Lazár D., Kromdijk J., Govindjee: Chlorophyll *a* fluorescence induction: Can just a one-second measurement be used to quantify abiotic stress responses? – Photosynthetica **56**: 86-104, 2018.
Strasser R.J., Tsimilli-Michael M., Srivastava A.: Analysis of the chlorophyll *a* fluorescence transient. – In: Papageorgiou, G.C., Govindjee (ed.): Chlorophyll *a* Fluorescence. Advances in Photosynthesis and Respiration, Vol. 19. Pp. 321-362. Springer, Dordrecht 2004.
Sukhov V.: Electrical signals as mechanism of photosynthesis regulation in plants. – Photosynth. Res. **130**: 373-387, 2016.
Tuberosa R.: Phenotyping for drought tolerance of crops in the genomics era. – Front. Physiol. **3**: doi: 10.3389/fphys.2012.00347, 2012.
Tyagi P.K., Singh D.P., Pannu R.K.: Effect of post-anthesis desiccation on plant-water relation, canopy temperature, photosynthesis and grain yield in wheat genotypes. – Ann. Biol. **16**: 111-119, 2000.
Wang L., Ruan Y.L.: Regulation of cell division and expansion by sugar and auxin signalling. – Front. Plant Sci. **4**: doi: 10.3389/fpls.2013.00163, 2013.
Wang R., Gao M., Ji S. *et al*.: Carbon allocation, osmotic adjustment, antioxidant capacity and growth in cotton under long-term soil drought during flowering and boll-forming period. – Plant Physiol. Bioch. **107**: 137-146, 2016.
Weber H., Heim U., Golombek S. *et al*: Expression of a yeast-derived invertase in developing cotyledons of *Vicia narbonensis* alters the carbohydrate state and affects storage functions. – Plant J. **16**: 163-172, 1998.
Zinselmeier C., Jeong B.R., Boyer J.S.: Starch and the control of kernel number in maize at low water potentials. – Plant Physiol. **121**: 25-35, 1999.

Plant Cell, Tissue and Organ Culture (PCTOC)
https://doi.org/10.1007/s11240-020-01825-2

ORIGINAL ARTICLE

GUS-reporter based analysis of the promoter activity of *Gossypium hirsutum* NAC transcription factor, *GhNAC4* that is induced by phytohormones and environmental stresses

Vikas Shalibhadra Trishla[1] · Sureshbabu Marriboina[1] · Prasanna Boyidi[1] · Pulugurtha Bharadwaja Kirti[2]

Received: 2 October 2019 / Accepted: 7 April 2020

Abstract

The expression analysis of *GhNAC4*, a NAC (*NAM, ATAF1-2*, and *CUC2*) domain-containing transcription factor of the upland cotton, *Gossypium hirsutum* was carried out. Its expression was up-regulated by abscisic acid, cytokinin, methyl jasmonic acid, gibberellic acid, auxin, and ethylene. Its expression was also highly induced by drought, osmotic, oxidative, salinity, high and low-temperature stresses, and wounding. To corroborate these observations, we cloned the promoter of *GhNAC4* and fused it transcriptionally with *uidA* (GUS) gene for studies in transgenic tobacco. Fluorometric GUS analysis of the transgenic plants revealed that it is also induced by various phytohormones and environmental stresses. The spatio-temporal analysis of the *GhNAC4* promoter revealed that GUS expression was active in all stages of plant development including the reproductive organs. In the mature plant, the *GhNAC4* is expressed at a higher level in vascular bundles and guard cells. We also observed intense expression in other cells upon wounding. These observations were supported by a detailed bioinformatic analysis of the *GhNAC4* promoter for identifying the *cis*-acting elements that are associated with the regulation of gene expression in a tissue-specific and induced manner.

Key message

GhNAC4 gene is induced by phytohormones and environmental stress treatments in cotton. It is expressed throughout a mature plant, including the reproductive organs, vascular bundles, and guard cells.

Keywords Fluorometric assay · Histochemical assay · Motif search analysis · Transgenic tobacco · Vascular bundle · Wounding

Abbreviations

4-MU	4-Methylumbelliferone
4-MUG/MUG	4-Methyl-umbelliferyl-β-D-glucuronide
ABA	Abscisic acid
BAP	6-Benzyl aminopurine
GA	Gibberellic acid
GUS	B-glucuronidase
IAA	Indole-3-acetic acid
JA	Jasmonic acid
MeJA	Methyl jasmonic acid
MV	Methyl viologen
NAC	NAM ATAF CUC
PEG	Polyethylene glycol
SA	Salicylic acid
TF	Transcription factor

Communicated by Barbara Mary Doyle Prestwich.

Electronic supplementary material The online version of this article (https://doi.org/10.1007/s11240-020-01825-2) contains supplementary material, which is available to authorized users.

✉ Vikas Shalibhadra Trishla
strishlajain@gmail.com

✉ Pulugurtha Bharadwaja Kirti
pbkirti@gmail.com; pbkirti@uohyd.ac.in

[1] Department of Plant Sciences, School of Life Sciences, University of Hyderabad, Hyderabad, Telangana 500046, India

[2] Agri Biotech Foundation, Rajendranagar, Telangana 500030, India

Published online: 13 April 2020

Introduction

NAC (*NAM, ATAF1-2*, and *CUC2*) transcription factors (TFs) constitute one of the largest plant-specific TF superfamilies with more than 100 members in *Arabidopsis*, rice (Nuruzzaman et al. 2010), Populus (Hu et al. 2010), soybean (Le et al. 2011) and foxtail millet (Puranik et al. 2013).

A typical NAC TF carries two domains—a conserved N-terminal domain and a highly divergent C-terminal domain (Olsen et al. 2005). The N-terminal domain is essential for the DNA binding property of NAC TFs (Ernst et al. 2004), while the C-terminal domain is vital for the trans-activating property of NAC TFs (Stender et al. 2015).

Previous studies have shown that NAC TFs play essential roles in regulating a wide variety of biological processes such as shoot apical meristem development (Souer et al. 1996), seed development (Sperotto et al. 2009), leaf senescence (Guo and Gan 2006), flower development (Sablowski and Meyerowitz 1998), fiber development (Ko et al. 2007), abiotic (Hu et al. 2006) and biotic stress responses (Nakashima et al. 2007).

Promoters of only a few NAC TFs from *Arabidopsis* and rice have been characterized for their induction and localization patterns so far. *OsNAC6* promoter-GUS fusion was induced by abscisic acid (ABA), jasmonic acid and various environmental stresses. Its promoter sequence exhibited different *cis*-acting elements that are known to be involved in responses to environmental stresses (Nakashima et al. 2007). *OsNAC5* promoter was induced by ABA and was localized to roots and leaves under ABA and NaCl treatments (Takasaki et al. 2010). The expression patterns of the *SNAC1* promoter was observed in callus, root, leaf, guard cells, ligule, stamen, and pistil (Hu et al. 2006). The promoter-GUS fusion of *NST1* localized to the anthers, filaments of stamens, carpels and vascular bundles of the leaf, while *NST2* was mostly localized to anther wall and pollen grains (Mitsuda et al. 2005). *ANAC012* was mainly localized to the vascular bundles, especially in the (pro) cambium region, xylem parenchyma cells along with shoot apical meristem (Ko et al. 2007).

In a genome-wide analysis, Sun et al. (2018) identified 283 NAC genes in *Gossypium hirsutum*, 147 in *G. arboreum*, 267 in *G. barbadense*, and 149 in *G. raimondii*. They have analyzed the expression of NAC TFs in *G. hirsutum* and identified that 38 and 124 NAC TFs were particularly important in fiber development and stress responses, respectively. They also identified the motifs enriched in these NAC TFs promoters. In another study, the promoters of *GhNAC8–GhNAC17* were isolated using genome walking and the *cis*-acting elements were predicted (Shah et al. 2013). To the best of our knowledge, the spatio-temporal localization of NAC TFs has not been carried out so far in cotton species. Hence, a GUS-reporter-aided approach was adopted to elucidate the promoter activity of *GhNAC4*, a NAC TF which is highly up-regulated during drought treatment (Meng et al. 2009) as a step in this direction. The promoter region was cloned, and the *cis*-acting elements were predicted. The histochemical analysis of *GhNAC4* expression was undertaken through promoter-GUS fusion in tobacco, which showed that it is active in most parts of the transgenic plant including reproductive tissues. In the mature plant, the expression was also seen at higher levels in vascular bundles and guard cells. The expression analysis of *GhNAC4* and induction of *GhNAC4* promoter under various environmental and phytohormonal treatments showed that the gene is differentially regulated suggesting a unique expression pattern during cotton growth and development.

Materials and methods

Plant material

Cotton (*Gossypium hirsutum* var. JK Durga) seeds were surface sterilized, germinated and grown for 2 weeks on sterile filter paper (Whatman no. 1) placed on top of half-strength Murashige and Skoog (1962) medium, denoted as 0.5 × MS salts.

Phytohormonal and stress treatments

Treatments were given as described by Wang et al. (2005) with minor modifications. For hormonal treatments, the filter paper (Whatman no. 1) on which the seedlings were grown was moistened singly with 100 µM abscisic acid (ABA), 100 µM methyl jasmonic acid (MeJA), 100 µM salicylic acid (SA), 20 µM 6-benzyl aminopurine (BAP), 20 µM gibberellic acid (GA_3) or 20 µM indole-3-acetic acid (IAA) and incubated for 24 h prior to sampling. As controls, untreated seedlings on filter paper moistened with water having the same quantity of sodium hydroxide or ethanol used for dissolving the hormones were also used. Ethylene treatment was carried out for 24 h by placing the seedlings on filter paper in a sealed container. Ethephon (Etherel 40%, HiMedia Laboratories, India) was added to the box and diluted to a final concentration of 10 ppm in distilled water. Seedlings in a similar container having air were used as control.

High salt and osmotic stresses were induced by moistening the filter paper (Whatman no. 1) with 0.25 M NaCl and 0.3 M mannitol separately and the seedlings were allowed to grow for 24 h. Oxidative and drought stresses were induced by moistening the filter paper with 10 µM methyl viologen

(MV) and 15% (w/v) polyethylene glycol (PEG) 8000 individually, followed by incubation for 24 h. Air drying stress was carried out by placing the seedlings on the surface of dry filter paper for 30 min. Flooding stress was achieved by immersing the seedlings in distilled water for 24 h. Wounding stress was provided by squeezing the leaves with a forceps and harvesting them after 30 min. Combination of dark and cold treatments was given by wrapping the seedlings in aluminum foil and incubating at 4 °C for 24 h, while the dark treatment was carried out at 25 °C for 24 h. High-temperature stress was achieved by subjecting the seedlings to 42 °C for 12 h. Following all the treatments, the leaves were quick-frozen in liquid nitrogen to analyze the expression levels of *GhNAC4* gene.

To determine the degree of promoter activation, T_2 tobacco seedlings were subjected to different hormonal treatments and environmental stresses following the same methodology as applied to cotton seedlings.

RNA isolation and real-time quantitative PCR

Total RNA was extracted from the leaves of control and treated cotton seedlings by the CTAB (Cetyltriethylammonium bromide) extraction procedure as described by Chang et al. (1993). One µg of total RNA was used for synthesizing the first-strand cDNA using RevertAid first strand cDNA synthesis kit (Thermo Fischer Scientific, USA) following the manufacturer's instructions. The constitutively expressing Ubiquitin gene (*GhUBQ7*, GenBank Accession No. DQ116441) of cotton was used as an internal reference gene. The primer sequences used to amplify the internal regions of *GhNAC4* (NAC4-RTF and NAC4-RTR) and *GhUBQ7* (UBQ7-RTF and UBQ7-RTR, Kuppu et al. 2013) are mentioned in Supplementary Table 1. The fold change was determined using the $\Delta\Delta C_T$ method (Livak and Schmittgen 2001). The experiments were performed in triplicates, and two independent biological replicates were used in the analyses.

Isolation and cloning of *GhNAC4* promoter from cotton

The full-length CDS of *GhNAC4* (GenBank Accession Number EU706342.1) was used as a query to retrieve the 5′-upstream sequence from Phytozome (https://phytozome.jgi.doe.gov/). Genomic DNA was used as a template for PCR amplification of the DNA fragment. The primer sequences (GhNACPRO-F, GhNACPRO-R) used for the amplification are mentioned in Supplementary Table 1. The amplicon was cloned into the promoter-less vector pCAMBIA 1381Z (Cambia, Australia) to generate a fusion gene having 5′ upstream region of *GhNAC4* and *uidA* gene (pPRO$_{GhNAC4}$:GUS). This construct was used for *Agrobacterium tumefaciens* (strain EHA105) mediated tobacco transformation.

Generation of transgenic tobacco plants

Transgenic tobacco plants carrying the PRO$_{GhNAC4}$:GUS or empty pCAMBIA 1381Z (vector control) were generated using the standard *Agrobacterium*-mediated leaf disc transformation method as described by Horsch et al. (1985).

Histochemical localization and fluorometric measurement of GUS activity

β-glucuronidase(GUS) activity was assayed as described by Jefferson (1989) with minor modifications. For histochemical staining, the tissues were vacuum infiltrated with the solution containing 1 mM X-Gluc (5-bromo-4-chloro-3-indolyl-β-D-glucuronide), 1 mM potassium ferrocyanide, 1 mM potassium ferricyanide, 1 mM EDTA and 0.1% Triton X-100 in 50 mM phosphate buffer (pH 7.0) and incubated at 37 °C for 12–14 h in the dark. After staining, they were fixed in a solution containing 4% formaldehyde in 50 mM phosphate buffer (pH 7.0) for 12 h at 4 °C and subsequently cleared in 70% ethanol. Photographs were taken using M165 FC and DM6B microscopes (Leica Microsystems, Germany).

For the fluorometric assay, the tissue was homogenized in 400 µL GUS extraction buffer containing 10 mM EDTA and 0.1% Triton X-100 in 50 mM phosphate buffer (pH 7.0). After centrifugation at 12,000 rpm (4 °C) for 15 min, 5 µL of homogenate was diluted with 95 µL of extraction buffer and mixed with 100 µL of extraction buffer having 2 mM 4-MUG (4-methyl-umbelliferyl-β-D-glucuronide, Duchefa, Netherlands) and incubated at 37 °C for 1 h. The reaction was terminated by adding 1.8 mL of 200 mM sodium carbonate. Total protein concentration in the homogenate was assessed by Bradford method (Bradford 1976) with bovine serum albumin as standard. Fluorescence (excitation 363 nm, emission 447 nm) was determined by Infinite 200 plate reader (Tecan, Switzerland) and GUS activity was expressed as pmol of 4-MU (4-methyl-umbelliferone, Sigma, USA) per µg protein per min. 4-MU in the range of 20 nM to 100 µM was used to generate a standard curve. Each MUG assay was performed in triplicate and repeated three times.

Bioinformatics analysis of *GhNAC4* promoter sequence

The transcription start site was predicted by the Softberry database (Shahmuradov et al. 2017, www.softberry.com) using the default settings. A search for the putative *cis*-acting regulatory elements in the promoter sequence was conducted

using the PlantPAN 2.0 (Chang et al. 2008, http://plantpan2.itps.ncku.edu.tw/), PLACE (Higo et al. 1999, https://www.dna.affrc.go.jp/PLACE/) and PlantCARE (Lescot et al. 2002, http://bioinformatics.psb.ugent.be/webtools/plantcare/html/) databases. Only statistically significant motifs (P value > 0.9) were selected.

Statistical analysis

All experiments were repeated at least three times, and the data were expressed as the mean ± SE. Data were analyzed by one-way analysis of variance (ANOVA) using SigmaPlot 11.0 software. ***P < 0.001, **P < 0.01 and *P < 0.05 represent significant differences at 0.1, 1 and 5% level respectively. 'ns' represents no significant difference.

Results and discussion

Responsiveness of *GhNAC4* gene to treatments with phytohormones and environmental stresses

To gain an insight into the impact of environmental stresses and phytohormones on the expression of *GhNAC4*, real-time expression analysis was carried out. Figures 1 and 2 demonstrate that *GhNAC4* responded differentially to several

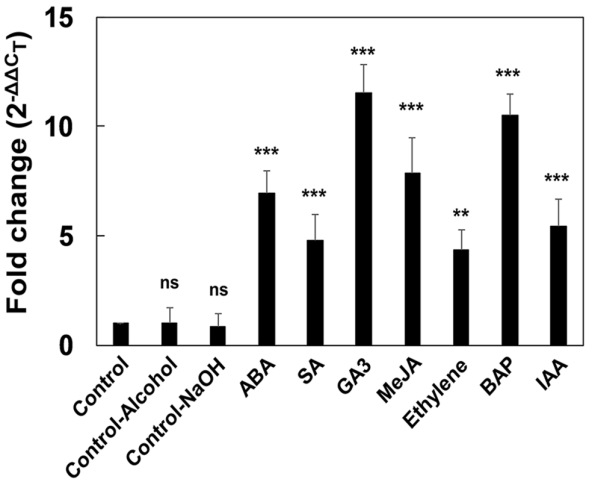

Fig. 1 Expression patterns of *GhNAC4* transcript in response to various phytohormones. qRT-PCR expression analysis of the *GhNAC4* gene in *G. hirsutum* leaves after ABA, MeJA, SA, 6-BAP, GA_3, IAA, or Ethephon treatment. Two weeks-old cotton seedlings incubated for 24 h under the treatment were used in the analysis. The mRNA levels of *GhNAC4* gene were normalized with that of Ubiquitin gene, *GhUBQ7*. The data are shown as the mean ± SE (n = 3). A statistical analysis with one-way ANOVA indicates significant differences (**P < 0.01, ***P < 0.001, *ns* not significant). *ABA* abscisic acid, *SA* salicylic acid, *GA3* 3-gibberellic acid, *MeJA* methyl jasmonic acid, *BAP* 6-benzyl aminopurine, *IAA* indole-3-acetic acid

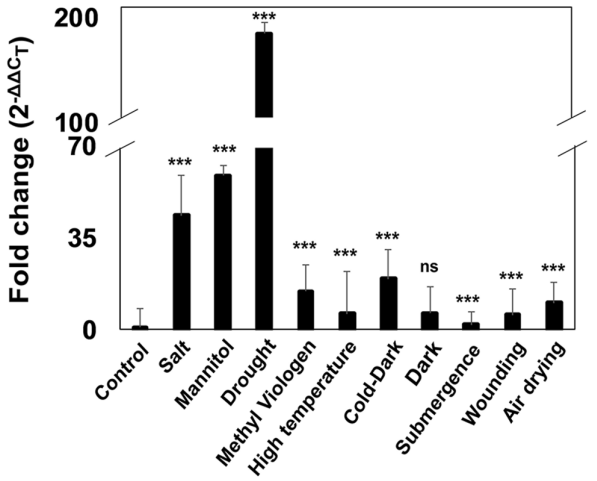

Fig. 2 Expression patterns of *GhNAC4* transcript in response to various environmental stresses. qRT-PCR expression analysis of the *GhNAC4* gene in *G. hirsutum* leaves after salt, mannitol, drought, methyl viologen, high temperature, air drying, submergence, wounding, dark or combination of dark and cold treatment. Two weeks-old cotton seedlings were used in the analysis. The mRNA levels of *GhNAC4* gene were normalized with that of Ubiquitin gene, *GhUBQ7*. The data are shown as the mean ± SE (n = 3). A statistical analysis with one-way ANOVA indicates significant differences (***P < 0.001, *ns* not significant)

phytohormones and environmental stresses. GA3 and BAP enhanced its expression by ~ 11.5 and 10.4 folds, respectively. The *GhNAC4* transcript levels were also up-regulated by MeJA and ABA to ~ 7.8 and 6.9 folds, respectively. IAA enhanced the expression by ~ 5.4 folds. However, other hormones like ethylene and SA triggered only a low level up-regulation of *GhNAC4* expression (~ four folds). ABA modulates plant abiotic stress responses, while MeJA, SA and ethylene play central roles in biotic stress responses. Role of auxin and cytokinin during environmental stress response is also emerging (Bielach et al. 2017). Cross-talk between various phytohormones results in antagonistic or synergistic interactions, which are necessary for plant response to environmental stress (Peleg and Blumwald 2011). Induction of expression of *GhNAC4* by these hormones suggests that the expression of *GhNAC4* is a possible node connecting multiple hormone signaling pathways.

The polyethylene glycol (PEG) induced drought stress treatment resulted in very high up-regulation of *GhNAC4* expression (~ 184 folds). Other abiotic stress treatments like high salinity and osmotic stresses also led to its high up-regulation (~ 43.6 and 58.7 folds respectively). Robust up-regulation of *GhNAC4* transcripts was also observed in air-drying and methyl viologen (MV) treatments (~ 10.2 and 14.5 folds). MV is known to generate ROS such as H_2O_2, which are important signaling molecules during environmental stress tolerance (Bhattacharjee 2005). Upregulation

of *GhNAC4* by MV suggests that it might be involved in the regulation of ROS-scavenging mechanism, playing a possible role in stress signaling pathway. Dark treatment caused ~6.2 folds increase in its expression and when this treatment was supplemented with low temperature, the expression was enhanced by ~19.4 folds suggesting an additive effect of the combination of two treatments. High temperature and wounding also increased *GhNAC4* expression by ~6.1 and 5.7 folds, respectively. The above expression profile suggests that fine-tuning of *GhNAC4* induction may require elaborate cross-talk between various signaling pathways via the involvement of phytohormones in cells.

Several NAC TFs are up-regulated by phytohormones and stress treatments. Furthermore, they function in diverse signaling pathways (Erpen et al. 2018). Auxin induces *AtNAC1* expression during lateral root formation (Xie et al. 2000). The expression of fine-stem stylo NAC TFs, *SgNAC1* and *SgNAC2* showed significant upregulation during cold stress (Zhan et al. 2018). The expression of rice *OsNAC6* is induced by ABA, JA, cold, drought, high salinity treatments and wounding (Ohnishi et al. 2005). Expression of tomato *SlNAC11* is induced by heat, dehydration and cold (Wang et al. 2017). Expression of wheat *TaNAC4* is up-regulated by ethylene, MeJA and ABA, cold, wounding and high salinity treatments (Xia et al. 2010). Various NAC TFs such as *SlNAC3* and *SbSNAC1* are also induced by drought and salinity (Al-Abdallat et al. 2015; Lu et al. 2013). Upregulation of *GhNAC4* by multiple stresses such as drought, salinity stress, osmotic stress, ROS, and wounding suggests it might play a potential role in multiple environmental stress signaling pathways.

Sequence analysis of *GhNAC4* promoter

A DNA fragment of 1612 bp corresponding to the upstream regulatory region (− 1492 bp to + 119 bp) of the *GhNAC4* was amplified from *G. hirsutum* genome. The composition of the GC content of *GhNAC4* promoter was 29.9%, which is as per the observed range for a plant promoter (Joshi 1987). The putative transcription start site (TSS) was located 119 bp upstream of the ATG translation start codon, which was consistent with the features of a eukaryotic promoter as shown in Supplementary Figure 1. The predicted TATA box was located 16 bp upstream of TSS, and a CAAT box was located 179 bp upstream of the TATA box.

Generation and analysis of tobacco transgenics of PRO_{GhNAC4}:GUS

To evaluate the promoter activity of *GhNAC4* gene, a total of 12 hygromycin resistant T_0 plants were generated and were confirmed by genomic PCR (GhNACPRO-F, GhNACPRO-R and HptII-F, HptII-R; Supplementary Table 1). To eliminate the effect of gene copy number on GUS activity, only single copy T_1 progenies, P7, P9, and P17 were used for further generation of T_2 seeds. The T_2 progenies of three lines, P7.1, P9.5, and P17.3, were used for histochemical and fluorometric assays.

GhNAC4 expresses in various tissues during growth and development

To precisely define the spatio-temporal expression patterns of *GhNAC4* promoter, we have used GUS staining analysis of PRO_{GhNAC4}:GUS transgenic tobacco plants. Figures 3 and 4 show the localization of GUS in vegetative and reproductive tissues. These GUS staining images are representative of at least three independent transgenic lines.

In early stages of tobacco growth (1 day old seedlings), GUS activity was first observed in emerging radicle (Fig. 3a), which was later detected in emerging cotyledons, root tip and shoot apex of 3 day old seedlings. However, GUS activity was relatively weaker in hypocotyl tissue (Fig. 3b). In 7, and 15 days old transformed tobacco seedlings, GUS expression was detected in leaf veins, petioles, stem, and root (Fig. 3c, d). Similar GUS activities were maintained in 1-month-old plants also (Fig. 3e).

The main and lateral roots showed GUS expression, which was absent in the root cap region and root hairs (Fig. 3f, g). Intense GUS staining was also observed in midrib and lateral veins, but leaf lamina showed scanty staining (Fig. 3h). We also observed GUS activity in guard cells (Fig. 3i) and developing mid rib regions of a young leaf (Fig. 3j). Figure 3k–m shows the staining of floral structures, which revealed that the GUS activity was present in sepals and to a lesser extent in the petal edges. GUS activity was also observed in anthers, pollen grains, and the stigma. However, it was absent in ovary and pedicel. No staining was detected in seedlings harboring a promoter-less GUS gene regardless of the developmental stage (Fig. 3n).

To obtain a better understanding of tissue specificity of GUS activity, thin cross-sections of various tissues were made using a razor blade. Intense GUS staining was detected in vascular bundles, especially in phloem of leaf veins, petiole, stem, and root (Fig. 4a–e). Both the abaxial and adaxial phloem tissues showed intense GUS staining. Other tissue types like pith, cortex, and epidermis, remained relatively unstained. However, cortex and epidermis also showed intense GUS expression upon wounding (Figs. 3k and 4f). The expression pattern of Passiflora *PmNAC1* transcripts was observed in root, shoot apex, floral bud and pro-vascular tissue especially the xylem cell specification (Rosa et al. 2013).

The occurrence of a unique pattern of *GhNAC4* promoter activity could be corroborated by the presence of several motifs responsible for tissue-specific expression

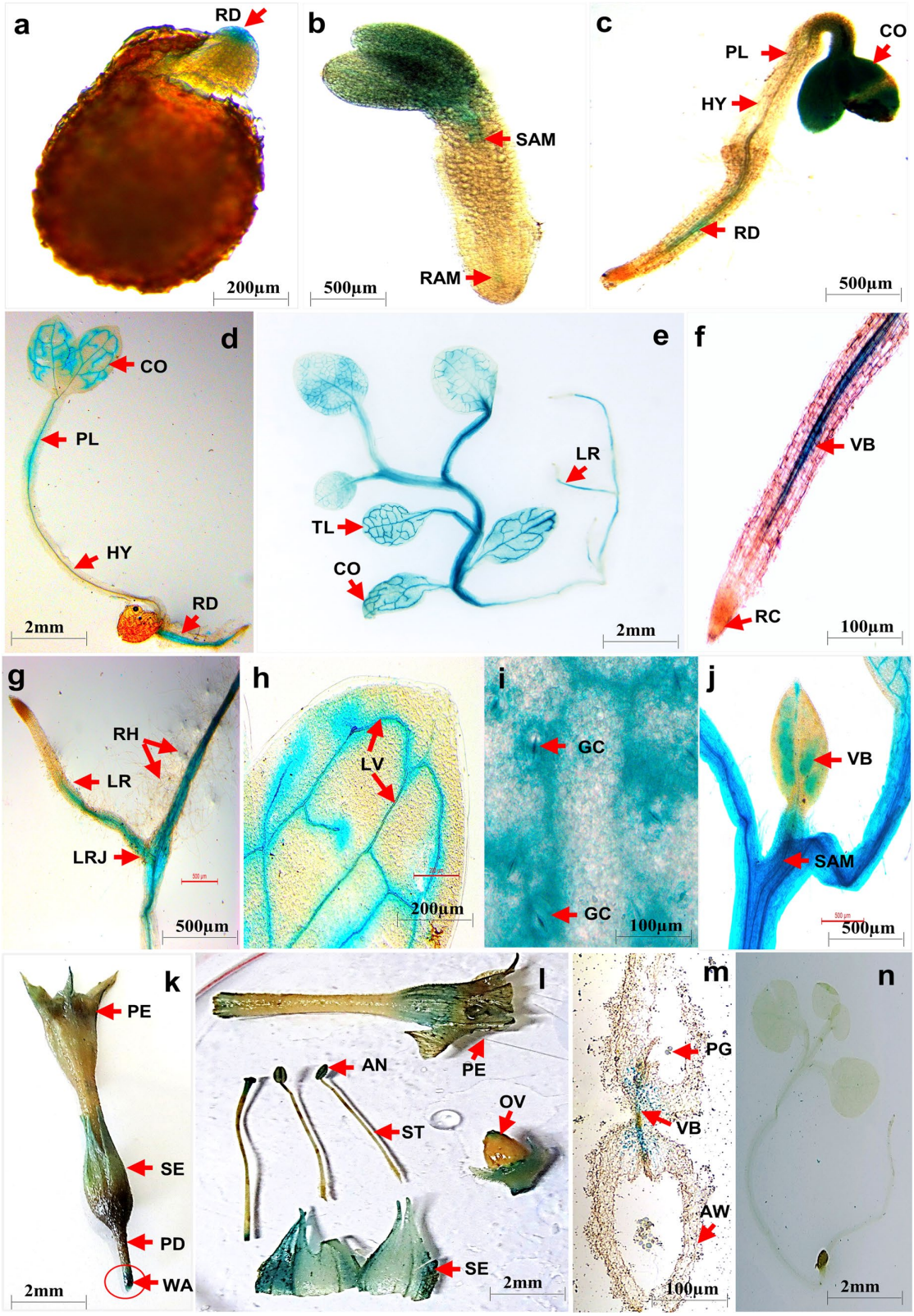
a
RD
200µm
b
SAM
RAM
500µm
c
CO
PL
HY
RD
500µm
d
CO
PL
HY
RD
2mm
e
LR
TL
CO
2mm
f
VB
RC
100µm
g
RH
LR
LRJ
500µm
h
LV
200µm
i
GC
GC
100µm
j
VB
SAM
500µm
k
PE
SE
PD
WA
2mm
l
PE
AN
OV
ST
SE
2mm
m
PG
VB
AW
100µm
n
2mm

◂**Fig. 3** Histochemical localization of GUS activity in tobacco transgenic plants containing PRO_{GhNAC4}:GUS construct. **a**–**e** seedlings grown on MS media with hygromycin at **a** day1; **b** day 3; **c** day 7; **d** day 15; **e** day 30. **f**–**j** Various tissues of a 30-day old transgenic tobacco plant **f** main root; **g** lateral root; **h** true leaf; **i** guard cells; **j** developing leaf. **k**–**m** floral structures **k** mature flower; **l** dissected flower showing various tissues; **m** cross-section of an anther. **n** 15 days old tobacco seedling carrying empty pCAMBIA 1381Z vector. *AW* anther wall, *CO* cotyledon, *GC* guard cell, *HY* hypocotyl, *LR* lateral root, *LRJ* lateral root junction, *LV* lateral vein, *OV* ovary, *PD* pedicel, *PE* petal, *PG* pollen grains, *PL* plumule, *RAM* root apical meristem, *RD* radicle, *RH* root hairs, *SAM* shoot apical meristem, *SE* sepal, *TL* true leaf, *VB* vascular bundle, *WA* wounded area. All arrows show strong GUS activity or no activity. Bars of each panel are as shown

patterns, as shown in Supplementary Table 2. Several copies of the developing embryo and seed-specific motifs such as SEF1MOTIF, SEF3MOTIFGM, and SEF4MOTIFGM7S motifs were observed in the *GhNAC4* promoter (Lessard et al. 1991) as also OSE1ROOTNODULE and OSE2ROOTNODULE motifs, which are root-specific elements (Fehlberg et al. 2005). Eleven copies of the ROOTMOTIFTAPOX1 element are predicted in the *GhNAC4* promoter, which has a distinct expression pattern in the root elongation zone and vascular bundle (Elmayan and Tepfer 1995). The CACTFTPPCA1 motif is a key component of mesophyll expression module 1 (MEM1) and is sufficient for high mesophyll-specific expression (Gowik et al. 2004). The TAAAGSTKST1 is a guard cell-specific motif and five copies were observed (Plesch et al. 2001).

Binding sites for quite a few other TFs known to play roles in organogenesis and tissue-specific expressions are also predicted such as GATA, MYBST1, DOFCOREZM, SBP TF, TCR TF, AT HOOK TF, and WOX TF. GATA motif plays a role in light responsiveness and tissue specificity and is involved in light-dependent development of phloem tissue (Yin et al. 1997). *GhNAC4* has 26 copies of DOFCOREZM motif, which is a binding site of DOF TFs. They regulate directly or indirectly the processes associated with the establishment and maintenance of vascular system (Le Hir and Bellini 2013).

Various motifs such as CARCGW8GAT, TGTCAC ACMCUCUMISIN and binding sites for MYBPZM and TCR TFs known to be important for flower and fruit development are found in the *GhNAC4* promoter. Several copies of the two pollen-specific motifs, POLLEN1LELAT52 (Bate and Twell 1998) and GTGANTG10 (Rogers et al. 2001) are also found in the *GhNAC4* promoter. Fang et al. (2008) carried out a systematic sequence analysis of NAC genes in rice and identified 12 particularly important tissue-specific NAC TFs. The promoters of these genes are predicted to have motifs such as SEF3MOTIFGM, ROOTMOTIFTAPOX1, and GTGANTG10.

GhNAC4 promoter is induced by various phytohormones

To explore the possible regulation of *GhNAC4* promoter by phytohormones, GUS activity was examined by fluorometric MUG assay. The corresponding results have been depicted in Fig. 5. The specific activity of GUS enzyme without any hormone treatments in PRO_{GhNAC4}:GUS seedlings was measured to be 2.4 ± 0.4 pmol μg^{-1} min^{-1}. This is in agreement with the histochemical staining results, where GUS staining was observed even in untreated seedlings. *GhNAC4* promoter was highly induced by BAP and ABA (~67.9% and 63.5%). IAA and MeJA treatment caused ~58.9% and 54.6% induction of the promoter activity, respectively. GA_3 and ethylene also enhanced the *GhNAC4* promoter activity by ~53.3% and 45.9% respectively. The pattern of *GhNAC4* promoter induction observed in phytohormonal treatments in tobacco seedlings is similar to the *GhNAC4* expression in cotton seedlings.

Evaluating the *cis*-elements present in the promoter region of the *GhNAC4* gene might allow us a better understanding of the differential regulation of *GhNAC4* by various phytohormones. *GhNAC4* promoter was predicted to have one copy of CPBCSPOR motif and 16 binding sites for Authentic Response Regulators1 (ARR1) as mentioned in Supplementary Table 2. CPBCSPOR motif is essential for cytokinin dependent transcriptional activation (Fusada et al. 2005). ARR1 is an important signaling component known to be involved in cytokinin-mediated differentiation of protoxylem (Yokoyama et al. 2007). Several motifs known for ABA responsiveness such as six copies of ACGTABREMOTIFA2OSEM, eight copies of ABRELATERD1 and one copy of ABREOSRAB21 motifs were predicted on the *GhNAC4* promoter. Mutation of the ABRE in the rice *OsNAC5* promoter led to the abolition of the activation of the promoter by ABA (Takasaki et al. 2010). Auxin responsive motifs such as AUXREPSIAA4, TGA element, GGTCCCATGMSAUR, and CATATGGMSAUR were predicted on the *GhNAC4* promoter. *Arabidopsis AtNAC1* plays a key role in promoting auxin-mediated lateral root formation (Xie et al. 2000). A plasma membrane-bound NAC TF, *NTM2* integrates auxin and salt signaling via the *IAA30* gene during seed germination in *Arabidopsis* (Park et al. 2011).

GhNAC4 promoter region is also predicted to contain JA responsive motifs such as T/GBOXATPIN2, TGACG, and CGTCA. JAMYC/AtMYC2 TF binds to the T/GBOXATPIN2 motif found in the promoter of JA responsive and wound-inducible Protease Inhibitor II (*PIN2*) gene (Boter et al. 2004). ANAC019 and ANAC055 act downstream of AtMYC2 as transcriptional activators to regulate JA-signaled defense responses (Bu et al. 2008). *GhNAC4* promoter is predicted to have four copies GAREAT and two copies of GARE1OSREP1 motifs, which are gibberellin responsive

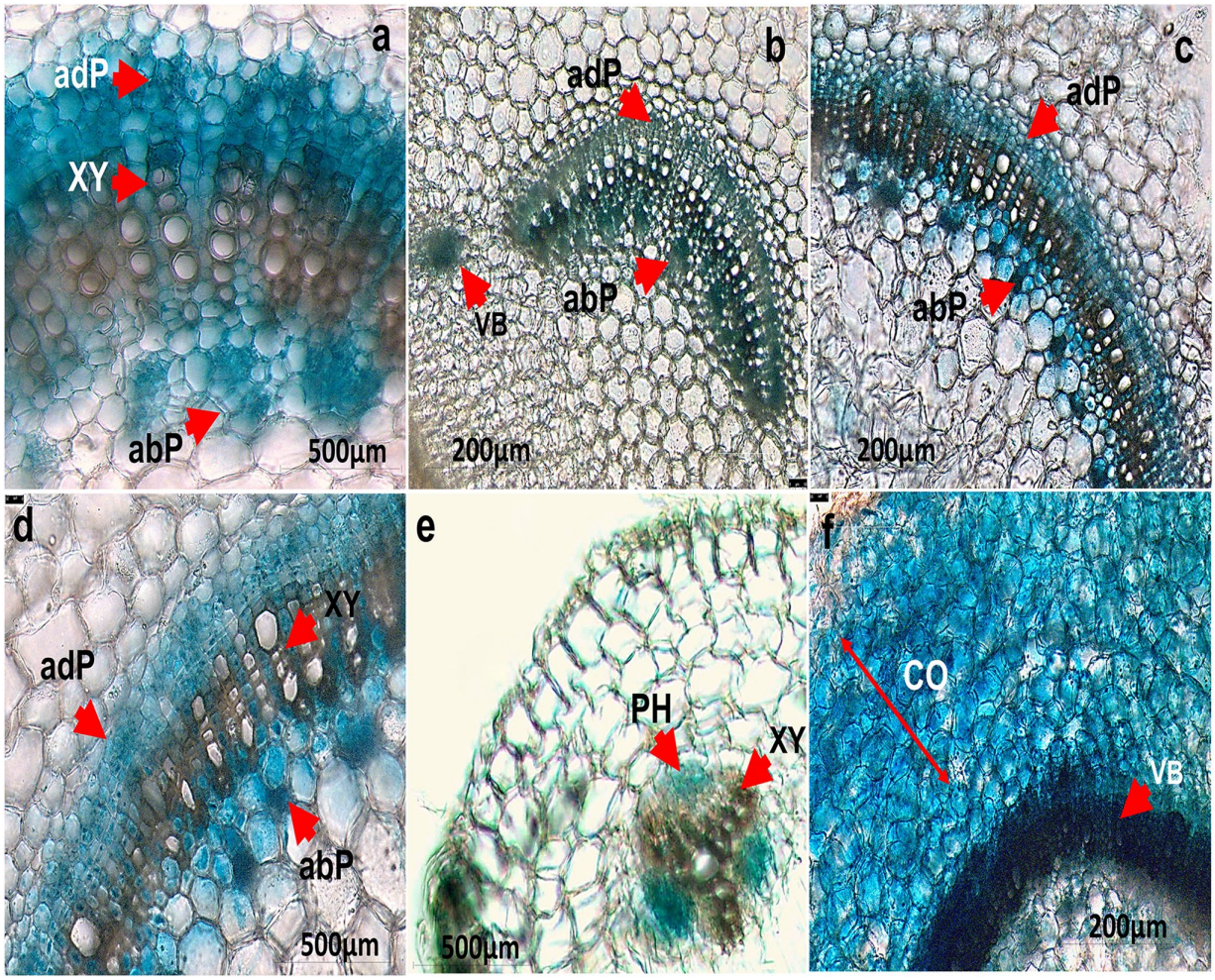

Fig. 4 GUS activity in free hand cross-sections tobacco transgenic plants containing PRO_{GhNAC4}:GUS construct. **a** leaf; **b** petiole; **c** stem **d** magnified view of the stem; **e** root; **f** wounded stem. *abP* abaxial phloem, *adP* adaxial phloem, *CO* cortex, *P* phloem, *VB* vascular bundle, *XY* xylem. All arrows show strong GUS activity or no activity. Bars of each panel are as shown

elements, GARE (Skriver et al. 1991). The above-mentioned sequences may function as phytohormone responsive motifs in the *GhNAC4* promoter.

GhNAC4 promoter is responsive to various environmental stress treatments

As we have observed that *GhNAC4* gene expression was regulated by various stresses, we studied the promoter activity by the fluorometric MUG assay as shown in Fig. 6. Drought stress treatment resulted in high induction of the *GhNAC4* promoter (~71%). Salinity and osmotic stress treatments also enhanced the promoter activity by ~68.5% and 69.5%, respectively. Oxidative stress and air-drying treatments up-regulated the promoter activity by ~68.2% and 66.6%, respectively. A combination of low-temperature stress and darkness treatment activated the *GhNAC4* promoter by ~59.3% as compared to darkness treatment alone (~43.1%) suggesting an additive effect of up-regulation of *GhNAC4* promoter induction. High-temperature and wounding stress treatments induced the promoter activity by ~42.1% and 41.7%, respectively. Flooding stress caused by submerging the seedlings in water also enhanced the promoter activity (~49.7%). The pattern of *GhNAC4* promoter induction observed by environmental stress treatments in tobacco seedlings is similar to the *GhNAC4* expression in cotton seedlings.

Evaluating the *cis*-elements present in the promoter region of the *GhNAC4* gene might help us with a better understanding of the differential regulation of *GhNAC4* by various environmental stresses. *GhNAC4* promoter region is predicted to contain many motifs like

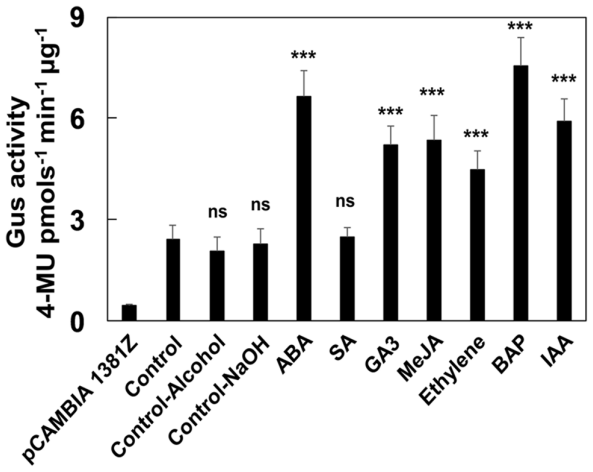

Fig. 5 Effect of various phytohormones on the GUS activity of PRO_{GhNAC4}:GUS tobacco transgenics. Fluorometric analysis of the GUS in tobacco seedlings after ABA, MeJA, SA, 6-BAP, GA_3, IAA, or Ethephon treatment. Two weeks-old PRO_{GhNAC4}:GUS tobacco transgenic seedlings incubated for 24 h under the treatment were used in the analysis. pCAMBIA 1381Z empty vector harboring tobacco seedlings were used as negative controls. The data are shown as the mean ± SE (n = 3). A statistical analysis with one-way ANOVA indicates significant differences (***P < 0.001, *ns* not significant). *ABA* abscisic acid, *SA* salicylic acid, *GA3* 3-gibberellic acid, *MeJA* methyl jasmonic acid, *BAP* 6-benzyl aminopurine, *IAA* indole-3-acetic acid

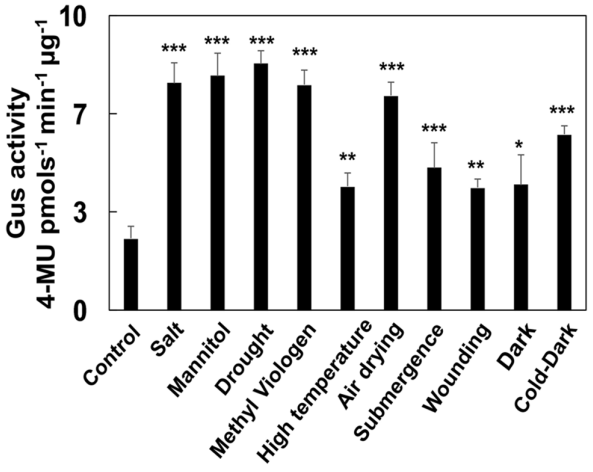

Fig. 6 Effect of various stresses on the GUS activity of PRO_{GhNAC4}:GUS tobacco transgenics. Fluorometric analysis of the GUS in tobacco seedlings after salt, mannitol, drought, methyl viologen, high temperature, air drying, submergence, wounding, dark or combination of dark and cold treatment. Two weeks-old PRO_{GhNAC4}:GUS tobacco transgenic seedlings, were used in the analysis. The data are shown as the mean ± SE (n = 3). A statistical analysis with one-way ANOVA indicates significant differences (*P < 0.05, **P < 0.01, ***P < 0.001)

MYB2CONSENSUSAT, C-REPEAT/DRE, DRECRTCOREAT, CSD, and CBFHV TF binding sites required for drought and cold responsiveness, as shown in Supplementary Table 2. Two copies of MYB2CONSENSUSAT motifs are found in the *GhNAC4* promoter, which is the binding site for AtMYB2 TF required for drought inducibility of *rd22* gene (Abe et al. 2003). Cold responsive motif, C-repeat (CRT) is responsible for the regulation of many cold-inducible genes in an ABA-independent manner. It is also involved in dehydration responsiveness (Stockinger et al. 1997). A fox-tail millet stress-responsive *SiNAC* promoter exhibits binding sites for MYB and MYC TFs and also contains CRT motif (Puranik et al. 2011). Three copies of the DRECRTCORE motif are found in the *GhNAC4* promoter. CBFHV motif is a binding site for an AP2 domain-containing cold-inducible TF, HvCBF1 characterized in barley (Xue 2002). Three copies of CBFHV motif are found in the *GhNAC4* promoter. Eight copies of binding site for cold shock domain (CSD) proteins are also found in the *GhNAC4* promoter that is highly activated during low-temperature stress. Promoter analysis of *MusaNAC68* by Negi et al. (2016) revealed the presence of various stress responsive motifs such as ACGTAT ERD1, MYB1AT, CBFHV and MYCCONSENSUSAT. Fang et al. (2008) carried out a systematic sequence analysis of NAC genes in rice and identified 20 particularly important stress-inducible NAC TFs. The promoters of these genes were predicted to have several stress-responsive motifs such as MYB1AT, MYB2CONSENSUSAT, MYCCONSENSUSAT, CBFHV, DRECRTCOREAT, and CRTDREHVCBF2.

Heat stress transcription factors (HSF) bind to the heat stress responsive element and modulate transcription during heat stress (Baniwal et al. 2004). Four copies of HSF binding site are present in the *GhNAC4* promoter. Binding sites for C2H2 TF are also identified in the *GhNAC4* promoter region. C2H2 TFs such as ZAT7, ZAT10, and ZPT2 are known to be important in regulating responses to abiotic and biotic stress tolerance (Kiełbowicz-Matuk 2012). *GhNAC4* promoter exhibited four copies of WBOXNTERF3 motifs. WRKY TFs binds to the WBOXNTERF3 motif in the promoter of *ERF3* gene of tobacco and causes its rapid activation upon wounding (Nishiuchi et al. 2004). The promoter of wound-inducible rice NAC gene, *OsNAC6* also exhibits four copies of W-box (Nakashima et al. 2007). The above-mentioned sequences may function as environmental stress-responsive motifs in the *GhNAC4* promoter.

Acknowledgements VST would like to acknowledge Vikas Kumar Jain and Manimaran Panneer Selvam for the critical reading of the manuscript. The authors are grateful to the Head, Department of Plant Sciences, University of Hyderabad for the facilities under various umbrella programs like DST-FIST and UGC-SAP-DRS.

Author contributions VST and PBK conceived and designed the experiments. VST, SM, and PB performed the experiments. VST analyzed the data. VST and PBK wrote the manuscript.

Funding VST would like to acknowledge the Council of scientific and industrial research (CSIR), New Delhi for research fellowship (20-6/2009(i)EU-IV).

Data availability All the data presented in the present manuscript are freely available to the interested researchers and would be made available upon request to the Corresponding author-VST (email- strishlajain@gmail.com).

Compliance with ethical standards

Conflict of interest The authors declare they have no conflict of interest.

Ethical approval This investigation does not necessitate the use of animals and hence, does not need the approval from the Animal Ethics Committee.

Consent to participate The present manuscript is the result of the participation of all the authors listed in it.

Consent for publication The authors of the manuscript hereby give their consent for publication of the manuscript in PCTOC.

References

Abe H, Urao T, Ito T, Seki M, Shinozaki K, Yamaguchi-Shinozaki K (2003) Arabidopsis AtMYC2 (bHLH) and AtMYB2 (MYB) function as transcriptional activators in abscisic acid signaling. Plant Cell 15:63–78. https://doi.org/10.1105/tpc.006130

Al-Abdallat AM, Ali-Sheikh-Omar MA, Alnemer LM (2015) Overexpression of two ATNAC3-related genes improves drought and salt tolerance in tomato (*Solanum lycopersicum* L.). Plant Cell Tiss Organ Cult 120:989–1001. https://doi.org/10.1007/s11240-014-0652-8

Baniwal SK, Bharti K, Chan KY, Fauth M, Ganguli A, Kotak S et al (2004) Heat stress response in plants: a complex game with chaperones and more than twenty heat stress transcription factors. J Biosciences 29:471–487. https://doi.org/10.1007/BF02712120

Bate N, Twell D (1998) Functional architecture of a late pollen promoter: pollen-specific transcription is developmentally regulated by multiple stage-specific and co-dependent activator elements. Plant Mol Biol 37:859–869. https://doi.org/10.1023/A:1006095023050

Bhattacharjee S (2005) Reactive oxygen species and oxidative burst: roles in stress, senescence and signal transduction in plants. Curr Sci 89:1113–1121

Bielach A, Hrtyan M, Tognetti VB (2017) Plants under stress: involvement of auxin and cytokinin. Int J Mol Sci 18:1427. https://doi.org/10.3390/ijms18071427

Boter M, Ruíz-Rivero O, Abdeen A, Prat S (2004) Conserved MYC transcription factors play a key role in jasmonate signaling both in tomato and Arabidopsis. Genes Dev 18:1577–1591. https://doi.org/10.1101/gad.297704

Bradford MM (1976) A rapid and sensitive method for the quantitation of microgram quantities of protein utilizing the principle of protein-dye binding. Anal Biochem 72:248–254. https://doi.org/10.1016/0003-2697(76)90527-3

Bu Q, Jiang H, Li CB, Zhai Q, Zhang J, Wu X et al (2008) Role of the Arabidopsis thaliana NAC transcription factors ANAC019 and ANAC055 in regulating jasmonic acid-signaled defense responses. Cell Res 18:756–767. https://doi.org/10.1038/cr.2008.53

Chang S, Puryear J, Cairney J (1993) A simple and efficient method for isolating RNA from pine trees. Plant Mol Biol Rep 11:113–116. https://doi.org/10.1007/BF02670468

Chang WC, Lee TY, Huang HD, Huang HY, Pan RL (2008) PlantPAN: plant promoter analysis navigator, for identifying combinatorial *cis*-regulatory elements with distance constraint in plant gene groups. BMC Genomics 9:561. https://doi.org/10.1186/1471-2164-9-561

Elmayan T, Tepfer M (1995) Evaluation in tobacco of the organ specificity and strength of the rolD promoter, domain A of the 35S promoter and the 35S2 promoter. Transgenic Res 4:388–396. https://doi.org/10.1007/BF01973757

Ernst HA, Olsen AN, Skriver K, Larsen S, Lo Leggio L (2004) Structure of the conserved domain of ANAC, a member of the NAC family of transcription factors. EMBO Rep 5:297–303. https://doi.org/10.1038/sj.embor.7400093

Erpen L, Devi HS, Grosser JW, Dutt M (2018) Potential use of the DREB/ERF, MYB, NAC and WRKY transcription factors to improve abiotic and biotic stress in transgenic plants. Plant Cell Tiss Organ Cult 132:1–125. https://doi.org/10.1007/s11240-017-1320-6

Fang Y, You J, Xie K, Xie W, Xiong L (2008) Systematic sequence analysis and identification of tissue-specific or stress-responsive genes of NAC transcription factor family in rice. Mol Genet Genomics 280:547–563. https://doi.org/10.1007/s00438-008-0386-6

Fehlberg V, Vieweg MF, Dohmann EMN, Hohnjec N, Pühler A, Perlick AM, Küster H (2005) The promoter of the leghaemoglobin gene VfLb29: functional analysis and identification of modules necessary for its activation in the infected cells of root nodules and in the arbuscule-containing cells of mycorrhizal roots. J Exp Bot 413:799–806. https://doi.org/10.1093/jxb/eri074

Fusada N, Masuda T, Kuroda H, Shimada H, Ohta H, Takamiya KI (2005) Identification of a novel *cis*-element exhibiting cytokinin-dependent protein binding in vitro in the 5′-region of NADPH-protochlorophyllide oxidoreductase gene in cucumber. Plant Mol Biol 59:631–645. https://doi.org/10.1007/s11103-005-0579-x

Gowik U, Burscheidt J, Akyildiz M, Schlue U, Koczor M, Streubel M, Westhoff P (2004) *cis*-regulatory elements for mesophyll-specific gene expression in the C 4 plant F*laveria trinervia*, the promoter of the C 4 phosphoenolpyruvate carboxylase gene. Plant Cell 16:1077–1090. https://doi.org/10.1105/tpc.019729

Guo Y, Gan S (2006) AtNAP, a NAC family transcription factor, has an important role in leaf senescence. Plant J 46:601–612. https://doi.org/10.1111/j.1365-313X.2006.02723.x

Higo K, Ugawa Y, Iwamoto M, Korenaga T (1999) Plant *cis*-acting regulatory DNA elements (PLACE) database: 1999. Nucleic Acids Res 27:297–300. https://doi.org/10.1093/nar/27.1.297

Horsch RB, Fry JE, Hoffmann NL, Eichholtz D, Rogers SG, Fraley RT (1985) A simple and general method for transferring genes into plants. Science 227:1229–1231. https://doi.org/10.1126/science.227.4691.1229

Hu H, Dai M, Yao J, Xiao B, Li X, Zhang Q, Xiong L (2006) Overexpressing a NAM, ATAF, and CUC (NAC) transcription factor enhances drought resistance and salt tolerance in rice. Proc Natl Acad Sci USA 103:12987–12992. https://doi.org/10.1073/pnas.0604882103

Hu R, Qi G, Kong Y, Kong D, Gao Q, Zhou G (2010) Comprehensive analysis of NAC domain transcription factor gene family in *Populus trichocarpa*. BMC Plant Biol 10:145. https://doi.org/10.1186/1471-2229-10-145

Jefferson RA (1989) The GUS reporter gene system. Nature 342:837–838. https://doi.org/10.1038/342837a0

Joshi CP (1987) An inspection of the domain between putative TATA box and translation start site in 79 plant genes. Nucleic Acids Res 15:6643–6653. https://doi.org/10.1093/nar/15.16.6643

Kiełbowicz-Matuk A (2012) Involvement of plant C2H2-type zinc finger transcription factors in stress responses. Plant Sci 185–186:78–85. https://doi.org/10.1016/j.plantsci.2011.11.015

Ko JH, Yang SH, Park AH, Lerouxel O, Han KH (2007) ANAC012, a member of the plant-specific NAC transcription factor family, negatively regulates xylary fiber development in *Arabidopsis thaliana*. Plant J 50:1035–1048. https://doi.org/10.1111/j.1365-313X.2007.03109.x

Kuppu S, Mishra N, Hu R, Sun L, Zhu X, Shen G et al (2013) Water-deficit inducible expression of a cytokinin biosynthetic gene IPT improves drought tolerance in cotton. PLoS ONE 8:e64190. https://doi.org/10.1371/journal.pone.0064190

Le DT, Nishiyama R, Watanabe Y, Mochida K, Yamaguchi-Shinozaki K, Shinozaki K, Tran LSP (2011) Genome-wide survey and expression analysis of the plant-specific NAC transcription factor family in soybean during development and dehydration stress. DNA Res 18:263–276. https://doi.org/10.1093/dnares/dsr015

Le Hir R, Bellini C (2013) The plant-specific Dof transcription factors family: new players involved in vascular system development and functioning in arabidopsis. Front Plant Sci 4:164. https://doi.org/10.3389/fpls.2013.00164

Lescot M, Dehais P, Thijs G, Marchal K, Van de Peer Y, Rouze P, Rombauts S (2002) PlantCARE, a database of plant *cis*-acting regulatory elements and a portal to tools for in silico analysis of promoter sequences. Nucleic Acids Res 30:325–327. https://doi.org/10.1093/nar/30.1.325

Lessard PA, Allen RD, Bernier F, Crispino JD, Fujiwara T, Beachy RN (1991) Multiple nuclear factors interact with upstream sequences of differentially regulated beta-conglycinin genes. Plant Mol Biol 16:397–413. https://doi.org/10.1007/BF00023991

Livak K, Schmittgen T (2001) Analysis of relative gene expression data using real-time quantitative PCR and the 2(T)(-Delta Delta C) method. Methods 25:402–408. https://doi.org/10.1006/meth.2001.1262

Lu M, Zhang DF, Shi YS, Song YC, Wang TY, Li Y (2013) Expression of SbSNAC1, a NAC transcription factor from sorghum, confers drought tolerance to transgenic Arabidopsis. Plant Cell Tiss Organ Cult 115:443–455. https://doi.org/10.1007/s11240-013-0375-2

Meng C, Cai C, Zhang T, Guo W (2009) Characterization of six novel NAC genes and their responses to abiotic stresses in *Gossypium hirsutum* L. Plant Sci 176:352–359. https://doi.org/10.1016/j.plantsci.2008.12.003

Mitsuda N, Seki M, Shinozaki K, Ohme-Takagi M (2005) The NAC transcription factors NST1 and NST2 of arabidopsis regulate secondary wall thickenings and are required for anther dehiscence. Plant Cell 17:2993–3006. https://doi.org/10.1105/tpc.105.036004

Murashige T, Skoog F (1962) A revised medium for rapid growth and bio assays with tobacco tissue cultures. Physiol Plant 15:473–497. https://doi.org/10.1111/j.1399-3054.1962.tb08052.x

Nakashima K, Tran LSP, Van Nguyen D, Fujita M, Maruyama K, Todaka D et al (2007) Functional analysis of a NAC-type transcription factor OsNAC6 involved in abiotic and *biotic stress-responsive gene expression in rice. Plant J 51:617–630. https://doi.org/10.1111/j.1365-313X.2007.03168.x

Negi S, Tak H, Ganapathi TR (2016) Expression analysis of MusaNAC68 transcription factor and its functional analysis by overexpression in transgenic banana plants. Plant Cell Tiss Organ Cult 125:59–70. https://doi.org/10.1007/s11240-015-0929-6

Nishiuchi T, Shinshi H, Suzuki K (2004) Rapid and transient activation of transcription of the ERF3 gene by wounding in tobacco leaves: possible involvement of NtWRKYs and autorepression. J Biol Chem 279:55355–55361. https://doi.org/10.1074/jbc.M409674200

Nuruzzaman M, Manimekalai R, Sharoni AM, Satoh K, Kondoh H, Ooka H, Kikuchi S (2010) Genome-wide analysis of NAC transcription factor family in rice. Gene 456:30–44. https://doi.org/10.1016/j.gene.2010.06.008

Ohnishi T, Sugahara S, Yamada T, Kikuchi K, Yoshiba Y, Hirano HY, Tsutsumi N (2005) OsNAC6, a member of the NAC gene family, is induced by various stresses in rice. Genes Genet Syst 80:135–139. https://doi.org/10.1266/ggs.80.135

Olsen AN, Ernst HA, Leggio LL, Skriver K (2005) NAC transcription factors: structurally distinct, functionally diverse. Trends Plant Sci 10:79–87. https://doi.org/10.1016/j.tplants.2004.12.010

Park J, Kim YS, Kim SG, Jung JH, Woo JC, Park CM (2011) Integration of auxin and salt signals by the NAC transcription factor NTM2 during seed germination in arabidopsis. Plant Physiol 156:537–549. https://doi.org/10.1104/pp.111.177071

Peleg Z, Blumwald E (2011) Hormone balance and abiotic stress tolerance in crop plants. Curr Opin Plant Biol 14:290–295. https://doi.org/10.1016/j.pbi.2011.02.001

Plesch G, Ehrhardt T, Mueller-Roeber B (2001) Involvement of TAAAG elements suggests a role for Dof transcription factors in guard cell-specific gene expression. Plant J 28:455–464. https://doi.org/10.1046/j.1365-313X.2001.01166.x

Puranik S, Bahadur RP, Srivastava PS, Prasad M (2011) Molecular cloning and characterization of a membrane associated NAC family gene, SiNAC from foxtail millet [*Setaria italica* (L.) P. Beauv]. Mol Biotechnol 49:138–150. https://doi.org/10.1007/s12033-011-9385-7

Puranik S, Sahu PP, Mandal SN, Parida SK, Prasad M (2013) Comprehensive genome-wide survey, genomic constitution and expression profiling of the NAC transcription factor family in foxtail millet (*Setaria italica* L.). PLoS ONE 8(5):64594. https://doi.org/10.1371/journal.pone.0064594

Rogers HJ, Bate N, Combe J, Sullivan J, Sweetman J, Swan C et al (2001) Functional analysis of *cis*-regulatory elements within the promoter of the tobacco late pollen gene g10. Plant Mol Biol 45:577–585. https://doi.org/10.1023/A:1010695226241

Rosa YBCJ, Aizza LCB, Bello CCM, Dornelas MC (2013) The PmNAC1 gene is induced by auxin and expressed in differentiating vascular cells in callus cultures of Passiflora. Plant Cell Tiss Organ Cult 115:275–283. https://doi.org/10.1007/s11240-013-0360-9

Sablowski RWM, Meyerowitz EM (1998) A homolog of NO APICAL MERISTEM is an immediate target of the floral homeotic genes APETALA3/PISTILLATA. Cell 531:220–234. https://doi.org/10.1016/j.gene.2013.09.007

Shah ST, Pang C, Fan S, Song M, Arain S, Yu S (2013) Isolation and expression profiling of GhNAC transcription factor genes in cotton (*Gossypium hirsutum* L.) during leaf senescence and in response to stresses. Gene 20:403–423. https://doi.org/10.1093/dnares/dst019

Shahmuradov IA, Umarov RK, Solovyev VV (2017) TSSPlant: a new tool for prediction of plant Pol II promoters. Nucleic Acids Res USA 88:7266–7270. https://doi.org/10.1073/pnas.88.16.7266

Skriver K, Olsen FL, Rogers JC, Mundy J (1991) *cis*-acting DNA elements responsive to gibberellin and its antagonist abscisic acid. Proc Natl Acad Sci USA 88:7266–7270. https://doi.org/10.1073/pnas.88.16.7266

Souer E, Van Houwelingen A, Kloos D, Mol J, Koes R (1996) The no apical Meristem gene of petunia is required for pattern formation in embryos and flowers and is expressed at meristem and primordia boundaries. Cell 85:159–170. https://doi.org/10.1016/S0092-8674(00)81093-4

Sperotto RA, Ricachenevsky FK, Duarte GL, Boff T, Lopes KL, Sperb ER et al (2009) Identification of up-regulated genes in flag leaves

during rice grain filling and characterization of OsNAC5, a new ABA-dependent transcription factor. Planta 230:985–1002. https://doi.org/10.1007/s00425-009-1000-9

Stender EG, O'Shea C, Skriver K (2015) Subgroup-specific intrinsic disorder profiles of arabidopsis NAC transcription factors: Identification of functional hotspots. Plant Signal Behav 10:6. https://doi.org/10.1080/15592324.2015.1010967

Stockinger EJ, Gilmour SJ, Thomashow MF (1997) Arabidopsis thaliana CBF1 encodes an AP2 domain-containing transcriptional activator that binds to the C-repeat. Proc Natl Acad Sci USA 94:1035–1040. https://doi.org/10.1073/pnas.94.3.1035

Sun H, Hu M, Li J, Chen L, Li M, Zhang S et al (2018) Comprehensive analysis of NAC transcription factors uncovers their roles during fiber development and stress response in cotton. BMC Plant Biol 18:1–15. https://doi.org/10.1186/s12870-018-1367-5

Takasaki H, Maruyama K, Kidokoro S, Ito Y, Fujita Y, Shinozaki K et al (2010) The abiotic stress-responsive NAC-type transcription factor OsNAC5 regulates stress-inducible genes and stress tolerance in rice. Mol Genet Genomics 284:173–183. https://doi.org/10.1007/s00438-010-0557-0

Wang NN, Shin MC, Li N (2005) The GUS reporter-aided analysis of the promoter activities of Arabidopsis ACC synthase genes AtACS4, AtACS5, and AtACS7 induced by hormones and stresses. J Exp Bot 56:909–920. https://doi.org/10.1093/jxb/eri083

Wang L, Hu Z, Zhu M, Zhu Z, Hu J, Qanmber G, Chen G (2017) The abiotic stress-responsive NAC transcription factor SlNAC11 is involved in drought and salt response in tomato (*Solanum lycopersicum* L.). Plant Cell Tiss Organ Cult 129:161–174. https://doi.org/10.1007/s11240-017-1167-x

Xia N, Zhang G, Liu XY, Deng L, Cai GL, Zhang Y et al (2010) Characterization of a novel wheat NAC transcription factor gene involved in defense response against stripe rust pathogen infection and abiotic stresses. Mol Biol Rep 37:3703–3712. https://doi.org/10.1007/s11033-010-0023-4

Xie Q, Frugis G, Colgan D, Chua NH (2000) Arabidopsis NAC1 transduces auxin signal downstream of TIR1 to promote lateral root development. Genes Dev 14:3024–3036. https://doi.org/10.1101/gad.852200

Xue GP (2002) An AP2 domain transcription factor HvCBF1 activates expression of cold-responsive genes in barley through interaction with a (G/a)(C/t)CGAC motif. BBA-Gene Regul Mech 1577:63–72. https://doi.org/10.1016/S0167-4781(02)00410-4

Yin Y, Chen L, Beachy R (1997) Promoter elements required for phloem-specific gene expression from the RTBV promoter in rice. Plant J 12:1179–1188. https://doi.org/10.1046/j.1365-313X.1997.12051179.x

Yokoyama A, Yamashino T, Amano YI, Tajima Y, Imamura A, Sakakibara H, Mizuno T (2007) Type-B ARR transcription factors, ARR10 and ARR12, are implicated in cytokinin-mediated regulation of protoxylem differentiation in roots of *Arabidopsis thaliana*. Plant Cell Physiol 48:84–96. https://doi.org/10.1093/pcp/pcl040

Zhan PL, Ke SW, Zhang PY, Zhou CC, Fu BL, Zhang XQ, Zhong TX, Chen S, Xie XM (2018) Overexpression of two cold-responsive ATAF-like NAC transcription factors from fine-stem stylo (*Stylosanthes guianensis* var. intermedia) enhances cold tolerance in tobacco plants. Plant Cell Tiss Organ 135:545–558. https://doi.org/10.1007/s11240-018-1486-6

Original article submitted to “Industrial Crops & Products”

Evaluation of High Salinity Tolerance in *Pongamia pinnata* (L.) Pierre by a Systematic Analysis of Hormone-Metabolic Network

Sureshbabu Marriboina[1], Kapil Sharma[2], Debashree Sengupta[1], Anurupa Devi Yadavalli[3], Rameshwar Prasad Sharma[2], Attipalli Ramachandra Reddy[1]*

[1]Department of Plant Sciences, School of Life Sciences, University of Hyderabad, Hyderabad-500046, India

[2]Repository of Tomato Genomics Resources, Department of Plant Sciences, School of Life Sciences, University of Hyderabad, Hyderabad-500046, India

[3]Department of Animal Biology, School of Life Sciences, University of Hyderabad, Hyderabad 500046, India

Abstract

Salinity stress results significant losses in plant productivity, and loss of cultivable lands. Although *Pongamia pinnata* is reported to be a salt tolerant semiarid biofuel tree crop, the adaptive mechanisms to saline environment are elusive. The present investigation describes alterations in hormonal and metabolic responses in correlation with physiological and molecular variations in leaves and roots of Pongamia at sea salinity level (3% NaCl) for 8days. At physiological level, salinity induced adjustments in plant morphology and leaf gas exchange patterns were observed. Our study also revealed that phytohormones including JAs and ABA play crucial role in promoting the salt adaptive strategies in Pongamia. Correlation studies demonstrated that hormones including ABA, JAs and SA showed a positive interaction with selective compatible metabolites (sugars, polyols and organic acids) to aid in maintaining osmotic balance and conferring salt tolerance to Pongamia. At the molecular level, our data showed that differential expression of transporter genes as well as antioxidant genes regulate the ionic and ROS homeostasis in Pongamia. Collectively, these results shed new insights on an integrated physiological, structural, molecular and metabolic adaptations conferring salinity tolerance to Pongamia.

Original article submitted to “Journal of Proteome Research”

Extensive Root Proteome Networks Revealed New Insights of Salt Tolerance Mechanisms in *Pongamia pinnata* L. Pierre

Authors: Sureshbabu Marriboina[1], Attipalli Ramachandra Reddy[1*]

[1]Department of Plant Sciences, School of Life Sciences, University of Hyderabad, Hyderabad-500046, India

ABSTRACT

Pongamia pinnata is being propagated as a potential tree species as a sustainable feed stock for biofuel and it is essential to understand the tolerance mechanisms of such trees to propagate on marginal lands. Pongamia roots provide determinant role to adapt the plant to sea saline concentration (3% NaCl). However, the tolerance mechanisms at cellular and proteome level are still inexplicit. In this study, Pongamia plants were grown hydroponically for 30 days and treated with 500 mM NaCl concentration for 4 days. Fresh roots were harvested for protein extraction and whole proteome was quantified by using free labelled nanoLC-MS/MS technique. A total number of 1062 proteins were identified with 130 differentially expressed proteins (DEPs). Protein homology studies have shown Pongamia sharing ~22% sequence similarity with *Glycine* and *Pisum*. Most of the DEPs belonged to flavonoid biosynthesis, CYP450 family proteins, seed storage proteins and carbohydrate metabolism. Interestingly, we recorded a significant increase in the chloroplast protective as well as glyoxylate cycle proteins. Our correlation network studies also clearly demonstrated a cross link between carbohydrate metabolism and amino acid metabolism. Collectively, for the first time, our data on whole root proteome have explored novel

insights into the salt tolerance mechanisms in *Pongamia pinnata* which are crucial to improve certain tree species to adapt for the fast changing and unfavourable climate regimes.

Original article submitted to "Photosynthesis Research"

Leaf gas exchange, Chlorophyll a fluorescence and biochemical responses depict High Salinity Tolerance in *Pongamia pinnata* (L.) pierre

Sureshbabu Marriboina[1], Kalva Madhana Sekhar[1], Attipalli Ramachandra Reddy*[1]
Department of Plant Sciences, School of Life Sciences, University of Hyderabad, Hyderabad-500046, India

Abstract

Saline lands and salinized arable lands are inadequate for plant growth and propagation. Cultivation of tree species such as Pongamia rehabilitate these lands towards economic gain, it is a well-known tree species for biofuel production. Without display of salt-induced morphological symptoms in plants grown 500 mM NaCl (3% NaCl; sea saline equivalent) for 30 days showed strong adaptive mechanisms operating under the extreme saline environment. Pongamia declined gas exchange parameters (net photosynthesis (A_{sat}), transpiration (E), and stomatal conductance (g_s)) about 50% at 15 DAS (day after salt-treatment) and maintained these levels for 30 days. Similar results were obtained in A_{sat}/Ci and A_{sat}/Q analysis. Analysis of polyphasic chl *a* fluorescence kinetics revealed well maintained structural and functional integrity of PSII. The characteristic negative L-band (which denotes grouping or connectivity among PSII units) was observed in both 300 and 500 mM NaCl treated plants at 30 DAS. A negative bell shaped K-band was recorded at 300 μs time interval in salt treated plants at 30 DAS. The JIP-test analysis and phenomenological fluxes showed salt induced photoacclimation responses including reduced electron transport and enhanced thermal dissipation of light energy from PSII. Proline levels were slightly increased in 300 and 500 mM salt treated plants at 30 DAS. Overall, for the first time, our data explored novel insights into underlying mechanisms which are responsible for unchanged leaf morphology characteristics in Pongamia under high saline environment.

Genetic, Physiological and Biochemical Responses to Salinity Stress in Pongamia pinnata (L.) Pierre, a Sustainable Feed Stock for Biofuel

by Marriboina Sureshbabu

Genetic, Physiological and Biochemical Responses to Salinity Stress in Pongamia pinnata (L.) Pierre, a Sustainable Feed Stock for Biofuel

ORIGINALITY REPORT

67%	8%	66%	3%
SIMILARITY INDEX	INTERNET SOURCES	PUBLICATIONS	STUDENT PAPERS

PRIMARY SOURCES

1	Sureshbabu Marriboina, Kapil Sharma, Debashree Sengupta, Anurupa Devi Yadavalli, Rameshwar Sharma, Attipalli Ramachandra Reddy. " Systematic hormone-metabolite network provides insights of high salinity tolerance in (L.) pierre ", Cold Spring Harbor Laboratory, 2020 Publication	34%
2	Sureshbabu Marriboina, Ramachandra Reddy Attipalli. "Hydrophobic cell-wall barriers and vacuolar sequestration of Na+ ions are among the key mechanisms conferring high salinity tolerance in a biofuel tree species, Pongamia pinnata L. pierre", Environmental and Experimental Botany, 2020 Publication	23%
3	Sureshbabu Marriboina, Debashree Sengupta, Sumit Kumar, Attipalli R. Reddy. "Physiological and molecular insights into the high salinity	5%

oxygen-induced cell death in HL-60 cells", Free Radical Research, 2009
Publication

28	Santisree Parankusam, Pooja Bhatnagar-Mathur, Kiran K. Sharma. "Heat responsive proteome changes reveal molecular mechanisms underlying heat tolerance in chickpea", Environmental and Experimental Botany, 2017 Publication	<1%
29	Parida, Asish K., Sairam K. Veerabathini, Asha Kumari, and Pradeep K. Agarwal. "Physiological, Anatomical and Metabolic Implications of Salt Tolerance in the Halophyte Salvadora persica under Hydroponic Culture Condition", Frontiers in Plant Science, 2016. Publication	<1%
30	repository.tudelft.nl Internet Source	<1%
31	S. Louati, M.S.J. Simmonds, R.J. Grayer, G.C. Kite, M. Damak. "Flavonoids from Eriobotrya japonica (Rosaceae) growing in Tunisia", Biochemical Systematics and Ecology, 2003 Publication	<1%
32	Submitted to University of Abertay Dundee Student Paper	<1%

Mariana Reginato. "The American Halophyte

18	"Salt Stress, Microbes, and Plant Interactions: Causes and Solution", Springer Science and Business Media LLC, 2019 Publication	<1%
19	"Reactive Oxygen, Nitrogen and Sulfur Species in Plants", Wiley, 2019 Publication	<1%
20	www.changbioscience.com Internet Source	<1%
21	www.publish.csiro.au Internet Source	<1%
22	"Salt Stress in Plants", Springer Science and Business Media LLC, 2013 Publication	<1%
23	journal.ashspublications.org Internet Source	<1%
24	link.springer.com Internet Source	<1%
25	"Ecophysiology and Responses of Plants under Salt Stress", Springer Nature, 2013 Publication	<1%
26	aspendb.uga.edu Internet Source	<1%
27	Sun Yee Kim, Su Min Lee, Jeen-Woo Park. "Antioxidant enzyme inhibitors enhance singlet	<1%

10	Submitted to Imperial College of Science, Technology and Medicine Student Paper	<1%
11	"Salt and Drought Stress Tolerance in Plants", Springer Science and Business Media LLC, 2020 Publication	<1%
12	Submitted to University of Hyderabad, Hyderabad Student Paper	<1%
13	"Salt Stress, Microbes, and Plant Interactions: Mechanisms and Molecular Approaches", Springer Science and Business Media LLC, 2019 Publication	<1%
14	www.frontiersin.org Internet Source	<1%
15	www.wildsoydb.org Internet Source	<1%
16	www.scsi.org.in Internet Source	<1%
17	"Molecular Stress Physiology of Plants", Springer Science and Business Media LLC, 2013 Publication	<1%

tolerance of Pongamia pinnata (L.) pierre, a potential biofuel tree species", Plant Science, 2017
Publication

4	www.biorxiv.org Internet Source	1%
5	Submitted to University of Wales Institute, Cardiff Student Paper	1%
6	B. B. V. Bindu, Mote Srinath, Aayeti Shailaja, Charu Chandra Giri. "Proteome analysis and differential expression by JA driven elicitation in Andrographis paniculata (Burm. f.) Wall. ex Nees using Q-TOF–LC–MS/MS", Plant Cell, Tissue and Organ Culture (PCTOC), 2019 Publication	<1%
7	Avnika Singh Anand, Urmila Gahlot, Dipti N. Prasad, Ekta Kohli. " Aluminum oxide nanoparticles mediated toxicity, loss of appendages in progeny of on chronic exposure ", Nanotoxicology, 2019 Publication	<1%
8	Submitted to University of Canterbury Student Paper	<1%
9	Submitted to University of Sheffield Student Paper	<1%

33	Prosopis strombulifera, a New Potential Source to Confer Salt Tolerance to Crops", Crop Production for Agricultural Improvement, 2012 Publication	<1%
34	Submitted to Higher Education Commission Pakistan Student Paper	<1%
35	Keita Tamura, Hikaru Seki, Hideyuki Suzuki, Mareshige Kojoma, Kazuki Saito, Toshiya Muranaka. "CYP716A179 functions as a triterpene C-28 oxidase in tissue-cultured stolons of Glycyrrhiza uralensis", Plant Cell Reports, 2016 Publication	<1%
36	T. Swaroopa Rani, Daisuke Takahashi, Matsuo Uemura, Appa Rao Podile. "Proteins Associated with Oxidative Burst and Cell Wall Strengthening Accumulate During Citrus-Xanthomonas Non-Host Interaction", Plant Molecular Biology Reporter, 2014 Publication	<1%
37	journals.plos.org Internet Source	<1%

I wish to bring to your kind notice that enclosed plagiarism report (62%) includes the contents of three papers published by us in reputed international Journals.

Exclude quotes On Exclude matches < 14 words

However, the total percent plagiarism excluding our publications (self) is only 5%.

Prof. Attipalli R. Reddy, FNASc
Dept. of Plant Sciences
University of Hyderabad